

FAROE-SHETLAND BASIN BASEMENT CHARACTERISATION AND THERMAL CALIBRATION DATABASE & REPORT

Project No.: 10006



**by
Applied Petroleum Technology (UK) Ltd.
14 Wynnstay Road, Colwyn Bay, LL29 8NB, UK
&
Chemostrat Ltd.
1 Ravenscroft Court, Buttington Cross Enterprise Park,
Welshpool, SY21 8SL, UK**

**January 2021
Copyright © APT UK Ltd. 2021**

Faroe-Shetland Basin Basement Characterisation and Thermal Calibration Database

Copyright of this document is vested in APT UK Ltd. and the document is issued in confidence for the purpose only for which it is supplied. It must not be reproduced in whole or in part except under an agreement or with the consent in writing of APT UK Ltd. and then only on the condition that this notice is included in any such reproduction.

Registered in England and Wales no. 5814934.

This copy of the above report has been licenced to:

.....

This report is for the sole use of the above company, parent company or wholly owned subsidiaries within the same group.

None of this report may be reproduced by or for any other company, organisation or individual without the written consent of
APPLIED PETROLEUM TECHNOLOGY (UK) LIMITED.

Warranty

In preparation of this report APT UK Ltd. has employed every reasonable endeavour to create a product that has been accurately prepared and follows accepted petroleum industry practices. The interpretation of the data and ideas expressed within are the best judgement of APT UK Ltd. The use of the report is at the sole discretion and judgement of the client and APT UK Ltd. shall not be held responsible or liable for any consequential loss or damages arising from the utilisation of this report.

Applied Petroleum Technology (UK) Ltd.

Unit 8, Tan-y-Graig, Parc Caer Seion, Conwy, LL32 8FA, UK

January 2021

REPORT

Text and Interpretation

Key Tables and Figures

CONTENTS

	PAGE
1 EXECUTIVE SUMMARY	1-1
1.1 Summary	1-1
2 INTRODUCTION	2-1
2.1 Summary	2-1
2.2 Scope and purpose of the study	2-1
2.3 Materials, analyses and database	2-2
2.4 Report structure	2-3
2.5 Personnel involved	2-4
2.6 Acknowledgements	2-4
3 INORGANIC GEOCHEMISTRY ANALYSES AND RESULTS	3-1
3.1 Introduction	3-1
3.2 Inorganic geochemical analyses results by well	3-2
3.2.1 Data and discussion for well 154/03-1	3-2
3.2.2 Data and discussion for well 164/25-2	3-2
3.2.3 Data and discussion for well 202/02-1	3-2
3.2.4 Data and discussion for well 202/08-1	3-2
3.2.5 Data and discussion for well 202/09-1	3-2
3.2.6 Data and discussion for well 204/10-1	3-3
3.2.7 Data and discussion for well 204/15-2	3-3
3.2.8 Data and discussion for well 204/23-1	3-3
3.2.9 Data and discussion for well 204/25-1	3-3
3.2.10 Data and discussion for well 204/26-1A	3-4
3.2.11 Data and discussion for well 204/27a-1	3-4
3.2.12 Data and discussion for well 204/28-1	3-4
3.2.13 Data and discussion for well 205/16-1	3-4
3.2.14 Data and discussion for well 205/20-1	3-4
3.2.15 Data and discussion for well 205/21-1A	3-5
3.2.16 Data and discussion for well 205/22-1A	3-5
3.2.17 Data and discussion for well 206/07a-2	3-5
3.2.18 Data and discussion for well 206/08-1A	3-5
3.2.19 Data and discussion for well 206/08-2	3-6
3.2.20 Data and discussion for well 206/08-7	3-6
3.2.21 Data and discussion for well 206/08-8	3-6
3.2.22 Data and discussion for well 06/09-2	3-6
3.2.23 Data and discussion for well 206/12-1	3-6
3.2.24 Data and discussion for well 207/01-3	3-7

3.2.25	Data and discussion for well 207/02-1	3-7
3.2.26	Data and discussion for well 208/23-1	3-7
3.2.27	Data and discussion for well 208/26-1	3-7
3.2.28	Data and discussion for well 208/27-1	3-7
3.2.29	Data and discussion for well 208/27-2	3-8
3.2.30	Data and discussion for well 209/09-1	3-8
3.2.31	Data and discussion for well 209/12-1	3-8
3.2.32	Data and discussion for well 214/09-1	3-8
3.2.33	Data and discussion for well 220/26-1	3-8
3.3	Basement mapping	3-9
3.4	Implications for petroleum exploration	3-11
3.4.1	Fractured basement	3-11
3.4.2	Provenance of sands in the FSB	3-11

4 APATITE THERMOCHRONOLOGY ANALYSES AND RESULTS

4-1

4.1	Summary	4-1
4.2	Introduction	4-3
4.3	Methods & Results of Apatite Fission Track Analyses	4-5
4.3.1	Quad 204 wells	4-10
4.3.1.1	Data and discussion for well 204/10a-5	4-10
4.3.2	Quad 205 wells	4-12
4.3.2.1	Data and discussion for well 205/09-1	4-12
4.3.2.2	Data and discussion for well 205/12-1	4-14
4.3.2.3	Data and discussion for well 205/14-2	4-17
4.3.2.4	Data and discussion for well 205/17b-2	4-19
4.3.3	Quad 206 wells	4-23
4.3.3.1	Data and discussion for well 206/11-1	4-23
4.3.4	Quad 207 wells	4-24
4.3.4.1	Data and discussion for well 207/01-2	4-24
4.3.5	Quad 208 wells	4-27
4.3.5.1	Data and discussion for well 208/17-2	4-27
4.3.5.2	Data and discussion for well 208/24-1A	4-28
4.3.5.3	Data and discussion for well 208/27-2	4-31
4.3.6	Quad 214 wells	4-35
4.3.6.1	Data and discussion for well 214/26-1	4-35
4.3.6.2	Data and discussion for well 214/28-1	4-37
4.4	Synopsis	4-44

5 OPTICAL MATURITY ANALYSES AND RESULTS

5-1

5.1	Summary	5-1
5.2	Introduction	5-3
5.3	Results of optical maturity analyses	5-4
5.3.1	Discussion for well 205/09-1	5-4
5.3.2	Discussion for well 205/12-1	5-4
5.3.3	Discussion for well 205/14-2	5-5
5.3.4	Discussion for well 205/14-3	5-6
5.3.5	Discussion for well 206/01-1A	5-6
5.3.6	Discussion for well 206/11-1	5-7

5.3.7	Discussion for well 207/01-2	5-8
5.3.8	Discussion for well 208/17-1	5-9
5.3.9	Discussion for well 207/17-2	5-9
5.3.10	Discussion for well 209/12-1	5-10
5.3.11	Discussion for well 214/26-1	5-11
5.3.12	Discussion for well 214/28-1	5-11

6 INTEGRATION OF NEW ANALYTICAL DATA AND REGIONAL COMPARISONS 6-1

6.1	Summary	6-1
6.2	Introduction	6-2
6.3	Geotrack Reports – GC503, GC540 & GC605 & Fluid inclusion data	6-3
	6.3.1 GeoTrack report synopsis and integration: What can we take from the GeoTrack reports?	6-5
	6.3.1.1 GC503 West of Shetlands (South)	6-5
	6.3.1.2 GC540 West of Shetlands (North)	6-6
	6.3.1.3 GC605 North of Shetlands	6-8
	6.3.1.4 GeoTrack & APT-Chemostrat data summary	6-9
	6.3.2 Evidence of ‘hot fluids’ from literature	6-11
	6.3.2.1 ‘Hot fluids’ Literature Summary & Implications	6-12
6.4	Basin context & evolution	6-14
	6.4.1 Lithosphere through time	6-14
	6.4.2 Iceland ‘plume’ and the impact on heat flow	6-15
	6.4.3 Crustal thickness	6-17
	6.4.4 Basement composition	6-18
	6.4.5 Depth conversion	6-19
	6.4.6 Late Tertiary uplift	6-20
6.5	1D Basin models	6-22
	6.5.1 Expulsion	6-22
	6.5.2 Model building	6-23
	6.5.3 Modelling volcanic areas	6-24
6.6	Faroe-Shetland Basin Petroleum Systems	6-26
	6.6.1 Charge timing – is there a problem?	6-26
	6.6.2 Misunderstanding of PSA, Faroe-Shetland Basin	6-27
	6.6.3 Oil vs. Gas Geochemistry	6-28
	6.6.4 Re-Os Isotopes	6-29

7 REFERENCES 7-1

DATA APPENDICES

APT and Chemostrat Geochemical Data - Analytical Tables and Figures

APPENDICES

APPENDIX 1 – INORGANIC GEOCHEMISTRY DATA

- Appendix 1.1 Summary of samples analysed for inorganic geochemistry
- Appendix 1.2 Radioactive heat production and Zircon/Apatite geochronology data
- Appendix 1.3 Petrology and X-Ray diffraction analysis summary
- Appendix 1.4 Mineral, fracture and bitumen point count analysis data

APPENDIX 2 – APATITE FISSION TRACK DATA

- Appendix 2.1 Summary of samples analysed for apatite fission track
- Appendix 2.2 Apatite fission track (AFT) data

APPENDIX 3 – OPTICAL MATURITY DATA

- Appendix 3.1 Summary of samples analysed for optical maturity
- Appendix 3.2 Vitrinite reflectivity (VR) data
- Appendix 3.3 Vitrinite reflectivity (VR) histograms, data and statistics
- Appendix 3.4 Spore colour index (SCI) data
- Appendix 3.5 List of abbreviations used in maturity data tables

APPENDIX 4 – PROVENANCE IMPLICATIONS

Discussion on the inorganic geochemistry data obtained for the sandstones (and basement) samples studied with regards to sediment provenance.

- Appendix 4.1 Zircon provenance
- Appendix 4.2 Apatite provenance

- Appendix 5.1 Analytical methods used in the Chemostrat laboratory (UK)
- Appendix 5.2 Analytical methods used in the Apatite.com laboratory (USA)
- Appendix 5.3 Analytical methods used in the APT AS laboratories (Norway) and APT UK laboratories (UK)

DATABASES

APT databases: optical maturity & AFT data

DATABASES

Database files

- Analytical data are fully report in Excel files listed below:
Optical maturity data 01 – APT-Chemostrat_WOSI II_VR-SCI_Database.xlsx
Apatite Fission Track data 02 – APT-Chemostrat_WOSI II_AFT_Database.xlsx
- Please refer to the first tab in each workbook for the reporting format (tab-name: dataKEYS).

Legacy database files

Three legacy non-proprietary reports, written by GeoTrack, have been released by the OGA:

- GC503 West of Shetlands (South): Thermal and tectonic development and hydrocarbon generation history assessed using apatite fission track analysis and vitrinite reflectance. – March 1995*
- GC540 West of Shetlands (North): Thermal and tectonic development and hydrocarbon generation history assessed using apatite fission track analysis and vitrinite reflectance. – February 1995*
- GC640 North Shetland Region: Thermal and tectonic development and hydrocarbon generation history assessed using apatite fission track analysis and vitrinite reflectance. – October 1996*

All the data from these reports has been digitised, assigned latitudes and longitudes and is included in this reported as Excel files – see:

- GeoTrack_legacy_reports_GC503-540-640_apatite_thermochronology_data.xlsx
- GeoTrack_legacy_reports_GC503-540-640_Vitrinite_reflectance_maturity_data.xlsx
- GeoTrack_legacy_reports_GC503-540-640_Bottom_hole_temperature_data.xlsx

This includes 357 temperature data points, largely comprising corrected bottom hole temperatures (BHT) and the 411 vitrinite reflectance measurements (by Keiraville Konsultants).

CHAPTER 1

EXECUTIVE SUMMARY

Alex Finlay, Chemostrat & Julian Moore, APT

1.1 SUMMARY

This study has generated a broad inter-disciplinary dataset that constrains the thermal evolution of the Faroe-Shetland Basin. The temperature history of a sedimentary basin is of importance to both the modelling of petroleum system (principally source rock maturation), reservoir fluid quality risk (biodegradation) and reservoir diagenesis.

The data reported in this study employed a wide range of inorganic and organic geochemical methods, mineralogical and organic petrology, and basin modelling. The basement samples were characterised using Inductively Coupled Plasma Optical Emission Spectroscopy (ICP-OES) & Inductively Coupled Plasma Mass Spectrometry (ICP-MS) analysis, petrology, Uranium-Lead (U-Pb) Zircon & U-Pb Apatite geochronology by Laser Ablation ICP-MS (LA-ICP-MS) methods. Shale samples were subject to kerogen isolation and microscopy analysis for vitrinite reflectance and spore colour indices. Sandstone samples were subject to High Resolution-Apatite Fission Track thermochronology (HR-AFT), where the apatite grains are sorted into distinct provenance groups using LA-ICP-MS data (REE concentrations and $^{206}\text{Pb}^*/^{238}\text{U}$ ages) and modelled as independent groups to yield group dependent time-temperature histories. This is the first time this method has been made available at a large scale commercially. The basement sample composition data was used to populate the crustal component of nine 1D models which were calibrated to both the new data generated in this report (apatite thermochronology derived time-temperature paths and % Ro) and the available legacy data.

The basement composition work revealed a clear compositional variation by displaying a trend from tonalitic dominated Neoarchean gneiss (quads 202, 204 and the west of 205) to more felsic Neoarchean gneisses of granitic/granodiorite composition (quads 206 & 208). Apatites contain within the gneisses displayed evidence of Laxfordian metamorphism. The data shows that basement samples in quads 214, 209 & 220 are of Caledonian plutonic granitic composition. Furthermore, two Neoarchean samples from the South East of quad 208 contain apatites that appear to have been reset by Caledonian metamorphism. This variation in basement composition results in a marked trend in heat flow and hence geothermal gradient from cool in the Southwest of the AOI (quads 202, 204) to 'hot' in the North East of the AOI (Quads 214, 209, 220).

The thermal calibration data (apatite thermochronology, %Ro/SCI) demonstrated that the basinal areas investigated tended to be at or close to their maximum temperatures present-day. Evidence for higher paleo-temperatures was sporadic and was indicated to occur in the Late Tertiary rather than the Early Tertiary when the intrusive igneous activity occurred (thought to be caused by decompression melting caused by the lithospheric thermal anomaly associated with the passing of the Icelandic plume). Models testing impact of thermal erosion of the lithosphere suggest that the impact on the temperature histories caused by this are very modest.

Heating associated with direct intrusive activity is of much greater magnitude but is thought to be relatively localised.

The results obtained from our 1D modelling, combined with appropriate expulsion modelling suggest that the charge timing ‘issue’ in the Faroe-Shetland Basin has been over-emphasised in previous studies. The integration of observations from across the petroleum system charge indicate that timing can be understood in terms of: Delayed expulsion – due to a function of cooler models (especially in the SW) and appropriate expulsion model(s); Migration ‘lag’ and the preservation of oil legs under leaking gas caps. The concept of a PSA critical moment is not a useful concept and should be discontinued (especially at the basin scale).

The study has implication for both exploration teams engaged in the modelling and prediction of the petroleum system in the Faroe-Shetland basins and for geoscientific researchers working on the processes involved in the basin evolution. While previously considered complex, it is believed that where the complexity is either miss-placed or miss understood in terms of the petroleum system then this can lead to poorer risking and a less clarity on the framework in which to assess new exploration opportunities. The objective is not to create a universal basin model or indeed a complete understanding of the petroleum system. Future work should look to carry out similar analyses particularly to the North and East of the study AOI. Additionally, further work on phase prediction integrating the analyses reported here with consideration of trap PT state, charge GOR, trap geometry and seal integrity would be of value to test the limits of predictability. Largely, further integration of gas and liquid geochemistry with charge histories and seal capacities to explore the interplay between these parameters is recommended.

CHAPTER 2

INTRODUCTION

Alex Finlay, Chemostrat & Julian Moore, APT

2.1 SUMMARY

Historically, petroleum system analysis in the Faroe Shetland Basin (FSB) has always struggled to match results with the observed geology. For example, the OGA petroleum systems chart for the West of Shetland and West of Hebrides, released as part of the 32nd licencing round, places the ‘critical moment’ for oil generation in the Mid to Late Cretaceous, before common Palaeogene reservoirs such as the Lamba and Vaila sands are deposited. Several explanations have been put forward to try and explain this mismatch between observed geology and modelled results, such as oil migrating into deeper holding reservoirs before re-migrating into the Palaeocene (e.g. the motel model; Lamer and Carmichael 1999) or overpressure retarding the expulsion of oil from source rock (e.g. Carr & Scotchman, 2003).

These published petroleum systems analysis studies do not account for all aspects of the petroleum system, one of particular relevance to the Faroe-Shetland basin is the variation in radioactive heat production (RHP) from basement. A focussed study around the Corona ridge demonstrated that basement here is “old and cold” (Gardiner *et al.* 2019) with basement RHP values averaging $\sim 1.6 \mu\text{W}/\text{m}^3$, significantly lower than the default values of upper-crust RHP in most basin modeling software (e.g., set at $\sim 2.8\text{--}3.2 \mu\text{W}/\text{m}^3$ in Genesis and PetroMod). By using these colder RHP values, Gardiner *et al.* (2019) produced a basin model that placed the critical moment for oil production around the Corona Ridge in the Palaeogene, after the deposition of local reservoirs. Is the ‘critical’ moment a useful concept? While all published basin modelling studies report ‘early’ (Cretaceous) generation for the Faroe-Shetland basin (e.g. Illiffe *et al.* 1999; Holms *et al.* 1999; Mark *et al.* 2005) can charge timing be an issue when numerous fields have been found? This study aims to help offer some answers to these questions (principally addressed in the integration Chapter 6).

This study has been produced with two main aims:

1. To produce a QA/QC controlled data base of the key data (RHP, apatite fission track and optical maturity data) needed to produce basin models across the FSB
2. To map basement and so understand how areas may be clumped or split when carrying out petroleum system analysis.
3. Provide a discussion based on the available legacy data, literature and the calibrated basin models produced in this study to describe how petroleum system may operate in a clear way.

2.2 SCOPE AND PURPOSE OF THE STUDY

This study aims to produce a set of fully quality assured/controlled key parameters needed for petroleum systems analysis across quads 154, 164, 202, 203, 204, 205, 206, 207, 208, 209, 214 & 220 in the FSB. It achieves this through:

- The production of RHP data for individual well and depths across the FSB for detailed petroleum systems analysis

- The mapping of basement
 - By age of formation (U-Pb Zircon geochronology)
 - By age of alteration by metamorphism (U-Pb apatite geochronology)
 - By texture and petrology (Petrography and X-Ray diffraction)
- The establishment of RHP values for mapped basement zones for regional petroleum systems analysis
- High resolution Apatite Fission Track Data (AFT) in Cretaceous and Palaeocene sands
- QA/QC of released OGA/GeoTrack AFT data
- New Optical maturity analysis data in shale units
- QA/QC of released OGA/GeoTrack VR data

In addition to this, the OGA released GeoTrack reports are discussed, as are considerations for basin model parameterisation. Finally, model selection for 1D models and new thoughts on source rock expulsion gained from the shale gas revolution are also discussed.

2.3 MATERIALS, ANALYSES AND DATABASE

All new samples analysed in this study were collected from the British Geological Surveys (BGS) Keywork corestore (Table *below*) and full results are presented in Appendix 1-3.

Well	RHP	U-Pb Zircon Geochronology	U-Pb Apatite Geochronology	Petrology	Apatite Fission Track	Optical Maturity
202/02-1	Y			Y		
202/08-1	Y			Y		
202/09-1	Y			Y		
204/10-1	Y	Y	Y	Y		
204/10a-5					Y	
205/9-1					Y	Y
205/12-1					Y	Y
205/14-2					Y	Y
205/14-3						Y
205/16-1	Y	Y	Y	Y		
205/17b-2					Y	
206/01-1A						Y
206/7a-2	Y	Y	Y	Y		
206/11-1					Y	Y
207/01-2					Y	Y
207/01-3	Y	Y	Y	Y		
207/02-1	Y	Y	Y	Y		
208/17-1						Y
208/17-2					Y	Y
208/23-1	Y	Y	Y	Y		
208/24-1A					Y	
208/27-2	Y	Y	Y	Y	Y	
209/09-1	Y	Y	Y	Y		
209/12-1	Y			Y		Y
214/26-1					Y	Y
214-28-1					Y	Y

New analyses have been undertaken at:

- Apatite.com laboratory (USA)
 - Apatite Fission Track
- APT UK laboratory (UK)
 - Optical Maturity
- Chemostrat laboratory (UK):
 - Elemental analysis to calculate RHP
 - U-Pb Zircon Geochronology
 - U-Pb Apatite Geochronology
 - Petrology (thin section analysis of core material and XRD analysis of cuttings material)

Full analytical protocols are recorded in Appendix 4.

In addition to the new analysis undertaken as part of this study, a literature search was conducted providing historical data for:

- Elemental data to enable RHP calculations: Chemostrat multiclient report: NE129, Chambers et al. (2005) & Finlay et al. (2018).
- U-Pb zircon geochronology: Ritchie et al. (2011), Chemostrat (2014) & Holdsworth et al. (2019)
- U-Pb apatite geochronology: Chemostrat (2014)
- Petrology: Chambers et al. (2005), Finlay et al. (2018) & Holdsworth et al. (2019).
- Apatite fission track & Optical Maturity data from OGA released GeoTrack studies GC503, GC540 & GC640

This data has been compiled into a new database (see appendix 1-3) and is discussed in Chapter 6.

2.4 REPORT STRUCTURE

Chapter 3 introduces the inorganic (elemental, geochronological and petrological) data and identifies what geological information can be gained from each technique. It then presents the new and historical data by well. This data is then used to split FSB basement into six zones, based on the age and geology of the basement. Finally, attention is drawn to how this data may be used to aid exploration in fractured basement plays.

Chapter 4 introduces the apatite thermochronology and results. Its objectives are to create an additional thermal calibration dataset for modelling and assess the evidence for anomalous thermal events in the Tertiary. Sample preparation and analytical methods are described as well as how this data can be used to produce time – temperature path models as well as understand what provenance information can be gained from this analysis. Data from wells are then clumped by quad and discussed individually.

Chapter 5 introduces the optical maturity analysis and results. Maturity analysis was carried out by vitrinite reflectivity, spore colouration and kerogen composition analysis. Results are presented and discussed by well.

Chapter 6 is an integration chapter, in which pertinent legacy apatite data (GeoTrack reports), maturity and fluid inclusion data are reviewed, and the geology and geophysical aspects of the

Faroe Shetland basin relevant to basin modelling are discussed. A series of 1D basin models are also briefly described. These models incorporate appropriate expulsion modelling, which is shown to impact both expelled products (i.e. petroleum phase) and timing. Finally, a discussion on Faroe-Shetland petroleum system is provided where some views, we believe to be misunderstandings of the petroleum system, are critiqued.

Chapter 7 contains a full list of references for this work with methods and data presented in Appendix 1-3. Finally, Appendix 4 discusses new implications on sediment provenance analyses produced by this study.

2.5 PERSONNEL INVOLVED

This report has been produced through the collaboration of Chemostrat Ltd and APT. No. Key staff are:

APT UK

- Dr. Julian Moore - study conception, project management, basin modelling, literature review, data analysis and report production
- Lloyd Jones – optical maturity analyses, table and figure drafting and report production
- Rick Harding – optical maturity QC
- Dr. Ray Doneick (subcontract – Apatite.com, apatite thermochronology)

Chemostrat:

- Dr. Alexander Finlay – study conception, RHP calculation, data interpretation and basement mapping, report production
- Dr. Brenton Fairey – U-Pb geochronology
- Mr. Guy Comfort - Petrology

2.6 ACKNOWLEDGEMENTS

Contributions regarding sample access and laboratory work have been made by the following people:

- Chemostrat laboratory staff
- British Geological Survey, and in particular Scott Renshaw for sample access

Well	Basin	Latitude (DD)	Longitude (DD)	Operator	Spud Year	Water Depth	RT/KB Elevation	Total Depth (m)	Flow Class	Mud System	Analytical Programme		
											IN GEO	AFT	MAT
154/03-1	West Lewis	58.930985	-7.566751	Conoco	1991	499.0	24.0	2459.0	Dry Hole	WBM (KCL/NaCl PHPA polymer)	y	-	-
164/25-2	North East Rockall	59.288309	-7.163316	BP	1990	697.0	26.0	1728.0	Dry Hole	?WBM	y	-	-
202/02-1	Solan	59.844750	-4.625028	Esso	1974	120.0	9.4	1220.0	Dry Hole	WBM (Seawater & gel)	y	-	-
202/08-1	Solan	59.792083	-4.531944	Shell	1974	122.0	25.0	1686.0	Dry Hole	?WBM	y	-	-
202/09-1	Solan	59.793417	-4.300472	Esso	1987	121.0	25.0	1640.0	Dry Hole	WBM (Seawater, gel & lignosulphonate)	y	-	-
204/10-1	Corona	60.802433	-4.162408	Amerada Hess	2002	1088.0	36.0	2523.0	Oil & Gas	WBM (KCl, bentonite & Aqua Drill)	y	-	-
204/10a-5	Corona	60.818643	-4.153971	Siccar Point	2018	1082.0	31.0	2442.0	Oil	Unknown	-	y	-
204/15-2	Westray	60.529463	-4.190930	Conoco	2001	749.0	36.0	4800.0	Oil Shows	WBM (KCl, Aquacol polymer)	y	-	-
204/23-1	Westray	60.238542	-4.497939	BP	1987	508.0	26.0	5883.0	Condensate	OBM (Fazeclean)	y	-	-
204/25-1	Rona	60.177585	-4.039954	Amerada Hess	1991	162.0	27.0	2902.0	Dry Hole	WBM (KCl polymer)	y	-	-
204/26-1A	Judd High	60.154833	-4.887500	Texaco	1995	632.0	25.0	2652.0	?Dry Hole	OBM (XP07)	y	-	-
204/27a-1	Judd High	60.159000	-4.652833	BP	1990	500.0	26.0	2180.0	Dry Hole	WBM (KCl polymer)	y	-	-
204/28-1	Judd High	60.158167	-4.533500	BP	1981	373.0	25.0	1974.0	Oil Shows	?WBM	y	-	-
205/09-1	Flett	60.806472	-3.372722	BP	1989	639.0	26.0	4750.0	Gas Shows	WBM (Bentonite & KCl polymer)	-	y	y
205/12-1	Flett	60.534358	-3.748417	Total	1995	498.0	24.0	3201.0	Dry Hole	WBM (KCl polymer)	-	y	y

TABLE 2.1 Well details and analytical well programme

Well	Basin	Latitude (DD)	Longitude (DD)	Operator	Spud Year	Water Depth	RT/KB Elevation	Total Depth (m)	Flow Class	Mud System	Analytical Programme		
											IN GEO	AFT	MAT
205/14-2	Flett	60.557475	-3.262725	Esso	1996	329.0	24.0	2727.0	Dry Hole	WBM (KCl polymer & Glycol)	-	y	y
205/14-3	Flett	60.659283	-3.279119	Amerada Hess	1997	464.0	24.0	3091.0	Dry Hole	WBM (KCl polymer & Glycol)	-	-	y
205/16-1	Rona	60.351000	-3.864639	BP	1986	312.0	26.0	4319.0	Dry Hole	OBM (Shaledrill)	y	-	-
205/17b-2	Flett Ridge	60.492308	-3.614158	BP	1995	407.0	26.0	2773.0	Dry Hole	WBM (KCl polymer)	-	y	-
205/20-1	Rona Ridge	60.456500	-3.116833	Elf	1974	216.0	26.0	2045.0	?Oil Shows	WBM (Seawater & FLC-LC polymer)	y	-	-
205/21-1A	Rona Ridge	60.182500	-3.843056	Shell	1974	152.0	25.0	1368.0	Oil Shows	?WBM	y	-	-
205/22-1A	Rona	60.268365	-3.768538	BP	1974	176.0	26.0	3231.0	?Dry Hole	WBM (Barite, CMC, lignite & FCL)	y	-	-
206/01-1A	Foula	60.849889	-2.837220	Britoil	1985	236.0	25.0	4620.0	Gas Shows	OBM (Inverkleen)	-	-	y
206/07a-2	Clair-Victory Ridge	60.687753	-2.611781	BP	1991	153.0	27.0	2650.0	Oil	OBM (BCM)	y	-	-
206/08-1A	Clair-Victory Ridge	60.692403	-2.542427	BP	1977	138.0	26.0	2327.0	Oil	WBM (Hicell & lignosulphonate)	y	-	-
206/08-2	Clair-Victory Ridge	60.735708	-2.481114	BP	1978	141.0	25.0	1890.0	Oil & Gas	?WBM	y	-	-
206/08-7	West Shetland	60.679313	-2.553053	BP	1985	139.0	25.0	2338.0	Oil	OBM (Enviromul)	y	-	-
206/08-8	Clair-Victory Ridge	60.690708	-2.544370	BP	1991	140.0	26.0	2502.0	Oil	OBM	y	-	-
206/09-2	Clair-Victory Ridge	60.784661	-2.367261	Mobil	1978	136.0	26.0	2465.0	Oil	WBM (Gel, FCL & IDFO)	y	-	-
206/11-1	Rona Ridge	60.607722	-2.942611	Elf	1977	236.0	25.0	4620.0	Gas	WBM	-	y	y

TABLE 2.1 Well details and analytical well programme

Well	Basin	Latitude (DD)	Longitude (DD)	Operator	Spud Year	Water Depth	RT/KB Elevation	Total Depth (m)	Flow Class	Mud System	Analytical Programme		
											IN GEO	AFT	MAT
206/12-1	Clair-Victory Ridge	60.597649	-2.767214	Esso	1972	171.0	9.0	1728.0	Dry Hole	WBM (Barite & lignosulphonate)	y	-	-
207/01-2	West Shetland	60.950028	-1.880828	Texaco	1977	142.0	26.0	1762.0	Dry Hole	WBM (Seawater, CMC, barite & lignosulphonate)	-	y	y
207/01-3	Clair-Victory Ridge	60.966539	-1.916458	Texaco	1977	158.0	26.0	1434.0	Gas	WBM (Seawater, gel & lignosulphonate)	y	-	-
207/02-1	West Shetland	60.978000	-1.736028	Shell	1974	142.0	25.0	2059.0	Dry Hole	?WBM	y	-	-
208/17-1	Northern Faroe-Shetland	61.456528	-1.789528	Amoco	1985	704.0	26.0	4846.0	Dry Hole	OBM (Invermul)	-	-	y
208/17-2	Northern Faroe-Shetland	61.399139	-1.665614	Amoco	1995	556.0	26.0	3679.0	Gas Shows	OBM (Aquamul)	-	y	y
208/23-1	Clair-Victory Ridge	61.170528	-1.514861	LASMO	1983	188.0	26.0	2075.0	Dry Hole	WBM (Seawater, gypsum & lignosulphonate)	y	-	-
208/24-1A	Northern Faroe-Shetland	61.191028	-1.350917	Amoco	1986	173.0	26.0	2160.0	Dry Hole	OBM (Invermul)	-	y	-
208/26-1	Foula	61.118056	-1.820500	Britoil	1983	300.0	23.0	3903.0	Oil Shows	WBM (KCl polymer)	y	-	-
208/27-1	Clair-Victory Ridge	61.091650	-1.718589	BNOC	1979	201.0	12.0	1525.0	Oil Shows	WBM (Polymer)	y	-	-
208/27-2	Clair-Victory Ridge	61.134544	-1.647175	BNOC	1982	217.0	25.0	1402.0	Oil Shows	WBM (Seawater & polymer mud)	y	y	-
209/09-1	Northern Faroe-Shetland	61.762306	-0.344219	BNOC	1979	229.0	25.0	2699.0	Dry Hole	WBM (Gypsum & CMC)	y	-	-
209/12-1	Northern Faroe-Shetland	61.630479	-0.739919	Marathon	1985	240.0	26.0	3513.0	Oil Shows	WBM (Seawater & polymer mud)	y	-	y
214/09-1	Northern Faroe-Shetland	61.804342	-2.200889	Mobil	2000	1556.0	29.0	4749.0	?Oil Shows	WBM (KCl silicate polymer)	y	-	-
214/26-1	Flett	61.119869	-2.829414	Conoco	1996	870.0	26.0	2743.0	Dry Hole	WBM (Sewater & polyglycol)	-	y	y

TABLE 2.1 Well details and analytical well programme

Well	Basin	Latitude (DD)	Longitude (DD)	Operator	Spud Year	Water Depth	RT/KB Elevation	Total Depth (m)	Flow Class	Mud System	Analytical Programme		
											IN GEO	AFT	MAT
214/28-1	Flett Ridge	61.113722	-2.492028	Esso	1984	653.0	10.0	5124.0	Oil Shows	OBM (Enviromul)	-	y	y
220/26-1	Northern Faroe-Shetland	62.072551	1.032030	BP	1985	325.0	26.0	5312.0	Dry Hole	OBM (Energol 8313)	y	-	-

AFT: Apatite Fission Track
MAT: Optical Maturity
IN GEO: Inorganic Geochemistry

TABLE 2.1 Well details and analytical well programme

CHAPTER 3

INORGANIC GEOCHEMISTRY ANALYSES AND RESULTS

Alex Finlay, Chemostrat

3.1 INTRODUCTION

Lithospheric crustal composition and structure acts as a primary control on the thermal regime in sedimentary basins, with up to 50% of surface heat flow originating from radioactive heat production (RHP) from the upper crystalline crust and basin infill (Vilà *et al.*, 2010). For example, across the Faroe-Shetland Basement (FSB) most models predict oil generation as occurring in the mid Cretaceous (e.g. Holmes *et al.*, 1999) before Late Cretaceous seals and Palaeocene reservoirs had been deposited. This has been explained using various methods to explain this (e.g. motels – Lamers and Carmichael, 1999 or overpressure delaying generation/expulsion Carr & Scotchman, 2003). However, Gardiner *et al.*, (2019) modelled oil generation around the Corona Ridge (utilising calculated values for basement RHP as removing Palaeocene sill thicknesses) as occurring in the Palaeocene, in agreement with observed geology. Therefore, to be able to accurately and precisely produce basin models in the FSB a thorough understanding of the basement is required.

The data presented in this chapter spans the FSB, and can be used to map the basement based on variations in its:

- RHP – Calculated from Potassium (K), Thorium (Th) and Uranium (U) abundances. Geochemical data has been produced either through a combined ICP-OES & ICPMS analysis for this study or taken from published data (see references).
- Petrography – Data for this study has been collected from thin section point count analysis (core), X-Ray Diffraction (XRD; cuttings) or taken from the from published literature (see references).
- Formation age – U-Pb Zircon geochronology data (which records the age zircons cooled below ~1000°C to 850°C) has either been collected through Laser Ablation ICP-MS methods or is taken from the from published literature (see references).
- Alteration age – U-Pb Apatite geochronology (which records the age apatites cooled below ~ 500°C) has been collected through Laser Ablation ICP-MS methods. This is the first time this has been applied to basement in the FSB.

A total of ninety four samples have been analysed across the FSB, full sample details and accompanying analytical programme are shown in Table 3.1.1. The distribution of wells analysed in this study are shown in Figure 3.1.1. The presented data is a mix of data newly generated for this study and data compiled from published literature, all data are shown in Tables 3.2.1 to 3.2.33, a series of maps integrating key study data are shown in Figures 3.2.1 to 3.2.8.

Well	Top depth	Bottom depth	Units (m/ft)	Stratigraphy	Age	Sample type	Washed (y/n)	Basin	Mud system	Anal. reason	Anal. status	RHP	Petro & XRD	Zircon Geo	Apatite Geo
154/03-1	-	8060.0	ft	Laxford Basement	Lax	COCH	-	West Lewis	WBM	IN GEO	P	y	y	-	-
164/25-2	2727.7	2727.8	m	Lewisian Basement	PrCam	COCH	-	NE Rockall	?WBM	IN GEO	P	-	y	-	-
202/02-1	-	3950.0	ft	Precambrian Basement	PrCam	DC	y	Solan	WBM	IN GEO	N	y	-	-	-
	-	4002.0	ft			COCH	-			IN GEO	P	y	y	y	-
202/08-1	-	5446.6	ft	Lewisian Basement	PrCam	COCH	-	Solan	?WBM	IN GEO	N	y	y	-	-
	-	5457.3	ft			COCH	-			IN GEO	N	y	y	-	-
	-	5500.0	ft			DC	n			IN GEO	N	y	y	-	-
	-	5510.0	ft			DC	n			IN GEO	N	y	y	-	-
	-	5520.0	ft			DC	n			IN GEO	N	y	y	-	-
202/09-1	-	5379.0	ft	Lewisian Basement	PrCam	COCH	-	Solan	WBM	IN GEO	N	y	y	-	-
204/10-1	-	2499.0	m	Precambrian Basement	PrCam	COCH	-	Corona	WBM	IN GEO	P	y	-	-	-
	-	2505.0	m			DC	y			IN GEO	N	y	-	y	y
	-	2508.0	m			DC	y			IN GEO	N	y	-		
	-	2511.0	m			DC	y			IN GEO	N	y	-		
	-	2514.0	m			DC	y			IN GEO	N	y	-		
204/15-2	7020.0	7270.0	ft	Balder	E1	DC	y	Westray	WBM	IN GEO	N	y	-	-	-
	7330.0	7990.0	ft	Flett	P3	DC	y			IN GEO	N	y	-	-	-
	8050.0	9550.0	ft	Lamba		DC	y			IN GEO	N	y	-	-	-
	9610.0	10810.0	ft	Vaila		DC	y			IN GEO	N	y	-	-	-
	10890.0	11610.0	ft	Coniacian-Albian	K2	DC	y			IN GEO	N	y	-	-	-
	11670.0	12390.0	ft	Volgian	J3	DC	y			IN GEO	N	y	-	-	-
	-	12450.0	ft	Precambrian Basement	PrCam	DC	Unkn.			IN GEO	P	y	y	-	-
	-	12467.0	ft	Precambrian Basement		DC	Unkn.			IN GEO	P	y	y	-	-
204/23-1	-	3847.2	m	Precam Basement	PrCam	COCH	-	Westray	OBM	IN GEO	P	y	y	-	-
204/25-1	-	9417.0	ft	Precam Basement	PrCam	COCH	-	Rona	WBM	IN GEO	P	y	y	y	-
204/26-1A	-	8689.9	ft	Lewisian Basement	PrCam	COCH	-	Judd High	OBM	IN GEO	P	-	y	y	-
204/27a-1	-	2136.3	m	Precam Basement	PrCam	COCH	-	Judd High	WBM	IN GEO	P	-	y	y	-
204/28-1	-	1941.6	m	Precam Basement	PrCam	COCH	-	Judd High	?WBM	IN GEO	P	-	y	y	-

TABLE 3.1.1 Analytical programme - Inorganic geochemistry analyses

Well	Top depth	Bottom depth	Units (m/ft)	Stratigraphy	Age	Sample type	Washed (y/n)	Basin	Mud system	Anal. reason	Anal. status	RHP	Petro & XRD	Zircon Geo	Apatite Geo
205/16-1	4172.0	4172.2	m	Lewisian Basement	PrCam	COCH	-	Rona	OBM	IN GEO	P	y	y	-	-
	-	4274.2	m			COCH	-			IN GEO	N	y	y	-	-
	-	4274.4	m			COCH	-			IN GEO	N	y	y	-	-
	-	4274.6	m			COCH	-			IN GEO	N	y	y	-	-
	-	4275.3	m			COCH	-			IN GEO	N	y	y	y	y
	-	4300.0	m			DC	y			IN GEO	N	y	y	y	y
	-	4305.0	m			DC	y			IN GEO	N	y			
	-	4310.0	m			DC	y			IN GEO	N	y			
	-	4314.0	m			DC	y			IN GEO	N	y			
	-	4314.0	m			DC	y			IN GEO	N	y			
205/20-1	-	2017.5	m	Lewisian Basement	PrCam	COCH	-	Rona Ridge	WBM	IN GEO	P	y	y	y	-
205/21-1A	-	4449.0	ft	Lewisian Basement	PrCam	COCH	-	Rona Ridge	?WBM	IN GEO	N, P	y	y	-	-
	-	4465.0	ft			COCH	-			IN GEO	N, P	y	y	-	-
205/22-1A	3225.5	3225.6	m	Precam Basement	PrCam	COCH	-	Rona	WBM	IN GEO	P	y	y	y	-
206/07a-2	-	2140.7	m	Lewisian Basement	PrCam	COCH	-	Clair-Victory Ridge	OBM	IN GEO	L	-	-	y	-
	-	2141.3	m			COCH	-			IN GEO	P	y	y	y	-
	-	2146.7	m			COCH	-			IN GEO	N	y	y	-	-
	-	2147.9	m			COCH	-			IN GEO	N	y	y	y	y
	-	2246.4	m			COCH	-			IN GEO	N	y	y	-	-
	-	2438.3	m			COCH	-			IN GEO	P	y	y	-	-
	-	2442.6	m			COCH	-			IN GEO	N	y	y	-	-
	-	2443.2	m			COCH	-			IN GEO	P	y	y	-	-
	-	2443.2	m			COCH	-			IN GEO	P	y	y	-	-
206/08-1A	-	2306.4	m	Precambrian Basement	PrCam	COCH	-	Clair-Victory Ridge	WBM	IN GEO	L	-	-	y	-
	-	2311.0	m			COCH	-			IN GEO	P	y	y	y	-
206/08-2	-	1859.0	m	Precambrian Basement	PrCam	COCH	-	Clair-Victory Ridge	?WBM	IN GEO	P	y	y	-	-
	-	1864.6	m			COCH	-			IN GEO	P	y	y	-	-
206/08-7	-	2320.5	m	Basement	PrCam	COCH	-	West Shetland	OBM	IN GEO	P	y	y	-	-
206/08-8	-	2499.0	m	Basement	PrCam	COCH	-	Clair-Victory Ridge	OBM	IN GEO	P	y	y	-	-
206/09-2	-	8084.0	ft	Lewisian Basement	PrCam	COCH	-	Clair-Victory Ridge	WBM	IN GEO	P	y	y	-	-

TABLE 3.1.1 Analytical programme - Inorganic geochemistry analyses

Well	Top depth	Bottom depth	Units (m/ft)	Stratigraphy	Age	Sample type	Washed (y/n)	Basin	Mud system	Anal. reason	Anal. status	RHP	Petro & XRD	Zircon Geo	Apatite Geo
206/12-1	-	5630.0	ft	Lewisian Basement	PrCam	COCH	-	Clair-Victory Ridge	WBM	IN GEO	P	y	y	-	-
	-	5632.0	ft			COCH	-			IN GEO	P	-	y	y	-
207/01-3	-	4576.3	ft	Precambrian Basement	PrCam	COCH	-	Clair-Victory Ridge	WBM	IN GEO	N	y	y	-	-
	-	4670.0	ft			DC	y			IN GEO	N	y	y	y	y
	-	4680.0	ft			DC	y			IN GEO	N	y			
	-	4690.0	ft			DC	y			IN GEO	N	y			
	-	4700.0	ft			DC	y			IN GEO	N	y			
	-	4706.0	ft			DC	y			IN GEO	N	y			
	-	4706.0	ft			DC	y			IN GEO	N	y			
207/02-1	-	6722.0	ft	Precambrian Basement	PrCam	COCH	-	West Shetland	?WBM	IN GEO	N	y	y	y	y
	-	6723.0	ft			COCH	-			IN GEO	N	y	y	y	y
	-	6724.0	ft			COCH	-			IN GEO	N	y	y	y	y
208/23-1	-	9795.5	ft	Lewisian Basement	PrCam	COCH	-	Clair-Victory Ridge	WBM	IN GEO	P	-	y	y	-
	-	9796.5	ft			COCH	-			IN GEO	N	y	y	y	y
	-	6799.2	ft			COCH	-			IN GEO	N	y	y	-	-
	-	6803.0	ft			COCH	-			IN GEO	N	y	y	-	-
	-	6806.1	ft			COCH	-			IN GEO	N	y	y	-	-
	-	6808.0	ft			COCH	-			IN GEO	N	y	y	-	-
	-	6808.0	ft			COCH	-			IN GEO	N	y	y	-	-
208/26-1	-	3894.0	m	Precam Basement	PrCam	COCH	-	Foula	WBM	IN GEO	P	y	y	-	-
208/27-1	-	1380.2	m	Precam Basement	PrCam	-	-	Clair-Victory Ridge	WBM	IN GEO	L	-	-	y	-
208/27-2	-	4452.5	ft	Lewisian Basement	PrCam	COCH	-	Clair-Victory Ridge	WBM	IN GEO	P	y	y	y	-
	-	4522.2	ft			COCH	-			IN GEO	N	y	y	-	-
	-	4527.5	ft			COCH	-			IN GEO	N	y	y	y	y
	-	4528.8	ft			COCH	-			IN GEO	P	y	y	-	-
	-	4531.2	ft			COCH	-			IN GEO	N	y	y	-	-
	-	4532.0	ft			COCH	-			IN GEO	N	y	y	-	-
209/09-1	-	8850.0	ft	Caledonian Basement	Sil	COCH	-	Northern Faroe-Shetland	WBM	IN GEO	N	y	y	-	-
	-	8854.0	ft			COCH	-			IN GEO	N	y	y	-	-
	-	8855.0	ft			COCH	-			IN GEO	N	y	y	y	y

TABLE 3.1.1 Analytical programme - Inorganic geochemistry analyses

Well	Top depth	Bottom depth	Units (m/ft)	Stratigraphy	Age	Sample type	Washed (y/n)	Basin	Mud system	Anal. reason	Anal. status	RHP	Petro & XRD	Zircon Geo	Apatite Geo
209/12-1	-	11385.7	ft	Caledonian Basement	Sil	COCH	-	Northern Faroe-Shetland	WBM	IN GEO	N	y	-	-	-
	-	11500.0	ft			DC	y			IN GEO	N	y	y	-	-
	-	11510.0	ft			DC	y			IN GEO	N	y			
	-	11520.0	ft			DC	y			IN GEO	N	y			
	-	11521.0	ft			DC	Unkn.			IN GEO	L	-	-	y	y
	-	11525.0	ft			COCH	y			IN GEO	N	y	y	-	-
	-	11526.0	ft			COCH	y			IN GEO	P	y	y	-	-
	-	11527.0	ft			COCH	y			IN GEO	N	y	y	-	-
214/09-1	-	11580.7	ft	Precam Basement	PrCam	DC	Unkn.	N Faroe-Shetland	WBM	IN GEO	P	y	y	-	-
220/26-1	-	5280.2	m	Cal Basement	Sil	COCH	y	N Faroe-Shetland	OBM	IN GEO	P	y	y	-	-
TOTAL:												84	67	27	12

Abbreviations/Key

DC: Ditch cuttings
COCH: Core chip
Unkn.: Unknown
WBM: Water base mud
OBM: Oil base mud
IN GEO: Inorganic geochemistry
N: New analyses for this study
P: Published data
L: Legacy Chemostrat data
RHP: Radioactive Heat Production
Petro & XRD: Petrography & XRD
Zircon Geo: Zircon Geochronology
Apatite Geo: Apatite Geochronology

Stratigraphy/Ages/Basins

Lax Basement: Laxfordian
Precam Basement: Precambrian Basement
Cal Basement: Caledonian Basement
E1: Early Eocene
P3: Late Paleocene
K2: Late Cretaceous
J3: Late Jurassic
Sil: Silurian
Lax: Laxfordian Basement
PrCam: Precambrian
NE Rockall: North-East Rockall
N Faroe-Shetland: Northern Faroe Shetland

TABLE 3.1.1 Analytical programme - Inorganic geochemistry analyses

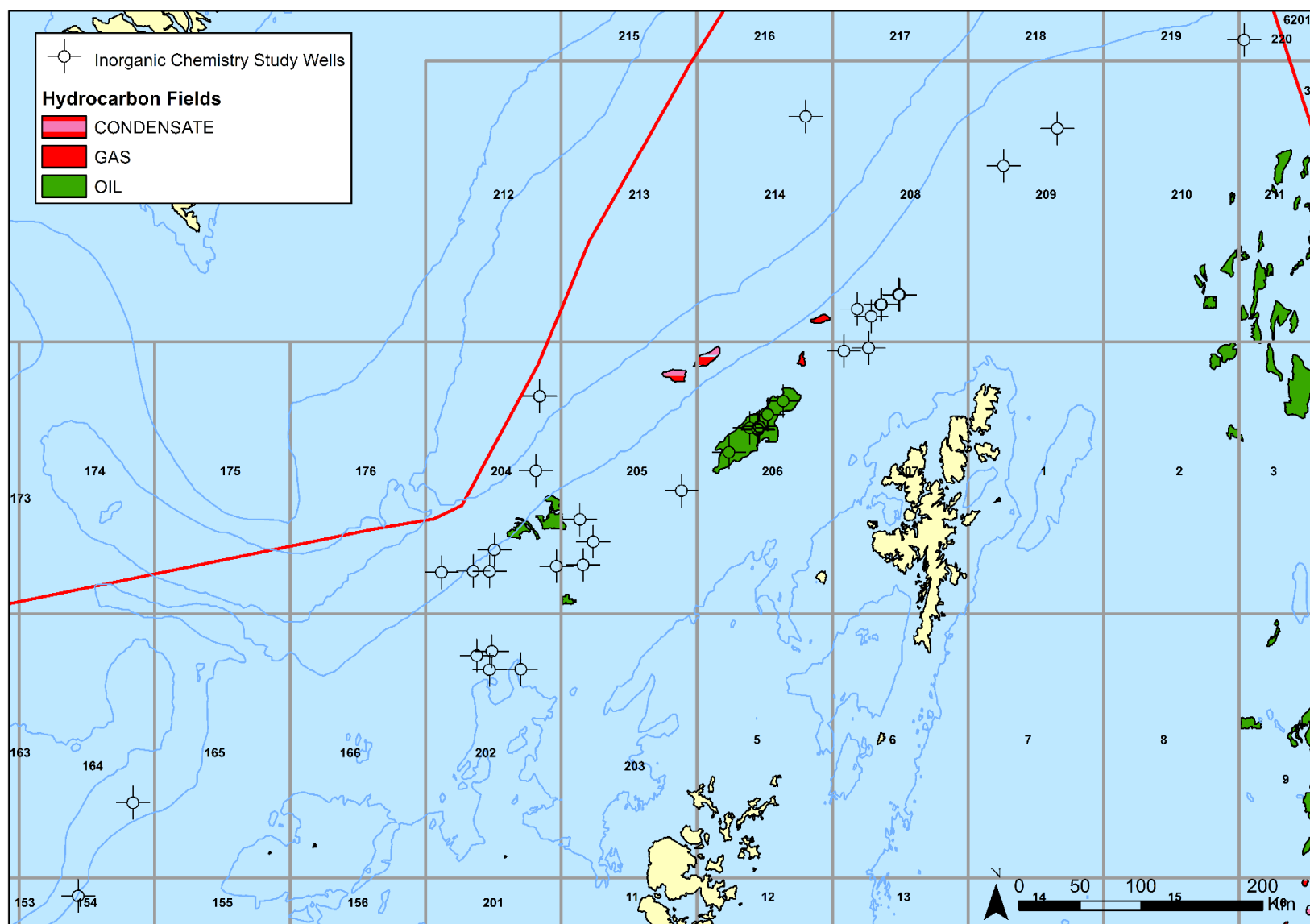


FIGURE 3.1.1 Location map of wells selected for inorganic geochemistry analyses

3.2 INORGANIC GEOCHEMISTRY ANALYSES RESULTS

3.2.1 Data and discussion for well 154/03-1 (Table 3.2.1)

Published data (Chambers *et al.*, 2005) are presented for one core sample from 8060.0ft MD, a summary of the key values are given below:

- RHP: 0.36 $\mu\text{W}/\text{m}^3$
- Composition: Amphibolite
- Crystal size: –
- Formation age: –
- Alteration age: –

3.2.2 Data and discussion for well 164/25-2 (Table 3.2.2)

Published data (Chambers *et al.*, 2005) are presented for one core sample from 2727.8m MD, a summary of the key values are given below:

- RHP: –
- Composition: Metabasic gneiss
- Crystal size: –
- Formation age: –
- Alteration age: –

3.2.3 Data and discussion for well 202/02-1 (Table 3.2.3)

Two sources of published data (Chambers *et al.*, 2005 & Ritchie *et al.*, 2011) and newly generated data from this study (one core and one cuttings) ranging from 3950.0-4002.0ft MD, a summary of the key values are given below:

- RHP: 0.90-1.80 $\mu\text{W}/\text{m}^3$
- Composition: Quartzofeldspathic gneiss
- Crystal size: –
- Formation age: Neoarchean
- Alteration age: –

3.2.4 Data and discussion for well 202/08-1 (Table 3.2.4)

Newly generated data from this study are presented for five samples (two core and three cuttings) ranging from 5447.0-5520.0ft MD, a summary of the key values are given below:

- RHP: 0.24-0.54 $\mu\text{W}/\text{m}^3$
- Crystal size: Medium-coarse
- Composition: Granodiorite, monzodiorite & tonalite
- Formation age: –
- Alteration age: –

3.2.5 Data and discussion for well 202/09-1 (Table 3.2.5)

Newly generated data from this study are presented for one core sample from 5379.0ft MD, a summary of the key values are given below:

- RHP: 0.70 $\mu\text{W}/\text{m}^3$
- Crystal size: Medium
- Composition: Diorite
- Formation age: –
- Alteration age: –

3.2.6 Data and discussion for well 204/10-1 (Table 3.2.6)

Published data (Finlay *et al.*, 2018) and newly generated data from this study are presented for five samples (one core and four cuttings) ranging from 2499.0-2514.0m MD, a summary of the key values are given below:

- RHP: 0.90-1.10 $\mu\text{W}/\text{m}^3$
- Composition: –
- Crystal size: –
- Formation age: Insufficient concordant zircons recovered for reliable age determination
- Alteration age: Laxfordian

3.2.7 Data and discussion for well 204/15-2 (Table 3.2.7)

Published data (Finlay *et al.*, 2018) and newly generated data from this study are presented for two basement cuttings samples ranging from 12450.0-12467.0ft. Additional RHP data for Balder, Flett, Lamba, Vaila, Cretaceous and Jurassic samples are also presented, a summary of the key values are given below:

- RHP (Basement): 0.20-0.51 $\mu\text{W}/\text{m}^3$
- RHP (Balder): 1.32 $\mu\text{W}/\text{m}^3$
- RHP (Flett): $\sim 0.89 \mu\text{W}/\text{m}^3$
- RHP (Lamba): $\sim 1.34 \mu\text{W}/\text{m}^3$
- RHP (Vaila): $\sim 0.96 \mu\text{W}/\text{m}^3$
- RHP (Cretaceous): $\sim 1.65 \mu\text{W}/\text{m}^3$
- RHP (Jurassic): $\sim 3.76 \mu\text{W}/\text{m}^3$
- Composition: –Tonalite
- Crystal size: –
- Formation age: –
- Alteration age: –

3.2.8 Data and discussion for well 204/23-1 (Table 3.2.8)

Published data (Chambers *et al.*, 2005) are presented for one core sample from 3847.2m MD, a summary of the key values are given below:

- RHP: 0.64 $\mu\text{W}/\text{m}^3$
- Composition: Quartzofeldspathic gneiss
- Crystal size: –
- Formation age: –
- Alteration age: –

3.2.9 Data and discussion for well 204/25-1 (Table 3.2.9)

Two sources of published data (Chambers *et al.*, 2005 & Holdsworth *et al.* 2019) are presented for one core sample from 9417.0ft MD, a summary of the key values are given below:

- RHP: 0.13 $\mu\text{W}/\text{m}^3$
- Composition: Tonalitic gneiss
- Crystal size: –
- Formation age: Neoarchean
- Alteration age: –

3.2.10 Data and discussion for well 204/26-1A (Table 3.2.10)

Published data (Holdsworth *et al.*, 2019) are presented for one core sample from 8689.9ft MD, a summary of the key values are given below:

- IRHP: –
- Composition: Granodioritic gneiss
- Crystal size: –
- Formation age: Neoarchean
- Alteration age: –

3.2.11 Data and discussion for well 204/27a-1 (Table 3.2.11)

Published data (Holdsworth *et al.*, 2019) are presented for one core sample from 2136.3m MD, a summary of the key values are given below:

- RHP: –
- Composition: Granite
- Crystal size : –
- Formation age: Neoarchean
- Alteration age: –

3.2.12 Data and discussion for well 204/28-1 (Table 3.2.12)

Published data (Holdsworth *et al.*, 2019) are presented for one core sample from 1941.6m MD, a summary of the key values are given below:

- RHP: –
- Composition: Granodioritic gneiss
- Crystal size: –
- Formation age: Neoarchean
- Alteration age: –

3.2.13 Data and discussion for well 205/16-1 (Table 3.2.13)

Published data (Chambers *et al.*, 2005) and newly generated data from this study are presented for nine samples (five core and four cuttings) ranging from 4172.2-4315.0m MD, a summary of the key values are given below:

- RHP: 0.41-2.36 $\mu\text{W}/\text{m}^3$
- Composition: Dioritic gneiss, granite, granodiorite & tonalite
- Crystal size: Medium-coarse
- Formation age: Neoarchean
- Alteration age: Laxfordian

3.2.14 Data and discussion for well 205/20-1 (Table 3.2.14)

Two sources of published data (Chambers *et al.*, 2005 & Holdsworth *et al.*, 2019) are presented for one core sample from 2017.5m MD, a summary of the key values are given below:

- RHP: 0.90 $\mu\text{W}/\text{m}^3$
- Composition: Granodioritic gneiss
- Crystal size: –
- Formation age: Neoarchean
- Alteration age: –

3.2.15 Data and discussion for well 205/21-1A (Table 3.2.15)

Published data (Finlay *et al.*, 2018) and newly generated data from this study are presented for two core samples ranging from 4449.0-4465.0ft MD, a summary of the key values are given below:

- RHP: 0.15 $\mu\text{W}/\text{m}^3$
- Composition: Granite & tonalite
- Crystal size: –
- Formation age: –
- Alteration age: –

3.2.16 Data and discussion for well 205/22-1A (Table 3.2.16)

Two sources of published data (Chambers *et al.*, 2005 & Holdsworth *et al.*, 2019) are presented for one core sample from 3225.6m MD, a summary of the key values are given below:

- RHP: 0.73 $\mu\text{W}/\text{m}^3$
- Composition: Dioritic gneiss
- Crystal size: –
- Formation age: Neoarchean
- Alteration age: –

3.2.17 Data and discussion for well 206/07a-2 (Table 3.2.17)

This well has been extensively studied as it has a long basement core section (enabling core heterogeneity to be understood) and also enables comparison of data produced in this study and published data. Four sources of published data (Chemostrat, 2014; Chambers *et al.*, 2005. Finlay *et al.*, 2018 & Holdsworth *et al.*, 2019) and newly generated data from this study are presented for seventeen core samples ranging from 2140.7-2598.1m MD, a summary of the key values are given below:

- RHP: 0.20-1.75 $\mu\text{W}/\text{m}^3$
- Composition: Granodioritic gneiss, tonalite & diorite
- Crystal size: Coarse
- Formation age: Neoarchean
- Alteration age: Laxfordian

3.2.18 Data and discussion for well 206/08-1A (Table 3.2.18)

Three sources of published data (Chemostrat, 2014, Chambers *et al.*, 2005 & Holdsworth *et al.*, 2019) are presented for two core samples ranging from 2306.4-2311.0m MD, a summary of the key values are given below:

- RHP: 0.64 $\mu\text{W}/\text{m}^3$
- Composition: Dioritic gneiss
- Crystal size: –
- Formation age: Neoarchean
- Alteration age: –

3.2.19 Data and discussion for well 206/08-2 (Table 3.2.19)

Two sources of published data (Finlay *et al.*, 2018 & Chambers *et al.*, 2005) are presented for two core samples ranging from 1859.0-1864.6m MD, a summary of the key values are given below:

- RHP: 1.92-2.27 $\mu\text{W}/\text{m}^3$
- Composition: Granodiorite & protomylonite
- Crystal size: –
- Formation age: –
- Alteration age: –

3.2.20 Data and discussion for well 206/08-7 (Table 3.2.20)

Published data (Chambers *et al.*, 2005) are presented for one core sample from 2320.5m MD, a summary of the key values are given below:

- RHP: 0.67 $\mu\text{W}/\text{m}^3$
- Composition: Amphibolite
- Crystal size: –
- Formation age: –
- Alteration age: –

3.2.21 Data and discussion for well 206/08-8 (Table 3.2.21)

Published data (Chambers *et al.*, 2005) are presented for one core sample from 2499.0m MD, a summary of the key values are given below:

- RHP: 0.25 $\mu\text{W}/\text{m}^3$
- Composition: Granitic gneiss
- Crystal size: –
- Formation age: –
- Alteration age: –

3.2.22 Data and discussion for well 206/09-2 (Table 3.2.22)

Published data (Finlay *et al.*, 2018) are presented for one core sample from 8084.0ft MD, a summary of the key values are given below:

- RHP: 2.68 $\mu\text{W}/\text{m}^3$
- Composition: Granite
- Crystal size: –
- Formation age: –
- Alteration age: –

3.2.23 Data and discussion for well 206/12-1 (Table 3.2.23)

Two sources of published data (Finlay *et al.*, 2018 & Holdsworth *et al.*, 2018) are presented for two core samples from 5630.0-5632.0ft MD, a summary of the key values are given below:

- RHP: 0.44 $\mu\text{W}/\text{m}^3$
- Composition: Granodioritic gneiss
- Crystal size: –
- Formation age: Neoarchean
- Alteration age: –

3.2.24 Data and discussion for well 207/01-3 (Table 3.2.24)

Newly generated data from this study are presented for six samples (one core and five cuttings) ranging from 4576.3-4706.0ft MD, a summary of the key values are given below:

- RHP: 0.94-1.39 $\mu\text{W}/\text{m}^3$
- Composition: Metasedimentary and granodiorite
- Crystal size: –
- Formation age: Neoarchean
- Alteration age: Laxfordian

3.2.25 Data and discussion for well 207/02-1 (Table 3.2.25)

Newly generated data from this study are presented for three core samples ranging from 6722.0-6724.0ft MD, a summary of the key values are given below:

- RHP: 0.76-0.86 $\mu\text{W}/\text{m}^3$
- Composition: Gneiss & syenogranite
- Crystal size: Coarse
- Formation age: Neoarchean
- Alteration age: Laxfordian

3.2.26 Data and discussion for well 208/23-1 (Table 3.2.26)

Published data (Holdsworth *et al.*, 2019) and newly generated data from this study are presented for six core samples ranging from 6795.5-6808.0ft MD, a summary of the key values are given below:

- RHP: 0.51-1.97 $\mu\text{W}/\text{m}^3$
- Composition: Granitic gneiss, granite, syenogranite, tonalite
- Crystal size: Fine-medium & coarse
- Formation age: Neoarchean
- Alteration age: Caledonian (lower intercept discordia age)

3.2.27 Data and discussion for well 208/26-1 (Table 3.2.27)

Published data (Finlay *et al.* 2018) are presented for one core sample from 3894.0m MD, a summary of the key values are given below:

- RHP: 0.20 $\mu\text{W}/\text{m}^3$
- Composition: Serpentinised granodiorite
- Crystal size: –
- Formation age: –
- Alteration age: –

3.2.28 Data and discussion for well 208/27-1 (Table 3.2.28)

Published data (Chemostrat. 2014) are presented for one core sample from 1380.2m MD, a summary of the key values are given below:

- RHP: –
- Composition: –
- Crystal size: –
- Formation age: Neoarchean
- Alteration age: –

3.2.29 Data and discussion for well 208/27-2 (Table 3.2.29)

Two sources of published data (Chambers *et al.*, 2005 & Holdsworth *et al.*, 2019) and newly generated data from this study are presented for six core samples ranging from 4452.5-4532.0ft MD, a summary of the key values are given below:

- RHP: 0.34-1.03 $\mu\text{W}/\text{m}^3$
- Composition: Mafic granitic gneiss, weathered granite, weathered syenogranite & granitic gneiss
- Crystal size: Coarse
- Formation age: Neoarchean
- Alteration age: Caledonian (lower intercept discordia age)

3.2.30 Data and discussion for well 209/09-1 (Table 3.2.30)

Newly generated data from this study are presented for three core samples ranging from 8850.0-8855.0ft MD, a summary of the key values are given below:

- RHP: 1.30-1.87 $\mu\text{W}/\text{m}^3$
- Composition: Tonalite, granodiorite & gneissic granite
- Crystal size: Coarse
- Formation age: Caledonian
- Alteration age: Caledonian

3.2.31 Data and discussion for well 209/12-1 (Table 3.2.31)

Two sources of published data (Chemostrat, 2014 & Chambers *et al.*, 2005) and newly generated data from this study are presented for eight samples (four core and four cuttings) ranging from 11385.7-11527.0ft MD, a summary of the key values are given below:

- RHP: 2.08-3.60 $\mu\text{W}/\text{m}^3$
- Composition: Granite, biotite granite, biotite schist
- Crystal size: Coarse
- Formation age: Insufficient recovery of concordant zircons
- Alteration age: Caledonian

3.2.32 Data and discussion for well 214/09-1 (Table 3.2.31)

Published data (Finlay *et al.*, 2018) are presented for one core sample from 15581.0ft MD, a summary of the key values are given below:

- RHP: 2.53 $\mu\text{W}/\text{m}^3$
- Composition: Granite
- Crystal size: –
- Formation age: –
- Alteration age: –

3.2.33 Data and discussion for well Well 220/26-1 (Table 3.2.33)

Published data (Chambers *et al.*, 2005) are presented for one core sample from 5280.2m MD, a summary of the key values are given below:

- RHP: 0.94 $\mu\text{W}/\text{m}^3$
- Composition: Quartzofeldspathic mylonite
- Crystal size: –
- Formation age: –
- Alteration age: –

Well	Bottom depth (ft)	Stratigraphy	Age	Sample type	Radioactive Heat		Petrography & XRD						Zircon Geochronology			Apatite Geochronology		
					RHP (μWm^3)	Data Source	Technique	Crystal Size	Texture	Natural Open Fractures (%)	Rock Classification (USGS)	Data Source	Age (Ma)	$\pm 2\sigma$ (Ma)	Data Source	Age (Ma)	$\pm 2\sigma$ (Ma)	Data Source
154/03-1	8060.0	Laxford Basement	Lax	COCH	0.36	Chambers <i>et al.</i> (2005)	Thin section	-	Amphibolite	-	Amphibolite	Chambers <i>et al.</i> (2005)	-	-	-	-	-	-

Lax: Laxfordian
COCH: Core chip

TABLE 3.2.1 Inorganic geochemistry data summary: 154/03-1

Well	Bottom depth (m)	Stratigraphy	Age	Sample type	Radioactive Heat		Petrography & XRD						Zircon Geochronology			Apatite Geochronology		
					RHP (μWm^3)	Data Source	Technique	Crystal Size	Texture	Natural Open Fractures (%)	Rock Classification (USGS)	Data Source	Age (Ma)	$\pm 2\sigma$ (Ma)	Data Source	Age (Ma)	$\pm 2\sigma$ (Ma)	Data Source
164/25-2	2727.8	Lewisian Basement	PrCam	COCH	-	-	Thin section	-	Gneissic	-	Metabasic gneiss	Chambers <i>et al.</i> (2005)	-	-	-	-	-	-

PrCam: Precambrian
COCH: Core chip

TABLE 3.2.2 Inorganic geochemistry data summary: 164/25-2

Well	Bottom depth (ft)	Stratigraphy	Age	Sample type	Radioactive Heat		Petrography & XRD						Zircon Geochronology			Apatite Geochronology		
					RHP (μWm^3)	Data Source	Technique	Crystal Size	Texture	Natural Open Fractures (%)	Rock Classification (USGS)	Data Source	Age (Ma)	$\pm 2\sigma$ (Ma)	Data Source	Age (Ma)	$\pm 2\sigma$ (Ma)	Data Source
202/02-1	3950.0	Precambrian Basement	PrCam	DC	1.80	NEW	-	-	-	-	-	-	-	-	-	-	-	-
	4002.0			COCH	0.90	Chambers <i>et al.</i> (2005)	Thin section	-	Gneissic	-	Quartzofeldspathic gneiss	Chambers <i>et al.</i> (2005)	2829.0	46.0	Ritchie <i>et al.</i> (2011)	-	-	-

PrCam: Precambrian

DC: Ditch cuttings

COCH: Core chip

NEW: Analysed in this study

TABLE 3.2.3 Inorganic geochemistry data summary: 202/02-1

Well	Bottom depth (ft)	Stratigraphy	Age	Sample type	Radioactive Heat		Petrography & XRD						Zircon Geochronology			Apatite Geochronology		
					RHP (μWm^3)	Data Source	Technique	Crystal Size	Texture	Natural Open Fractures (%)	Rock Classification (USGS)	Data Source	Age (Ma)	$\pm 2\sigma$ (Ma)	Data Source	Age (Ma)	$\pm 2\sigma$ (Ma)	Data Source
202/08-1	5447.0	Lewisian Basement	PrCam	COCH	0.38	NEW	Thin section	Medium - Coarse	Gneissic	0.05	Monzodiorite	NEW	-	-	-	-	-	-
	5457.0			COCH	0.24		Thin section	Medium	Gneissic	1.33	Tonalite		-	-	-	-	-	-
	5500.0			DC	0.41		XRD	-	-		Granodiorite		-	-	-	-	-	-
	5510.0			DC	0.54		XRD	-	-		Granodiorite		-	-	-	-	-	-
	5520.0			DC	0.43		XRD	-	-		Granodiorite		-	-	-	-	-	-

PrCam: Precambrian
COCH: Core chip

DC: Ditch cuttings
NEW: Analysed in this study

XRD: X-ray diffraction

TABLE 3.2.4 Inorganic geochemistry data summary: 202/08-1

Well	Bottom depth (ft)	Stratigraphy	Age	Sample type	Radioactive Heat		Petrography & XRD						Zircon Geochronology			Apatite Geochronology		
					RHP (μWm^3)	Data Source	Technique	Crystal Size	Texture	Natural Open Fractures (%)	Rock Classification (USGS)	Data Source	Age (Ma)	$\pm 2\sigma$ (Ma)	Data Source	Age (Ma)	$\pm 2\sigma$ (Ma)	Data Source
202/09-1	5379.0	Lewisian Basement	PrCam	COCH	0.70	NEW	Thin section	Medium	Gneissic	0.00	Diorite	NEW	-	-	-	-	-	-

PrCam: Precambrian

COCH: Core chip

NEW: Analysed in this study

TABLE 3.2.5 Inorganic geochemistry data summary: 202/09-1

Well	Bottom depth (m)	Stratigraphy	Age	Sample type	Radioactive Heat		Petrography & XRD						Zircon Geochronology			Apatite Geochronology		
					RHP (μWm³)	Data Source	Technique	Crystal Size	Texture	Natural Open Fractures (%)	Rock Classification (USGS)	Data Source	Age (Ma)	± 2σ (Ma)	Data Source	Age (Ma)	± 2σ (Ma)	Data Source
204/10-1	2499.0	Precambrian Basement	PrCam	COCH	1.10	Finlay <i>et al.</i> (2018)	-	-	-	-	-	-	-	-	-	-	-	-
	2505.0			DC	1.00	NEW	-	-	-	-	-	-	Insufficient concordant Zircon recovery	1792.0	73.0	NEW		
	2508.0			DC	1.00		-	-	-	-	-	-						
	2511.0			DC	0.90		-	-	-	-	-	-						
	2514.0			DC	1.00		-	-	-	-	-	-					-	
							-	-	-	-	-	-					-	

PrCam: Precambrian
COCH: Core chip

DC: Ditch cuttings
NEW: Analysed in this study

TABLE 3.2.6 Inorganic geochemistry data summary: 204/10-1

Well	Bottom depth (ft)	Stratigraphy	Age	Sample type	Radioactive Heat		Petrography & XRD						Zircon Geochronology			Apatite Geochronology		
					RHP (μWm^3)	Data Source	Technique	Crystal Size	Texture	Natural Open Fractures (%)	Rock Classification (USGS)	Data Source	Age (Ma)	$\pm 2\sigma$ (Ma)	Data Source	Age (Ma)	$\pm 2\sigma$ (Ma)	Data Source
204/15-2	7270.0	Balder	E1	DC	1.32	NEW	-	-	-	-	-	-	-	-	-	-	-	-
	7990.0	Flett		DC	0.89		-	-	-	-	-	-	-	-	-	-	-	-
	9550.0	Lamba	P3	DC	1.34		-	-	-	-	-	-	-	-	-	-	-	-
	10810.0	Vaila		DC	0.96		-	-	-	-	-	-	-	-	-	-	-	-
	11610.0	Coniacia-Albian	K2	DC	1.65		-	-	-	-	-	-	-	-	-	-	-	-
	12390.0	Volgian	J3	DC	3.76		-	-	-	-	-	-	-	-	-	-	-	-
	12450.0	Precambrian Basement	PrCam	DC	0.51	Finlay <i>et al.</i> (2018)	Thin section	-	Gneissic	-	Tonalite	Finlay <i>et al.</i> (2018)	-	-	-	-	-	-
	12476.0			DC	0.20		Thin section	-	Gneissic	-	Tonalite		-	-	-	-	-	-

PrCam: Precambrian
E1: Early Eocene

P3: Late Paleocene
K2: Late Cretaceous

J3: Late Jurassic
DC: Ditch cuttings

NEW: Analysed in this study

TABLE 3.2.7 Inorganic geochemistry data summary: 204/15-2

Well	Bottom depth (m)	Stratigraphy	Age	Sample type	Radioactive Heat		Petrography & XRD						Zircon Geochronology			Apatite Geochronology		
					RHP (μWm^3)	Data Source	Technique	Crystal Size	Texture	Natural Open Fractures (%)	Rock Classification (USGS)	Data Source	Age (Ma)	$\pm 2\sigma$ (Ma)	Data Source	Age (Ma)	$\pm 2\sigma$ (Ma)	Data Source
204/23-1	3847.2	Precambrian Basement	PrCam	COCH	0.64	Chambers <i>et al.</i> (2005)	Thin section	-	Gneissic	-	Quartzofeldspathic gneiss	Chambers <i>et al.</i> (2005)	-	-	-	-	-	-

PrCam: Precambrian
COCH: Core chip

TABLE 3.2.8 Inorganic geochemistry data summary: 204/23-1

Well	Bottom depth (ft)	Stratigraphy	Age	Sample type	Radioactive Heat		Petrography & XRD						Zircon Geochronology			Apatite Geochronology		
					RHP (μWm^3)	Data Source	Technique	Crystal Size	Texture	Natural Open Fractures (%)	Rock Classification (USGS)	Data Source	Age (Ma)	$\pm 2\sigma$ (Ma)	Data Source	Age (Ma)	$\pm 2\sigma$ (Ma)	Data Source
204/25-1	9417.0	Precambrian Basement	PrCam	COCH	0.13	Chambers <i>et al.</i> (2005)	Thin section	-	Gneissic	-	Tonalitic gneiss	Chambers <i>et al.</i> (2005)	2729.0	12.0	Holdsworth <i>et al.</i> (2019)	-	-	-

PrCam: Precambrian
COCH: Core chip

TABLE 3.2.9 Inorganic geochemistry data summary: 204/25-1

Well	Bottom depth (ft)	Stratigraphy	Age	Sample type	Radioactive Heat		Petrography & XRD						Zircon Geochronology			Apatite Geochronology		
					RHP (μWm^3)	Data Source	Technique	Crystal Size	Texture	Natural Open Fractures (%)	Rock Classification (USGS)	Data Source	Age (Ma)	$\pm 2\sigma$ (Ma)	Data Source	Age (Ma)	$\pm 2\sigma$ (Ma)	Data Source
204/26-1A	8689.9	Lewisian Basement	PrCam	COCH	-	-	Thin section	-	Gneissic	-	Granodioritic gneiss	Holdsworth <i>et al.</i> (2019)	2733.0	14.0	Holdsworth <i>et al.</i> (2019)	-	-	-

PrCam: Precambrian
COCH: Core chip

TABLE 3.2.10 Inorganic geochemistry data summary: 204/26-1A

Well	Bottom depth (m)	Stratigraphy	Age	Sample type	Radioactive Heat		Petrography & XRD						Zircon Geochronology			Apatite Geochronology		
					RHP (μWm^3)	Data Source	Technique	Crystal Size	Texture	Natural Open Fractures (%)	Rock Classification (USGS)	Data Source	Age (Ma)	$\pm 2\sigma$ (Ma)	Data Source	Age (Ma)	$\pm 2\sigma$ (Ma)	Data Source
204/27a-1	2136.3	Precambrian Basement	PrCam	COCH	-	-	Thin section	-	-	-	Granite	Holdsworth <i>et al.</i> (2019)	2745.0	15.0	Holdsworth <i>et al.</i> (2019)	-	-	

PrCam: Precambrian
COCH: Core chip

TABLE 3.2.11 Inorganic geochemistry data summary: 204/27a-1

Well	Bottom depth (m)	Stratigraphy	Age	Sample type	Radioactive Heat		Petrography & XRD						Zircon Geochronology			Apatite Geochronology		
					RHP (μWm^3)	Data Source	Technique	Crystal Size	Texture	Natural Open Fractures (%)	Rock Classification (USGS)	Data Source	Age (Ma)	$\pm 2\sigma$ (Ma)	Data Source	Age (Ma)	$\pm 2\sigma$ (Ma)	Data Source
204/28-1	1941.6	Precambrian Basement	PrCam	COCH	-	-	Thin section	-	Gneissic	-	Granodioritic gneiss	Holdsworth <i>et al.</i> (2019)	2762.0	13.0	Holdsworth <i>et al.</i> (2019)	-	-	-

PrCam: Precambrian
COCH: Core chip

TABLE 3.2.12 Inorganic geochemistry data summary: 204/28-1

Well	Bottom depth (m)	Stratigraphy	Age	Sample type	Radioactive Heat		Petrography & XRD						Zircon Geochronology			Apatite Geochronology		
					RHP (μWm ³)	Data Source	Technique	Crystal Size	Texture	Natural Open Fractures (%)	Rock Classification (USGS)	Data Source	Age (Ma)	± 2σ (Ma)	Data Source	Age (Ma)	± 2σ (Ma)	Data Source
205/16-1	4172.2	Lewisian Basement	PrCam	COCH	1.21	Chambers <i>et al.</i> (2005)	Thin section	-	Gneissic	-	Dioritic gneiss	Chambers <i>et al.</i> (2005)	-	-	-	-	-	-
	4274.2			COCH	0.82	NEW	Thin section	Medium	Gneissic	0.00	Tonalite	NEW	-	-	-	-	-	-
	4274.4			COCH	0.96		Thin section	Medium	Gneissic	0.33	Tonalite		-	-	-	-	-	-
	4274.6			COCH	0.41		Thin section	Medium - Coarse	Gneissic	Tr	Granodiorite		-	-	-	-	-	-
	4275.3			COCH	2.36		Thin section	Medium - Coarse	Gneissic	Tr	Granodiorite		2738	6.0	NEW	1783	44.0	NEW
	4300.0			DC	0.96		XRD	-	-	-	Granite		2742.00	6.0		1905.00	41.0	
	4305.0			DC	0.90													
	4310.0			DC	0.89													
	4315.0			DC	0.67													

PrCam: Precambrian
COCH: Core chip

DC: Ditch cuttings
XRD: X-ray diffraction

NEW: Analysed in this study
Tr: Trace

TABLE 3.2.13 Inorganic geochemistry data summary: 205/16-1

Well	Bottom depth (m)	Stratigraphy	Age	Sample type	Radioactive Heat		Petrography & XRD						Zircon Geochronology			Apatite Geochronology		
					RHP (μWm^3)	Data Source	Technique	Crystal Size	Texture	Natural Open Fractures (%)	Rock Classification (USGS)	Data Source	Age (Ma)	$\pm 2\sigma$ (Ma)	Data Source	Age (Ma)	$\pm 2\sigma$ (Ma)	Data Source
205/20-1	2017.5	Lewisian Basement	PrCam	COCH	0.90	Chambers <i>et al.</i> (2005)	Thin section	-	Gneissic	-	Granodioritic gneiss	Holdsworth <i>et al.</i> (2019)	2806.0	8.0	Holdsworth <i>et al.</i> (2019)	-	-	-

PrCam: Precambrian
COCH: Core chip

TABLE 3.2.14 Inorganic geochemistry data summary: 205/20-1

Well	Bottom depth (ft)	Stratigraphy	Age	Sample type	Radioactive Heat		Petrography & XRD						Zircon Geochronology			Apatite Geochronology		
					RHP (μWm^3)	Data Source	Technique	Crystal Size	Texture	Natural Open Fractures (%)	Rock Classification (USGS)	Data Source	Age (Ma)	$\pm 2\sigma$ (Ma)	Data Source	Age (Ma)	$\pm 2\sigma$ (Ma)	Data Source
205/21-1A	4449.0	Lewisian Basement	PrCam	COCH	0.15	NEW	Thin section	-	Gneissic	0.33	Granite	Finlay <i>et al.</i> (2018)	-	-	-	-	-	-
	4465.0			COCH	0.15		Thin section	-	Gneissic	0.33	Tonalite		-	-	-	-	-	-

PrCam: Precambrian
COCH: Core chip

NEW: Analysed in this study

TABLE 3.2.15 Inorganic geochemistry data summary: 205/21-1A

Well	Bottom depth (m)	Stratigraphy	Age	Sample type	Radioactive Heat		Petrography & XRD						Zircon Geochronology			Apatite Geochronology		
					RHP (μWm^3)	Data Source	Technique	Crystal Size	Texture	Natural Open Fractures (%)	Rock Classification (USGS)	Data Source	Age (Ma)	$\pm 2\sigma$ (Ma)	Data Source	Age (Ma)	$\pm 2\sigma$ (Ma)	Data Source
205/22-1A	3225.6	Precambrian Basement	PrCam	COCH	0.73	Chambers <i>et al.</i> (2005)	Thin section	-	Genissic	-	Dioritic gneiss	Chambers <i>et al.</i> (2005)	2700.0	13.0	Holdsworth <i>et al.</i> (2019)	-	-	-

PrCam: Precambrian
COCH: Core chip

TABLE 3.2.16 Inorganic geochemistry data summary: 205/22-1A

Well	Bottom depth (m)	Stratigraphy	Age	Sample type	Radioactive Heat		Petrography & XRD						Zircon Geochronology			Apatite Geochronology		
					RHP (μWm^3)	Data Source	Technique	Crystal Size	Texture	Natural Open Fractures (%)	Rock Classification (USGS)	Data Source	Age (Ma)	$\pm 2\sigma$ (Ma)	Data Source	Age (Ma)	$\pm 2\sigma$ (Ma)	Data Source
206/07a-2	2140.7	Precambrian Basement	PrCam	COCH	-	-	-	-	-	-	-	-	2809.2	20.8	Chemostrat (2014)	-	-	-
	2141.3			COCH	0.90	Chambers <i>et al.</i> (2005)	Thin section	Coarse	Gneissic	-	Granodioritic gneiss	Holdsworth <i>et al.</i> (2019)	2806.0	8.0	Holdsworth <i>et al.</i> (2019)	-	-	-
	2146.7			COCH	0.20	NEW	Thin section	Coarse	Gneissic	-	Tonalite	NEW	-	-	-	-	-	-
	2147.9			COCH	0.30		Thin section	Coarse	Gneissic	0.33	Tonalite		2851.0	18.0	NEW	1748.2	79.6	NEW
	2246.4			COCH	1.10		Thin section	-	Gneissic	0.00	Tonalite		-	-	-	-	-	-
	2438.3			COCH	0.60	Finlay <i>et al.</i> (2018)	Thin section	Coarse	Gneissic	0.67	Tonalite	Finlay <i>et al.</i> (2018)	-	-	-	-	-	-
	2442.6			COCH	0.50	NEW	Thin section	-	Gneissic	0.00	Tonalite-diorite	NEW	-	-	-	-	-	-
	2443.2			COCH	1.70	Finlay <i>et al.</i> (2018)	Thin section	Coarse	Gneissic	0.33	Diorite	Finlay <i>et al.</i> (2018)	-	-	-	-	-	-

PrCam: Precambrian
COCH: Core chip

NEW: Analysed in this study

TABLE 3.2.17 Inorganic geochemistry data summary: 206/07a-2

Well	Bottom depth (m)	Stratigraphy	Age	Sample type	Radioactive Heat		Petrography & XRD						Zircon Geochronology			Apatite Geochronology		
					RHP (μWm^3)	Data Source	Technique	Crystal Size	Texture	Natural Open Fractures (%)	Rock Classification (USGS)	Data Source	Age (Ma)	$\pm 2\sigma$ (Ma)	Data Source	Age (Ma)	$\pm 2\sigma$ (Ma)	Data Source
206/08-1A	2306.4	Precambrian Basement	PrCam	COCH	-	-	-	-	-	-	-	-	2691.0	28.0	Chemostrat (2014)	-	-	-
	2311.0			COCH	0.64	Chambers <i>et al.</i> (2005)	Thin section	-	Gneissic	-	Dioritic gneiss	Chambers <i>et al.</i> (2005)	2801.7	5.0	Holdsworth <i>et al.</i> (2019)	-	-	-

PrCam: Precambrian
COCH: Core chip

TABLE 3.2.18 Inorganic geochemistry data summary: 206/08-1A

Well	Bottom depth (m)	Stratigraphy	Age	Sample type	Radioactive Heat		Petrography & XRD						Zircon Geochronology			Apatite Geochronology		
					RHP (μWm^3)	Data Source	Technique	Crystal Size	Texture	Natural Open Fractures (%)	Rock Classification (USGS)	Data Source	Age (Ma)	$\pm 2\sigma$ (Ma)	Data Source	Age (Ma)	$\pm 2\sigma$ (Ma)	Data Source
206/08-2	1859.0	Precambrian Basement	PrCam	COCH	2.27	Finlay <i>et al.</i> (2018)	Thin Section	-	Gneissic	0.05	Granodiorite	Finlay <i>et al.</i> (2018)	-	-	-	-	-	-
	1864.6			COCH	1.92	Chambers <i>et al.</i> (2005)	Thin Section	-	-	0.00	Protomylonite	Chambers <i>et al.</i> (2005)	-	-	-	-	-	-

PrCam: Precambrian
COCH: Core chip

TABLE 3.2.19 Inorganic geochemistry data summary: 206/08-2

Well	Bottom depth (m)	Stratigraphy	Age	Sample type	Radioactive Heat		Petrography & XRD						Zircon Geochronology			Apatite Geochronology		
					RHP (μWm^3)	Data Source	Technique	Crystal Size	Texture	Natural Open Fractures (%)	Rock Classification (USGS)	Data Source	Age (Ma)	$\pm 2\sigma$ (Ma)	Data Source	Age (Ma)	$\pm 2\sigma$ (Ma)	Data Source
206/08-7	2320.5	Basement	PrCam	COCH	0.67	Chambers <i>et al.</i> (2005)	Thin section	-	Amphibolite	-	Amphibolite	Chambers <i>et al.</i> (2005)	-	-	-	-	-	-

PrCam: Precambrian
COCH: Core chip

TABLE 3.2.20 Inorganic geochemistry data summary: 206/08-7

Well	Bottom depth (m)	Stratigraphy	Age	Sample type	Radioactive Heat		Petrography & XRD						Zircon Geochronology			Apatite Geochronology		
					RHP (μWm^3)	Data Source	Technique	Crystal Size	Texture	Natural Open Fractures (%)	Rock Classification (USGS)	Data Source	Age (Ma)	$\pm 2\sigma$ (Ma)	Data Source	Age (Ma)	$\pm 2\sigma$ (Ma)	Data Source
206/08-8	2499.0	Basement	PrCam	COCH	0.25	Chambers <i>et al.</i> (2005)	Thin section	-	Gneissic	-	Granitic gneiss	Chambers <i>et al.</i> (2005)	-	-	-	-	-	-

PrCam: Precambrian
COCH: Core chip

TABLE 3.2.21 Inorganic geochemistry data summary: 206/08-8

Well	Bottom depth (ft)	Stratigraphy	Age	Sample type	Radioactive Heat		Petrography & XRD						Zircon Geochronology			Apatite Geochronology		
					RHP (μWm^3)	Data Source	Technique	Crystal Size	Texture	Natural Open Fractures (%)	Rock Classification (USGS)	Data Source	Age (Ma)	$\pm 2\sigma$ (Ma)	Data Source	Age (Ma)	$\pm 2\sigma$ (Ma)	Data Source
206/09-2	8084.0	Lewisian Basement	PrCam	COCH	2.68	Finlay <i>et al.</i> (2018)	Thin section	-	Gneissic	0.33	Granite	Finlay <i>et al.</i> (2018)	-	-	-	-	-	-

PrCam: Precambrian
COCH: Core chip

TABLE 3.2.22 Inorganic geochemistry data summary: 206/09-2

Well	Bottom depth (ft)	Stratigraphy	Age	Sample type	Radioactive Heat		Petrography & XRD						Zircon Geochronology			Apatite Geochronology		
					RHP (μWm^3)	Data Source	Technique	Crystal Size	Texture	Natural Open Fractures (%)	Rock Classification (USGS)	Data Source	Age (Ma)	$\pm 2\sigma$ (Ma)	Data Source	Age (Ma)	$\pm 2\sigma$ (Ma)	Data Source
206/12-1	5630.0	Lewisian Basement	PrCam	COCH	0.44	Finlay <i>et al.</i> (2018)	Thin section	-	Gneissic	0.33	Granodioritic gneiss	Finlay <i>et al.</i> (2018)	-	-	-	-	-	-
	5632.0			COCH	-	-	Thin section	-	Gneissic	0.00	Granodioritic gneiss	Holdsworth <i>et al.</i> (2019)	2748.0	6.0	Holdsworth <i>et al.</i> (2019)	-	-	-

PrCam: Precambrian
COCH: Core chip

TABLE 3.2.23 Inorganic geochemistry data summary: 206/12-1

Well	Bottom depth (ft)	Stratigraphy	Age	Sample type	Radioactive Heat		Petrography & XRD						Zircon Geochronology			Apatite Geochronology		
					RHP (μWm^3)	Data Source	Technique	Crystal Size	Texture	Natural Open Fractures (%)	Rock Classification (USGS)	Data Source	Age (Ma)	$\pm 2\sigma$ (Ma)	Data Source	Age (Ma)	$\pm 2\sigma$ (Ma)	Data Source
207/01-3	4576.3	Precambrian Basement	PrCam	COCH	0.94	NEW	Thin section	0.0	Schistose	0.33	Metasedimentary (metasandstone)	NEW	-	-	-	-	-	-
	4670.0			DC	1.10		XRD	-	-	-	Granodiorite	NEW	2738.0	16.0	NEW	1425.0	99.0	NEW
	4680.0			DC	0.89													
	4690.0			DC	1.39													
	4700.0			DC	1.03													
	4706.0			DC	1.00													

PrCam: Precambrian
COCH: Core chip

DC: Ditch cuttings
NEW: Analysed in this study

XRD: X-ray diffraction

TABLE 3.2.24 Inorganic geochemistry data summary: 207/01-3

Well	Bottom depth (ft)	Stratigraphy	Age	Sample type	Radioactive Heat		Petrography & XRD						Zircon Geochronology			Apatite Geochronology		
					RHP (μWm^3)	Data Source	Technique	Crystal Size	Texture	Natural Open Fractures (%)	Rock Classification (USGS)	Data Source	Age (Ma)	$\pm 2\sigma$ (Ma)	Data Source	Age (Ma)	$\pm 2\sigma$ (Ma)	Data Source
207/02-1	6722.0	Precambrian Basement	PrCam	COCH	0.76	NEW	Thin section	Coarse	Gneissic	0.33	Granite	NEW	2732.0	4.0	NEW	1761.0	25.0	NEW
	6723.0			COCH	0.77		Thin section	Coarse	Gneissic	0.33	Syenogranite		2735.0	5.0		1761.0	28.0	
	6724.0			COCH	0.86		Thin section	Coarse	Gneissic	1.00	Granite		2734.6	4.0		1762.0	26.0	

PrCam: Precambrian
COCH: Core chip

NEW: Analysed in this study

TABLE 3.2.25 Inorganic geochemistry data summary: 207/02-1

Well	Bottom depth (ft)	Stratigraphy	Age	Sample type	Radioactive Heat		Petrography & XRD						Zircon Geochronology			Apatite Geochronology		
					RHP (μWm^3)	Data Source	Technique	Crystal Size	Texture	Natural Open Fractures (%)	Rock Classification (USGS)	Data Source	Age (Ma)	$\pm 2\sigma$ (Ma)	Data Source	Age (Ma)	$\pm 2\sigma$ (Ma)	Data Source
208/23-1	6795.5	Precambrian Basement	PrCam	COCH	-	-	Thin section	-	Gneissic	-	Granitic gneiss	Holdsworth <i>et al.</i> (2019)	2776.0	12.0	Holdsworth <i>et al.</i> (2019)	-	-	-
	6796.5			COCH	1.72	NEW	Thin section	Coarse	Gneissic	-	Granite	NEW	2782.0	6.0	NEW	~450	LIR	NEW
	6799.2			COCH	0.56		Thin section	Coarse	Gneissic	-	Fractured syenogranite		-	-	-	-	-	-
	6803.0			COCH	0.51		Thin section	Coarse	Gneissic	-	Syenogranite		-	-	-	-	-	-
	6806.1			COCH	1.97		Thin section	Coarse	Gneissic	-	Tonalite		-	-	-	-	-	-
	6808.0			COCH	1.10		Thin section	Fine - Medium	Gneissic	-	Tonalite		-	-	-	-	-	-

PrCam: Precambrian
COCH: Core chip

NEW: Analysed in this study
LIR: Lower intercept range

TABLE 3.2.26 Inorganic geochemistry data summary: 208/23-1

Well	Bottom depth (m)	Stratigraphy	Age	Sample type	Radioactive Heat		Petrography & XRD						Zircon Geochronology			Apatite Geochronology		
					RHP (μWm^3)	Data Source	Technique	Crystal Size	Texture	Natural Open Fractures (%)	Rock Classification (USGS)	Data Source	Age (Ma)	$\pm 2\sigma$ (Ma)	Data Source	Age (Ma)	$\pm 2\sigma$ (Ma)	Data Source
208/26-1	3894.0	Precambrian Basement	PrCam	COCH	0.20	Finlay <i>et al.</i> (2018)	Thin section	-	Gneissic	0.67	Serpentinised granodiorite	Finlay <i>et al.</i> (2018)	-	-	-	-	-	-

PrCam: Precambrian
COCH: Core chip

TABLE 3.2.27 Inorganic geochemistry data summary: 208/26-1

Well	Bottom depth (m)	Stratigraphy	Age	Sample type	Radioactive Heat		Petrography & XRD						Zircon Geochronology			Apatite Geochronology		
					RHP (μWm^3)	Data Source	Technique	Crystal Size	Texture	Natural Open Fractures (%)	Rock Classification (USGS)	Data Source	Age (Ma)	$\pm 2\sigma$ (Ma)	Data Source	Age (Ma)	$\pm 2\sigma$ (Ma)	Data Source
208/27-1	1380.2	Precambrian Basement	PrCam	COCH	-	-	-	-	-	-	-	-	2738.7	22.0	Chemostrat (2014)	-	-	-

PrCam: Precambrian
COCH: Core chip

TABLE 3.2.28 Inorganic geochemistry data summary: 208/27-1

Well	Bottom depth (ft)	Stratigraphy	Age	Sample type	Radioactive Heat		Petrography & XRD						Zircon Geochronology			Apatite Geochronology		
					RHP (μWm^3)	Data Source	Technique	Crystal Size	Texture	Natural Open Fractures (%)	Rock Classification (USGS)	Data Source	Age (Ma)	$\pm 2\sigma$ (Ma)	Data Source	Age (Ma)	$\pm 2\sigma$ (Ma)	Data Source
208/27-2	4452.5	Lewisian Basement	PrCam	COCH	-	-	Thin section	-	Gneissic	-	Mafic granitic gneiss	Holdsworth <i>et al.</i> (2019)	2789.0	8.0	Holdsworth <i>et al.</i> (2019)	-	-	-
	4522.2			COCH	0.34	NEW	Thin section	Coarse	Gneissic (weathered)	0.00	Weathered granite	NEW	-	-	-	-	-	-
	4527.5			COCH	0.74		Thin section	Coarse	Gneissic (weathered)	0.00	Weathered granite		2742.0	6.0	NEW	~450	LIR	NEW
	4528.8			COCH	1.03	Chambers <i>et al.</i> (2005)	Thin section	-	Gneissic	-	Granitic gneiss	Chambers <i>et al.</i> (2005)	-	-	-	-	-	-
	4531.2			COCH	0.37	NEW	Thin section	Coarse	Gneissic (weathered)	0.00	Weathered granite	NEW	-	-	-	-	-	-
	4532.0			COCH	0.49		Thin section	Coarse	Gneissic (weathered)	0.00	Weathered syenogranite		-	-	-	-	-	-

PrCam: Precambrian
COCH: Core chip

NEW: Analysed in this study
LIR: Lower intercept range

TABLE 3.2.29 Inorganic geochemistry data summary: 208/27-2

Well	Bottom depth (ft)	Stratigraphy	Age	Sample type	Radioactive Heat		Petrography & XRD						Zircon Geochronology			Apatite Geochronology		
					RHP (μWm^3)	Data Source	Technique	Crystal Size	Texture	Natural Open Fractures (%)	Rock Classification (USGS)	Data Source	Age (Ma)	$\pm 2\sigma$ (Ma)	Data Source	Age (Ma)	$\pm 2\sigma$ (Ma)	Data Source
209/09-1	8850.0	Caledonian Basement	Sil	COCH	1.94	NEW	Thin section	Coarse	Igneous	-	Tonalite (biotite enriched)	NEW	-	-	-	-	-	-
	8854.0			COCH	1.87		Thin section	Coarse	Igneous	-	Granodiorite		-	-	-	-	-	-
	8855.0			COCH	1.30		Thin section	Coarse	Igneous	-	Gneissic quartz rich granitoid (biotite enriched)		463.0	10.0	NEW	417.2	17.0	NEW

Sil: Silurian
COCH: Core chip

NEW: Analysed in this study

TABLE 3.2.30 Inorganic geochemistry data summary: 209/09-1

Well	Bottom depth (ft)	Stratigraphy	Age	Sample type	Radioactive Heat		Petrography & XRD						Zircon Geochronology			Apatite Geochronology		
					RHP (μWm³)	Data Source	Technique	Crystal Size	Texture	Natural Open Fractures (%)	Rock Classification (USGS)	Data Source	Age (Ma)	± 2σ (Ma)	Data Source	Age (Ma)	± 2σ (Ma)	Data Source
209/12-1	11385.7	Caledonian Basement	Sil	COCH	3.60	NEW	-	-	-	-	-	-	-	-	-	-	-	-
	11500.0			DC	2.08		XRD	-	-	-	Granite	NEW	-	-	-	-	-	-
	11510.0			DC	2.18													
	11520.0			DC	2.14													
	11521.0			DC	-	-	-	-	-	-	-	Insufficient concordant Zircon recovery			425.0	21.0	NEW	
	11525.0			COCH	2.07	NEW	Thin section	Coarse	Igneous	-	Biotite granite - syenogranite	-	-	-	-	-	-	-
	11526.0			COCH	2.68	Chambers <i>et al.</i> (2005)	Thin section	-	-	-	Biotite schist	-	-	-	-	-	-	-
	11527.0			COCH	2.29	NEW	Thin section	Coarse	Igneous	-	Alkali feldspar biotite granite	-	-	-	-	-	-	-

Sil: Silurian
COCH: Core chip

DC: Ditch cuttings
XRD: X-ray diffraction

NEW: Analysed in this study

TABLE 3.2.31 Inorganic geochemistry data summary: 209/12-1

Well	Bottom depth (ft)	Stratigraphy	Age	Sample type	Radioactive Heat		Petrography & XRD						Zircon Geochronology			Apatite Geochronology		
					RHP (μWm^3)	Data Source	Technique	Crystal Size	Texture	Natural Open Fractures (%)	Rock Classification (USGS)	Data Source	Age (Ma)	$\pm 2\sigma$ (Ma)	Data Source	Age (Ma)	$\pm 2\sigma$ (Ma)	Data Source
214/09-1	11581.0	Precambrian Basement	PrCam	DC	2.53	Finlay <i>et al.</i> (2018)	Thin section	-	Igneous	0.05	Granite	Finlay <i>et al.</i> (2018)	-	-	-	-	-	-

PrCam: Precambrian
DC: Ditch cuttings

NEW: Analysed in this study

TABLE 3.2.32 Inorganic geochemistry data summary: 214/09-1

Well	Bottom depth (m)	Stratigraphy	Age	Sample type	Radioactive Heat		Petrography & XRD						Zircon Geochronology			Apatite Geochronology		
					RHP (μWm^3)	Data Source	Technique	Crystal Size	Texture	Natural Open Fractures (%)	Rock Classification (USGS)	Data Source	Age (Ma)	$\pm 2\sigma$ (Ma)	Data Source	Age (Ma)	$\pm 2\sigma$ (Ma)	Data Source
220/26-1	5280.2	Caledonian Basement	Sil	COCH	0.94	Chambers <i>et al.</i> (2005)	Thin section	-	-	-	Quartzofeldspathic mylonite	Chambers <i>et al.</i> (2005)	-	-	-	-	-	-

Sil: Silurian
COCH: Core chip

NEW: Analysed in this study

TABLE 3.2.33 Inorganic geochemistry data summary: 220/26-1

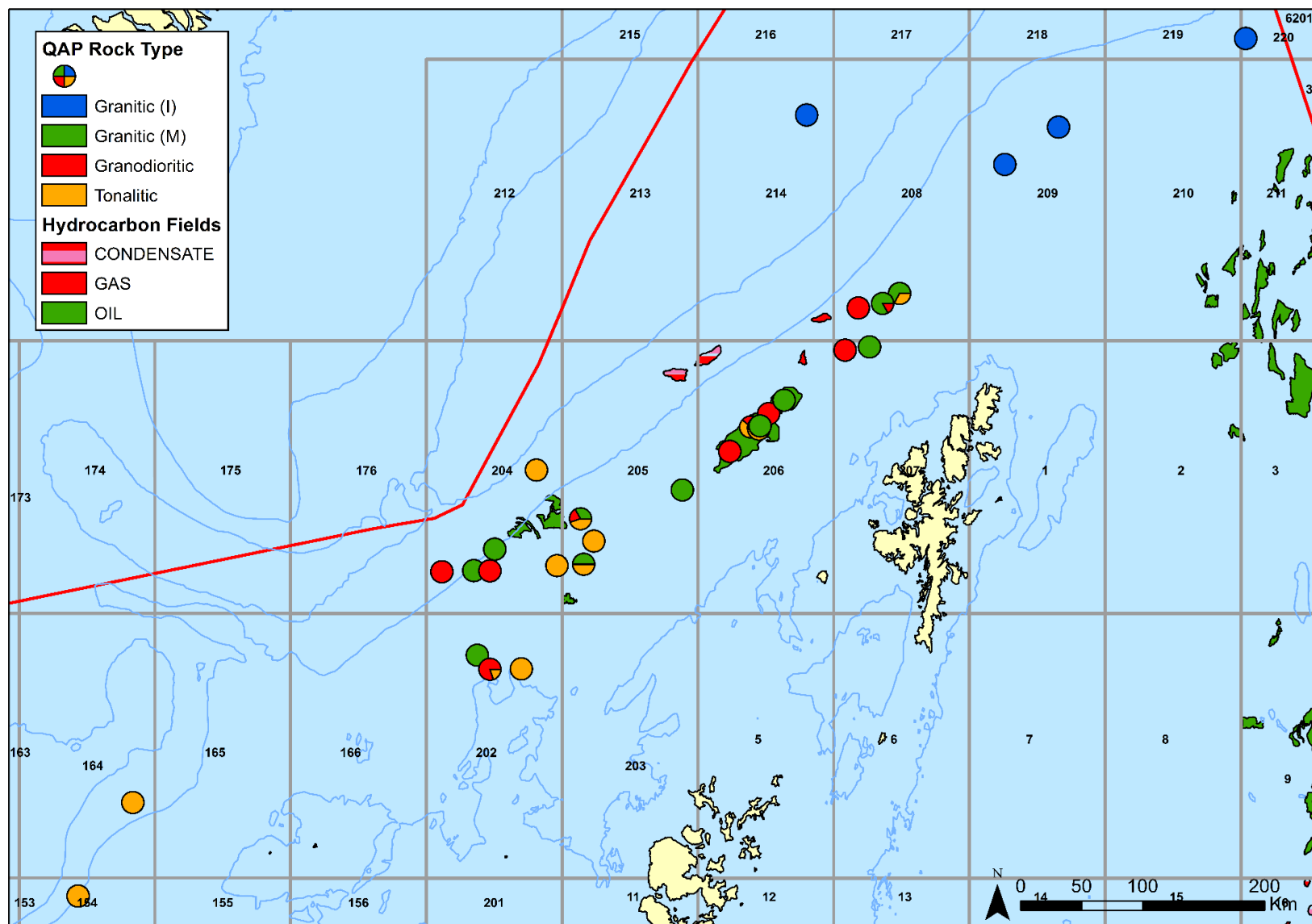


FIGURE 3.2.1 Basement composition

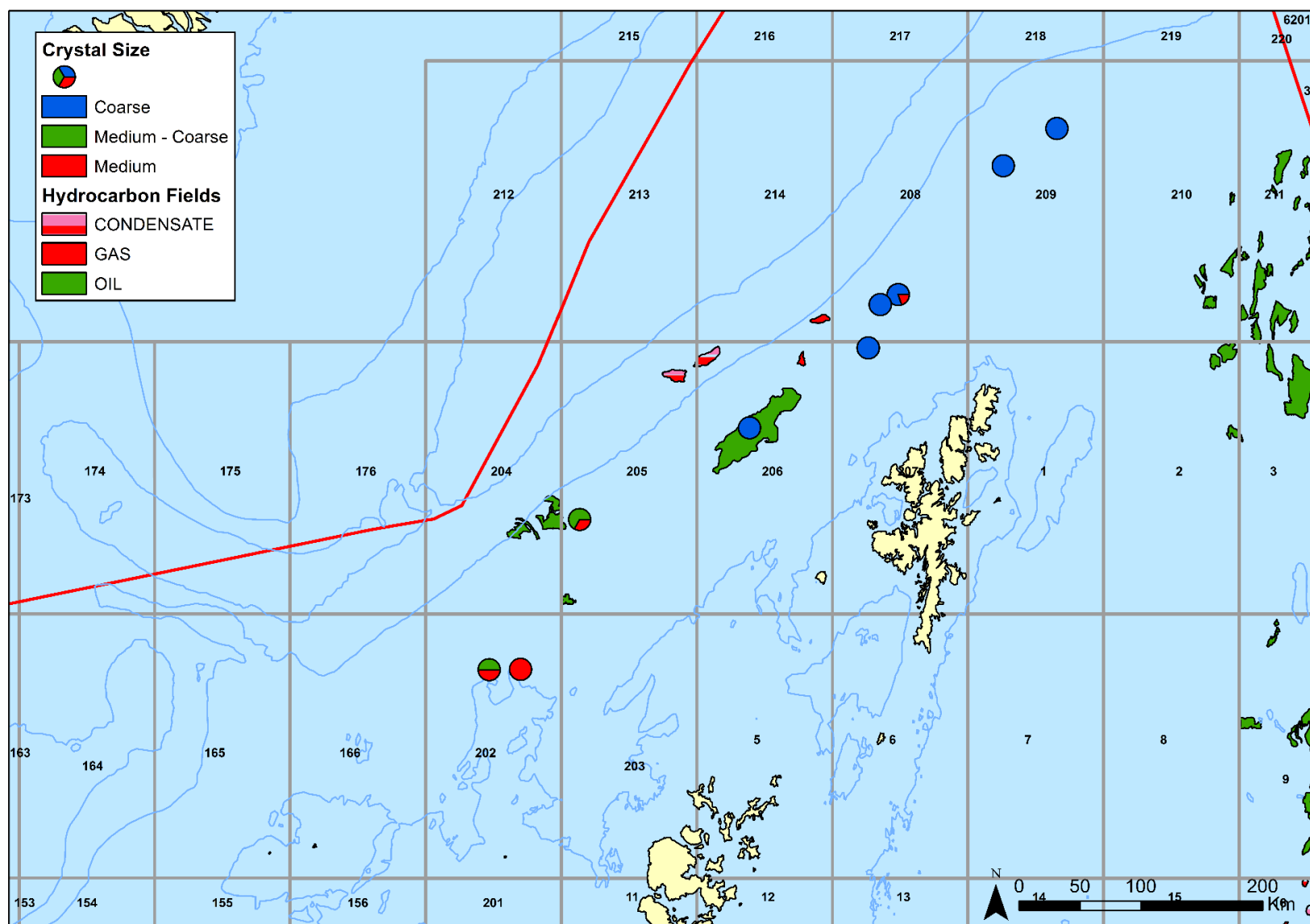


FIGURE 3.2.2 Crystal size distribution

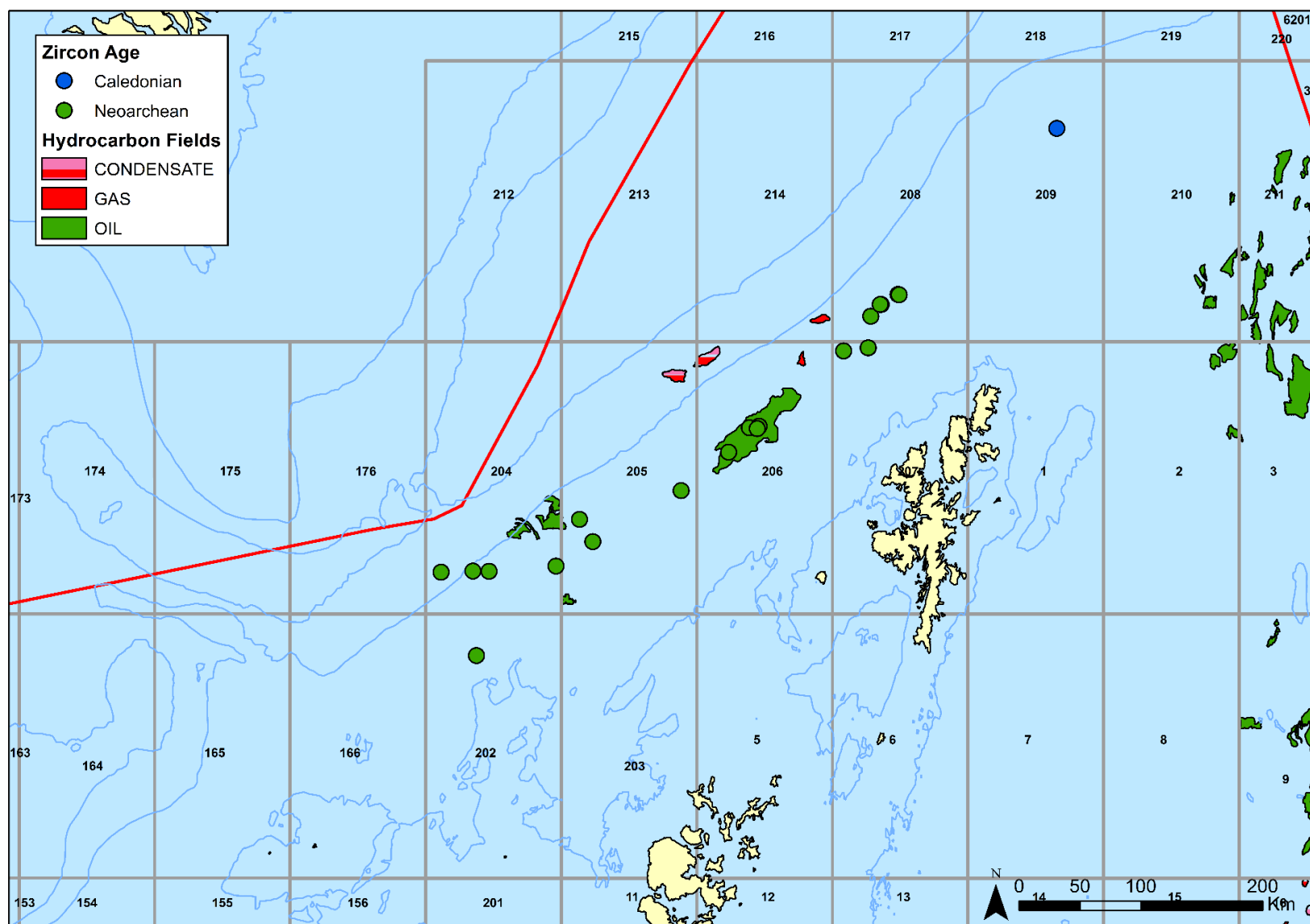


FIGURE 3.2.3 UPb Zircon geochronology

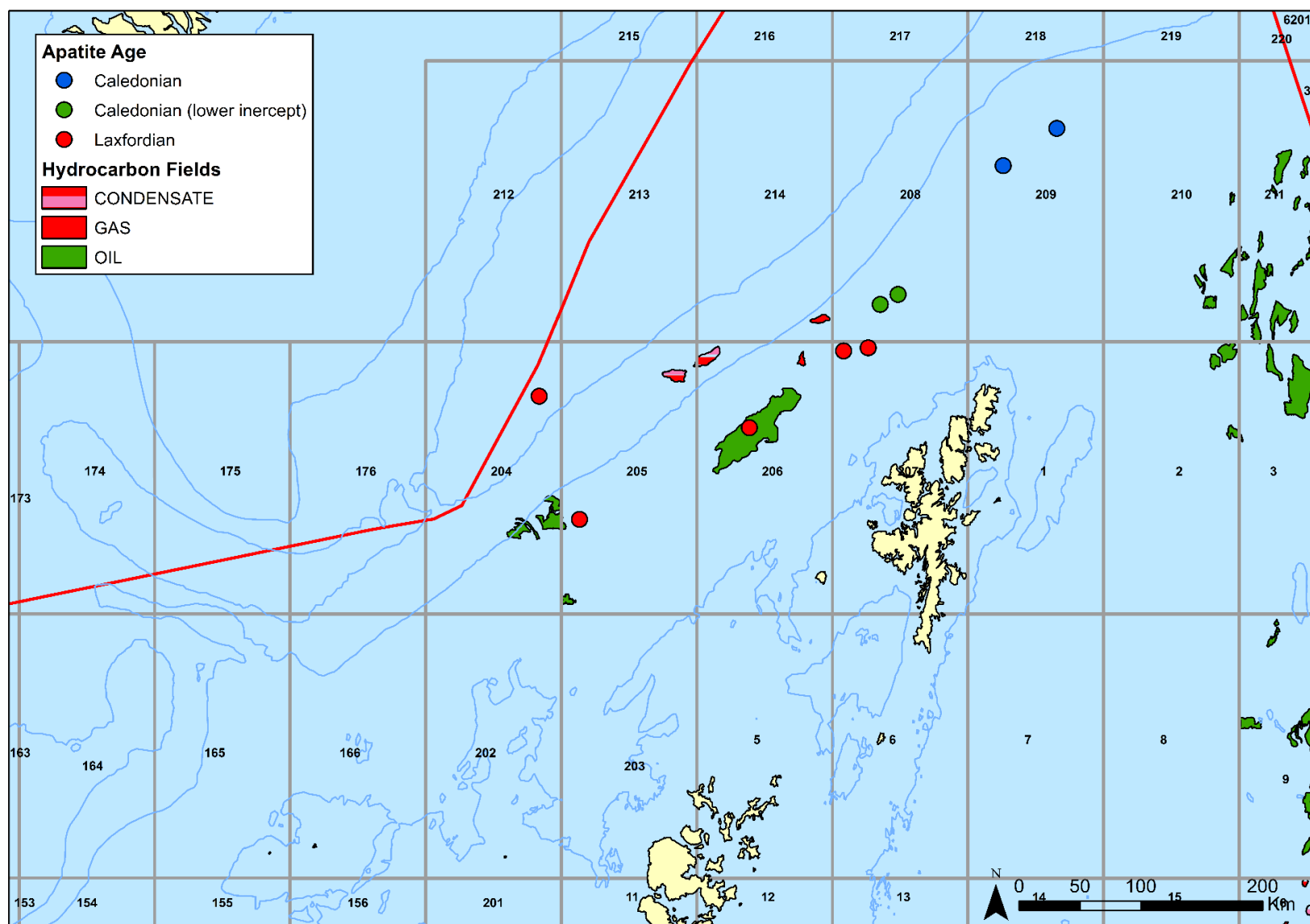


FIGURE 3.2.4 UPb Apatite geochronology

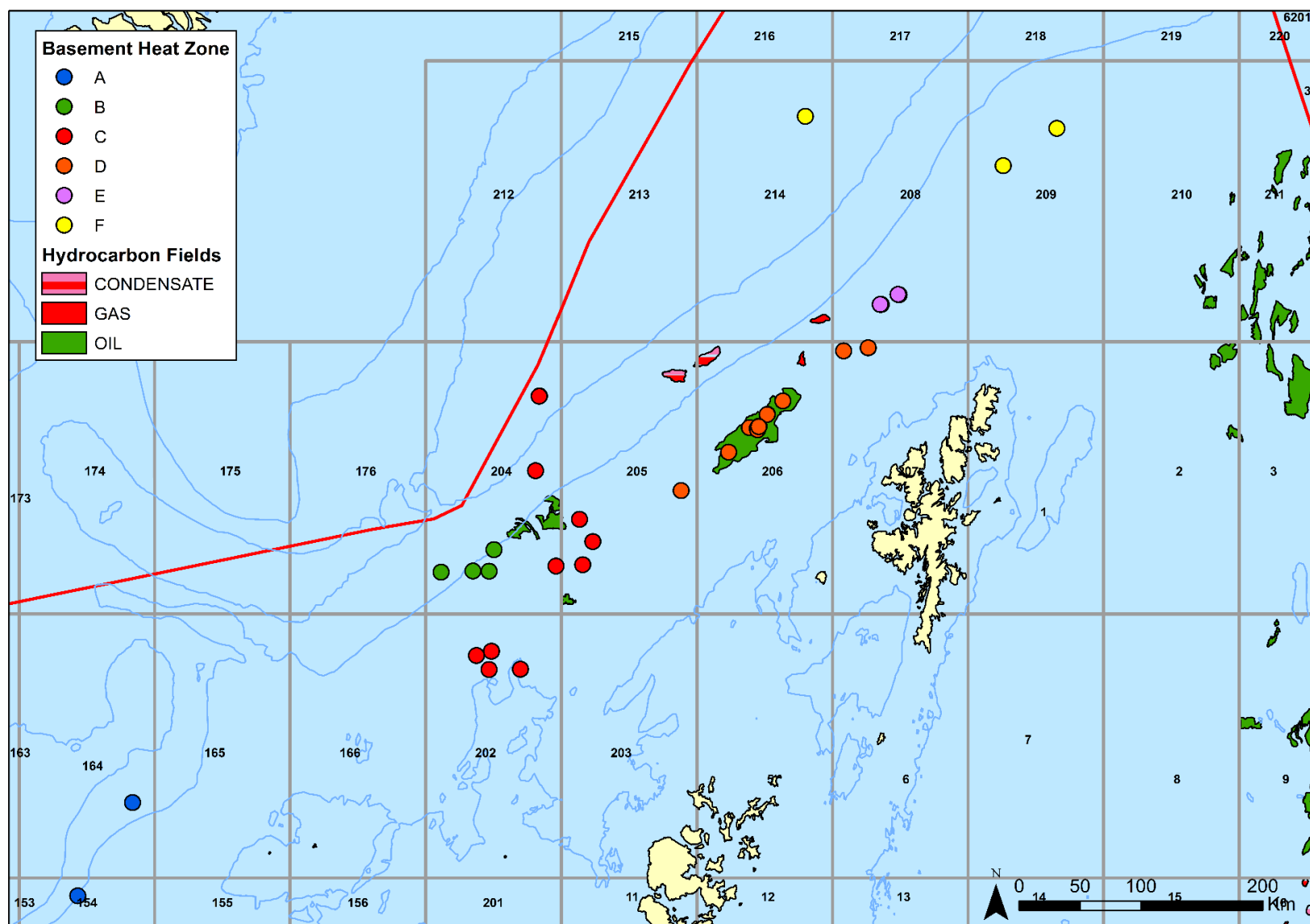
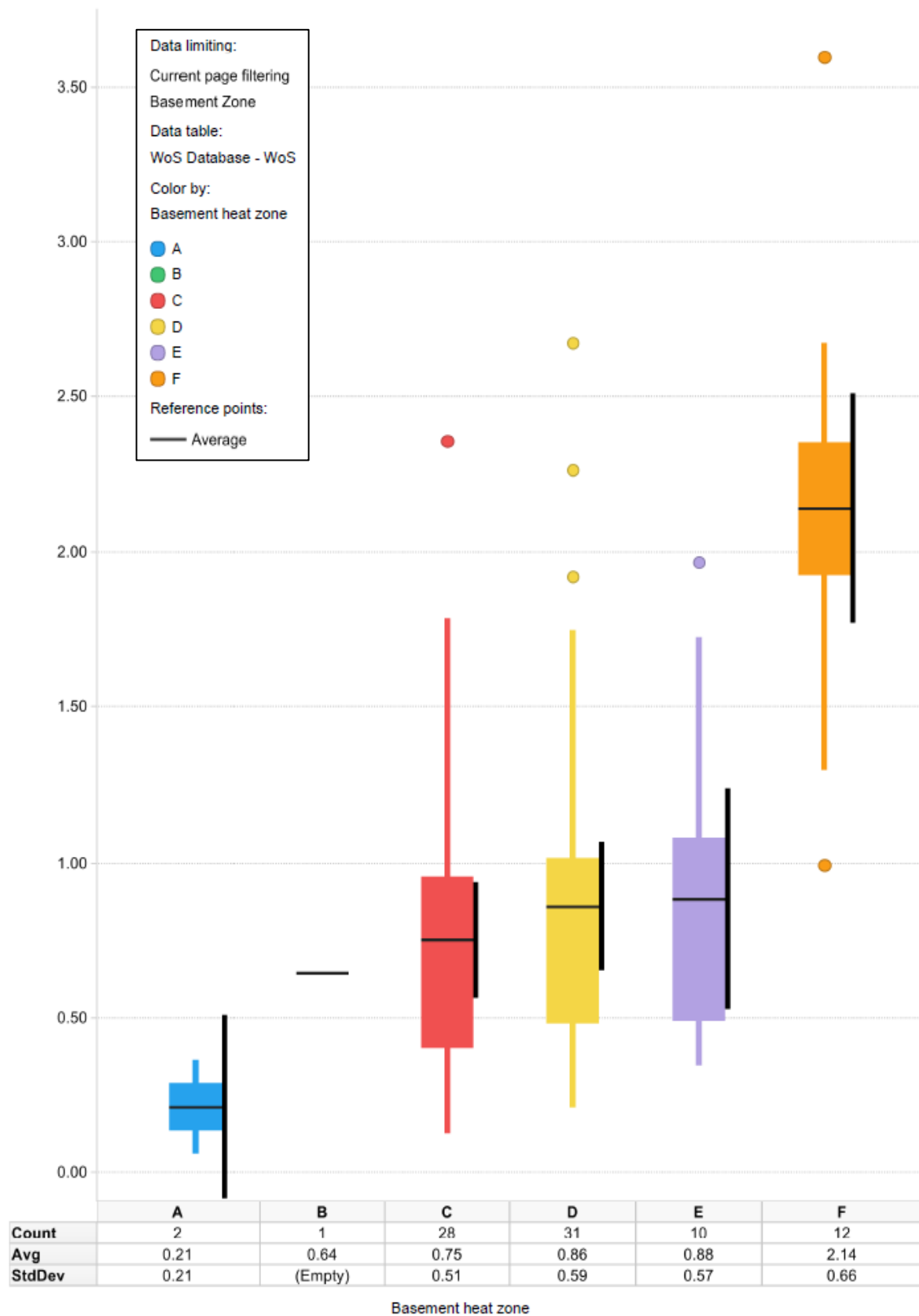


FIGURE 3.2.5 Faroe-Shetland Basin basement heat zones



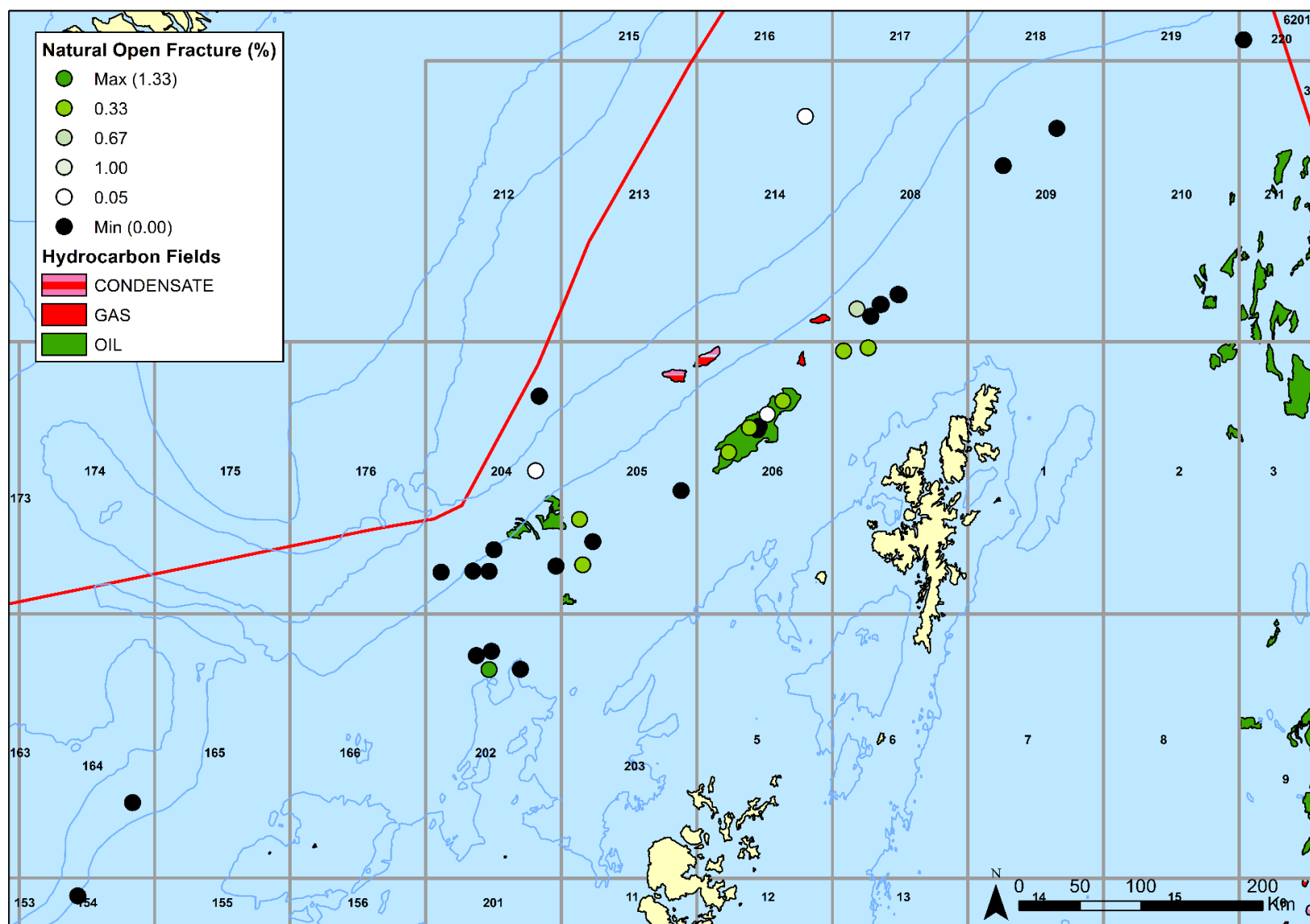


FIGURE 3.2.7 Natural open fracture (%) distribution

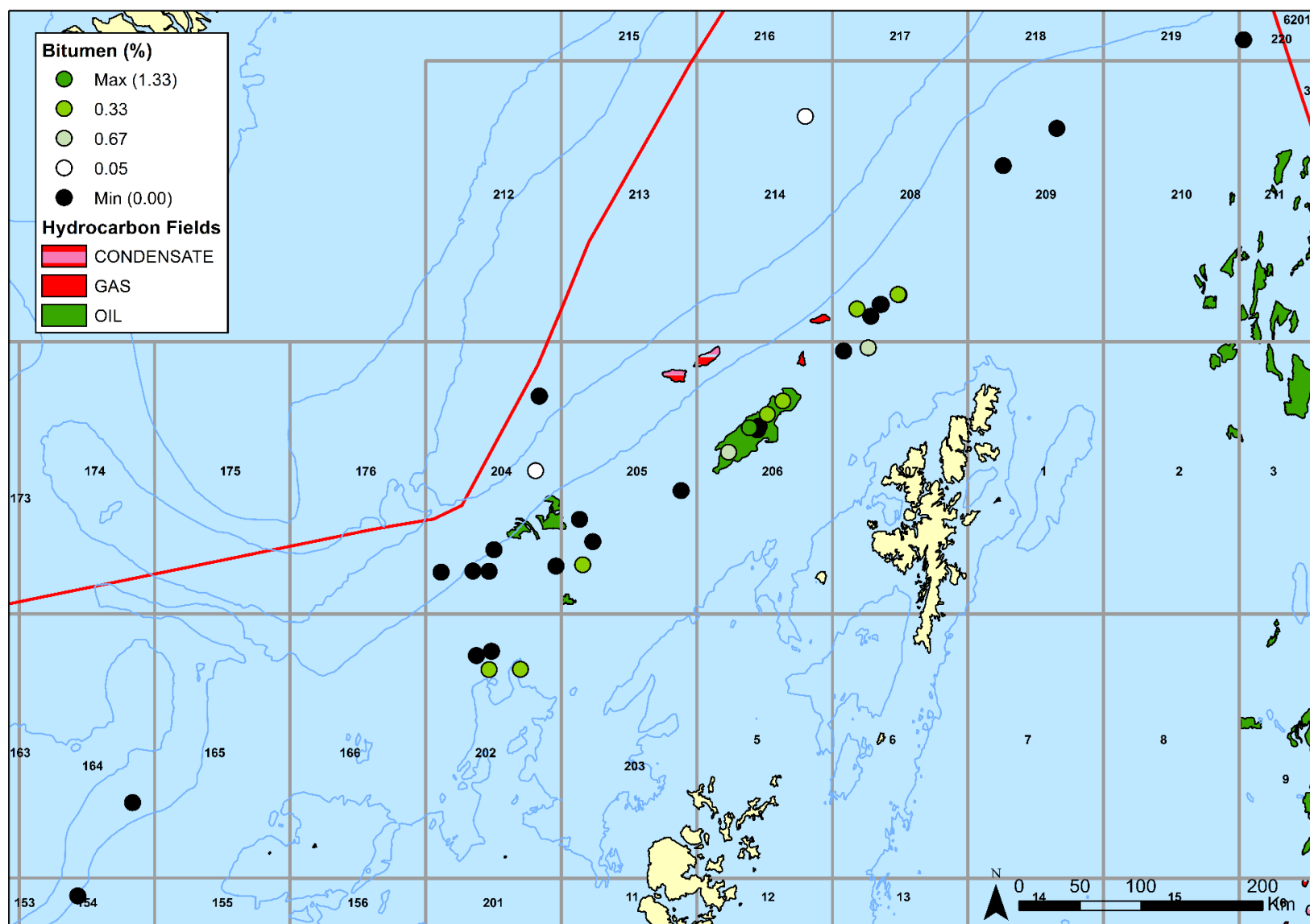


FIGURE 3.2.8 Bitumen (%) proportion distributions

3.3 BASEMENT MAPPING

This study has been designed to enable the licensee to integrate the data with any proprietary data they possess on any scale across the FSB. We present a regional basement map based on changes in the size, composition, age and metamorphic history of basement material presented in this study.

The compositional and geochronological variation in basement in the FSB is presented in Figures 3.2.1 to 3.2.8. The compositional variation in basement (Figure 3.2.1) displays a trend from gneiss dominated by tonalitic material (quads 202, 204 and the west of 205) to more felsic gneisses of granitic/granodiorite composition (quads 206 & 208). Furthermore, the data shows that basement samples in quads 214, 209 & 220 are of plutonic granitic composition. Crystal size data is only available for a subset of samples analysed as part of this study (Figure 3.2.2) and shows a coarsening in crystal size, from medium crystalline material found in quads 202 & 205 to coarsely crystalline material found in quads 206, 207, 208 & 209.

The U-Pb Zircon geochronology (Figure 3.2.3) confirms that the majority of basement in the FSB is Neoarchean aged and shows no sign of a Laxfordian event. Furthermore, the plutonic material in quad 209 has been shown to be Caledonian in age. The U-Pb Apatite ages do however shed significant new geochronological information for the basement of the FSB (Figure 3.2.4). Across quads 205, 206 & 207 the U-Pb ages show evidence for a medium temperature (300-500°C) Laxfordian event. Investigation of these apatites suggest that they have not been subjected to high grade metamorphism, therefore it is hypothesised that this age is recording burial beneath a Laxfordian orogenic belt which no longer exists.

The apatite geochronology recorded in the two basement samples from the south west of quad 208 differs from the rest of the Neoarchean basement and record a Caledonian U-Pb apatite lower intercept discordia ages. Furthermore, the granitic plutonic material samples in quad 209 records a Caledonian age. Therefore, the Caledonian front (and possible terrane boundary) lies south west of wells 208/23-1 & 208/27-2 and North East of wells 207/01-3 & 207/02-1.

It is therefore suggested that the basement in the FSB can be split into six zones (Figure 3.2.5):

- Zone A. Basement from quads 154 & 164. Dominated by tonalitic material south west of the “Laxfordian front” postulated by Holdsworth *et al.*, (2019)
- Zone B. Basement from the South Western wells in quad 204. Dominated by granodioritic and granitic material of Neoarchean ages. North East of the “Laxfordian front” postulated by Holdsworth *et al.*, (2019)
- Zone C. Basement from wells in Quad 202, east of quad 204 and south west of quad 205. Dominated by more tonalitic, medium crystalline material of Neoarchean age, recording a medium temperature Laxfordian event
- Zone D. Basement from the Rona Ridge in the East of quad 205, 206 and 207. Dominated by granitic to granodioritic, coarsely crystalline material of Neoarchean age, recording a medium temperature Laxfordian event.
- Zone E. Basement from the south west of quad 208. Dominated by granitic to granodioritic, coarsely crystalline material of Neoarchean age, recording a medium temperature Caledonian event. Split from zone D by the proposed Caledonian deformation front.
- Zone F. Basement from Quads 209 and 214. Dominated by Caledonian granitic igneous material

Importantly for basin modelling each of these basement zones have different RHP values ranging from coolest in the South West to warmest in the North East (Figure 3.2.6).

Mapped Basement Zone	Basement Heat Zone	Mean RGHP (mWm3)	$\pm(2\sigma)$
A	H1	0.21	0.08
B	H2	0.8	0.6
C			
D	H3	0.9	0.7
E			
F	H4	2.1	1.8

The integration of this work with the 1D basin modelling done is further discussed in Chapter 6.

3.4 IMPLICATIONS FOR PETROLEUM EXPLORATION

3.4.1 FRACTURED BASEMENT

Holdsworth *et al.*, (2019) demonstrated how fractures in this section can be used to predict permeability and porosity in the fractured basement of the Lancaster field. As part of the point counting undertaken for this study, both fracture and bitumen data was collected (Figure. 3.2.7 and 3.2.8 respectively) and can be related to the basement zones identified in this study.

- Zone A. No data
- Zone B. No data
- Zone C. Natural, open fractures and trace amounts of bitumen recorded
- Zone D. Natural, open fractured and bitumen recorded
- Zone E. No natural open fractures recorded, but bitumen is recorded.
- Zone F. Negligible natural open fractures and bitumen recorded.

This (small dataset) suggests that Zones C and D are best for unconventional fractured basement exploration.

CHAPTER 4

APATITE THERMOCHRONOLOGY ANALYSES AND RESULTS

Julian Moore, APT

4.1 SUMMARY

A total of nine wells across the Faroe-Shetland Basin have been subject to apatite thermochronology. The wells were selected to provide constraint across a range of structural settings, in particular in basinal areas where existing coverage of apatite thermochronology data was limited. The samples have also been selected from a wide range of geological ages from Pre-Cambrian basement to Eocene aged sands; with the majority of the samples being Tertiary in age.

The objectives of this work were twofold:

- 1) Create an additional thermal calibration dataset for modelling (in addition to present-day measured temperatures and vitrinite reflectance).
- 2) Assess the evidence for anomalous thermal events in the Tertiary.

The individual well results are summarised in the Table below and discussed in detail in this chapter. Samples from 4 wells (in bold in the summary Table) have possible evidence for paleo-temperatures being hotter in the past: 205/9-1, 208/27-2, 214/26-1 and 214/28-1. With the exception of 208/27-2 all these wells occur in the Flett sub-basin. The result for the 208/27-2 well is low confidence. For 205/9-1, 214/26-1 and 214/28-1 samples the temperature increase is in the range 18-27°C. The timing of the elevated temperature is most consistent with the onset of Late Tertiary uplift.

A small number of samples have results that have estimated a cooler peak temperature than that measured at present-day and are therefore treated with caution, as they are almost certainly in error. These wells are in red text in the summary table below.

Overall, the majority of results indicate that the sections sampled are at or close to maximum burial and hence temperature present-day. While paleo-thermal events may have occurred based on evidence from other analyses (cf. Parnell, *et al.* 1999, 2005; Wycherley *et al.* 2003; Baron *et al.* 2008) no evidence for increased temperatures during the Iceland plume event has been found in this data. The principal evidence for thermal anomalies all resides in microthermometric, petrographic and isotopic data that is restricted to Paleocene samples (in particular unzoned quartz cements) and is interpreted as reflecting lateral focusing of hot fluids (cf. Wycherley *et al.* 2003). Further discussion is provided in Chapter 6. These events seem to have had limited, if any, impact on the apatite thermochronology data and suggests that neither was there any material impact on the maturation of the Upper Jurassic source rock.

Well	Sample Number	Stratigraphy	Age	Setting	Pooled Age (Ma)	Mean Track Length (μm)	Present Day Temp (°C)	Peak Temp Time (Ma)	Peak Temp (°C)	ΔT
204/10a-5	P10012_013	Hildasay	E1	Corona	235.39	12.32	52	28±37	52.2±9.3	0.2
205/09-1	P10012_001	Sele	E1	Flett	283	10.85	75	1±38	75.9±38	0.9
	P10012_002	Lista (D1) Sand	P3		59.52	9.98	95	27±29	122±29	27.0
205/12-1	P10012_003	Lamba	P3	Flett	173	12.18	66	1±6	65.2±6	-0.8
	P10012_004	Shetland	K2		219	10.98	87	1±76	89.2±12	2.2
205/14-2	P10012_005	Unit IV Upper	P3	Flett	234	12.23	60	1±18	64.3±7	4.3
205/17b-2	P10012_006	Lista	P3	Flett Ridge	292	12.04	67	1±4	65.3±7	-1.7
206/11-1	P10012_007	Early Cret Sands	K1	Rona Ridge	5	5.51	137	±31	138.7±7	1.7
207/01-2	P10011_003	Victory	K1	West Shetland	190	11.93	70	32±40	59.8±8	-10.0
	P10011_004	PrCam Basement	PrCam		250	11.68	72	1±32	57±6	-15.0
208/17-2	P10012_008	Westerhouse	P3	N Faroe-Shetland	216	11.29	83	31±28	83±13	0.0
208/24-1A	P10011_006	Victory	K1	N Faore-Shetland	220	11.28	73	36.5±30	76±8	3.0
	P10011_007				168	10.94	77	56±19	75±10	-2.0
208/27-2	P10011_009	Shetland	K2	Clair-Victory Ridge	189	13.48	50	29±43	66±43	16.0
	P10011_011	PrCam Basement	PrCam		203	12.61	57	±32	56±8	-1.0
	P10011_013	Caved Shetland	K2		197	12.48	56	42±32	61±13	5.0
214/26-1	P10012_009	Lewis Fan Envelope	E2	Flett	232	11.28	49	1±32	67±12	18.0
214/28-1	P10012_010	Late Paleocene	P3	Flett Ridge	165	11.08	77	22±36	70±8	-7.0
	P10012_011	Middle Eocene	P2		4	7.75	110	25±21	133±4	23.0
	P10012_012	Early-Middle Eocene	P1		2	8.05	132	18±23	133±8	1.0

Summary of results for wells analysed with apatite thermochronology; samples in plane text have a modelled peak temperature \approx measured temperature present-day; samples in **bold text** modelled peak temperature $>$ measured temperature present-day; samples in *red text* modelled peak temperature $<$ measured temperature present-day (caved or unreliable?).

4.2 INTRODUCTION

A total of nine wells were selected for Apatite Fission Track (AFT) analysis. Well selection was principally determined by distribution across the West of Shetland (WOS) area, location in their respective basin (basin centre vs flank or uplifted areas) and to corroborate the vitrinite reflectivity analyses (Chapter 5). A summary of the wells analysed, and sample numbers are shown in the table below and the distribution of analysed wells shown in Figure 4.1.1.

Well	Basin	AFT Analyses.	Sample No.	Analysed during this Study (Y/N)
204/10a-5	Corona Ridge	Y	1	Y
205/09-1	Flett	Y	2	Y
205/12-1	Flett	Y	2	Y
205/14-2	Foula	Y	1	Y
205/17b-2	Rona Ridge	Y	1	Y
206/11-1	Rona Ridge	Y	1	Y
208/17-2	Northern Faroe-Shetland	Y	1	Y
214/26-1	Flett	Y	1	Y
214/28-1	Flett	Y	3	Y
207/01-2	West Shetland	Y	2	N
208/24-1A	Northern Faroe-Shetland	Y	2	N
208/27-2	Clair/Victory Ridge	Y	3	N

Apatite fission track analysis was carried out on a total of thirteen samples, apatite thermochronology data from a further three wells (six samples) have been incorporated from APT UK's proprietary database. Mineral separation using gravimetric and magnetic techniques to isolate apatite grains recovered varying quantities of apatite grains. A summary of the apatite yield and number of grain mounts prepared are shown in the table below.

Well	Depth	Apatite Sample No.	Apatite Sub-Groups (Y/N)	Apatite Yield	Grain Mounts
204/10a-5	2361.8-2383.5m	P10012 013	Y	1000s	1
205/09-1	2798-2807m	P10012 001	N	10s	1
	2704-3719m	P10012 002	N	100s	1
205/12-1	2570m	P10012 003	Y	1000s	1
	3175m	P10012 004	N	10s	1
205/14-2	7430ft	P10012 005	N	100s	1
205/17b-2	2443.8m	P10012 006	Y	1000s	1
206/11-1	4370-7376m	P10012 007	N	100s	1
207/01-2	5590-5620ft	P10011 003	Y	100s	1
	5740-5750ft	P10011 004	Y	100s	1
208/17-2	7871.0-7946.8ft	P10012 008	Y	100s	1
208/24-1A	5900-6000ft	P10011 006	Y	100s	1
	6230-6300	P10011 007	Y	100s	1
208/27-2	3960-3990ft	P10011 009	N	10s	1
	4540ft	P10011 011	Y	1000s	1
	4300-4590ft	P10011 013	N	1000s	1
214/26-1	7516-7539ft	P10012 009	N	10s	1
214/28-1	8374.3ft	P10012 010	Y	100s	1
	11900-11920ft	P10012 011	N	100s	1
	14310.0-14334.4ft	P10012 012	N	100s	1

Prepared grain mounts underwent two sessions of laser ablation-inductively coupled plasma-mass spectrometry (LA-ICP-MS) to count surface fission tracks (SFT) and measure confined fission tracks (CFT) and etch figure dimensions (Dpar and Dper). The apatite grain mounts were irradiated with ^{242}Cf derived fission fragments to increase the amount of CFT measurements.

Thermochronological modelling to determine fission track ages and temperature were calculated using the equations of Donelick *et al.* (2005). UThPb ages were calculated for each spore using the general principles described in Donelick *et al.* (2009). Chemical composition values were calculated using the methods described in Donelick and Donelick (2014). The full methods used in the apatite fission analysis process are described in Appendix 4.2.

Apatite fission track analyses are summarised in Tables 4.2.1 to 4.2.3. Apatite fission track age and length data are given in Appendix 2.2. The measured pooled AFT ages, Median U-Pb Ages and the U content (ppm) are cross-plotted in Figure 4.2.1a as a QA-QC. The apatite fission track lengths for each sample are summarised in Figure 4.2.1b. The present-day temperature, apatite age and mean track lengths for each of the study wells are presented in Figures 4.2.2 to 4.2.13. Thermal history data inverted from each of the samples are presented in Figures 4.3.1 to 4.3.25.

In the following section the method used is described, and then for each of the study wells the results are described and the implications of the time-temperature history discussed.

Well	Top depth	Bottom depth	Units (m/ft)	Stratigraphy	Age	Sample type	Washed (y/n)	Basin	Mud system	Anal. reason	Anal. status	Sample ID.	Apatite fission track analyses
204/10a-5	2361.8	2383.5	m	Hildasay	E1	COCH	-	Corona	WBM	AFT	NEW	P10012_013	y
205/09-1	2798.0	2807.0	m	Sele	E1	DC	y	Flett	WBM	AFT	NEW	P10012_001	y
	3704.0	3719.0	m	Lista (D1 Sand)	P3	DC	y			AFT	NEW	P10012_002	y
205/12-1	-	2570.0	m	Lamba	P3	DC	y	Flett	WBM	AFT	NEW	P10012_003	y
	-	3175.0	m	Shetland	K2	DC	y			AFT	NEW	P10012_004	y
205/14-2	-	7430.0	ft	Unit IV Upper	P3	DC	y	Flett	WBM	AFT	NEW	P10012_005	y
205/17b-2	-	2443.8	m	Lista	P3	COCH	-	Flett Ridge	WBM	AFT	NEW	P10012_006	y
206/11-1	4370.0	4376.0	m	Early Cretaceous Sands	K1	DC	y	Rona Ridge	WBM	AFT	NEW	P10012_007	y
207/01-2	5590.0	5620.0	ft	Victory	K1	DC	y	West Shetland	WBM	AFT	APT Prop	P10011_003	y
	5740.0	5750.0	ft	Precambrian	PrCam	DC	y			AFT	APT Prop	P10011_004	y
208/17-2	7871.0	7946.8	ft	Waterhouse	P3	COCH	-	N Faroe-Shetland	OBM	AFT	AFT	P10012_008	y
208/24-1A	5900.0	6000.0	ft	Victory	K1	DC	n	Northern Faroe-Shetland	OBM	AFT	APT Prop	P10011_006	y
	6530.0	6300.0	ft			DC	n			AFT	APT Prop	P10011_007	y
208/27-2	4960.0	3990.0	ft	Shetland	K2	DC	y	Clair-Vicotry Ridge	WBM	AFT	APT Prop	P10011_009	y
	-	4540.0	ft	Precambrian	PrCam	DC	y			AFT	APT Prop	P10011_011	y
	4300.0	4590.0	ft	Caved Shetland	K2	DC	y			AFT	APT Prop	P10011_013	y
214/26-1	7516.0	7539.0	ft	Lewis Fan Envelope (Lobe 2)	E2	DC		Flett	WBM	AFT	NEW	P10012_009	y
214/28-1	-	8374.3	ft	Late Paleocene	P3	COCH	-	Flett Ridge	OBM	AFT	NEW	P10012_010	y
	11900.0	11920.0	ft	Middle Paleocene	P2	DC	n			AFT	NEW	P10012_011	y
	14310.0	14334.4	ft	Early-Middle Paleocene	P1	COCH	-			AFT	NEW	P10012_012	y

Abbreviations/Key

DC: Ditch cuttings
COCH: Core chip
WBM: Water base mud
OBM: Oil base mud
AFT: Apatite fission track
NEW: New analyses for this study
APT Prop: Data from APT proprietary AFT database

Stratigraphy/Ages/Basins

E2: Middle Eocene
E1: Early Eocene
P3: Late Paleocene
P2: Middle Paleocene
P1: Early Paleocene
K2: Late Cretaceous Shale III
K1: Early Cretaceous Turbidite

TOTAL:**20****PrCam:** Precambrian**N Faroe-Shetland:** Northern Faroe Shetland**TABLE 4.1.1 Analytical programme - Apatite fission track analyses**

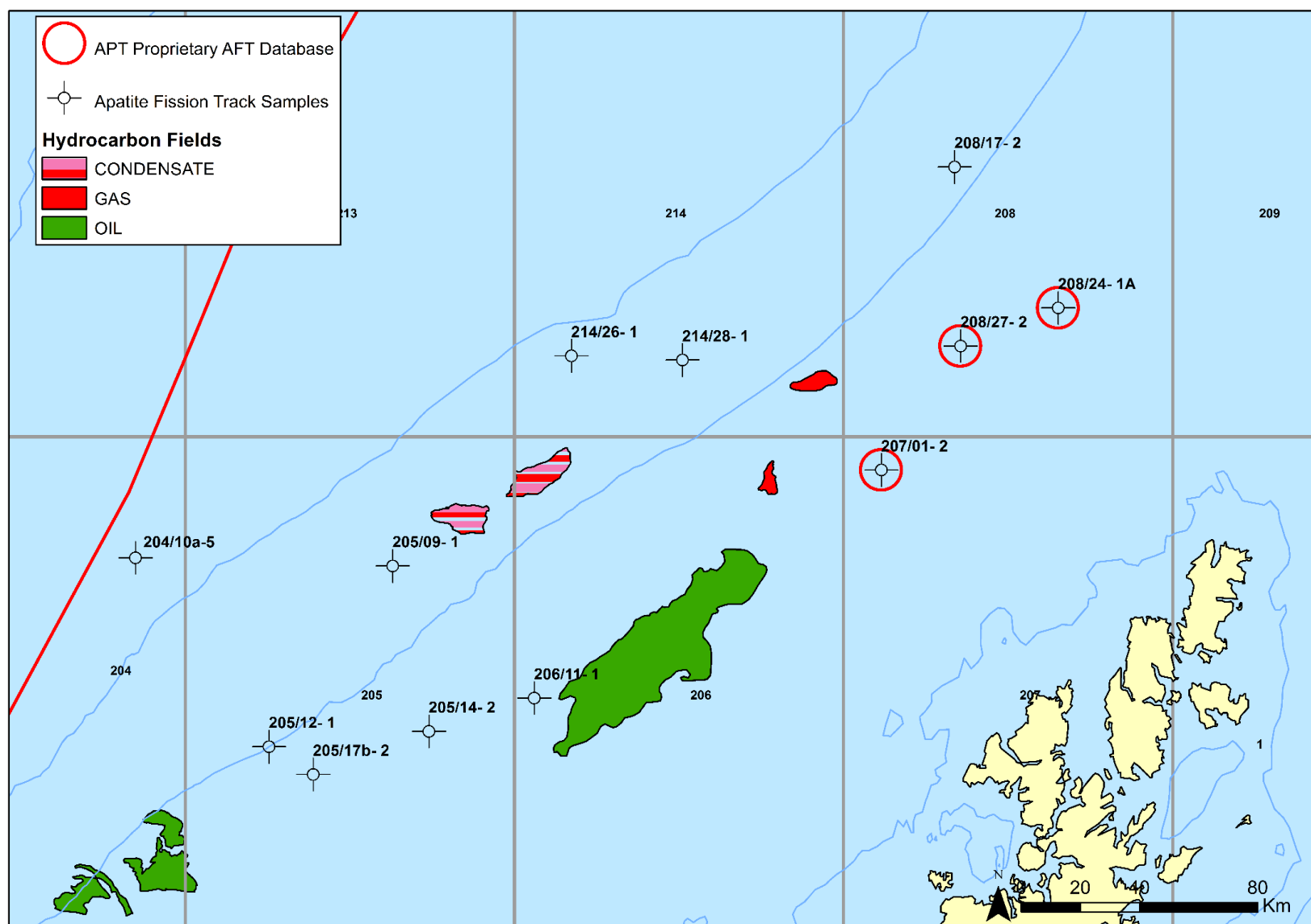


FIGURE 4.1.1 Location map of wells selected for apatite fission track analyses

4.3 METHODS & RESULTS OF APATITE FISSION TRACK ANALYSES

The following section first reviews the technical basis of the technique, secondly summarises the data overall and finally describes each of the individual wells analysed in some detail.

Introduction to the technique

The reader is referred to Chew & Donelick (2012) and references therein for a detailed review of the methods briefly reviewed here. Fission track dating is based on the spontaneous decay of ^{238}U which creates linear defects (“fission tracks”) in the lattice of U-bearing minerals (typically apatite, zircon and titanite as they contain sufficient U of $>10\text{ppm}$). The tracks are chemically etched to make them visible using an optical microscope. Since ^{238}U decays at a known rate, the density of the fission tracks with a known (measured) ^{238}U content allows an apparent age to be calculated; this age provides an estimate of the time that has elapsed since the mineral cooled through a temperature window (the partial annealing zone or PAZ) specific to the mineral and the mineral composition. For apatite the PAZ occurs approximately between 60–110°C. At higher temperatures there is enough energy to completely anneal the fission tracks via thermal diffusion, at temperatures lower than the PAZ there is not enough energy to repair the tracks, within the range of the PAZ the tracks are repaired at a rate dependent on composition (discussed below).

To estimate the apparent fission track age of an apatite sample one needs to:

- i. Estimate the amount of ^{238}U decay recorded by the mineral lattice – given by the spontaneous fission track density.
- ii. Estimate the amount of ^{238}U (the parent isotope) in the sample.

The spontaneous fission track density is estimated by measuring etched fission tracks using a microscope.

While the fission track age which yields information on the timing of cooling through the PAZ, the apatite fission track method also yields information on the nature of the cooling path. This information is obtained from the distribution of confined fission track lengths in a sample (Gleadow *et al.* 1986a). Confined fission tracks are horizontal (or $<10^\circ$ from horizontal) tracks that lie in a c-axis prismatic section, such that both ends of the track are visible entirely within the polished and etched apatite crystal without altering the focal depth. Unannealed, spontaneous fission track lengths in natural apatite grains typically range between ~ 14.5 and $15.5\ \mu\text{m}$ depending on its chemical composition (Gleadow *et al.* 1986a). For example, an apatite grain which exhibits a fission track population with mean track lengths in this range and a narrow variation in track length distribution (e.g., $<1.5\ \mu\text{m}$), would be interpreted to have cooled relatively rapidly from a temperature $\geq 110^\circ\text{C}$ to a temperature $\leq 60^\circ\text{C}$ at the time indicated by the apparent apatite fission track age. A shorter mean track length with a broad standard distribution indicates that the sample resided in the PAZ for a significant period of time since the formation of the oldest fission tracks (Gleadow *et al.* 1986b). The apatite fission track age and track length distribution can be combined to construct time–temperature paths by inverse and/or forward modelling of the fission track age and length data (e.g. Ketcham 2005).

To go from a track length distribution to a thermal history we need to know the controls on the rate of annealing. Rates of thermal annealing of fission tracks in apatite depend strongly upon

the chemical composition of the host crystal. If neglected, this sensitivity of annealing rates to apatite chemistry may severely limit the precision of thermal histories derived from partially annealed fission-track populations in apatite crystals with a range of composition, because models for thermal annealing calibrated by experiments on a single apatite will not accurately predict the annealing behaviour of fission tracks in a compositionally diverse population (Carlson *et al.* 1999). Equally, if the variation in annealing behaviour for apatites of different composition could be quantified, the range of temperature over which apatite fission tracks serve as recorders of thermal history could be extended and the precision of thermal histories could be improved; more resistant apatites could be used to probe the higher-temperature portions of a rock's history, whereas less-resistant apatites could be used to monitor the lower-temperature portions (Carlson *et al.* 1999).

Measurements of initial fission-track length, a parameter of considerable importance to the derivation of time-temperature paths from fission-track data, reveal substantial variations from one apatite to another; initial lengths are best predicted from the etch figures.

Carlson *et al.* (1999) presented functions that relate initial mean track length ($l_{0,m}$) and initial modeled c-axis projected track length ($l_{0,c,mod}$; cf. Ketcham *et al.* 1999) to etch-pit diameter (Dpar) and chlorine content. Dpar is the arithmetic mean fission track etch figure diameter parallel to the crystallographic c-axis (in μm). It is an estimator of annealing rate of an individual apatite grain (Barbarand *et al.*, 2003). The correlations of $l_{0,m}$ and $l_{0,c,mod}$ with Dpar can be understood in terms of apatite bulk-etching characteristics and are the primary source of the variations in the initial mean track lengths (Carlson *et al.* 1999).

Various attempts have been made to correlate apatite annealing rates from composition, apatite structure or etching rates. Clearly factors influencing annealing rates are complex; Carlson *et al.* (1999) demonstrated that their experimental data cannot be accounted for by a single control, such as Cl content as advocated by Green *et al.* (1986). Similarly, using Dpar to infer relative resistance to annealing accounts for some but not all of the variability observed (Carlson *et al.* 1999).

To account for this variability in annealing behaviour Carlson *et al.* (1999) proposed a parameter, r_{mr0} , which characterises the annealing behaviour of any chosen apatite in comparison with the most resistant apatite in the dataset. Correlation of the r_{mr0} parameter to other parameters proved to be complex; Carlson *et al.* (1999) produced an empirical best fit of the annealing data to a functional combination of the compositional variables; in this study this correlation is used to convert compositional data from the LA-ICP-MS analysis to an estimate of the r_{mr0} parameter.

Time-temperature path modelling

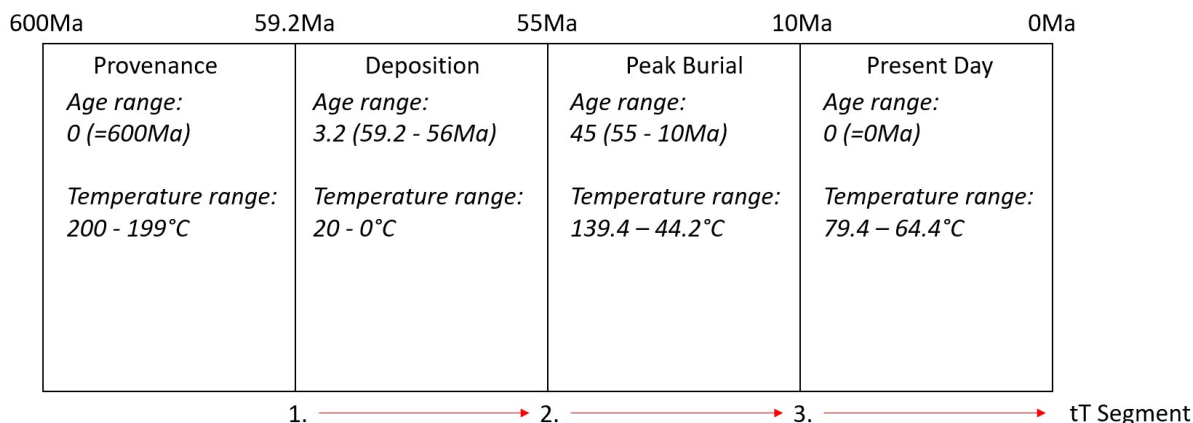
To aid in the clear communication of the results obtained, the approach to determining the time-temperature (tT) histories is described briefly.

All modelling has been performed in FT³, Apatite.com Partners' software package for calculating thermal histories based on conventional AFT and HR-AFT data. The philosophy of this software is similar to that of AFTSolve (Ketcham *et al.*, 2000) but allows provenance history to vary among modelled apatite grain populations. FT³ uses the experimental data of Donelick (unpublished), Donelick (1988), Donelick *et al.* (1990), Donelick (1991), Vrolijk *et al.* (1992), Carlson *et al.* (1999), and the calibration of Rmr0 provided by Ketcham *et al.* (1999).

All confined fission track (CFT) data are projected onto the c-axis using the model of Donelick (1991) after Donelick *et al.* (1999). The initial model realisations are given some constrain based upon their age and present-day temperature. The assumptions and constraints for each individual sample / well are given in the individual well summaries (see below).

The tT history is split into four “boxes” relating to the provenance, deposition (age), peak burial and present-day. Each box is joined by a tT segment node. Each box has a specified age and temperature range, a random number generator picks an age and temperature within this range for each of the apatite sub-groups being modelled. For most of the study samples 3 tT segments were considered. The three tT path segments are then combined into an overall tT path. Fission track parameters are then calculated for each complete tT path and compared to measured values for each sub-group-population yielding the GOF values. In all models, at least some of the old tracks are annealed to zero (ensured by starting tT box 1 in the range 200.0 to 199.0 degC). The age of the oldest fission track for each sub-group-population is noted, and all tT points prior to the age of the oldest fission track are discarded.

Example tT generation for sample P10012_001 (205/9-1 – 2798-2807m):



FT³ yields tT paths with corresponding AFT age goodness-of-fit (GOF) and confined fission track (CFT) length GOF values for each population. Models are deemed acceptable when all GOF values are ≥ 0.05 . The best fit model is the model yielding the greatest product of all GOF values. A number of statistical tests could be used to estimate the GOR values (e.g. the Kolmogorov–Smirnov test); in this project Kuipers statistic is preferred since it is better fitting tails.

In summary the results of each of the tT inversions are reported in two ways:

- The average tT of the acceptable paths (which are given in the individual well summaries (see below).
- The ‘best-fit’ tT model is the tT path that has the greatest overall product of the GOF values (Table 4.2.3).

High resolution apatite fission track thermochronology: Sub-groups & populations

The apatite data collected are sorted into both sub-groups and populations. The sub-groups here are sub-sets of apatite grains based on specific criteria, in this project the criteria are based on the REE composition and the U-Pb age. For High Resolution-AFT (HR-AFT), the apatite grains are sorted into groups using the following steps:

- 1) for each of approximately 9 different apatite standard species analysed during a LA-ICP-MS session, measure REE concentrations and $^{206}\text{Pb}^*/^{238}\text{U}$ ages and calculate the mean and standard deviation for each measured value for each standard,
- 2) derive a session-specific, best-fit line for each measured value that gives standard deviation as a function of mean among all standards,
- 3) for each unknown apatite grain (from an unknown group), use the derived best-fit lines to define an apatite grain group centred at the measured values for the unknown grain and bounded by 2 standard deviations about the measured values, and
- 4) search for and isolate other unknown apatite grains that exhibit measured values that fall within the bounds of the defined apatite grain group.

The sub-groups are selected so as to maximise the amount of AFT data per sub-group by minimizing the number of sub-groups to be used in the time-temperature (tT) modelling. The broad age groups are:

- 0 $\sim < 325$ Ma,
- 1 $\sim 325\text{-}800$ Ma,
- 2 $\sim 800\text{-}1750$ Ma,
- 3 $\sim > 1750$ Ma.

Eight sub-groups were recognised: 0, 1A, 1B, 2A,2B,2C,3A,3B. The term ‘population’ to describe a set of apatite grains characterized by a) a single tT history (same provenance) and b) a single AFT annealing kinetics (median r_{mr0}). Because of a), a ‘population’ is almost always limited to a single sample. This term as defined is used by the broader fission track community.

While not the focus of this study, provenance groups were also identified. The selection of these provenance groups differed from the selection of the sub-groups for tT modelling. The groups were selected manually, to find all unique sub-groups in terms of Eu anomaly, overall REE pattern, and UPb age. They were selected without regard to the amount of AFT data per sub-group. This method led to the best sub-group resolution (in the sense of provenance) and these data are intended to find provenance connections between samples. This identified 14 provenance sub-groups:

- A $\sim < 325$ Ma
- B $\sim 325\text{-}800$ Ma
- B1 $\sim 325\text{-}800$ Ma, strong negative Eu anomaly
- B2 $\sim 325\text{-}800$ Ma, weak negative Eu anomaly
- C $\sim 800\text{-}1750$ Ma
- C1 $\sim 800\text{-}1300$ Ma
- C11 $\sim 800\text{-}1300$ Ma, strong negative Eu anomaly
- C12 $\sim 800\text{-}1300$ Ma, weak negative Eu anomaly
- C2 $\sim 1300\text{-}1750$ Ma
- C21 $\sim 1300\text{-}1750$ Ma, strong negative Eu anomaly
- C22 $\sim 1300\text{-}1750$ Ma, weak negative Eu anomaly
- D $\sim > 1750$ Ma
- D11 $\sim > 1750$ Ma, strong negative Eu anomaly
- D12 $\sim > 1750$ Ma, weak negative Eu anomaly

These groups and their distribution with regards well and stratigraphic age are outlined in Appendix 4.2

Points to Remember:

- U-Pb Ages: provide constraint on the high temperature thermal history and information on discrete detrital apatite groups.
- Apatite uranium fission track ages (UFT): represent an estimate of the time elapsed since cooling below the PAZ (~110-120°C – dependent on composition).
- Apatite (confined) fission track lengths (measured in a c-axis prismatic section) yields information on the nature of the cooling path. This information is obtained from the distribution of confined fission track lengths in a sample (Gleadow *et al.* 1986a).
- Samples with mean track lengths of 14.5 – 16µm with a narrow variation in track length distribution (e.g., <1.5µm), would be interpreted to have cooled relatively rapidly from a temperature $\geq 110^{\circ}\text{C}$ to a temperature $\leq 60^{\circ}\text{C}$ at the time indicated by the apparent apatite fission track age.
- Samples with shorter track lengths (<14.5µm) indicates that the sample resided in the PAZ for a significant period of time since the formation of the oldest fission tracks.
- The apatite fission track age and track length distribution can be combined to construct time–temperature paths by inverse and/or forward modelling of the fission track age and length data.

Results summary

The UFT ages range from ~0 to ~378Ma. The mean track length (MTL) ranges from 5.51 to ~14µm (1 SE) with standard deviations of between 0.65 and 5.06µm. The etch parameter, Dpar, ranges from 1.46 to 2.56µm, which illustrates some significant spread relative to the Durango apatite standard (mean Dpar measured for the same etching protocol is 1.61µm).

For the AFT Age grains the U content (ppm) ranges between 2 to 46.6ppm. The highest U content is from the 208/24-2 Lower Cretaceous sample from ~1910 mD (P10011_007). The lowest U content is from the AFT Age grain 204/10a-5 Paleocene sample from 2372m mD (P10012_013).

The U-Pb Ages for the samples range between 151 to 2709Ma. The youngest U-Pb is also from the 214/28-1 Paleocene sample from ~3630m mD (P10012_011). The oldest U-Pb Age for the samples was measured in the 207/1-2 Lower Cretaceous sample from ~1708m mD (P10011_003). As noted previously, there is no clear correlation between the pooled AFT ages, the Median U-Pb Ages or the U content (ppm) as shown in [Figure 4.2.1](#) suggesting the data is robust. For all samples studied, HR-AFT with r_{mr0} were used, the weighted mean temperature ranges listed in [Table 4.2.3](#) are narrower (e.g., higher resolution) than the temperature ranges calculated using conventional AFT with r_{mr0} .

4.3.1 Quad 204 wells

4.3.1.1 Data and discussion for well 204/10a-5

A single core sample was collected from the Paleocene interval penetrated in the 204/10a-5 well. Sample details are given in the table below.

Well	Top Depth	Bottom Depth	Units (m/ft)	Stratigraphy	Age	Sample Type	Sample ID.	Apatite Grains
204/10a-5	2361.8	2383.5	m	Hildasay	E1	COCH	P10012 013	1000s

The bulk sample for the Hildasay Sand core sample yielded a median common lead corrected U-Pb Age of 1537.7Ma. The pooled AFT Age is ~235.39Ma. Four sub-populations were identified to which distinct model ages were assigned (see below). The bulk sample has a mean track length of $12.32\mu\text{m} \pm 1.4$ with a median Dpar of $1.84\mu\text{m}$ and a median $R_{\text{mr}0}$ of 0.8513. Four apatite sub-populations are recognised based on U-Pb ages and REE chemistry:

- Sub-Group 1
 - Median U-Pb Age: 482.6 Ma
 - Best fit model - Oldest AFT Age: 244.0 Ma
 - Measured Pooled AFT Age: 163.96 Ma
 - Mean track length: $13.19 \pm 1.14 \mu\text{m}$
 - Median Dpar: $1.84 \mu\text{m}$
 - Median $R_{\text{mr}0}$: 0.8491
- Sub-Group 2A
 - Median U-Pb Age: 977.7 Ma
 - Best fit model - Oldest AFT Age: 390.0 Ma
 - Measured Pooled AFT Age: 245.45 Ma
 - Mean track length: -
 - Median Dpar: $1.86 \mu\text{m}$
 - Median $R_{\text{mr}0}$: 0.8574
- Sub-Group 2B
 - Median U-Pb Age: 1480.9 Ma
 - Best fit model - Oldest AFT Age 395.0 Ma
 - Measured Pooled AFT Age: 272.31 Ma
 - Mean track length: $11.74 \pm 1.56 \mu\text{m}$
 - Median Dpar: $1.92 \mu\text{m}$
 - Median $R_{\text{mr}0}$: 0.8314
- Sub-Group 2C
 - Median U-Pb Age: 1607.3 Ma
 - Best fit model - Oldest AFT Age 332.0 Ma
 - Measured Pooled AFT Age: 232.13 Ma
 - Mean track length: $12.29 \pm 1.27 \mu\text{m}$
 - Median Dpar: $1.83 \mu\text{m}$
 - Median $R_{\text{mr}0}$: 0.852

These results are consistent with a wholly provenance related apatite thermochronology signature. The sub-group 1 samples have a U-Pb age consistent with cooling in the earliest

Ordovician. For the sub-group 2 samples, the U-Pb ages are all consistent with the provenance of these sediments being cooled below ~450–550°C in the Pre-Cambrian (cf. Chamberlain & Bowring 2000 and Schoene & Bowring 2007, for U-Pb closure temperatures). The AFT ages for both samples indicate cooling below the apatite closure temperature (120°C) in the Permian to Mid-Jurassic. The apatites then remained below 60°C until erosion and transport into the basin in the Lower Tertiary. There was some discrepancy between the reported test temperature and the BHT data; the latter indicated a GTG of ~45 deg C-km⁻¹ which was viewed as anomalously hot. The PVT test temperature (~52°C) estimates a GTG of ~40°C/km⁻¹ which is still relatively hot. The temperature data put the data just below the lower boundary of the partial annealing zone (PAZ) for apatite (60 - 110°C).

The time-temperature constraints used for the FT³ modelling are given below:

Well	Sample ID.	Initial		Deposition		Peak Burial		Present Day	
		Age (Ma)	Temp (°C)	Age (Ma)	Temp (°C)	Age (Ma)	Temp (°C)	Age (Ma)	Temp (°C)
204/10a-5 2361.8-2383.5m	P10012_013	600.0	199.0- 200.0	56.0- 59.2	0.0- 20.0	10.0- 55.0	21.6- 110.6	0.0	41.6- 50.6

A plot showing the integration of sample age, temperature and mean apatite fission track length is shown in Figure 4.2.1. The time-temperature histories for the 204/10a-5 samples are shown in Figures 4.3.1. The thermal history implications from the time-temperature (tT) modelling of the 204/10a-5 apatite data are summarised in the table below:

Well	Sample ID.	Peak Burial Time t (Ma)	Peak Burial Temp T (°C)	Temp at 1 Ma (°C)	Temp at 5 Ma (°C)	Temp at 10 Ma (°C)	Temp at 25 Ma (°C)	Temp at 50 Ma (°C)
204/10a-5 2361.8-2383.5m	P10012_013	28.0	52.2	46.8	47.4	47.7	48.5	26.6

A vitrinite reflectivity equivalent of 0.33-0.38% Ro is given for the Hildasay sample

The results indicate that the timing of the peak temperature is poorly constrained (with a 2sigma of 37Ma). The absolute peak temperature (52°C ±9.3) is close to the reported present-day temperature recorded from the PVT report where formation temperature (at 2401.2 m MDBRT) was reported as 52.1 - 53.7°C (cf. Core Lab report RFLA 201801920, Rev 2).

There is no vitrinite data available for calibration of the 204/10a-5 well.

The modelled temperature history for the Hildasay samples suggests rapid heating (burial) between 50-40Ma after, the flat nature of the tT path post ~40Ma is indicative of samples at or close to maximum burial (R. Donelick, *Pers. Comm*). Inspection of Figure 4.3.1 shows that the Genesis time-temperature history and the apatite tT paths are in reasonable agreement. Integration of the 204/10a-5 apatite thermochronology data together with the calibration data (measured temperature) and 1D basin modelling is considered further in Chapter 6.

4.3.2 Quad 205 wells

4.3.2.1 Data and discussion for well 205/09-1

Two ditch cuttings samples were collected from Eocene and Paleocene intervals penetrated in the 205/09-1 well. Sample details are given in the table below.

Well	Top Depth	Bottom Depth	Units (m/ft)	Stratigraphy	Age	Sample Type	Sample ID.	Apatite Grains
205/09-1	2798.0	2807.0	m	Sele	E1	DC	P10012 001	10s
	3704.0	3719.0		Lista (D1) Sand	P3	DC	P10012 002	100s

The Sele Formation sample is a composite of ditch cuttings over the 2798-2807m interval; no sub-groups were recognised, and the provenance make up of this sample is poorly constrained. Three populations were recognised (cf. definition on p. 4-6 – 4.7); a ‘population’ is used to describe a set of apatite grains characterized by: a) a single tT history (same provenance) and b) a single UFT annealing kinetics (median R_{mr0} in this project). The sample yields a median U-Pb Age of 1406.2Ma, which potentially indicates a sourcing origination from the Laxfordian terrane. The pooled UFT Age is ~283Ma; the oldest model UFT ages range between 455-544Ma, the measured UFT Ages 228-321Ma. The bulk sample has a Mean track length is $10.85 \pm 1.1 \mu\text{m}$ with a median Dpar of $1.63 \mu\text{m}$ and a median R_{mr0} of 0.7806.

The apatite fission track ages for the Sele Formation suggest a provenance signature. The U-Pb ages are consistent with the provenance of these sediments being cooled below ~450–550°C in the Grenvillian-Laxfordian stage (sub-group 2 ~ 800-1700Ma) (cf. Chamberlain & Bowring 2000 and Schoene & Bowring 2007, for U-Pb closure temperatures).

The Lista (D1) Sand Formation sample yields apatite grains comprising of four sub-groups to which distinct model ages were assigned (see below). The bulk sample had a median common lead corrected U-Pb Age of ~1070.8Ma. The pooled UFT Age is ~59.52Ma. The bulk sample Mean track length is $9.98 \pm 1.96 \mu\text{m}$ with a median Dpar of $1.74 \mu\text{m}$ and a median R_{mr0} of 0.8094. Again, the track length data would suggest a significant period within the PAZ. This sample has a relatively short mean length and a higher standard deviation. This indicates that the sample resided in the PAZ (60-120°C) for a significant period of time since the formation of the oldest fission tracks (Gleadow et al. 1986b). Four apatite sub-populations are recognised based on U-Pb ages and REE chemistry in this sample:

- Sub-Group 0
 - Median U-Pb Age: 178.2 Ma
 - Best fit model - Oldest UFT Age: Pop1: 21.0 Ma. Pop2: 150.0 Ma
 - Measured Pooled UFT Age: 21.08 Ma
 - Mean track length: $14.00 \pm 0.00 \mu\text{m}$
 - Median Dpar: $1.9 \mu\text{m}$
 - Median R_{mr0} : 0.8231
- Sub-Group 1
 - Median U-Pb Age: 667.3 Ma
 - Best fit model - Oldest UFT Age: Pop1 19.0 Ma
 - Measured Pooled UFT Age: 54.28 Ma
 - Mean track length: $9.78 \pm 1.08 \mu\text{m}$
 - Median Dpar: $1.75 \mu\text{m}$

- Median R_{mr0} : 0.8055
- Sub-Group 2
 - Median U-Pb Age: 1006.6 Ma
 - Best fit model - Oldest UFT Age: Pop1 22.0Ma. Pop2: 140.0Ma. Pop3: 150.0Ma
 - Measured Pooled UFT Age: 117.69 Ma
 - Mean track length: $9.51 \pm 0.49 \mu\text{m}$
 - Median Dpar of $1.75 \mu\text{m}$
 - Median R_{mr0} : 0.7951
- Sub-Group 3
 - Median U-Pb Age: 2267.0 Ma
 - Best fit model - Oldest UFT Age: Pop3: 19.0 Ma
 - Measured Pooled UFT Age: 0.0 Ma
 - Mean track length: $10.26 \pm 0.93 \mu\text{m}$
 - Median Dpar of $1.8 \mu\text{m}$
 - Median R_{mr0} : 0.8340

The U-Pb ages for the Lista sample both incorporate a wide range of ages of cooling below $\sim 450\text{--}550^\circ\text{C}$ (cf. Chamberlain & Bowring 2000 and Schoene & Bowring 2007, for U-Pb closure temperatures) which may indicate sediment sourced from the following terrane groups:

Sub-group 0: 178Ma These Mesozoic ages are some of the youngest recorded. This period is known as a phase of extensional activity, however, local foot-wall related uplift and denudation is thought to involve insufficient cooling i.e. this process will not involve rocks buried to the U-Pb closure temperature, exhume them and re-sediment them since the magnitudes of cooling required are deemed too great, so this must presumably relate to the continued denudation of the source terrane external to the basin.

- Sub-group 1: 667Ma ~Caledonian (too old?)
- Sub-group 2: 1006-1446Ma ~Grenvillian to Laxfordian (800 – 1900Ma)
- Sub-group 3: ~2267Ma ~NeoArchean Lewisian (2000 – 2800Ma)

Provenance is further discussed in Appendix 4.

The Lista Formation apatite fission track ages generally suggest cooling below the apatite closure temperature (120°C) in early Miocene, with the exception being sub-group 2 which record Mesozoic cooling ages. This likely reflects the ‘resistive’ apatite kinetics of this particular group as indicated by the R_{mr0} of 0.7951.

The time-temperature constraints for the FT³ thermal modelling are summarised below:

Well	Sample ID.	Initial		Deposition		Peak Burial		Present Day	
		Age (Ma)	Temp ($^\circ\text{C}$)	Age (Ma)	Temp ($^\circ\text{C}$)	Age (Ma)	Temp ($^\circ\text{C}$)	Age (Ma)	Temp ($^\circ\text{C}$)
205/09-1 2798.0-2807.0m	P10012_001	600.0	199.0-200.0	56.0-59.2	0.0-20.0	10.0-55.0	44.2-139.4	0.0	64.2-79.4
205/09-1 3704.0-3719.0m	P10012_002	600	199.0-200.0	56.0-59.2	0.0-20.0	10.0-55.0	67.9-169.4	0.0	87.9-109.4

A plot showing the integration of sample age, temperature and mean apatite fission track length is shown in Figure 4.2.2. The time-temperature histories for the 205/9-1 samples are shown in

Figures 4.3.2, 4.3.3 & 4.3.4. The thermal history implications from the time-temperature (tT) modelling of the 205/9-1 apatite data are summarised in the table below:

Well	Sample ID.	Peak Burial Time t (Ma)	Peak Burial Temp T (°C)	Temp at 1 Ma (°C)	Temp at 5 Ma (°C)	Temp at 10 Ma (°C)	Temp at 25 Ma (°C)	Temp at 50 Ma (°C)
205/09-1 2798.0-2807.0m	P10012_001	1.0	75.9	72.0	72.0	71.8	69.0	32.0
205/09-1 3704.0-3719.0m	P10012_002	27.0	≥122.9	97.0	101.0	106.4	116.1	45.9

*A vitrinite reflectivity equivalent of 0.43-0.48% Ro is given for the Sele sample
A vitrinite reflectivity equivalent of 0.64-≥0.71% Ro is given for the Lista (D1) Sand sample*

The modelled temperature history for the shallower Sele Formation sample (2798-2807m) suggests maximum heating occurred during the last 50Ma, with 2sigma vale of ~38Ma indicating the constrain on timing is weak; the peak temperature is estimated to be ~75°C±15 i.e within the range of the present-day temperature. The reported best fit model (based of GOF) (p.1-38) estimates a peak temp of ~75°C at 45Ma.

The modelled temperature history for the deeper Lista Formation sample (3704-3719m) also suggests maximum heating occurred during the last 50Ma. The averaged time – temperature history (Table 1.1) yields a time of peak temperature at 27Ma±29Ma and a peak temperature of >122°C±23. The reported best fit models (based of GOF) (p.1-40) estimates a peak temp of ~116-153°C at 19-30Ma. Both of which are hotter than the estimated present-day temperature of ~95°C. These results would be consistent with maximum burial prior to Late Tertiary uplift. Conversely, it is plausible that the heating recorded is reflecting the movement of hot fluids (cf. Parnell *et al.*, 1999, 2005; Baron *et al.* 2008). The timing of the peak temperature has a simpler correspondence with the regional estimate of peak burial, but the 205/09-1 well is located in a basinal area thought to have experience modest uplift (cf. Tassone *et al.* 2014) likely insufficient to wholly account for the higher paleotemperatures.

The correspondence between the measured vitrinite reflectivity and the modelled reflectivity from the apatite thermochronology is very good (Figure 5.2.1). The Lista sample does trend to higher values using the EasyRo kinetics, however the BasinRo (Nielsen., *et al.*) and the EasyDL kinetics are in close agreement with the measured values.

4.3.2.2 Data and discussion for well 205/12-1

Two ditch cuttings samples were collected from Paleocene and Cretaceous intervals penetrated in the 205/12-1 well. Samples details are given in the table below.

Well	Top Depth	Bottom Depth	Units (m/ft)	Stratigraphy	Age	Sample Type	Sample ID.	Apatite Grains
205/12-1	-	2570.0	m	Lamba	P3	DC	P10012_003	1000s
	-	3175.0		Shetland	K2	DC	P10012_004	10s

The Lamba Formation sample is a single ditch cuttings sample from 2570.0m; the bulk sample yielded a median common lead corrected U-Pb Age of 1536.2Ma. The pooled UFT Age is ~173Ma, four of sub-populations were identified to which distinct model ages were assigned (see below). The bulk sample has a Mean track length is 12.18±1.43µm with a median Dpar of 1.75µm and a median R_{mr0} of 0.8045. The relatively narrow variation in track length distribution (e.g., <1.5 µm), would be interpreted to have cooled relatively rapidly from a temperature ≥

110°C to a temperature $\leq 60^\circ\text{C}$ at the time indicated by the apparent apatite fission track age. Four apatite sub-populations are recognised based on U-Pb ages and REE chemistry in this sample:

- Sub-Group 0
 - Median U-Pb Age: 388.5 Ma
 - Best fit model - Oldest UFT Age: Pop1: 296.0 Ma. Pop2: 345.0 Ma
 - Pooled UFT Age: 178.9 Ma
 - Mean track length: $12.42 \pm 1.31 \mu\text{m}$
 - Median Dpar: 1.82 μm
 - Median $R_{\text{mr}0}$: 0.7342
- Sub-Group 1
 - Median U-Pb Age: 722.1 Ma
 - Best fit model - Oldest UFT Age: Pop1: 125.0 Ma. Pop3: 447.0 Ma
 - Pooled UFT Age: 233.34 Ma
 - Mean track length: $12.04 \pm 1.46 \mu\text{m}$
 - Median Dpar: 1.73 μm
 - Median $R_{\text{mr}0}$: 0.7359
- Sub-Group 2A
 - Median U-Pb Age: 1597.5 Ma
 - Best fit model - Oldest UFT Age: Pop1: 273.0 Ma. Pop3: 419.0 Ma
 - Pooled UFT Age: 208.32 Ma
 - Mean track length: $12.17 \pm 1.61 \mu\text{m}$
 - Median Dpar: 1.79 μm
 - Median $R_{\text{mr}0}$: 0.749
- Sub-Group 2B
 - Median U-Pb Age: 1661.5 Ma
 - Best fit model - Oldest UFT Age: Pop1: 215.0 Ma. Pop2: 246.0 Ma. Pop3 277.0 Ma. Pop4: 568.0 Ma
 - Pooled UFT Age: 145.61 Ma
 - Mean track length: $12.21 \pm 1.37 \mu\text{m}$
 - Median Dpar: 1.71 μm
 - Median $R_{\text{mr}0}$: 0.823

The Shetland Formation sample is a single ditch cuttings sample from 3175.0m; the bulk sample yielded a median common lead corrected U-Pb Age of ~454Ma, with a pooled UFT Age of ~219Ma. The bulk sample Mean track length is $10.98 \pm 1.39 \mu\text{m}$ with a median Dpar of 1.6 μm and a median $r_{\text{mr}0}$ of 0.7898. Three apatite sub-populations are recognised based on U-Pb ages and REE chemistry in this sample:

- Sub-Group 0
 - Median U-Pb Age: 246.1 Ma
 - Best fit model - Oldest UFT Age: 319.0 Ma
 - Pooled UFT Age: 209.26 Ma
 - Mean track length: $11.86 \pm 0.78 \mu\text{m}$
 - Median Dpar: 1.71 μm

- Median R_{mr0} : 0.7734
- Sub-Group 1
 - Median U-Pb Age: 533.3 Ma
 - Best fit model - Oldest UFT Age: 345.0 Ma
 - Pooled UFT Age: 209.31 Ma
 - Mean track length: $10.11 \pm 0.68 \mu\text{m}$
 - Median Dpar: $1.57 \mu\text{m}$
 - Median R_{mr0} : 0.7399
- Sub-Group 2
 - Median U-Pb Age: 1552.7 Ma
 - Best fit model - Oldest UFT Age: -
 - Pooled UFT Age: 252.3 Ma
 - Mean track length: No track lengths could be measured
 - Median Dpar: $1.59 \mu\text{m}$
 - Median R_{mr0} : 0.8068

The UFT ages for both the Paleocene and Cretaceous samples suggest a provenance signature i.e. the apatite in these samples cooled below the apatite closure temperature (120°C) prior to their deposition and have not since been heated above this temperature. The U-Pb ages for the two samples both incorporate a wide range of ages of cooling below $\sim 450\text{--}550^\circ\text{C}$ (cf. Chamberlain & Bowring 2000 and Schoene & Bowring 2007, for U-Pb closure temperatures) which may indicate sediment sourced from the following terrane groups:

- Sub-group 0: 246 – 388Ma ~Acadian-Variscan (*sensu* Mendum, BGS)
 - The majority of the apatite UFT ages also fall in the range 345-219Ma.
- Sub-group 1: 533 – 722Ma ~Caledonian-Laxfordian?
- Sub-group 2: 1552-1661Ma ~Grenvillian to Laxfordian (800 – 1900Ma)

Provenance is further discussed in Appendix 4.

The time-temperature constraints for the FT³ thermal modelling are summarised below:

Well	Sample ID.	Initial		Deposition		Peak Burial		Present Day	
		Age (Ma)	Temp ($^\circ\text{C}$)	Age (Ma)	Temp ($^\circ\text{C}$)	Age (Ma)	Temp ($^\circ\text{C}$)	Age (Ma)	Temp ($^\circ\text{C}$)
205/12-1 2570.0m	P10012_003	600.0	199.0- 200.0	56.0- 59.2	0.0- 20.0	10.0- 55.0	41.9- 136.4	0.0	61.9- 76.4
205/12-1 3175.0m	P10012_004	600	199.0- 200.0	139.8- 145.0	0.0- 20.0	10.0- 130.0	57.6- 156.3	0.0	77.6- 96.3

A plot showing the integration of sample age, temperature and mean apatite fission track length is shown in Figure 4.2.4. The time-temperature histories for the 205/12-1 samples are shown in Figures 4.3.5, 4.3.6 & 4.3.7. The thermal history implications from the time-temperature (tT) modelling of the 205/12-1 apatite data are summarised in the table below:

Well	Sample ID.	Peak Burial Time t (Ma)	Peak Burial Temp T (°C)	Temp at 1 Ma (°C)	Temp at 5 Ma (°C)	Temp at 10 Ma (°C)	Temp at 25 Ma (°C)	Temp at 50 Ma (°C)
205/12-1 2570.0m	P10012_003	1.0	65.2	65.2	63.1	60.0	51.3	22.8
205/12-1 3175.0m	P10012_004	0.0	89.2	85.4	85.0	84.2	83.3	79.3

*A vitrinite reflectivity equivalent of 0.38-0.42% Ro is given for the Lamba sample
A vitrinite reflectivity equivalent of 0.50-0.60% Ro is given for the Shetland sample*

The modelled temperature history for both samples is consistent with progressive heating throughout the Tertiary; agreement with the Genesis model is generally good (cf. Figures 4.3.5 & 6). The tT modelling for the 3175m is poorly constrained in time but estimates a peak of ~89°C (±12°C) which is approximately equal to the present-day temperature. The shallower 2570m sample is much better constrained in time, indicating maximum temperature was reached ~1Ma (±6Ma), the peak temperature is ~65°C (±6°C); the reported best fit model (based of GOF) estimates a peak temp of ~66°C at 1Ma. Essentially the data indicate the maximum temperature has been reached geologically recently.

Integration of the 205/12-1 apatite thermochronology data together with the vitrinite reflectivity thermal calibration data is shown in Figure 5.2.2 and are in good agreement. Integration with and 1D basin modelling and expulsion timing is considered further in Chapter 6.

4.3.2.3 Data and discussion for well 205/14-2

A single ditch cuttings sample was collected from the Paleocene interval penetrated in the 205/14-2 well. Sample details are given in the table below

Well	Top Depth	Bottom Depth	Units (m/ft)	Stratigraphy	Age	Sample Type	Sample ID.	Apatite Grains
205/14-2	-	7430.0	ft	Unit IV Upper	P3	DC	P10012_005	100s

The Unit IV Upper (Vaila) Formation sample is a single ditch cuttings sample from 7430.0ft; the bulk sample yielded a median common lead corrected U-Pb Age of 1093.5Ma. The pooled UFT Age is ~234Ma. The bulk sample has a Mean track length is 12.23±1.64 µm with a median Dpar of 1.79µm and a median R_{mr0} of 0.8262. Four apatite sub-populations are recognised based on U-Pb ages and REE chemistry in this sample:

- Sub-Group 0
 - Median U-Pb Age: 152.3 Ma
 - Best fit model - Oldest UFT Age: -
 - Pooled UFT Age: 123.0 Ma
 - Mean track length: 12.05±1.64µm
 - Median Dpar: 1.62 µm
 - Median R_{mr0}: 0.8193
- Sub-Group 1
 - Median U-Pb Age: 533.5 Ma
 - Best fit model - Oldest UFT Age: Pop1: 208.0Ma. Pop2: 449.0Ma. Pop3: 391Ma
 - Pooled UFT Age: 264.0 Ma
 - Mean track length: 12.95±1.46µm
 - Median Dpar: 1.88 µm

- Median R_{mr0} : 0.8131
- Sub-Group 2
 - Median U-Pb Age: 1421.4 Ma
 - Best fit model - Oldest UFT Age: pop1: 487 Ma
 - Pooled UFT Age: 224.0 Ma
 - Mean track length: $12.16 \pm 1.51 \mu\text{m}$
 - Median Dpar: $1.67 \mu\text{m}$
 - Median R_{mr0} : 0.8278
- Sub-Group 3
 - Median U-Pb Age: 2206.0 Ma
 - Best fit model - Oldest UFT Age: Pop1 313.0 Ma. Pop2: 506.0 Ma
 - Pooled UFT Age: 292.0 Ma
 - Mean track length: $11.65 \pm 1.69 \mu\text{m}$
 - Median Dpar: $1.79 \mu\text{m}$
 - Median R_{mr0} : 0.8304

The UFT ages for the Paleocene sample indicate a provenance signature i.e. the apatite in the sample cooled below the apatite closure temperature (120°C) prior to its deposition and have not since been heated above this temperature. The U-Pb ages are consistent either with a Caledonian ($\sim 400\text{--}600\text{Ma}$) or Acadian-Variscan ($\sim 250\text{--}400\text{Ma}$) age. The exception is the Sub-Group 0 which has an Early Cretaceous age. The U-Pb ages cover all the sub-groups identified in this study, and may be related to source terranes from:

Sub-group 0: 152Ma Local foot-wall uplift related to foot-wall-uplift would involve insufficient cooling, so this must presumably relate to the continued denudation of the source terrane.

- Sub-group 1: 533Ma \sim Caledonian
- Sub-group 2: 1421Ma \sim Grenvillian to Laxfordian (800 – 1700Ma)
- Sub-group 3: 2206Ma NeoArchean Lewisian (2000 – 2800Ma)

Provenance is further discussed in Appendix 4.

The time-temperature constraints for the FT³ thermal modelling are summarised below:

Well	Sample ID.	Initial		Deposition		Peak Burial		Present Day	
		Age (Ma)	Temp ($^\circ\text{C}$)	Age (Ma)	Temp ($^\circ\text{C}$)	Age (Ma)	Temp ($^\circ\text{C}$)	Age (Ma)	Temp ($^\circ\text{C}$)
205/14-2 7430.0ft	P10012_005	600.0	199.0- 200.0	56.0- 59.2	0.0- 20.0	10.0- 55.0	38.3- 131.9	0.0	58.3- 71.9

A plot showing the integration of sample age, temperature and mean apatite fission track length is shown in Figure 4.2.5. The time-temperature histories for the 205/14-2 samples is shown in Figure 4.3.8. The thermal history implications from the time-temperature (tT) modelling of the 205/14-2 apatite data are summarised in the table below:

Well	Sample ID.	Peak Burial Time t (Ma)	Peak Burial Temp T ($^\circ\text{C}$)	Temp at 1 Ma ($^\circ\text{C}$)	Temp at 5 Ma ($^\circ\text{C}$)	Temp at 10 Ma ($^\circ\text{C}$)	Temp at 25 Ma ($^\circ\text{C}$)	Temp at 50 Ma ($^\circ\text{C}$)
205/14-2 7430.0ft	P10012_005	1.0	64.3	63.4	61.5	60.2	52.5	22.1

A vitrinite reflectivity equivalent of 0.38-0.42% Ro is given for the Unit IV Upper (Vaila) sample

The tT model indicates that maximum temperature was reached ~1Ma (± 17 Ma), the peak temperature is $\sim 64^{\circ}\text{C}$ ($\pm 7^{\circ}\text{C}$); the reported best fit model (based of GOF) estimates a peak temp of $\sim 65^{\circ}\text{C}$ at 1Ma. Essentially the data indicate the maximum temperature has been reached geologically recently.

Integration of the 205/14-2 apatite thermochronology data together with the % Ro thermal calibration data is shown in Figure 5.2.3 and are in good agreement. Integration with and 1D basin modelling and expulsion timing is considered further in Chapter 6.

4.3.2.4 Data and discussion for well 205/17b-2

A single core sample was collected from the Paleocene interval penetrated in the 205/17b-2 well. Sample details are given in the table below

Well	Top Depth	Bottom Depth	Units (m/ft)	Stratigraphy	Age	Sample Type	Sample ID.	Apatite Grains
205/17b-2	-	2443.8	m	Lista	P3	COCH	P10012 006	1000s

The bulk AFT sample for the Lista Formation sample yielded a median common lead corrected U-Pb Age of 1419Ma; the composite sample pooled UFT Age is ~ 292 Ma. The bulk sample has a Mean track length is $12.04 \pm 1.56 \mu\text{m}$ with a median Dpar of $1.81 \mu\text{m}$ and a median $r_{\text{mr}0}$ of 0.8334. Four apatite sub-populations are recognised based on U-Pb ages and REE chemistry in this sample:

- Sub-Group 0
 - Median U-Pb Age: 232.0 Ma
 - Best fit model - Oldest UFT Age: Pop2: 377.0 Ma
 - Pooled UFT Age: 287.0 Ma
 - Mean track length: $12.29 \pm 1.11 \mu\text{m}$
 - Median Dpar: $1.73 \mu\text{m}$
 - Median $R_{\text{mr}0}$: 0.809
- Sub-Group 1
 - Median U-Pb Age: 433.0 Ma
 - Best fit model - Oldest UFT Age: Pop1: 380.0 Ma. Pop2: 381.0 Ma
 - Pooled UFT Age: 237.0 Ma
 - Mean track length: $12.3 \pm 1.38 \mu\text{m}$
 - Median Dpar: $1.9 \mu\text{m}$
 - Median $R_{\text{mr}0}$: 0.8276
- Sub-Group 2A
 - Median U-Pb Age: 1038.0 Ma
 - Best fit model - Oldest UFT Age: Pop1: 405.0 Ma
 - Pooled UFT Age: 237.0 Ma
 - Mean track length: $12.46 \pm 1.11 \mu\text{m}$
 - Median Dpar: $1.77 \mu\text{m}$
 - Median $R_{\text{mr}0}$: 0.8445
- Sub-Group 2B
 - Median U-Pb Age: 1794.0 Ma

- Best fit model - Oldest UFT Age: Pop1: 492.0 Ma. Pop2: 582.0 Ma
- Pooled UFT Age: 237.0 Ma
- Mean track length: $11.68 \pm 1.75 \mu\text{m}$
- Median Dpar $1.81 \mu\text{m}$
- Median R_{mr0} : 0.8398
- Sub-Group 2C
 - Median U-Pb Age: 1970.0 Ma
 - Best fit model - Oldest UFT Age: Pop1: 524.0 Ma
 - Pooled UFT Age: 237.0 Ma
 - Mean track length: $12.04 \pm 1.57 \mu\text{m}$
 - Median Dpar: $1.85 \mu\text{m}$
 - Median R_{mr0} : 0.8382

The UFT ages for the Paleocene sample indicate a provenance signature i.e. the apatite in the sample cooled below the apatite closure temperature (120°C) prior to its deposition and have not since been heated above this temperature. The majority of the U-Pb ages are consistent with a Caledonian ($\sim 400\text{--}600\text{Ma}$) and/or Acadian-Variscan ($\sim 250\text{--}400\text{Ma}$) age. The U-Pb ages, indicating cooling below $\sim 450\text{--}550^\circ\text{C}$ (cf. Chamberlain & Bowring 2000 and Schoene & Bowring 2007, for U-Pb closure temperatures) range across all the sub-groups identified in this study, and may indicate source terranes related to:

- Sub-group 0: 232Ma This age is too young to be Variscan. As discussed for 205/9-1 it seems unlikely footwall uplift and denudation can be responsible associated with any extension; therefore, this must presumably relate to the continued denudation of the source terrane.
- Sub-group 1: 433Ma \sim Caledonian
- Sub-group 2A-2B: 1038-1794Ma \sim Grenvillian to Laxfordian (800 – 1700Ma)
- Sub-group 3: $\sim 1970\text{Ma}$ NeoArchean Lewisian (2000 – 2800Ma)

Provenance is further discussed in Appendix 4.

The time-temperature constraints for the FT³ thermal modelling are summarised below:

Well	Sample ID.	Initial		Deposition		Peak Burial		Present Day	
		Age (Ma)	Temp ($^\circ\text{C}$)	Age (Ma)	Temp ($^\circ\text{C}$)	Age (Ma)	Temp ($^\circ\text{C}$)	Age (Ma)	Temp ($^\circ\text{C}$)
205/17b-2 2443.8m	P10012_006	600.0	199.0- 200.0	56.0- 59.2	0.0- 20.0	10.0- 55.0	41.0- 135.2	0.0	61.0- 75.2

A plot showing the integration of sample age, temperature and mean apatite fission track length is shown in Figure 4.2.6. The time-temperature history for the 205/17b-2 samples is shown in Figure 4.3.9. The thermal history implications from the time-temperature (tT) modelling of the 205/17b-2 apatite data are summarised in the table below:

Well	Sample ID.	Peak Burial Time t (Ma)	Peak Burial Temp T ($^\circ\text{C}$)	Temp at 1 Ma ($^\circ\text{C}$)	Temp at 5 Ma ($^\circ\text{C}$)	Temp at 10 Ma ($^\circ\text{C}$)	Temp at 25 Ma ($^\circ\text{C}$)	Temp at 50 Ma ($^\circ\text{C}$)
205/17b-2 2443.8m	P10012_006	1.0	65.3	65.1	62.1	58.9	47.5	19.2

A vitrinite reflectivity equivalent of 0.37-0.42% Ro is given for the Lista sample

The modelled temperature history for both samples is consistent with progressing heating to temperatures $<100^{\circ}\text{C}$ through the Tertiary. The timing of peak temperature is relatively well constrained by the apatite data, with the average of the accepted paths having an age of $\sim 1\text{Ma}(\pm 4\text{Ma})$, and a maximum temperature of $\sim 65\pm 7^{\circ}\text{C}$. The reported best fit model (based of GOF) estimates a peak temp of $\sim 64^{\circ}\text{C}$ at 1Ma.

The 1D Genesis basin model indicates more rapid heating (due to rapid burial in the Lower Tertiary), but both the apatite thermochronology and basin model are in broad agreement regarding the timing of maximum temperature close to present-day. Integration with and 1D basin modelling and expulsion timing is considered further in Chapter 6.

4.3.3 Quad 206 wells

4.3.3.1 Data and discussion for well 206/11-1

A single ditch cuttings sample was collected from the undifferentiated Cretaceous interval penetrated in the 206/11-1 well. Sample details are given in the table below.

Well	Top Depth	Bottom Depth	Units (m/ft)	Stratigraphy	Age	Sample Type	Sample ID.	Apatite Grains
206/11-1	4370.0	4376.0	m	Early Cret Sands	K1	DC	P10012_007	100s

The Early Cretaceous Sands sample is a composite of ditch cuttings over the 4370-4376m interval; the bulk sample yield a median common lead corrected U-Pb Age of 1291Ma. The pooled UFT Age is ~5Ma. The bulk sample has a Mean track length of $5.51 \pm 0.0 \mu\text{m}$ with a median Dpar of $1.8 \mu\text{m}$ and a median $r_{\text{mr}0}$ of 0.8334. Two apatite sub-populations are recognised based on U-Pb ages and REE chemistry in this sample:

- Sub-Group 1
 - Median U-Pb Age: 524.0Ma
 - Best fit model - Oldest UFT Age: Pop1: 6.0Ma
 - Pooled UFT Age: 0.0 Ma
 - Mean track length: -
 - Median Dpar: $1.8 \mu\text{m}$
 - Median $R_{\text{mr}0}$: 0.7406
- Sub-Group 2
 - Median U-Pb Age: 1350.0 Ma
 - Best fit model - Oldest UFT Age: Pop1: 1.0Ma. Pop: 2 5 Ma. Pop3: 10.0 Ma
 - Pooled UFT Age: 5.8 6Ma
 - Mean track length: $5.51 \pm 0.0 \mu\text{m}$
 - Median Dpar: $1.81 \mu\text{m}$
 - Median $R_{\text{mr}0}$: 0.8348

The UFT age for the Cretaceous sample suggests indicates that the sample is at or close to maximum burial present day, although there are some complexities in the data as the measured apatite kinetic parameters are variable (discussed below). The U-Pb ages, indicating cooling below ~450–550°C (cf. Chamberlain & Bowring 2000 and Schoene & Bowring 2007, for U-Pb closure temperatures) fall into two sub-groups that may indicate source from the following source terranes:

- Sub-group 1: 524Ma ~Caledonian
- Sub-group 2: 1350Ma ~Grenvillian to Laxfordian (800 – 1700Ma)

Provenance is further discussed in Appendix 4.

The time-temperature constraints for the FT³ thermal modelling are summarised below:

Well	Sample ID.	Initial		Deposition		Peak Burial		Present Day	
		Age (Ma)	Temp (°C)	Age (Ma)	Temp (°C)	Age (Ma)	Temp (°C)	Age (Ma)	Temp (°C)
206/11-1 4370-4376m	P10012_007	600.0	199.0-200.0	100.5-113.0	0.0-20.0	10.0-65.0	80.0-204.5	0.0	100.0-144.5

A plot showing the integration of sample age, temperature and mean apatite fission track length is shown in Figure 4.2.7. The time-temperature history for the 206/11-1 samples is shown in Figure 4.3.10. The thermal history implications from the time-temperature (tT) modelling of the 206/11-1 apatite data are summarised in the table below:

Well	Sample ID.	Peak Burial Time t (Ma)	Peak Burial Temp T (°C)	Temp at 1 Ma (°C)	Temp at 5 Ma (°C)	Temp at 10 Ma (°C)	Temp at 25 Ma (°C)	Temp at 50 Ma (°C)
206/11-1 4370-4376m	P10012_007	33.0	≥138.7	124.4	126.8	128.7	133.4	133.4

A vitrinite reflectivity equivalent of 0.72-≥1.01% Ro is given for the Early Cretaceous Sands sample

The tT modelling in terms of the average of the acceptable tT paths indicates that the timing of peak temperature is relatively poorly constrained, with an estimate of 33±31Ma (i.e. maximum temperature could have occurred from 64 – 2Ma within 2sigma). The magnitude of the peak temperature has greater constraint at >138±7°C. This is in good agreement with the 1D Genesis basin model (Figure 4.3.10). This well was included in Tassone *et al.*'s (2014) study of Tertiary exhumation using sediment velocities; for this well a modest ~183m of exhumation was estimated so a slight cooling would be expected on the basis of this data, although such a small number is likely below the resolution of the apatite thermochronology technique.

The best fit models obtained varied as the kinetics of the apatite samples were observed to vary (cf. R_{mr0} values):

- Sub-Group 1; population 1- Best Fit Model: Oldest UFT 6Ma; SFT GOF: 0.922; Peak temperature 6Ma, peak temperature 162°C. Measured UFT Age 0Ma; R_{mr0} : 0.7404
- **Sub-Group 2; population 1- Best Fit Model: Oldest UFT 1Ma; SFT GOF: 0.0815; Peak temperature 1Ma, Peak temperature 112°C. Measured UFT Age 10.3Ma; R_{mr0} : 0.842**
- Sub-Group 2; population 2- Best Fit Model: Oldest UFT 5Ma; SFT GOF: 0.8999; Peak temperature 5Ma, Peak temperature 152°C. Measured UFT Age 0Ma; R_{mr0} : 0.773
- Sub-Group 2; population 3- Best Fit Model: Oldest UFT 10Ma; SFT GOF: 0.8554; Peak temperature 10Ma, Peak temperature 182°C. Measured UFT Age 0Ma; R_{mr0} : 0.6783

Lower R_{mr0} numbers indicate higher activation energy for the apatite to anneal which pushes the upper limit of the PAZ to hotter temperatures. The numbers above 150°C could well be model artefacts and should probably be ignored (Ray Donelick, *Pers. Comm*), therefore sub-group 2, population 1 is viewed at the most reliable result. This indicates that the maximum temperature was reached close to present-day. This well was also analysed by GeoTrack in their GC540 Report (“*West of Shetlands (North): Thermal and tectonic development and hydrocarbon generation history assessed using apatite fission track analysis and vitrinite reflectance. – February 1995*”) which also concluded that the AFTA and vitrinite reflectivity data was most consistent with maximum temperature (and burial) at or close to present-day.

Integration of the 206/11-1 apatite thermochronology data together with the vitrinite reflectivity thermal calibration data is shown in Figure 5.2.6 and are in good agreement. Integration with and 1D basin modelling and expulsion timing is considered further in Chapter 6.

4.3.4 Quad 207 wells

4.3.4.1 Data and discussion for well 207/01-2

Two ditch cuttings samples were collected from Cretaceous and Basement intervals penetrated in the 207/01-2 well. Sample details are given in the table below.

Well	Top Depth	Bottom Depth	Units (m/ft)	Stratigraphy	Age	Sample Type	Sample ID.	Apatite Grains
207/01-2	5590.0	5620.0	ft	Victory	K1	DC	P10011 003	100s
	5740.0	5750.0		PrCam Basement	PrCam	DC	P10011 004	100s

The Victory Formation sample is a composite of cuttings over the 5590-5620ft interval; the bulk sample yields a median common lead corrected U-Pb Age of 538Ma; the pooled UFT Age is ~190Ma. The bulk sample has a Mean track length of $11.93 \pm 1.61 \mu\text{m}$ with a median Dpar of $1.83 \mu\text{m}$ and a median $r_{\text{mr}0}$ of 0.8315. Two apatite sub-populations are recognised based on U-Pb ages and REE chemistry in this sample:

- Sub-Group 1A
 - Median U-Pb Age: 547.0 Ma
 - Best fit model - Oldest UFT Age: Pop1: 300.0 Ma. Pop2: 234.0 Ma
 - Pooled UFT Age: 189.0 Ma
 - Mean track length: $11.87 \pm 1.68 \mu\text{m}$
 - Median Dpar: $1.79 \mu\text{m}$
 - Median $R_{\text{mr}0}$: 0.8310
- Sub-Group 1B
 - Median U-Pb Age: 462.0 Ma
 - Best fit model - Oldest UFT Age: Pop1: 342.0 Ma
 - Pooled UFT Age: 222.0 Ma
 - Mean track length: $11.87 \pm 1.68 \mu\text{m}$
 - Median Dpar: $2.0 \mu\text{m}$
 - Median $R_{\text{mr}0}$: 0.8302

The Precambrian Basement sample is a composite of cuttings over the 5740-5750ft interval; the bulk sample yields a median common lead corrected U-Pb Age of 800Ma and a pooled UFT Age of ~250Ma. The bulk sample has a Mean track length of $11.68 \pm 1.55 \mu\text{m}$ with a median Dpar of $1.76 \mu\text{m}$ and a median $r_{\text{mr}0}$ of 0.8439. Four apatite sub-populations are recognised based on U-Pb ages and REE chemistry in this sample:

- Sub-Group 1A
 - Median U-Pb Age: 545.0 Ma
 - Best fit model - Oldest UFT Age: Pop1: 306.0Ma. Pop2: 433.0Ma. Pop3: 378Ma
 - Pooled UFT Age: 303.0 Ma
 - Mean track length: $12.12 \pm 1.13 \mu\text{m}$
 - Median Dpar: $1.81 \mu\text{m}$
 - Median $R_{\text{mr}0}$: 0.8409
- Sub-Group 1B
 - Median U-Pb Age: 412.0 Ma
 - Best fit model - Oldest UFT Age: Pop1: 438.0 Ma

- Pooled UFT Age: 321.0 Ma
- Mean track length: $11.84 \pm 1.33 \mu\text{m}$
- Median Dpar: $1.79 \mu\text{m}$
- Median $R_{\text{mr}0}$: 0.8462
- Sub-Group 2A
 - Median U-Pb Age: 1530.0 Ma
 - Best fit model - Oldest UFT Age: Pop1: 407.0 Ma
 - Pooled UFT Age: 202.0 Ma
 - Mean track length: $10.75 \pm 1.33 \mu\text{m}$
 - Median Dpar: $1.77 \mu\text{m}$
 - Median $R_{\text{mr}0}$: 0.8478
- Sub-Group 2B
 - Median U-Pb Age: 1736.0 Ma
 - Best fit model - Oldest UFT Age: Pop1: 363.0Ma. Pop2: 387.0Ma. Pop4: 529.0 Ma
 - Pooled UFT Age: 284.0 Ma
 - Mean track length: $10.76 \pm 1.92 \mu\text{m}$
 - Median Dpar: $1.76 \mu\text{m}$
 - Median $R_{\text{mr}0}$: 0.8418

The UFT age for the Cretaceous and Basement samples both suggest a provenance signature. For both the Cretaceous and the Basement sample this would indicate that the apatite in the sample cooled below the apatite closure temperature (120°C) prior to its deposition and have not since been heated above this temperature. The U-Pb ages, indicating cooling below ~ 450 – 550°C (cf. Chamberlain & Bowring 2000 and Schoene & Bowring 2007, for U-Pb closure temperatures) fall into two sub-groups that may indicate source from the following source terranes:

- Sub-group 1: 412 - 547Ma ~Caledonian
- Sub-group 2: 1530 - 1736Ma ~Grenvillian to Laxfordian (800 – 1700Ma).

On the basis of this data the Cretaceous sample only contains apatite derived from Caledonian aged sources. Whereas the ‘basement’ contains apatite from both Caledonian and Laxfordian sources. Provenance is further discussed in Appendix 4.

The time-temperature constraints for the thermal modelling are summarised below:

Well	Sample ID.	Initial		Deposition		Peak Burial		Present Day	
		Age (Ma)	Temp ($^\circ\text{C}$)	Age (Ma)	Temp ($^\circ\text{C}$)	Age (Ma)	Temp ($^\circ\text{C}$)	Age (Ma)	Temp ($^\circ\text{C}$)
207/01-2 5590.0-5620.0ft	P10011_003	600.0	199.0-200.0	100.5-145.0	0.0-20.0	10.0-65.0	28.8-119.8	0.0	48.8-59.8
207/01-2 5740.0-5750.0ft	P10011_004	600.0	199.0-200.0	100.5-145.0	0.0-20.0	10.0-65.0	29.9-121.2	0.0	49.9-61.2

A plot showing the integration of sample age, temperature and mean apatite fission track length is shown in Figure 4.2.8. The time-temperature history for the 207/1-2 samples is shown in Figures 4.3.11, 4.3.12 & 4.3.13. The thermal history implications from the time-temperature (tT) modelling of the 207/1-2 apatite data are summarised in the table below:

Well	Sample ID.	Peak Burial Time t (Ma)	Peak Burial Temp T (°C)	Temp at 1 Ma (°C)	Temp at 5 Ma (°C)	Temp at 10 Ma (°C)	Temp at 25 Ma (°C)	Temp at 50 Ma (°C)
207/01-2 5590.0-5620.0ft	P10011_003	32.0	59.8	54.6	55.4	56.2	57.0	55.0
207/01-2 5740.0-5750.0ft	P10011_004	1.0	57.0	56.0	55.3	54.7	52.7	45.9

*A vitrinite reflectivity equivalent of 0.38-0.43% Ro is given for the Victory sample
A vitrinite reflectivity equivalent of 0.36-0.40% Ro is given for the Precambrian Basement sample*

For the Lower Cretaceous sample, the tT modelling in terms of the average of the acceptable tT paths indicates that the timing of peak temperature is relatively poorly constrained, with an estimate of 32 ± 40 Ma (i.e. maximum temperature could have occurred from 72 – 0 Ma within 2sigma). The magnitude of the peak temperature has greater constraint at $>59.8 \pm 8^\circ\text{C}$. The reported best fit model (based of GOF) estimates a peak temp of $\sim 64^\circ\text{C}$ at 18 Ma. Both the averaged result and the best-fit model have temperatures that are cooler than the present-day measured temperature to which the 1D Genesis model is calibration (cf. Figure 4.3.11). The raw bht temperatures in this well were 57-63.3°C and the corrected temperature (using the Carstens & Finstad (1981) correction) were estimated to be 69-70°C. In order for the apatite thermochronology data and the measured temperatures to match one would have to accept the raw bht data in this case needed little correction.

A similar result was obtained for the Basement sample, with the tT modelling in terms of the average of the acceptable tT paths indicates that the timing of peak temperature is relatively poorly constrained, with an estimate of 1 ± 32 Ma (i.e. maximum temperature could have occurred from 32 – 0 Ma within 2sigma). Combining the results from the two samples suggests peak temperature must have been obtained within the last 32 Ma if the results are to be mutually consistent. The magnitude of the peak temperature has greater constraint at $>56.95 \pm 6^\circ\text{C}$. The reported best fit model (based of GOF) estimates a peak temp of $\sim 54^\circ\text{C}$ at 1 Ma. This would be cooler than even the uncorrected bottom-hole temperatures and which seems unlikely to be correct, thus the Basement (P10011_004) apatite tT paths are viewed with caution. There is the possibility that apatite-bearing sands have caved into the sample contaminating it with apatite from a shallower (cooler) part of the sedimentary column.

Integration of the 207/01-2 apatite thermochronology data together with the vitrinite reflectivity thermal calibration data is shown in Figure 5.2.7; for this sample only a single APT sample was available, taken in the shallow section to constrain potential uplift, which was confirmed by the measured value of $\sim 0.25\%$ Ro (virgin vitrinite at surface conditions would have a reflectivity of $\sim 0.18\%$ Ro).

The legacy data showed a wide spread of values, the apatite thermochronology based model results suggest the lower values in the legacy data are most robust. Integration with and 1D basin modelling and expulsion timing is considered further in Chapter 6.

4.3.5 Quad 208 wells

4.3.5.1 Data and discussion for well 208/17-2

A single core sample was collected from the Palaeocene interval penetrated in the 208/17-2 well. Sample details are given in table below.

Well	Top Depth	Bottom Depth	Units (m/ft)	Stratigraphy	Age	Sample Type	Sample ID.	Apatite Grains
208/17-2	7871.0	7946.8	ft	Waterhouse	P3	COCH	P10012 008	100s

The bulk sample yielded a median common lead corrected U-Pb Age of 577Ma; the pooled UFT Age is ~216Ma. The bulk sample has a Mean track length of $11.29 \pm 1.47 \mu\text{m}$ with a median Dpar of $1.84 \mu\text{m}$ and a median $R_{\text{mr}0}$ of 0.7745. Four apatite sub-populations are recognised based on U-Pb ages and REE chemistry in this sample:

- Sub-Group 0
 - Median U-Pb Age: 260.2 Ma
 - Best fit model - Oldest UFT Age: Pop1: 351.0 Ma. Pop2: 548.0 Ma
 - Pooled UFT Age: 123.0 Ma
 - Mean track length: $11.18 \pm 1.47 \mu\text{m}$
 - Median Dpar: $1.74 \mu\text{m}$
 - Median $R_{\text{mr}0}$: 0.7772
- Sub-Group 1A
 - Median U-Pb Age: 593.0 Ma
 - Best fit model - Oldest UFT Age: Pop1: 303.0 Ma. Pop2: 482.0 Ma. Pop3: 441.0 Ma. Pop4: 519.0 Ma
 - Pooled UFT Age: 264.0 Ma
 - Mean track length: $11.27 \pm 1.34 \mu\text{m}$
 - Median Dpar: $1.89 \mu\text{m}$
 - Median $R_{\text{mr}0}$: 0.7815
- Sub-Group 1B
 - Median U-Pb Age: 574.0 Ma
 - Best fit model - Oldest UFT Age: Pop3: 380.0 Ma
 - Pooled UFT Age: 224.0 Ma
 - Mean track length: $11.16 \pm 1.69 \mu\text{m}$
 - Median Dpar: $1.9 \mu\text{m}$
 - Median $R_{\text{mr}0}$: 0.7553
- Sub-Group 2
 - Median U-Pb Age: 1251Ma
 - Best fit model - Oldest UFT Age: Pop1: 271.0 Ma. Pop2: 417.0 Ma
 - Pooled UFT Age: 292.0 Ma
 - Mean track length: $11.8 \pm 1.65 \mu\text{m}$
 - Median Dpar: $1.96 \mu\text{m}$
 - Median $R_{\text{mr}0}$: 0.7732

The UFT ages for the Paleocene sample indicate a provenance signature i.e. the apatite in the sample cooled below the apatite closure temperature (120°C) prior to its deposition and have

not since been heated above this temperature. The reported U-Pb ages cover all the sub-groups identified in this study, potentially relating to source terranes from:

- Sub-group 0: ~260Ma. This age probably is too young to be Variscan. As discussed for 205/09-1 it seems unlikely footwall uplift and denudation can be responsible associated with any extension; therefore, this must presumably relate to the continued denudation of the source terrane.
- Sub-group 1A-B: 574-593Ma ~Caledonian
- Sub-group 2: 1251Ma ~Grenvillian to Laxfordian (800 – 1700Ma)

Provenance is further discussed in Appendix 4.

The time-temperature constraints for the FT³ thermal modelling are summarised below:

Well	Sample ID.	Initial		Deposition		Peak Burial		Present Day	
		Age (Ma)	Temp (°C)	Age (Ma)	Temp (°C)	Age (Ma)	Temp (°C)	Age (Ma)	Temp (°C)
208/17-2 7871.0-7946.8ft	P10012_008	600.0	199.0-200.0	56.0-59.2	0.0-20.0	10.0-55.0	36.2-129.2	0.0	562.-59.2

A plot showing the integration of sample age, temperature and mean apatite fission track length is shown in Figure 4.2.9. The time-temperature history for the 208/17-2 samples is shown in Figure 4.3.14. The thermal history implications from the time-temperature (tT) modelling of the 208/17-2 apatite data are summarised in the table below:

Well	Sample ID.	Peak Burial Time t (Ma)	Peak Burial Temp T (°C)	Temp at 1 Ma (°C)	Temp at 5 Ma (°C)	Temp at 10 Ma (°C)	Temp at 25 Ma (°C)	Temp at 50 Ma (°C)
208/17-2 7871.0-7946.8ft	P10012_008	1.0	57.0	56.1	55.3	54.7	52.7	45.9

A vitrinite reflectivity equivalent of 0.45-0.51% Ro is given for the Waterhouse sample

For the Upper Paleocene sample the tT modelling in terms of the average of the acceptable tT paths indicates that the timing of peak temperature is relatively moderately constrained, with an estimate of 1 ± 17.65 Ma (i.e. maximum temperature could have occurred from ~19 – 0Ma within 2sigma). The magnitude of the peak temperature has greater constraint at $\sim 83 \pm 13^\circ\text{C}$. The reported best fit model (based of GOF) estimates a peak temp of $\sim 82^\circ\text{C}$ at 1Ma. These results indicate that the sample is at maximum burial and temperature at present day (The measured temperature $\sim 80^\circ\text{C}$) to which the 1D Genesis model is calibrated (cf. Figure 4.3.14). The temperature time path indicated by the apatite thermochronology suggests more progressive heating through the Tertiary relative to the 1D basin model which, because of the stratigraphic zonation, implies rapid burial and hence heating in the Lower Tertiary followed by long period of little variation.

The correspondence between the measured % Ro and modelled % Ro from the apatite thermochronology is very good (Figure 5.2.9); integration with and 1D basin modelling and expulsion timing is considered further in Chapter 6.

4.3.5.2 Data and discussion for well 208/24-1A

Two ditch cuttings samples were collected from the Cretaceous interval penetrated in the 208/24-1 well. Sample details are given in the table below.

Well	Top Depth	Bottom Depth	Units (m/ft)	Stratigraphy	Age	Sample Type	Sample ID.	Apatite Grains
208/24-1A	5900.0	6000.0	ft	Victory	K1	DC	P10011 006	100s
	6230.0	6300.0				DC	P10011 007	100s

The shallower Victory Formation (Santonian) bulk sample yielded a median common lead corrected U-Pb Age of 527Ma; the pooled UFT Age is ~220Ma. The bulk sample has a Mean track length of $11.28 \pm 1.63 \mu\text{m}$ with a median Dpar of $1.83 \mu\text{m}$ and a median $R_{\text{mr}0}$ of 0.8031. Three apatite sub-populations are recognised based on U-Pb ages and REE chemistry in this sample:

- Sub-Group 1A:
 - Median U-Pb Age: 536.0 Ma
 - Best fit model - Oldest UFT Age: Pop1: 452.0Ma. Pop2: 306.0Ma. Pop3: 498Ma
 - Pooled UFT Age: 218.0 Ma
 - Mean track length: $11.37 \pm 1.68 \mu\text{m}$
 - Median Dpar: $1.85 \mu\text{m}$
 - Median $R_{\text{mr}0}$: 0.7950
- Sub-Group 1B:
 - Median U-Pb Age: 500.0 Ma
 - Best fit model - Oldest UFT Age: Pop1: 404.0Ma. Pop2: 522.0Ma. Pop3: 332Ma
 - Pooled UFT Age: 225.0 Ma
 - Mean track length: $11.09 \pm 1.5 \mu\text{m}$
 - Median Dpar: $1.76 \mu\text{m}$
 - Median $r_{\text{mr}0}$: 0.8241
- Sub-Group 2
 - Median U-Pb Age: 1472Ma
 - Best fit model - Oldest UFT Age: Pop1: 171.0 Ma. Pop2: 511.0 Ma
 - Pooled UFT Age: 217.0 Ma
 - Mean track length: $11.09 \pm 1.5 \mu\text{m}$
 - Median Dpar: $1.68 \mu\text{m}$
 - Median $R_{\text{mr}0}$: 0.8286

The deeper Victory Formation (Hauterivian-Barremian) bulk sample yielded a median common lead corrected U-Pb Age of 553Ma; the pooled UFT Age is ~168Ma. The bulk sample has a Mean track length of $10.94 \pm 1.67 \mu\text{m}$ with a median Dpar of $1.85 \mu\text{m}$ and a median $R_{\text{mr}0}$ of 0.8202. Three apatite sub-populations are recognised based on U-Pb ages and REE chemistry in this sample:

- Sub-Group 1A:
 - Median U-Pb Age: 546.0 Ma
 - Best fit model - Oldest UFT Age: Pop1: 481.0 Ma. Pop2: 399.0 Ma
 - Pooled UFT Age: 174.0 Ma
 - Mean track length: $11.08 \pm 1.81 \mu\text{m}$
 - Median Dpar: $1.81 \mu\text{m}$
 - Median $R_{\text{mr}0}$: 0.8205
- Sub-Group 1B:
 - Median U-Pb Age: 482.0 Ma

- Best fit model - Oldest UFT Age: Pop2: 263.0 Ma. Pop3: 375.0Ma
- Pooled UFT Age: 152.0 Ma
- Mean track length: $10.67 \pm 1.37 \mu\text{m}$
- Median Dpar: 2.0 μm
- Median $R_{\text{mr}0}$: 0.7971
- Sub-Group 2
 - Median U-Pb Age: 1179.0 Ma
 - Best fit model - Oldest UFT Age: Pop1: 445.0 Ma
 - Pooled UFT Age: 197.0 Ma
 - Mean track length: $11.38 \pm 1.53 \mu\text{m}$
 - Median Dpar: 2.0 μm
 - Median $R_{\text{mr}0}$: 0.8024

The UFT ages for the Paleocene sample indicate a provenance signature i.e. the apatite in the sample cooled below the apatite closure temperature (120°C) prior to its deposition and have not since been heated above this temperature. The U-Pb ages from the shallower (Lower Santonian) sample are consistent with an Acadian-Variscan (~250-400Ma) age; however, the deeper Hauterivian-Barremian sample have a younger age range of 152-197Ma. This may record unroofing associated with flank uplift during Mesozoic rifting? The U-Pb ages cover all the sub-groups bar sub-group zero (the youngest aged apatite) identified in this study, and may be related to source terranes from:

- Sub-group 1A-B: 482-546Ma ~Caledonian
- Sub-group 2: 1179-1472Ma ~Grenvillian to Laxfordian (800 – 1700Ma)

Provenance is further discussed in Appendix 4.

The time-temperature constraints for the FT³ thermal modelling are summarised below:

Well	Sample ID.	Initial		Deposition		Peak Burial		Present Day	
		Age (Ma)	Temp (°C)	Age (Ma)	Temp (°C)	Age (Ma)	Temp (°C)	Age (Ma)	Temp (°C)
208/24-1A 5900.0-6000.0ft	P10011_006	600.0	199.0-200.0	83.6-86.3	0.0-20.0	10.0-65.0	30.6-122.1	0.0	50.6-62.1
208/24-1A 6230.0-6300.0ft	P10011_007	600.0	199.0-200.0	125.0-129.4	0.0-20.0	10.0-65.0	33.1-125.3	0.0	53.1-65.3

A plot showing the integration of sample age, temperature and mean apatite fission track length is shown in Figure 4.2.10. The time-temperature history for the 208/24-1A samples is shown in Figures 4.3.15, 4.3.16 & 4.3.17. The thermal history implications from the time-temperature (tT) modelling of the 208/24-1A apatite data are summarised in the table below:

Well	Sample ID.	Peak Burial Time t (Ma)	Peak Burial Temp T (°C)	Temp at 1 Ma (°C)	Temp at 5 Ma (°C)	Temp at 10 Ma (°C)	Temp at 25 Ma (°C)	Temp at 50 Ma (°C)
208/24-1A 5900.0-6000.0ft	P10011_006	36.5	76.4	57.6	60.0	62.6	67.9	61.7
208/24-1A 6230.0-6300.0ft	P10011_007	56.0	76.1	58.0	58.8	60.2	64.1	73.2

A vitrinite reflectivity equivalent of 0.43-0.48% Ro is given for the Victory sample
A vitrinite reflectivity equivalent of 0.44-0.50% Ro is given for the Victory sample

For the Victory (Santonian) sample, the tT modelling in terms of the average of the acceptable tT paths indicates that the timing of peak temperature is moderately constrained, with an estimate of 36.5 ± 30 Ma (i.e. maximum temperature could have occurred from 66 – 6 Ma within 2sigma). The magnitude of the peak temperature has greater constraint at $\sim 76 \pm 8^\circ\text{C}$. The reported best fit model (based of GOF) estimates a peak temperature of $\sim 88^\circ\text{C}$ at 1 Ma. Both the averaged result and the best-fit model have temperatures that are marginally hotter than the present-day measured temperature ($\sim 73^\circ\text{C}$) to which the 1D Genesis model is calibrated (cf. Figure 4.3.15).

For the Victory (Hauterivian-Barremian) sample, the tT modelling in terms of the average of the acceptable tT paths indicates that the timing of peak temperature is accurately constrained, with an estimate of 1 ± 2.7 Ma (i.e. maximum temperature could have occurred from 3.7 – 1 Ma within 2sigma). The magnitude of the peak temperature has greater constraint at $\sim 75 \pm 10^\circ\text{C}$. The reported best fit model (based of GOF) estimates a peak temperature of $\sim 73^\circ\text{C}$ at 1 Ma.

The correspondence between the measured vitrinite reflectivity and the modelled reflectivity from the apatite thermochronology is very good (Figure 5.2.10); integration with and 1D basin modelling and expulsion timing is considered further in Chapter 6.

4.3.5.3 Data and discussion for well 208/27-2

Three ditch cuttings samples were collected and analysed from the Cretaceous and Basement interval penetrated in 208/27-2 well. Sample details are given in the table below.

Well	Top Depth	Bottom Depth	Units (m/ft)	Stratigraphy	Age	Sample Type	Sample ID.	Apatite Grains
208/27-2	3960.0	3990.0	ft	Shetland	K2	DC	P10011 009	10s
	-	4540.0		PrCam Basemnt	PrCam	DC	P10011 011	1000s
	4300.0	4590.0		Caved Shetland	K2	DC	P10011 013	100s

The Shetland Group (Campanian) bulk sample yielded a median common lead corrected U-Pb Age of 1276 Ma; the pooled UFT Age is ~ 189 Ma. The bulk sample has a Mean track length of $13.48 \pm 1.59 \mu\text{m}$ with a median Dpar of $1.82 \mu\text{m}$ and a median $R_{\text{mr}0}$ of 0.8083. Two apatite sub-populations are recognised based on U-Pb ages and REE chemistry in this sample:

- Sub-Group 1
 - Median U-Pb Age: 566.0 Ma
 - Best fit model - Oldest UFT Age: -
 - Pooled UFT Age: 285.0 Ma
 - Mean track length: -
 - Median Dpar: $1.77 \mu\text{m}$
 - Median $R_{\text{mr}0}$: 0.81
- Sub-Group 2
 - Median U-Pb Age: 1441.0 Ma
 - Best fit model - Oldest UFT Age: Pop2: 186.0 Ma
 - Pooled UFT Age: 168.0 Ma
 - Mean track length: $13.48 \pm 1.59 \mu\text{m}$
 - Median Dpar: $1.81 \mu\text{m}$
 - Median $R_{\text{mr}0}$: 0.8078

The Precambrian Basement bulk sample yielded a median common lead corrected U-Pb Age of 1558Ma; the pooled UFT Age is ~203Ma. The bulk sample has a Mean track length of $12.61 \pm 1.46 \mu\text{m}$ with a median Dpar of $1.75 \mu\text{m}$ and a median $R_{\text{mr}0}$ of 0.8202. Three apatite sub-populations are recognised based on U-Pb ages and REE chemistry in this sample:

- Sub-Group 1
 - Median U-Pb Age: 567.0 Ma
 - Best fit model - Oldest UFT Age: -
 - Pooled UFT Age: 270.0 Ma
 - Mean track length: -
 - Median Dpar: $1.62 \mu\text{m}$
 - Median $R_{\text{mr}0}$: 0.8110
- Sub-Group 2A
 - Median U-Pb Age: 1558.0 Ma
 - Best fit model - Oldest UFT Age: Pop1: 393.0Ma. Pop2: 268.0Ma, Pop3: 348Ma
 - Pooled UFT Age: 211.0 Ma
 - Mean track length: $12.7 \pm 1.49 \mu\text{m}$
 - Median Dpar: $1.83 \mu\text{m}$
 - Median $R_{\text{mr}0}$: 0.8283
- Sub-Group 2B
 - Median U-Pb Age: 1558.0 Ma
 - Best fit model - Oldest UFT Age: Pop1: 240.0 Ma
 - Pooled UFT Age: 181.0 Ma
 - Mean track length: $12.02 \pm 1.1 \mu\text{m}$
 - Median Dpar: $1.64 \mu\text{m}$
 - Median $R_{\text{mr}0}$: 0.8477

The caved Shetland Group (Campanian) bulk sample yielded a median common lead corrected U-Pb Age of 1517Ma; the pooled UFT Age is ~197Ma. The bulk sample has a Mean track length of $12.48 \pm 1.67 \mu\text{m}$ with a median Dpar of $1.85 \mu\text{m}$ and a median $R_{\text{mr}0}$ of 0.7992. Three apatite sub-populations are recognised based on U-Pb ages and REE chemistry in this sample:

- Sub-Group 1
 - Median U-Pb Age: 705.0 Ma
 - Best fit model - Oldest UFT Age: -
 - Pooled UFT Age: 144.0 Ma
 - Mean track length: $12.64 \pm 0.8 \mu\text{m}$
 - Median Dpar: $2.0 \mu\text{m}$
 - Median $R_{\text{mr}0}$: 0.7853
- Sub-Group 2A
 - Median U-Pb Age: 1546.0 Ma
 - Best fit model - Oldest UFT Age: Pop1: 382.0Ma. Pop2: 211.0Ma, Pop3: 494Ma
 - Pooled UFT Age: 211.0 Ma
 - Mean track length: $12.46 \pm 1.7 \mu\text{m}$
 - Median Dpar: $1.83 \mu\text{m}$
 - Median $R_{\text{mr}0}$: 0.7947

- Sub-Group 2B
 - Median U-Pb Age: 1538.0 Ma
 - Best fit model - Oldest UFT Age: Pop1: 330.0 Ma. Pop2: 370.0 Ma
 - Pooled UFT Age: 184.0 Ma
 - Mean track length: $12.63 \pm 1.63 \mu\text{m}$
 - Median Dpar: $1.82 \mu\text{m}$
 - Median R_{mro} : 0.8241

The UFT ages for all the samples analysed indicate a provenance signature i.e. the apatite in the sample cooled below the apatite closure temperature (120°C) prior to its deposition and have not since been heated above this temperature. Most of the U-Pb ages are consistent either with a Caledonian or Grenvillian-Laxfordian age:

- Sub-group 1A-B: 566-705Ma ~Caledonian
- Sub-group 2A/B: 1441 - 1558Ma ~Grenvillian to Laxfordian (800 – 1700Ma)

Provenance is further discussed in Appendix 4.

The time-temperature constraints for the FT³ thermal modelling are summarised below:

Well	Sample ID.	Initial		Deposition		Peak Burial		Present Day	
		Age (Ma)	Temp ($^\circ\text{C}$)	Age (Ma)	Temp ($^\circ\text{C}$)	Age (Ma)	Temp ($^\circ\text{C}$)	Age (Ma)	Temp ($^\circ\text{C}$)
208/27-2 3960.0-3990.0ft	P10011_009	600.0	199.0-200.0	72.1-83.6	0.0-20.0	10.0-65.0	14.0-101.0	0.0	34.0-41.0
208/27-2 4540.0ft	P10011_011	600.0	199.0-200.0	72.1-83.6	5.6-25.6	10.0-65.0	18.4-106.6	0.0	38.4-46.6
208/27-2 4300.0-4590.0ft	P10011_013	600.0	199.0-200.0	72.1-83.6	0.0-20.0	10.0-65.0	17.7-105.7	0.0	37.7-45.7

A plot showing the integration of sample age, temperature and mean apatite fission track length is shown in Figure 4.2.11. The time-temperature histories for the 208/27-2 samples is shown in Figures 4.3.18, 4.3.19 & 4.3.20. The thermal history implications from the time-temperature (tT) modelling of the 208/17-2 apatite data are summarised in the table below:

Well	Sample ID.	Peak Burial Time t (Ma)	Peak Burial Temp T ($^\circ\text{C}$)	Temp at 1 Ma ($^\circ\text{C}$)	Temp at 5 Ma ($^\circ\text{C}$)	Temp at 10 Ma ($^\circ\text{C}$)	Temp at 25 Ma ($^\circ\text{C}$)	Temp at 50 Ma ($^\circ\text{C}$)
208/27-2 3960.0-3990.0ft	P10011_009	29.5	66.0	38.3	39.5	41.8	50.0	44.6
208/27-2 4540.0ft	P10011_011	41.0	56.3	42.8	44.5	46.2	50.4	49.1
208/27-2 4300.0-4590.0ft	P10011_013	42.0	61.2	42.0	43.7	45.9	52.8	51.7

A vitrinite reflectivity equivalent of 0.38-0.42% Ro is given for the Shetland sample

A vitrinite reflectivity equivalent of 0.35-0.39% Ro is given for the Precambrian Basement sample

A vitrinite reflectivity equivalent of 0.37-0.42% Ro is given for the Caved Shetland sample

For The Shetland Group (Campanian) sample, the tT modelling in terms of the average of the acceptable tT paths indicates that the timing of peak temperature is relatively poorly constrained, with an estimate of $29.5 \pm 43.13\text{Ma}$ (i.e. maximum temperature could have occurred from $\sim 73 - 0\text{Ma}$ within 2sigma). The magnitude of the peak temperature has is also poorly

constrained at $\sim 66 \pm 43^\circ\text{C}$. The reported best fit model (based of GOF) is cooler but still within the range of uncertainty with an estimate of a peak temp of $\sim 38^\circ\text{C}$ at 29Ma. Taking the average of the acceptable path temperatures ($\sim 66^\circ\text{C}$) does suggest hotter temperatures in the past relative to the present-day temperature $\sim 50^\circ\text{C}$; if valid, it is plausible that the heating recorded is reflecting the movement of hot fluids (cf. Parnell *et al.*, 1999, 2005; Baron *et al.* 2008).

For the Precambrian Basement sample, the tT modelling in terms of the average of the acceptable tT paths indicates that the timing of peak temperature is also relatively poorly constrained, with an estimate of $41 \pm 32\text{Ma}$ (i.e. maximum temperature could have occurred from $\sim 73 - 9\text{Ma}$ within 2sigma). The magnitude of the peak temperature has is also more tightly constrained at $\sim 56 \pm 8^\circ\text{C}$ and corresponds much more closely with the measured temperature present-day. The reported best fit model (based of GOF) is in range of uncertainty with an estimate of a peak temp of $\sim 56^\circ\text{C}$ at 44Ma.

Similarly, for the caved Shetland Group sample, the tT modelling, in terms of the average of the acceptable tT paths indicates that the timing of peak temperature is again poorly constrained, with an estimate of $42 \pm 32\text{Ma}$ (i.e. maximum temperature could have occurred from $\sim 74 - 10\text{Ma}$ within 2sigma). The magnitude of the peak temperature has is also better constrained at $\sim 61 \pm 13^\circ\text{C}$ and corresponds much more closely with the measured temperature present-day. The reported best fit model (based of GOF) is in range of uncertainty with an estimate of a peak temp of $\sim 61^\circ\text{C}$ at 51Ma.

The correspondence between the measured vitrinite reflectivity and the modelled reflectivity from the apatite thermochronology is relatively poor and suggests that the legacy vitrinite reflectivity trend has not been picked on indigenous vitrinite leading to an overestimation of maturity (Figure 5.2.11); integration with and 1D basin modelling and expulsion timing is considered further in Chapter 6.

4.3.6 Quad 214 wells

4.3.6.1 Data and discussion for well 214/26-1

A single ditch cuttings sample was collected and analysed from the Eocene interval penetrated in the 214/26-1 well. Sample details are given in the table below.

Well	Top Depth	Bottom Depth	Units (m/ft)	Stratigraphy	Age	Sample Type	Sample ID.	Apatite Grains
214/26-1	7516.0	7539.0	ft	Lewis Fan	E2	DC	P10012_009	10s

The bulk sample (P10012_009) yields a median common lead corrected U-Pb Age of 1620Ma; the pooled UFT Age is ~232Ma. The bulk sample has a Mean track length of $11.28 \pm 1.8 \mu\text{m}$ with a median Dpar of $1.73 \mu\text{m}$ and a median $R_{\text{mr}0}$ of 0.8467. Four apatite sub-populations are recognised based on U-Pb ages and REE chemistry in this sample:

- Sub-Group 1
 - Median U-Pb Age: 362.0 Ma
 - Best fit model - Oldest UFT Age: Pop1: 322.0 Ma. Pop2: 284.0 Ma
 - Pooled UFT Age: 202.0 Ma
 - Mean track length: $11.89 \pm 1.32 \mu\text{m}$
 - Median Dpar: $1.72 \mu\text{m}$
 - Median $R_{\text{mr}0}$: 0.8356
- Sub-Group 2A
 - Median U-Pb Age: 1193.5 Ma
 - Best fit model - Oldest UFT Age: Pop1: 337.0 Ma
 - Pooled UFT Age: 221.0 Ma
 - Mean track length: $13.38 \pm 0.65 \mu\text{m}$
 - Median Dpar: $1.78 \mu\text{m}$
 - Median $R_{\text{mr}0}$: 0.8363
- Sub-Group 2B
 - Median U-Pb Age: 1782.0 Ma
 - Best fit model - Oldest UFT Age: Pop1: 481.0 Ma. Pop2: 355.0 Ma
 - Pooled UFT Age: 291.0 Ma
 - Mean track length: $11.94 \pm 1.1 \mu\text{m}$
 - Median Dpar: $1.94 \mu\text{m}$
 - Median $R_{\text{mr}0}$: 0.842
- Sub-Group 2C
 - Median U-Pb Age: 1679.0 Ma
 - Best fit model - Oldest UFT Age: Pop1: 360.0Ma. Pop2: 226.0 Ma
 - Pooled UFT Age: 211.0 Ma
 - Mean track length: $10.37 \pm 1.95 \mu\text{m}$
 - Median Dpar: $1.67 \mu\text{m}$
 - Median $R_{\text{mr}0}$: 0.8525

The UFT ages for all the samples analysed indicate a provenance signature i.e. the apatite in the sample cooled below the apatite closure temperature (120°C) prior to its deposition and have not since been heated above this temperature.

The recorded U-Pb ages (which reflect of cooling below ~450–550°C (cf. Chamberlain & Bowring 2000 and Schoene & Bowring 2007)) cover a wide range of ages indicative of a heterogeneous sediment source(s) and may indicate sediment sourced from the following terrane groups:

- Sub-group 1: ~362Ma ~Acadian-Variscan (*sensu* Mendum, BGS)
- Sub-group 2A: 1194Ma ~ Grenvillian? (Park *et al.* 2003)
- Sub-group 2B-C: 1679-1782Ma ~ Laxfordian (800 – 1900Ma)

Provenance is further discussed in Appendix 4.

The time-temperature constraints for the FT³ thermal modelling are summarised below:

Well	Sample ID.	Initial		Deposition		Peak Burial		Present Day	
		Age (Ma)	Temp (°C)	Age (Ma)	Temp (°C)	Age (Ma)	Temp (°C)	Age (Ma)	Temp (°C)
214/26-1 7516.0-7539.0ft	P10012_009	600.0	199.0-200.0	56.0-59.2	0.0-20.0	10.0-55.0	36.2-129.2	0.0	56.2-69.2

A plot showing the integration of sample age, temperature and mean apatite fission track length is shown in Figure 4.2.12. The time-temperature history for the 214/26-1 sample is shown in Figure 4.3.21. The thermal history implications from the time-temperature (tT) modelling of the 214/26-1 apatite data are summarised in the table below:

Well	Sample ID.	Peak Burial Time t (Ma)	Peak Burial Temp T (°C)	Temp at 1 Ma (°C)	Temp at 5 Ma (°C)	Temp at 10 Ma (°C)	Temp at 25 Ma (°C)	Temp at 50 Ma (°C)
214/26-1 7516.0-7539.0ft	P10012_009	1.0	65.7	63.5	63.3	63.1	60.4	30.1

A vitrinite reflectivity equivalent of 0.39-0.43% Ro is given for the Lewis Fan sample

The modelled temperature history for both samples is consistent with progressive heating throughout the Tertiary; although the agreement with the Genesis model is only modest (cf. Figure 4.3.21). The tT modelling in terms of the average of the acceptable tT paths indicates that the timing of peak temperature is relatively poorly constrained, with an estimate of 18±38Ma (i.e. maximum temperature could have occurred from ~56 – 0Ma within 2sigma). The magnitude of the peak temperature has is better constrained at ~67±12°C which is hotter than the estimated present-day temperature of 49°C. The reported best fit model (based of GOF) is cooler but still within the range of uncertainty with an estimate of a peak temp of ~68°C at 33Ma.

The data suggests that the sample was hotter in the past than present day, albeit it has always been wholly within the PAZ. The hotter paleotemperatures would most likely correspond with burial prior to Late Tertiary uplift (cf. Tassone *et al.* 2014) or it is plausible that the heating recorded is reflecting the movement of hot fluids (cf. Parnell *et al.*, 1999, 2005; Baron *et al.* 2008).

Integration of the 214/26-1 apatite thermochronology data together with the legacy % Ro thermal calibration data is shown in Figure 5.2.13 and are in good agreement. Note: there are some apparently local high maturity values that would appear to be related to intrusives; however, none are reported on the comp log. They are deemed to be of only local significance

since the maturity depth-trend appears to be unaffected. Integration with and 1D basin modelling and expulsion timing is considered further in Chapter 6.

4.3.6.2 Data and discussion for well 214/28-1

Two core and 1 ditch cuttings samples were collected and analysed from the Paleocene interval penetrated in the 214/28-1 well. Sample details are given in the table below.

Well	Top Depth	Bottom Depth	Units (m/ft)	Stratigraphy	Age	Sample Type	Sample ID.	Apatite Grains
214/28-1	-	8374.3	ft	Late Paleocene	P3	COCH	P10012 010	100s
	11900.0	11920.0		Middle Paleocene	P2	DC	P10012 011	100s
	14310.0	14334.4		Early-Middle Pal	P1	COCH	P10012 012	100s

The Late Paleocene bulk sample yielded a median common lead corrected U-Pb Age of 582Ma with a pooled UFT Age of ~165Ma. The bulk sample has a Mean track length of $11.08 \pm 1.52 \mu\text{m}$ with a median Dpar of $1.88 \mu\text{m}$ and a median $R_{\text{mr}0}$ of 0.8391. Three apatite sub-populations are recognised based on U-Pb ages and REE chemistry in this sample:

- Sub-Group 1A
 - Median U-Pb Age: 453.0 Ma
 - Best fit model - Oldest UFT Age: Pop1: 382.0 Ma
 - Pooled UFT Age: 226.0 Ma
 - Mean track length: $11.07 \pm 1.68 \mu\text{m}$
 - Median Dpar: $1.91 \mu\text{m}$
 - Median $R_{\text{mr}0}$: 0.8351
- Sub-Group 1B
 - Median U-Pb Age: 515.0 Ma
 - Best fit model - Oldest UFT Age: Pop1: 255.0 Ma. Pop2: 133.0 Ma
 - Pooled UFT Age: 137.0 Ma
 - Mean track length: $11.23 \pm 1.48 \mu\text{m}$
 - Median Dpar: $1.87 \mu\text{m}$
 - Median $R_{\text{mr}0}$: 0.8462
- Sub-Group 2
 - Median U-Pb Age: 1707.0 Ma
 - Best fit model - Oldest UFT Age: Pop1: 302.0Ma. Pop2: 568.0Ma. Pop3: 487Ma
 - Pooled UFT Age: 177.0 Ma
 - Mean track length: $10.87 \pm 1.34 \mu\text{m}$
 - Median Dpar: $1.85 \mu\text{m}$
 - Median $R_{\text{mr}0}$: 0.8391

The UFT ages for the Upper Paleocene sample analysed indicate a provenance signature i.e. the apatite in the sample cooled below the apatite closure temperature (120°C) prior to its deposition and have not since been heated above this temperature.

The Middle Paleocene bulk sample yielded a median common lead corrected U-Pb Age of 798Ma with a pooled UFT Age of ~4Ma. The bulk sample has a Mean track length of

7.75±1.92µm with a median Dpar of 1.69µm and a median R_{mr0} of 0.8327. Four apatite sub-populations are recognised based on U-Pb ages and REE chemistry in this sample:

- Sub-Group 0
 - Median U-Pb Age: 151.0 Ma
 - Best fit model - Oldest UFT Age: -
 - Pooled UFT Age: 13.8 Ma
 - Mean track length: -
 - Median Dpar: 1.49 µm
 - Median R_{mr0} : 0.7838
- Sub-Group 1
 - Median U-Pb Age: 554.0 Ma
 - Best fit model - Oldest UFT Age: Pop1: 7.0 Ma. Pop2: 10.0 Ma. Pop3: 22.0 Ma
 - Pooled UFT Age: 4.38 Ma
 - Mean track length: 11.23±1.48µm
 - Median Dpar: 1.69 µm
 - Median R_{mr0} : 0.8344
- Sub-Group 2A
 - Median U-Pb Age: 969.0 Ma
 - Best fit model - Oldest UFT Age: Pop1: 7.0 Ma. Pop2: 13.0 Ma. Pop3: 487.0Ma
 - Pooled UFT Age: 6.63 Ma
 - Mean track length: 6.44±0µm
 - Median Dpar: 1.73 µm
 - Median R_{mr0} : 0.8125
- Sub-Group 2B
 - Median U-Pb Age: 1917.0 Ma
 - Best fit model - Oldest UFT Age: Pop1: 8.0 Ma. Pop2: 19.0 Ma
 - Pooled UFT Age: 1.71 Ma
 - Mean track length: -
 - Median Dpar: 1.64 µm
 - Median R_{mr0} : 0.8267

The Early-Middle Paleocene bulk sample yielded a median common lead corrected U-Pb Age of 1815Ma with a pooled UFT Age of ~2Ma. The bulk sample has a Mean track length of 8.05±3.23µm with a median Dpar of 1.81µm and a median R_{mr0} of 0.8246. Five apatite sub-populations are recognised based on U-Pb ages and REE chemistry in this sample:

- Sub-Group 0
 - Median U-Pb Age: 161.0 Ma
 - Best fit model - Oldest UFT Age: -
 - Pooled UFT Age: 51.9 Ma
 - Mean track length: 6.42±0.00µm
 - Median Dpar: 2.56 µm
 - Median R_{mr0} : 0.8320
- Sub-Group 1
 - Median U-Pb Age: 534.0 Ma

- Best fit model - Oldest UFT Age: Pop1: 7.0 Ma. Pop2: 10.0 Ma. Pop3: 22.0 Ma
- Pooled UFT Age: 0.38 Ma
- Mean track length: -
- Median Dpar: 1.54 μm
- Median R_{mr0} : 0.7931
- Sub-Group 2
 - Median U-Pb Age: 1599.0 Ma
 - Best fit model - Oldest UFT Age: Pop1: 7.0 Ma, Pop2: 13.0 Ma; Pop3: 487.0Ma
 - Pooled UFT Age: 0.0 Ma
 - Mean track length: $7.44 \pm 5.06 \mu\text{m}$
 - Median Dpar: 1.58 μm
 - Median R_{mr0} : 0.8267
- Sub-Group 3A
 - Median U-Pb Age: 2249.0 Ma
 - Best fit model - Oldest UFT Age: Pop1: 8.0 Ma. Pop2: 19.0 Ma
 - Pooled UFT Age: 0.0 Ma
 - Mean track length: $6.04 \pm 0 \mu\text{m}$
 - Median Dpar: 1.72 μm
 - Median R_{mr0} : 0.8246
- Sub-Group 3B
 - Median U-Pb Age: 1981.0 Ma
 - Best fit model - Oldest UFT Age: Pop1: 8.0 Ma. Pop2: 19.0 Ma
 - Pooled UFT Age: 1.03 Ma
 - Mean track length: $10.48 \pm 2.7 \mu\text{m}$
 - Median Dpar: 1.9 μm
 - Median R_{mr0} : 0.7882

The UFT ages for the Middle Paleocene & lower-Middle Paleocene samples analysed indicate a that the samples have passed the through the PAZ in the geologically recent past (i.e. the samples are at or close to maximum burial present-day).

The U-Pb ages cover a very wide range and indicate that sediment sourcing to the Paleocene section at the 214/28-1 was from a diverse set of sources. The U-Pb ages for the two samples both incorporate a wide range of ages of cooling below $\sim 450\text{--}550^\circ\text{C}$ (cf. Chamberlain & Bowring 2000 and Schoene & Bowring 2007, for U-Pb closure temperatures) which may indicate sediment sourced from the following terrane groups:

Sub-group 0: 151 - 178Ma These Mesozoic ages are some of the youngest recorded. This period is known as a phase of extensional activity, however, local foot-wall related uplift and denudation is thought to involve insufficient cooling i.e. this is process will not involve rocks buried to the U-Pb closure temperature, exhume them and re-sediment them, so this must presumably relate to the continued denudation of the source terrane.

- Sub-group 1: 453-554Ma \sim Caledonian
- Sub-group 2A: 969Ma \sim Grenvillian (1000Ma) (Middle Paleocene sample only)
- Sub-group 2 – 2B: 1599-1707-1917Ma \sim Laxfordian
- Sub-group 3A: \sim 2267Ma \sim NeoArchean Lewisian (2000 –2800Ma)

- Sub-group 3B: ~1981Ma ~NeoArchean Lewisian with Laxfordian overprint? (lower-Middle Paleocene sample only)

Provenance is further discussed in Appendix 4.

The time-temperature constraints for the FT³ thermal modelling are summarised below:

Well	Sample ID.	Initial		Deposition		Peak Burial		Present Day	
		Age (Ma)	Temp (°C)	Age (Ma)	Temp (°C)	Age (Ma)	Temp (°C)	Age (Ma)	Temp (°C)
214/28-1 8374.3ft	P10012_010	600.0	199.0-200.0	56.0-59.2	0.0-20.0	10.0-55.0	37.4-130.7	0.0	57.4-70.7
214/28-1 11900.0-11920.0ft	P10012_011	600.0	199.0-200.0	59.2-61.6	0.0-20.0	10.0-55.0	65.4-166.2	0.0	85.4-106.2
214/28-1 14310.0-14334.4ft	P10012_012	600.0	199.0-200.0	59.2-66.0	0.0-20.0	10.0-55.0	80.0-190.5	0.0	100.0-130.5

A plot showing the integration of sample age, temperature and mean apatite fission track length is shown in Figure 4.2.13. The time-temperature histories for the 214/28-1 samples are shown in Figures 4.3.22 to 4.3.25. The thermal history implications from the time-temperature (tT) modelling of the 214/28-1 apatite data are summarised in the table below:

Well	Sample ID.	Peak Burial Time t (Ma)	Peak Burial Temp T (°C)	Temp at 1 Ma (°C)	Temp at 5 Ma (°C)	Temp at 10 Ma (°C)	Temp at 25 Ma (°C)	Temp at 50 Ma (°C)
214/28-1 8374.3ft	P10012_010	22.0	70.0	64.9	65.9	66.3	65.7	35.9
214/28-1 11900.0-11920.0ft	P10012_011	25.0	≥133.0	99.2	407.3	119.1	129.7	65.0
214/28-1 14310.0-14334.4ft	P10012_012	18.0	≥133.3	120.2	125.7	127.9	141.8	87.7

A vitrinite reflectivity equivalent of 0.41-0.45% Ro is given for the Late Paleocene sample

A vitrinite reflectivity equivalent of 0.69-≥0.89% Ro is given for the Middle Paleocene sample

A vitrinite reflectivity equivalent of 0.69-≥0.89% Ro is given for the Early-Middle Paleocene sample

The modelled temperature history for the Late Paleocene sample is consistent with progressive heating throughout the Tertiary; although the agreement with the Genesis model is only modest (cf. Figure 4.3.22). The tT modelling in terms of the average of the acceptable tT paths indicates that the timing of peak temperature is relatively poorly constrained, with an estimate of 22±36Ma (i.e. maximum temperature could have occurred from ~58 – 0Ma within 2sigma). The magnitude of the peak temperature has is more tightly constrained at ~70±8°C. The reported best fit model (based of GOF) is hotter with an estimate of a peak temp of ~74°C at 44Ma and sits outside of the acceptable paths plotted from FT³. In this sample the model results are cooler than the estimated present-day temperature of ~77°C. Since the sample is a core this discrepancy cannot be ascribed to the impact of caving. The cause of the different remains uncertain, however since the modelled values uncertainty bounds largely overlap with the estimated present-day temperature it is not viewed as overly detrimental.

For the Middle Paleocene sample the agreement with the Genesis model is improved compared with the shallow sample (cf. Figure 4.3.22 & 23). The tT modelling in terms of the average of the acceptable tT paths indicates that the timing of peak temperature is only modestly constrained, with an estimate of 25±21Ma (i.e. maximum temperature could have occurred

from $\sim 46 - 4\text{Ma}$ within 2sigma). The magnitude of the peak temperature has is more tightly constrained at $\sim \geq 133 \pm 4^\circ\text{C}$. For this sample individual sub-groups had distinct best fit models (based of GOF):

- Sub-Group 1 population 1 $\sim 144^\circ\text{C}$ at 7Ma. (Surface fission track (SFT) GOF=0.42; Confined fission track (CFT) GOF = n/a – no confined tracks present.)
- Sub-Group 1 population 2 $\sim 131^\circ\text{C}$ at 10Ma. (SFT GOF = 0.97; CFT GOF = n/a – no confined tracks present.)
- Sub-Group 1 population 3 $\sim 157^\circ\text{C}$ at 22Ma. (SFT GOF = 0.42; CFT GOF = n/a – no confined tracks present.)
- Sub-Group 2A population 1 $\sim 114^\circ\text{C}$ at 7Ma. (SFT GOF = 0.85; CFT GOF = n/a – no confined tracks present.)
- Sub-Group 2A population 1 $\sim 134^\circ\text{C}$ at 13Ma. (SFT GOF = 0.21; CFT GOF = 0.92)
- Sub-Group 2B population 1 $\sim 123^\circ\text{C}$ at 8Ma. (SFT GOF = 0.62; CFT GOF = n/a – no confined tracks present.)
- Sub-Group 2B population 2 $\sim 156^\circ\text{C}$ at 19Ma. (SFT GOF = 0.92; CFT GOF = n/a – no confined tracks present.)

For the Early-Middle Paleocene sample the agreement with the Genesis model is reasonable (cf. Figure 4.3.24). The tT modelling in terms of the average of the acceptable tT paths indicates that the timing of peak temperature is again only modestly constrained, with an estimate of $18 \pm 23\text{Ma}$ (i.e. maximum temperature could have occurred from $\sim 41 - 0\text{Ma}$ within 2sigma). The magnitude of the peak temperature has is estimated to be $\sim \geq 133 \pm 8^\circ\text{C}$. For this sample individual sub-groups had distinct best fit models:

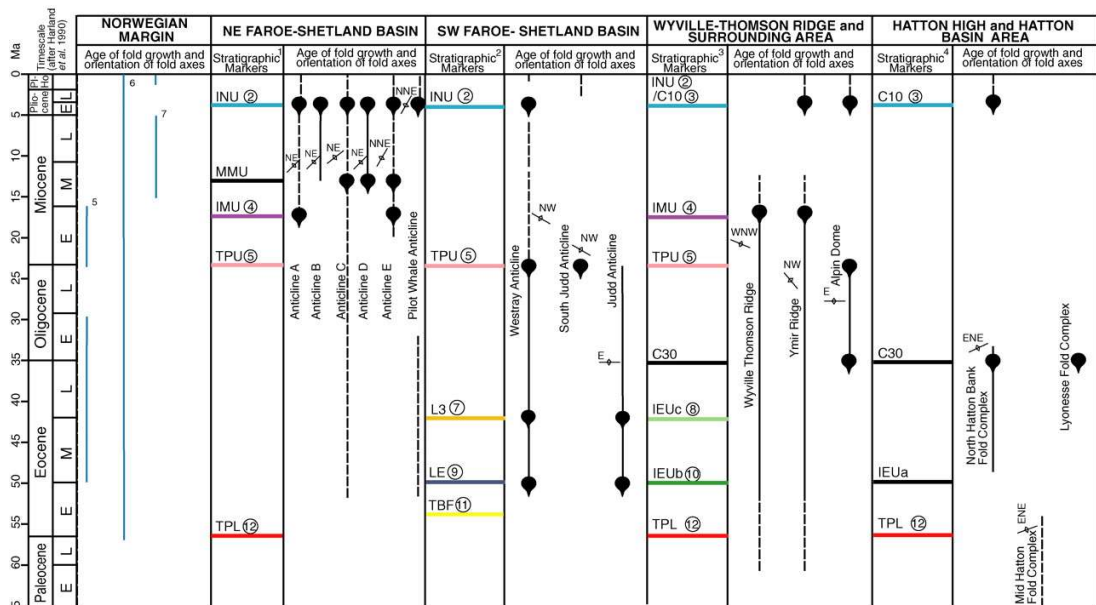
- Sub-Group 0 population 1 $\sim 117^\circ\text{C}$ at 2Ma. (SFT GOF=0.97; CFT GOF = 0.99)
- Sub-Group 1 population 1 $\sim 117^\circ\text{C}$ at 2Ma. (SFT GOF = 0.53; CFT GOF = n/a – no confined tracks present.)
- Sub-Group 1 population 2 $\sim 159^\circ\text{C}$ at 7Ma. (SFT GOF = 0.65; CFT GOF = n/a – no confined tracks present.)
- Sub-Group 2 population 1 $\sim 117^\circ\text{C}$ at 2Ma. (SFT GOF = 0.88; CFT GOF = 0.99)
- Sub-Group 2 population 2 $\sim 137^\circ\text{C}$ at 13Ma. (SFT GOF = 0.82; CFT GOF = 0.94)
- Sub-Group 3A population 1 $\sim 117^\circ\text{C}$ at 2Ma. (SFT GOF = 0.85; CFT GOF 0.99)
- Sub-Group 3A population 2 $\sim 157^\circ\text{C}$ at 6Ma. (SFT GOF = 0.65; CFT GOF = n/a – no confined tracks present.)
- Sub-Group 3B population 1 $\sim 117^\circ\text{C}$ at 2Ma. (SFT GOF = 0.53; CFT GOF = n/a – no confined tracks present.)
- Sub-Group 3B population 2 $\sim 160^\circ\text{C}$ at 9Ma. (SFT GOF = n/a; CFT GOF = n/a – no confined tracks present.)

Overall, for both the Middle and lower-Middle Paleocene samples, the models with lower temperatures reaching peak temperature at more recent geological times typically have better goodness of fit values. The data suggests that the sample was hotter in the past than present day with the UFT ages generally falling within the age range of burial. This well was included in Tassone *et al.*'s (2014) study of Tertiary exhumation using sediment velocities, which concluded that there was no Tertiary uplift at this well location. If this result is accepted then

the hotter paleotemperatures cannot have been a result of deeper burial. An alternative explanation may be that the structuration associated with the late Tertiary compression may have initiated fluid movement from hotter (more basinal) areas to structurally higher areas.

This well was also analysed by GeoTrack in their GC540 Report (“*West of Shetlands (North): Thermal and tectonic development and hydrocarbon generation history assessed using apatite fission track analysis and vitrinite reflectance. – February 1995*”) which also concluded that the well was at maximum burial present-day but also exhibits the effects of localised heating. The GeoTrack sample was taken from the same section at the Late Paleocene sample (P10012_010) considered here. The apatite thermochronology data was very similar: the Apatite.Inc data has a pooled UFT Age of ~165Ma compared with the GeoTrack AFTA age of 163.6 ± 16.5 Ma. The Apatite.Inc bulk sample has a Mean track length of $11.08 \pm 1.52 \mu\text{m}$ compared the GeoTrack measured mean length of $11.08 \pm 0.14 \mu\text{m}$. The similarity in analytical results is encouraging and demonstrates those differences that exist are in interpretation and not in the fundamental data.

It is plausible that the heating reflects the passage of hot fluids associated with the Icelandic plume (cf. Parnell *et al.*, 1999, 2005; Baron *et al.* 2008); however, the estimated times are significantly younger than the timing of the Icelandic plume event, and would be more consistent temporally with the late Tertiary compressional activity (cf. summary chart below from Ritchie *et al.* 2008).



Summary chart of the timing/duration of Cenozoic fold growth development within the Faroe-Shetland Basin and adjacent areas within the NE Atlantic margin (modified from Ritchie *et al.* 2003 and Johnson *et al.* 2005). Abbreviations: C10, Early Pliocene Unconformity; C30, Late Eocene Unconformity; IEUa, b and c, Intra-Eocene unconformities; IMU, Intra-Miocene Unconformity; INU, Intra-Neogene (Early Pliocene) Unconformity; L3, Mid Eocene (late Lutetian); LE, Early Eocene (latest Ypresian) Unconformity; MMU, Mid Miocene Unconformity; TBF, Top Balder Formation; TPL, Top Palaeogene lavas; TPU, Top Palaeogene Unconformity. From Ritchie *et al.* (2008).

The samples recording the highest temperatures relate to those with the most resistive apatite (lowest r_{mro} values); caution is urged with respect to samples indicated temperatures $>130^\circ\text{C}$ since these would fall outside of what is observed globally for apatite kinetics (R.Donelick, *Pers. Comm.*).

Integration of the 214/28-1 apatite thermochronology data together with the legacy vitrinite reflectivity thermal calibration data is shown in Figure 5.2.14 and are in good agreement, in regard to the BasinRo (Nielsen *et al.*) and the EasyDL kinetics, whereas the EasyRo kinetics would suggest higher maturities than those measured. Integration with and 1D basin modelling and expulsion timing is considered further in Chapter 6.

Well	Top Depth	Bottom Depth	Units (m/ft)	Stratigraphy	Age	Sample Type	Sample ID.	Peak Burial Time t (Ma)	Peak Burial Temp T (°C)	Temp at 1Ma (°C)	Temp at 5Ma (°C)	Temp at 10Ma (°C)	Temp at 25Ma (°C)	Temp at 50Ma (°C)	VR Equiv (%)
204/10a-5	2361.8	2383.5	m	Hildasay	E1	COCH	P10012_013	28.0	52.2	46.8	47.4	47.7	48.5	26.6	0.33-0.38
205/09-1	2798.0	2807.0	m	Sele	E1	DC	P10012_001	1.0	75.9	72.2	71.9	71.8	69.0	32.3	0.43-0.48
	3704.0	3719.0		Lista (D1 Sand)	P3	DC	P10012_002	27.0	≥122.9	97.0	101.0	106.4	116.1	45.9	0.64-≥0.79
205/12-1	-	2570.0	m	Lamba	P3	DC	P10012_003	1.0	65.2	65.2	63.1	60.0	51.3	22.8	0.38-0.42
	-	3175.0		Shetland	K2	DC	P10012_004	1.0	89.2	85.4	85.0	84.2	83.3	79.3	0.50-0.60
205/14-2	-	7430.0	ft	Unit IV Upper	P3	DC	P10012_005	1.0	64.3	63.4	61.5	60.2	52.5	22.1	0.38-0.42
205/17b-2	-	2443.8	m	Lista	P3	COCH	P10012_006	1.0	65.3	65.1	62.1	58.9	47.5	19.2	0.37-0.42
206/11-1	4370.0	4376.0	m	Early Cret Sands	K1	DC	P10012_007	33.0	≥138.7	124.4	126.8	128.7	133.4	133.4	0.72-≥1.01
207/01-2	5590.0	5620.0	ft	Victory	K1	DC	P10011_003	32.0	59.8	54.6	55.4	56.2	57.0	55.0	0.38-0.43
	5740.0	5750.0		PrCam Basement	PrCam	DC	P10011_004	1.0	57.0	56.1	55.3	54.7	52.7	45.9	0.36-0.40
208/17-2	7871.0	7946.8	ft	Waterhouse	P3	COCH	P10012_008	31.0	80.1	64.7	66.8	69.2	73.3	34.2	0.45-0.51
208/24-1A	5900.0	6000.0	ft	Victory	K1	DC	P10011_006	36.5	76.4	57.6	60.0	62.6	67.9	61.7	0.43-0.48
	6230.0	6300.0		Victory	K1	DC	P10011_007	56.0	76.1	58.0	58.8	60.2	64.1	73.2	0.44-0.50
208/27-2	3960.0	3990.0	ft	Shetland	K2	DC	P10011_009	29.5	66.0	38.3	39.5	41.8	50.0	44.6	0.38-0.42
	-	4540.0		PrCam Basement	PrCam	DC	P10011_011	41.0	56.3	42.8	44.5	46.2	50.4	49.1	0.35-0.39
	4300.0	4590.0		Caved Shetland	K2	DC	P10011_013	42.0	61.2	42.0	43.7	45.9	52.8	51.7	0.37-0.42
214/26-1	7516.0	7539.0	ft	Lewis Fan Env	E2	DC	P10012_009	1.0	65.7	63.5	63.3	63.1	60.4	30.1	0.39-0.43
214/28-1	-	8374.3	ft	Late Paleocene	P3	COCH	P10012_010	22.0	70.0	64.9	65.9	66.3	65.7	35.9	0.41-0.45
	11900.0	11920.0		M Paleocene	P2	DC	P10012_011	25.0	≥133.0	99.2	107.3	119.1	129.7	65.0	0.69-≥0.89
	14310.0	14334.4		E-M Paleocene	P1	COCH	P10012_012	18.0	≥133.3	120.2	125.7	127.9	141.8	87.7	0.69-≥0.89

Stratigraphy/Ages

Early Cret Sands: Early Cretaceous Sands

PrCam Basement: Precambrian Basement

Lewis Fan Env: Lewis Fan Envelope (Lobe 2)

M Paleocene: Middle Paleocene

E-M Paleocene: Early-Middle Paleocene

TABLE 4.2.1 Thermal history reconstruction

Well	Top Depth	Bottom Depth	Units (m/ft)	Stratigraphy	Age	Sample Type	Sample ID.	Model Time-Temperature Constraints							
								Initial		Deposition		Maximum Burial		Present Day	
								Age (Ma)	Temp (°C)	Age (Ma)	Temp (°C)	Age (Ma)	Temp (°C)	Age (Ma)	Temp (°C)
204/10a-5	2361.8	2383.5	m	Hildasay	E1	COCH	P10012_013	600.0	199.0-200.0	56.0-59.2	0.0-20.0	10.0-55.0	21.6-110.6	0.0	41.6-50.6
205/09-1	2798.0	2807.0	m	Sele	E1	DC	P10012_001	600.0	199.0-200.0	56.0-59.2	0.0-20.0	10.0-55.0	44.2-139.4	0.0	64.2-79.4
	3704.0	3719.0		Lista (D1 Sand)	P3	DC	P10012_002	600.0	199.0-200.0	56.0-59.2	0.0-20.0	10.0-55.0	67.9-169.4	0.0	87.9-109.4
205/12-1	-	2570.0	m	Lamba	P3	DC	P10012_003	600.0	199.0-200.0	56.0-59.2	0.0-20.0	10.0-55.0	41.9-136.4	0.0	61.9-76.4
	-	3175.0		Shetland	K2	DC	P10012_004	600.0	199.0-200.0	139.8-145.0	0.0-20.0	10.0-130.0	57.6-156.3	0.0	77.6-96.3
205/14-2	-	7430.0	ft	Unit IV Upper	P3	DC	P10012_005	600.0	199.0-200.0	56.0-59.2	0.0-20.0	10.0-55.0	38.3-131.9	0.0	58.3-71.9
205/17b-2	-	2443.8	m	Lista	P3	COCH	P10012_006	600.0	199.0-200.0	56.0-59.2	0.0-20.0	10.0-55.0	41.0-135.2	0.0	61.0-75.2
206/11-1	4370.0	4376.0	m	Early Cret Sands	K1	DC	P10012_007	600.0	199.0-200.0	100.5-113.0	0.0-20.0	10.0-65.0	80.0-204.5	0.0	100.0-144.5
207/01-2	5590.0	5620.0	ft	Victory	K1	DC	P10011_003	600.0	199.0-200.0	100.5-145.0	0.0-20.0	10.0-65.0	28.8-119.8	0.0	48.8-59.8
	5740.0	5750.0		PrCam Basement	PrCam	DC	P10011_004	600.0	199.0-200.0	100.5-145.0	0.0-20.0	10.0-65.0	29.9-121.2	0.0	49.9-61.2
208/17-2	7871.0	7946.8	ft	Waterhouse	P3	COCH	P10012_008	600.0	199.0-200.0	56.0-59.2	0.0-20.0	10.0-55.0	36.2-129.2	0.0	56.2-69.2
208/24-1A	5900.0	6000.0	ft	Victory	K1	DC	P10011_006	600.0	199.0-200.0	83.6-86.3	0.0-20.0	10.0-65.0	30.6-122.1	0.0	50.6-62.1
	6230.0	6300.0		Victory	K1	DC	P10011_007	600.0	199.0-200.0	125.0-129.4	0.0-20.0	10.0-65.0	33.1-125.3	0.0	53.1-65.3
208/27-2	3960.0	3990.0	ft	Shetland	K2	DC	P10011_009	600.0	199.0-200.0	72.1-83.6	0.0-20.0	10.0-65.0	14.0-101.0	0.0	34.0-41.0
	-	4540.0		PrCam Basement	PrCam	DC	P10011_011	600.0	199.0-200.0	72.1-83.6	5.6-25.6	10.0-65.0	18.4-106.6	0.0	38.4-46.6
	4300.0	4590.0		Caved Shetland	K2	DC	P10011_013	600.0	199.0-200.0	72.1-83.6	0.0-20.0	10.0-65.0	17.7-105.7	0.0	37.7-45.7
214/26-1	7516.0	7539.0	ft	Lewis Fan Env	E2	DC	P10012_009	600.0	199.0-200.0	56.0-59.2	0.0-20.0	10.0-55.0	36.2-129.2	0.0	56.2-69.2
214/28-1	-	8374.3	ft	Late Paleocene	P3	COCH	P10012_010	600.0	199.0-200.0	56.0-59.2	0.0-20.0	10.0-55.0	37.4-130.7	0.0	57.4-70.7
	11900.0	11920.0		M Paleocene	P2	DC	P10012_011	600.0	199.0-200.0	59.2-61.6	0.0-20.0	10.0-55.0	65.4-166.2	0.0	85.4-106.2
	14310.0	14334.4		E-M Paleocene	P1	COCH	P10012_012	600.0	199.0-200.0	59.2-66.0	0.0-20.0	10.0-55.0	80.0-190.5	0.0	100.0-130.5

Near surface

Stratigraphy/Ages

Early Cret Sands: Early Cretaceous Sands

PrCam Basement: Precambrian Basement

Lewis Fan Env: Lewis Fan Envelope (Lobe 2)

M Paleocene: Middle Paleocene

E-M Paleocene: Early-Middle Paleocene

TABLE 4.2.2 Apatite fission track time-temperature constraints

Well	Top depth	Bottom depth	Units (m/ft)	Stratigraphy	Age	Sample Type	Sample ID	Sub Group	Pop.	Modelled Parameters								Measured Parameters						
										Oldest UFT (Ma)	Surface Fission Track GOF	Confined Fission Track GOF	Stratigraphy Age (Ma)	Peak Burial Time t (Ma)	Peak Burial Temp T (°C)	UFT Age (Ma)	Vitrinite Reflectivity Equivalent (% Ro)	UFT Age (Ma)	Chemical Ionisation -95%	Chemical Ionisation +95%	Spots	Confined Fission Tracks	UPb Age (Ma)	
204/10a-5	2361.8	2383.5	m	Hildasay	E1	COCH	P10012_013	1	1	244.0	0.53	0.58	57.0	1.0	48.0	182.0	0.32-0.37	153.0	35.7	46.3	4	37	515.0	
								2A	1	390.0	0.91	1.00	57.0	1.0	48.0	254.9	0.32-0.37	245.5	62.9	84.1	5	0	978.0	
								2B	2	395.0	0.62	0.36	57.0	1.0	48.0	281.4	0.32-0.37	303.4	44.9	52.5	3	48	1470.0	
								2C	1	332.0	0.94	0.25	57.0	1.0	48.0	227.5	0.32-0.37	225.5	24.6	27.6	16	121	1605.0	
205/09-1	2798.0	2807.0	m	Sele	E1	DC	P10012_001	2	1	455.0	0.78	1.00	58.0	45.0	75.0	205.4	0.44-0.50	228.9	85.1	134.0	3	2	1601.0	
								2	2	544.0	0.59	0.63	58.0	45.0	75.0	270.8	0.44-0.50	321.1	93.1	129.8	5	5	1209.0	
								3	491.0	0.96	0.63	58.0	45.0	75.0	321.8	0.44-0.50	302.5	168.0	367.4	1	1	2266.0		
	3704.0	3719.0	m	Lista (D1 Sand)	P3	DC	P10012_002	0	1	21.0	0.71	1.00	21.0	21.0	121.0	9.5	0.58-0.72	15.1	-15.1	30.1	5	1	161.0	
								2	150.0	0.69	1.00	59.0	30.0	153.0	43.5	0.85-1.19	24.3	16.7	52.9	1	0	226.0		
								1	1	19.0	0.94	0.91	19.0	19.0	116.0	7.9	0.54-0.66	8.5	-8.5	4.3	4	3	718.0	
								2	1	22.0	0.16	0.67	22.0	22.0	123.0	10.4	0.59-0.71	47.3	26.4	59.7	3	6	1181.0	
									2	140.0	0.98	1.00	59.0	30.0	153.0	19.6	0.85-1.19	18.4	12.6	40.0	2	0	1175.0	
									3	150.0	1.00	0.90	59.0	30.0	153.0	42.8	0.85-1.19	0.0	0.0	0.0	0	5	844.0	
								3	1	19.0	0.74	0.64	19.0	19.0	116.0	7.9	0.54-0.66	0.0	0.0	23.4	3	7	2346.0	
205/12-1	-	2570.0	m	Lamba	P3	DC	P10012_003	0	1	296.0	0.26	1.00	56.0	1.0	66.0	202.7	0.37-0.42	62.9	-62.9	124.0	1	11	332.0	
								2	345.0	0.67	0.18	56.0	1.0	66.0	222.2	0.37-0.42	189.1	55.6	78.2	2	6	435.0		
								1	1	125.0	0.40	0.93	56.0	1.0	66.0	85.9	0.37-0.42	145.1	70.7	136.4	2	5	615.0	
									3	447.0	0.70	0.70	56.0	1.0	66.0	291.1	0.37-0.42	258.6	63.3	83.4	3	25	722.0	
								2A	1	273.0	0.59	0.31	56.0	1.0	66.0	162.3	0.37-0.42	189.6	50.3	68.2	1	27	1494.0	
									3	419.0	0.42	0.07	56.0	1.0	66.0	297.8	0.37-0.42	239.1	55.8	72.4	2	12	1599.0	
								2B	1	215.0	0.18	0.43	56.0	1.0	66.0	130.4	0.37-0.42	176.0	34.1	42.1	5	58	1648.0	
									2	246.0	0.91	0.64	56.0	1.0	66.0	149.8	0.37-0.42	144.0	39.3	53.9	3	20	1808.0	
	3	277.0	0.80	0.09	56.0	1.0	66.0	177.5	0.37-0.42	188.5	42.7	54.9	4	12	1479.0									
	4	568.0	0.87	0.96	56.0	1.0	66.0	211.3	0.37-0.42	178.5	94.7	198.9	1	4	2085.0									
-	3175.0	m	Shetland	K2	DC	P10012_004	0	1	319.0	0.93	1.00	143.0	1.0	85.0	173.3	0.49-0.58	178.7	65.2	101.8	2	3	221.0		
							1	1	345.0	0.77	0.70	143.0	1.0	85.0	197.4	0.49-0.58	219.7	77.0	117.6	2	5	504.0		
205/14-2	-	7430.0	ft	Unit IV Upper	P3	DC	P10012_005	1	1	208.0	0.50	0.47	58.0	1.0	65.0	117.3	0.37-0.41	178.4	91.0	183.1	3	15	598.0	
									2	449.0	0.78	1.00	58.0	1.0	65.0	314.8	0.37-0.41	269.4	101.7	161.3	1	4	491.0	
									3	391.0	0.75	0.62	58.0	1.0	65.0	258.6	0.37-0.41	280.1	67.2	87.8	3	5	487.0	
								2	1	487.0	0.81	0.70	58.0	1.0	65.0	357.6	0.37-0.41	324.2	96.9	136.8	2	9	1312.0	
									3	1	313.0	0.65	0.87	58.0	1.0	65.0	213.0	0.37-0.41	239.6	59.0	77.8	2	23	2193.0
										2	506.0	0.84	1.00	58.0	1.0	65.0	368.9	0.37-0.41	389.0	101.0	135.1	4	5	2218.0
205/17b-2	-	2443.8	m	Lista	P3	COCH	P10012_006	0	2	377.0	0.64	0.86	57.0	1.0	64.0	269.2	0.38-0.42	291.5	47.0	55.7	5	32	243.0	
								1	1	380.0	0.39	0.97	57.0	1.0	64.0	258.9	0.38-0.42	193.9	54.7	75.8	4	22	447.0	
									2	381.0	0.42	1.00	57.0	1.0	64.0	261.8	0.38-0.42	340.6	98.4	137.0	1	17	526.0	
								2A	1	405.0	0.45	1.00	57.0	1.0	64.0	250.1	0.38-0.42	194.9	53.7	73.7	5	5	1087.0	
								2B	1	492.0	0.36	0.18	57.0	1.0	64.0	331.8	0.38-0.42	378.7	51.6	59.4	10	46	1752.0	
									2	582.0	1.00	0.42	57.0	1.0	64.0	441.0	0.38-0.42	0.0	0.0	0.0	0	7	1835.0	
								2C	1	524.0	0.95	0.10	57.0	1.0	64.0	359.2	0.38-0.42	354.2	63.2	76.5	6	58	1970.0	
206/11-1	4370.0	4376.0	m	Early Cretaceous Sands	K1	DC	P10012_007	1	1	6.0	0.92	1.00	6.0	6.0	162.0	2.0	0.79-1.14	0.0	0.0	20.7	4	0	524.0	
								2	1	1.0	0.08	1.00	1.0	1.0	112.0	0.2	0.52-0.63	10.3	5.8	13.1	9	1	1397.0	
									2	5.0	0.90	1.00	5.0	5.0	152.0	1.5	0.71-0.99	0.0	0.0	11.8	3	0	1752.0	
									3	10.0	0.86	1.00	10.0	10.0	182.0	2.9	1.48-2.90	0.0	0.0	15.8	2	0	1843.0	

Chemical Ionisation -95%: Chemical ionisation (CI) -95%=95% confidence interval (2 sigma) in the negative direction for asymmetrical UFT age error

Chemical Ionisation +95%: Chemical ionisation (CI) +95%=95% confidence interval (2 sigma) in the positive direction for asymmetrical UFT age error

TABLE 4.2.3 Apatite fission track modelled and measured parameters

Well	Top depth	Bottom depth	Units (m/ft)	Stratigraphy	Age	Sample Type	Sample ID	Sub Group	Pop.	Modelled Parameters								Measured Parameters					
										Oldest UFT (Ma)	Surface Fission Track GOF	Confined Fission Track GOF	Stratigraphy Age (Ma)	Peak Burial Time t (Ma)	Peak Burial Temp T (°C)	UFT Age (Ma)	Vitrinite Reflectivity Equivalent (% Ro)	UFT Age (Ma)	Chemical Ionisation -95%	Chemical Ionisation +95%	Spots	Confined Fission Tracks	UPb Age (Ma)
207/01-2	5590.0	5620.0	ft	Victory	K1	DC	P10011_003	1A	1	300.0	0.78	0.31	117.0	18.0	64.0	192.6	0.38-0.43	197.8	18.9	20.9	19	76	554.0
									2	234.0	0.68	0.92	117.0	18.0	64.0	150.8	0.38-0.43	159.9	22.1	25.6	6	54	532.0
								1B	1	342.0	0.67	0.06	117.0	18.0	64.0	240.0	0.38-0.43	221.7	36.3	43.3	6	43	462.0
									2	205.0	0.89	1.00	117.0	18.0	64.0	138.0	0.38-0.43	143.1	35.2	46.6	1	9	2709.0
	5740.0	5750.0		PreCambrian Basement	PrCam	DC	P10011_004	1A	1	306.0	0.06	0.19	103.0	1.0	54.0	211.4	0.36-0.40	292.5	42.7	49.8	6	88	570.0
									2	433.0	0.32	0.91	103.0	1.0	54.0	292.4	0.36-0.40	373.2	81.1	102.8	2	18	546.0
									3	378.0	0.73	0.17	103.0	1.0	54.0	248.5	0.36-0.40	273.5	72.1	97.2	1	7	550.0
								1A	1	438.0	0.74	0.21	103.0	1.0	54.0	300.2	0.36-0.40	321.1	63.9	79.2	2	28	412.0
			2A					1	407.0	0.52	0.37	103.0	1.0	54.0	245.7	0.36-0.40	201.7	51.7	69.1	4	8	1531.0	
			2B					1	363.0	0.17	0.12	103.0	1.0	54.0	228.4	0.36-0.40	183.8	27.8	32.7	8	42	1698.0	
								2	387.0	0.75	0.12	103.0	1.0	54.0	248.6	0.36-0.40	220.7	63.6	88.7	1	14	2009.0	
								4	529.0	0.93	0.97	102.0	1.0	54.0	147.3	0.36-0.40	139.6	54.2	87.9	2	2	1548.0	
208/17-2	7871.0	7946.8	ft	Waterhouse	P3	COCH	P10012_008	0	1	351.0	1.00	0.55	59.0	15.0	76.0	199.7	0.43-0.48	0.0	0.0	0.0	0	1	220.0
									2	548.0	0.96	0.99	59.0	15.0	76.0	374.0	0.43-0.48	379.4	99.2	132.9	4	6	274.0
								1A	1	303.0	0.47	1.00	59.0	15.0	76.0	184.7	0.43-0.48	224.7	55.3	72.9	2	9	526.0
									2	482.0	0.57	0.74	59.0	15.0	76.0	310.2	0.43-0.48	384.4	132.3	198.6	1	32	490.0
									3	441.0	0.86	0.86	59.0	15.0	76.0	284.9	0.43-0.48	270.0	64.5	84.1	3	50	697.0
									4	519.0	1.00	0.19	59.0	15.0	76.0	307.0	0.43-0.48	0.0	0.0	0.0	0	8	597.0
								1B	3	380.0	0.72	0.10	59.0	15.0	76.0	187.0	0.43-0.48	199.2	33.9	40.8	3	32	573.0
								2	1	271.0	0.75	0.79	59.0	15.0	76.0	127.8	0.43-0.48	103.0	44.7	78.4	1	9	2167.0
									2	417.0	0.64	0.44	59.0	15.0	76.0	278.1	0.43-0.48	313.6	75.7	99.1	2	10	985.0
208/24-1A	5900.0	6000.0	ft	Victory	K1	DC	P10011_006	1A	1	438.0	0.50	0.94	85.0	25.0	74.0	259.0	0.42-0.46	217.6	48.4	61.9	4	58	506.0
									2	328.0	0.62	0.59	85.0	25.0	74.0	221.9	0.42-0.46	204.5	30.1	35.2	7	28	532.0
									3	476.0	0.12	0.14	85.0	25.0	74.0	293.7	0.42-0.46	231.0	34.7	40.7	3	52	586.0
								1B	1	431.0	0.45	0.86	85.0	25.0	74.0	220.6	0.42-0.46	247.2	35.2	40.9	4	31	502.0
									2	371.0	0.31	0.25	85.0	25.0	74.0	204.3	0.42-0.46	252.9	47.5	58.3	4	19	497.0
									3	311.0	0.80	0.08	85.0	25.0	74.0	183.1	0.42-0.46	191.5	33.1	39.8	4	7	504.0
								2	1	283.0	0.63	0.99	85.0	25.0	74.0	179.3	0.42-0.46	92.0	-92.0	180.2	1	31	1709.0
									2	444.0	0.56	0.15	85.0	25.0	74.0	291.2	0.42-0.46	228.6	73.2	106.8	1	23	1266.0
	6230.0	6300.0		Victory	K1	DC	P10011_007	1A	1	293.0	0.16	0.12	129.0	63.0	78.0	170.8	0.45-0.51	211.6	28.7	33.1	8	75	539.0
									2	400.0	0.87	0.65	129.0	63.0	78.0	253.6	0.45-0.51	259.9	39.7	46.7	4	52	551.0
								1B	2	304.0	0.69	0.17	128.0	63.0	78.0	142.8	0.45-0.51	134.2	18.5	21.4	7	22	503.0
									3	352.0	0.53	0.11	128.0	63.0	78.0	227.8	0.45-0.51	201.0	35.4	42.9	3	26	452.0
									4	538.0	1.00	0.57	128.0	63.0	78.0	328.8	0.45-0.51	0.0	0.0	0.0	0	8	418.0
								2	1	491.0	0.59	0.14	128.0	63.0	78.0	206.8	0.45-0.51	234.1	50.0	63.3	5	4	1532.0
3	489.0	1.00	0.09	129.0	63.0	78.0	302.3	0.45-0.51	0.0	0.0	0.0	0	8	827.0									
208/27-2	3960.0	3990.0	ft	Shetland	K2	DC	P10011_009	2	2	186.0	0.95	0.98	74.0	29.0	38.0	141.7	0.29-0.33	137.9	42.7	61.5	3	6	1605.0
	-	PreCambrian Basement		PrCam	DC	P10011_011	2A	1	393.0	0.79	0.69	81.0	44.0	56.0	262.9	0.35-0.39	251.2	36.9	43.2	6	74	1510.0	
								2	268.0	0.69	0.42	80.0	44.0	56.0	186.1	0.35-0.39	196.5	26.4	30.4	8	31	1544.0	
								3	348.0	0.91	0.33	81.0	44.0	56.0	195.0	0.35-0.39	190.6	33.6	40.7	5	25	1827.0	
	4300.0	4590.0		Caved Shetland	K2	DC	P10011_013	2A	1	240.0	0.46	0.06	80.0	44.0	56.0	166.9	0.35-0.39	188.5	28.9	34.0	10	20	1678.0
									1	382.0	0.55	0.64	81.0	51.0	61.0	243.4	0.37-0.41	215.9	38.1	46.1	10	70	1548.0
									2	211.0	0.90	0.94	81.0	51.0	61.0	153.8	0.37-0.41	147.1	39.4	53.6	3	24	1214.0

Chemical Ionisation -95%: Chemical ionisation (CI) -95%=95% confidence interval (2 sigma) in the negative direction for asymmetrical UFT age error

Chemical Ionisation +95%: Chemical ionisation (CI) +95%=95% confidence interval (2 sigma) in the positive direction for asymmetrical UFT age error

TABLE 4.2.3 Apatite fission track modelled and measured parameters

Well	Top depth	Bottom depth	Units (m/ft)	Stratigraphy	Age	Sample Type	Sample ID	Sub Group	Pop.	Modelled Parameters								Measured Parameters					
										Oldest UFT (Ma)	Surface Fission Track GOF	Confined Fission Track GOF	Stratigraphy Age (Ma)	Peak Burial Time t (Ma)	Peak Burial Temp T (°C)	UFT Age (Ma)	Vitrinite Reflectivity Equivalent (% Ro)	UFT Age (Ma)	Chemical Ionisation -95%	Chemical Ionisation +95%	Spots	Confined Fission Tracks	UPb Age (Ma)
208/27-2	4300.0	4590.0	ft	Caved Shetland	K2	DC	P10011_013	2A	3	494.0	0.44	0.49	81.0	51.0	61.0	315.9	0.37-0.41	262.2	54.9	69.0	4	63	1670.0
									4	298.0	0.57	0.63	81.0	51.0	61.0	194.4	0.37-0.41	167.9	37.0	47.3	8	22	1439.0
								2B	1	330.0	0.85	0.92	81.0	51.0	61.0	215.2	0.37-0.41	233.1	93.0	153.0	2	10	1637.0
									2	370.0	0.25	1.00	81.0	51.0	61.0	251.3	0.37-0.41	167.0	51.5	74.0	4	5	1580.0
214/26-1	7516.0	7539.0	ft	Lewis Fan Envelop	E2	DC	P10012_009	1	1	322.0	0.74	0.95	58.0	33.0	68.0	192.9	0.39-0.44	212.7	60.2	83.4	3	4	369.0
									2	284.0	0.80	1.00	58.0	33.0	68.0	208.8	0.39-0.44	174.0	77.0	136.8	5	0	304.0
								2A	1	337.0	0.41	0.44	57.0	33.0	68.0	209.5	0.39-0.44	268.6	72.2	98.0	3	3	1252.0
									1	481.0	0.56	0.52	58.0	33.0	68.0	291.0	0.39-0.44	340.7	84.4	111.3	4	11	1900.0
								2B	2	355.0	0.87	0.77	58.0	33.0	68.0	251.5	0.39-0.44	234.4	73.7	106.7	2	6	1681.0
									1	360.0	0.45	0.82	58.0	33.0	68.0	213.4	0.39-0.44	258.5	59.2	76.3	9	19	1683.0
								2C	2	226.0	0.48	1.00	57.0	33.0	68.0	151.0	0.39-0.44	90.3	44.2	85.8	3	1	1574.0
214/28-1	-	8374.3	ft	Late Paleocene	P3	COCH	P10012_010	1A	1	382.0	0.93	0.81	58.0	44.0	74.0	224.9	0.41-0.46	219.6	45.9	57.7	2	78	435.0
									1B	1	255.0	0.71	0.65	58.0	44.0	74.0	164.3	0.41-0.46	151.4	28.5	35.0	10	46
								2		133.0	0.15	0.83	58.0	44.0	74.0	88.7	0.41-0.46	124.1	24.6	30.6	5	28	551.0
								2		1	302.0	0.99	1.00	58.0	44.0	74.0	177.8	0.41-0.46	177.3	30.2	36.3	10	32
									2	568.0	0.49	0.06	58.0	44.0	74.0	363.5	0.41-0.46	166.9	105.9	283.7	1	20	2148.0
									3	487.0	1.00	0.41	58.0	44.0	74.0	317.0	0.41-0.46	0.0	0.0	0.0	0	5	945.0
	11900.0	11920.0		Middle Paleocene	P2	DC	P10012_011	1	1	7.0	0.42	0.93	7.0	7.0	114.0	3.2	0.53-0.65	5.5	2.9	6.3	8	3	541.0
									2	10.0	0.97	1.00	10.0	10.0	131.0	4.6	0.64-0.78	4.3	-4.3	8.5	2	0	521.0
									3	22.0	0.42	1.00	22.0	22.0	157.0	7.6	0.84-1.18	0.0	0.0	9.5	2	0	586.0
								2A	1	7.0	0.86	1.00	7.0	7.0	114.0	2.8	0.53-0.65	3.4	-3.4	6.7	6	0	1046.0
									2	13.0	0.21	0.92	13.0	13.0	134.0	5.2	0.68-0.85	35.2	24.1	76.2	2	1	931.0
								2B	1	8.0	0.62	1.00	8.0	8.0	123.0	3.7	0.58-0.72	1.8	1.2	3.8	8	0	1937.0
									2	19.0	0.92	1.00	19.0	19.0	156.0	7.0	0.75-1.11	0.0	0.0	72.0	1	0	1914.0
								14310.0	14334.4	Early-Middle Paleocene	P1	COCH	P10012_012	0	1	2.0	0.98	1.00	2.0	2.0	117.0	0.6	0.55-0.66
	1	1		2.0	0.53	1.00	2.0								2.0	117.0	0.6	0.55-0.66	1.6	-1.6	3.2	3	0
		2		7.0	0.66	1.00	7.0							7.0	159.0	2.3	0.79-1.15	0.0	0.0	5.1	3	0	550.0
		2		1	2.0	0.89	1.00							2.0	2.0	117.0	0.4	0.55-0.66	0.0	0.0	3.2	5	1
	2			4.0	0.83	0.95	4.0							4.0	137.0	1.2	0.67-0.82	0.0	0.0	5.4	3	1	1477.0
	3A	1		2.0	0.85	1.00	2.0							2.0	117.0	0.6	0.55-0.66	0.0	0.0	3.2	7	1	2245.0
		2		6.0	0.66	1.00	6.0							6.0	157.0	2.1	0.74-1.11	0.0	0.0	4.8	2	0	2233.0
	3B	1		2.0	0.53	1.00	2.0							2.0	117.0	0.4	0.55-0.66	1.0	-1.0	2.1	8	0	1920.0
		2		9.0	1.00	1.00	9.0							9.0	160.0	2.5	0.88-1.21	0.0	0.0	0.0	0	2	2042.0

Chemical Ionisation -95%: Chemical ionisation (CI) -95%=95% confidence interval (2 sigma) in the negative direction for asymmetrical UFT age error

Chemical Ionisation +95%: Chemical ionisation (CI) +95%=95% confidence interval (2 sigma) in the positive direction for asymmetrical UFT age error

TABLE 4.2.3 Apatite fission track modelled and measured parameters

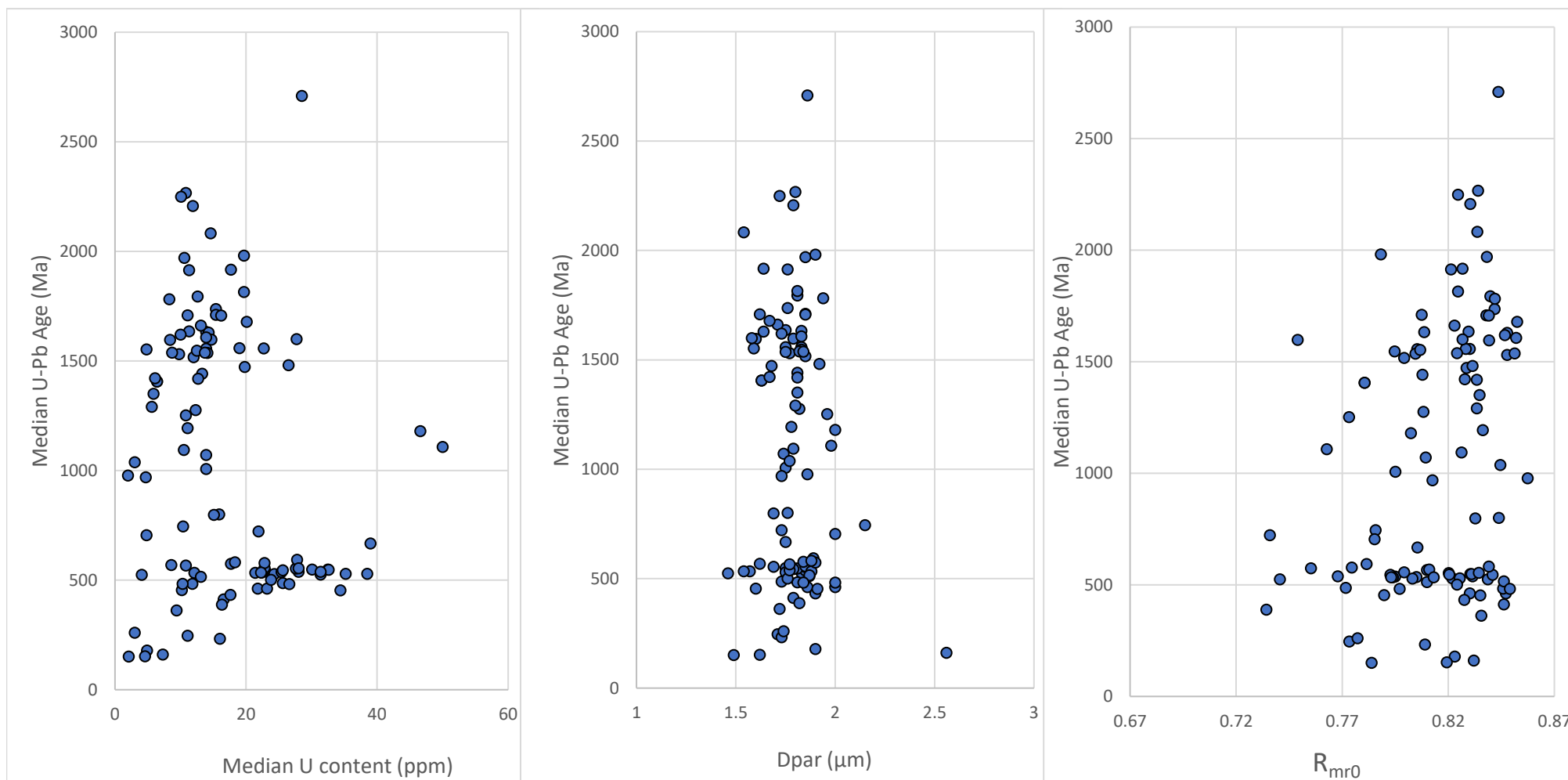
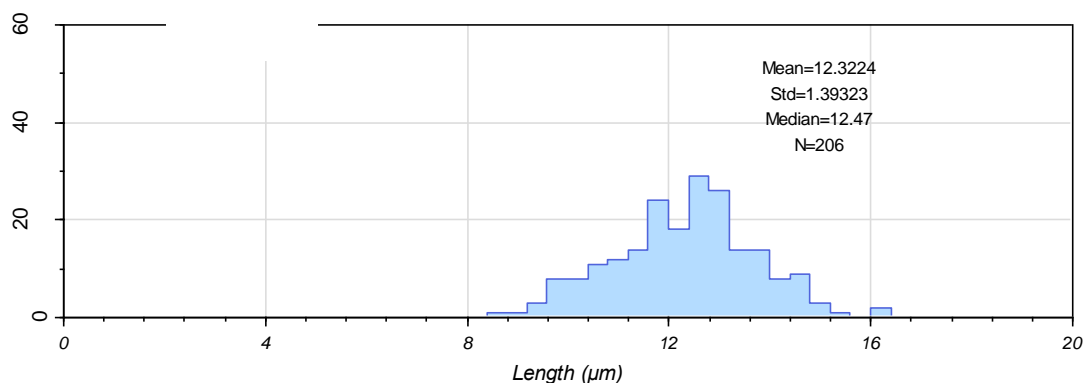
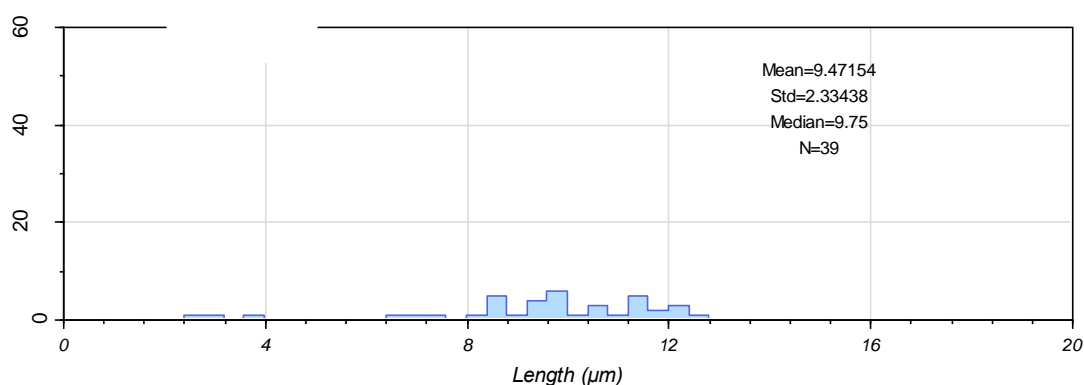


FIGURE 4.2.1a West of Shetland pooled UFT Age (Ma) vs. Median U-Pb Age (Ma), Median U content (ppm) and Dpar (μm)

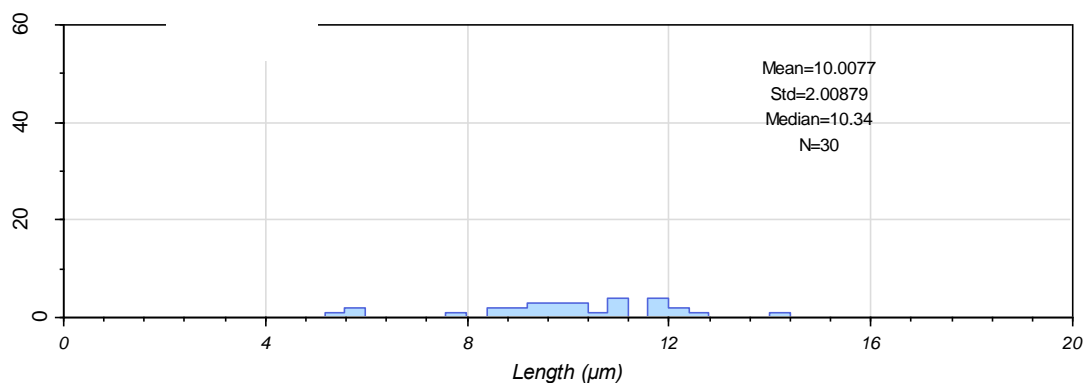
204/10a-5 (2361.8-2383.5m) - Hildasay (E1): Corona Basin - P10012_013



205/09-1 (2798-2807m) - Sele (E1): Flett Basin - P10012_001



205/09-1 (3704-3719m) - Lista (D1 Sand) (P3): Flett Basin - P10012_002



205/12-1 (2570m) - Lamba (P3): Flett Basin - P10012_003

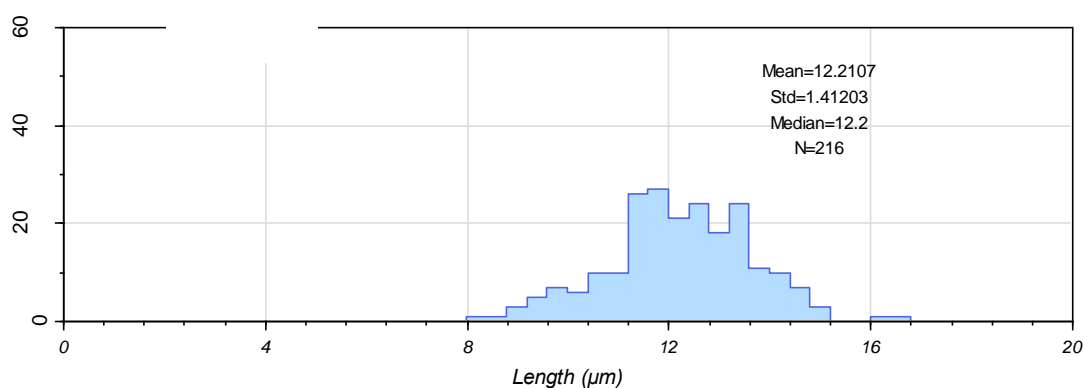


FIGURE 4.2.1b Apatite fission track length (μm) histograms

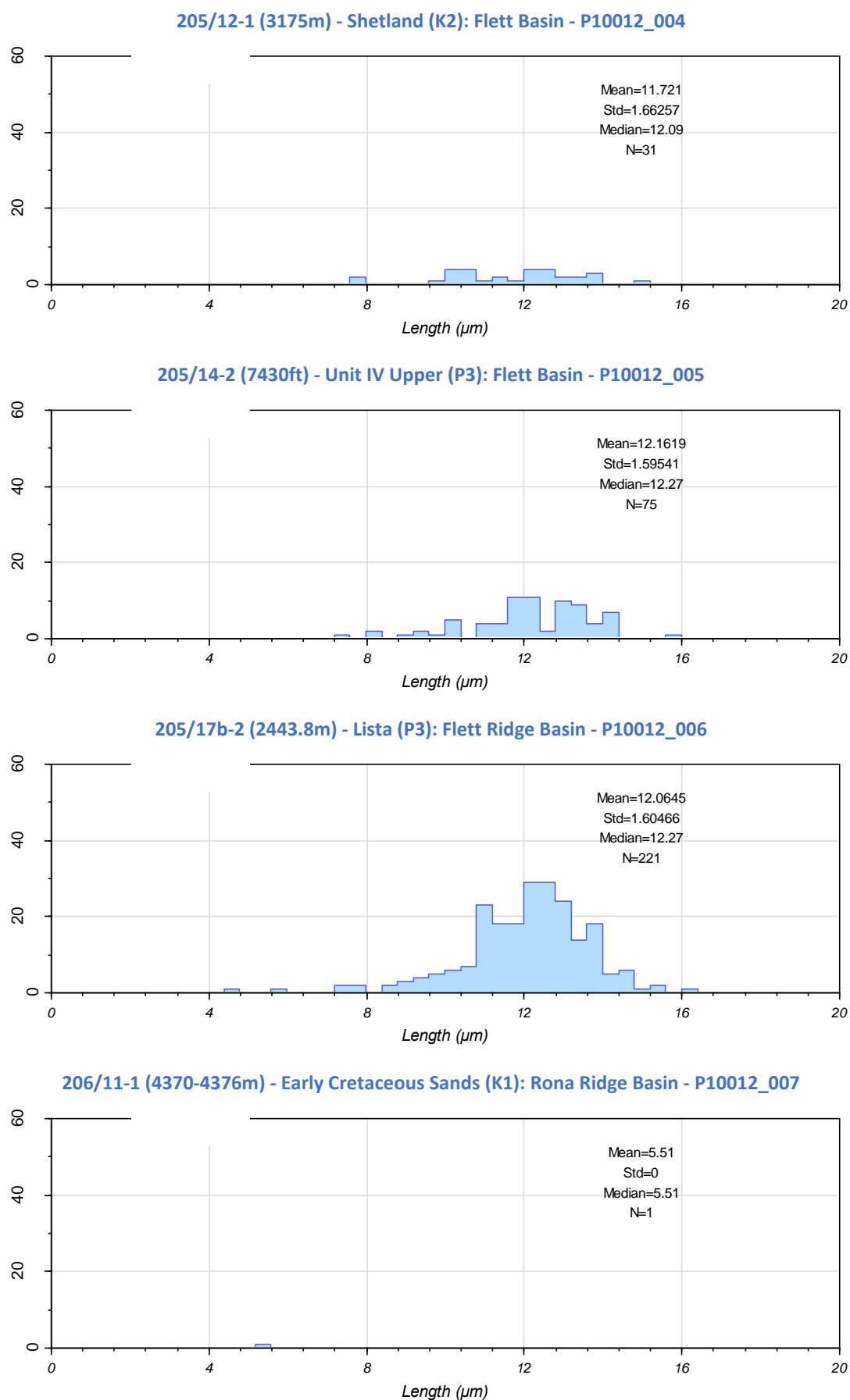
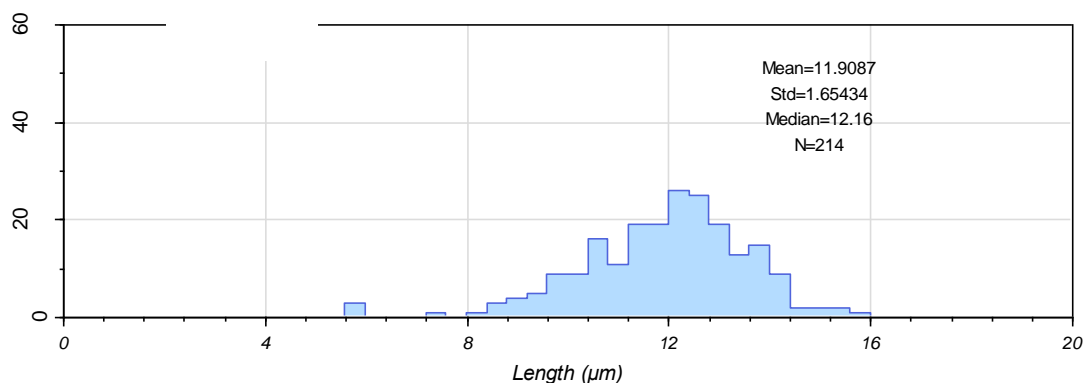
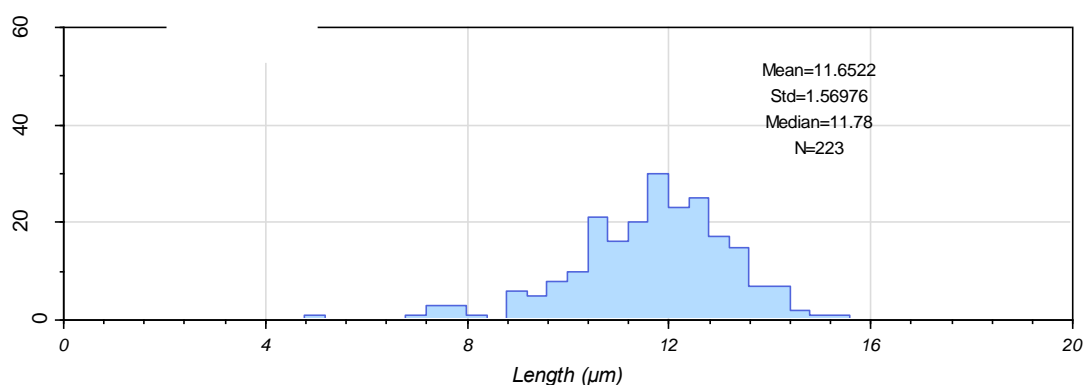


FIGURE 4.2.1b Apatite fission track length (μm) histograms

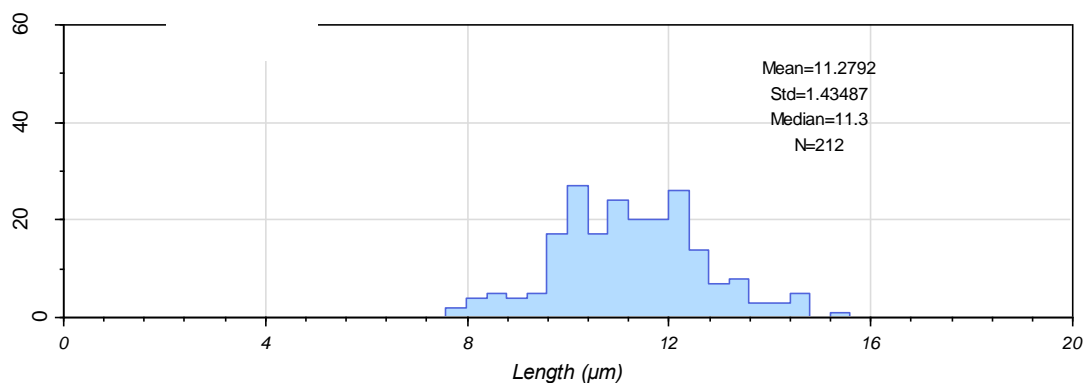
207/01-2 (5590-5620ft) - Victory (K1): West Shetland Basin - P10011_003



207/01-2 (5740-5750ft) - Precambrian Basement (PrCam): West Shetland Basin - P10011_004



208/17-2 (7871-7946.8ft) - Waterhouse (P3): N Faroe-Shetland Basin - P10012_008



208/24-1A (5900-6000ft) - Victory (K1): Northern Faroe-Shetland Basin - P10011_006

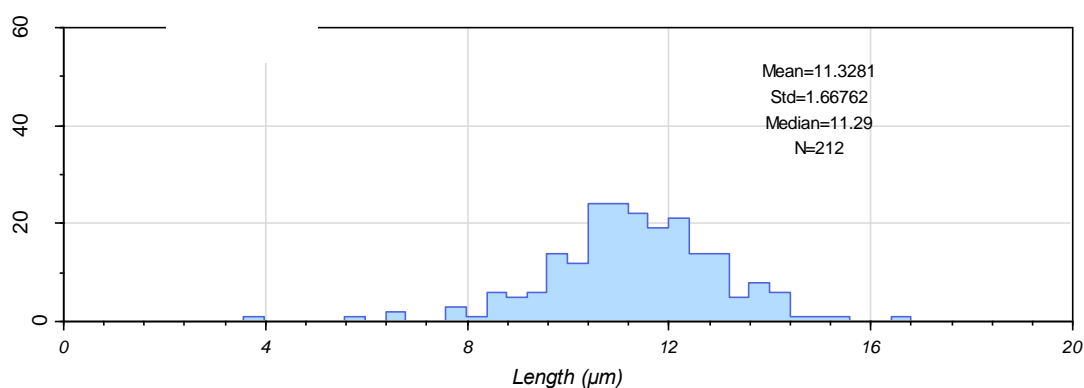


FIGURE 4.2.1b Apatite fission track length (μm) histograms

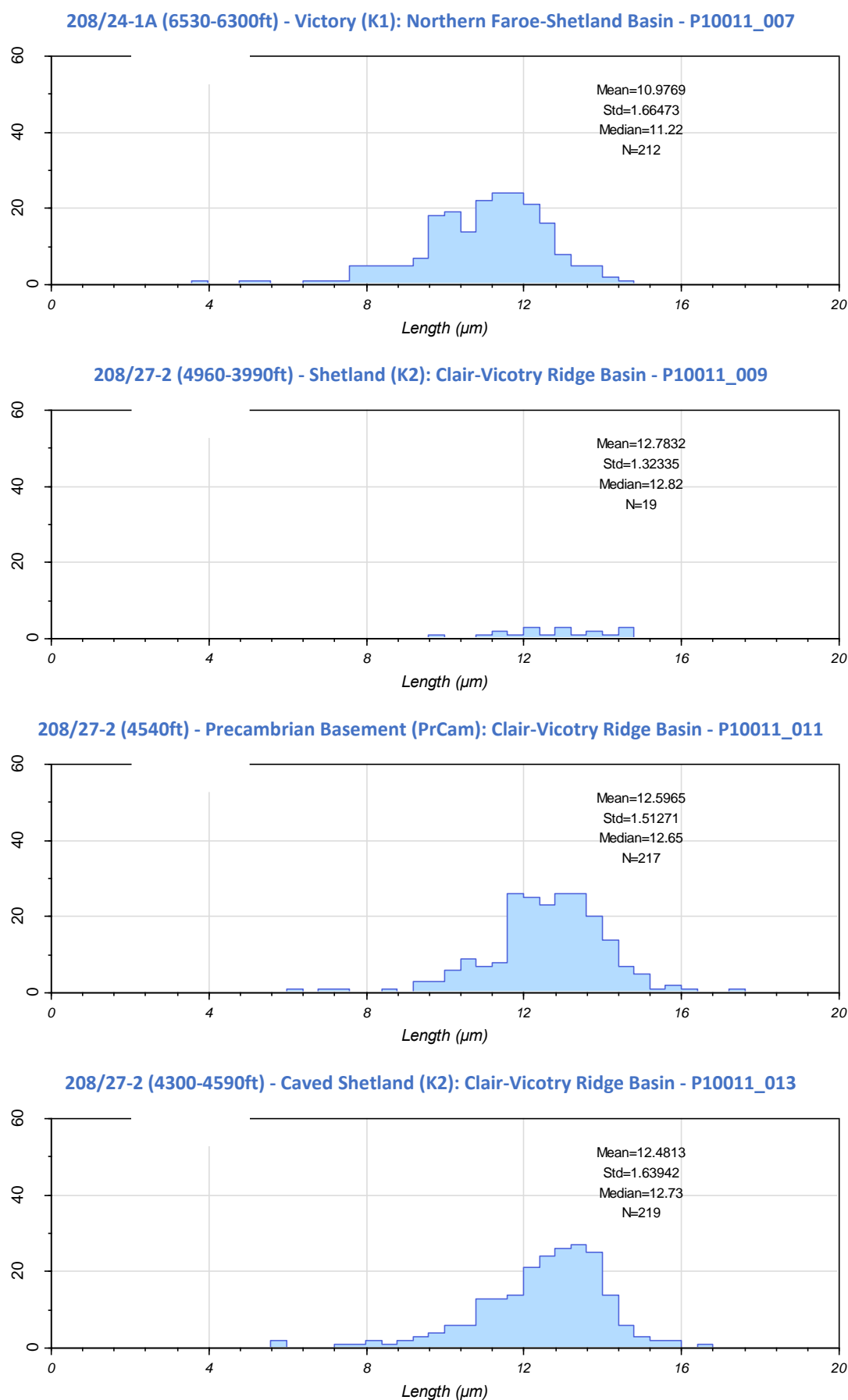


FIGURE 4.2.1b Apatite fission track length (μm) histograms

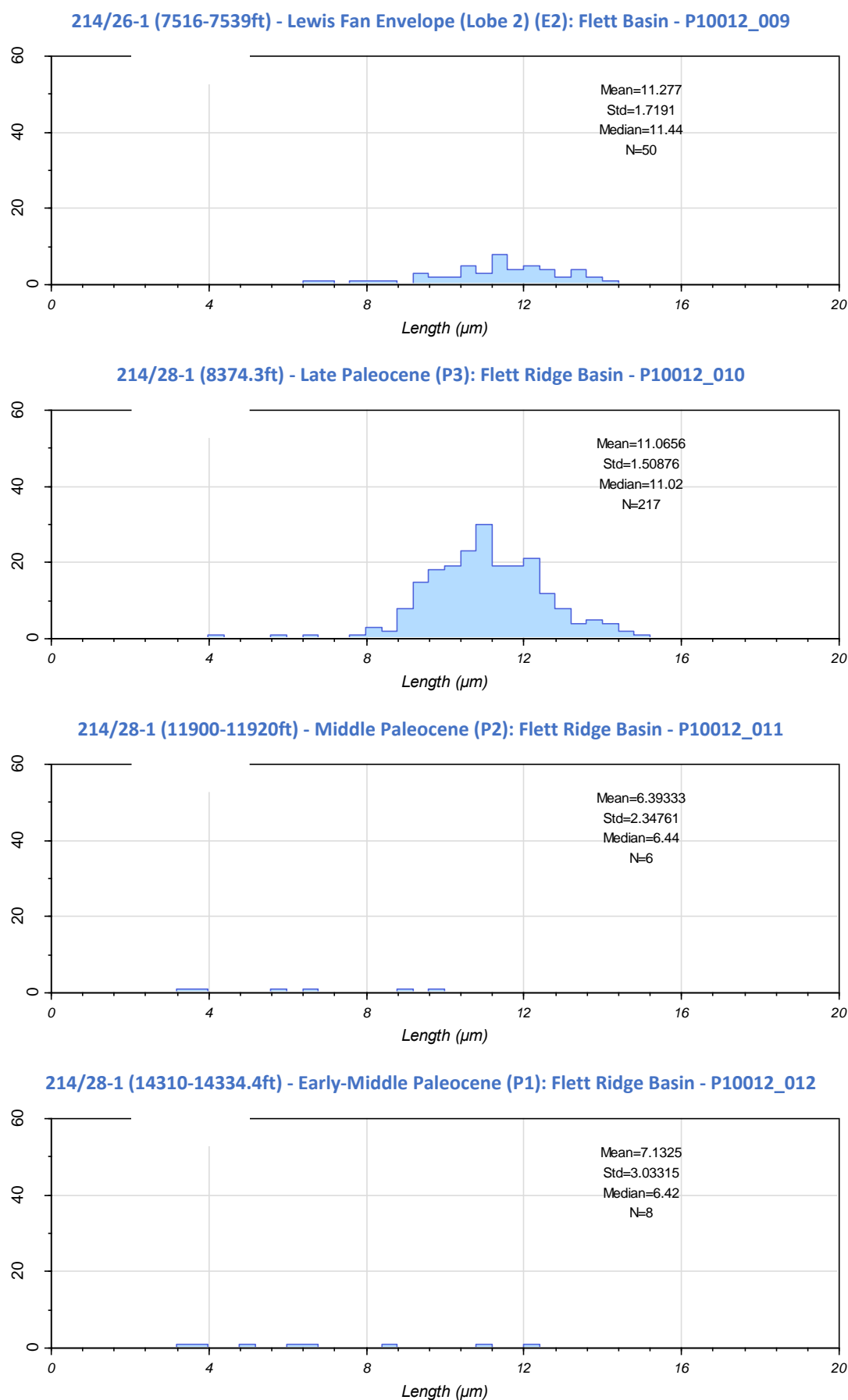


FIGURE 4.2.1b Apatite fission track length (μm) histograms

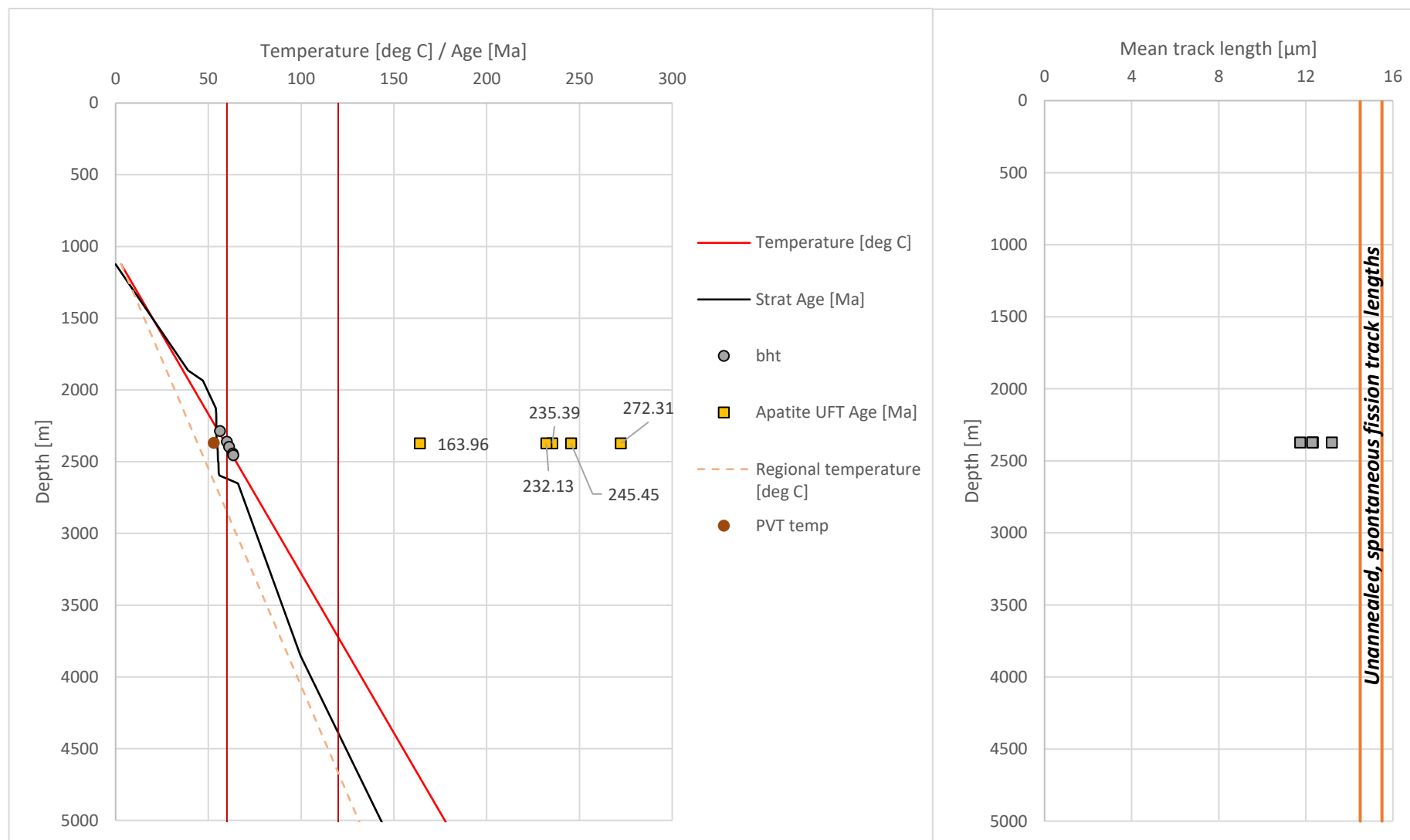


FIGURE 4.2.2 Apatite thermochronology parameters plotted against depth, stratigraphic age and temperature for well 204/10a-5

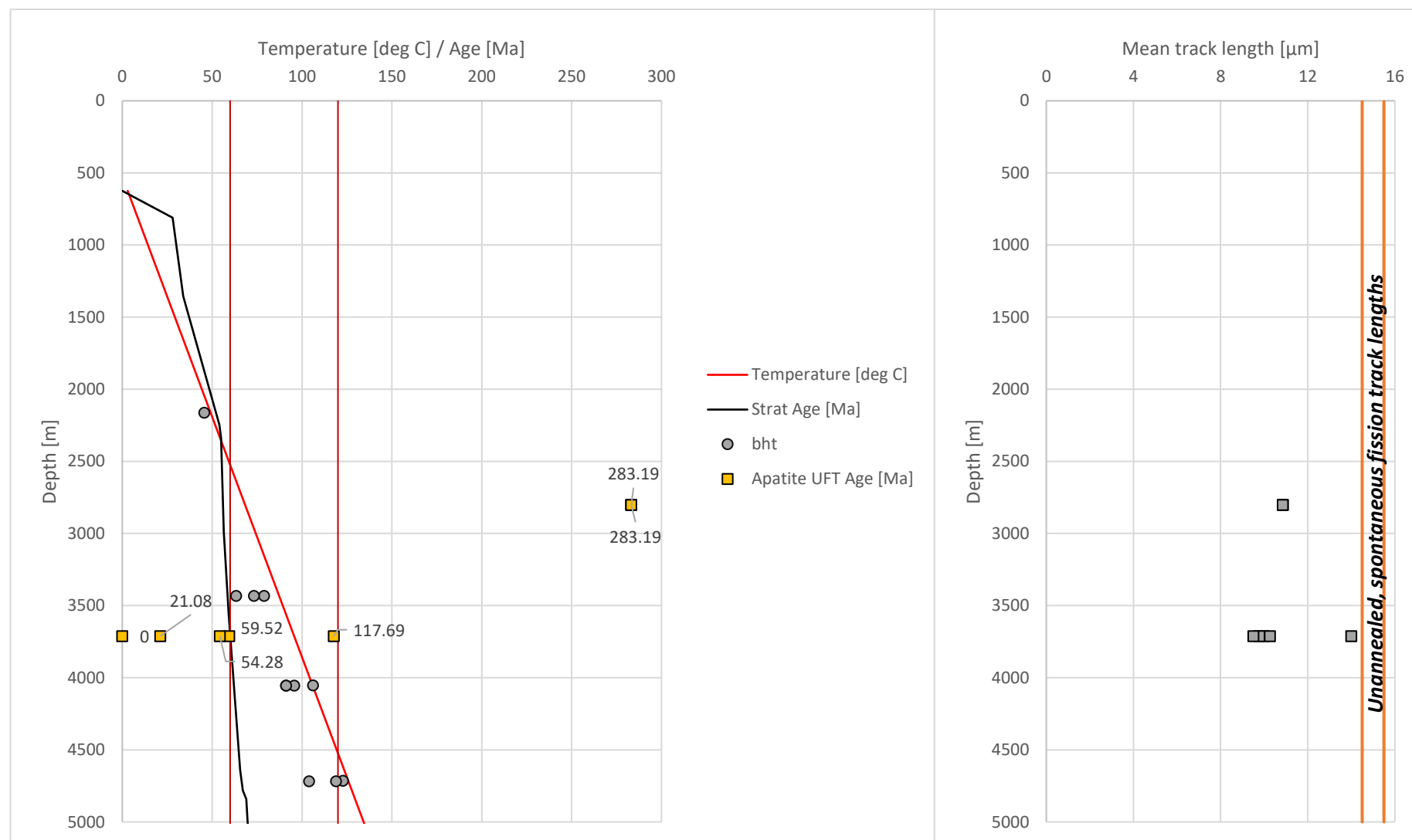


FIGURE 4.2.3 Apatite thermochronology parameters plotted against depth, stratigraphic age and temperature for well 205/09-1

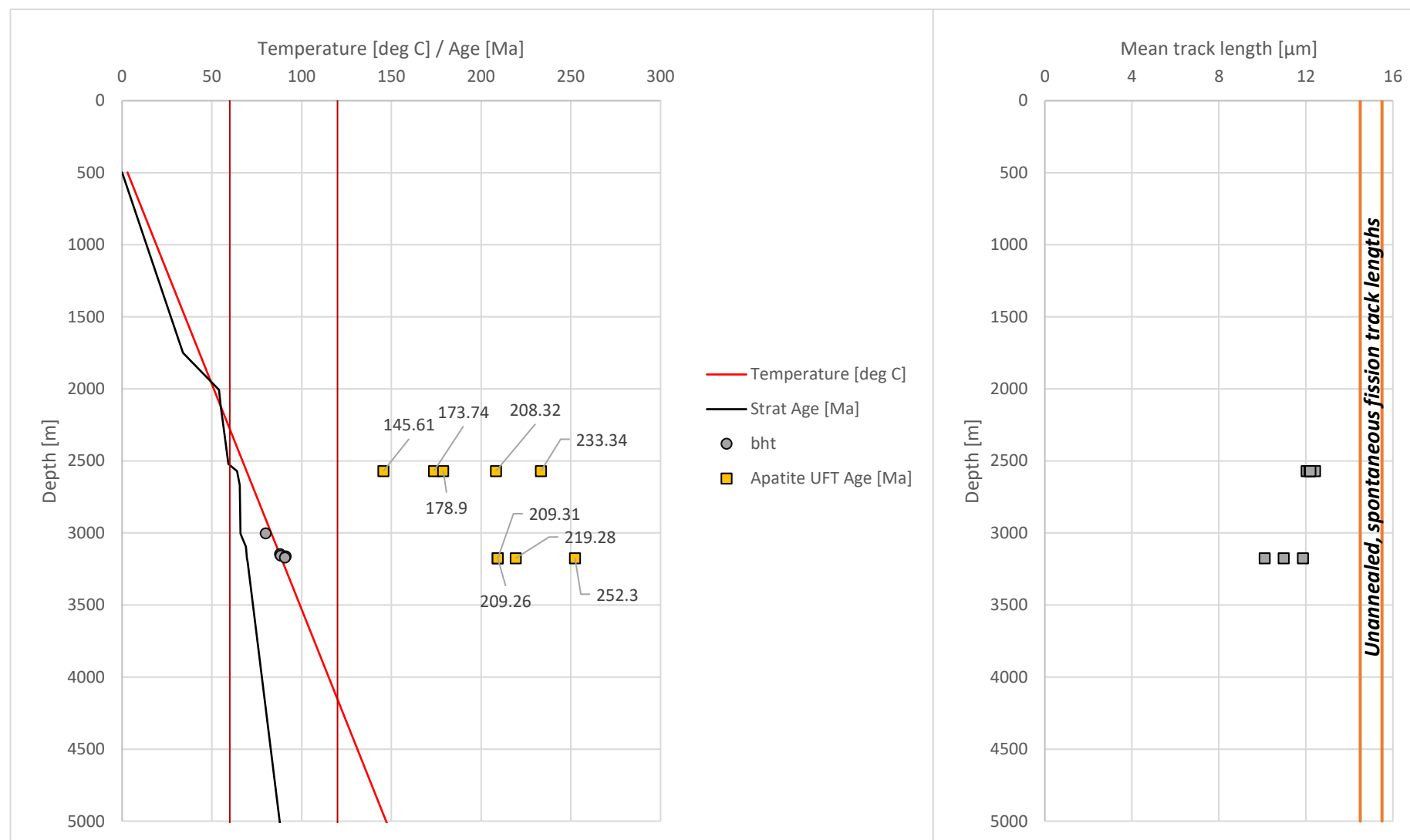


FIGURE 4.2.4 Apatite thermochronology parameters plotted against depth, stratigraphic age and temperature for well 205/12-1

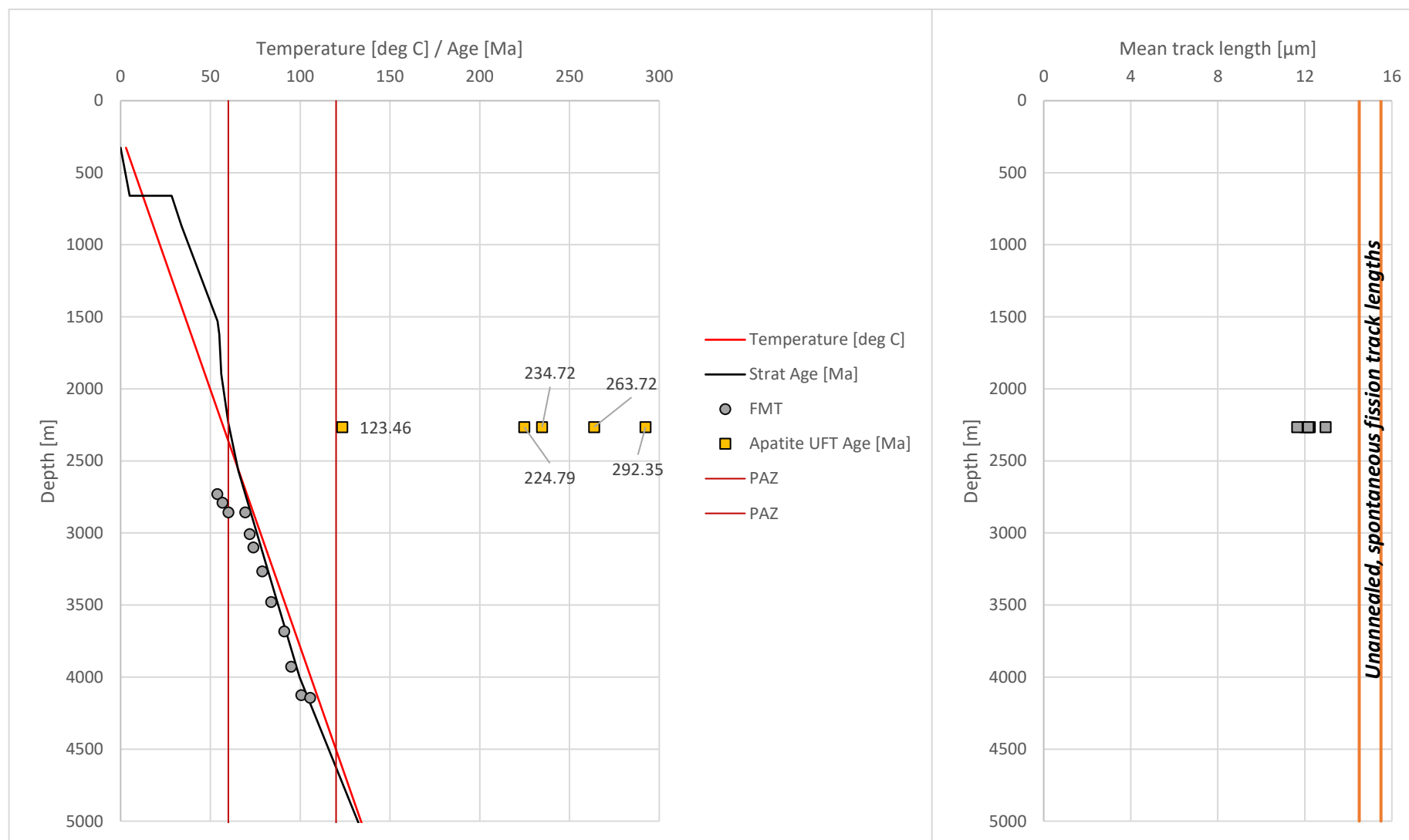


FIGURE 4.2.5 Apatite thermochronology parameters plotted against depth, stratigraphic age and temperature for well 205/14-2

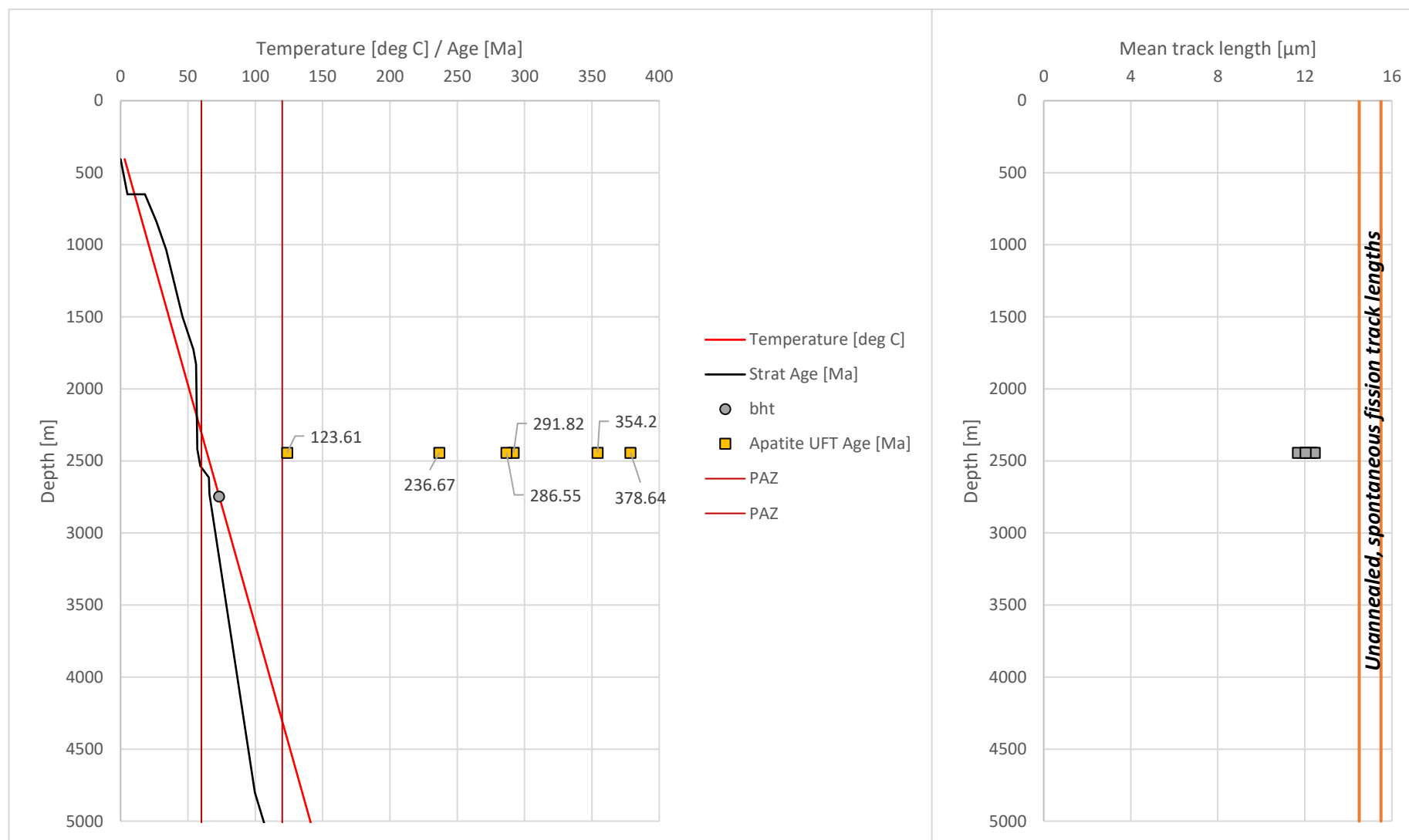


FIGURE 4.2.6 Apatite thermochronology parameters plotted against depth, stratigraphic age and temperature for well 205/17b-2



FIGURE 4.2.7 Apatite thermochronology parameters plotted against depth, stratigraphic age and temperature for well 206/11-1

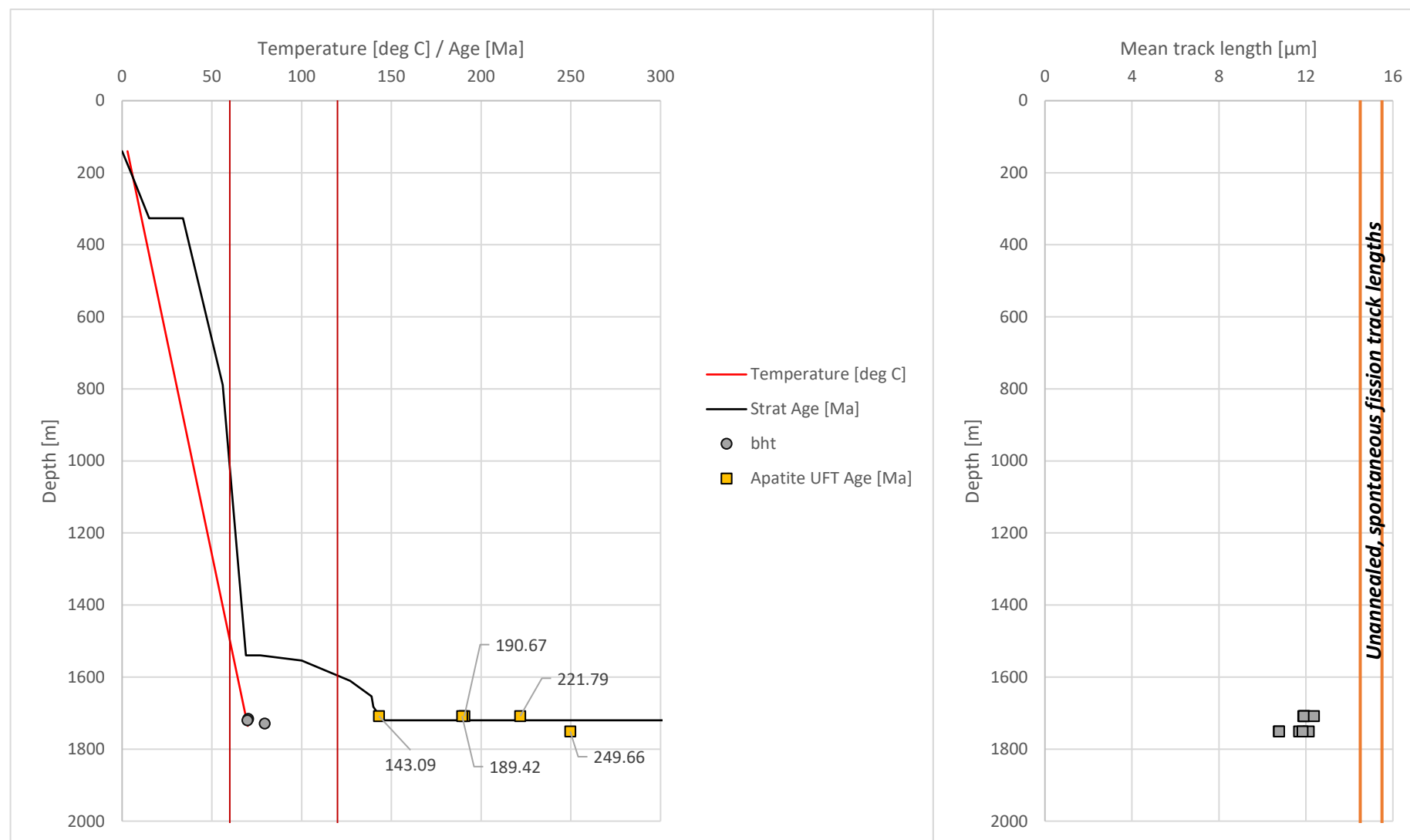


FIGURE 4.2.8 Apatite thermochronology parameters plotted against depth, stratigraphic age and temperature for well 207/01-2

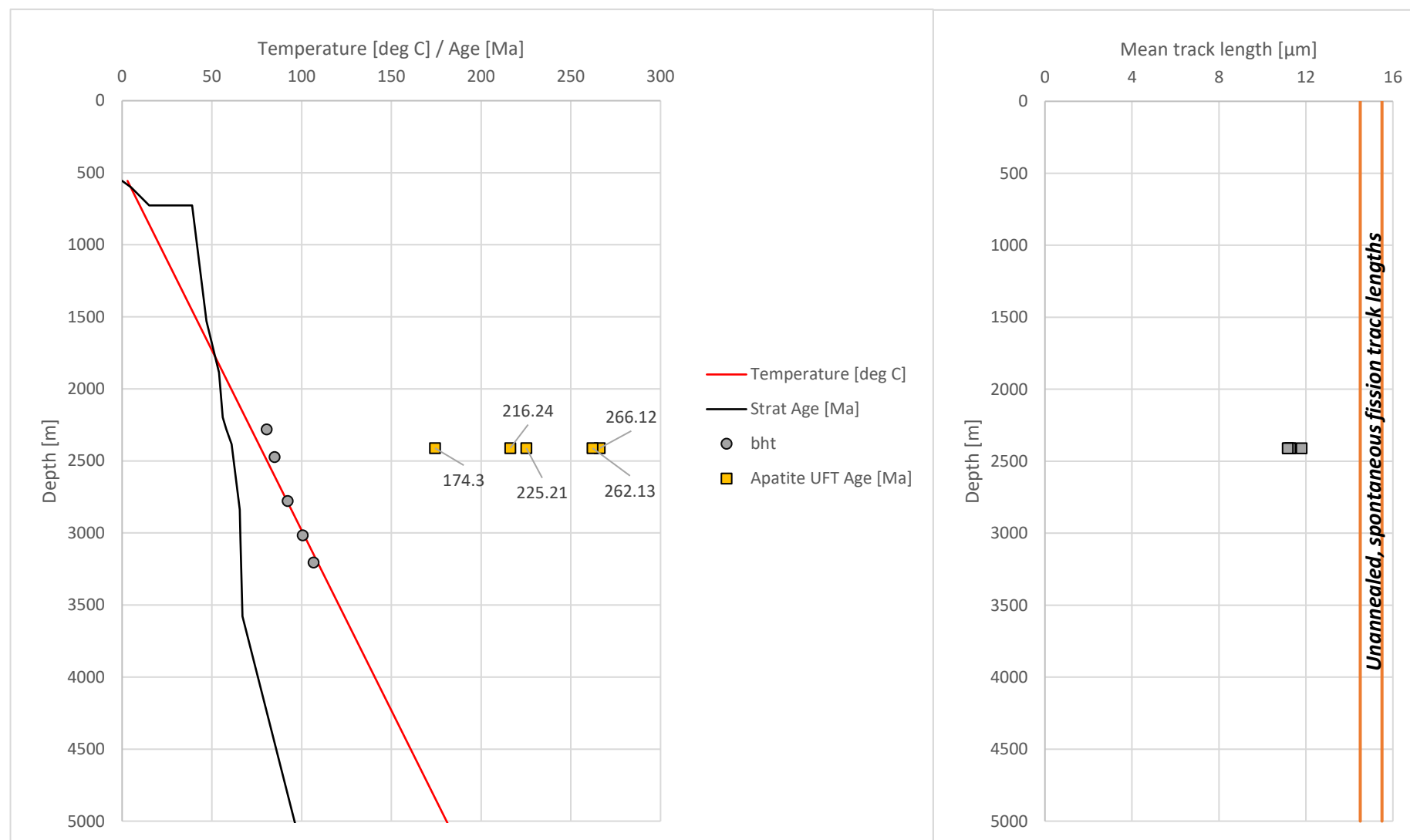


FIGURE 4.2.9 Apatite thermochronology parameters plotted against depth, stratigraphic age and temperature for well 208/17-2

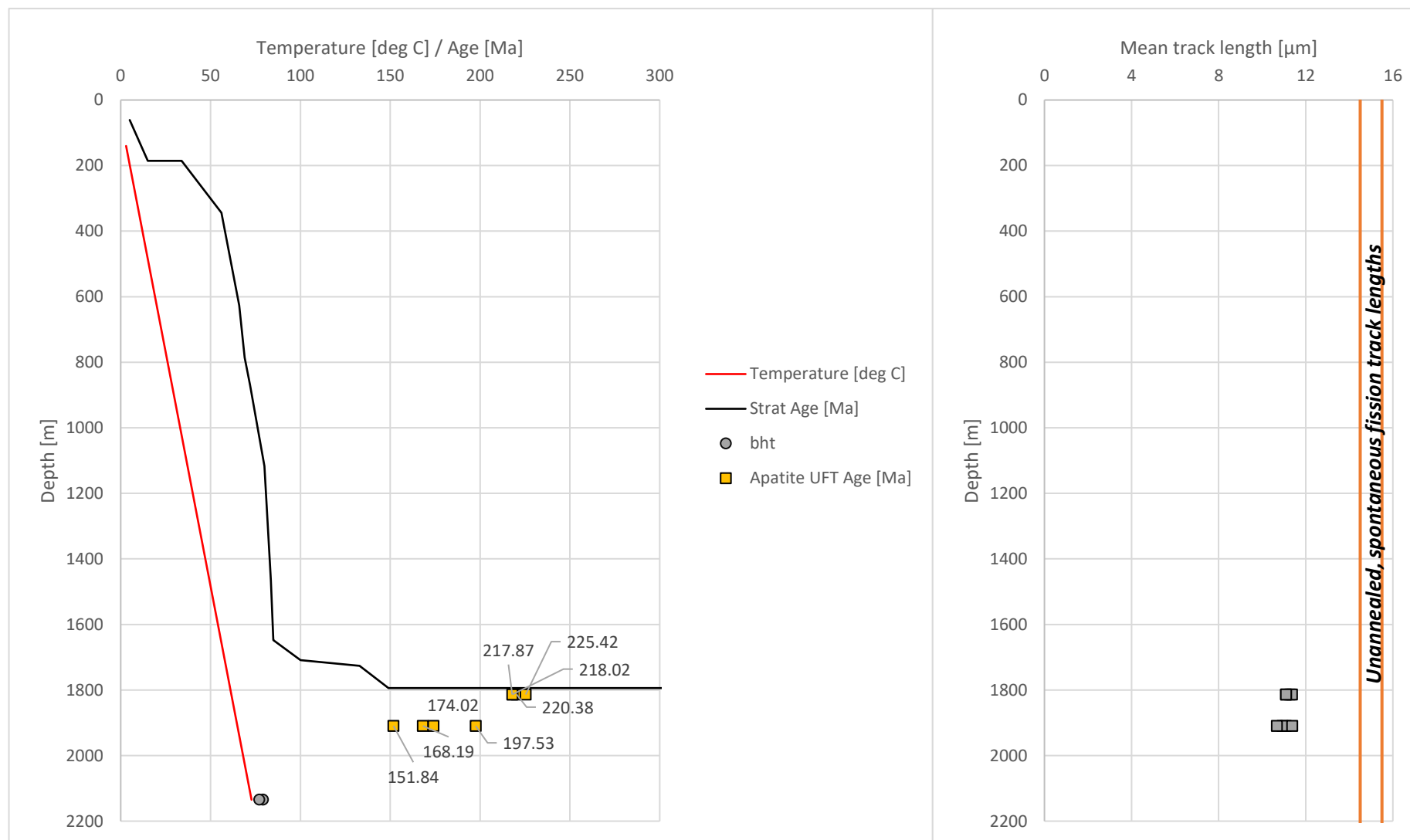


FIGURE 4.2.10 Apatite thermochronology parameters plotted against depth, stratigraphic age and temperature for well 208/24-1A

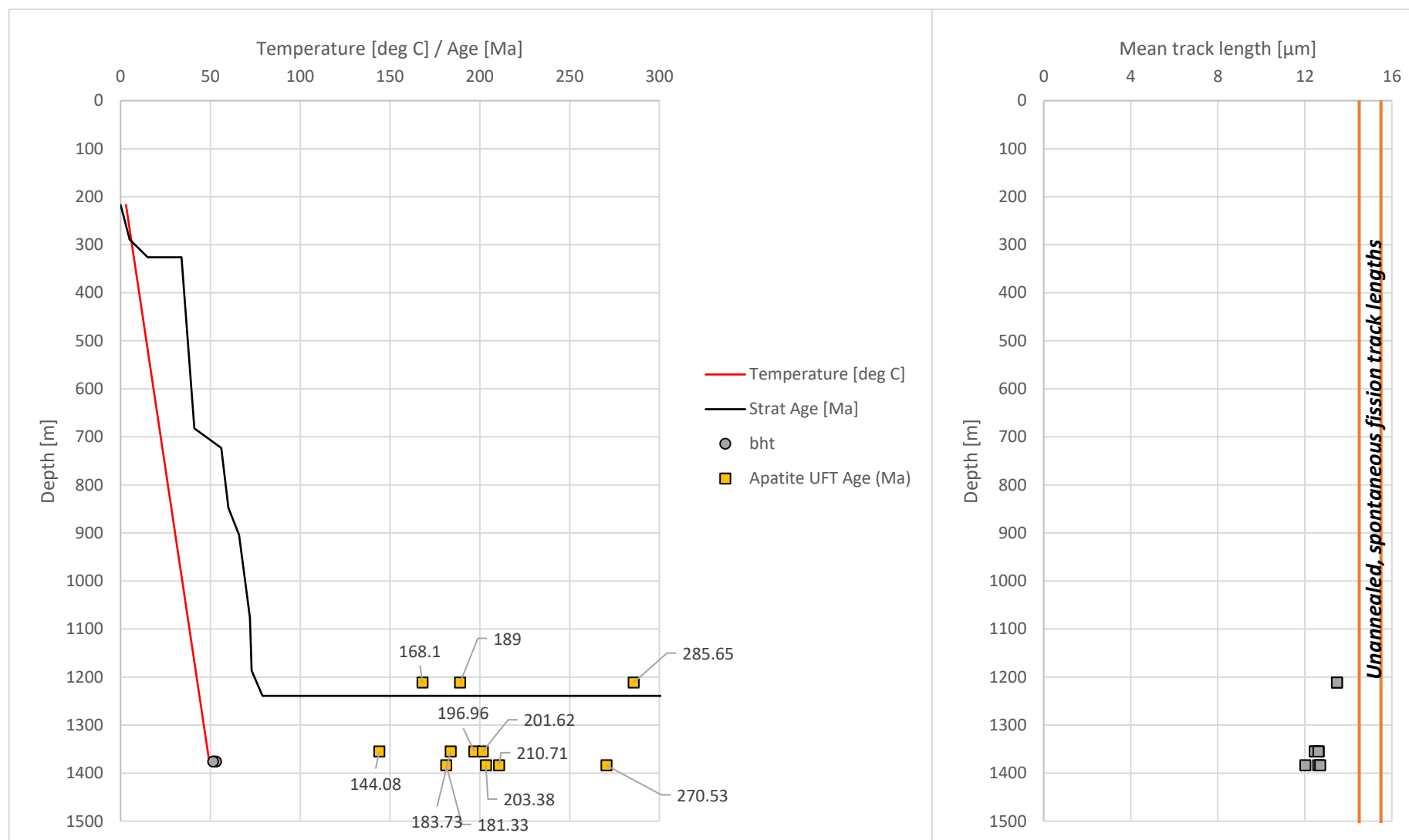


FIGURE 4.2.11 Apatite thermochronology parameters plotted against depth, stratigraphic age and temperature for well 208/27-2

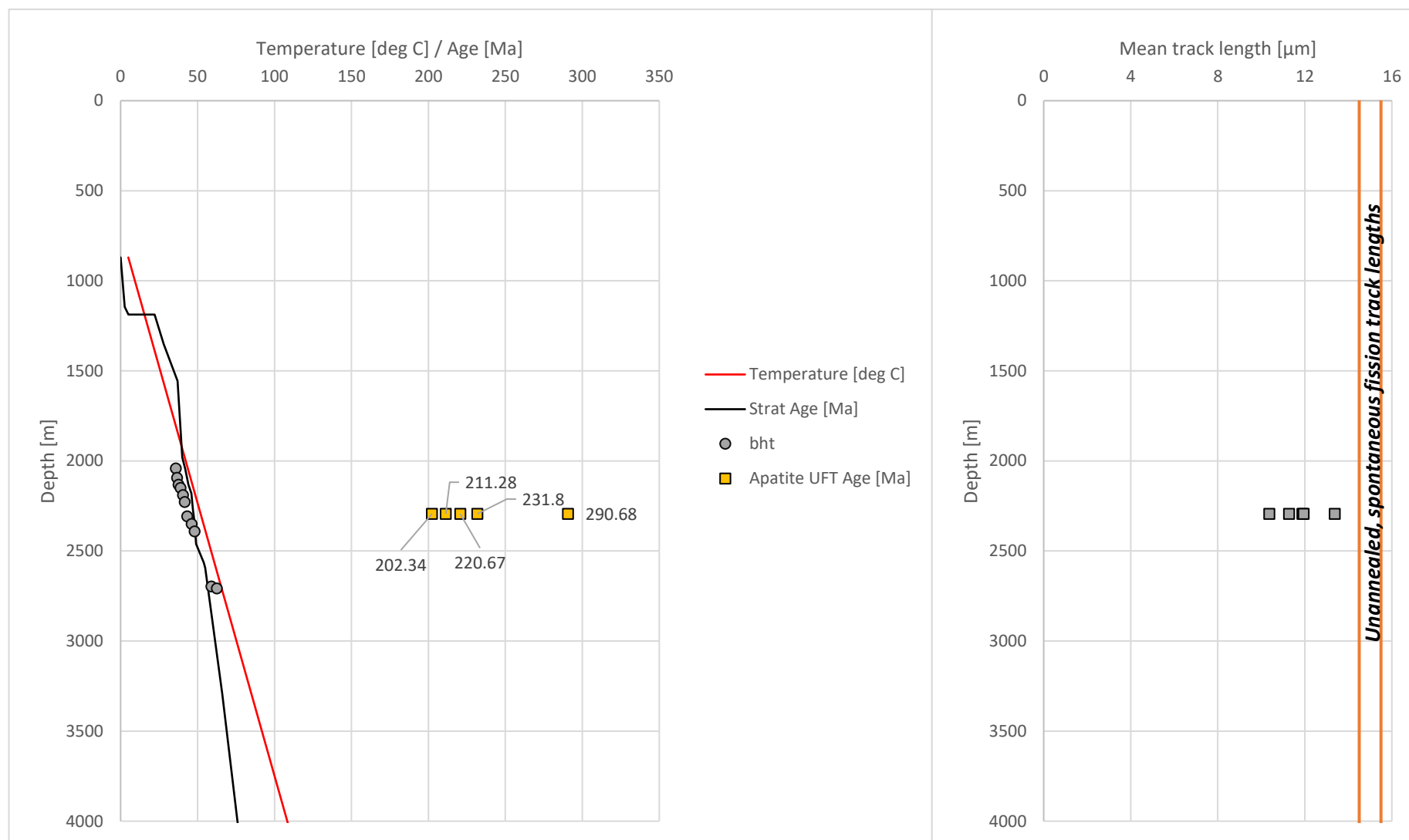


FIGURE 4.2.12 Apatite thermochronology parameters plotted against depth, stratigraphic age and temperature for well 214/26-1

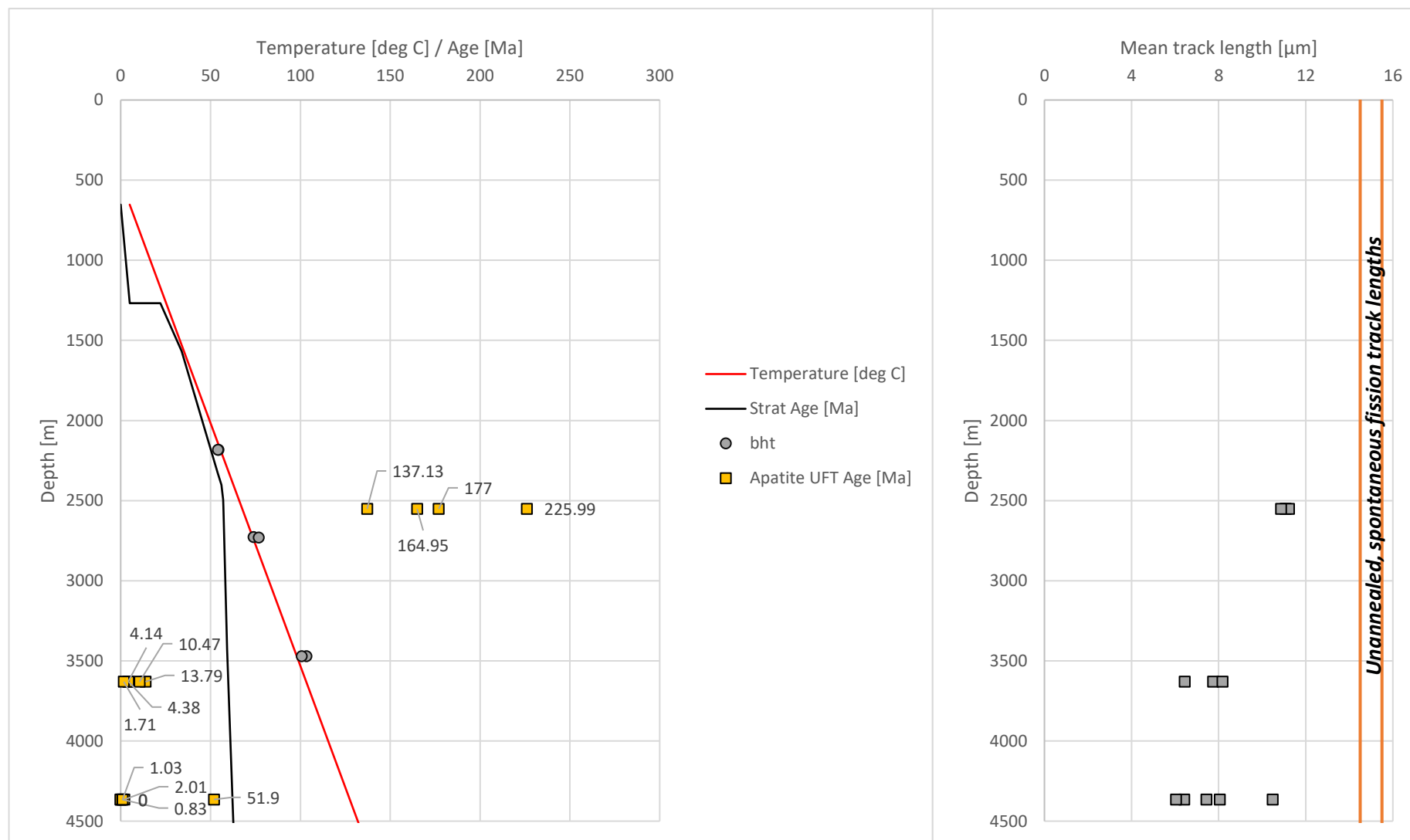


FIGURE 4.2.13 Apatite thermochronology parameters plotted against depth, stratigraphic age and temperature for well 214/28-1

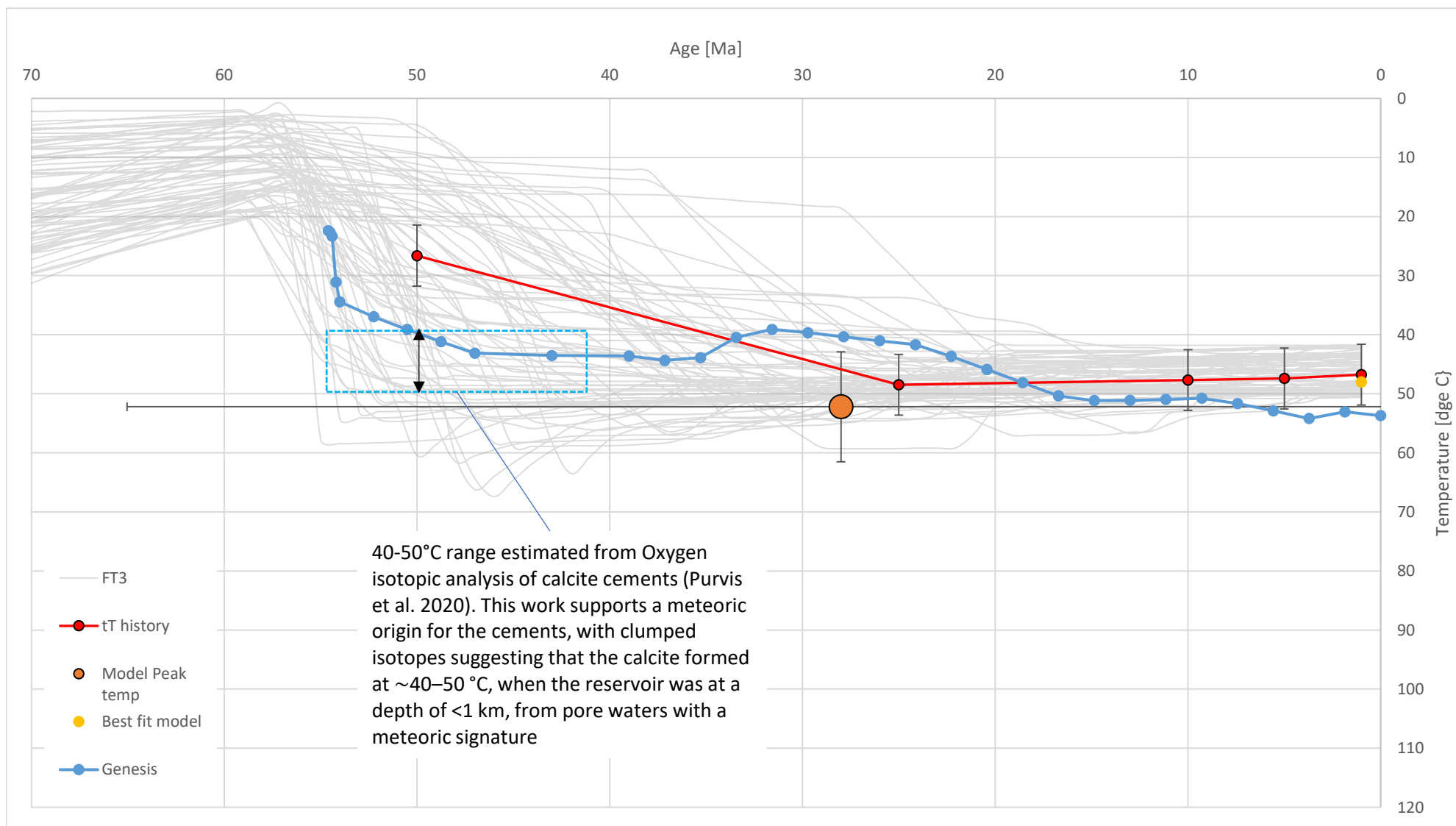


FIGURE 4.3.1 Thermal history data derived from the Apatite.Inc modelling for well 204/10a-5 sample depth 2372.6m

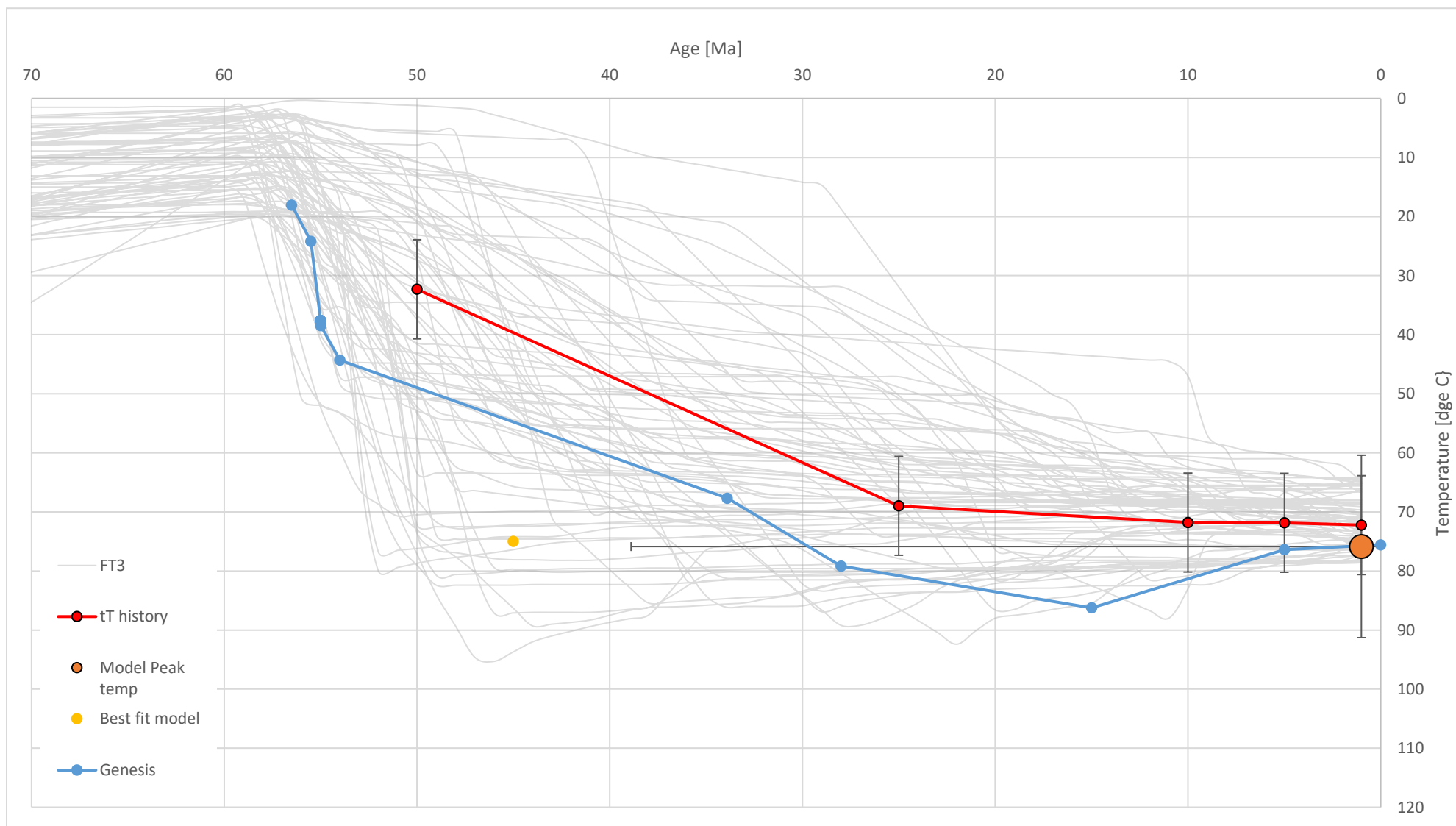


FIGURE 4.3.2 Thermal history data derived from the Apatite.Inc modelling for well 205/09-1 sample depth 2802.5m

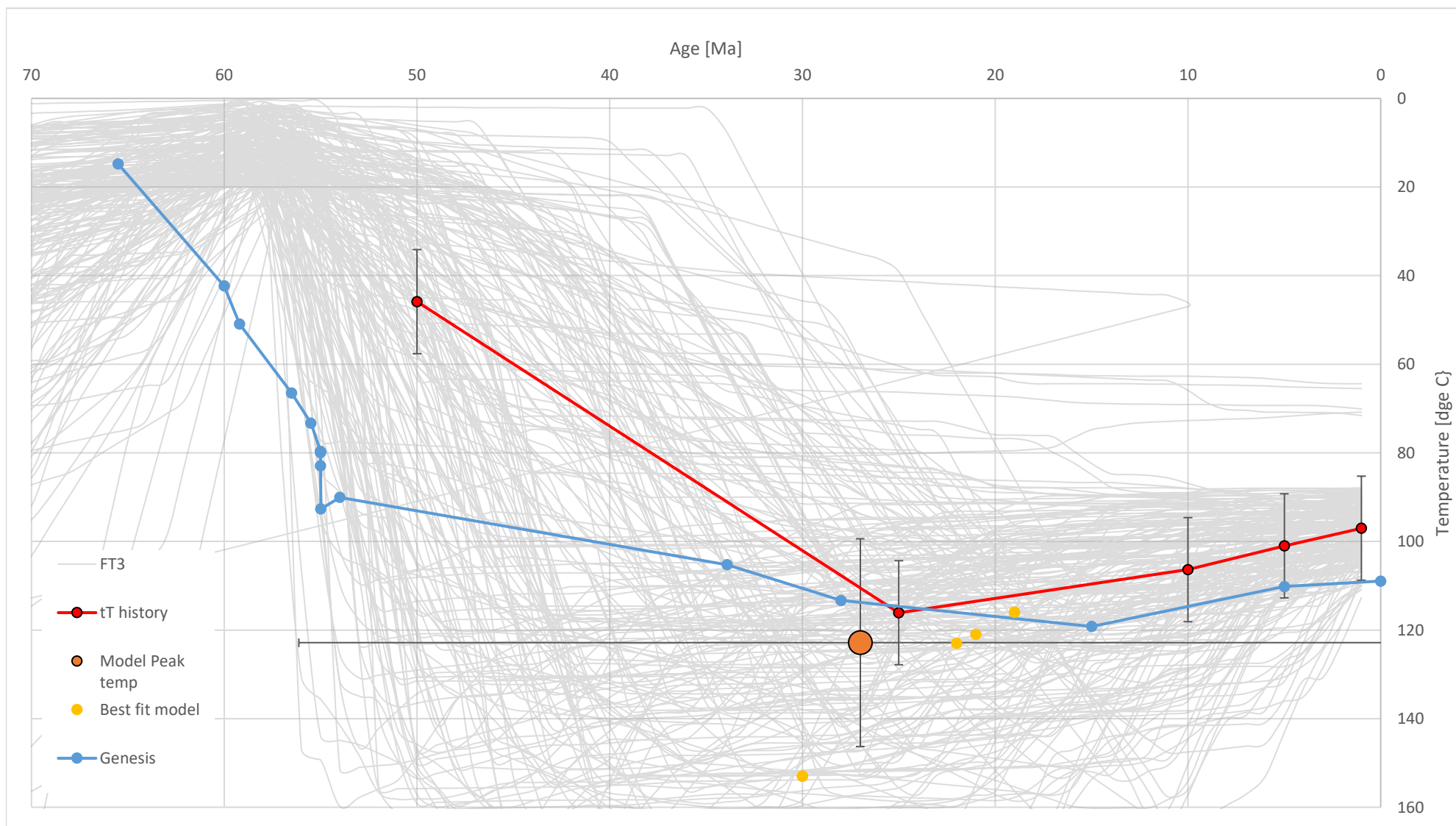


FIGURE 4.3.3 Thermal history data derived from the Apatite.Inc modelling for well 205/09-1 sample depth 3711.5m

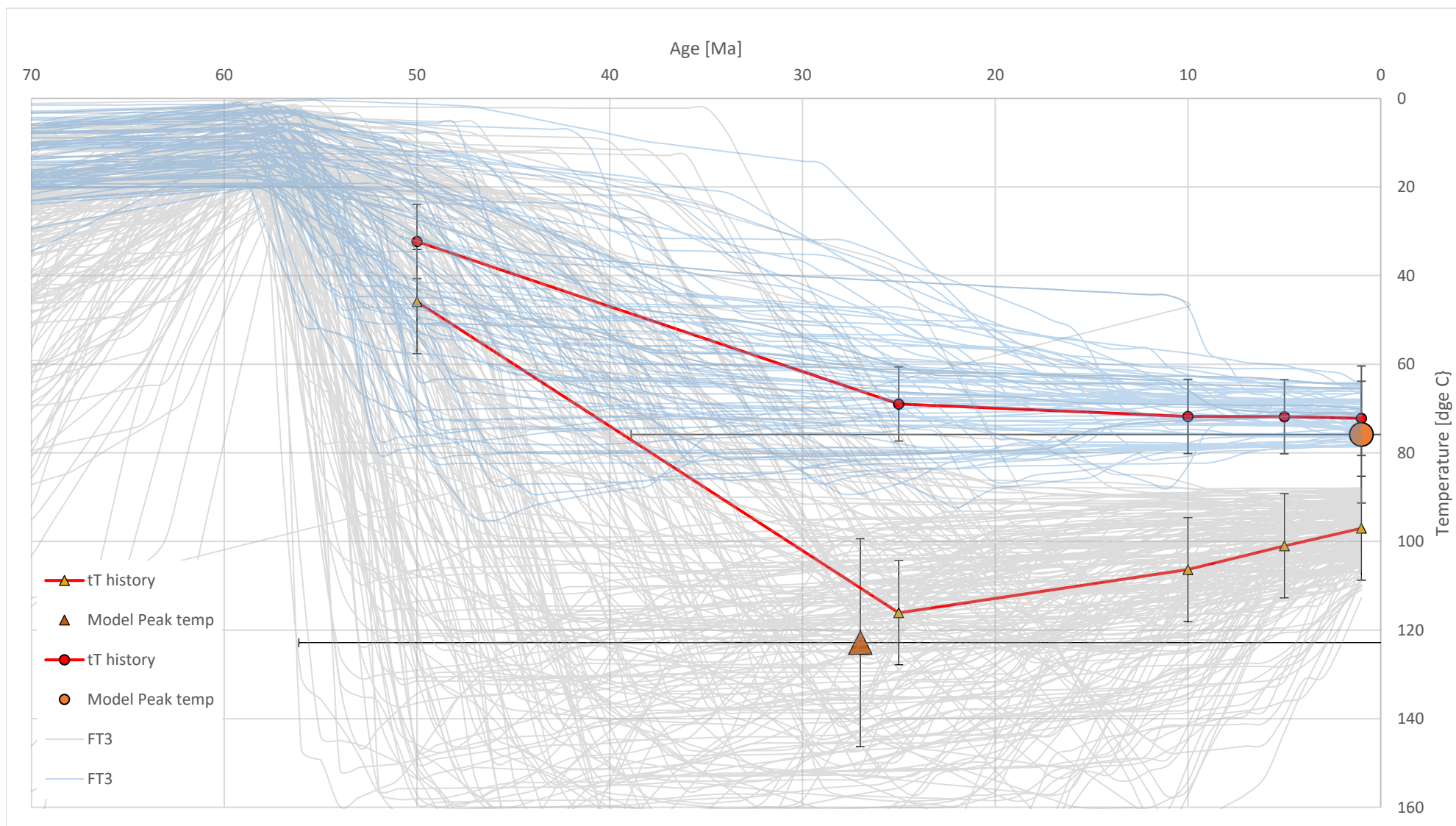


FIGURE 4.3.4 Combined thermal history 205/09-1 from samples 2802.5m & 3711.5m

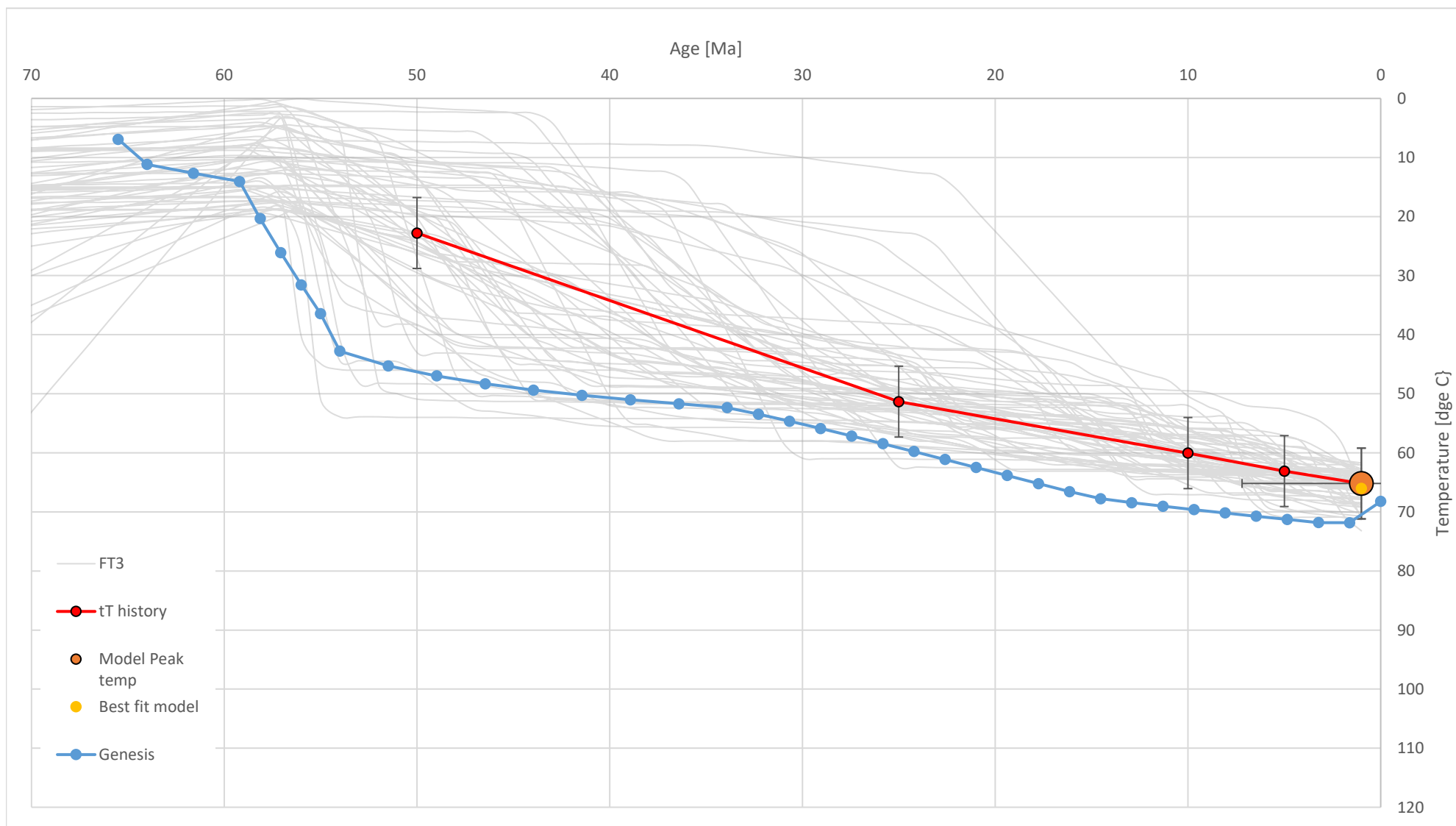


FIGURE 4.3.5 Thermal history data derived from the Apatite.Inc modelling for well 205/12-1 sample depth 2570m

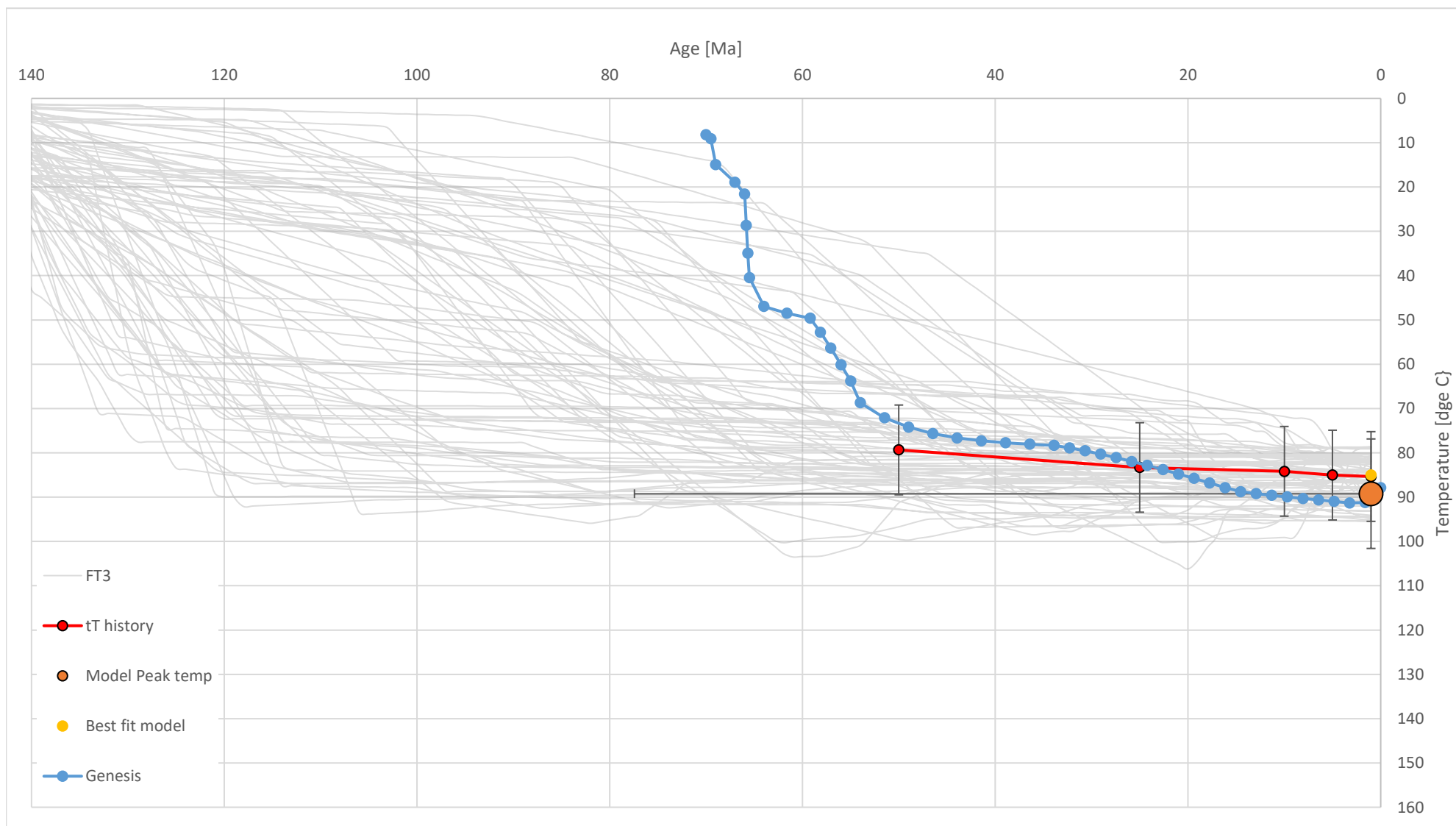


FIGURE 4.3.6 Thermal history data derived from the Apatite.Inc modelling for well 205/12-1 sample depth 3175m

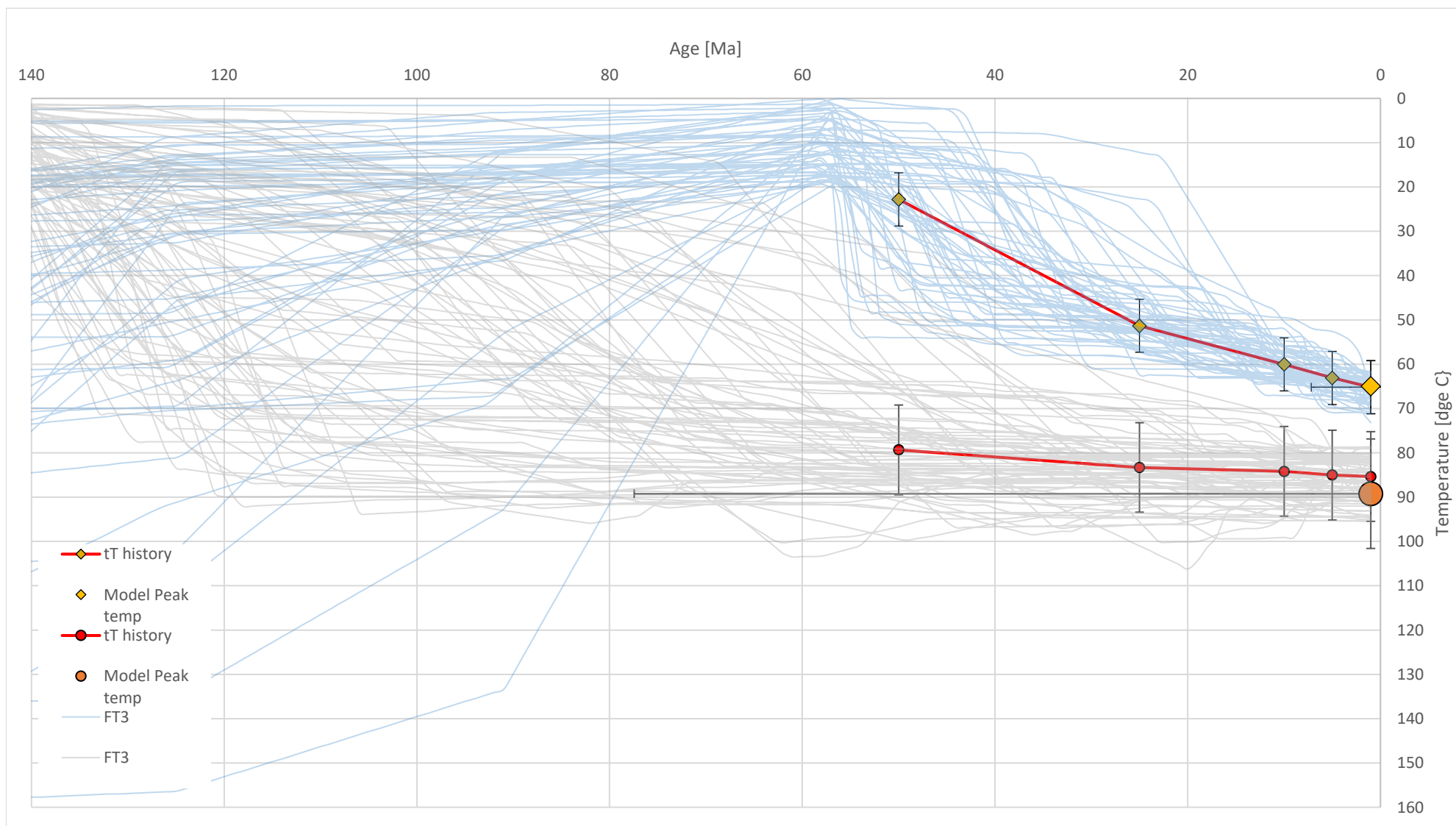


FIGURE 4.3.7 Combined thermal history 205/12-1 from samples 2570m & 3175m

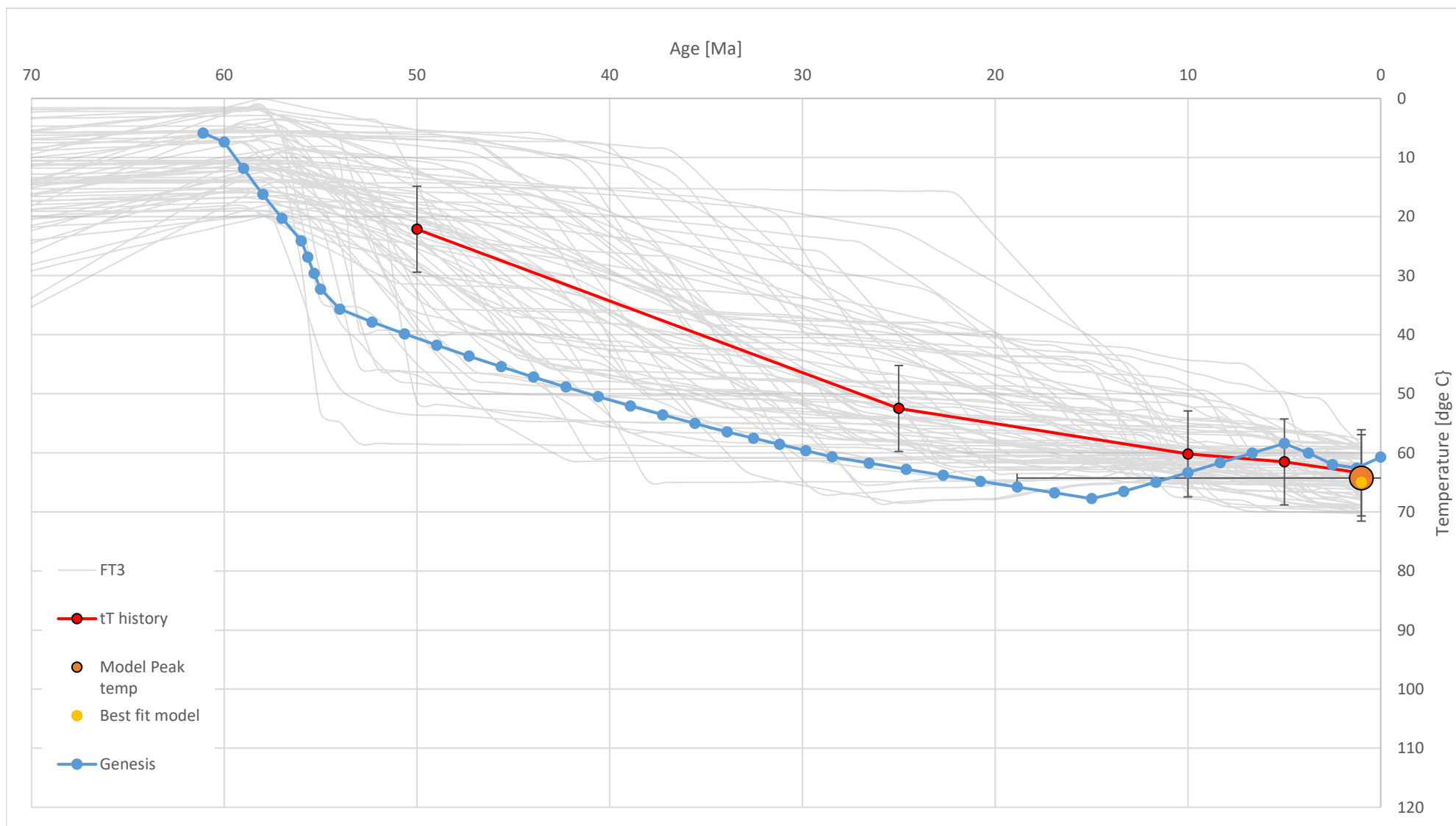


FIGURE 4.3.8 Thermal history data derived from the Apatite.Inc modelling for well 205/14-2 sample depth 2265m

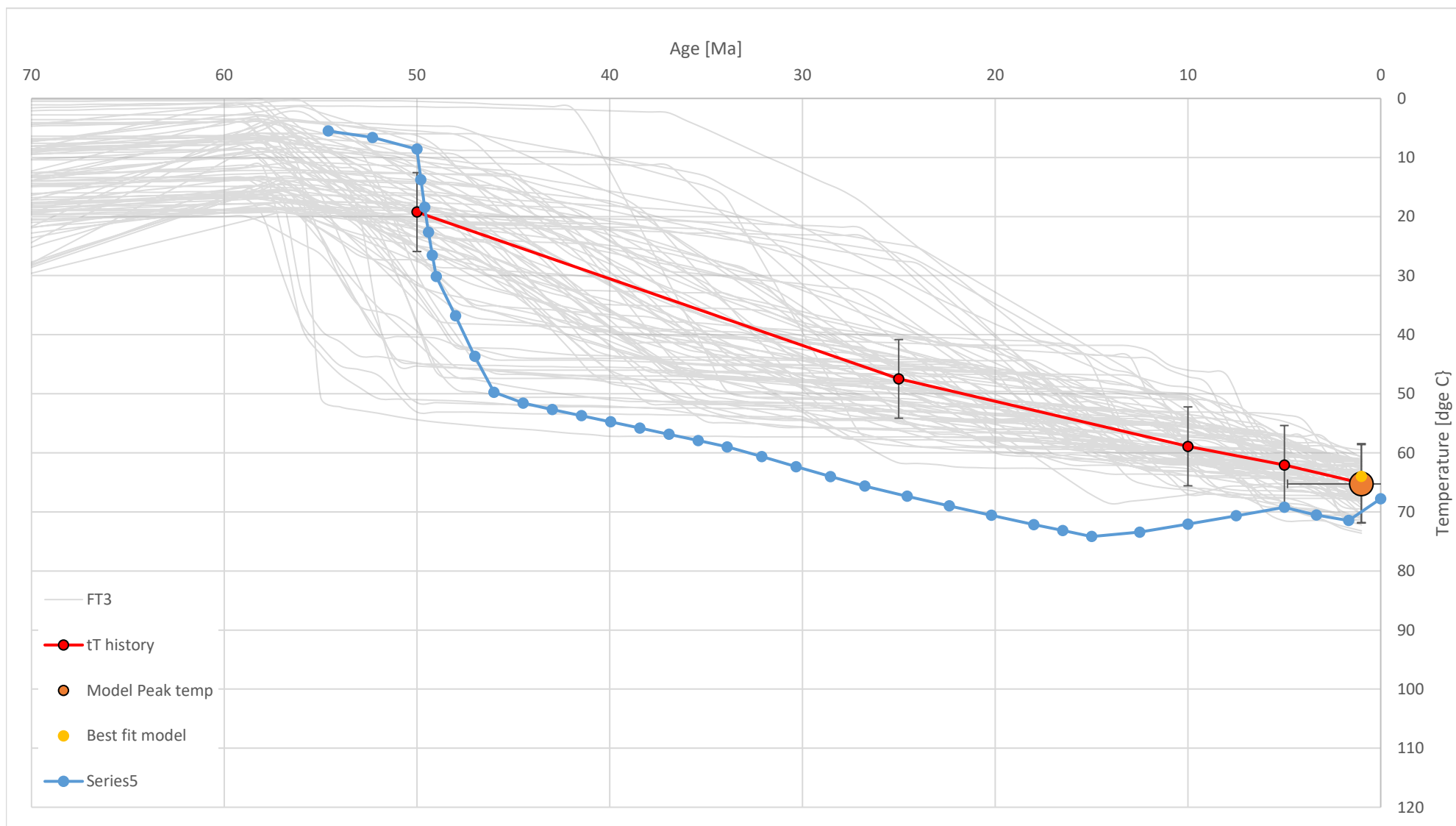


FIGURE 4.3.9 Thermal history data derived from the Apatite.Inc modelling for well 205/17b-2 sample depth 2443.8m

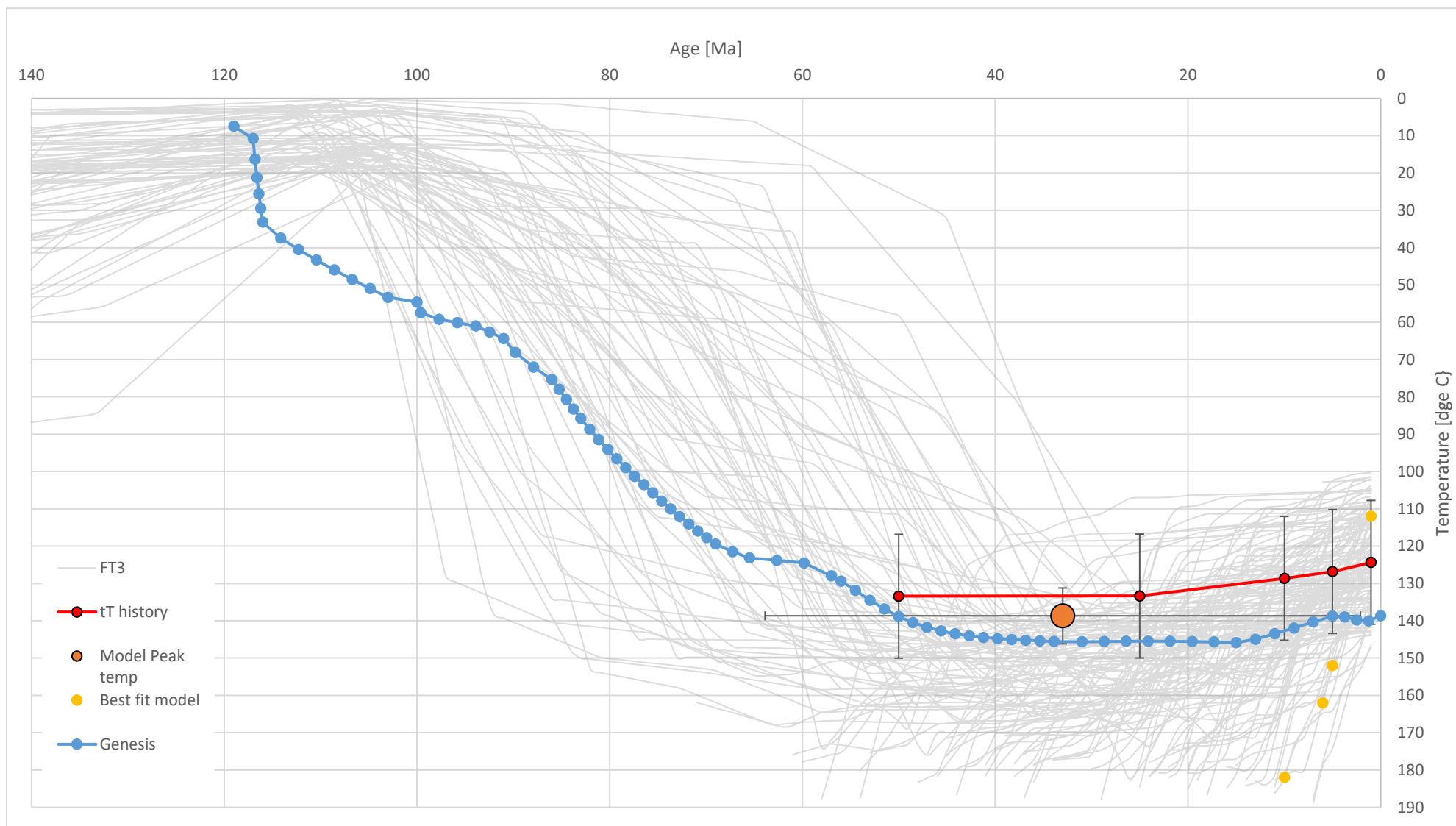


FIGURE 4.3.10 Thermal history data derived from the Apatite.Inc modelling for well 206/11-1 sample depth 4373m

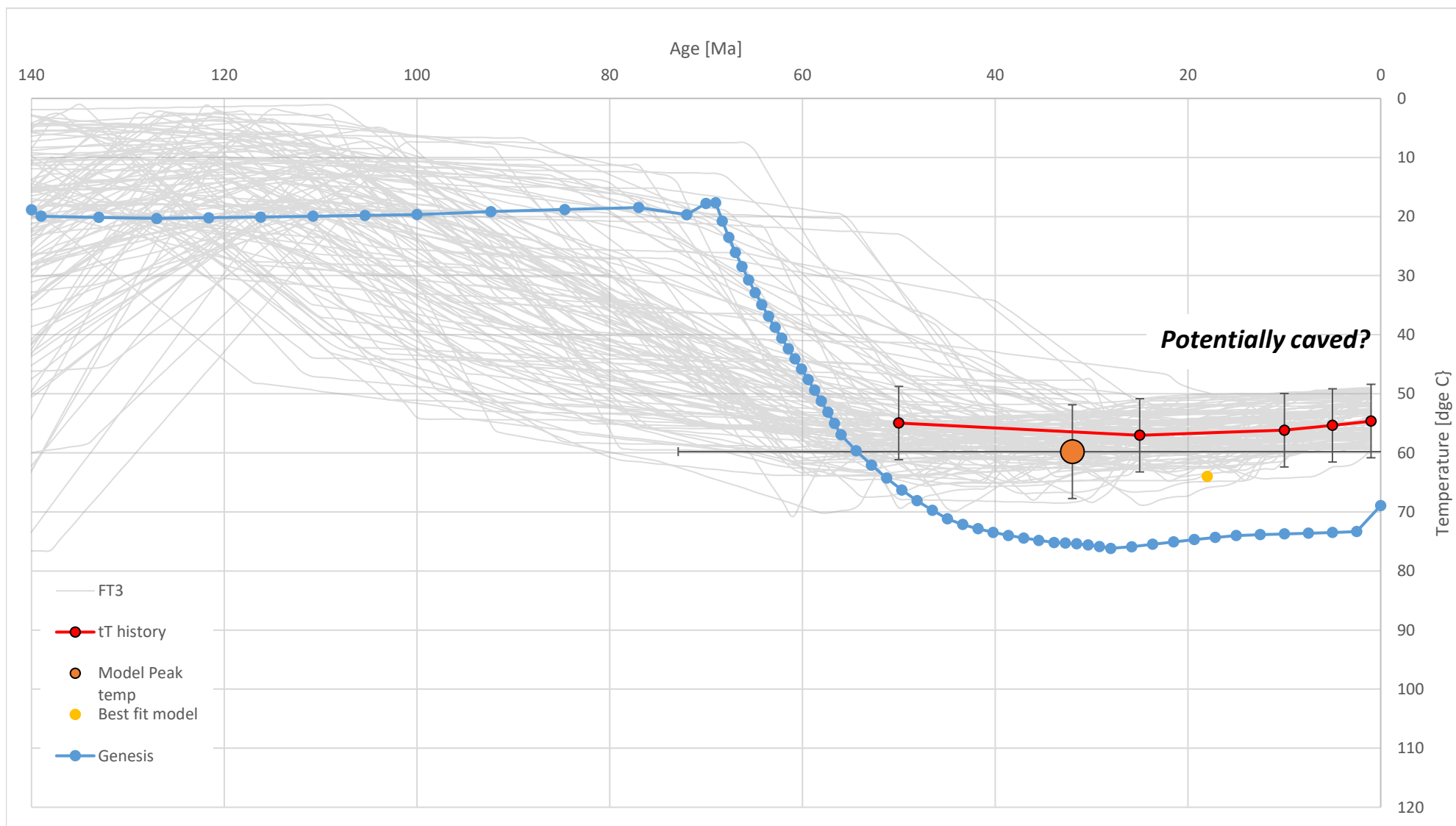


FIGURE 4.3.11 Thermal history data derived from the Apatite.Inc modelling for well 207/1-2 sample depth 1708.404m

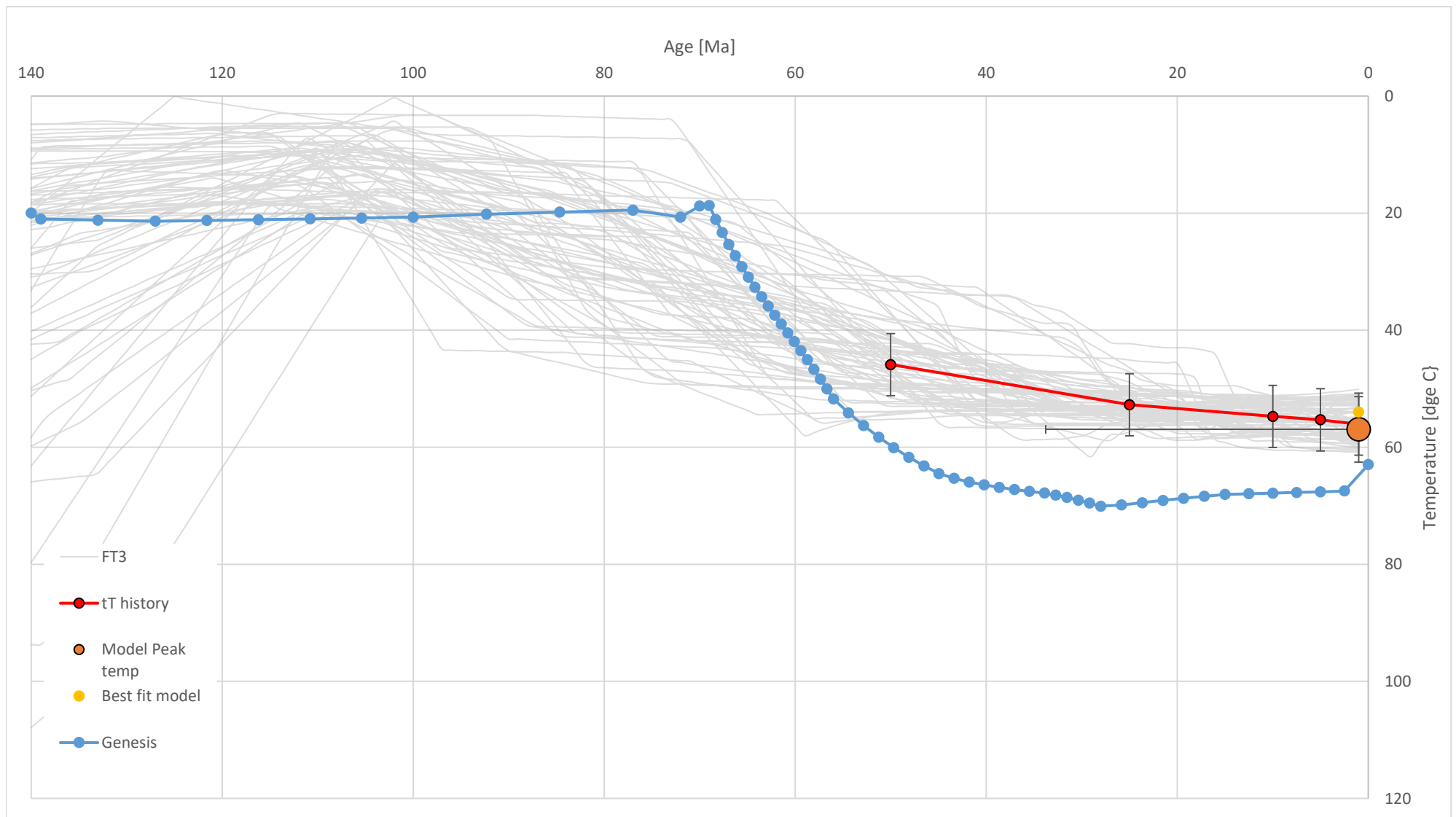


FIGURE 4.3.12 Thermal history data derived from the Apatite.Inc modelling for well 207/1-2 sample depth 1751m

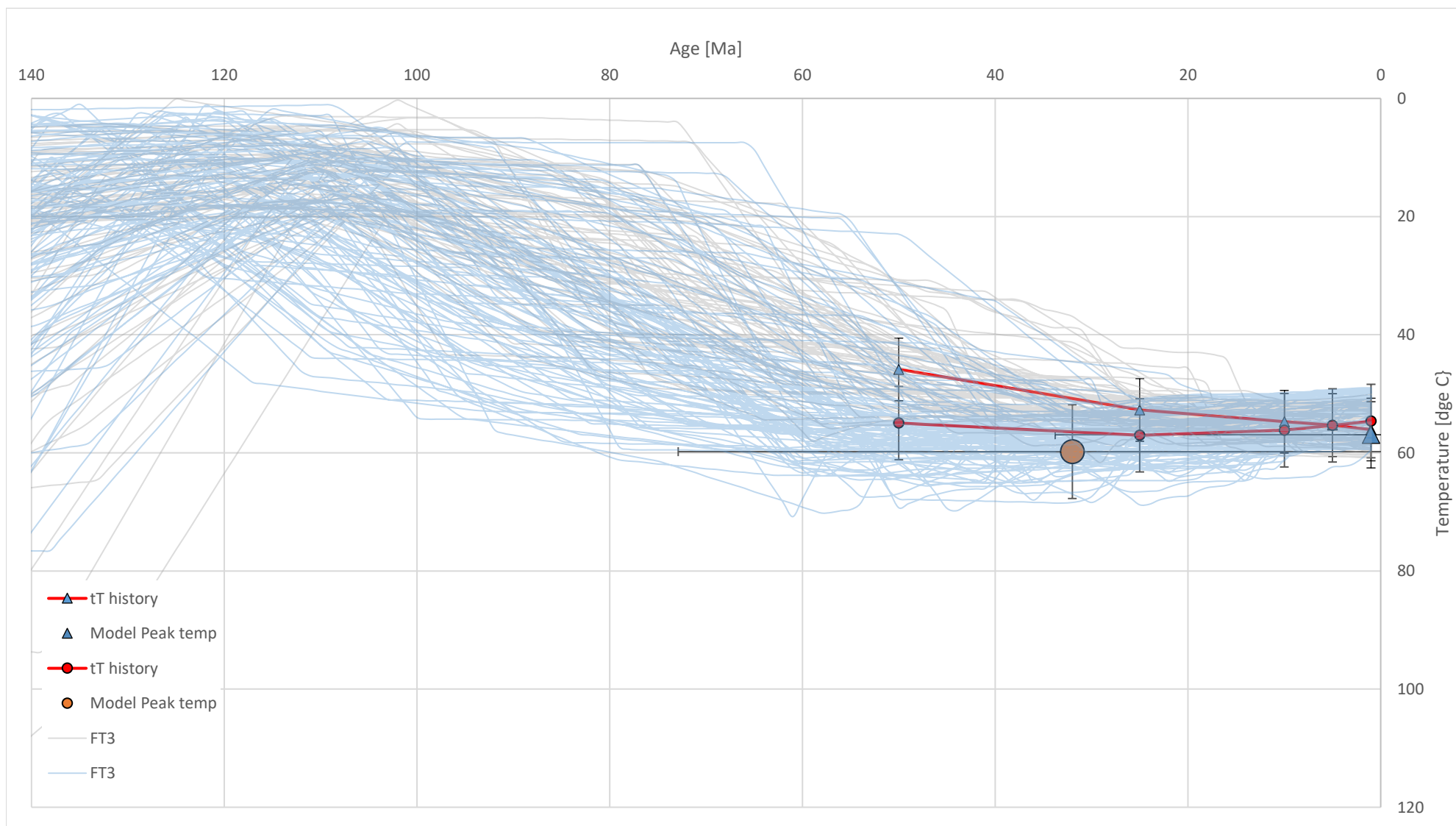


FIGURE 4.3.13 Combined thermal history 207/1-2 from samples 1708.404m & 1751m

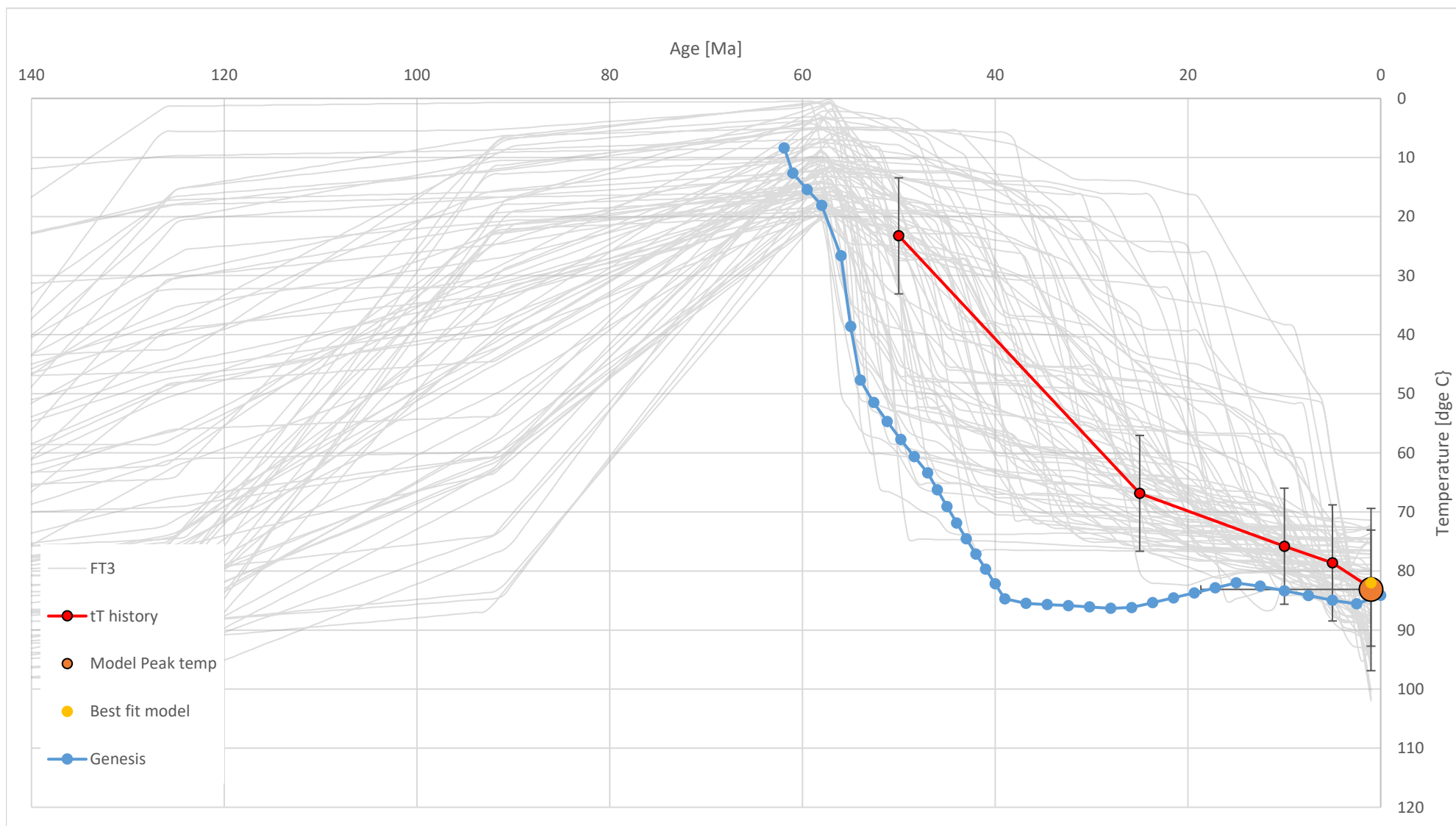


FIGURE 4.3.14 Thermal history data derived from the Apatite.Inc modelling for well 208/17-2 sample depth 2411m

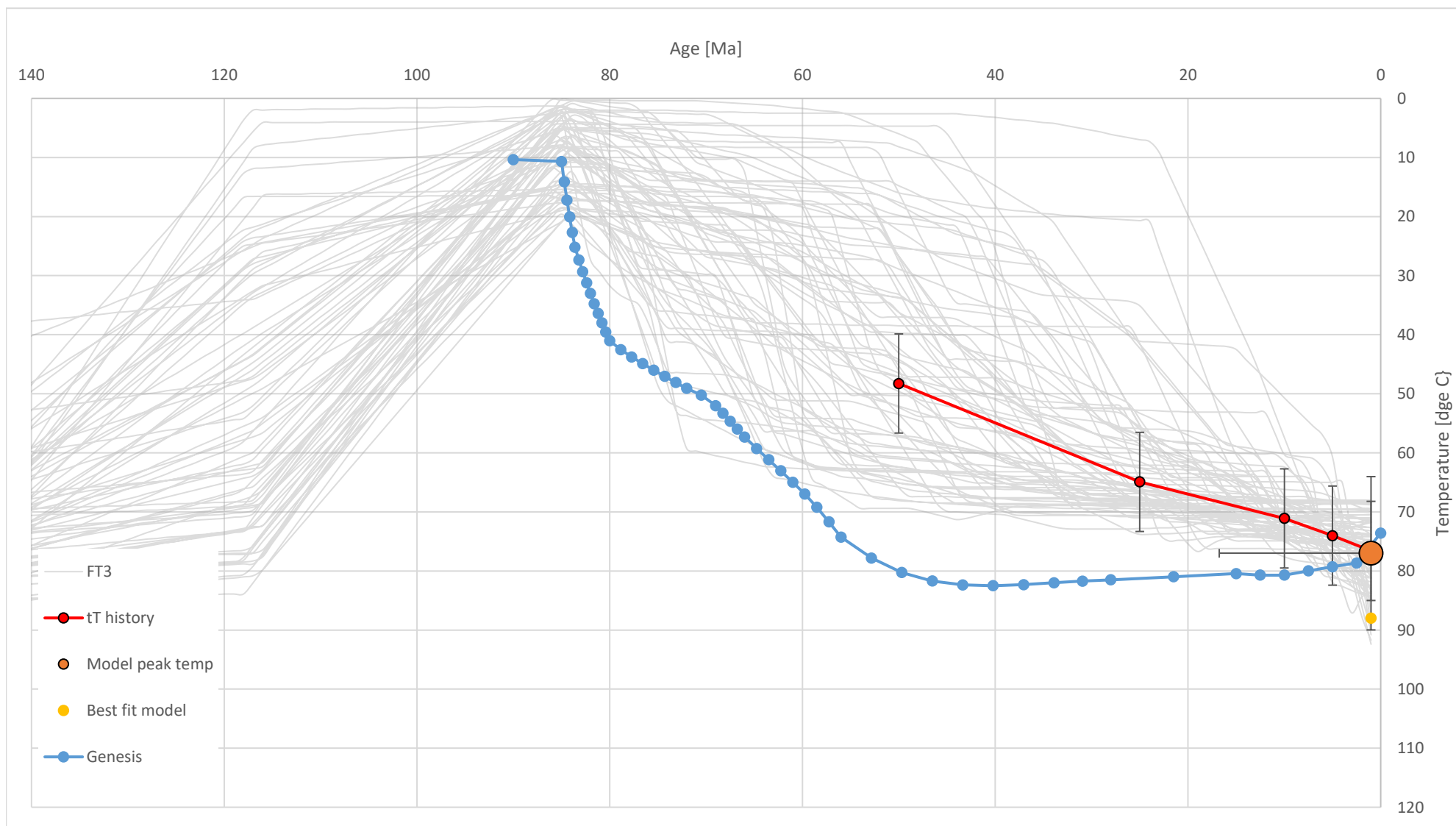


FIGURE 4.3.15 Thermal history data derived from the Apatite.Inc modelling for well 208/24-1 sample depth 1813.5m

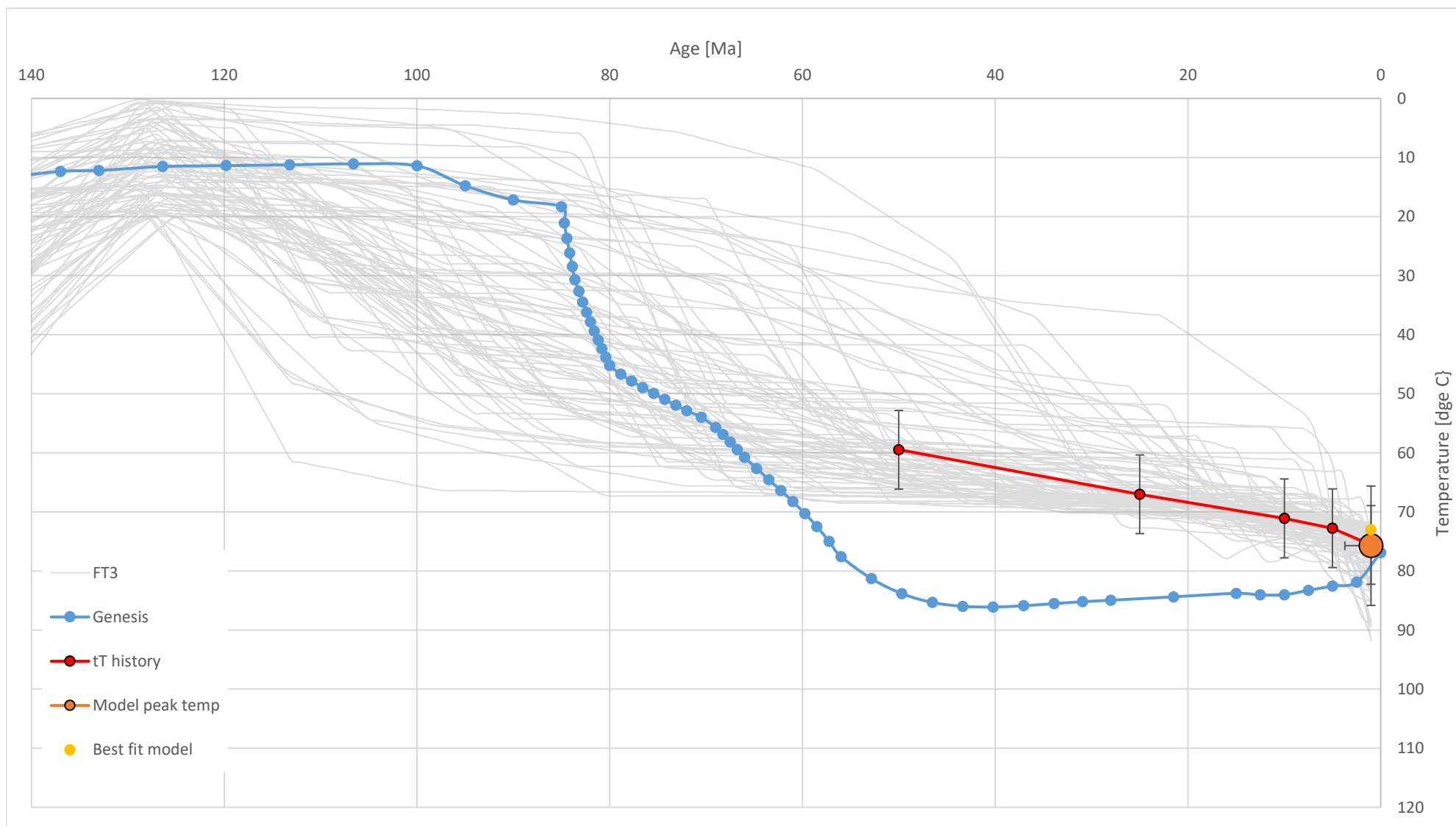


FIGURE 4.3.16 Thermal history data derived from the Apatite.Inc modelling for well 208/24-1 sample depth 1909.572m

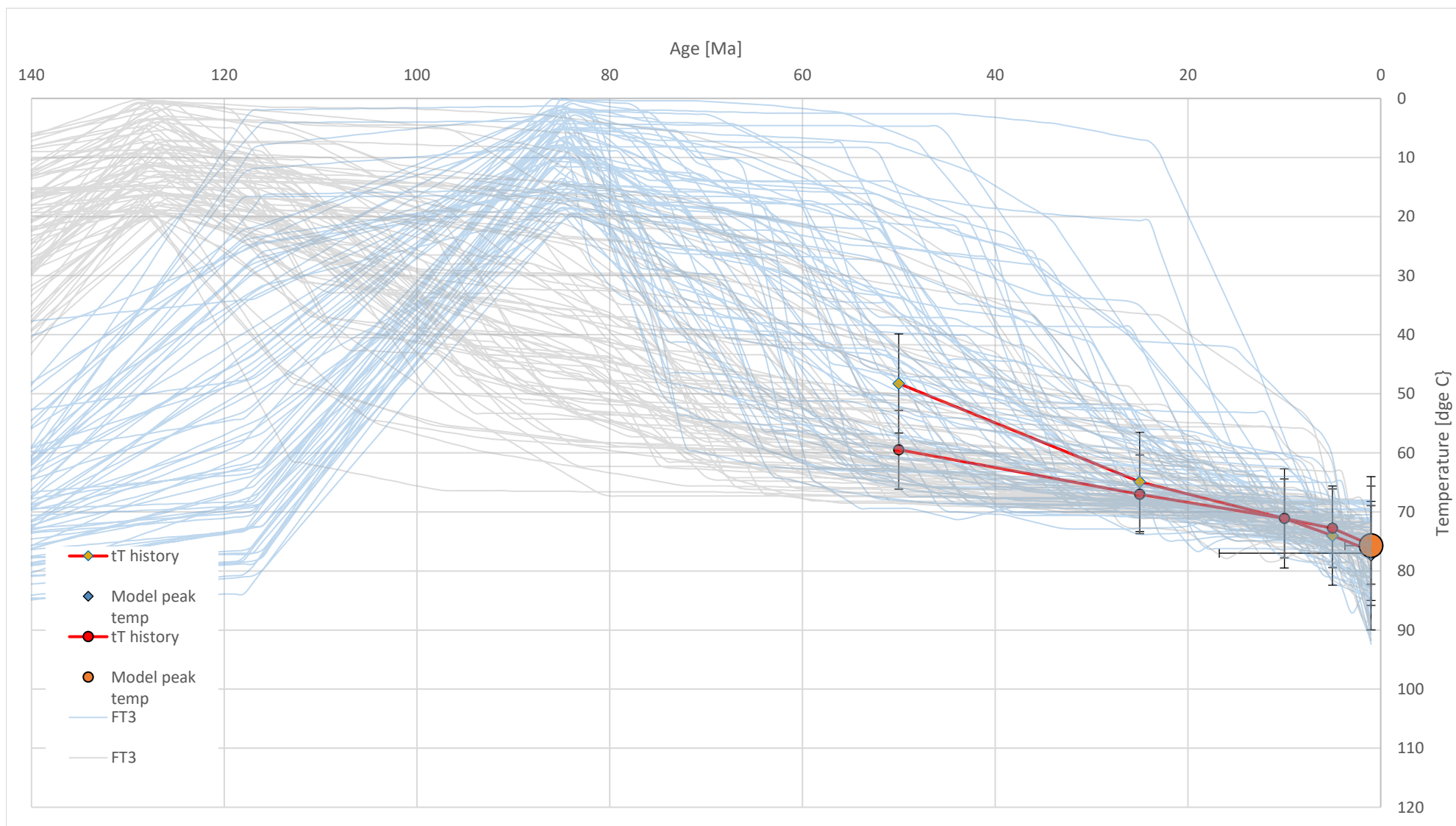


FIGURE 4.3.17 Combined thermal history 208/24-1 from samples 1813.5m & 1909.572m

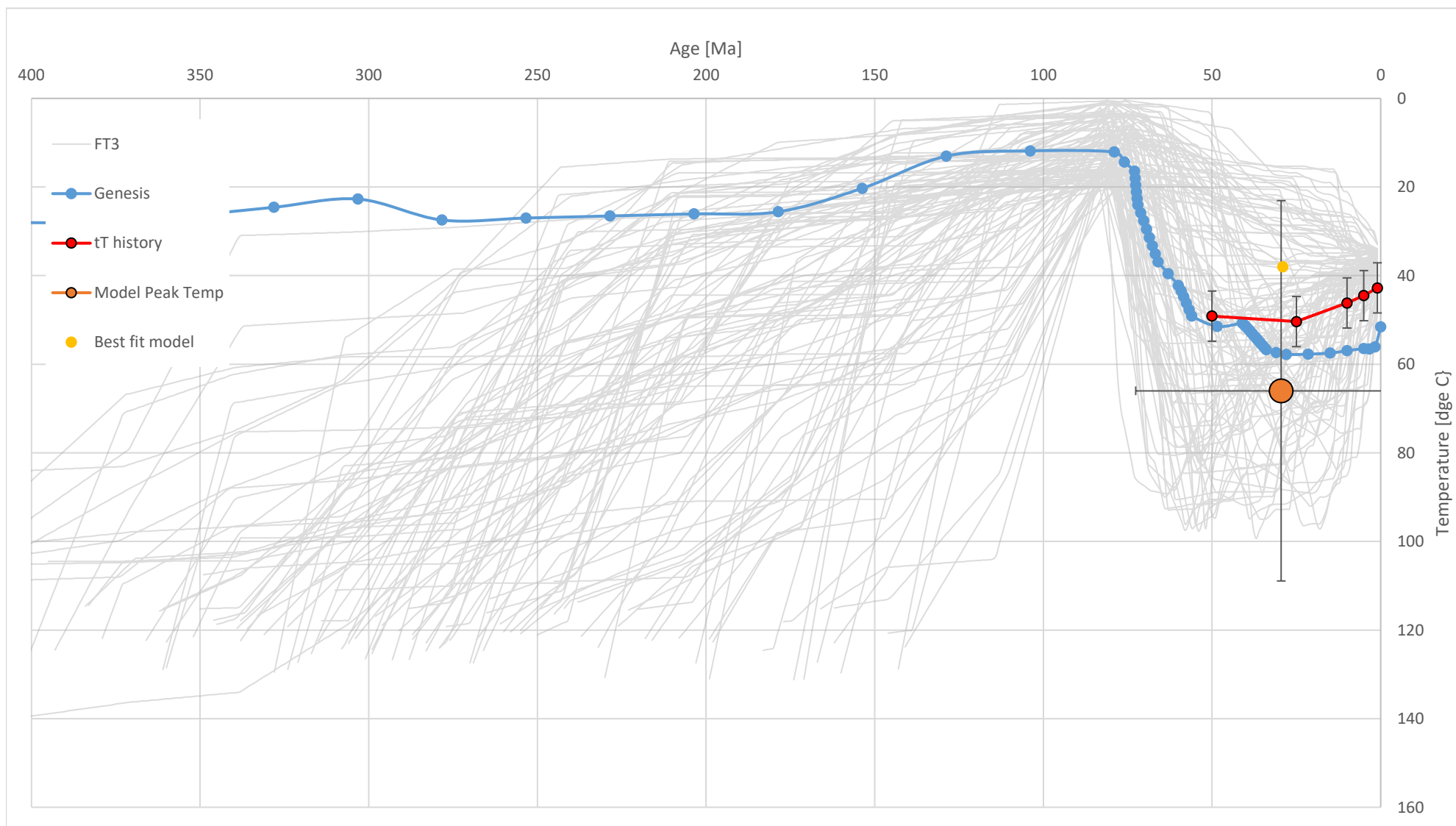


FIGURE 4.3.18 Thermal history data derived from the Apatite.Inc modelling for well 208/27-2 sample depth 1211.58m

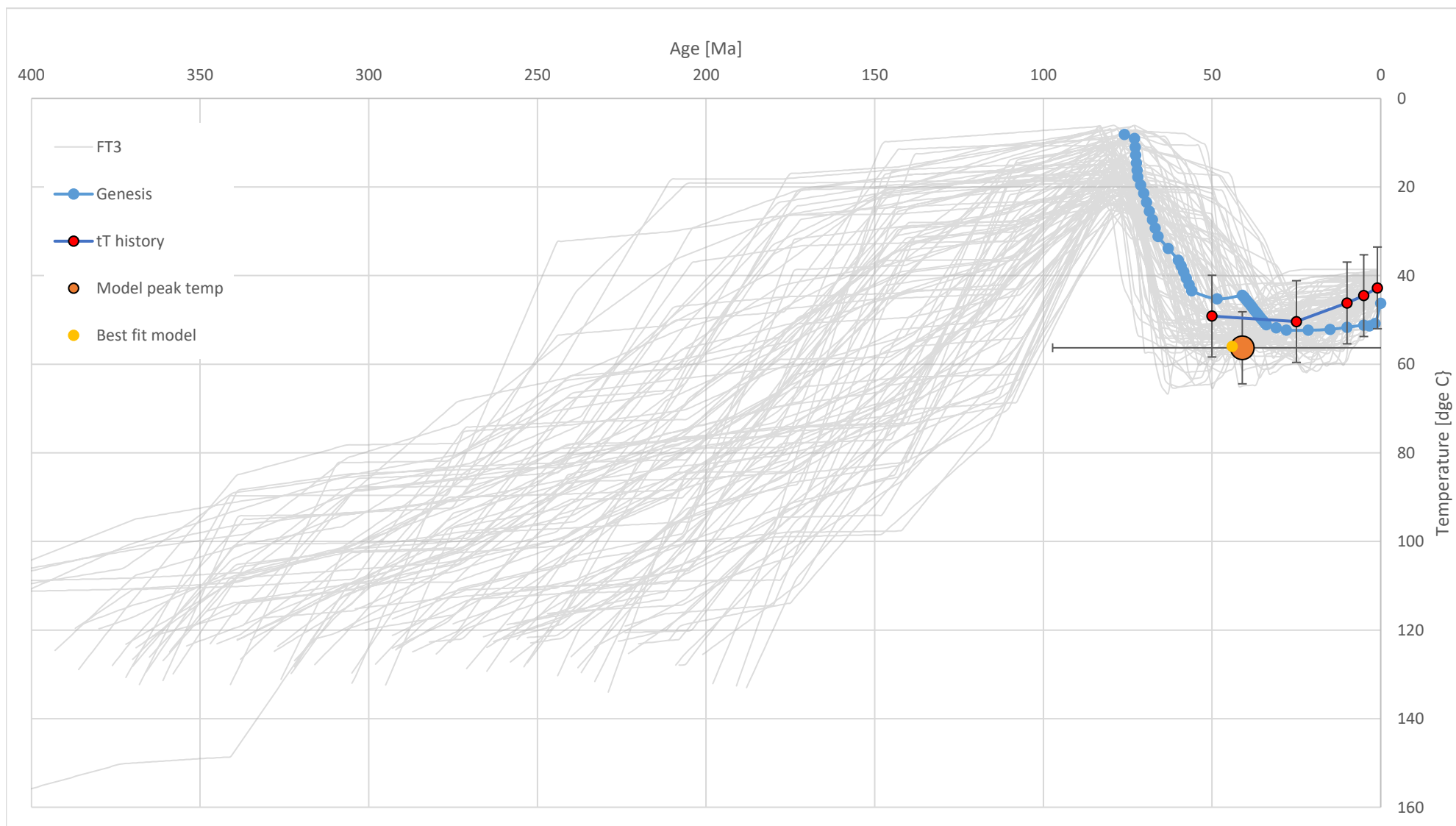


FIGURE 4.3.19 Thermal history data derived from the Apatite.Inc modelling for well 208/27-2 sample depth 1383m

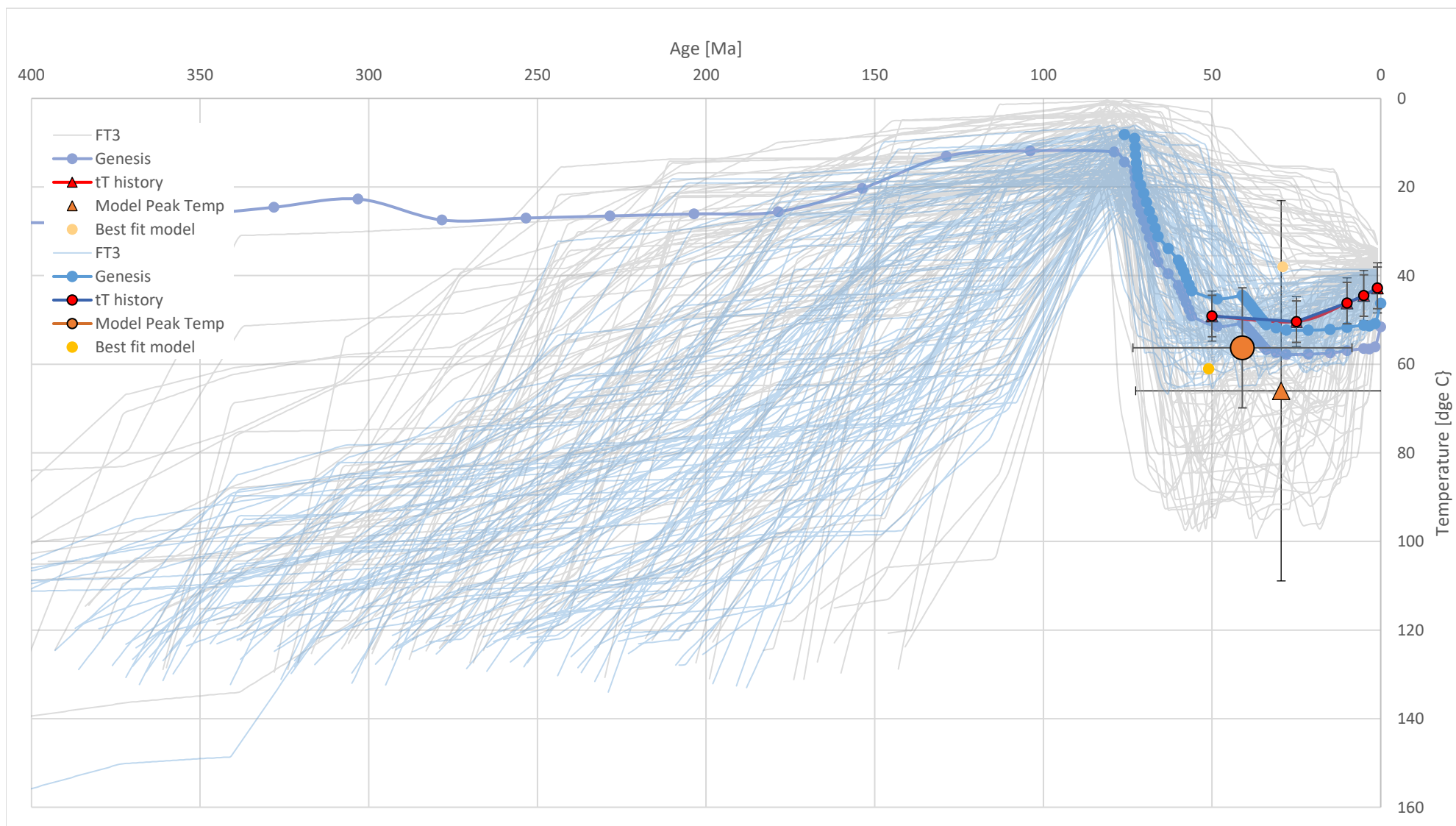


FIGURE 4.3.20 Combined thermal history 208/27-2 from samples 1211.58m & 1383m

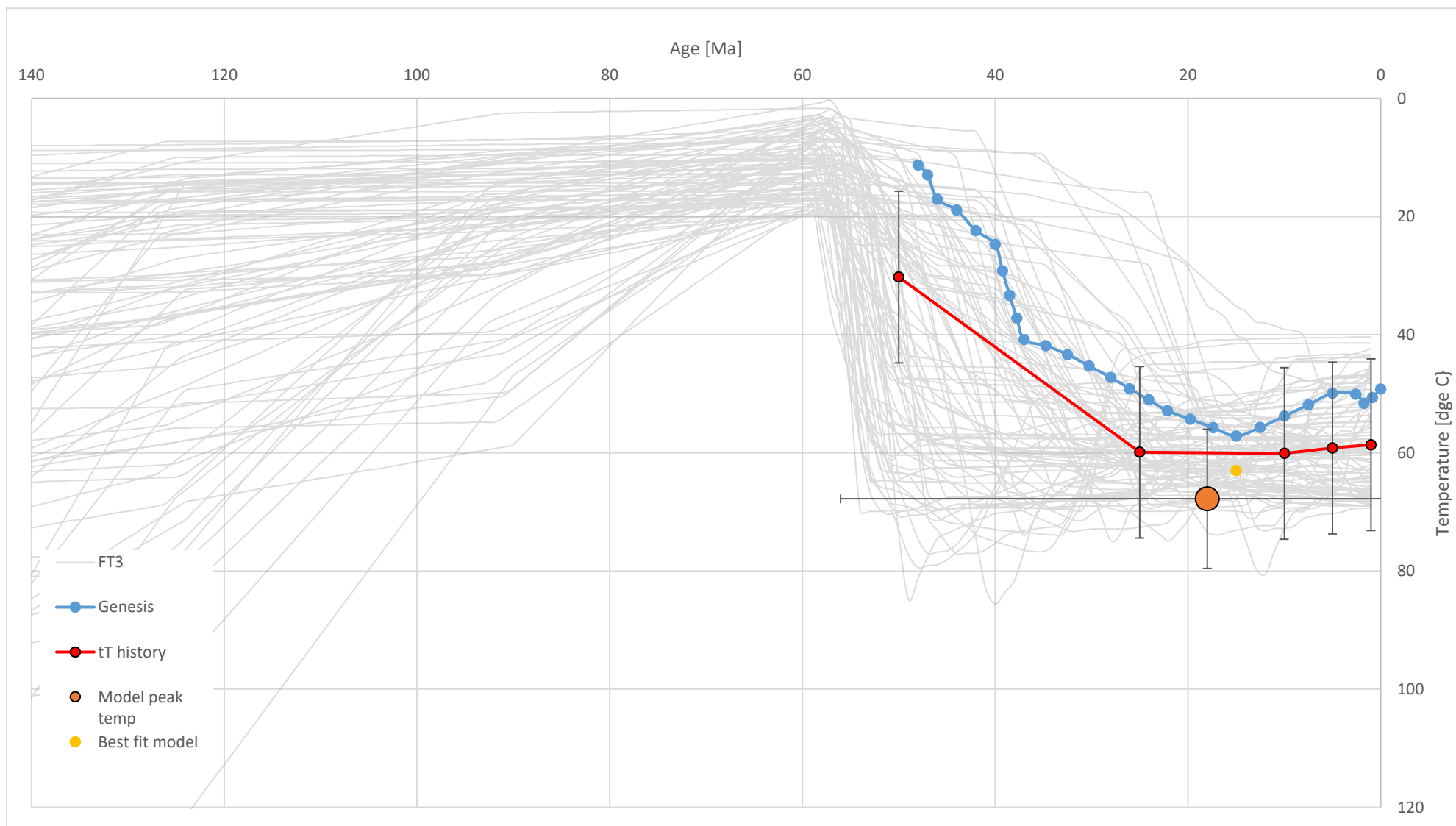


FIGURE 4.3.21 Thermal history data derived from the Apatite.Inc modelling for well 214/26-1 sample depth 2294m

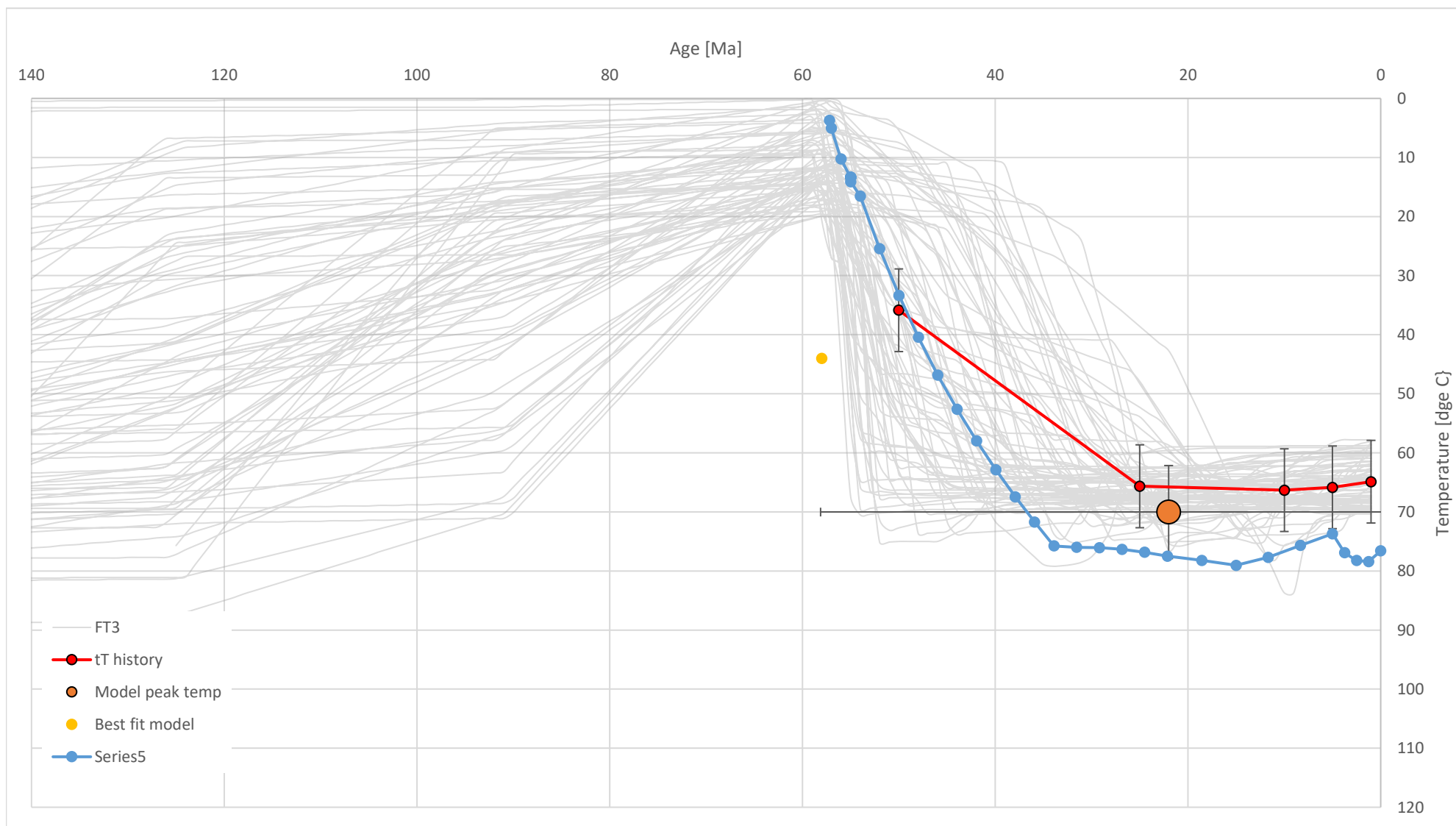


FIGURE 4.3.22 Thermal history data derived from the Apatite.Inc modelling for well 214/28-1 sample depth 2552m

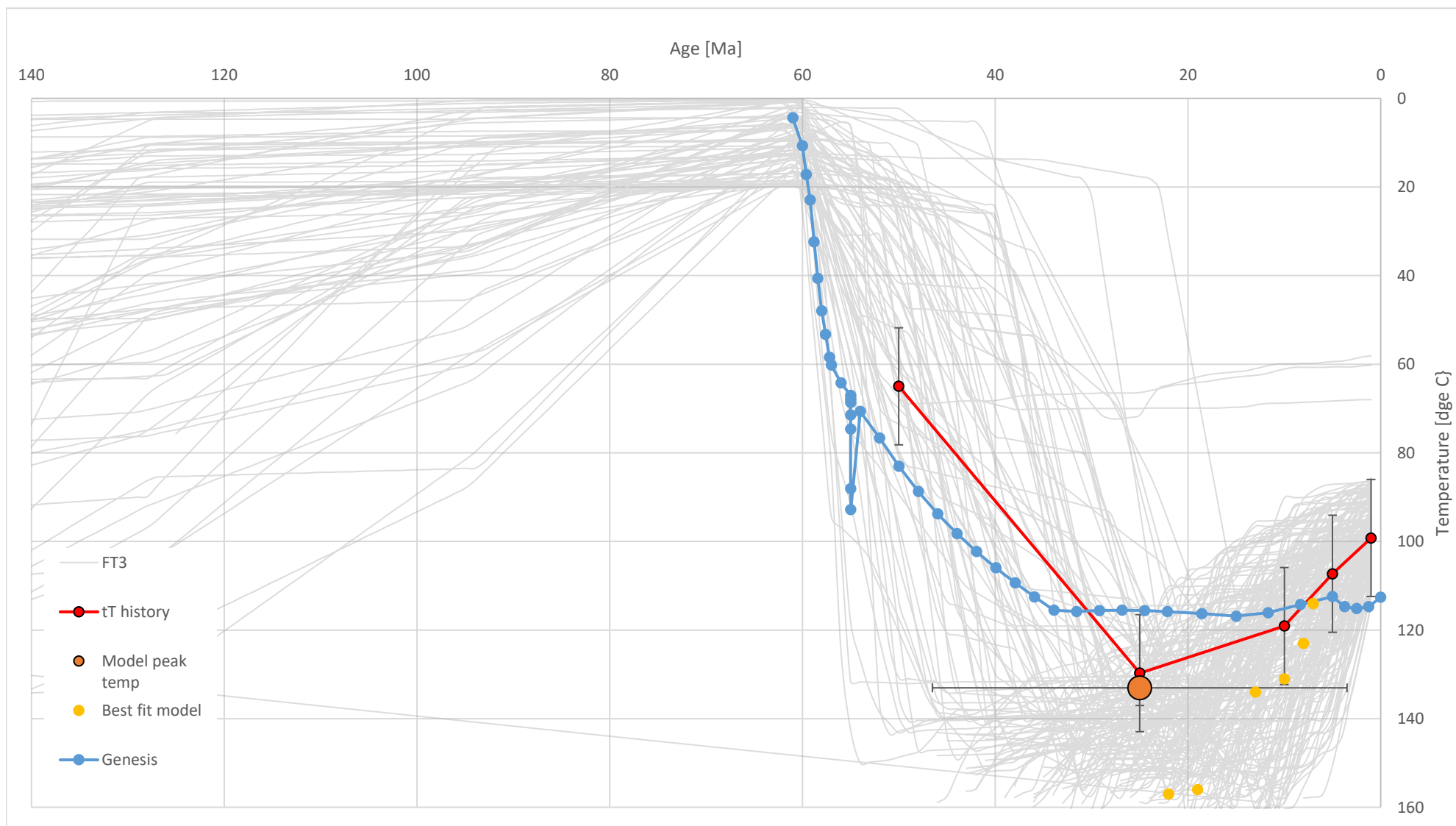


FIGURE 4.3.23 Thermal history data derived from the Apatite.Inc modelling for well 214/28-1 sample depth 3630m

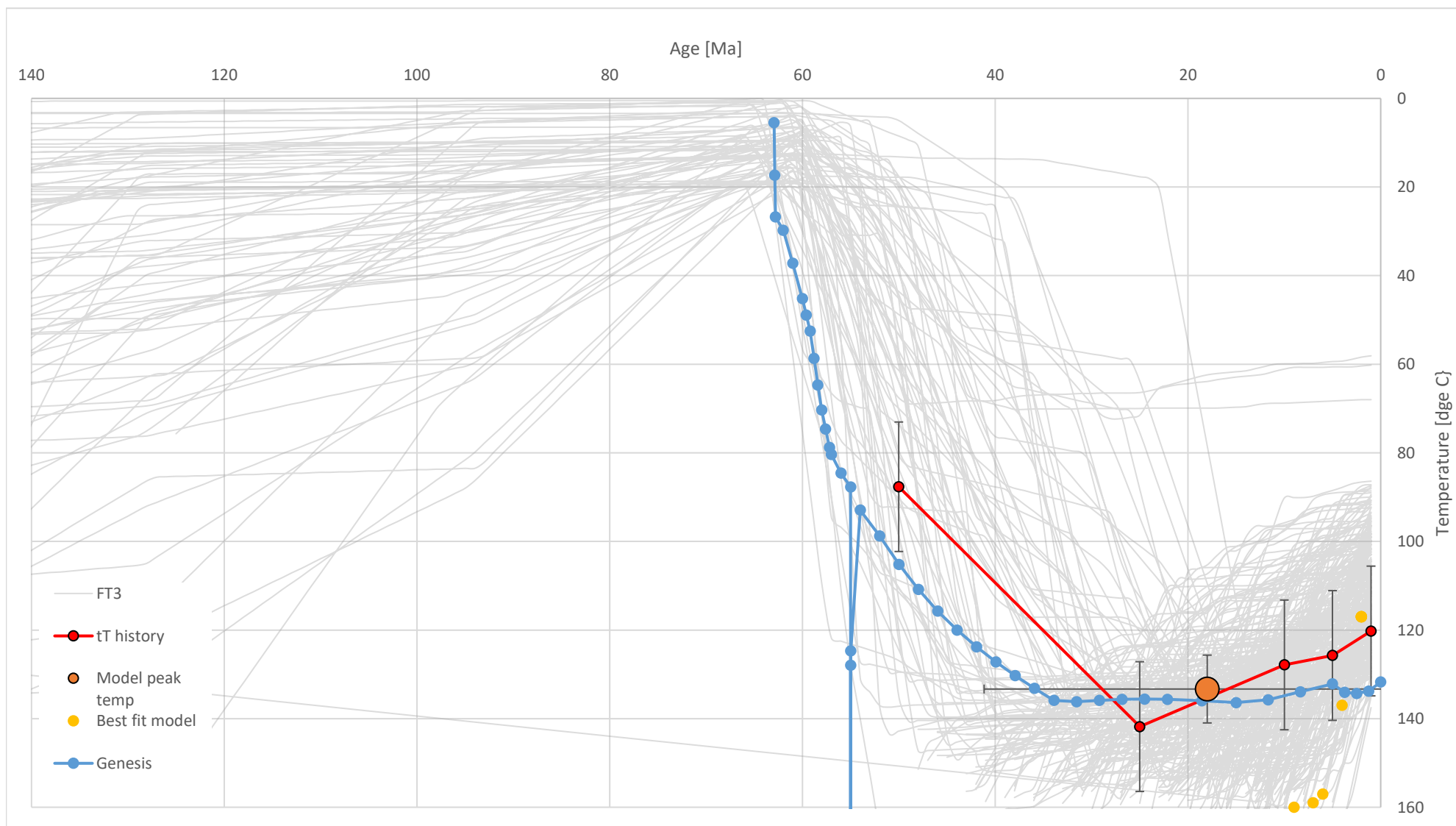


FIGURE 4.3.24 Thermal history data derived from the Apatite.Inc modelling for well 214/28-1 sample depth 4365m

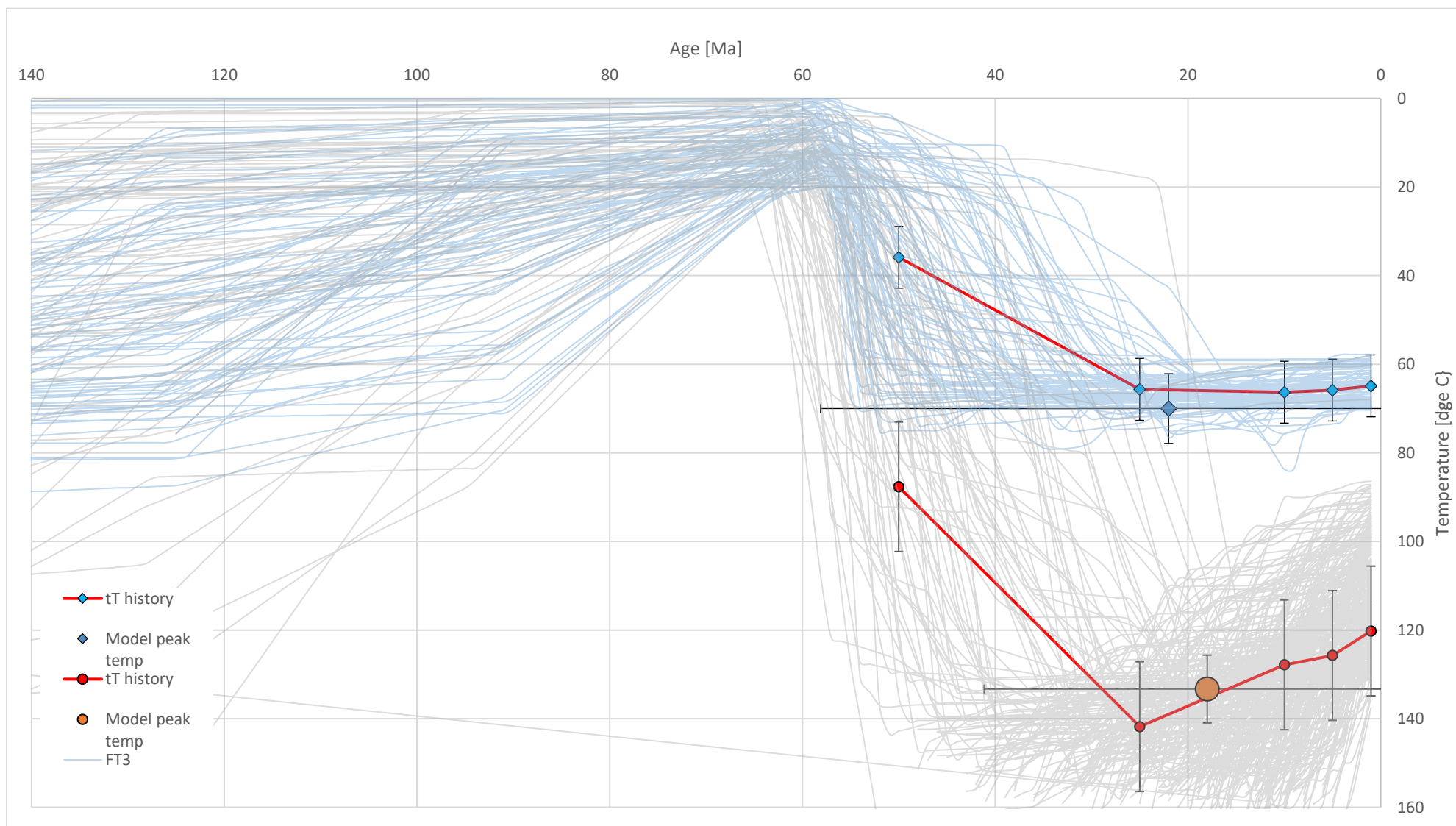


FIGURE 4.3.25 Combined thermal history 214/28-1 from samples 2552m & 4365m

4.4 SYNOPSIS

While a lot of relatively complex data has been presented on the apatite thermochronology data in this section, relatively simple conclusions can be drawn by cross plotting the measured present-day temperatures of the samples with the modelled peak temperatures inverted from the apatite age and track length data, as shown in Figure 4.4.1. In this figure the estimated present-day temperature is cross plotted against the modelled peak temperature from the apatite fission track data. In the plot it can clearly be seen that the majority of samples fall on or close to the one-to-one line indicated the samples present-day are at or close to their maximum temperatures.

Four wells show some evidence of hotter paleo-temperatures from the apatite fission track data; three of these wells (205/9-1, 214/26-1, 214/28-1) are in outboard locations away from where significant Tertiary exhumation is anticipated. The estimates ages of peak temperature are:

205/9-1 – Upper Paleocene (Lista Formation) sample (3704-3719m): $27\text{Ma} \pm 29\text{Ma}$. Present day temperature $\sim 95^\circ\text{C}$. Peak temperature $> 122^\circ\text{C} \pm 23$.

214/26-1 – Eocene sample (2290-2297m): $18 \pm 38\text{Ma}$. Present day temperature $\sim 49^\circ\text{C}$. Peak temperature $\sim 67 \pm 12^\circ\text{C}$.

214/28-1 – Middle Paleocene sample (3627-3633m): $25 \pm 21\text{Ma}$. Present day temperature $\sim 110^\circ\text{C}$. Peak temperature $\sim 133 \pm 4^\circ\text{C}$.

The ages do not generally correspond with the time expecting for heating associated with the Iceland plume and temporally are more consistent with Late Tertiary compression. The obvious problem is that these wells, being located out in the basin, are not thought to have experienced material uplift. The wells are located on structures though and so may have been a focus of hot fluids moving in response to the structuration. If this mechanism is accepted then the impact on the petroleum system would be expected to be limited, particularly in regard to source rock maturation.

The fourth sample that showed a hotter paleotemperature was the Shetland Group (Campanian) sample from 208/27-2 which is located on or close to the Rona Ridge, and is therefore more likely to have experienced some uplift; however for this well both the timing ($29.5 \pm 43.13\text{Ma}$) and maximum temperature estimate ($\sim 66 \pm 43^\circ\text{C}$ vs an estimated present day temperature of 50°C) are very poorly constrained and thus only very limited constrain is provided by the apatite data here.

Two wells, 207/01-2 and 214/28-1 show modelled temperatures that are cooler than present-day temperatures – which is clearly problematic!

207/01-2 – two samples, comprising of cuttings from the Lower Cretaceous (1703 – 1712m) and basement (1749 – 1752m) were selected for analysis. Both results returned modelled temperatures cooler than those measured at the sample depths present-day, which clearly cannot be genuine. The most likely explanation for the discrepancy is the contamination of the apatites with those from younger (cooler) sediments caved into the sample from shallower in the well. In 207/01-1 the 13 3/8" casing point was at 2496ft / 760m, the well was then drilled to a TD of

~5780ft / 1761m, so there was about 1000m of open hole providing ample opportunity for caving.

214/28-1 – the shallowest Paleocene sample from this well (8504ft / 2592m) was taken from a core chip so caving cannot be the explanation for the model results. The apatite model peak temperature was estimated to be $70\pm 8^{\circ}\text{C}$ whereas the measured temperature was $\sim 77^{\circ}\text{C}$ thus the discrepancy was not huge and is not thought to be of material significance.

In the project the intent was to sample wells in basinal locations as much as possible (since wells are typically drilled on structural highs) with the reason being that these wells are most representative of the kitchens of interest. As noted above the majority of samples indicate the sections analysed are at or close to maximum temperature present-day.

Some limited evidence of higher paleotemperatures are indicated in a number of wells (205/9-1, 214/26-1, 214/28-1), which although not especially well constrained, the timing of which would be most consistent with the mid to late Tertiary events (from IMU, Intra-Miocene Unconformity to the TPU, Top Palaeogene Unconformity (cf. Ritchie et al. (2008)). It is presumed this heating reflects advective heat transport associated with fluids migrating within carrier beds from deeper to shallower settings and is not thought to be of significance for source rock maturation. Integration and discussion of the petroleum system is provided in Chapter 6.

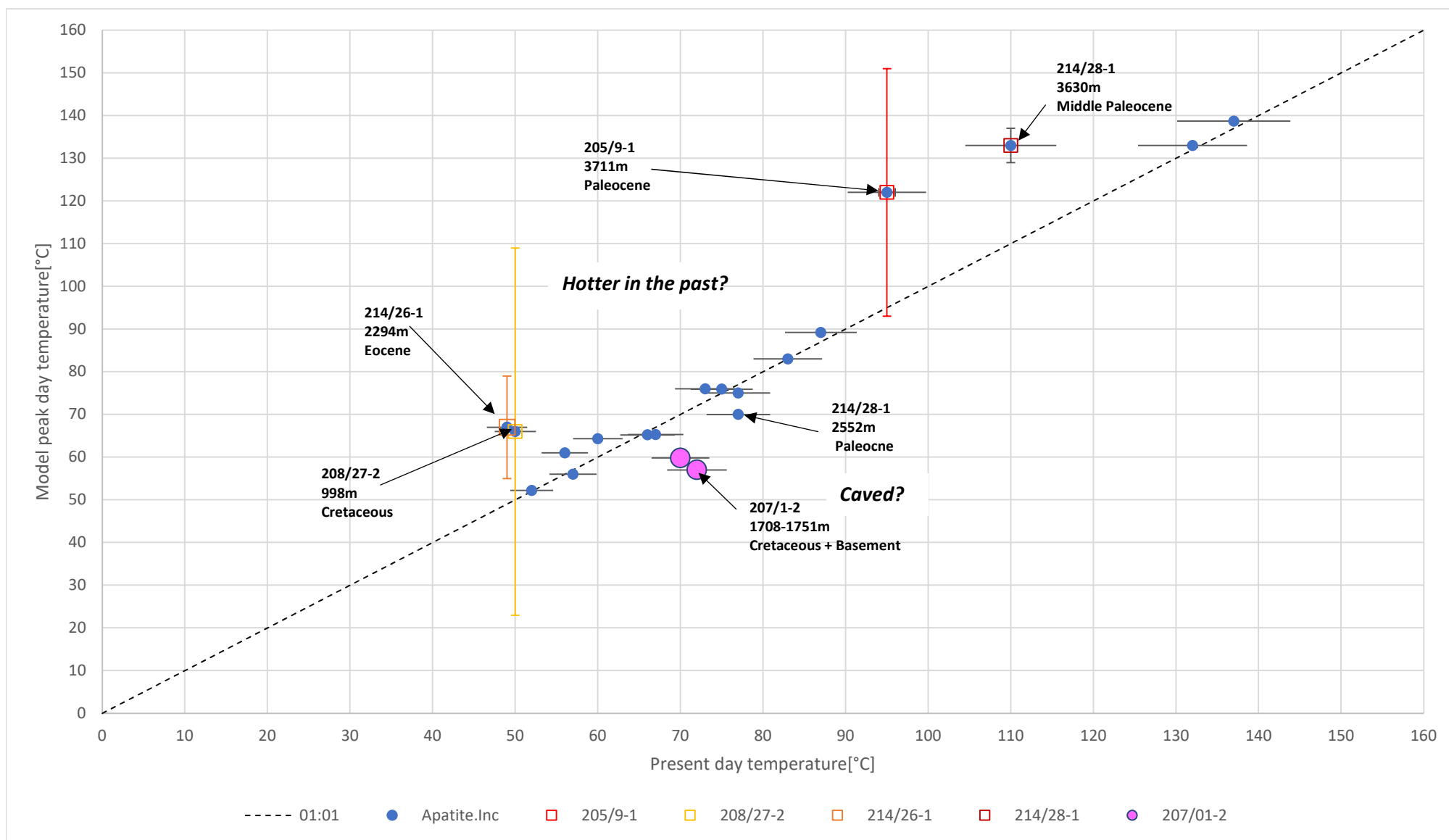


FIGURE 4.4.1 Measured present day temperature vs. Apatite thermochronology modelled peak temperature

CHAPTER 5

OPTICAL MATURITY ANALYSES AND RESULTS

Lloyd Jones & Rick Harding, APT

5.1 SUMMARY

The thermal maturity of twelve wells west of Shetland were analysed by vitrinite reflectivity and spore colour analysis, supplemented by observation of exinite fluorescence in near ultraviolet blue light excitation. Kerogen composition was also determined. These analyses have resulted in the following findings,

205/9-1

Samples ranging from Early Eocene to the Late Cretaceous in age were analysed. The top of the oil window is placed at 3500m by vitrinite reflectivity and at 4000m by SCI data. The kerogen contained in samples analysed consisted mainly of gas-prone organic matter.

205/12-1

Samples ranging from Early Eocene to the Early Cretaceous in age were analysed. The top of the oil window is placed at 3200m and 3800m by vitrinite reflectivity and SCI respectively. Oil-prone kerogen was present in Stronsay Group samples, although they are unlikely to attain maturity in the region. Gas-prone kerogen predominates in all samples below 2010m.

205/14-2

Samples ranging from Early Eocene to the Late Cretaceous in age were analysed. The top of the oil window is placed at 10200ft by reflectivity data, but at 11400ft by SCI data. Vitrinite reflectivity is thought to provide the more accurate reflection of maturity. Tertiary sediments contain mainly gas-prone kerogen; the Maastrichtian sample contains oil-prone kerogen.

205/14-3

Samples ranging from Tertiary (undifferentiated) to the Late Cretaceous in age were analysed. The top of the oil window was placed at 11500ft by vitrinite reflectivity and at 12200m by SCI data. All samples contained gas-prone kerogen except for that from the Balder Formation., which contained mainly oil-prone kerogen.

206/01-1A

Samples ranging from Late Eocene to the Late Cretaceous in age were analysed. The top of the oil window was placed at 10500ft and 12800ft by vitrinite reflectivity and SCI data respectively. The spore colour data are, however, of poor quality and vitrinite reflectivity is considered to define maturity more accurately.

206/11-1

Samples ranging from Tertiary (undifferentiated) to the Early Cretaceous in age were analysed. The top of the oil window was placed at 3200m and 4000m by vitrinite reflectivity and SCI data respectively; however, vitrinite reflectivity data are considered to provide the more accurate assessment of thermal maturity.

207/01-2

A single Tertiary sample from 1260ft was analysed. A Mean SCI of 3.0 SCI and mean vitrinite reflectivity of 0.23% Ro shows the sample to be immature for hydrocarbon generation. The organic matter is gas-prone.

208/17-1

Samples ranging from Middle Eocene to the Late Cretaceous in age were analysed. The top of the oil window was placed at 12500ft and 9000ft by vitrinite reflectivity and SCI data respectively; however, the spore colour results are highly anomalous when viewed alongside other data from this study and the interpretation from vitrinite reflectivity is preferred. All sediments analysed contain mainly gas-prone kerogen.

208/17-2

Samples ranging from Tertiary (undifferentiated) to the Late Cretaceous in age were analysed. Vitrinite reflectivity and SCI data place the top of the oil window at 10000ft, but do confirm that the analysed interval is immature for hydrocarbon generation. The topmost sample contains oil-prone kerogen but all deeper samples are gas-prone.

209/12-1

Three samples of Oxfordian/?Berriasian age between 11383.9ft and 11385.7ft were analysed. SCI data were not available as the samples were devoid of miospores, but reflectivity data showed the interval to be post-mature for oil generation and well into the gas window. Due to high maturity and severe alteration, the original nature of the kerogen could not be ascertained.

214/26-1

Samples ranging from Middle to Early Eocene in age were analysed. Spore colour indices increased over the interval from 3.0 SCI to 4.5 SCI and vitrinite reflectivity from 0.24% Ro to 0.48% Ro; however, in each case, there values increase briefly just below 6000ft to 0.58% Ro 7.5 SCI. The distribution of reflectivity and SCI values suggests igneous intrusive activity in this part of the well section. The top of the oil window is variously projected to lie at 11400ft and 12000ft by vitrinite reflectivity and spore colour data. All samples contain gas-prone kerogen except in the Middle Eocene at 7760ft.

214/28-1

Samples ranging from Early Oligocene to Late Cretaceous were analysed. The oil window was variously placed at 11400ft by vitrinite reflectivity and at 12000ft by SCI data. Kerogen in these samples was gas-prone except in a Middle Eocene sample from 7300ft.

With the exception of the 206/01-1A well, there is no evidence of significant uplift and erosion at the top of the sections of these wells. Vitrinite data from 206/01-1A well suggests that about 3000ft of sediment has been eroded from top of that section.

5.2 INTRODUCTION

A total of twelve wells were selected for optical maturity analyses (vitrinite reflectivity and spore colouration). Seven of these wells were also selected for Apatite Fission Track (AFT) analysis. Well selection was principally determined by distribution across the West of Shetland (WOS) area, location in their respective basin (centre/flank or uplifted areas). A summary of the wells analysed and sample numbers are shown in the table below with full sample details reported in Table 5.1.1. The distribution of analysed wells are shown in Figure 5.1.1.

Well	Basin	Optical Maturity Analyses.	Sample No.	AFT Analyses Undertaken
205/09-1	Flett	Y	9	Y
205/12-1	Flett	Y	7	Y
205/14-2	Foula	Y	8	Y
205/14-3	Flett	Y	8	N
206/01-1A	Foula	Y	7	N
206/11-1	Rona Ridge	Y	9	Y
207/01-2	West Shetland	Y	1	Y
208/17-1	Northern Faroe-Shetland	Y	12	N
208/17-2	Northern Faroe-Shetland	Y	7	Y
209/12-1	Northern Faroe-Shetland	Y	3	N
214/26-1	Flett	Y	10	Y
214/28-1	Flett Ridge	Y	13	Y

Maturity determination was undertaken on a total of ninety-four samples by optical methods in both transmitted light (spore colour indices) and reflected light (vitrinite reflectivity). Vitrinite reflectivity analyses were carried out on polished, isolated kerogen (sieved and unsieved) mounted in resin. Spore colouration and kerogen typing were carried out on strewn mounts on glass microscope slides and supplemented by observation of fluorescence colours of exinite under near ultra-violet blue light excitation. The full microscopy methods are detailed in Appendix 4.2.

Vitrinite reflectivity and spore colour index (SCI) data are summarised in Tables 5.2.1 to 5.2.12. and accompanying vitrinite reflectivity and SCI depth plots in Figures 5.2.1.1 to 5.2.1.12 and 5.2.2.1 to 5.2.2.12 respectively. Detailed vitrinite reflectivity and spore colour and kerogen composition data are given in Appendices 3.2 and 3.4 respectively, along with vitrinite reflectivity histograms, data and statistics in Appendix 3.3.

Spore colour data are reported as Spore Colour Indices (Collins, 1990), wherein progressively darker colours (from translucent through orange to black) are assigned values from 1.0 to 10.0, increasing by half integer steps. The main oil generation window coincides with spore colour indices between 5.0 and 8.5.

Well	Bottom depth	Units (m/ft)	Stratigraphy	Age	Sample type	Washed (y/n)	Block No.	Basin	Mud system	Anal. reason	Anal. status	Screening Analyses			
												Vitrinite reflectivity	Spore Colour Index	Visual kerogen	
205/09-1	2110.0	m	Hordaland	E1	DC	y	19-862	Flett	WBM	MAT	NEW	y	y	y	
	2384.0	m	Sele		DC	y	19-863			MAT	NEW	y	y	y	
	2774.0	m		Lista	P3	DC	y			19-864	MAT	NEW	y	y	y
	3143.0	m	DC			y	19-865			MAT	NEW	y	y	y	
	3452.0	m	DC			y	19-866			MAT	NEW	y	y	y	
	3803.0	m	DC			y	19-867			MAT	NEW	y	y	y	
	4136.0	m	Undiff.			DC	y			19-868	MAT	NEW	y	y	y
	4535.0	m	Maureen			P1	DC			y	19-869	MAT	NEW	y	y
	4709.0	m	Shetland	K2	DC	y	19-870			MAT	NEW	y	y	y	
	205/12-1	1990.0	m	Stronsay	E1	DC	y			19-871	Flett	WBM	MAT	NEW	y
2010.0		m	DC			y	19-872	MAT	NEW	y			y	y	
2300.0		m	Lamba	P3	DC	y	19-873	MAT	NEW	y			y	y	
2515.0		m			DC	y	19-874	MAT	NEW	y			y	y	
2800.0		m	Vaila		DC	y	19-875	MAT	NEW	y			y	y	
2990.0		m			DC	y	19-876	MAT	NEW	y			y	y	
3125.0		m	Shetland	K1	DC	y	19-877	MAT	NEW	y			y	y	
205/14-2		5150.0	ft	Balder	E1	DC	y	19-878	Foula	WBM			MAT	NEW	y
	5660.0	ft	DC			y	19-879	MAT			NEW	y	y	y	
	6110.0	ft	Unit II	P3	DC	y	19-880	MAT			NEW	y	y	y	
	6830.0	ft			DC	y	19-881	MAT			NEW	y	y	y	
	7520.0	ft	Unit IV Upper		DC	y	19-882	MAT			NEW	y	y	y	
	7940.0	ft	Unit IV Lower		DC	y	19-883	MAT			NEW	y	y	y	
	8630.0	ft	Unit V	P1	DC	y	19-884	MAT			NEW	y	y	y	
	8947.0	ft	Cretaceous	K2	DC	y	19-885	MAT			NEW	y	y	y	
	205/14-3	3840.0	ft	Undiff.	Ter	DC	y	19-886			Flett	WBM	MAT	NEW	y
5250.0		ft	Stronsay	DC		y	19-887	MAT	NEW	y			y	y	
6600.0		ft	Balder	E1	DC	y	19-888	MAT	NEW	y			y	y	
6900.0		ft			DC	y	19-889	MAT	NEW	y			y	y	

TABLE 5.1.1 Analytical programme - Optical maturity analyses

Well	Bottom depth	Units (m/ft)	Stratigraphy	Age	Sample type	Washed (y/n)	Block No.	Basin	Mud system	Anal. reason	Anal. status	Screening Analyses		
												Vitrinite reflectivity	Spore Colour Index	Visual kerogen
205/14-3	7320.0	ft	Hildasay	E1	DC	y	19-890	Flett	WBM	MAT	NEW	y	y	y
	8840.0	ft	Ketla Tuff	P3	DC	y	19-891			MAT	NEW	y	y	y
	9770.0	ft	Sullom	P2	DC	y	19-892			MAT	NEW	y	y	y
	10100.0	ft	Jorsalfare	K2	DC	y	19-893			MAT	NEW	y	y	y
206/01-1A	3350.0	ft	Undiff.	E3	DC	y	19-894	Foula	OBM	MAT	NEW	y	y	y
	4580.0	ft		E2	DC	y	19-895			MAT	NEW	y	y	y
	5570.0	ft			DC	y	19-896			MAT	NEW	y	y	y
	7100.0	ft	Sele	P3	DC	y	19-897			MAT	NEW	y	y	y
	7740.0	ft			DC	y	19-898			MAT	NEW	y	y	y
	7780.0	ft			DC	y	19-899			MAT	NEW	y	y	y
	9290.0	ft	Shetland	K2	DC	y	19-900			MAT	NEW	y	y	y
206/11-1	1250.0	m	Undiff.	Ter	DC	y	19-901	Rona Ridge	WBM	MAT	NEW	y	y	y
	1825.0	m	Late	K2	DC	y	19-902			MAT	NEW	y	y	y
	2380.0	m	Cretaceous		DC	y	19-903			MAT	NEW	y	y	y
	2900.0	m	Shale I		DC	y	19-904			MAT	NEW	y	y	y
	3244.0	m	L. Cret Shale III		DC	y	19-905			MAT	NEW	y	y	y
	3606.0	m	Early	K1	DC	y	19-906			MAT	NEW	y	y	y
	3934.0	m	Cretaceous		DC	y	19-907			MAT	NEW	y	y	y
	4258.0	m	Sandstone		DC	y	19-908			MAT	NEW	y	y	y
	4586.0	ft	E. Cret Turbidite		DC	y	19-909			MAT	NEW	y	y	y
207/01-2	1260.0	ft	Undiff.	Ter	DC	y	19-910	West Shetland	WBM	MAT	NEW	y	y	y
208/17-1	4680.0	ft	Middle Eocene	E2	DC	y	19-911	Northern Faroe-Shetland	OBM	MAT	NEW	y	y	y
	5880.0	ft			DC	y	19-912			MAT	NEW	y	y	y
	6720.0	ft			DC	y	19-913			MAT	NEW	y	y	y
	7300.0	ft	Early Eocene	E1	DC	y	19-914			MAT	NEW	y	y	y
	8610.0	ft	Late Paleocene	P3	DC	y	19-915			MAT	NEW	y	y	y
	9760.0	ft			DC	y	19-916			MAT	NEW	y	y	y
	10550.0	ft			DC	y	19-917			MAT	NEW	y	y	y

TABLE 5.1.1 Analytical programme - Optical maturity analyses

Well	Bottom depth	Units (m/ft)	Stratigraphy	Age	Sample type	Washed (y/n)	Block No.	Basin	Mud system	Anal. reason	Anal. status	Screening Analyses		
												Vitrinite reflectivity	Spore Colour Index	Visual kerogen
208/17-1	11840.0	y	Early Paleocene	P1	DC	y	19-918	Northern Faroe-Shetland	OBM	MAT	NEW	y	y	y
	12760.0	y			DC	y	19-919			MAT	NEW	y	y	y
	13980.0	y			DC	y	19-920			MAT	NEW	y	y	y
	14740.0	y			DC	y	19-921			MAT	NEW	y	y	y
	15860.0	y	Late Cret	K2	DC	y	19-922			MAT	NEW	y	y	y
208/17-2	5400.0	y	Stronsay	Ter	DC	y	19-923	Northern Faroe-Shetland	OBM	MAT	NEW	y	y	y
	6280.0	y	Balder	E1	DC	y	19-924			MAT	NEW	y	y	y
	7290.0	y	Flett		DC	y	19-925			MAT	NEW	y	y	y
	9470.0	y	Vaila	P2	DC	y	19-926			MAT	NEW	y	y	y
	10600.0	y	Sullom	P1	DC	y	19-927			MAT	NEW	y	y	y
	11710.0	y			DC	y	19-928			MAT	NEW	y	y	y
	12050.0	y	Shetland	K2	DC	y	19-929			MAT	NEW	y	y	y
209/12-1	11383.9	y	Humber	J3	COCH	-	19-930	Northern Faroe-Shetland	WBM	MAT	NEW	y	y	y
	11385.1	y			COCH	-	19-931			MAT	NEW	y	y	y
	11385.7	y			COCH	-	19-932			MAT	NEW	y	y	y
214/26-1	5350.0	y	Hordaland	E2	DC	y	19-933	Flett	WBM	MAT	NEW	y	y	y
	5710.0	y			DC	y	19-934			MAT	NEW	y	y	y
	6010.0	y			DC	y	19-935			MAT	NEW	y	y	y
	6390.0	y			DC	y	19-936			MAT	NEW	y	y	y
	6760.0	y	Lewis Fan		DC	y	19-937			MAT	NEW	y	y	y
	7140.0	y	Lewis Lobe		DC	y	19-938			MAT	NEW	y	y	y
	7960.0	y			DC	y	19-939			MAT	NEW	y	y	y
	8230.0	y	Base Lewis Lobe	E1	DC	y	19-940			MAT	NEW	y	y	y
	8510.0	y	Balder		DC	y	19-941			MAT	NEW	y	y	y
	8910.0	y	Sele		DC	y	19-942			MAT	NEW	y	y	y
214/28-1	4560.0	y	Lower Oligocene	O1	DC	n	19-943	Flett Ridge	OBM	MAT	NEW	y	y	y
	5850.0	y	Late Eocene	E3	DC	n	19-944			MAT	NEW	y	y	y
	6540.0	y	Middle Eocene	E2	DC	n	19-945			MAT	NEW	y	y	y

TABLE 5.1.1 Analytical programme - Optical maturity analyses

Well	Bottom depth	Units (m/ft)	Stratigraphy	Age	Sample type	Washed (y/n)	Block No.	Basin	Mud system	Anal. reason	Anal. status	Screening Analyses		
												Vitrinite reflectivity	Spore Colour Index	Visual kerogen
214/28-1	7300.0	ft	Middle Eocene	E2	DC	n	19-946	Flett Ridge	OBM	MAT	NEW	y	y	y
	8200.0	ft	Early Eocene	E1	DC	n	19-947			MAT	NEW	y	y	y
	9630.0	ft	Middle Paleocene	P2	DC	n	19-948			MAT	NEW	y	y	y
	10660.0	ft			DC	n	19-949			MAT	NEW	y	y	y
	11540.0	ft			DC	n	19-950			MAT	NEW	y	y	y
	12510.0	ft	Early Paleocene	P1	DC	n	19-951			MAT	NEW	y	y	y
	13460.0	ft			DC	n	19-952			MAT	NEW	y	y	y
	14600.0	ft			DC	n	19-953			MAT	NEW	y	y	y
	15470.0	ft			DC	n	19-954			MAT	NEW	y	y	y
	16960.0	ft	Maastrichtian	K2	DC	n	19-955			MAT	NEW	y	y	y
	TOTAL:											94	94	94

Abbreviations/Key

DC: Ditch cuttings
COCH: Core chip
WBM: Water base mud
OBM: Oil base mud
MAT: Maturity
NEW: New analyses for this study

Stratigraphy/Ages

Undiff.: Undifferentiate
L. Cret Shale III: Late Cretaceous Shale III
E. Cret Turbidite: Early Cretaceous Turbidite
Ter: Tertiary
O1: Lower Oligocene
E3: Late Eocene
E2: Middle Eocene
E1: Early Eocene
P3: Late Paleocene
P2: Middle Paleocene
P1: Early Paleocene
K2: Late Cretaceous Shale III
K1: Early Cretaceous Turbidite
J3: Late Jurassic

TABLE 5.1.1 Analytical programme - Optical maturity analyses

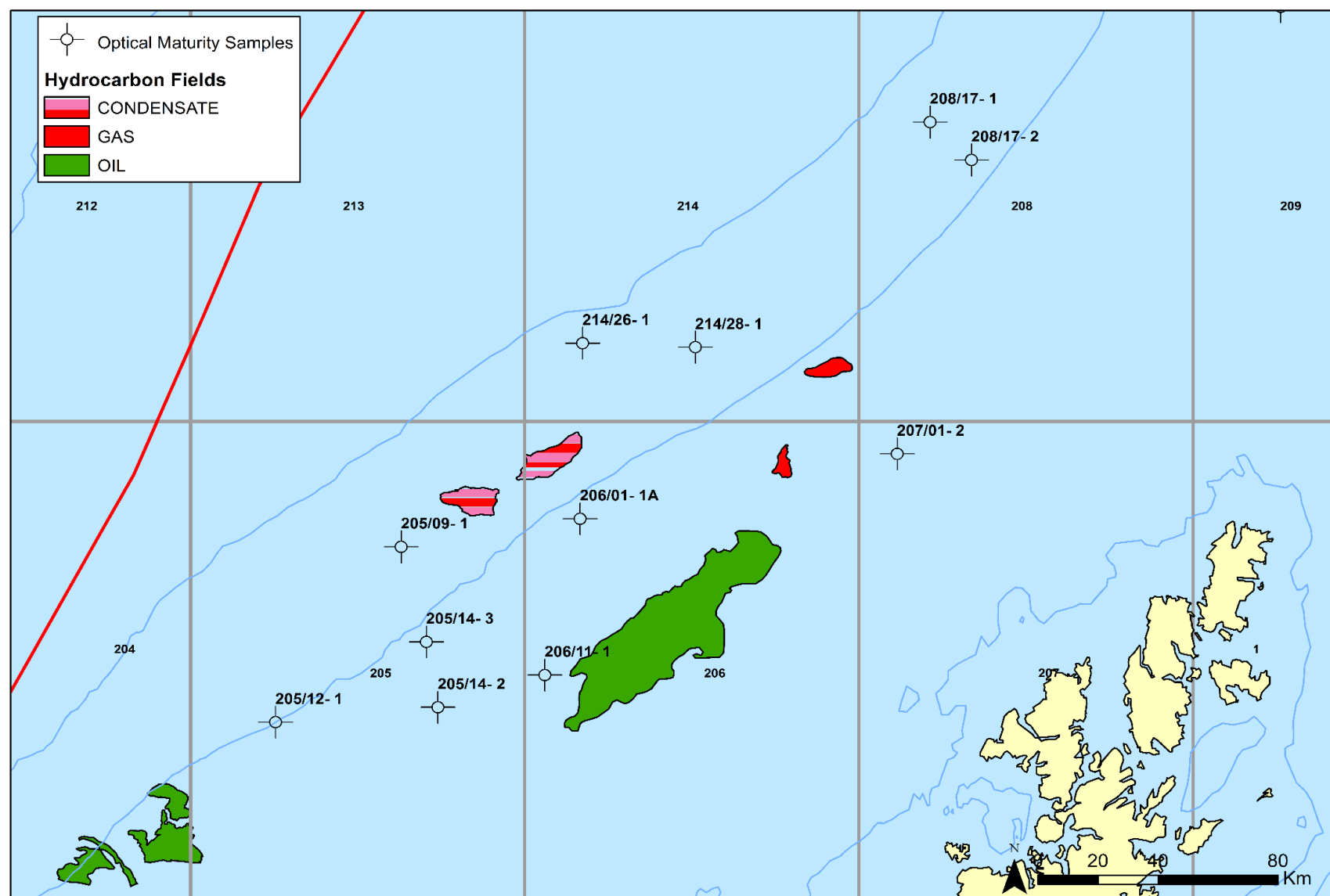


FIGURE 5.1.1 Location map of wells selected for optical maturity analyses

5.3 RESULTS OF OPTICAL MATURITY ANALYSES

5.3.1 Discussion for well 205/09-1

Nine samples ranging in age from Early Eocene to Late Cretaceous between 2100m and 4709m were analysed for vitrinite reflectivity, spore colouration and kerogen composition.

Spore Colour Indices (SCI)

Spore colour data quality was fair to good despite overall poor palynomorph preservation in samples from the Sele, Lista and Maureen Formations. Data quality was very poor in the Hordaland and Sele Formation samples due to low palynomorph recovery and poor preservation. Data quality from the Shetland Group sample was particularly poor as preservation precluded confident identification of palynomorphs as miospores. Miospore recovery was greatest in the Lista Formation and undifferentiated Paleocene.

Spore colour indices increase with depth from 3.0 SCI at 2110m to 7.0 SCI at 4709m. Despite the variable quality, the resulting depth plot (Figure 5.2.2.1) shows a steady increase in SCI with depth. The gradient suggests that the top of the oil window (5.0 SCI) lies at ~4000m. Upward extrapolation of the gradient indicates an intercept near the base value of 1.0 SCI at seafloor, indicating that no significant erosion has occurred at the top of the well section.

Vitrinite Reflectivity

Vitrinite reflectivity data quality was fair to excellent in all samples, and particularly high quality between 2110m and 4136m. The appearance of low reflecting populations was noted at in samples from 3452m down to the base of the analysed interval. Reflectivity increases with depth from 0.35% Ro at 2100m to 0.75% Ro at the base of the analysed interval. The gradient shown in Figure 5.2.1.1 intersects the onset of hydrocarbon generation (0.50% Ro) at ~3400m. This is ~600m shallower than the depth indicated by the spore colour data. Given the better quality of the vitrinite data throughout the analysed interval, it is likely to more accurately reflect the true level of maturity in the well.

Kerogen Composition

Miospores in the uppermost two samples of the interval fluoresced yellow-orange, changing to orange at 3452m, and orange brown at 3803m. No miospore fluorescence was observed in the Shetland Group sample. These colours are somewhat redder than what is suggested by the reflectivity and spore colour data; and is likely due to preservation rather than maturation.

Kerogen composition throughout the analysed interval is dominated by non-fluorescing amorphous organic matter (AOM) with secondary amounts of humic organic matter, which is primarily vitrinite between 2110m and 3143m. Inertinite (coaly) becomes more common at 3143m. The analysed interval therefore appears to be gas-prone rather than oil-prone.

5.3.2 Discussion for well 205/12-1

Seven samples ranging in age from Early Eocene to Early Cretaceous between 1990m and 3125m were analysed for vitrinite reflectivity, spore colouration and kerogen composition.

Spore Colour Indices (SCI)

All samples contained sufficient miospores with fair preservation to provide good, reliable data. SCI values increased with depth from 2.5 SCI at 199m to 4.0 SCI at the base of the analysed interval, indicating that the analysed interval is entirely immature for hydrocarbon generation.

Downward extrapolation of gradient shown in Figure 5.2.2.2 suggests the onset of hydrocarbon generation lies at depth greater than ~4000m.

Vitrinite Reflectivity

Vitrinite particles are common to abundant in most samples, with reflectivity populations essentially unimodal, generating reliable data. Reflectivity increases steadily with depth from 0.28% Ro at 19990m to 0.51% Ro at the base of the analysed interval. The deepest sample (3125m – Shetland Group) is marginally mature, indicating the top oil window lies at this depth. Downward extrapolation of the gradient shown in Figure 5.2.1.2 suggests the main gas window lies at ~4500m. The oil window lies ~850m shallower than the depth indicated by the spore colour data. Given the better quality of the vitrinite data throughout the analysed interval, it is likely to more accurately reflect the true level of maturity in the well.

Kerogen Composition

Miospores throughout the analysed interval fluoresce yellow, although some dull orange-yellow fluorescence was noted at 3125m. Consistent with the reflectivity and SCI data.

Kerogen in Middle Eocene Stronsay Group samples was dominated by fluorescing AOM. Fluorescence was strong at 1990m but became weaker at 2010m. Although fluorescing AOM is oil-prone, these sediments are unlikely to have attained sufficient maturity for oil generation in the basin. Samples below 2010m were generally dominated by gas-prone humic organic matter.

5.3.3 Discussion for well 205/14-2

Eight samples ranging in age from Early Eocene to Late Cretaceous between 5150ft and 8917ft were analysed for vitrinite reflectivity, spore colouration and kerogen composition.

Spore Colour Indices (SCI)

Spores were common in all samples, although interpretation of the data was complicated by the presence of caved, reworked and/or stained miospores. Spore colour indices generally increase with depth from 3.0 SCI to 4.5 SCI through the analysed interval. SCI data indicates the entire analysed interval is immature for hydrocarbon generation. Downward extrapolation of the gradient shown in Figure 5.2.2.3 intersects the top of the oil window at ~11400ft.

Vitrinite Reflectivity

Vitrinite particles are common throughout the analysed interval and data are of fair to good quality. Reflectivity increases steadily with depth from 0.28% R to 0.43% Ro at the base of the analysed interval suggesting the interval is immature for oil generation. Downward extrapolation of the gradient shown in Figure 5.2.1.3 intersects the onset of hydrocarbon generation at ~10200ft, significantly shallower than that estimated by the spore colour data. Upward extrapolation of both the reflectivity and SCI gradients intercept near base values at sea floor, indicating no significant erosion has occurred at the top of the well section.

A small break in the data is apparent between 5660ft and 6100ft, which coincides with an unconformity indicated on the completion log. This should be viewed with caution as there are only two data points above the break, and a break is not corroborated by reflectivity data.

Kerogen Composition

Miospore fluorescence is yellow at the top of the interval, changing to orange brown at the base. The colours at the base of analysed interval are somewhat redder than suggested by the reflectivity and spore colour data; and is likely be due to preservation rather than maturation.

Samples from the Tertiary interval are dominated by gas-prone to inert (coaly) humic organic matter, although a small amount (0%-20%) of oil-prone fluorescing AOM is present. Samples from The Upper Cretaceous interval contain 70% fluorescing AOM and can be considered oil-prone.

5.3.4 Discussion for well 205/14-3

Eight samples ranging in age from Eocene to Late Cretaceous between 3850ft and 10100ft were analysed for vitrinite reflectivity, spore colouration and kerogen composition.

Spore Colour Indices (SCI)

Miospores, while never super abundant throughout the analysed, are present in sufficient quantities to provide good quality data. SCI values increased steadily with depth from 2.0 SCI to 4.5 SCI from 3840ft to 10100ft respectively, indicating that the interval is immature for oil generation. The gradient shown in Figure 5.2.2.4 suggests the top of the oil window lies at ~12200ft.

Vitrinite Reflectivity

Vitrinite data from the Tertiary interval are fair to good, with abundant vitrinite, with large and coaly particles. Data from the Jorsalfare Formation was poor, due rare *in situ* vitrinite and the assemblage swamped by reworked vitrinite. Very bright inertinite was the most common humic component.

Reflectivity values throughout the analysed interval increased steadily with depth from 0.25% Ro to 0.48% Ro at the base of the analysed interval, confirming that the analysed interval is immature for hydrocarbon generation. Downward extrapolation of the gradient shown in Figure 5.2.1.4 suggests that the onset of hydrocarbon generation occurs at depths greater than 11500ft, ~700ft shallower than that suggested by SCI data.

Kerogen Composition

Most miospores displayed yellow fluorescence at the top of the interval, which changed to yellow orange towards the base of the Tertiary interval. Miospores from the Late Cretaceous sample fluoresced orange and are fairly consistent with the reflectivity and SCI data.

Kerogen from Stronsay Group sample is comprised mainly of gas-prone humic (woody and coaly) organic matter. The Balder Formation samples, comprised mainly of oil-prone fluorescing AOM. The Late Paleocene sample was dominated by a mixture of non-fluorescing AOM and humic organic matter, primarily inert (coaly) organic matter. The Late Cretaceous sample comprised mainly of gas-prone non-fluorescing AOM.

5.3.5 Discussion for well 206/01-1A

Seven samples ranging in age from Late Eocene to Late Cretaceous between 3350ft and 9290ft were analysed for vitrinite reflectivity, spore colouration and kerogen composition.

Spore Colour Indices (SCI)

Spore colour data quality throughout the Eocene interval was poor, with two samples practically devoid of miospores and, where present, identification uncertain. Data quality improved through the Late Paleocene interval, miospores are observed with at least fair preservation and are relatively common.

SCI values increase with depth from 2.5 SCI to 4.0 SCI, indicating that the entire interval is immature for hydrocarbon generation. The gradient shown in Figure 5.2.2.5 suggests the top of the oil window lies at ~12800ft. Upward extrapolation of gradient intersects the seafloor at ~2.0 SCI, suggesting a small amount (~2000ft) of uplift and erosion has occurred at the top of the well section.

Vitrinite Reflectivity

Vitrinite reflectivity data quality is generally good throughout the analyses interval, vitrinite is abundant and all Tertiary populations are unimodal. The Shetland Group sample has a bimodal distribution which complicates interpretation, and is unclear if this reflects the presence of cavings or oxidation.

Vitrinite reflectivity increases steadily throughout the analysed interval from 0.30% Ro to 0.45% Ro at the base of the analyses interval. Downward extrapolation of the gradient shown in Figure 5.2.1.5 suggests the onset of hydrocarbon generation occurs at depths greater than ~10500ft, significantly shallower than that suggested by the SCI data. Upward extrapolation of the gradient intersects the seafloor at ~0.25% Ro, corroborating the conclusion derived from the SCI data that substantial uplift and erosion (~3000ft) has occurred at the top of the well section.

Kerogen Composition

Miospores fluoresce yellow throughout the Tertiary interval, confirming the immaturity of the interval. Rare orange miospore fluorescence are observed in the Shetland Group sample, dinocysts fluoresce orange-yellow.

The two uppermost samples are dominated by gas-prone non-fluorescing AOM. Lower proportions of oil-prone fluorescing AOM are observed in the Middle Eocene sample at 5570ft, although this sample shows an increasingly terrestrial fingerprint with large woody particles becoming common, and are present in all deeper Tertiary samples. By contrast, kerogen in the Shetland Group sample is entirely marine, although gas-prone non-fluorescing AOM is the dominant component.

Discrepancies are apparent between the vitrinite reflectivity and spore colour data, the reflectivity data indicates the oil window to be ~2300ft shallower than that suggested by the SCI data. The vitrinite reflectivity data also indicates greater uplift and erosion at the top of the well section; ~3000ft rather than 2000ft. Given the poor quality spore colour data in the upper part of the analysed interval, it is likely that the reflectivity data be a more accurate representation of maturity in the well.

5.3.6 Discussion for well_206/11-1

Nine samples ranging in age from undifferentiated Tertiary to Early Cretaceous between 1250m and 4586m were analysed for vitrinite reflectivity, spore colouration and kerogen composition.

Spore Colour Indices (SCI)

Spore colour data quality is generally poor throughout the analysed interval. Miospores were relatively lean, with poor preservation and palynomorph identification uncertain. Improved miospore preservation was observed in the deepest Early Cretaceous Turbidite sample in which well-preserved brownish orange miospores are common.

SCI values increase steadily between 1250m to 3934m from 3.0 SCI to 4.5 SCI respectively, but a relatively noticeable increase in SCI values are observed in the bottom two samples. SCI values plotted against depth (Figure 5.2.2.6) show the shallower section of the analysed interval is immature for hydrocarbon generation, but a dogleg in the gradient is observed in the lower part of the Early Cretaceous interval and at peak oil maturity. The gradient intersects the oil window at ~4000m. Upward extrapolation of the gradient above 3934m intersects the seafloor at ~2.0 SCI, suggesting that up to 1000m of sediment has been uplifted and eroded. This is not corroborated, however, by reflectivity data.

Vitrinite Reflectivity

Vitrinite reflectivity data quality are variable throughout the analysed interval, with reflectivity populations in most samples dominated by reworked and/or oxidised particles. Improved data quality are observed in samples at 1250m (Tertiary) and 3934m (Early Cretaceous).

The gradient shown in Figure 5.2.1.6 is not comparable to the gradient derived from the SCI data. Mean indigenous reflectivity values increase from 0.30% Ro to 0.65% Ro at 4586m, no *in situ* vitrinite is recorded at 4586m. Extrapolation of the gradient to 4586m, suggests a reflectivity at this depth to be 0.80% Ro, aligning with the SCI data. These data indicate that the top of the oil window lies at 3200m, some 800m shallower than indicated by SCI data. Upward extrapolation of the gradient intersects the seafloor at near base values for vitrinite reflectivity, suggesting that little or no uplift has occurred at the top of the well section.

Kerogen Composition

Miospores fluoresce yellow-orange at the top of the interval, becoming dull orange at 3606m, and brown at 3934m. No fluorescence are observed in miospores at the base of the analysed interval, consistent with the reflectivity data.

Kerogen in these samples comprises mainly gas-prone non-fluorescing AOM and inert (coaly) organic matter. There is no evidence of significant oil source potential in these sediments.

Discrepancies are apparent between the vitrinite reflectivity and spore colour data, SCI data places the top of the oil window at ~4000m, significantly deeper than the reflectivity data (~3200m). There is also a suggestion from the SCI data of ~1000m of uplift and erosion, whereas reflectivity data indicates none. A comparison of reflectivity data from this well parallels the data derived from the other wells in this study, whereas the dogleg in the SCI data appears anomalous and is seen in none of the other wells. Furthermore, the observed exinite fluorescence aligns more fully to the reflectivity data than the SCI, and it is therefore concluded that reflectivity provides the more reliable indication of maturity in the well. It is likely that much of the spore colour data in the Late Cretaceous interval and the upper part of Early Cretaceous interval has resulted from the presence of caved miospores.

5.3.7 Discussion for well 207/01-2

One undifferentiated Tertiary sample, from 1250ft, was analysed for vitrinite reflectivity, spore colouration and kerogen composition.

Spore Colour Indices (SCI)

Spore colour data was of poor quality as only five miospores were observed. A tentative SCI of 3.0 SCI suggests the sample to be immature for hydrocarbon generation. Miospores fluoresce pale yellow to yellow-orange.

Vitrinite Reflectivity

Vitrinite was abundant in the sample and generated good quality, reliable data. The resulting reflectivity of 0.23% Ro suggests the sample to be very immature, lower than that indicated by the SCI data.

Kerogen Composition

The organic matter comprises mainly degraded vitrinite and is therefore considered to be mainly gas-prone.

5.3.8 Discussion for well 208/17-1

Twelve samples ranging in age from Middle Eocene to Late Cretaceous between 4680ft to 15860ft were analysed for vitrinite reflectivity, spore colouration and kerogen composition.

Spore Colour Indices (SCI)

Spore colour data was of very poor quality throughout the analysed interval, due to very low miospore abundance and poor miospore preservation. Only six of the twelve samples yielded SCI data. Samples from the Middle Eocene interval yielded data based on one and three measurements respectively. No data was recorded between 6720ft to 9760ft. Adjacent Late and Early Paleocene samples at 10550ft and 11840ft, yielded six and eight measurements respectively with SCI values of 6.0 SCI and 6.5 SCI respectively and are considered the most reliable samples from the well. Based on the intermittent data coverage, the gradient displayed in Figure 5.2.2.8 intersects the top of the oil window at 9000ft. Data from nearby wells analysed in this study suggests that an oil window at this relatively shallow depth is unlikely.

Vitrinite Reflectivity

Vitrinite reflectivity data from the uppermost section of the well (Middle Eocene) are of good quality. Organic matter recovery and data quality declines below this, but still provides reliable data when compared to the SCI data. Reflectivity values increase steadily from 0.28% Ro to 0.57% Ro at the base of the analysed interval. The gradient displayed in Figure 5.2.1.8 intersects the top of the oil window at ~12500ft, and aligns with data from the other wells in this study.

Kerogen Composition

Due to the paucity of miospores, there was little miospore fluorescence observed for corroboration.

Organic matter in these samples consisted almost entirely of gas-prone non-fluorescing AOM.

5.3.9 Discussion for well 208/17-2

Twelve samples ranging in age from undifferentiated Tertiary to Late Cretaceous between 5400ft and 12050ft were analysed for vitrinite reflectivity, spore colouration and kerogen composition.

Spore Colour Indices (SCI)

Spore colour data quality was variable, with two distinct SCI populations, the miospores with low values, appear anomalously low with respect to bottom hole temperatures (BHT) and the

newly generated AFT data, so therefore the higher SCI populations are believed to best reflect the maturity of the interval. SCI increases steadily from 3.5 SCI at the top of the analysed interval to 76.5 SCI at 11710ft. The deepest sample (12050ft – Shetland Group) was barren of identifiable miospores. The data suggests the 5400ft to 9470ft interval is immature for hydrocarbon generation, with the gradient shown in Figure 5.2.2.9 indicating the top oil window lies at 9800ft.

Vitrinite Reflectivity

Vitrinite reflectivity data are of fair to good quality between 5400ft and 9470ft, data quality reduces noticeably 10600ft. Indigenous vitrinite populations data cluster tightly around the regression and are likely to be a fair reflection of maturity.

Vitrinite reflectivity increases from 0.28% Ro at 5400ft to 0.60% Ro at the base of the analysed interval. The gradient shown in Figure 5.2.1.9 suggests the top of the oil window lies at ~9800ft, conforming with the SCI data. Upward extrapolation of the gradient intersects the seafloor at ~0.25% Ro, indicating that a small amount of uplift and erosion has occurred at this location.

Kerogen Composition

Miospore fluorescence changed from yellow orange at the top of the interval to orange brown at the base, indicating somewhat greater maturity than the reflectivity data and probably reflects preservation rather than maturity.

Kerogen in the uppermost sample (Middle Eocene) consists almost entirely of oil-prone fluorescing AOM, although it is unlikely that these sediments will attain maturity in the West of Shetland area. Deeper samples consist mainly of gas-prone non-fluorescing AOM.

5.3.10 Discussion for well 209/12-1

Three samples of Oxfordian/?Berriasian age between 11383.9ft and 11385.7ft were analysed for vitrinite reflectivity, spore colouration and kerogen composition.

Spore Colour Indices (SCI)

No miospores were present in these samples, but the overall dark brown to black colour of the kerogen is consistent with spore colour indices between 8.5 SCI and 9.5 SCI, which suggests that the interval is post-mature for oil generation and into the (?dry) gas window.

Vitrinite Reflectivity

Vitrinite reflectivity data quality was fair in all samples, and although relatively rare, of sufficient amounts to provide reliable data. Reflectivity values varied from 2.75% Ro and 2.72% Ro between 11383.9ft and 11385.1ft respectively. Reflectivity dropped to 2.33% Ro at 11385.7. The combined factors of anomalously high reflectivities in all three samples (well above the regional gradient) and a reduction in reflectivity for the deepest sample suggest that the interval has been affected by igneous intrusive activity.

There was no fluorescing organic matter in any of these samples.

Non-fluorescing AOM dominates the kerogen in these samples, but they are too severely altered to determine their original character.

5.3.11 Discussion for well 214/26-1

Ten samples ranging in age from Middle to Early Eocene between 5350ft to 8910 were analysed for vitrinite reflectivity, spore colouration and kerogen composition.

Spore Colour Indices (SCI)

Spore colour data quality was generally poor and interpretation of the results complicated by the presence of abundant dark miospores that may represent either reworked palynomorphs or palynomorphs darkened by igneous intrusive activity.

SCI values increase steadily from 3.0 SCI at 5350ft to 4.5 SCI at the base of the analysed interval. However, anomalously high values were recorded at 6010ft and 6390ft of 7.0 SCI and 6.5 SCI respectively. SCI values plotted against depth (Figure 5.2.2.11) show the high values recorded between 6010-6390ft are suggestive of an increase in maturity resulting from an igneous intrusion. Downward extrapolation of the gradient shown in Figure 5.2.2.11 suggest the top of the oil window lies at ~10000ft.

Vitrinite Reflectivity

Vitrinite reflectivity data quality was generally good, common to abundant vitrinite was observed in several of the samples although interpretation was also complicated by anomalously high values similar to that displayed in the SCI data. Mean indigenous reflectivities of 0.24% Ro at the top of the analysed interval rapidly increase to 0.58% Ro and 0.52% Ro at 6010ft and 6390ft respectively, dropping back to 0.34% Ro at 6760ft and then steadily increasing to 0.48% Ro at the bottom of the analysed interval. Downward extrapolation of the gradient shown in Figure 5.2.1.11 suggests that the onset of hydrocarbon generation occurs at depths greater than ~9500ft. Upward extrapolation of the gradient intersects the seafloor at near base values, indicating little or no erosion.

Kerogen Composition

Miospores display yellow orange fluorescence at the top of the interval which changes to orange at the anomalously high value interval (6010-6390ft), becoming yellow orange again below this and then changing to orange at the base of the analysed interval.

Kerogen throughout the analysed interval is principally dominated by gas-prone non-fluorescing AOM, except in the Lewis Lobe sample at 6760ft Fan (E2) which is dominated by oil-prone fluorescing AOM.

5.3.12 Discussion for well 214/28-1

Thirteen samples ranging in age from Early Oligocene to Late Cretaceous between 4560ft to 16960 were analysed for vitrinite reflectivity, spore colouration and kerogen composition.

Spore Colour Indices (SCI)

Spore colour data quality was generally poor throughout the analysed interval, due to low miospores abundance. A noticeable increase in miospore abundance at 7300ft (Middle Eocene) and 9630ft (Middle Paleocene) generated good, reliable data. SCI values increase rather erratically from 3.0 SCI at 4560ft to 5.0 SCI at the base of the analysed interval. Data quality is of significantly reduced below 11540ft, and should be interpreted cautiously. The gradient shown in Figure 5.2.2.12 indicates that the top of the oil window lies at ~12000ft. Upward extrapolation of the gradient suggests some uplift and erosion, up to ~2000ft. This is not, however, corroborated by reflectivity data.

Vitrinite Reflectivity

Vitrinite reflectivity data quality varies from fair to good between 4560ft and 11540ft, organic matter recovery is poor to barren below 11540ft and subsequently generates poor quality data. Mean indigenous reflectivity values also increase erratically from 0.27% Ro at 4560ft to 0.73% Ro at 14600ft. The gradient shown in Figure 5.2.1.12 intersects the top of the oil window at ~11400ft. Upward extrapolation intersects the seafloor at near base values, indicating that no significant uplift or erosion has occurred at the top of the interval.

Kerogen Composition

Miospore fluorescence changes from yellow orange at the top of the interval to brown by 12500ft.

The kerogen in most samples mainly comprises of gas-prone non-fluorescing AOM, except in the Middle Eocene interval at 7300m, which is dominated by oil-prone fluorescing AOM. In all samples, where humic organic matter is observed, it is commonly inert (coaly) organic matter.

Well	Bottom Depth (m)	Stratigraphy	Age	Sample Type	Sample Prep.	Indigenous VR Pop.		Indigenous SCI Pop.		UV Fluorescence		Maturity
						Av. % Ro	No.	Av. SCI	No.	Form	Colour	
205/09-1	2110.0	Hordaland	E1	DC	KC	0.35	40	3.0	5	Miosp	Yel orn - ?brn	Immature
										Sph	Pl yel	
										AOM	Brn - N.F.	
	2384.0	Sele		DC	KC	0.34	40	3.5	22	Miosp	Orn-yel	
										Dino	Yel orn - ?brn	
										AOM	Brn - N.F.	
	2774.0		P3	DC	KC	0.42	44	4.0	8	Miosp	Yel orn - N.F.	
										AOM	N.F.	
										-	-	
	3143.0	DC		KC	0.46	40	4.0	3	Miosp	Yel orn		
									Dino	?Brn		
									AOM	DI brn - N.F.		
	3452.0	Lista		DC	KC	0.51	41	4.0	14	Miosp	Orn	
										AOM	N.F.	
										-	-	
	3803.0			DC	KC	0.56	50	5.0	18	Miosp	Orn - brn	
										Dino	Brn - N.F.	
										AOM	N.F.	
	4136.0	Undiff.		DC	KC	0.61	40	5.0	14	Miosp	?N.F.	
										Dino	Wk yel orn	
										AOM	N.F.	
	4535.0	Maureen	P1	DC	KC	0.67	26	6.0	8	Miosp	N.F.	
										Dino	N.F.	
										AOM	N.F.	
	4709.0	Shetland	K2	DC	KC	0.75	27	7.0	8	Miosp	N.F.	
										AOM	N.F.	
										-	-	

TABLE 5.2.1 Optical maturity data summary: 205/09-1

Well	Bottom Depth (m)	Stratigraphy	Age	Sample Type	Sample Prep.	Indigenous VR Pop.		Indigenous SCI Pop.		UV Fluorescence		Maturity
						Av. % Ro	No.	Av. SCI	No.	Form	Colour	
205/12-1	1990.0	Stronsay	E1	DC	KC	0.28	30	2.5	23	Miosp	Yel	Immature
										Dino	Yel - grn	
										AOM	Pl yel	
	2010.0			DC	KC	0.29	37	2.5	19	Miosp	Yel	
										Dino	Yel - grn	
										AOM	Brn	
	2300.0	Lamba	P3	DC	KC	0.33	40	3.0	17	Miosp	Yel - yel grn	
										Dino	Yel - brn	
										AOM	N.F	
	2515.0			DC	KC	0.40	38	3.5	26	Miosp	Yel	
										Dino	Yel - brn	
										AOM	Brn	
	2800.0	Vaila		DC	KC	0.44	34	3.5	22	Miosp	Orn - yel	
										AOM	N.F	
										-	-	
	2990.0			DC	KC	0.47	20	3.5	16	Miosp	N.F	
										AOM	N.F	
										-	-	
	3125.0	Shetland	K1	DC	KC	0.51	32	4.0	21	Miosp	Yel - dl orn yel	Middle Mature (Early Oil Window)
										AOM	N.F	
										-	-	

TABLE 5.2.2 Optical maturity data summary: 205/12-1

Well	Bottom Depth (ft)	Stratigraphy	Age	Sample Type	Sample Prep.	Indigenous VR Pop.		Indigenous SCI Pop.		UV Fluorescence		Maturity
						Av. % Ro	No.	Av. SCI	No.	Form	Colour	
205/14-2	5150.0	Balder	E1	DC	KC	0.29	52	3.0	14	Miosp	DI yel - dl orn	Immature
										AOM	DI orn	
										-	-	
	5660.0			DC	KC	0.28	55	3.0	36	Miosp	DI yel - dl orn	
										AOM	DI orn	
										-	-	
	6110.0	Unit II	P3	DC	KC	0.31	45	3.5	27	Miosp	N.F.	
										AOM	N.F.	
										-	-	
	6830.0			DC	KC	0.33	47	3.5	19	Miosp	N.F.	
										AOM	N.F.	
										-	-	
	7520.0	Unit IV Upper SS		DC	KC	0.36	49	4.0	15	Miosp	Orn - brn	
										AOM	Brn	
										-	-	
	7940.0	Unit IV Lower SS		DC	KC	0.39	43	4.0	24	Miosp	Orn	
										AOM	Brn	
										-	-	
	8630.0	Unit V	P1	DC	KC	0.43	19	4.0	27	Miosp	Orn - brn	
										Dino	DI yel	
										AOM	?Brn	
	8947.0	Cretaceous	K2	DC	KC	0.43	29	4.5	6	Miosp	Brn	
										Dino	DI orn	
										AOM	DI brn - N.F.	

TABLE 5.2.3 Optical maturity data summary: 205/14-2

Well	Bottom Depth (ft)	Stratigraphy	Age	Sample Type	Sample Prep.	Indigenous VR Pop.		Indigenous SCI Pop.		UV Fluorescence		Maturity
						Av. % Ro	No.	Av. SCI	No.	Form	Colour	
205/14-3	3840.0	Undiff.	Ter	DC	KC	0.25	22	2.0	15	Miosp	Orn yel - yel	Immature
										AOM	N.F.	
										-	-	
	5250.0	Stronsay	Ter	DC	KC	0.32	55	3.0	23	Miosp	Orn - yel	
										Dino	Grn	
										AOM	Wk brn	
	6600.0	Balder	E1	DC	KC	0.32	40	3.0	19	Miosp	Yel	
										AOM	Orn brn - yel	
										-	-	
	6900.0			DC	KC	0.33	40	3.5	18	Miosp	Yel	
										AOM	Orn brn - yel	
										-	-	
	7320.0	Hildasay		DC	KC	0.31	40	3.5	19	Miosp	Yel orn	
										AOM	N.F.	
										-	-	
	8840.0	Ketla Tuff	P3	DC	KC	0.35	40	3.5	19	Miosp	Yel orn	
										AOM	Brn - yel - orn	
										-	-	
	9770.0	Sullom	P2	DC	KC	0.39	40	3.5	20	Miosp	Yel - orn	
										AOM	Orn - N.F.	
										-	-	
	10100.0	Jorsalfare	K2	DC	KC	0.48	32	4.5	19	Miosp	Orn	
										AOM	N.F.	
										-	-	

TABLE 5.2.4 Optical maturity data summary: 205/14-3

Well	Bottom Depth (ft)	Stratigraphy	Age	Sample Type	Sample Prep.	Indigenous VR Pop.		Indigenous SCI Pop.		UV Fluorescence		Maturity
						Av. % Ro	No.	Av. SCI	No.	Form	Colour	
206/01-1A	3350.0	Undiff.	E3	DC	KC	0.30	21	2.5	2	Miosp	Yel	Immature
										Dino	Yel	
										AOM	N.F.	
	4580.0		E2	DC	KC	0.37	42	3.0	12	Miosp	Yel	
										AOM	N.F.	
										-	-	
	5570.0		E2	DC	KC	0.36	30	3.0	2	Miosp	Yel	
										Dino	N.F.	
										AOM	N.F.	
	7100.0	Sele	P3	DC	KC	0.36	40	3.0	17	Miosp	Yel	
										AOM	Orn - brn	
										-	-	
	7740.0			DC	KC	0.40	47	3.5	23	Miosp	Yel	
										AOM	N.F.	
										-	-	
	7780.0			DC	KC	0.45	46	3.5	17	Miosp	Yel	
										AOM	N.F.	
										-	-	
	9290.0	Shetland	K2	DC	KC	0.47	36	4.0	10	Miosp	Orn	
										Dino	Orn - yel	
										AOM	N.F.	

TABLE 5.2.5 Optical maturity data summary: 206/01-1A

Well	Bottom Depth (m)	Stratigraphy	Age	Sample Type	Sample Prep.	Indigenous VR Pop.		Indigenous SCI Pop.		UV Fluorescence		Maturity
						Av. % Ro	No.	Av. SCI	No.	Form	Colour	
206/11-1	1250.0	Undiff.	Ter	DC	KC	0.30	46	3.0	10	Miosp	DI yel orn	Immature
										Dino	N.F.	
										AOM	N.F.	
	1825.0	Late Cretaceous Shale I	K2	DC	KC	0.35	12	3.5	8	Miosp	Yel orn - N.F.	
										Dino	Yel orn - orn	
										AOM	N.F.	
	2380.0			DC	KC	0.43	13	4.0	14	Miosp	DI yel orn - N.F.	
										Dino	N.F.	
										AOM	N.F.	
	2900.0			DC	KC	0.46	12	4.5	2	Miosp	Yel orn - dl orn	
										Dino	Orn	
										AOM	N.F.	
	3244.0	Late Cretaceous Shale III		DC	KC	-	-	4.5	3	Miosp	Yel orn - dl orn	
										Dino	?N.F.	
										AOM	N.F.	
	3606.0	Early Cretaceous Sandstone	K1	DC	KC	0.52	17	5.0	6	Miosp	DI orn - N.F.	
										Dino	N.F.	
										AOM	N.F.	
	3934.0			DC	KC	0.62	26	5.0	1	Miosp	Brn - N.F.	
										Dino	?N.F.	
										AOM	N.F.	
	4258.0			DC	KC	0.65	12	6.5	6	Miosp	Brn - N.F.	
										Sph	DI yel orn	
										AOM	N.F.	
	4586.0	Early Cretaceous Turbidite		DC	KC	-	-	7.5	7	Miosp	N.F.	
										Dino	N.F.	
										AOM	N.F.	

TABLE 5.2.6 Optical maturity data summary: 206/11-1

Well	Bottom Depth (ft)	Stratigraphy	Age	Sample Type	Sample Prep.	Indigenous VR Pop.		Indigenous SCI Pop.		UV Fluorescence		Maturity
						Av. % Ro	No.	Av. SCI	No.	Form	Colour	
207/01-2	1260.0	Undiff.	Ter	DC	KC	0.25	55	3.0	5	Miosp	Pl yel - yel orn	Immature
										AOM	N.F.	
										-	-	

TABLE 5.2.7 Optical maturity data summary: 207/01-2

Well	Bottom Depth (ft)	Stratigraphy	Age	Sample Type	Sample Prep.	Indigenous VR Pop.		Indigenous SCI Pop.		UV Fluorescence		Maturity
						Av. % Ro	No.	Av. SCI	No.	Form	Colour	
208/17-1	4680.00	Middle Eocene	E2	DC	KC	0.28	40	3.0	3	Miosp	Orn - yel	Immature
										Dino	Yel	
										AOM	N.F.	
	5880.00			DC	KC	0.29	30	2.5	1	Miosp	Yel	
										AOM	N.F.	
										-	-	
	6720.00			DC	KC	0.29	30	-	-	AOM	N.F.	
										-	-	
										-	-	
	7300.00	Early Eocene	E1	DC	KC	-	-	-	-	AOM	N.F.	
										-	-	
										-	-	
	8610.00	Late Paleocene	P3	DC	KC	0.33	13	-	-	AOM	N.F.	
										-	-	
										-	-	
	9760.00			DC	KC	0.42	18	-	-	AOM	N.F.	
										-	-	
										-	-	
	10550.0			DC	KC	0.47	12	5.0	4	Miosp	N.F.	
										AOM	N.F.	
										-	-	
	11840.0	Early Paleocene	P1	DC	KC	0.46	5	6.0	6	Miosp	N.F.	
										Dino	Brn	
										AOM	N.F.	
	12760.0			DC	KC	-	-	-	-	AOM	N.F.	
										-	-	
										-	-	
	13980.0			DC	KC	-	-	-	-	AOM	N.F.	
										-	-	
										-	-	

TABLE 5.2.8 Optical maturity data summary: 208/17-1

Well	Top Depth (ft)	Stratigraphy	Age	Sample Type	Sample Prep.	Indigenous VR Pop.		Indigenous SCI Pop.		UV Fluorescence		Maturity
						Av. % Ro	No.	Av. SCI	No.	Form	Colour	
208/17-1	14740.0	Early Paleocene	P1	DC	KC	0.79	5	-	-	AOM	N.F.	Middle Mature (Main Oil Window)
										-	-	
										-	-	
	15860.0	Late Cretaceous	K2	DC	KC	-	-	-	-	AOM	N.F.	
										-	-	
										-	-	

TABLE 5.2.8 Optical maturity data summary: 208/17-1

Well	Bottom Depth (ft)	Stratigraphy	Age	Sample Type	Sample Prep.	Indigenous VR Pop.		Indigenous SCI Pop.		UV Fluorescence		Maturity
						Av. % Ro	No.	Av. SCI	No.	Form	Colour	
208/17-2	5400.0	Stronsay	Ter	DC	KC	0.28	25	3.5	5	Miosp	Yel - ?orn	Immature
										AOM	?Ft orn	
										-	-	
	6280.0	Balder	E1	DC	KC	0.39	23	4.0	16	Miosp	Yel - orn	
										Dino	Ft orn	
										AOM	Yel - orn	
	7290.0	Flett		DC	KC	0.43	38	4.0	24	Miosp	?Brn - orn	
										AOM	Orn - yel	
										-	-	
	9470.0	Vaila	P2	DC	KC	0.46	30	4.5	17	Miosp	Brn - bt orn	Middle Mature (Main Oil Window)
										Dino	Orn - yel	
										AOM	Bt orn - N.F.	
	10600.0	Sullom	P1	DC	KC	0.52	12	5.0	9	Miosp	Orn - brn	
										AOM	?Brn - orn	
										-	-	
	11710.0			DC	KC	0.58	9	?6.5	2	Miosp	?Brn	
										Dino	N.F.	
										AOM	Ra orn - N.F.	
	12050.0	Shetland	K2	DC	KC	0.60	4	-	-	Dino	N.F.	
										AOM	Ra ft brn - N.F.	
										-	-	

TABLE 5.2.9 Optical maturity data summary: 208/17-2

Well	Bottom Depth (ft)	Stratigraphy	Age	Sample Type	Sample Prep.	Indigenous VR Pop.		Indigenous SCI Pop.		UV Fluorescence		Maturity
						Av. % Ro	No.	Av. SCI	No.	Form	Colour	
209/12-1	11383.9	Humber	J3	COCH	KC	2.75	24	-	-	AOM	N.F.	Post Mature (Main Dry Gas Window)
										-	-	
										-	-	
	11385.1			COCH	KC	2.72	39	-	-	AOM	N.F.	
										-	-	
										-	-	
	11385.7			COCH	KC	2.33	34	-	-	AOM	N.F.	
										-	-	
										-	-	

TABLE 5.2.10 Optical maturity data summary: 209/12-1

Well	Bottom Depth (ft)	Stratigraphy	Age	Sample Type	Sample Prep.	Indigenous VR Pop.		Indigenous SCI Pop.		UV Fluorescence		Maturity	
						Av. % Ro	No.	Av. SCI	No.	Form	Colour		
214/26-1	5350.0	Hordaland	E2	DC	KC	0.24	26	3.0	20	Miosp	Yel - orn	Immature	
	AOM									Orn - brn - N.F.			
	-									-			
	5710.0			DC	KC	0.33	20	3.5	7	Miosp	Orn		
										Dino	Orn		
										AOM	Orn - N.F.		
	6010.0			DC	KC	0.58	23	7.0	15	Miosp	?N.F.		?Middle Mature (Main Oil Window)
										Dino	?Orn - brn		
										AOM	Ra yel - orn		
	6390.0	DC		KC	0.52	22	6.5	2	Miosp	N.F.			
									Dino	?Bl			
									AOM	?Ft orn - N.F.			
	6760.0	Lewis Fan Envelope		DC	KC	0.34	18	3.5	19	Miosp	Orn - yel	Immature	
										Dino	Ft orn		
										AOM	Orn		
	7140.0	Lewis Lobe		DC	KC	0.41	21	4.0	6	Miosp	Orn - brn - N.F.		
										Dino	Orn		
										AOM	?Bt orn - brn		
	7960.0	Lewis Lobe		DC	KC	-	-	4.0	11	Miosp	Orn - N.F.		
										Dino	N.F.		
										AOM	Brn - yel - orn		
	8230.0	Base Lewis Fan Envelope		DC	KC	-	-	4.5	10	Miosp	Ft orn - N.F.		
										Dino	Ft orn - brn - N.F.		
										AOM	Orn - brn - N.F.		
8510.0	Balder	DC	KC	0.41	30	4.0	7	Miosp	Brn - Ft orn - N.F.				
								Dino	Orn - brn				
								AOM	Orn - N.F.				
8910.0	Sele	DC	KC	0.48	19	4.5	9	Miosp	Orn - brn - N.F.				
								Dino	Brn				
								AOM	Orn - brn				

TABLE 5.2.11 Optical maturity data summary: 214/26-1

Well	Bottom Depth (ft)	Stratigraphy	Age	Sample Type	Sample Prep.	Indigenous VR Pop.		Indigenous SCI Pop.		UV Fluorescence		Maturity
						Av. % Ro	No.	Av. SCI	No.	Form	Colour	
214/28-1	4560.0	Lower Oligocene	O1	DC	KC	0.27	45	3.0	4	Miosp	?Yel orn	Immature
										Dino	?Yel orn	
										AOM	N.F.	
	5850.0	Late Eocene	E3	DC	KC	0.27	30	3.5	1	Miosp	?Orn	
										Dino	?Yel orn	
										AOM	Yel - brn - N.F.	
	6540.0	Middle Eocene	E2	DC	KC	0.30	26	3.5	4	Miosp	?Orn	
										Dino	?Yel orn	
										AOM	Yel - brn - N.F.	
	7300.0			DC	KC	0.37	46	3.5	10	Miosp	Yel orn - ?orn	
										Dino	Yel orn - orn	
										AOM	N.F.	
	8200.0	Early Eocene	E1	DC	KC	0.37	10	3.0	34	Miosp	Yel orn - orn	
										Dino	Yel orn	
										AOM	DI brn - N.F.	
	9630.0	Middle Paleocene	P2	DC	KC	0.36	45	4.0	12	Miosp	Yel orn	
										Dino	DI yel orn	
										AOM	Orn - N.F.	
	10660.0			DC	KC	0.43	19	4.5	4	Miosp	Orn - N.F.	
										Sph	Yel orn	
										AOM	Ra dl brn - N.F.	
	11540.0			DC	KC	0.50	13	5.0	2	Miosp	DI orn - N.F.	Middle Mature (Main Oil Window)
										Sph	?Orn	
										AOM	N.F.	
	12510.0	Early Paleocene	P1	DC	KC	-	-	4.5	4	Miosp	Brn - N.F.	
										Sph	DI orn - N.F.	
										AOM	N.F.	
	13460.0			DC	KC	-	-	4.5	1	Miosp	?Brn	
										AOM	N.F.	
										-	-	

TABLE 5.2.12 Optical maturity data summary: 214/28-1

Well	Top Depth (ft)	Stratigraphy	Age	Sample Type	Sample Prep.	Indigenous VR Pop.		Indigenous SCI Pop.		UV Fluorescence		Maturity
						Av. % Ro	No.	Av. SCI	No.	Form	Colour	
214/28-1	14600.0	Early Paleocene	P1	DC	KC	0.73	2	4.5	1	Miosp	?DI brn	Middle Mature (Main Oil Window)
										AOM	N.F.	
										-	-	
	15470.0	Early Paleocene	P1	DC	KC	-	-	5.0	3	Miosp	N.F.	
										AOM	N.F.	
										-	-	
	16960.0	Maastrichtian	K2	DC	KC	-	-	-	-	AOM	N.F.	
										-	-	
										-	-	

TABLE 5.2.12 Optical maturity data summary: 214/28-1

Population type: Vitrinite reflectivity

N.D.P.: No determination possible
I: Indigenous
C: Caved
L: Low reflecting
R: Reworked
B: Bitumen
E: Excinite
Z: Zooclast

Population type: Spore colouration

N.D.P.: No determination possible
Indg: Indigenous
Cav: Caved/bleached
St: Stained
Rwk: Reworked
e: estimate based on acritarch or overall kerogen colour/fluorescence

Colour

lt: Light
pl: Pale
bt: Bright
dl: Dull
wk: Weak
dk: Dark
brn: Brown
orn: Orange
yl: Yellow
grn: Green
rd: Red
ra: Rare
N.F: Non Fluorescent

Form

AOM: Amorphous organic matter
Paly: Palynomorphs
Indet: Indeterminate
Mio: Misopores
Dino: Dinocysts
Sph: Sphaeromorphs
Bisa: Bisaccate
Acrit: Acritarchs
FDOM: Finely disseminated organic matter
SOM: Structured organic matter

Kerogen types: six component system

FA: Fluoramorphinite - fluorescent amorphous material
HA: Hebamorphinite - non-fluorescent or weakly fluorescent amorphous material.
AL: Algal organic matter/phytoplankton - identifiable algae and phytoplankton, including dinocysts
HE: Herbaceous Organic Matter - identifiable species and fragments of spores, pollen and cuticles
WO: Woody Organic Matter - translucent, structured woody tissues
CO: Coaly Organic Matter - completely opaque, usually angular material
SP: Identifiable species and fragments of spores and pollen
CUT: Cuticular organic matter (cutinite)
Humic: Structured humic organic matter (huminite, vitrinite) - translucent, structured woody tissues.
Inert: Inert organic matter (inertinite)- completely opaque, usually angular material

Kerogen types: three component system

Sap: Includes alginite, sporinite, cuticle and liptodetrinite and organic matter interpreted to have originated as fluoramorphinite.
Vit: Includes vitrinite and vitridetrinite and organic matter interpreted to have originated as hebamorphinite.
Inert: Inert organic matter (inertinite)- completely opaque, usually angular material.
Am: Amorphous organic matter (used as a modifier for sapropel and vitrinite).

Quantities

Tr: Trace
Mn: Minor
V: Very
Abn: abundant

TABLE 5.2KEY Optical maturity summary table - key

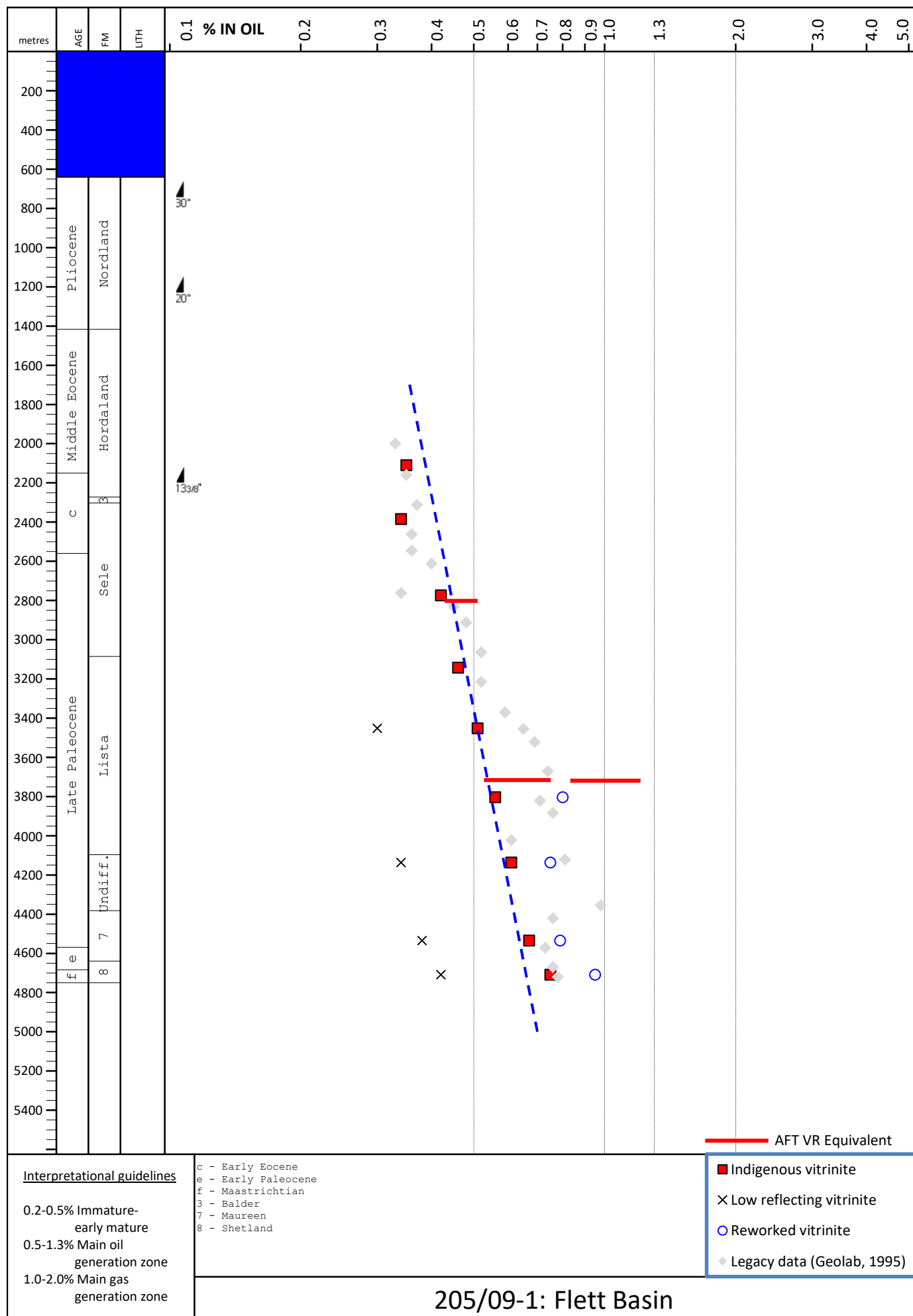


FIGURE 5.2.1.1 Vitrinite reflectivity against depth - 205/09-1

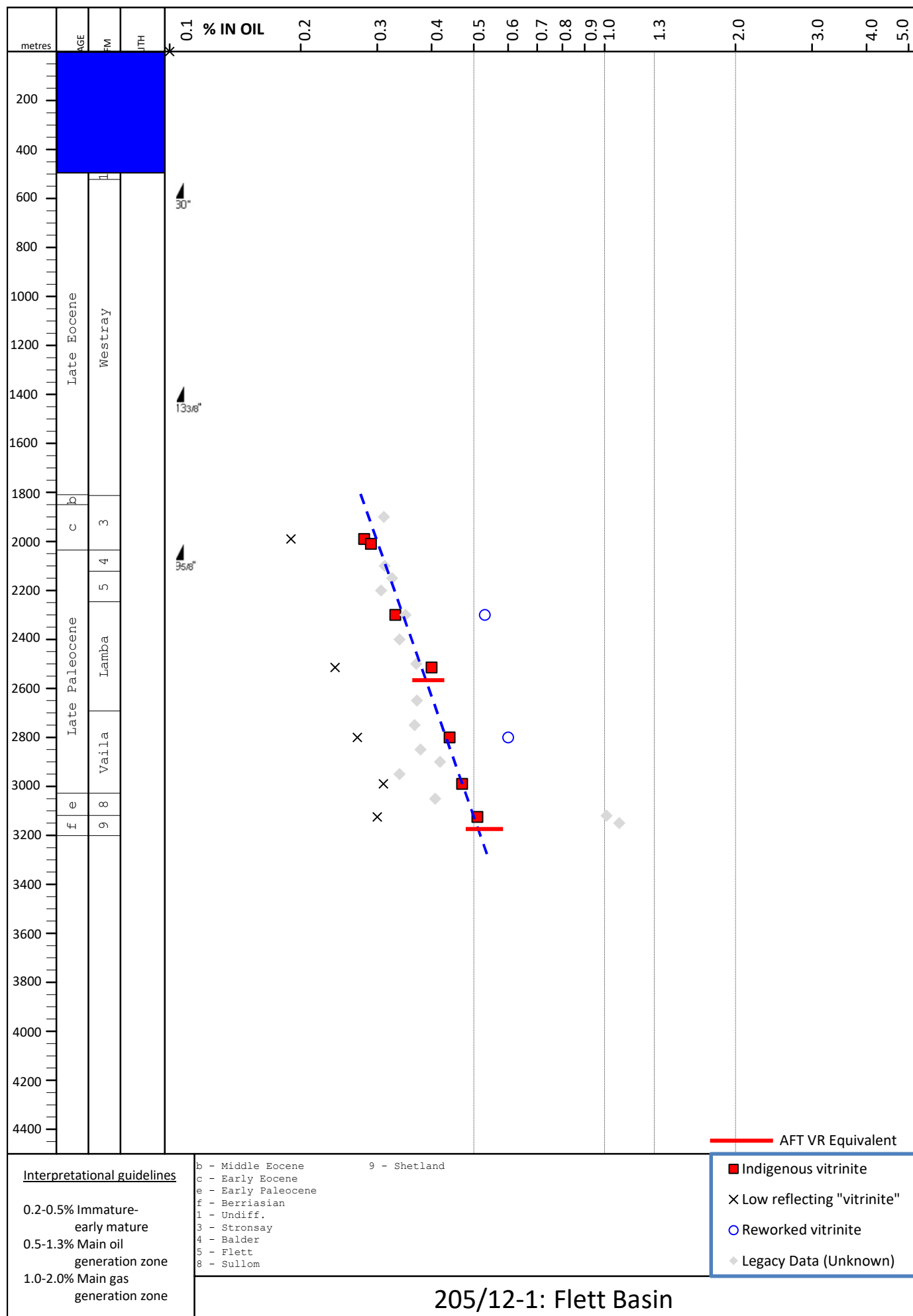


FIGURE 5.2.1.2 Vitrinite reflectivity against depth - 205/12-1

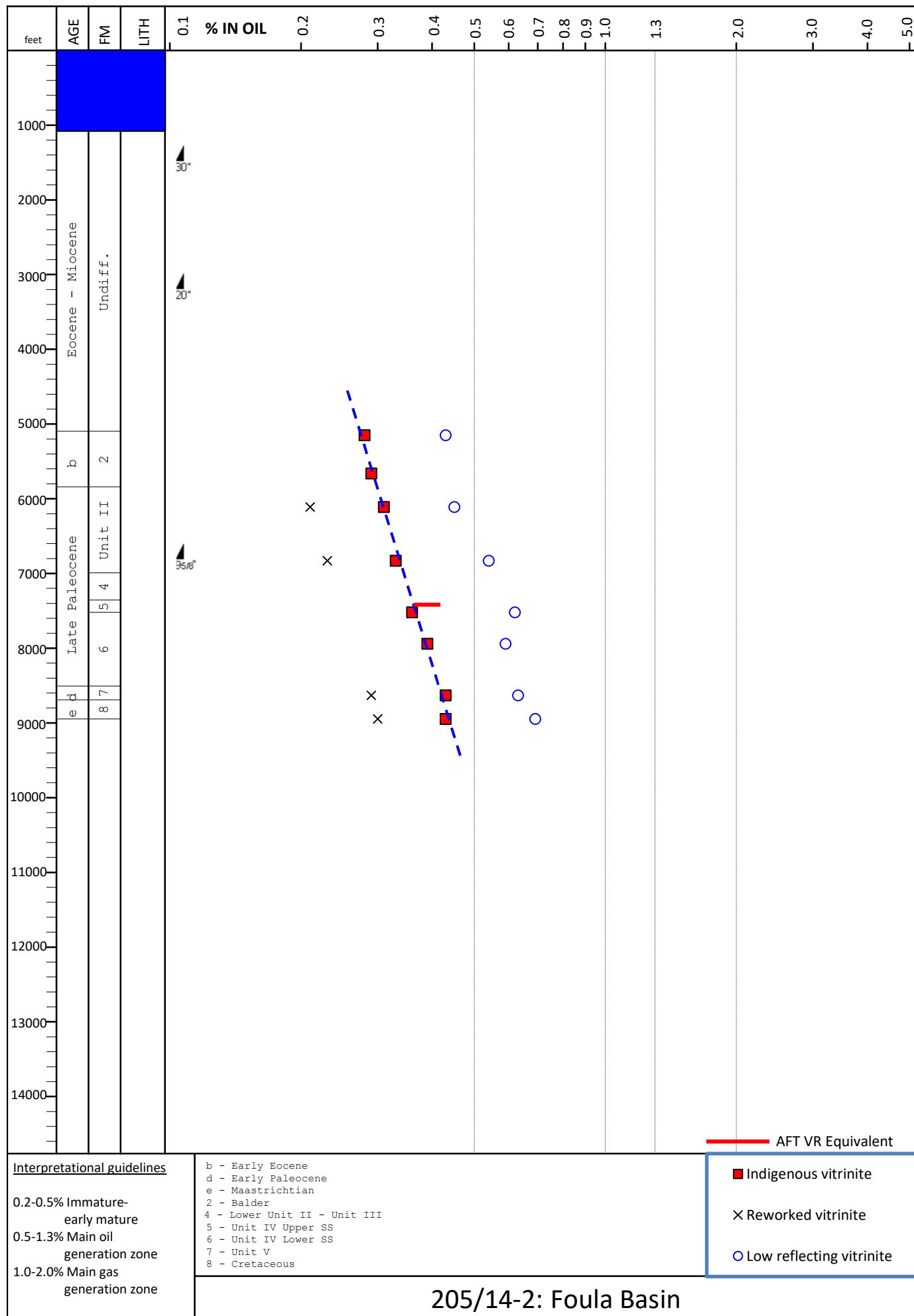


FIGURE 5.2.1.3 Vitrinite reflectivity against depth - 205/14-2

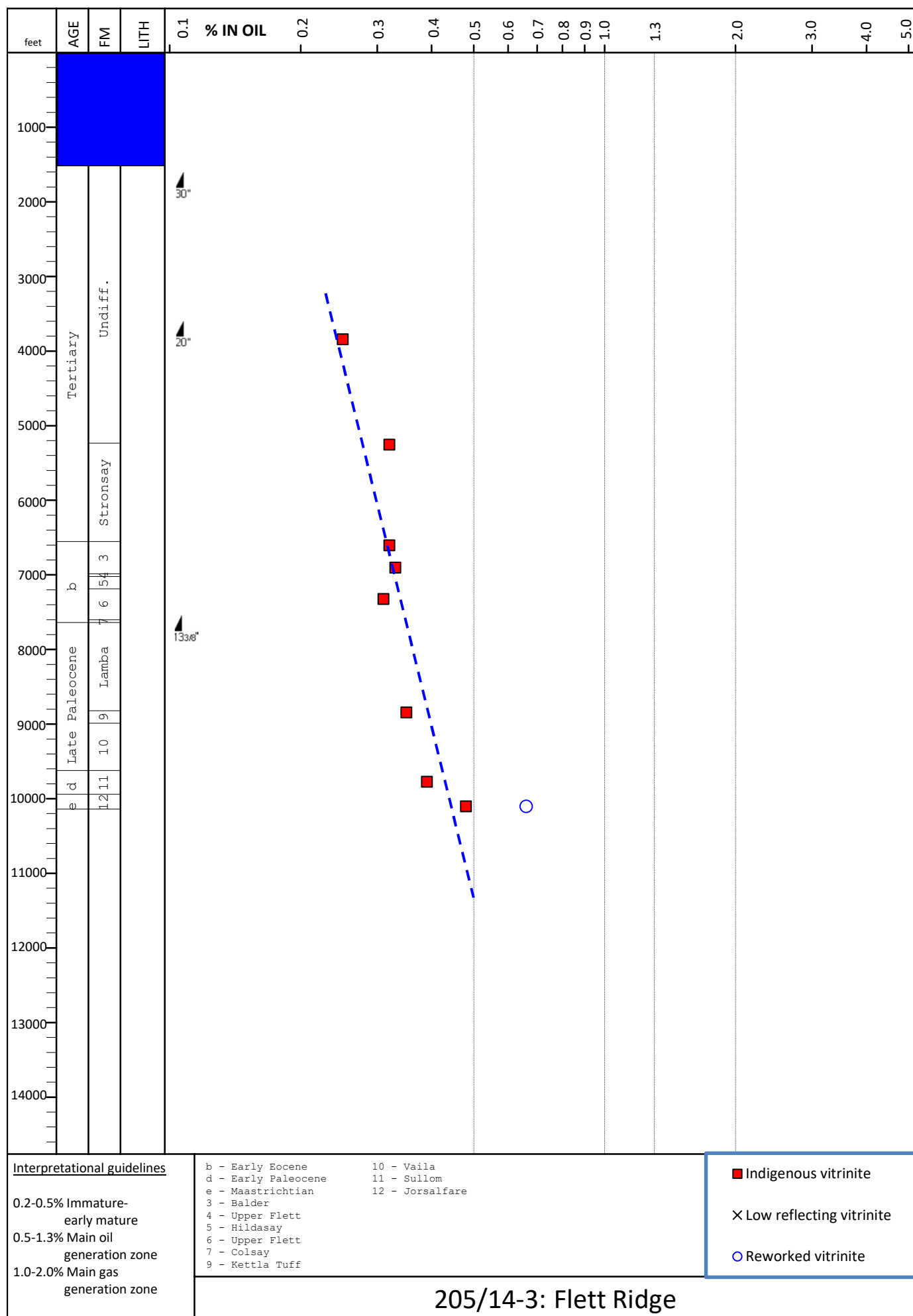


FIGURE 5.2.1.4 Vitrinite reflectivity against depth - 205/14-3

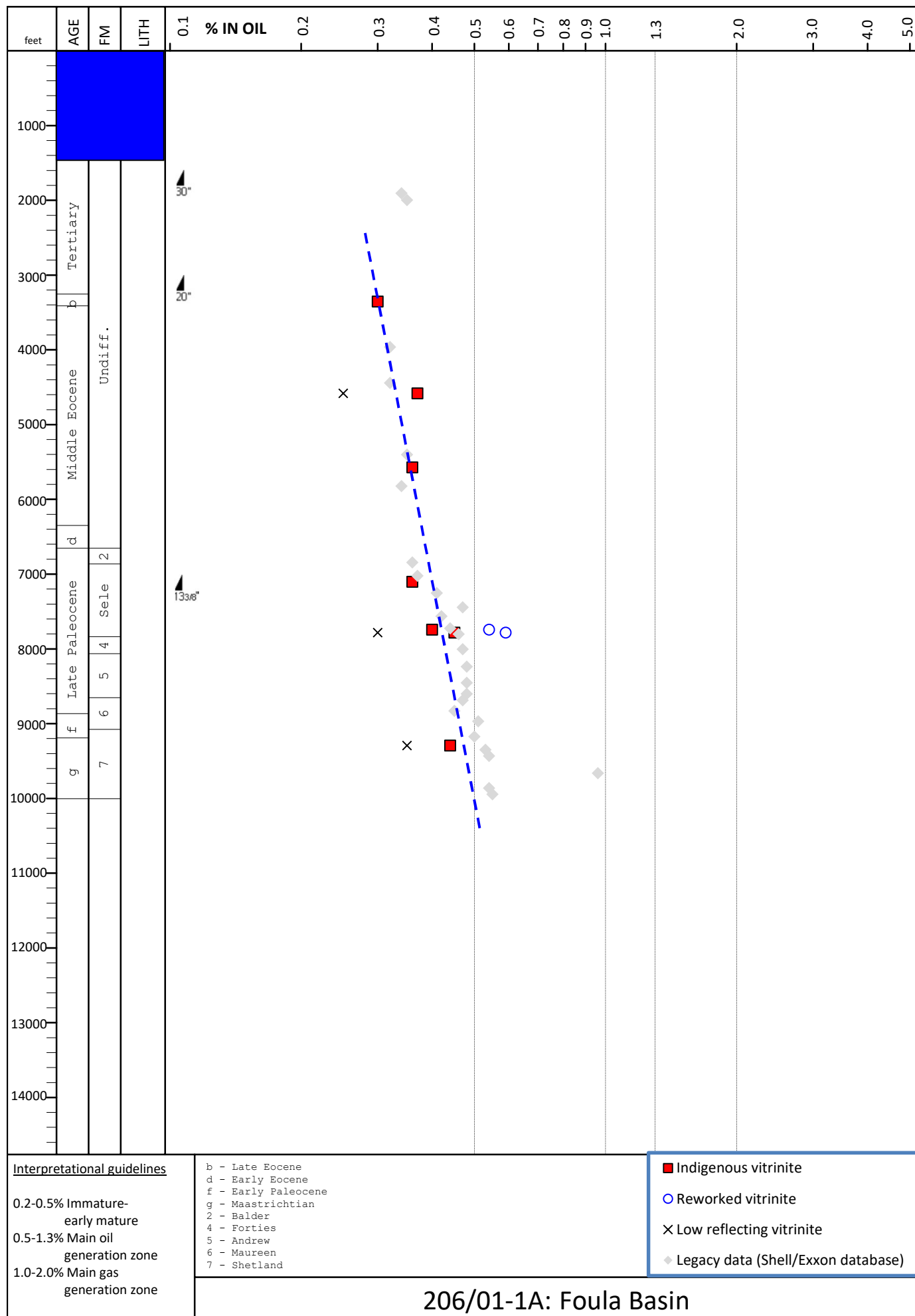


FIGURE 5.2.1.5 Vitrinite reflectivity against depth - 206/01-1A

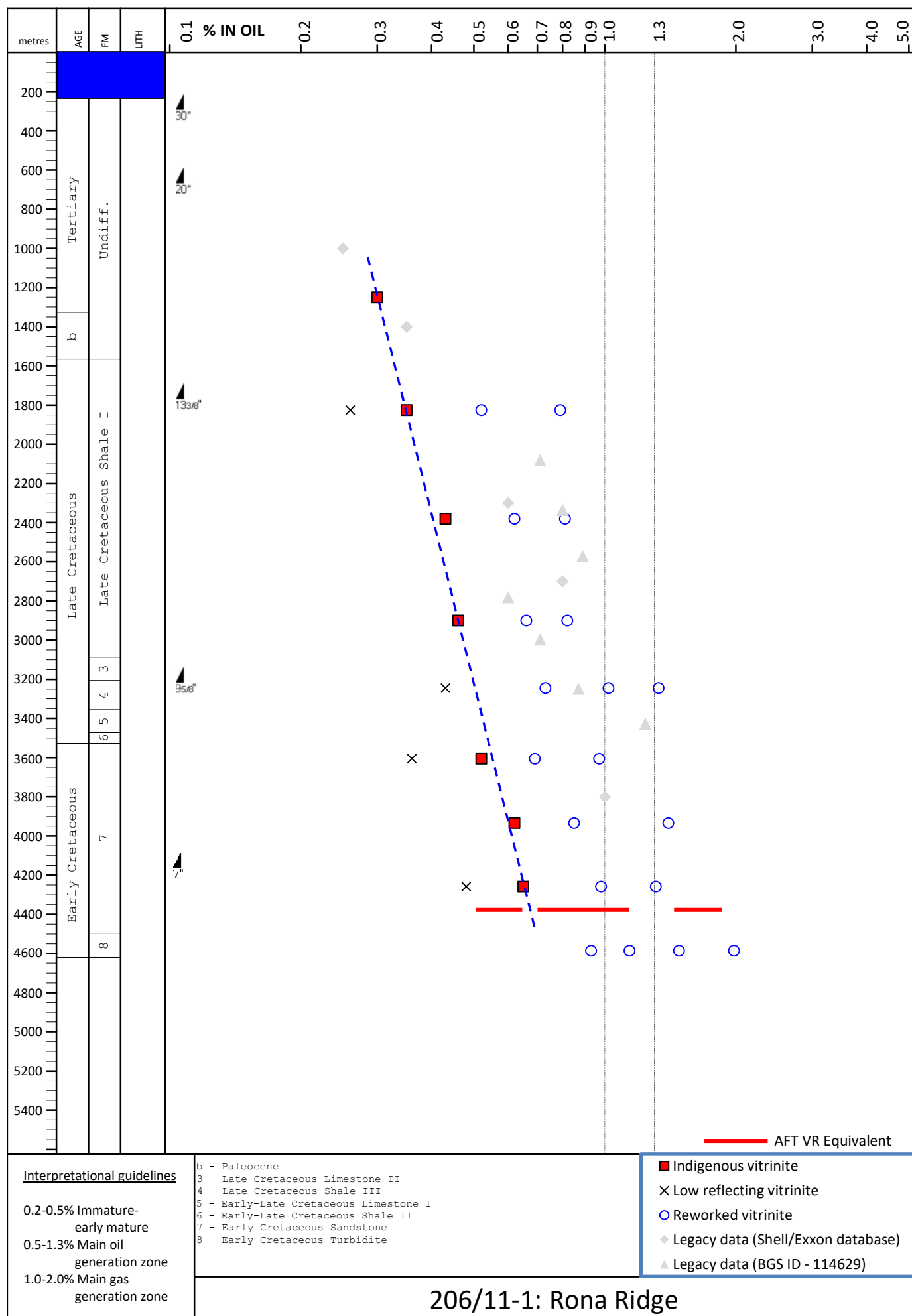


FIGURE 5.2.1.6 Vitrinite reflectivity against depth - 206/11-1

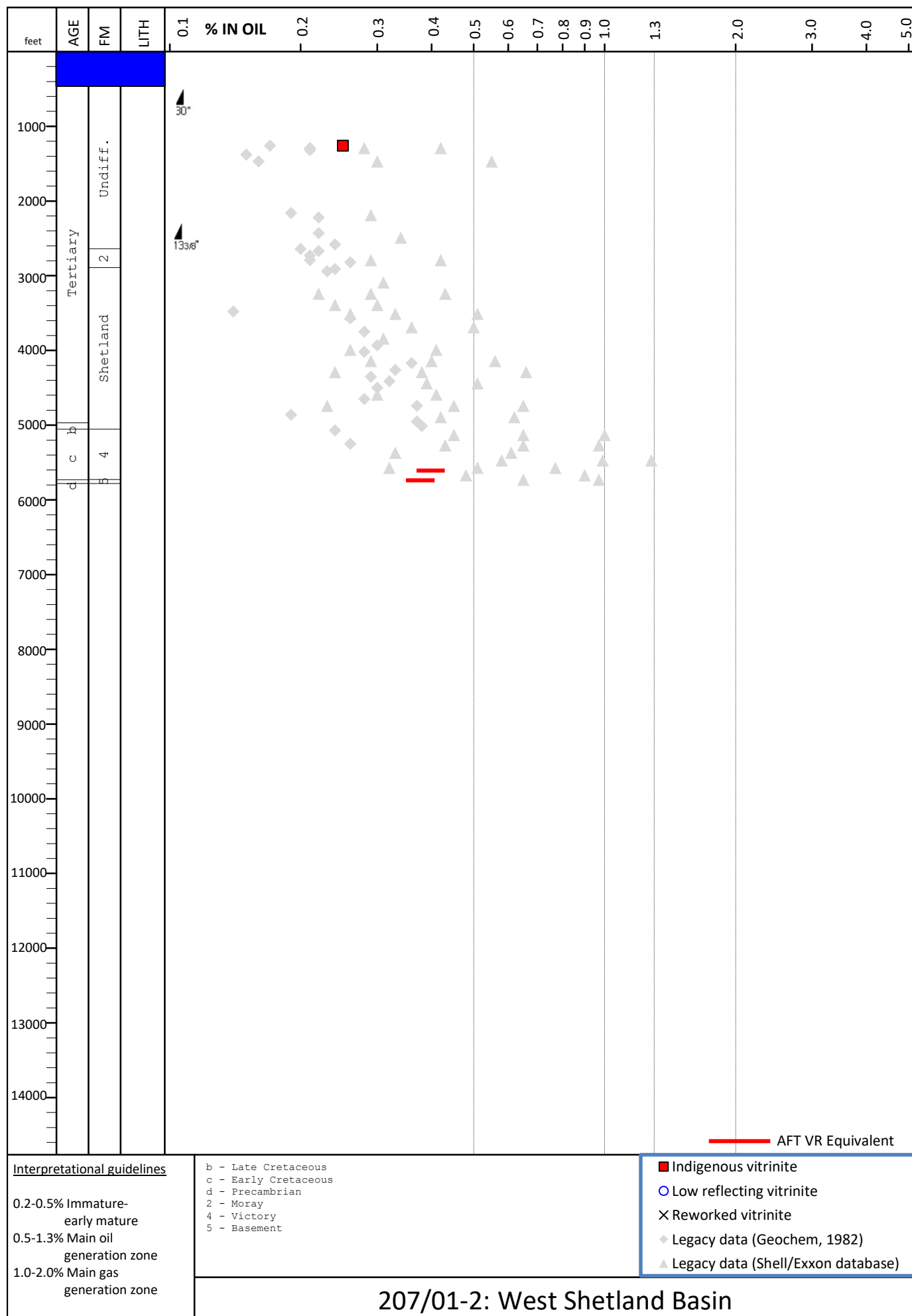


FIGURE 5.2.1.7 Vitrinite reflectivity against depth - 207/01-2

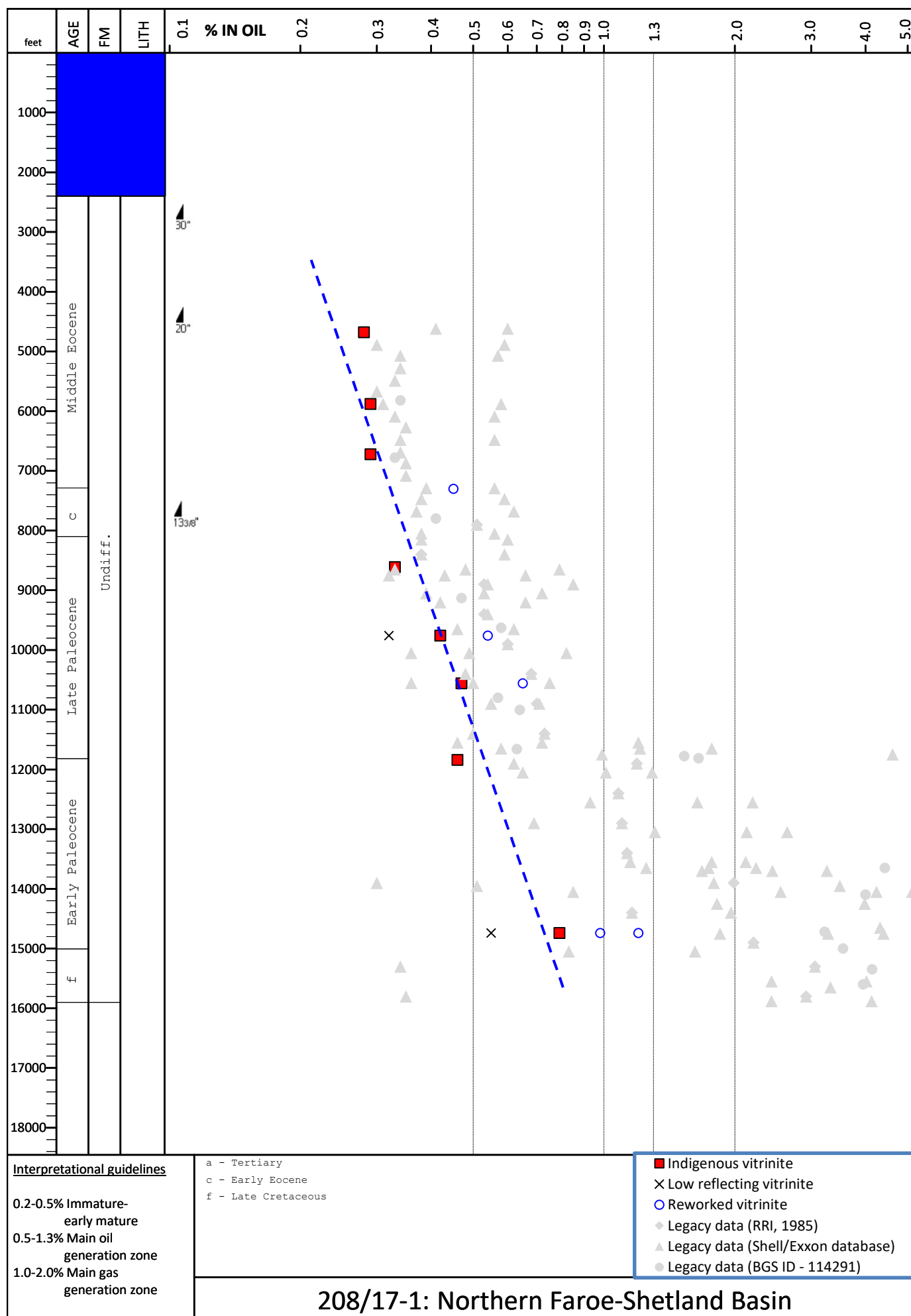


FIGURE 5.2.1.8 Vitrinite reflectivity against depth - 208/17-1

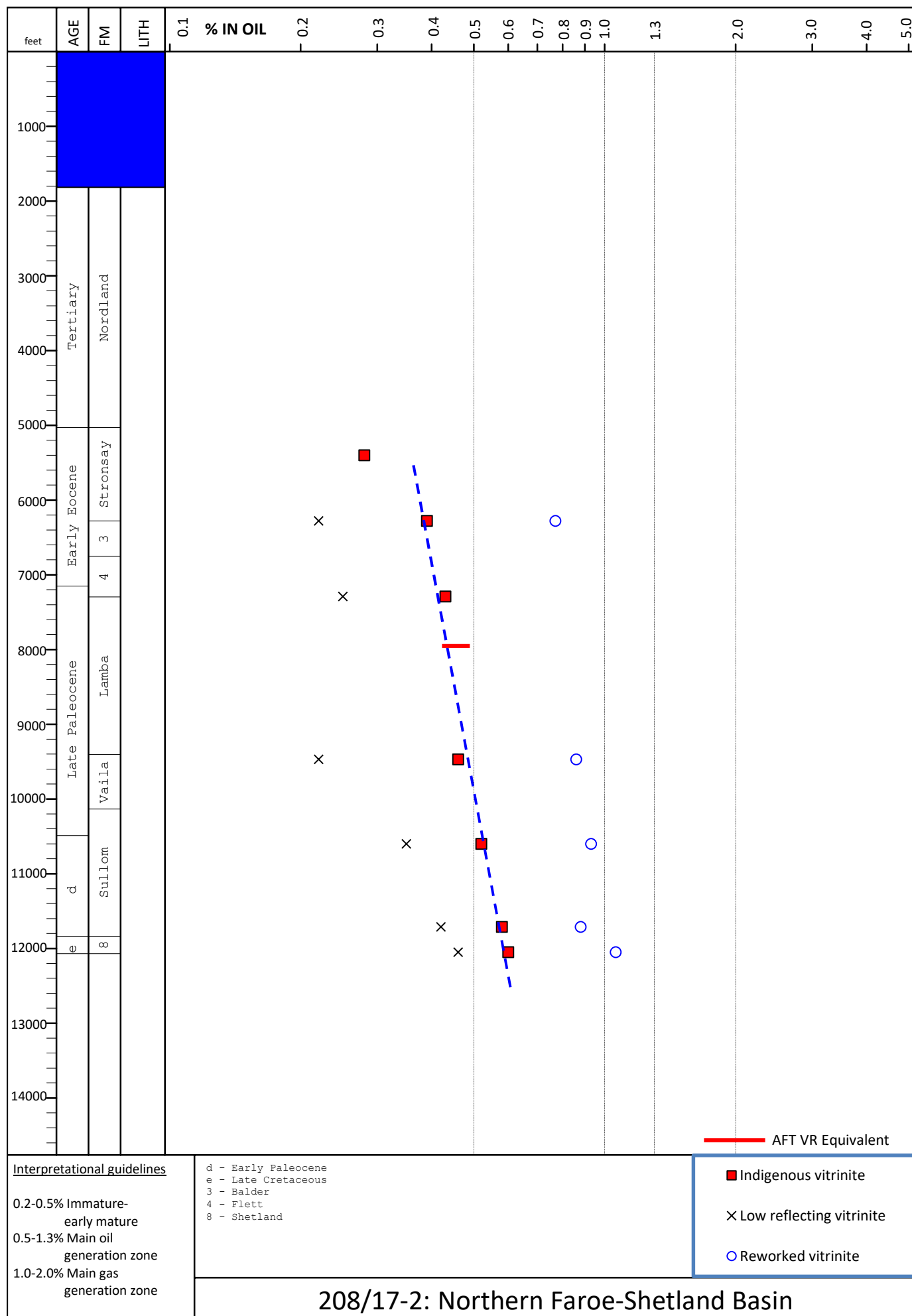


FIGURE 5.2.1.9 Vitrinite reflectivity against depth - 208/17-2

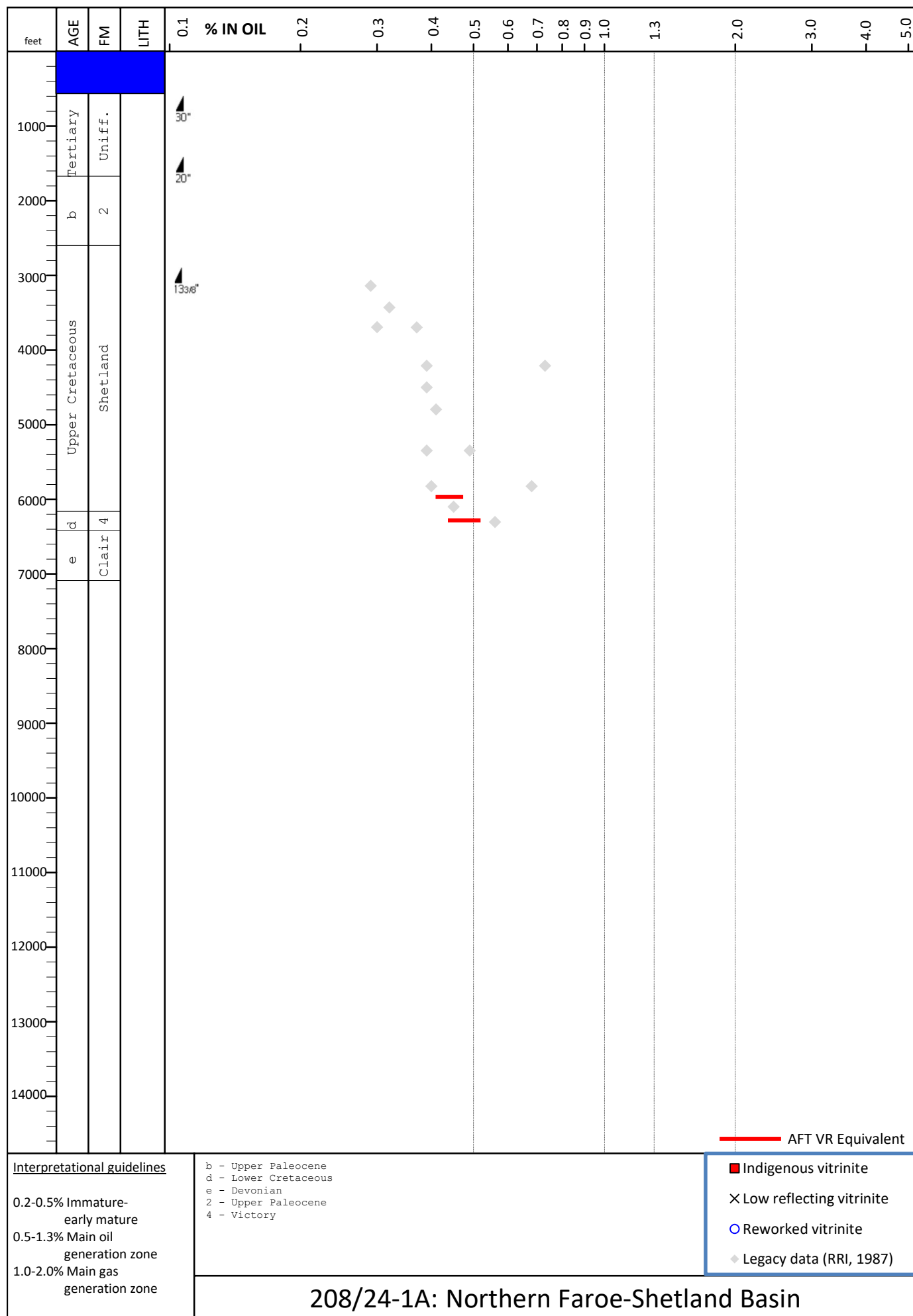


FIGURE 5.2.1.10 Vitrinite reflectivity against depth - 208/24-1A

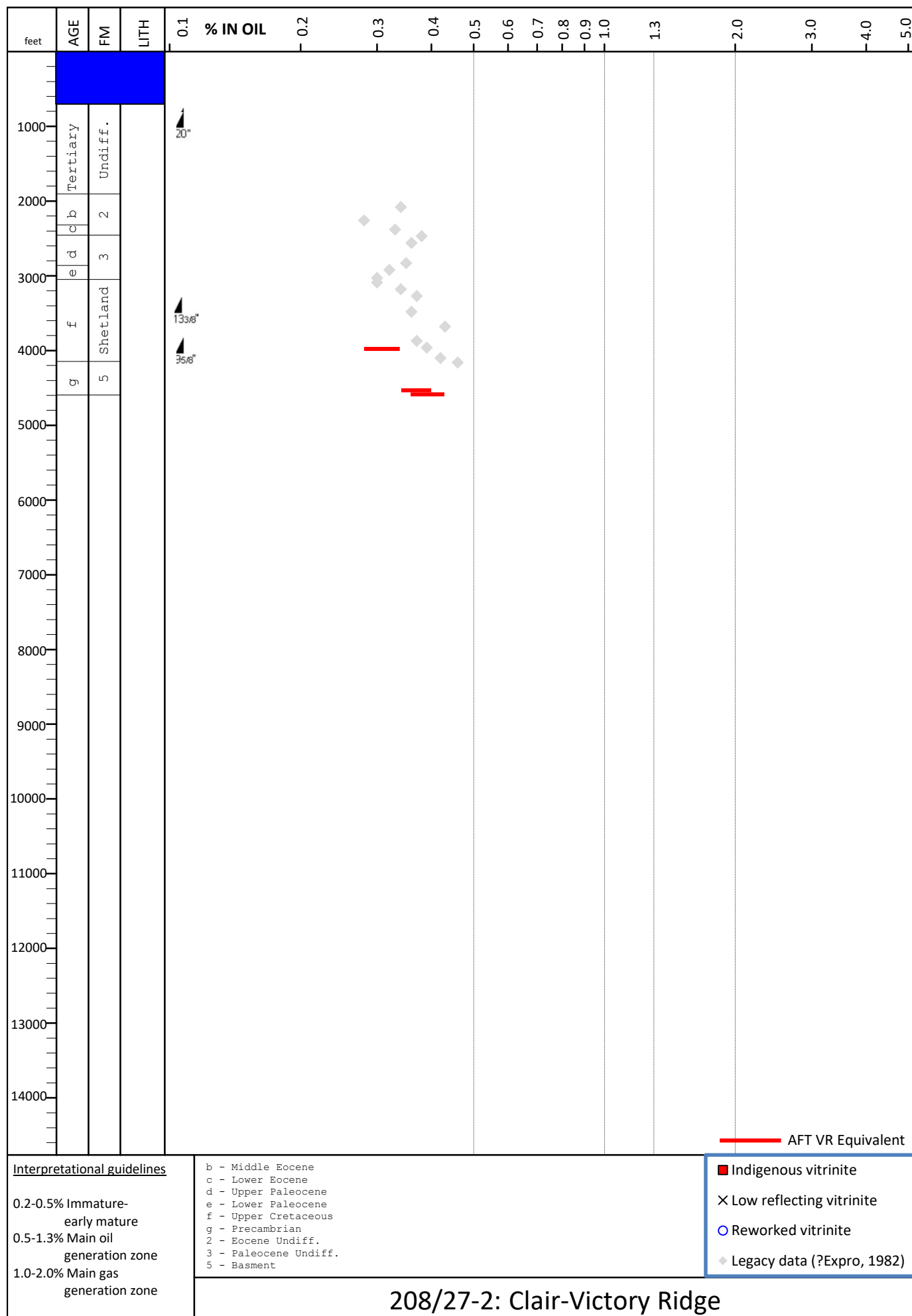


FIGURE 5.2.1.11 Vitrinite reflectivity against depth - 208/27-2

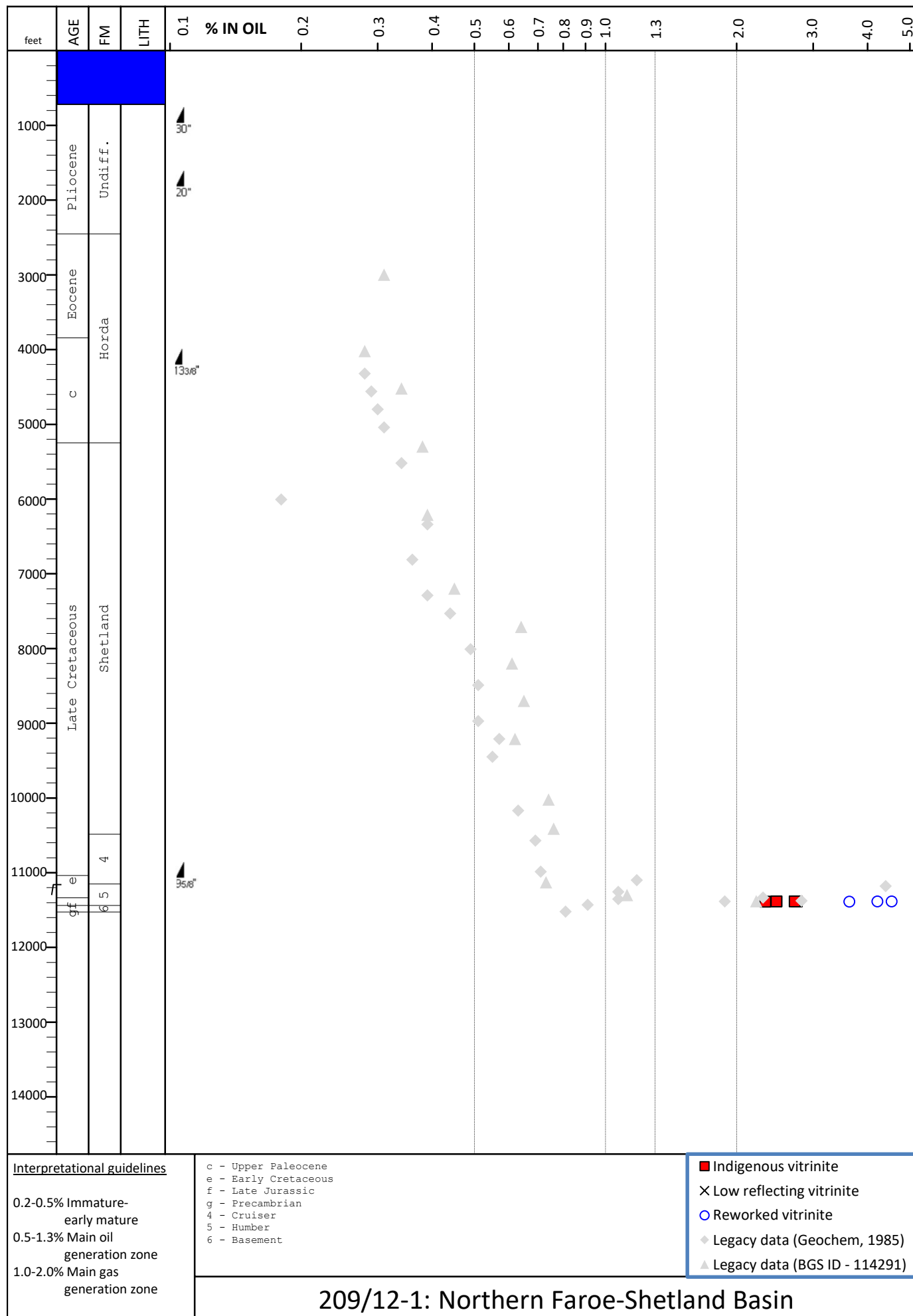


FIGURE 5.2.1.12 Vitrinite reflectivity against depth - 209/12-1

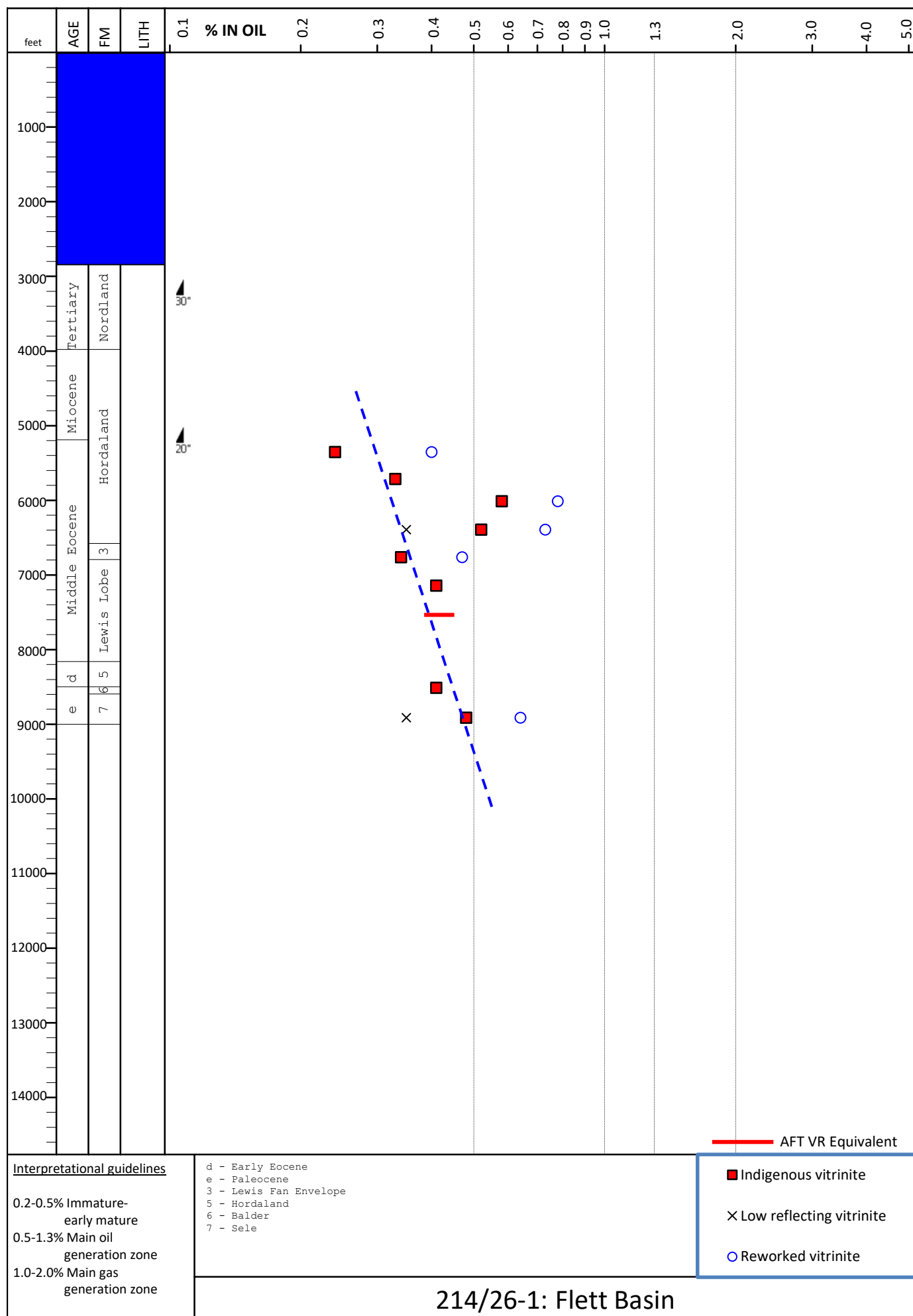


FIGURE 5.2.1.13 Vitrinite reflectivity against depth - 214/26-1

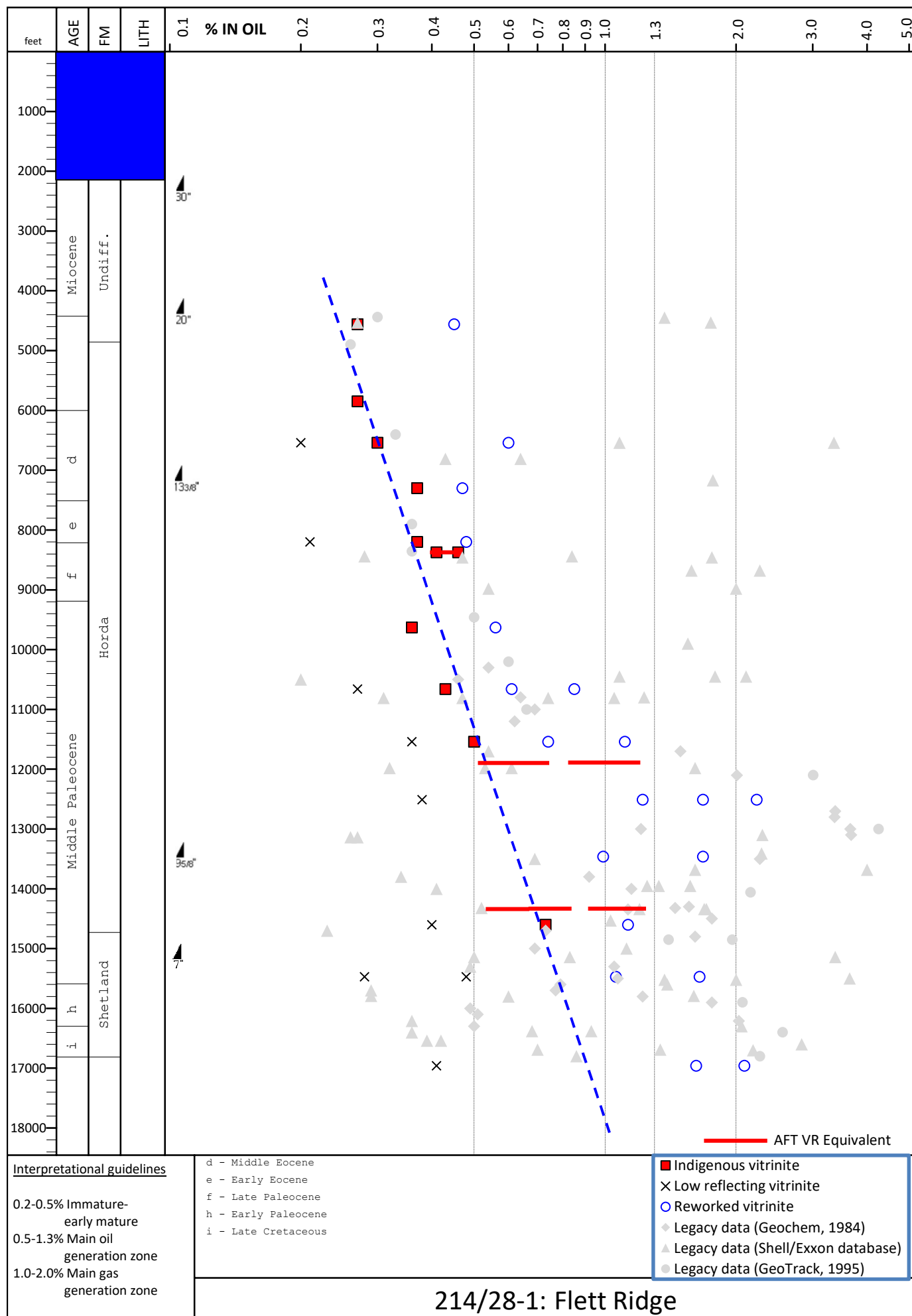


FIGURE 5.2.1.14 Vitrinite reflectivity against depth - 214/28-1

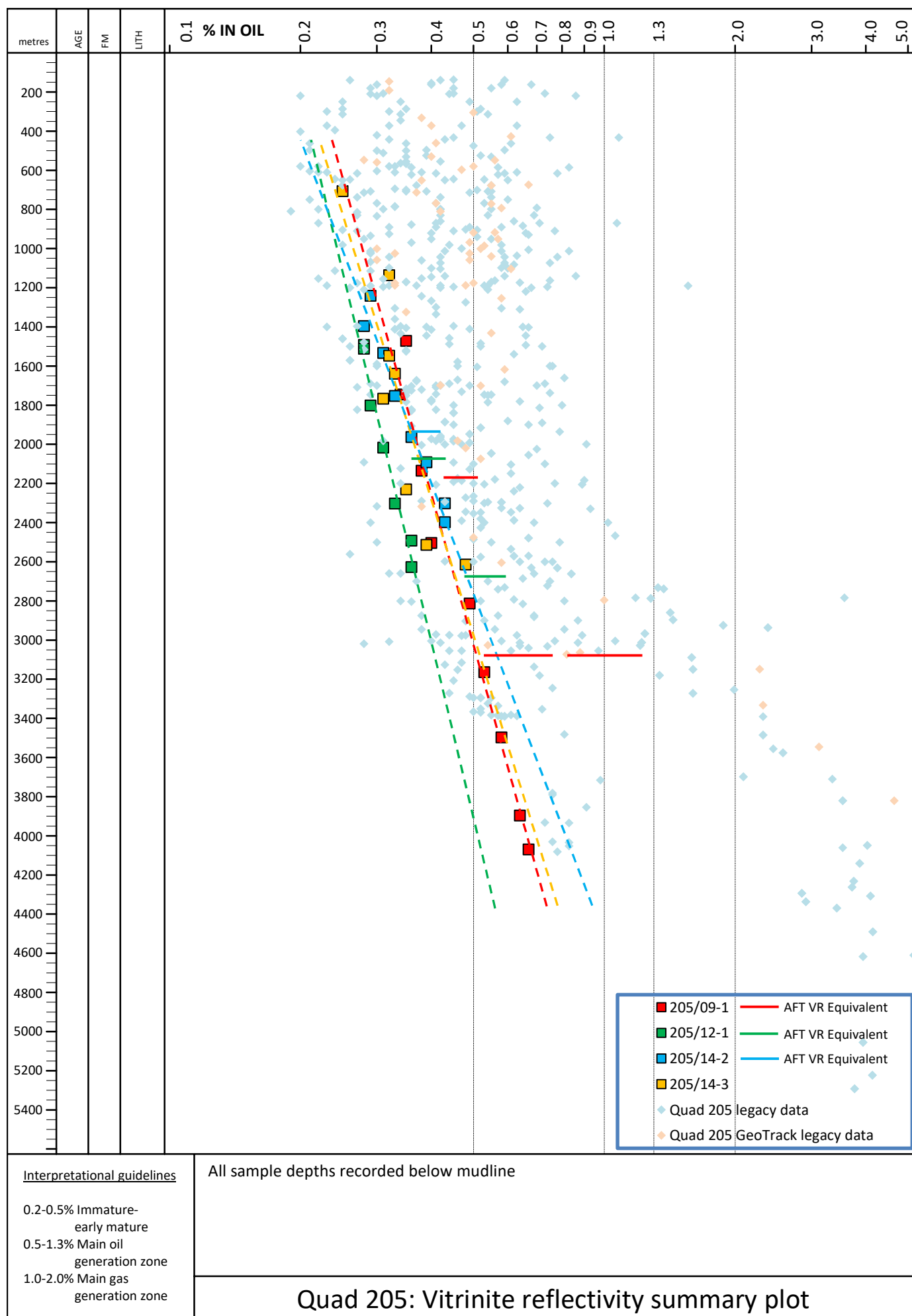


FIGURE 5.2.1.15 Vitrinite reflectivity against depth - Quad 205 summary plot

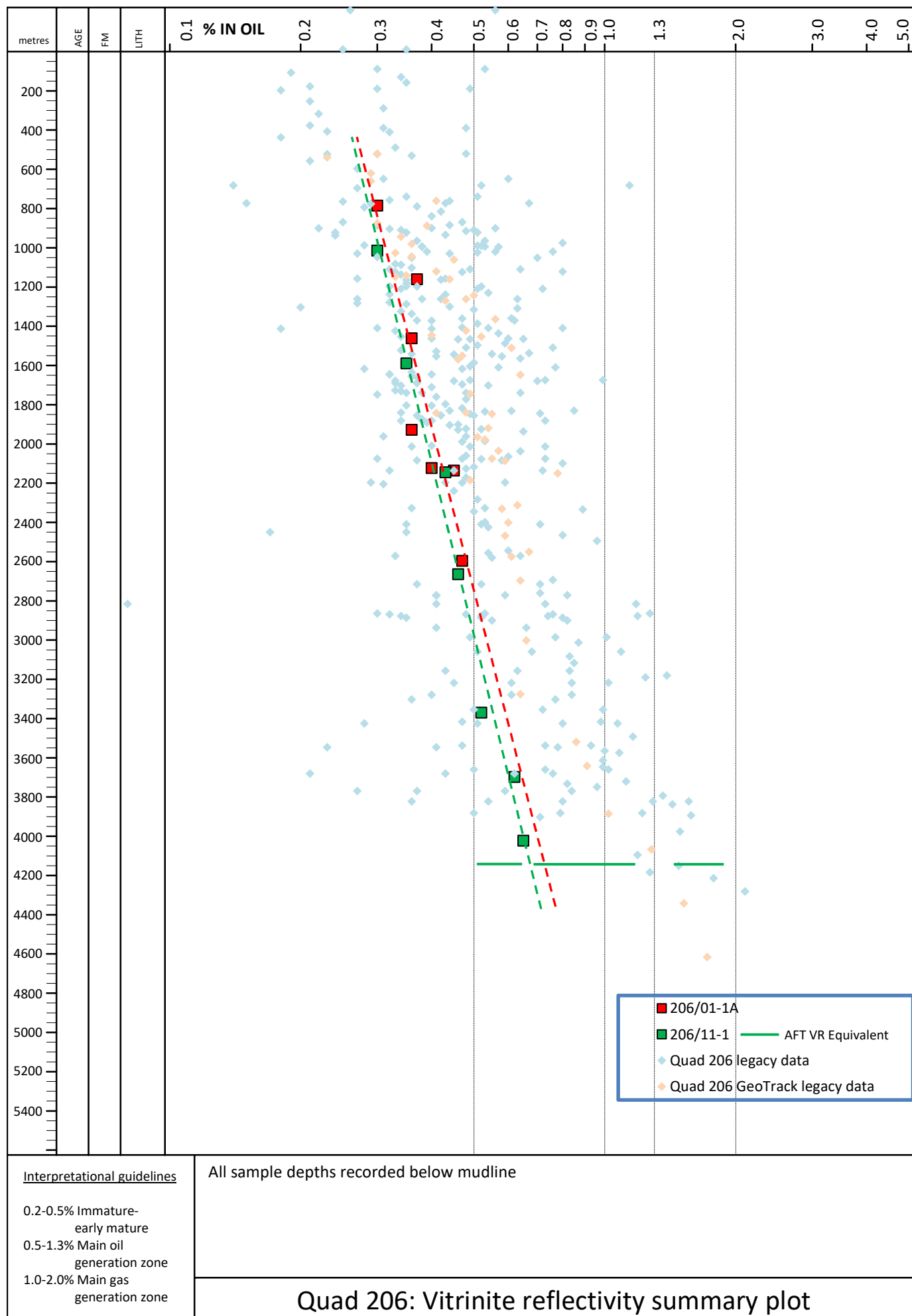


FIGURE 5.2.1.16 Vitrinite reflectivity against depth - Quad 206 summary plot

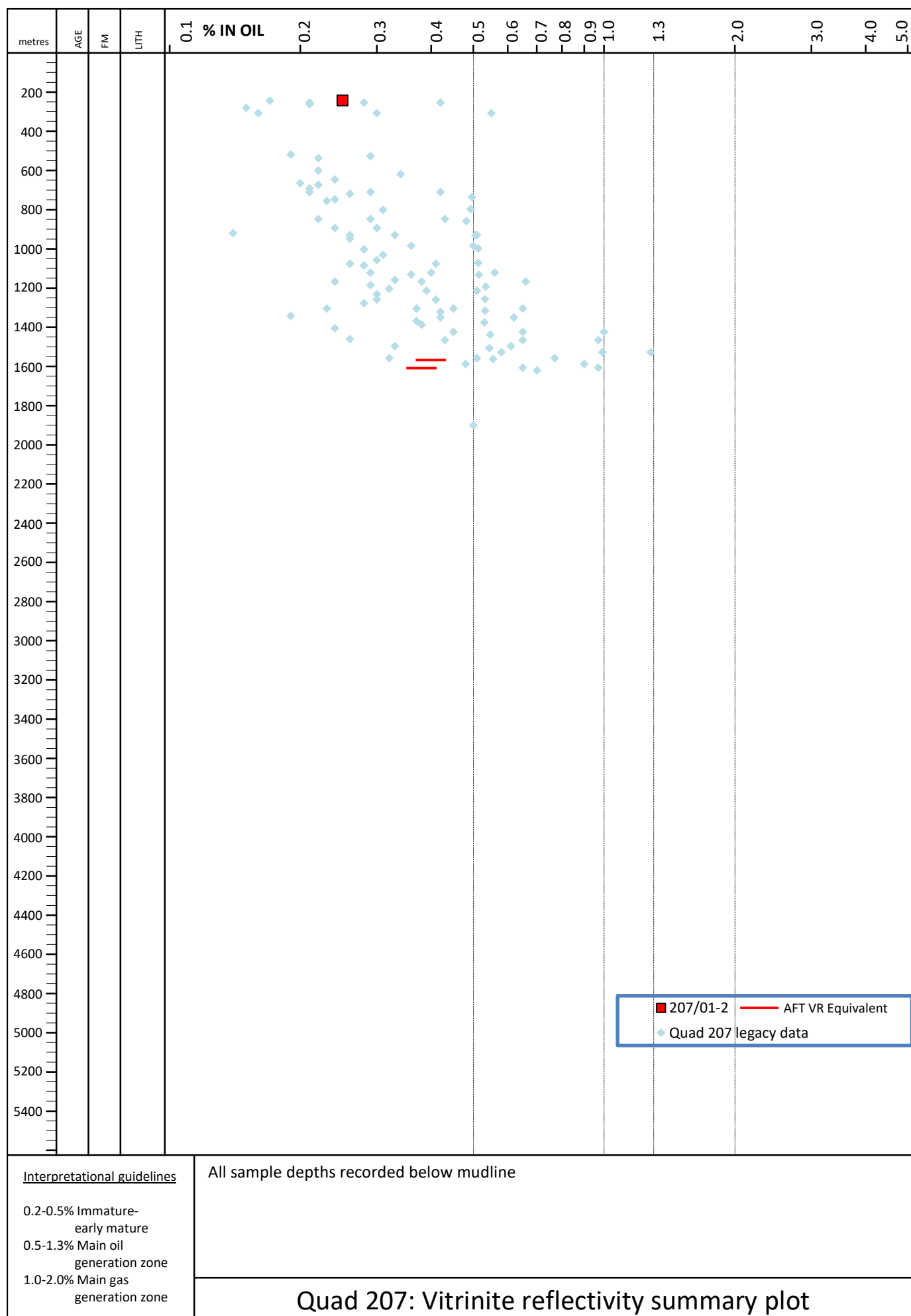


FIGURE 5.2.1.17 Vitrinite reflectivity against depth - Quad 207 summary plot

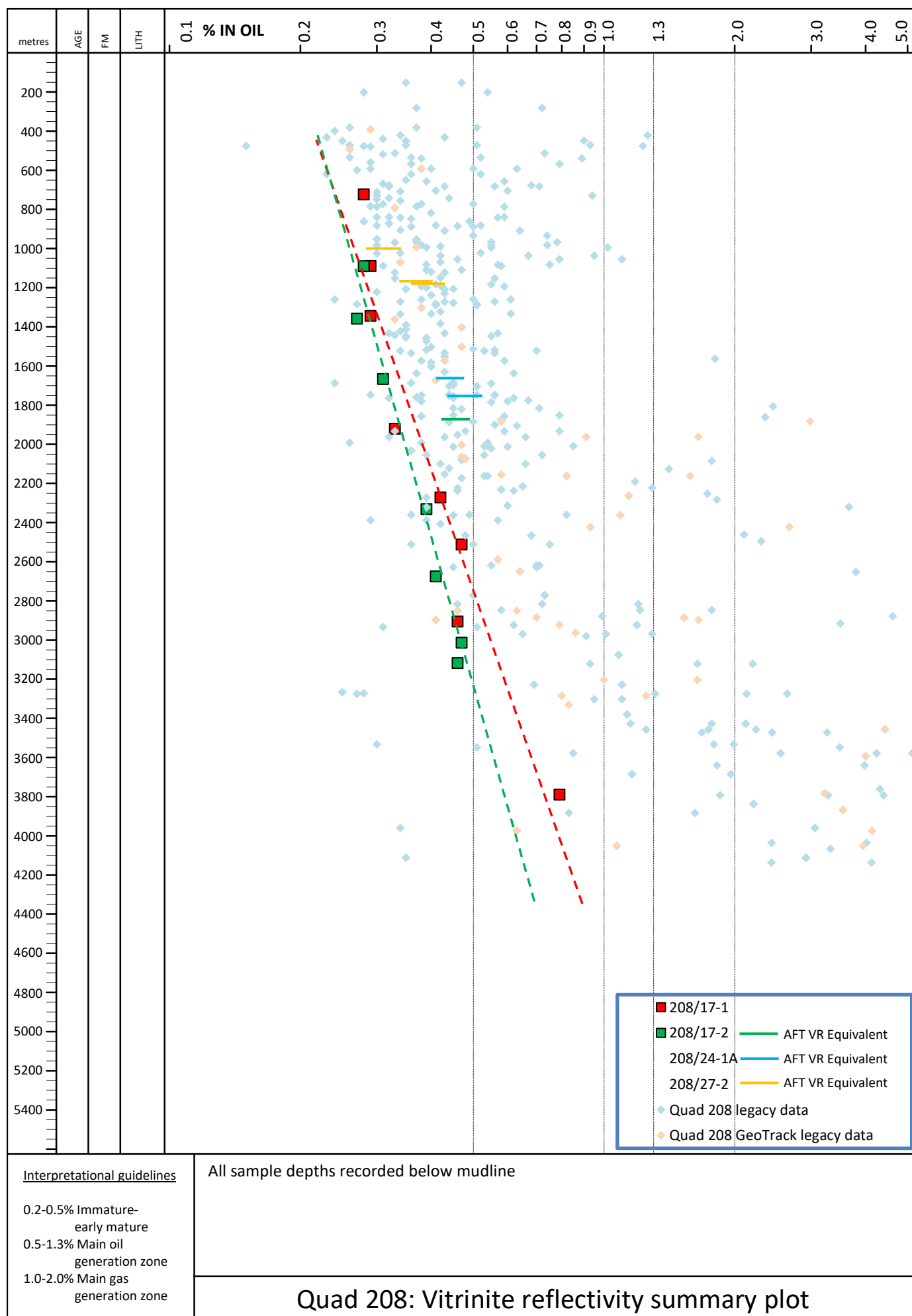


FIGURE 5.2.1.18 Vitrinite reflectivity against depth - Quad 205 summary plot

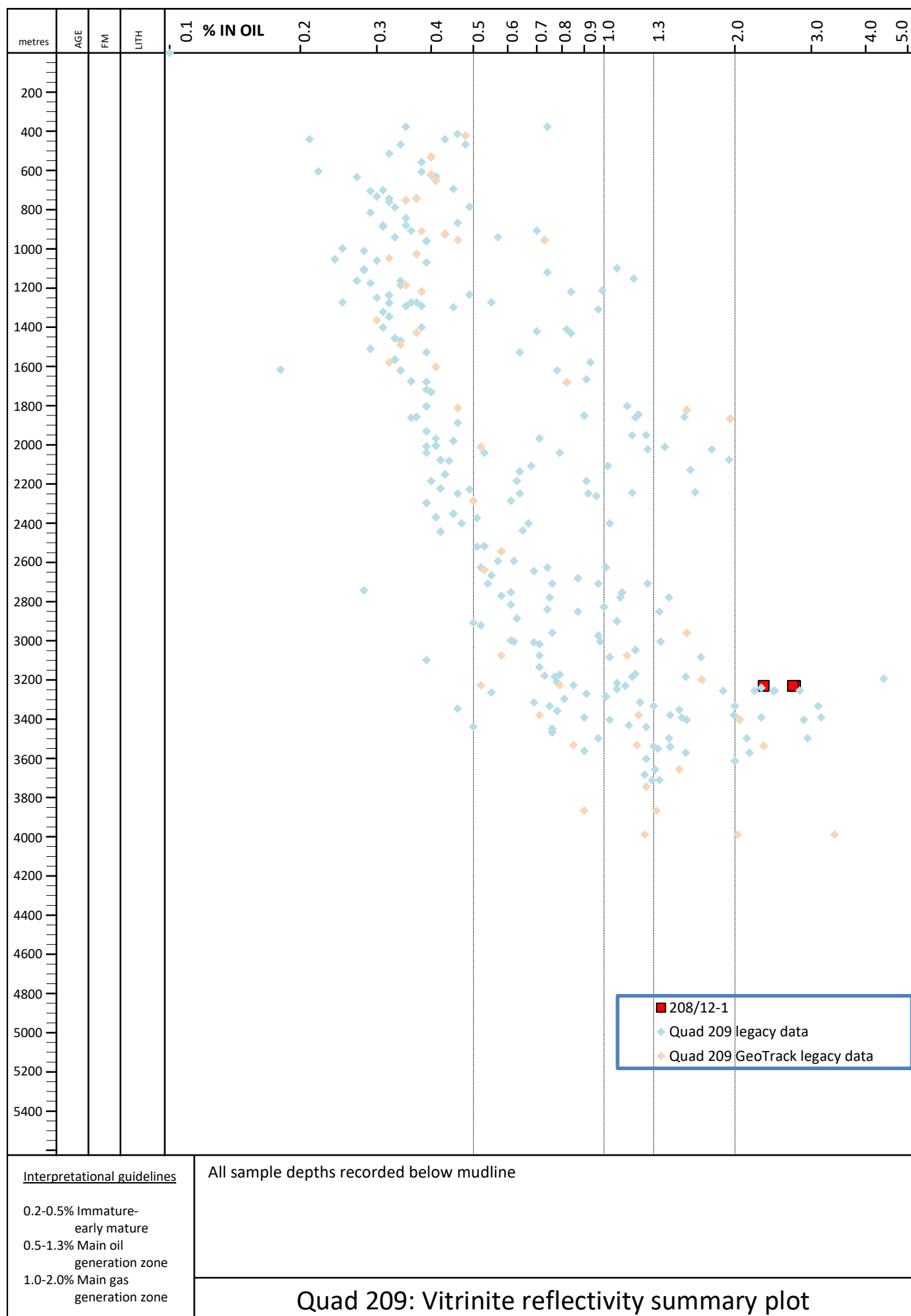


FIGURE 5.2.1.19 Vitrinite reflectivity against depth - Quad 209 summary plot

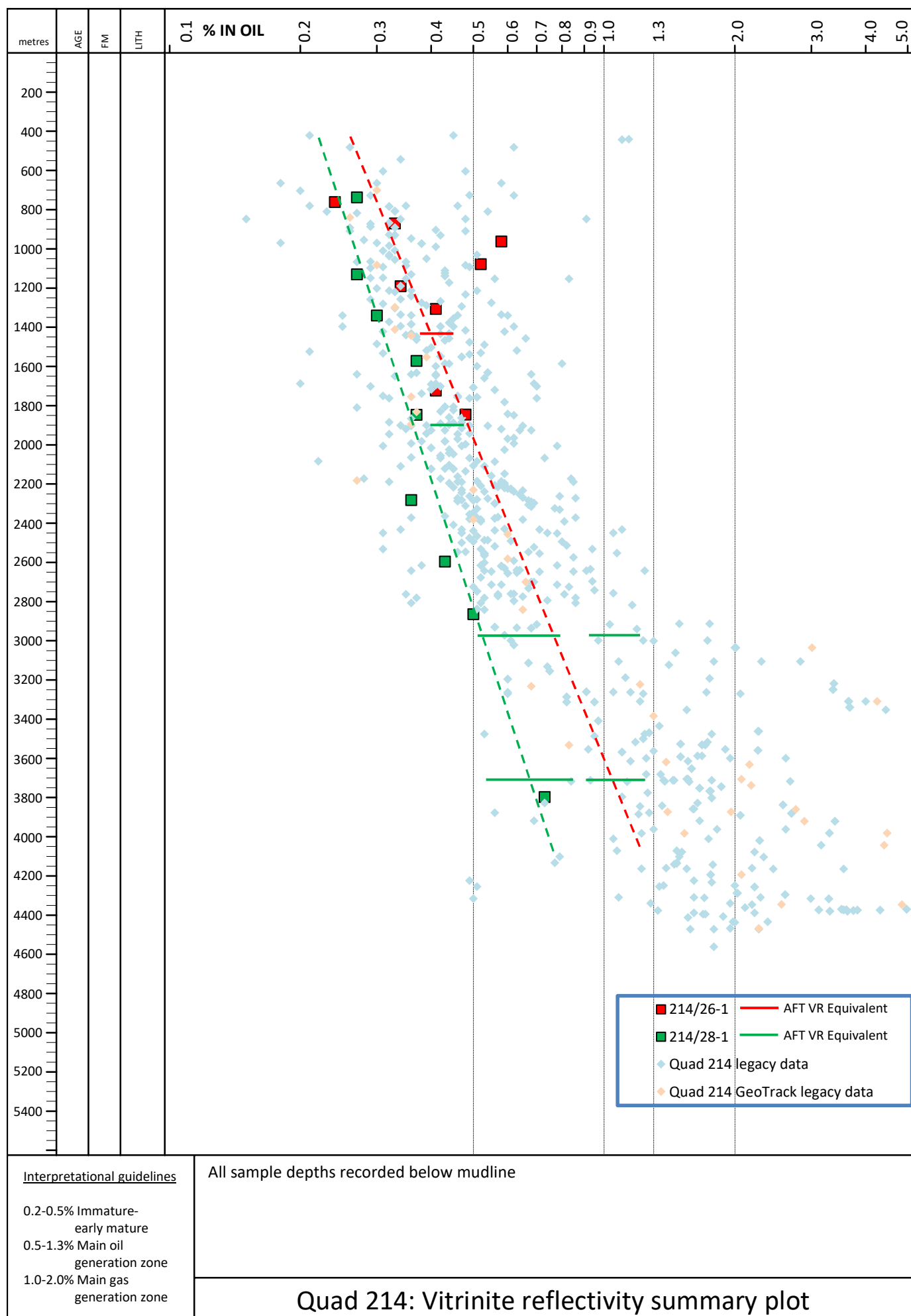


FIGURE 5.2.1.20 Vitrinite reflectivity against depth - Quad 214 summary plot

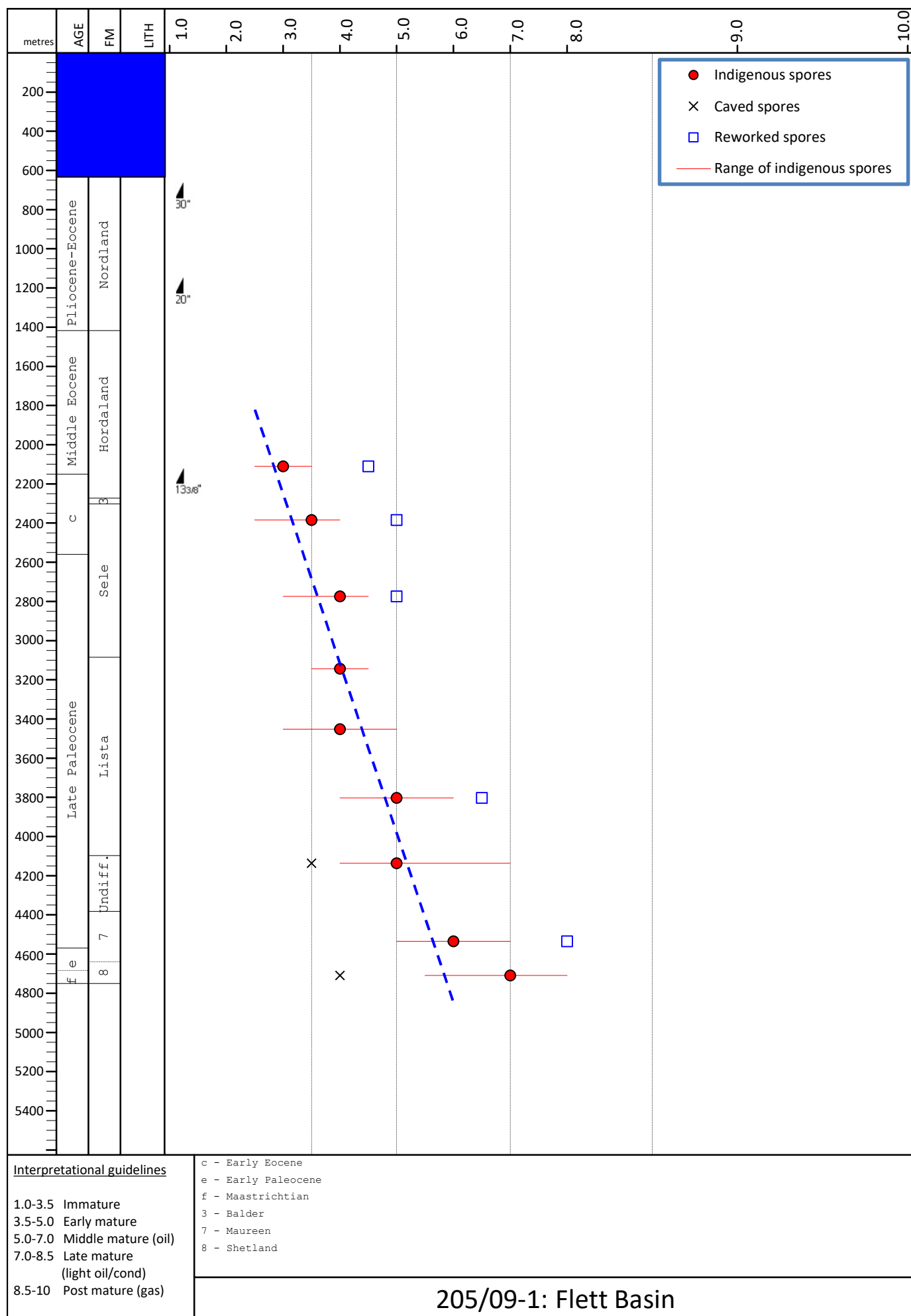
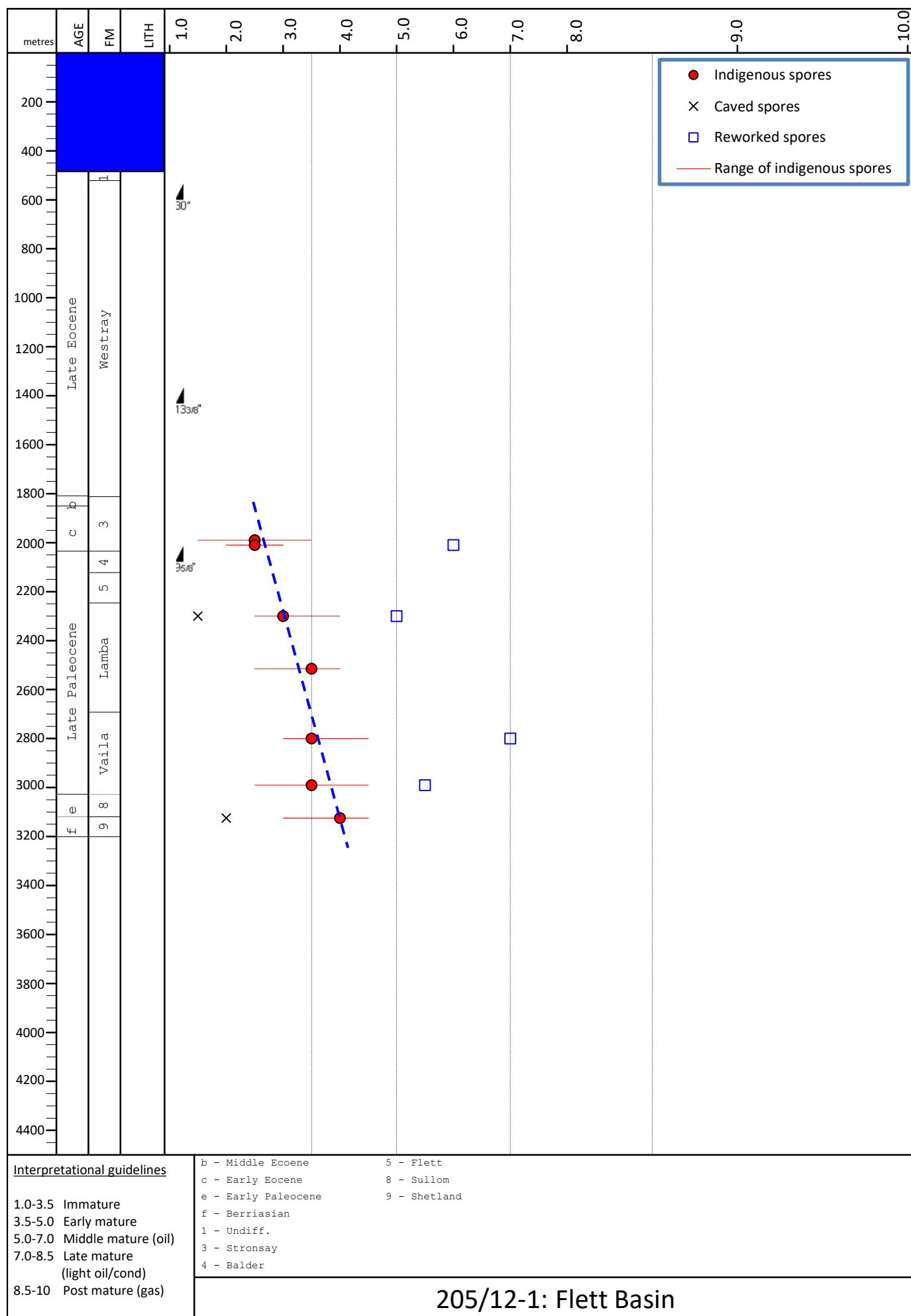


FIGURE 5.2.2.1 Spore colour index against depth - 205/09-1


FIGURE 5.2.2.2 Spore colour index against depth - 205/12-1

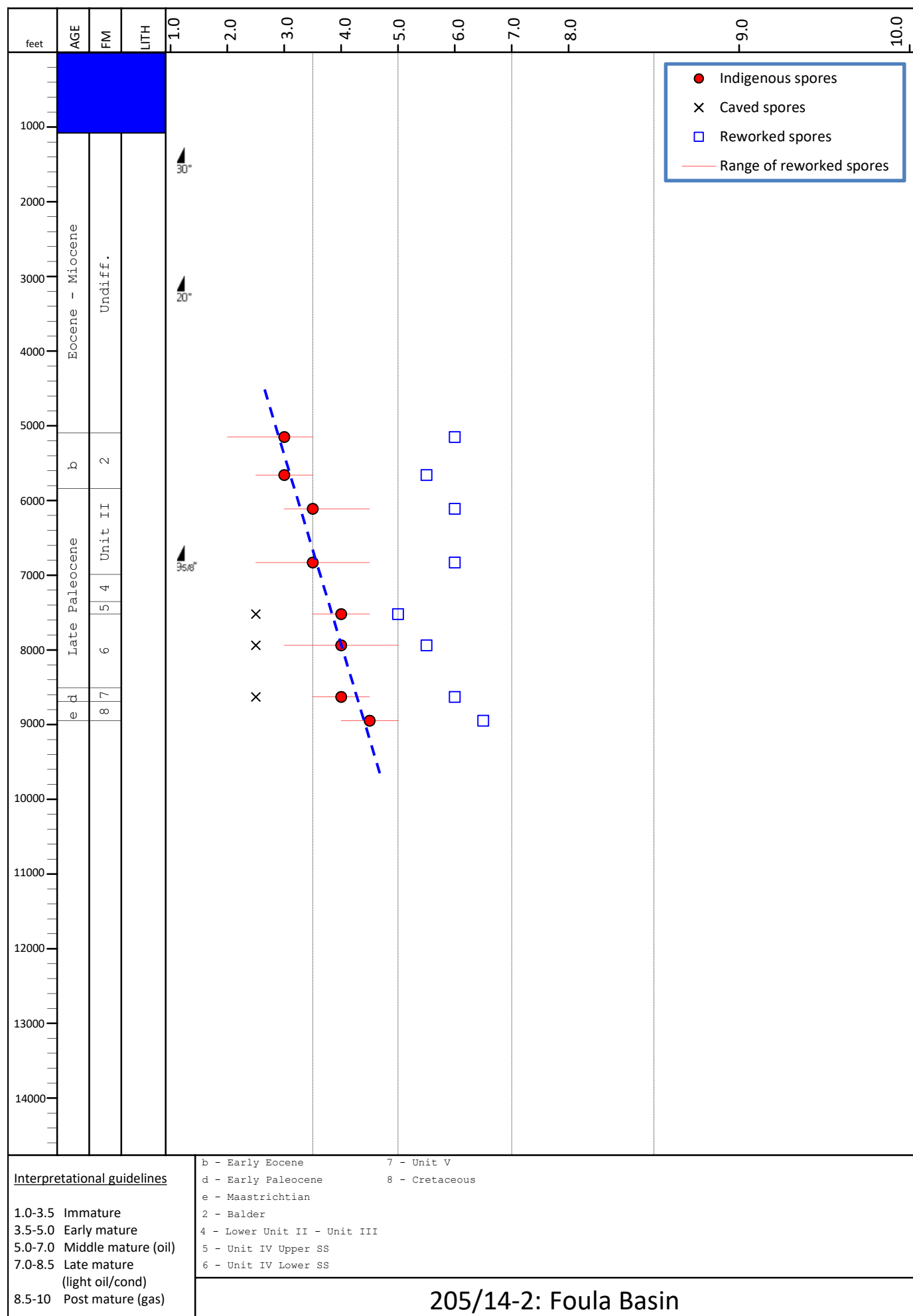


FIGURE 5.2.2.3 Spore Colour Index (SCI) against depth - 205/14-2

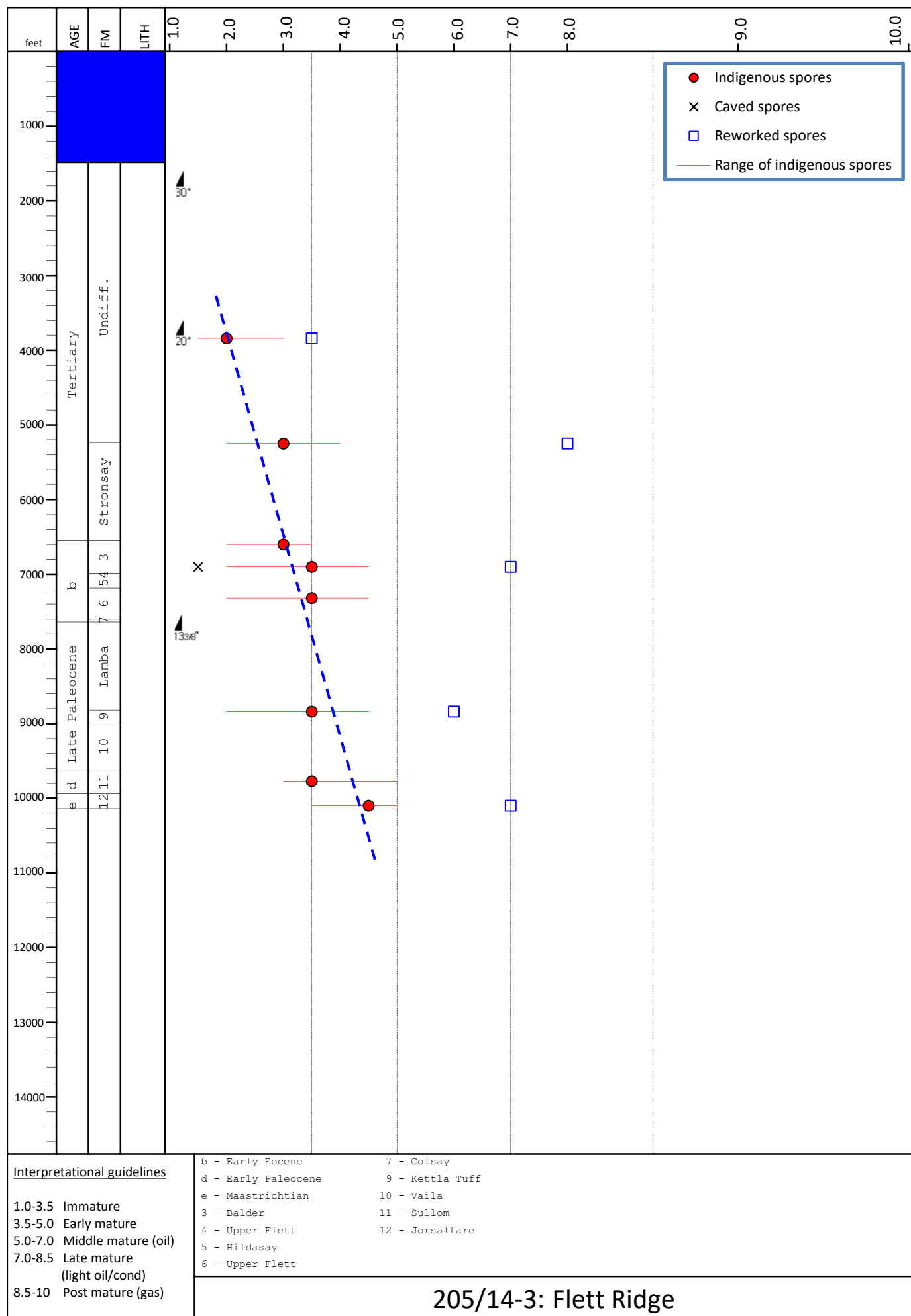


FIGURE 5.2.2.4 Spore Colour Index (SCI) against depth - 205/14-3

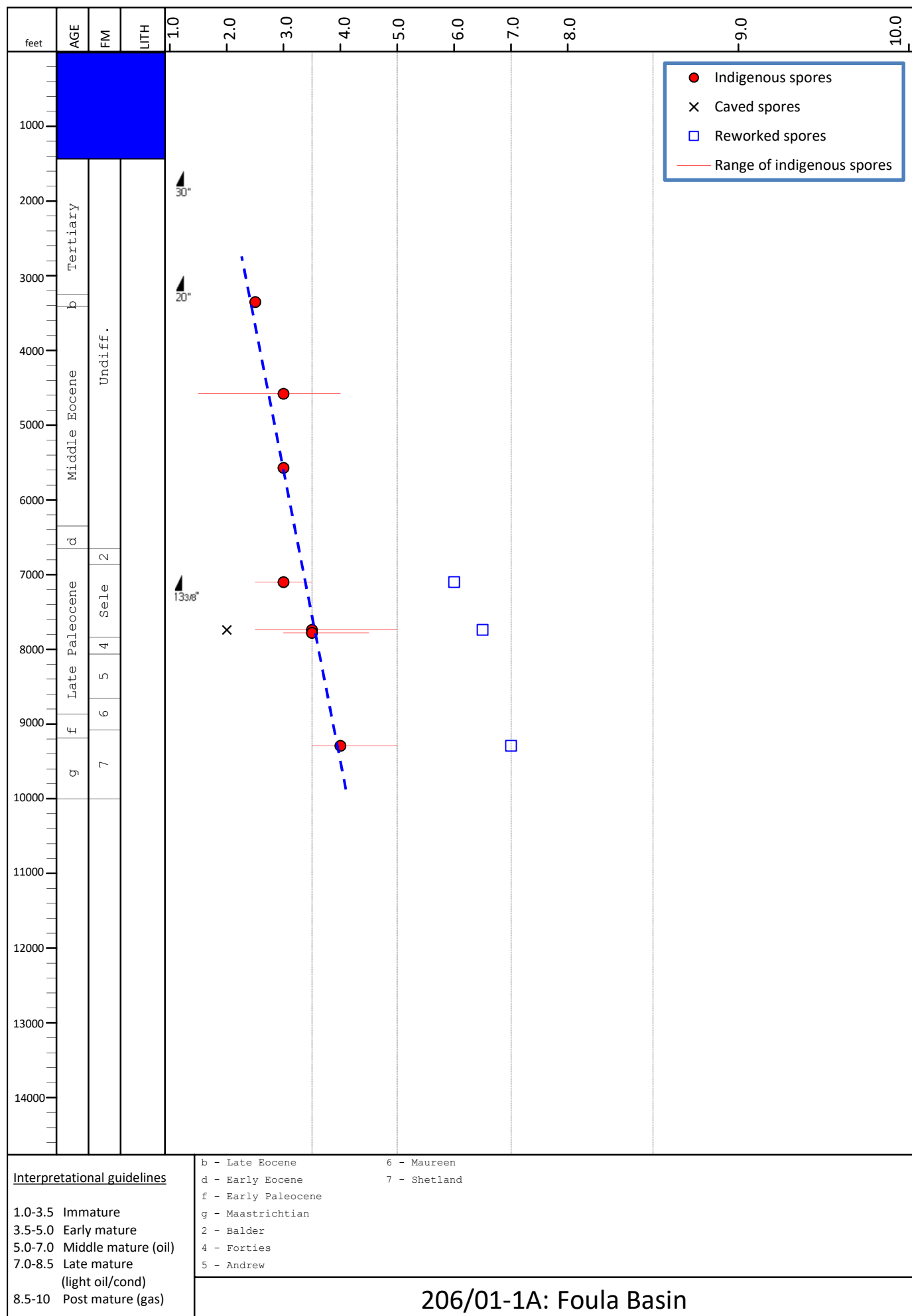


FIGURE 5.2.2.5 Spore Colour Index (SCI) against depth - 206/01-1A

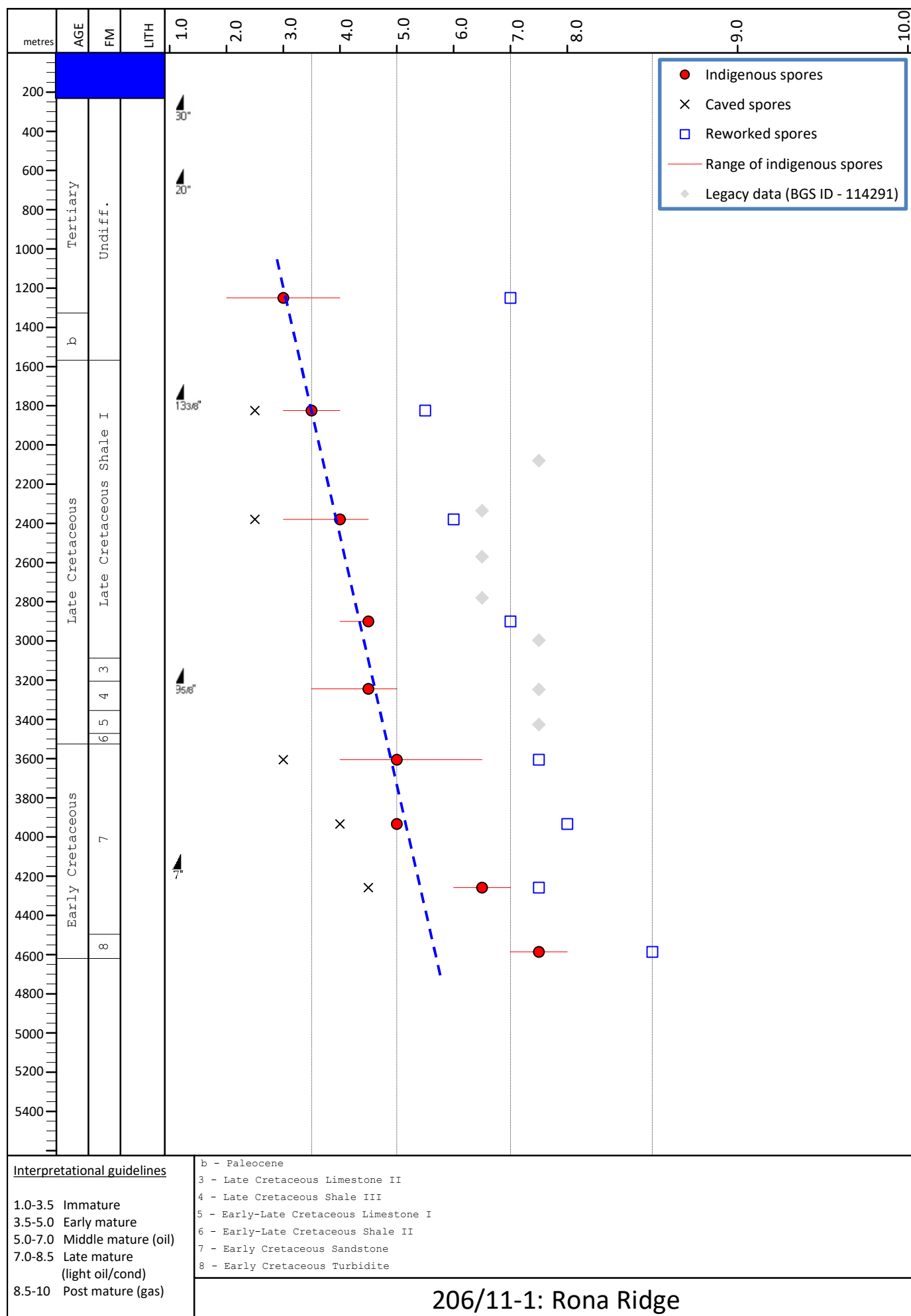


FIGURE 5.2.2.6 Spore colour index against depth - 206/11-1

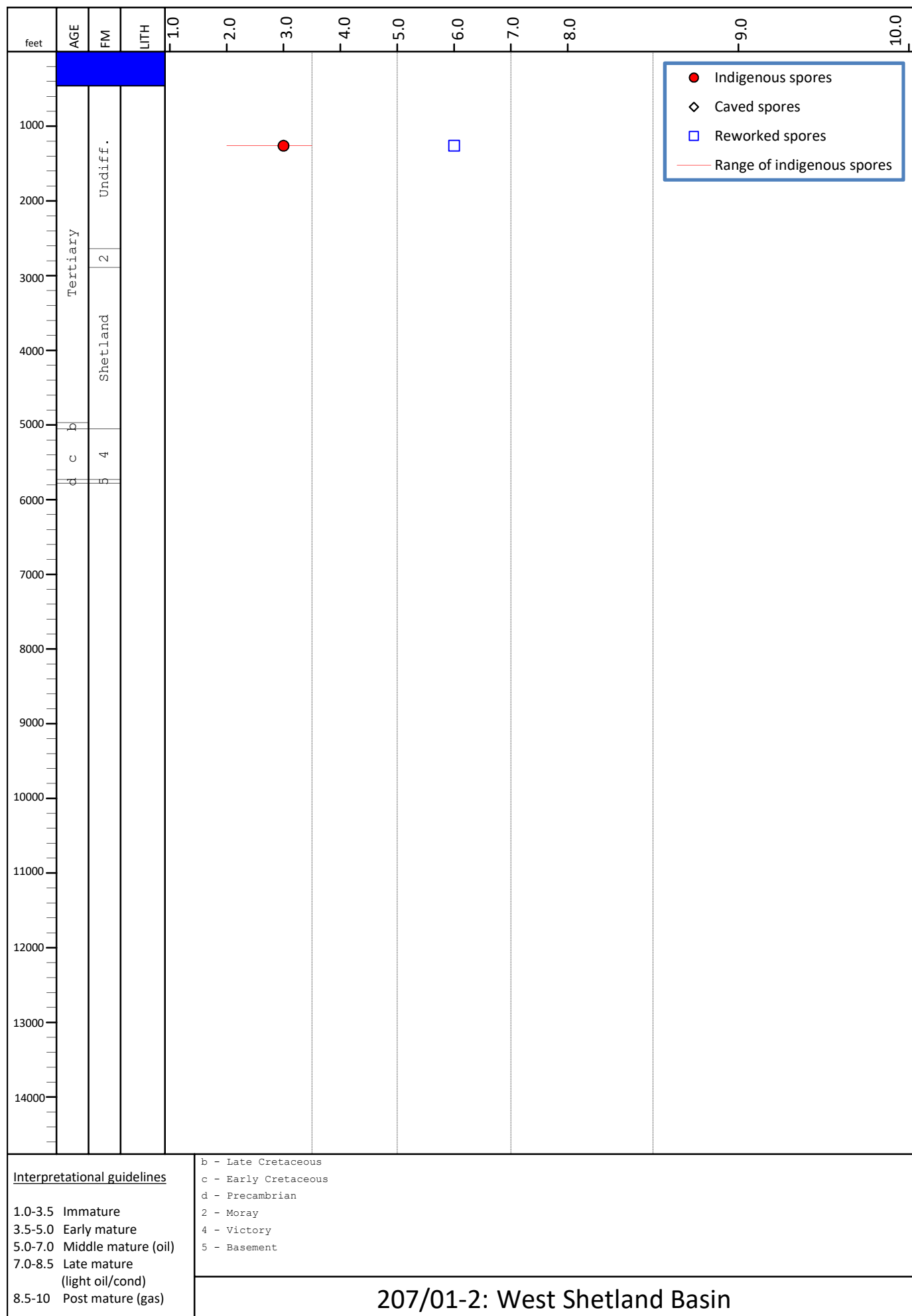


FIGURE 5.2.2.7 Spore Colour Index (SCI) against depth - 207/01-2

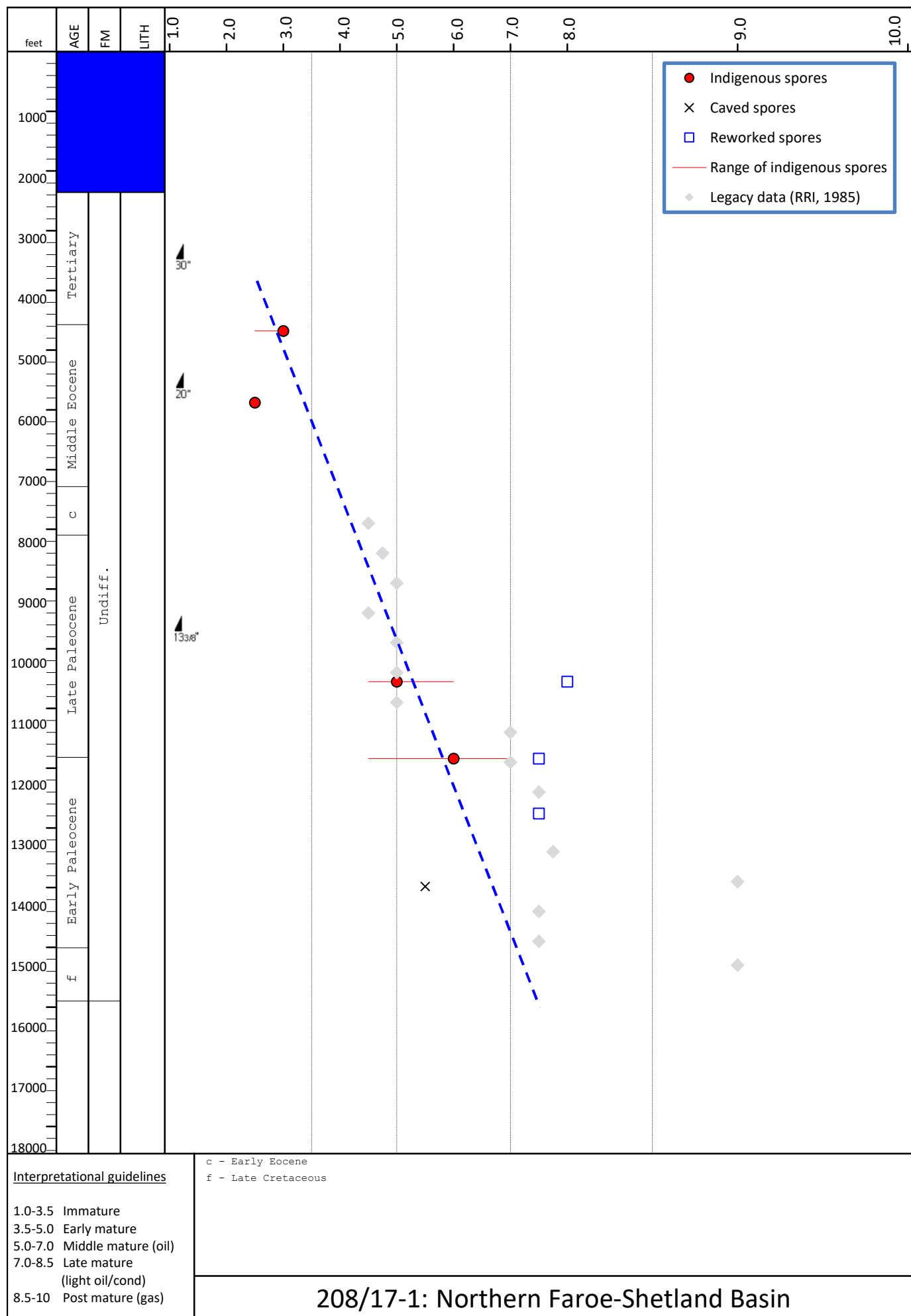


FIGURE 5.2.1.8 Spore Colour Index (SCI) against depth - 208/17-1

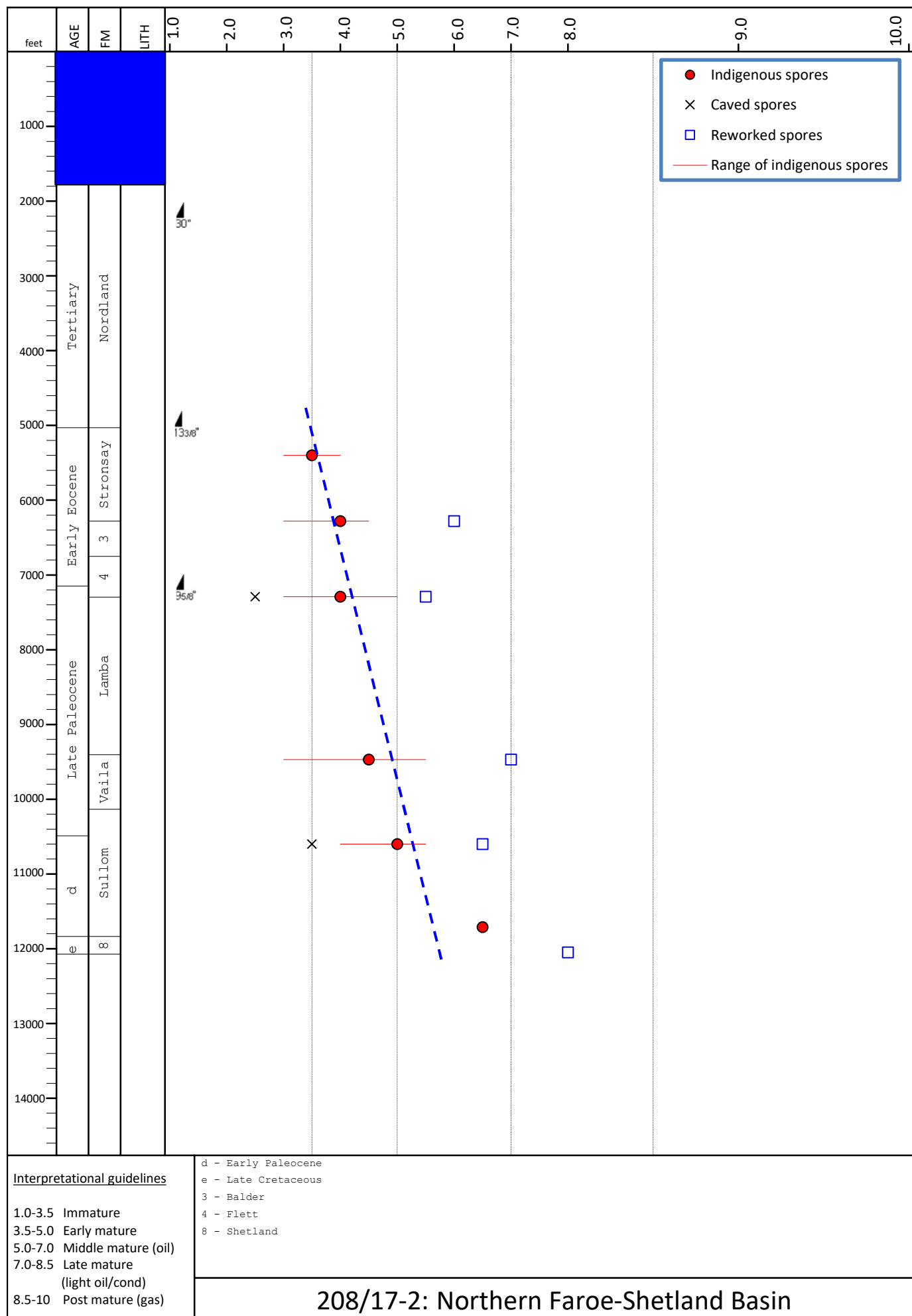


FIGURE 5.2.2.9 Spore Colour Index (SCI) against depth - 208/17-2

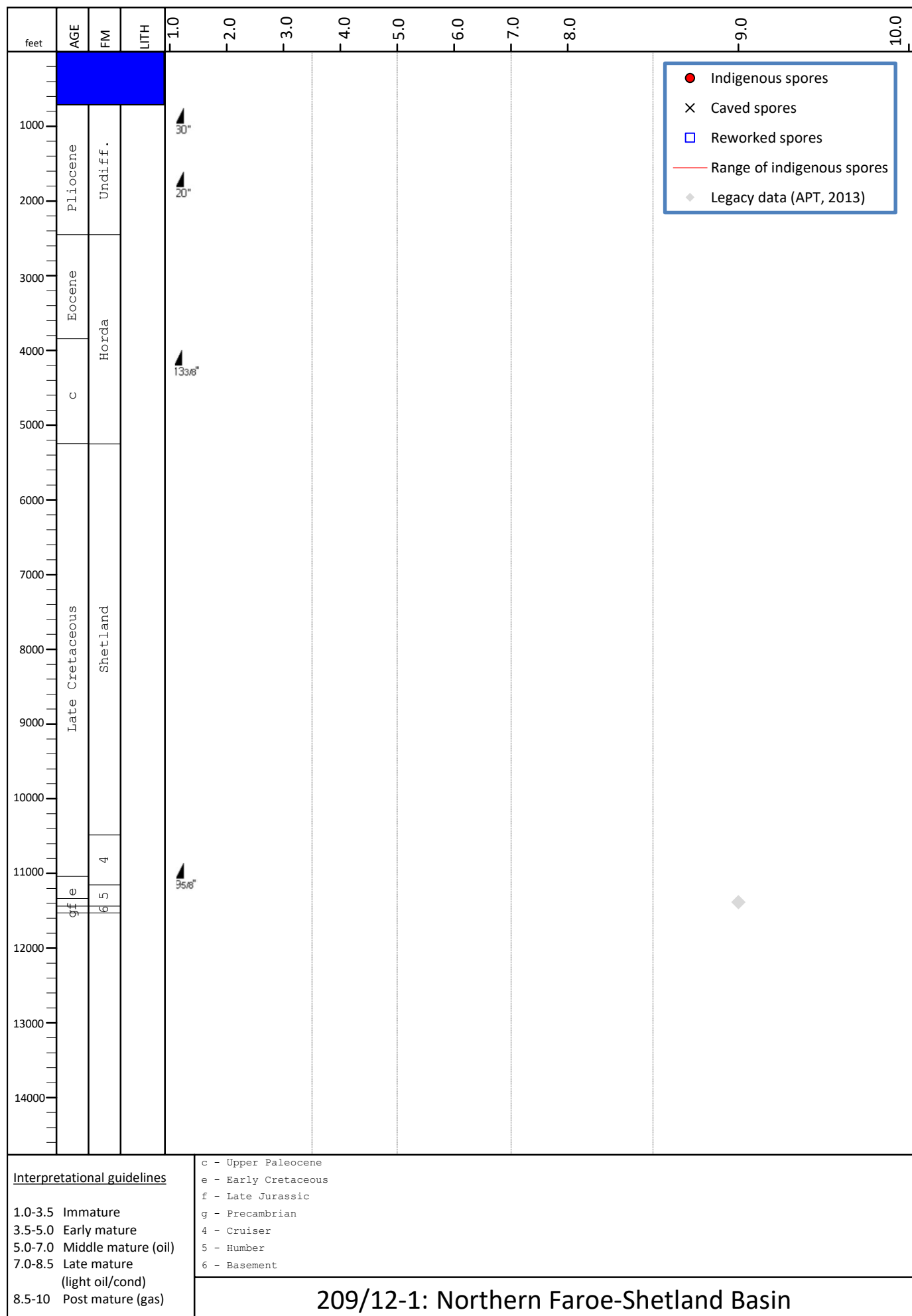


FIGURE 5.2.2.10 Spore Colour Index (SCI) against depth - 209/12-1

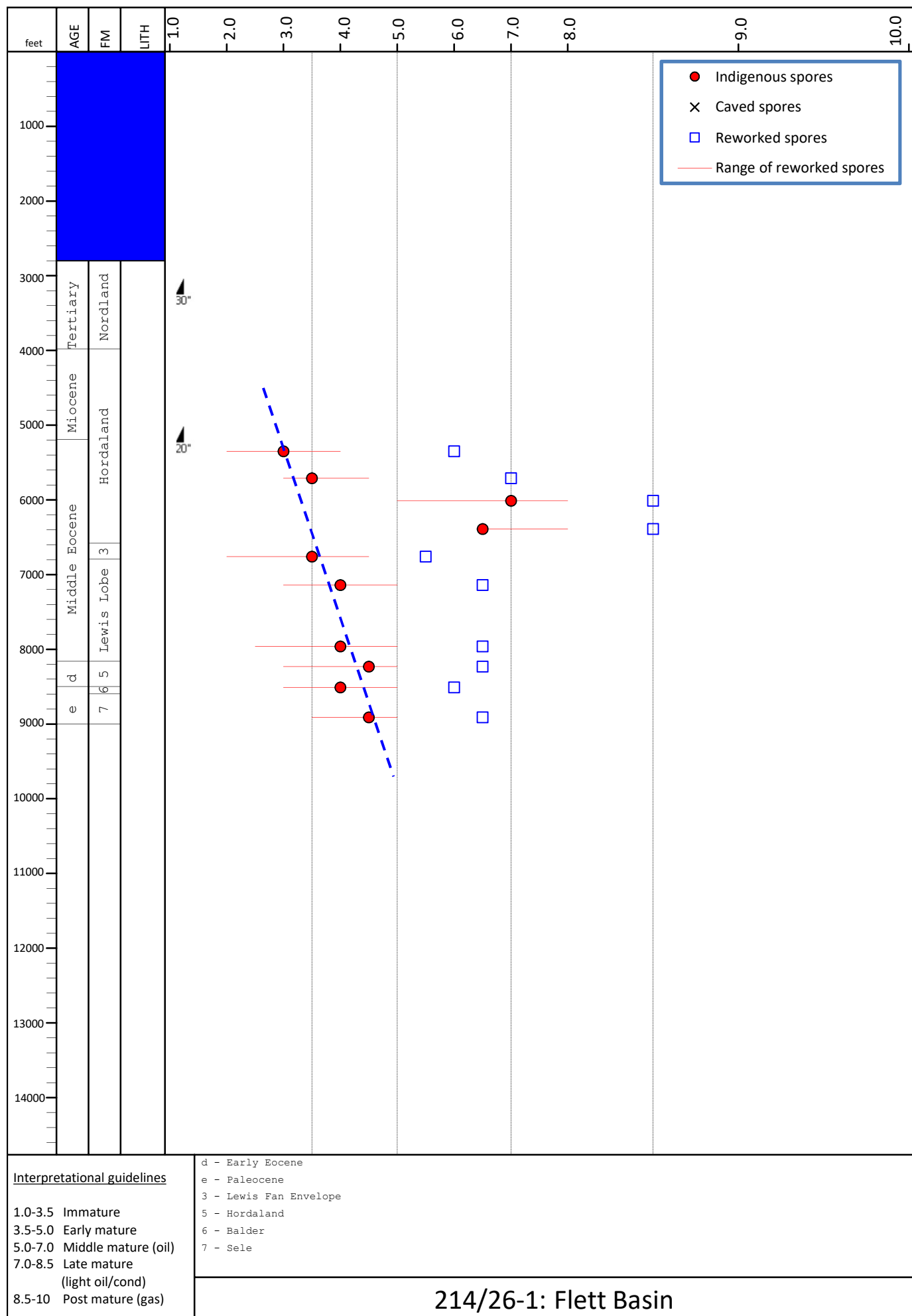


FIGURE 5.2.2.11 Spore Colour Index (SCI) against depth - 214/26-1

FIGURE 5.2.2.12 Spore Colour Index (SCI) against depth - 205/09-1

CHAPTER 6

INTEGRATION

Julian Moore, APT

6.1 SUMMARY

In this integration chapter the objectives are four-fold:

- 1) Review and summarise relevant previous studies in public domain, in particular the pertinent released non-proprietary GeoTrack reports and published fluid-inclusion based research (section 6.3)
- 2) Review the geology and geophysical aspects of the basin of importance to basin modelling (section 6.4)
- 3) Describe the construction and results of 1D basin modelling carried out in this study (calibrated to the data described in chapters 3, 4 & 5; Section 6.5).
- 4) Clarify our understanding of the petroleum system operating in Faroe-Shetland basin area (Section 6.6).

The data generated in this study is largely in agreement with that generated in the GeoTrack reports but infills gaps for the basinal areas where the principal kitchens are located. The thermal calibration data taken together indicate that much of the basin is at, or is close to, maximum burial at the present-day. Flanking settings have been affected by both Late Tertiary exhumation (focused in the South and Southwest), locally Late Tertiary advective heat flow (outboard of the Rona Ridge), and Early Tertiary contact metamorphism. There is little evidence of significantly higher heat flows in the geological past and models describing a dynamic Lithosphere-Asthenosphere Boundary (LAB) during the Icelandic plume event suggest the thermal effects are subtle. Intrusive volcanic effects are of a much greater magnitude but are thought to be much more localised.

The West of Shetland has a variable heat flow from the Basement, in particular it is cooler in the Southwest which, when parameterised correctly, means generation occurs relative to previous studies. The low heat flow area in the Southwest transitions to a higher heat flow character in the Northeast, thought to reflect the increasing occurrence of Caledonian granitic pluton material within the crust.

1D models have been constructed by integrating new robust calibration data together with a geological and geophysical understanding of the basin and source rock expulsion model. The new results seem to fit well with observations from the petroleum system, data measured from fluid inclusions and Re-Os isotope studies of the oil.

It is thought the charge timing issue has been over-emphasised in previous studies. By modelling appropriately and integrating observations from across the petroleum system charge timing can be understood in terms of: Delayed expulsion – due to a function of cooler models (especially in the SW) and appropriate expulsion model(s); Migration ‘lag’ and the preservation of oil legs under leaking gas caps. The concept of a Petroleum system analysis (PSA) critical moment is not a useful concept and should be discontinued (especially at the basin scale).

6.2 INTRODUCTION

The West of Shetland area is a geologically complex area which imparts a degree of complexity to the petroleum system. Aspects of the basin geology that are important to consider when modelling the petroleum system include the age and composition of the basement, the influence of Tertiary volcanism / intrusion (cf. Gardiner et al. 2019), late Tertiary uplift (cf. Tassone et al. 2014) and the influence of migration lag effects (cf. He, 2016). Additionally, some published assertions reflect a fundamental misunderstanding of source rocks and what they expel through the maturity window which has led to apparent complexity that can be accounted without the need for exotic models.

This section of the report is split into 4 sections. The first focuses on the integration of apatite thermochronology data, both published and the new data from this study and on published data derived from fluid-inclusion studies. The second section reviews what geological and geophysical considerations must be made in building a set of geologically and geophysically driven thermal models appropriate for the west of Shetland area. The next section discusses a small number of 1D basin models both in terms of appropriate parameterization and in terms of the relevance of the model predictions for the Petroleum system. The final section discusses the results obtained and the petroleum system of the Faroe Shetland basin more broadly. The supposed problem of charge timing is discussed, and some myths proposed about the nature of the system debunked.

6.3 GEOTRACK REPORTS – GC503, GC540 & GC605 & FLUID INCLUSION DATA

Three relevant legacy non-proprietary reports, written by GeoTrack, have been released by the OGA:

- GC503 West of Shetlands (South): Thermal and tectonic development and hydrocarbon generation history assessed using apatite fission track analysis and vitrinite reflectance. – March 1995
- GC540 West of Shetlands (North): Thermal and tectonic development and hydrocarbon generation history assessed using apatite fission track analysis and vitrinite reflectance. – February 1995
- GC605 North Shetland Region: Thermal and tectonic development and hydrocarbon generation history assessed using apatite fission track analysis and vitrinite reflectance. – October 1996.

All the data from these reports has been digitised, assigned latitudes and longitudes and is included as Excel files in this studies data package – see:

‘apt GeoTrack Report GC503-540-605_report_integrated_AFTA_data FINAL.xlsx’

‘apt GeoTrack_report_Well_lat-long.xlsx’

In addition to the large amount of apatite thermochronology data and analysis these reports contain, they also contain a significant amount of high-quality temperature and vitrinite data (performed by Keiraville Konsultants). In summary, the 357 temperature data points, largely comprising corrected bottom hole temperatures (bht) and the 411 vitrinite reflectance measurements have been digitised, assigned latitudes and longitudes and are made available as part of this report as Excel files – see:

‘apt GeoTrack Report GC503-540-605_report_%Ro_data FINAL.xlsx’

‘apt GeoTrack Report GC503-540-605_report_bht_data FINAL.xlsx’

The Geotrack reports are useful in that they provide a lot of data over a wide geographical area. Unfortunately, the Geotrack reports are unwieldy to use, invoke a lot of complexity, physical anomalies and contradictions which make them difficult to understand and practically use in petroleum systems studies.

A map of the GeoTrack geothermal gradients derived from their corrected bottom-hole temperatures is shown in Figure 6.3.1; the variation at first sight appears quite random with no obvious trends. It is thought that in part this reflects the quality of the data. In Figure 6.3.2 the estimated geothermal gradient from the GeoTrack data is plotted against depth; the samples with high geothermal gradients are often shallow and often located on structural highs. There are also some issues with GeoTrack data itself. In Figure 6.3.3a the GeoTrack corrected data are compared with the Carstens & Finstad (1981) corrected data, in our experience this correction works well in the West of Shetland (unsurprising as it calibrated for the Northern North Sea); it can be observed that at cooler temperatures the Carstens & Finstad corrections are generally hotter whereas at higher temperatures the GeoTrack corrected data are typically hotter. While the data generally appear to be reliable, some of the bottom-hole-corrected temperatures are in our view over-corrected. Figure 6.3.3b plots the time-since-circulation (TSC in hours) versus the measured temperature for the 204/9-1 well (the 202/3-2 data is plotted

for comparison). The uncorrected 204/9-1 temperature data vary between $\sim 58\text{--}70^\circ\text{C}$. The highest temperature was recorded at the maximum TSC (35 hours). However, GeoTrack have used the two temperatures measured after the shortest duration (5.7 & 8 hours) to estimate the corrected temperatures (66 & 83°C) despite the maximum recorded temperature after 35 hours only being 70°C ; by this time the formation fluid should have equilibrated, therefore the GeoTrack data here are viewed with some caution. This potential for overcorrection may account for some of the high gradients observed. Additionally, it is likely that at least a proportion of the higher gradients, particularly in the Southwest corner of the AOI, are thought to be related to advective flow and heating, rather than representing the regional temperature gradient.

There are also inconsistencies in how the apatite fission track data are described. For example in GC605 the summary provided for well 208/17-1 states that the AFTA and %Ro data indicate no uplift, no detectable Late Tertiary thermal events and a constant GTG of $\sim 35.3^\circ\text{C}\cdot\text{km}^{-1}$ (GC605, p.22); however in the GeoTrack report Figure 2.1 (GC605, p.15) the very same well is included on a plot which purportedly reports timing constraints for two cooling episodes Late Cretaceous to Early Tertiary ($70\text{--}55\text{Ma}$) and Late Tertiary ($20\text{--}0\text{Ma}$). This presents a challenge to extracting meaning from the full dataset.

Furthermore, we have reservations regarding the approach employed by GeoTrack which is thought to result in the over-interpretation of the generated data. Studies utilising fission track data for time-temperature histories have faced two principal challenges; the reproducibility of track length measurements and the variability of annealing kinetics. These amongst other methodological and geological challenges to the method used are summarised below:

Kinetics: Use of a single set of reference kinetics. The GeoTrack kinetic model is unpublished and therefore cannot be independently scrutinised; the references cited essentially invoke the behaviour of a single type of apatite, such as Durango apatite (e.g. Green *et al.*, 1986). However, Carlson *et al.* (1999) showed that annealing behaviour cannot be accounted for purely based on the Cl content of a single apatite as proposed (cf. Green *et al.* 1986). The results of this study suggest as many as five distinct apatite groups can be recognised in a sample. These groups are distinct in composition and hence their kinetics and should therefore be modelled individually rather than as a single type as apparently done by GeoTrack.

Track length orientation: GeoTrack report raw fission track length and not ‘c-axis’ projection lengths, which are now universally accepted. It is suspected that some variance seen in the GeoTrack track lengths is as a result of the orientation. Mean length parallel to c-axis is longer than mean length perpendicular and this relationship is elliptical, parallel to optical indicatrix. The GeoTrack mean fission track lengths are commonly shorter than our data, GeoTrack invokes cooling to explain it, but it may simply be because they have not measured length perpendicular to the c-axis. Another possibility is that GeoTrack “microns” do not equal Apatite.com “microns”. The best way to assess this is to obtain mean track length data for widely available standards such as Durango apatite or Fish Canyon Tuff apatite (natural fission tracks and induced fission tracks) and use this to calibrate the measurements as done in our data. The most serious problem with GeoTrack data is that it is produced by multiple analysts. This will unavoidably introduce variation, both in the skill of the analyst and in the subjective decisions that need to be taken while making the measurements. This can easily result in $0.5\mu\text{m}$ shift in mean track lengths among analysts, and worse among insufficiently skilled and tested analysts (R. Donelick, *Pers. comm.*).

Use of default thermal histories: by defining a thermal history *a priori* they almost certainly introduce unconscious bias.

Use of linear geothermal gradients: there is a heavy reliance upon linear geothermal gradients, and significant complexity invoking multiple, highly varying gradients are frequently referred to in the reconstruction of the palaeo-geothermal gradients. It is difficult to judge how realistic this is. Experience suggests that the available regional temperature datasets rarely, if ever, demonstrate the degree of variation (and hence the complexity) invoked in the GeoTrack reports (although this may reflect the generally infrequent temperature datapoints available in most well datasets). In their analysis, GeoTrack, impose high frequency changes in the gradient (which can occur locally) to the entire geotherm which is unrealistic. Our view is that to determine the thermal history of a basin through time, the gross geotherm needs to be considered, accepting that local departures (limited in z) will occur but have a minor if any impact on the maturation of source rocks at depth (the principal objective of most thermal studies).

Burial histories: As noted previously, the proposed burial histories can appear un-geological – rapid burial immediately followed by rapid uplift (e.g. GC640, Figure 3.2; p.26) without any apparent regard to the forces driving basin formation (and exhumation).

6.3.1 GeoTrack report synopsis and integration: What can we take from the GeoTrack reports?

Notwithstanding the comments and concerns held regarding the GeoTrack reports, the data is generally of good quality and insights are there, if reported in a rather dense and at times obfuscated manner. A summary of the results, conclusions, commonalities and comparison with the data generated in this study, where possible, is given in the following text.

6.3.1.1 GC503 West of Shetlands (South)

The GC503 West of Shetlands (South) GeoTrack report included data from 18 hydrocarbon exploration wells, 13 shallow boreholes and 14 outcrop locations from the northern Scottish coast and the Orkneys:

GC503			
Q202	Q204	Q205	Borehole
202/2-1	204/19-1	205/21a-1	BH77/09
202/3-1	204/28-1	205/22-1A~	BH/82/02
202/3-2	204/29-1	205/23-1+	BH78/07
202/3a-3	204/30-1	205/26-1	BH77/08
202/8-1		205/26a-2	BH72/34
202/9-1+		205/27-1	BH73/31
202/19-1		205/30-1~	BH73/29
			BH72/25

+ = hot fluids? i.e. evidence of higher temperatures but no igneous intrusions present

~ = local effects?

^ = igneous intrusives present

This report describes the southern region, incorporating the southern portion of Quadrants 204 and 205, the northern portion of Quad 202 and the adjacent continental shelf extending to the Scottish Coast. There was no overlap between the current APT-Chemostrat study and the wells in the GC503 report. The GeoTrack analysis broadly indicates four episodes of heating and cooling:

- 270 to 250 Ma (late Paleozoic),
- 160 to 130 Ma (late Jurassic to early Cretaceous), and
- 75 to 60 Ma (late Cretaceous to early Tertiary)
- 20 to 0Ma (late Tertiary) – possible, only seen in the exploration wells.

The report summary refers to low geothermal gradients ($\sim 25^{\circ}\text{C}/\text{km}^{-1}$) which would be consistent with the basement composition and heat flow mapping for this area carried out in this report (cf. Chapter 3). However, in the detail, the report accounts for the ‘low’ geothermal gradients extracted from the data as reflecting input of heat shallow in the section. This is counter to the fact that in shallow settings geothermal gradients are consistently higher. For example Stranne & O’Regan, (2015) showed shallow gradients in one study are higher by on average $19^{\circ}\text{C km}^{-1}$ (consistent with higher porosity and generally lower thermal conductivity in near-seafloor sediments). Thus, the inference made in the report is difficult to reconcile with known physical behaviour and makes it much more difficult to confidently extract meaning from the data and conclusions presented.

In the report only two wells, 202/19-1 and 205/30-1, are suggested to have data that suggest that the additional heating detected in the data is due to additional depth of burial.

In terms of the petroleum system, the report supposes that in many of the wells analysed from Quads 202 and 205, the Upper Jurassic source rocks reached maximum maturity during the purported ‘*late Jurassic to early Cretaceous heating episode*’. The maximum maturity attained lies in the range ~ 0.5 to 0.6% suggesting the Jurassic source rock is early mature at best and is unlikely to have expelled material volumes of oil, although if more carbonate-prone (Type IIS, Class A) facies occur (with lower activation energies) this may be more favourable (cf. Herries et al. 1999), particularly where Tertiary burial is sufficient to push the Upper Jurassic into the oil window. In that regard, the report concludes that in Quadrant 204, the northern portion of Quad 202 and Quad 205 north of the Rona Ridge, the situation is more favourable for generation of hydrocarbons from Upper Jurassic source rocks - this could be concluded by simply inspecting an appropriate seismic section.

One positive that is noted in the reports is that the low reported paleo-geothermal gradients, and assigned to the GeoTrack heating episodes, allowed preservation of generation potential, which may have been realised in areas where later burial was sufficient to produce higher maturation levels. Our study agrees with this view but relates it to the fundamental geology of the crust in this area.

6.3.1.2 GC540 West of Shetlands (North)

The GC540 West of Shetlands (North) GeoTrack report included data from 15 hydrocarbon exploration wells:

GC540			
Q205	Q206	Q208	Q214
205/10-2b^	206/3-1	208/26-1 ^	214/27-1^
205/20-1	206/5-1		214/28-1#^
	206/7-1		214/29-1^
	206/8-2		
	206/8-5		
	206/9-1		
	206/9-2		
	206/10-1		
	206/11-1#		

+ = hot fluids? i.e. evidence of higher temperatures but no igneous intrusions present

~ = local effects?

^ = igneous intrusives present

= APT-Chemostrat study well

This report describes the northern region, dealing mainly with the northern half of Quadrant 206 and adjacent portions of Quads 205, 208 and 214 and is a companion to the Geotrack Report #503 described above.

The Geotrack analysis broadly indicates four episodes of heating and cooling:

- 265 to 245 Ma (late Paleozoic),
- 160 to 130 Ma (*late Jurassic to early Cretaceous*) – reported in GC503 but not seen in the GC540 Wells
- 75 to 60 Ma (late Cretaceous to early Tertiary)
- 20 to 0Ma (late Tertiary)

The description in the GeoTrack report is quite complex, however, the report conclusions can be simplified to the following: The majority of the wells outboard, including 205/10-2, 206/11-1, 206/3-1, 206/5-1, 208/26-1, 214/27-1, 214/28-1, and 214/29-1 are at maximum burial (temperature) present-day with wells with igneous intrusions showing local effects at depth. In contrast, wells located on the Rona Ridge, including 206/8-5, 206/8-2, 206/9-2 and 206/10-1, have experienced higher temperatures in the past as a result of exhumation and/or heating associated with fluid flow (advective) effects. These wells cluster around the Clair field where independent methods, principally based on data derived from fluid inclusions, have verified these results, examples include Baron *et al.* (2008) and Mark *et al.* (2008) the results of which are summarised in Section 6.3.2 below.

Two wells have been analysed both in the Geotrack GC540 study and the current APT-Chemostrat study: 206/11-1 and 214/28-1.

For well 206/11-1 both the GeoTrack dataset and the dataset reported in this study have been interpreted to indicate that the section is at or close to maximum burial present-day (cf. Section 4.3.3.1 of this report, p. 4-22 – 4-23); the closest samples from each study where offset by ~50m. The analytical results from each study where different – as summarised below:

Sample	Depth	Lab	AFT Age Ma	±Ma	Mean Length μm	± μm
P10012_007	4373M	Apatite.Inc	5.51	0.0	5.51	0.00
GC254-39	4325M	GeoTrack	18.40	8.5	10.63	0.96

Despite the analytical data differences the interpretations were essentially equivalent.

For well 214/28-1 the samples overlapped closely in depth and the recovered analytical data was very similar:

Sample	Depth	Lab	AFT Age Ma	±Ma	Mean Length μm	± μm
P10012_010	2552m	Apatite.Inc	165.00	21.0	11.08	1.52
GC540-157	2557m	GeoTrack	163.00	16.5	11.08	0.14

The GeoTrack data was equivocally interpreted with the sample providing no direct evidence of being hotter in the past; the measured fission track length was shorter than the estimated GeoTrack default thermal history (12.2 μm) which could either be indicative of some heating, or it could simply be due to GeoTracks use of raw fission track length rather than 'c-axis' projection lengths (cf. p. 6-5). The interpretation of our Apatite.Inc data was more complex; the modelled time-temperature path results are cooler than the estimated present-day temperature of ~77°C, and the result from the Late Palaeocene sample (P10012_010) was in contrast to the results obtained from two deeper samples from this well (cf. p. 4-40 – p4-43).

The overall interpretations from both this and the GeoTrack study were consistent, i.e. the 214/28-1 well is at maximum burial present-day but exhibits some evidence of higher temperatures in the past, likely reflecting both contact heating associated with the intrusions deeper in the well (early Tertiary) and potentially advective heating (Late Tertiary?).

6.3.1.3. GC605 North of Shetlands

The GC605 North of Shetlands GeoTrack report included data from 17 hydrocarbon exploration wells:

GC605				
Q208	Q209	Q210	Q214	Q219
208/15-1a^	209/3-1a^	210/4-1	214/27-1 ^	219/20-1^
208/17-1^	209/4-1a^	210/5-1	214/28-1#^	219/27-1
208/17-2#	209/6-1^		214/29-1^	219/28-1
208/19-1^	209/12-1^			219/28-2^
208/26-1				

+ = hot fluids? i.e. evidence of higher temperatures but no igneous intrusions present

~ = local effects?

^ = igneous intrusives present

This report describes the lightly explored area north of the Shetland Islands, encompassing wells from Quads 208, 209, 210, 214 and 219. There was no overlap between the current APT-Chemostrat study and the wells in the GC605 report. The Geotrack analysis broadly indicates two episodes of heating and cooling:

- “Early Tertiary” episode (~55Ma) mainly due to effects of Early Tertiary intrusives but more extensive hydrothermal activity is possible in several wells.
- “Late Tertiary” episode (20 to 0Ma) characterised in most wells by non-linear paleotemperature profiles and apparently due chiefly to movement of hot fluids. According to GeoTrack, no cooling effects can be attributed to uplift and erosion following deeper burial.

The report commented that the resolution of the two previous studies (GC503 & GC540) was insufficient to resolve both the Tertiary results. The paleotemperature profiles recovered were described as falling into five categories, with type 1 & 2 most prevalent:

- Type 1 – most of the section at maximum burial present-day, but samples from within the Early Tertiary show evidence of paleotemperatures attributed to the effects of contact heating.
- Type 2 (cyan) – in addition to Early Tertiary section contact heating effects, the section immediately above the intruded zone also shows heating effects attributed to late Tertiary effects.

6.3.1.4. GeoTrack & APT-Chemostrat data summary

A number of summary maps have been created that present the GeoTrack data by sample age with a legend that demarks each data into three categories:

- 1 no evidence of higher paleo-temperatures (i.e. at maximum temperature (burial) today)
- 2 evidence from AFTA age data for higher paleo-temperatures
- 3 evidence from AFTA fission track length data for higher paleo-temperatures

Figure 6.3.4 maps the GeoTrack Cretaceous samples. The majority of samples show no evidence of higher paleotemperatures; a subset of samples from along the Rona Ridge show evidence from the apatite fission track length data for higher temperatures in the past – this could as a result of either exhumation or advective heat flow focused onto the ridge. In Figure 6.3.5 the Jurassic & Triassic samples included in the Geotrack studies are mapped. While there are relatively fewer samples, the signal is similar to that taken from the Cretaceous samples in this study. For samples on, or close to, the Rona Ridge, evidence for elevated paleo-temperatures occurs either in the apatite age data or in the fission track length data (but only one sample has evidence in both – the Triassic aged sample from 205/27-1).

The Basement samples analysed by GeoTrack are mapped in Figure 6.3.6. Nearly all the GeoTrack basement samples, which have a wide-ranging distribution from onshore northern Scotland to the Basement sample in well 219/28-1, show evidence of higher paleotemperatures in both the Apatite age data and the fission track length data.

Figure 6.3.7. compares the uplift estimates from the combined AFTA & % Ro approach of GeoTrack with the shale-velocity based approach of Tassone *et al.* (2014). The absolute correspondence is relatively poor, although it does improve in the more basinal wells outboard of the Rona Ridge where uplift estimated tend to be modest (<500m). Along the ridge and in the Southwest corner of the study AOI (northern Quad 202) uplift estimates are generally higher in the GeoTrack reports, but not universally so. The lack of correspondence between the

methods is to be expected given the multiple assumptions required in each of the approaches. What we can say is (from thinking structurally and assessing the geometry of the basin) the Rona Ridge and other structural lineaments (Corona, Flett, Westray etc) are focus of structuration and the associated exhumation whereas the basinal areas have had much less influence of exhumation, which broadly increases southwards.

The apatite thermochronology data from the GeoTrack reports is directly compared with data from this study in Figure 6.3.8. A ‘boomerang’ plot, which plots the pooled apatite age (Ma) versus the mean track length, for both this studies and the compiled GeoTrack data is shown in Figure 6.3.8a. Samples that are >150Ma and have track lengths greater than ~11 μm would be interpreted as principally having a provenance signature. Samples with younger ages and shorter track lengths reflect the progressive heating as burial proceeds in the basin. Samples with track lengths >10 μm and younger ages would be interpreted as having been rapidly uplifted out of the partial annealing zone (PAZ) to temperatures <60°C freezing the fission track distributions (these samples are only found in the GeoTrack data). Figure 6.3.8b plots the present-day sample temperature versus the measured mean fission track length (μm); the Apatite.Inc data generated in this study have a strongly linear correspondence giving confidence to the kinetic model(s) employed. The GeoTrack data show a much greater degree of scatter, this likely reflects both the larger dataset and issues arising from the GeoTrack methods (cf. p. 6-5 – 6-6). In Figure 6.3.8c the measured present-day temperatures of the study samples are plotted against the modelled peak temperatures inverted from the apatite age and track length data (not available for the GeoTrack data), which clearly illustrates that the majority of samples fall on or close to the one-to-one line indicated the samples present-day are at or close to their maximum temperatures (cf. Section 4.4, p. 4-44 – 4-45 for a discussion).

In Figure 6.3.9 a ‘boomerang’ plot (as described above) for all data is mapped and those samples falling into the area on the plot representative of uplifted samples are highlighted. Additionally, the independently derived exhumation estimates of Tassone *et al.* (2014) are also plotted. Overall, the correspondence is relatively weak, although the “uplift” samples do fall onto a general NE-SW trend aligned with the Rona Ridge. The lack of correspondence is thought to, impart, reflect the modest uplift amount, relative to the resolution of the techniques employed here - most of the uplift is likely <1km. The ‘boomerang’ plot is of more use in assessing areas of compressional tectonics and active mountain building where the magnitudes of exhumation are greater than those observed here.

Both this and GeoTrack studies have identified modest evidence of thermal anomalies in the Late Tertiary – however, the origin of these anomalies is uncertain. Possible models include the advection of deep, ‘hot’ fluids driven by Late Tertiary compression (cf. Ritchie *et al.* 2008) or alternatively, fluids heated by Early Tertiary intrusions being somehow lagged in geological time to be recorded as Late Tertiary effects (requiring a ‘lag’ of 30-40Ma). The latter highly complex lag model seems to be favoured by GeoTrack, however, the degree of lag required seems unlikely. For example, Sydnes *et al.* (2019) modelled the transient impact of intrusions and estimated the effects could last several million years, a factor of 10 to 20 less than that observed. Aside from apatite thermochronology data, there are numerous studies of various fluid-inclusion methods that record thermal events in the basin which appear to actually have a relatively wide-ranging distribution through geological time. These studies are briefly reviewed in the following section.

6.3.2 Evidence of ‘hot fluids’ from literature

Seven key papers have published microthermometric, petrographic and isotopic data that provide alternative constraints for the thermal history of the basin. The distribution of the data is shown in Figure 6.3.10 and the key information from these papers is summarised below:

Parnell *et al.* (1999). Hydrocarbon migration history, West of Shetland: integrated fluid inclusion and fission track studies

Wells/Age: 204/24-1a / Tertiary

Wells/Age: 204/27-1; 204/28-1; 205/22-1; 205/26-1 / Jurassic

Result: “The integrated AFTA, VR and fluid inclusion data presented in this study show clear and consistent evidence for multiple episodes of fluid flow in the West of Shetland region throughout the Mesozoic and Tertiary. We interpret these results to reflect repeated expulsion of fluids emanating from basinal areas onto adjacent flanking highs, where their thermal effects have been preserved because of the relative stability of these regions through Mesozoic and Tertiary times”

West Shetland & East Solan Basins (inboard of Rona Ridge) were mature in the Mesozoic (provides additional source of early charge) – e.g. 205/30-1

Temperature: 105 – 135°C (Calcite veins); Quartz grain trails 160-225°C

Dating: Late Mesozoic (rifting?) to Late Tertiary (Miocene uplift)

Wycherley *et al.* (2003). Indicators of hot fluid migration in sedimentary basins: evidence from the UK Atlantic Margin

Wells: 164/25-1; 204/22-1; 204/28-1; 205/22-1a; 206/5-1; 206/5-2; 208/26-1; 208/27-1; 214/29-1

Results: “New data presented here show that temperatures are hotter by c. 40°C in Tertiary samples than in the underlying Jurassic and Cretaceous sediments in wells 204/28-1, 206/5-2, 208/27-1, especially in cements from samples as young as mid–upper Eocene in age.”

Temperature: 80-100°C

Dating: Paleocene to Upper Eocene

Parnell *et al.* (2005). Thermal history and oil charge on the UK Atlantic margin

Wells: 204/19-1 / Eocene – Devonian

Result: “Fluid inclusion data indicate that Paleocene–Eocene sandstones have experienced temperatures much higher than can be explained by burial alone. Temperatures up to 200°C indicate the passage of hot fluid through Cenozoic sandstones, which by-passed the pre-Cenozoic section in this and other wells. The hot fluid event must have been of very brief duration (up to 100 years) to show no record in the fission track and reflectance data, implying that the fluids migrated through fracture systems.”

Temperature: up to 200°C

Dating: Paleocene - very brief ~100 years.

Mark *et al.* (2005). Dating of Multistage Fluid Flow in Sandstones

Wells/Age: 207/01a-5 / Lower Cretaceous – Victory Formation

Results: “Characterization of fluid inclusions within K-feldspar cement in sandstones permits the integration of homogenization temperature data with high-resolution Ar-Ar ages (assuming the basin thermal history does not disturb the Ar isotope system). By 63 Ma, the Victory reservoir had cooled to ~50°C, and K-feldspar authigenesis ceased ~54 Ma. [Basin modelling of Pseudo-well in a basinal location indicates oil migration from 115Ma (~Aptian)]

Temperature: up to 125°C

Dating: 83Ma ~Santonian

Baron *et al.* (2008). Evolution of hydrocarbon migration style in a fractured reservoir deduced from fluid inclusion data, Clair Field, west of Shetland, UK

Wells/Age: 206/8-1a; 206/8-7; 206/8-8 / Devonian-Carboniferous

Results: “New data presented here show that temperatures are hotter by c. 40°C in Tertiary samples than in the underlying Jurassic and Cretaceous sediments in wells 204/28-1, 206/5-2, 208/27-1, especially in cements from samples as young as mid–upper Eocene in age.”

Temperature: up to 180°C

Dating: mid-Cretaceous to Paleocene?

Mark *et al.* (2008). Late Palaeozoic hydrocarbon migration through the Clair field, West of Shetland, UK Atlantic margin

Wells/Age: 206/8-1a; 206/8-7; 206/8-8 / Devonian-Carboniferous

Results: Dates early phase of fluid flow and oil charge to the Clair field – the aqueous and oil-bearing inclusions are dated prior to deposition of both the principal KCF source rock and the Cretaceous top-seal providing evidence of prior Palaeozoic petroleum system.

Temperature: 90 - 110°C

Dating: 264 - 247Ma ~Late Permian – Early Triassic

Mark *et al.* (2010). $^{40}\text{Ar}/^{39}\text{Ar}$ dating of oil generation and migration at complex continental margins

Wells/Age: 204/28-1 / Late Jurassic – Rona Sandstone Member

Results: Oil-bearing fluid inclusions hosted in potassium (K) feldspars are dated to the Aptian ~ 113.2±3.5Ma. The oil is assumed to be Jurassic in origin, however the paucity of data on alternative source rocks (Middle Jurassic lacustrine; Devonian lacustrine) suggests the confidence in oil-source correlation remains uncertain.

Temperature: 158 - 170°C

Dating: 113.2±3.5Ma ~Aptian – Albian

6.3.2.1 ‘Hot fluid’ Literature Summary & Implications

Together this research indicates that there is abundant evidence in the microthermometric, petrographic and isotopic data of hot fluids interacting with Paleozoic, Mesozoic and Tertiary aged reservoirs in the West of Shetland.

Mark *et al.* 2010 advocate an early migration event based on fluid inclusion analysis of potassium feldspars collected from a Jurassic Rona Sandstone sample in well 204/28-1. This data includes $^{40}\text{Ar}/^{39}\text{Ar}$ dating and homogenisation temperatures of authigenic K-feldspars and oil-bearing fluid inclusions contained within these crystals. The $^{40}\text{Ar}/^{39}\text{Ar}$ dates range 113.2±3.5Ma (2σ) and the homogenisation temperatures range from 158-170°C.

The confidence in the assignment of the source rock age from the oil-inclusion data is modest at best; middle Jurassic and Devonian lacustrine source rocks could be present and a Paleozoic petroleum system has been claimed to have been proved by Mark *et al.* (2008).

The authors claim that their data can be used to ‘constrain the timing of maturation for the Faroe-Shetland basin source rocks’. From such a small amount of data this is a rather bold claim. Clearly the basin is dynamic through time and different areas will achieve maturity at different times. Furthermore, through exclusively using the K-feldspar $^{40}\text{Ar}/^{39}\text{Ar}$ system they

are only viewing one component of the diagenetic sequence. K-feldspars have been shown to occur early in the diagenetic sequence (cf. Parnell *et al.* 1999; Baron *et al.* 2008) and hence they are only constraining that part of the system, not its entirety (Figure 6.3.11). It is thought most likely that the oil-inclusions originated inboard from the Solan and West Shetland basins which are more dominated by Mesozoic burial (and hence maturation) relative to the Faroe-Shetland basin, which is dominated by Tertiary burial. Thus, the claims made by Mark *et al.* (2010) are somewhat misleading.

In terms of the stratigraphy impacted by the occurrence of hot fluids – Parnell *et al.* 2005 and Wycherley *et al.* 2003 report that the influence of the hot fluids are restricted to Paleocene sediments – the wells studied by these authors are typically outboard of the Rona Ridge (204/19-1, 204/22-1, 206/5-2, 214/29-1). The studies that report the influence of hot fluids in older stratigraphy appear restricted to the Rona Ridge or the basins inboard of the ridge (West Shetland and East Solan Basins). This may well reflect a sampling bias (since outboard the Mesozoic is typically much deeper and therefore less represented); however, Parnell *et al.*'s (2005) dataset extended to the Jurassic and Devonian and all samples purportedly had evidence of paleotemperatures higher than those measured present-day.

The basin has a long and relatively complex history which varies through time from location to location, thus some hot fluids may relate to Mesozoic rifting inboard, others may relate to Early Tertiary igneous intrusions and others to Late Tertiary events. Occam's Razor means it is expected that the probability of occurrence will increase with proximity to the origin of the fluids, hence those of Mesozoic origin would be expected to be found in the Mesozoic rifts and the areas proximal to them, while those associated with the Early Tertiary intrusive activity would be found close to these intrusions and around the Tertiary volcanic centres. Since hot fluids migrate some will undoubtedly be found distal to their origin but at reduced probability.

The influence of these hot fluids upon the petroleum system is harder to ascertain with confidence. Based on current data there seems to be minimal influence upon the maturation of source rocks at the basin scale. The influences may be more important for reservoir quality issues, however that is beyond the scope of this study.

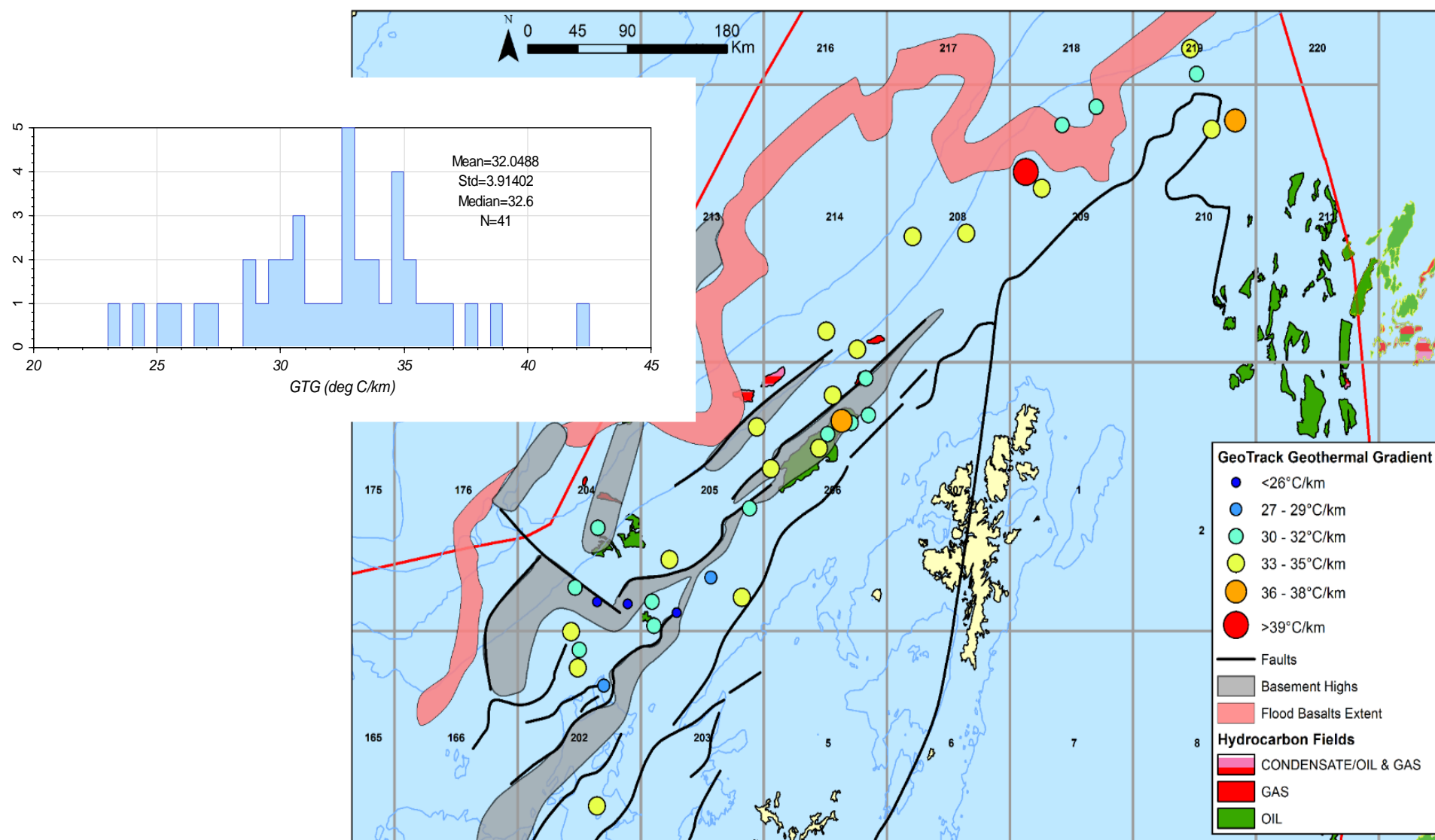


FIGURE 6.3.1 Estimated geothermal gradient (GTG) based on QA/QC legacy GeoTrack data

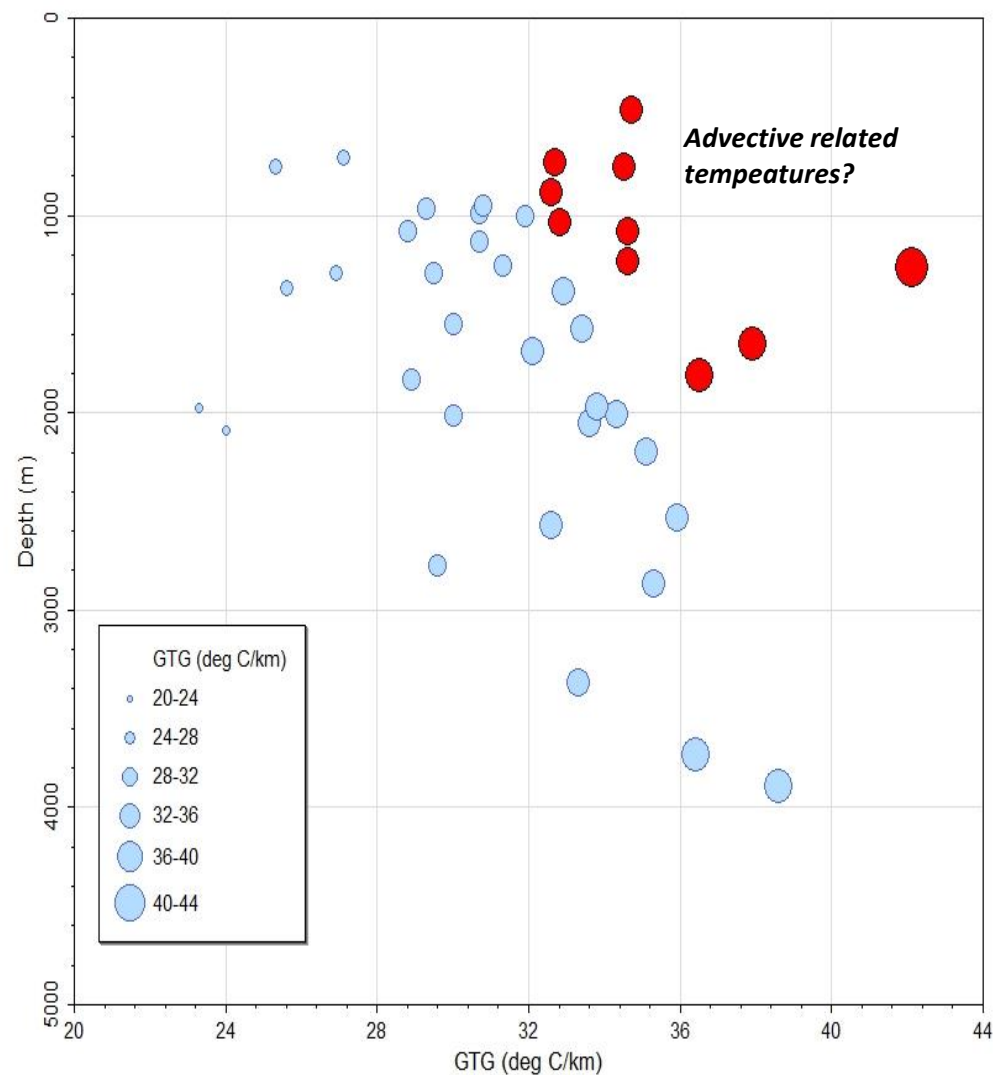
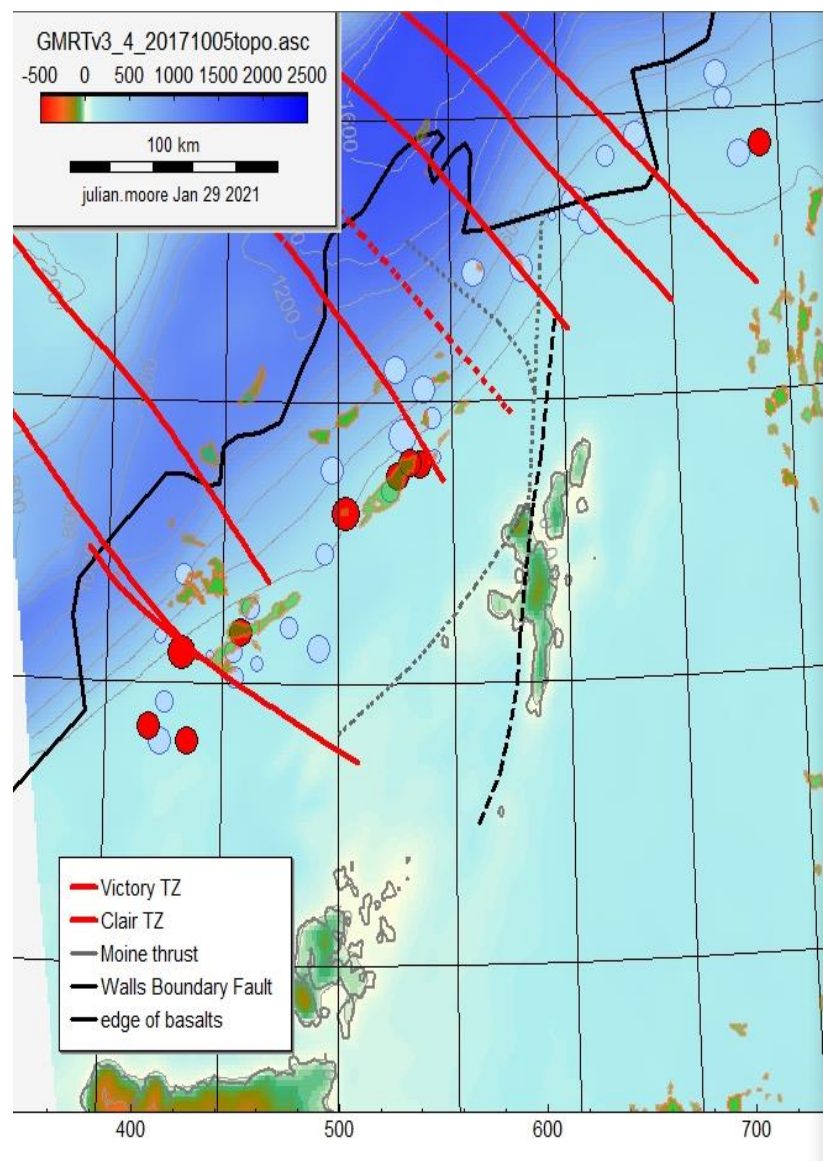


FIGURE 6.3.2 QA/QC of GeoTrack bht data, highlighting high GTG at shallow depths

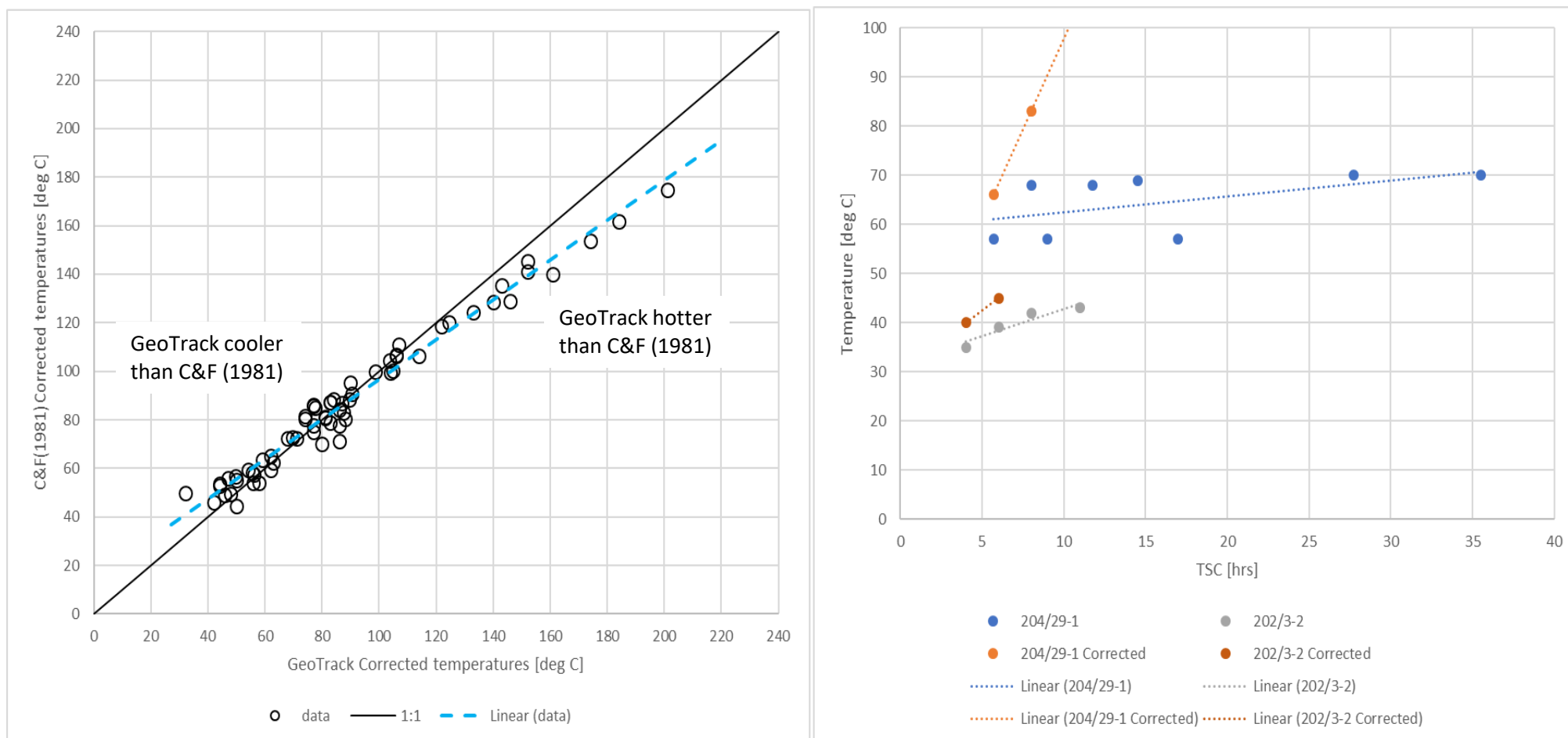


FIGURE 6.3.3 (a) Cross plot of the GeoTrack corrected bht temperatures vs those corrected using Carstens & Finstad (1981); (b) example of suspected over-correction in 204/29-1 GeoTrack data

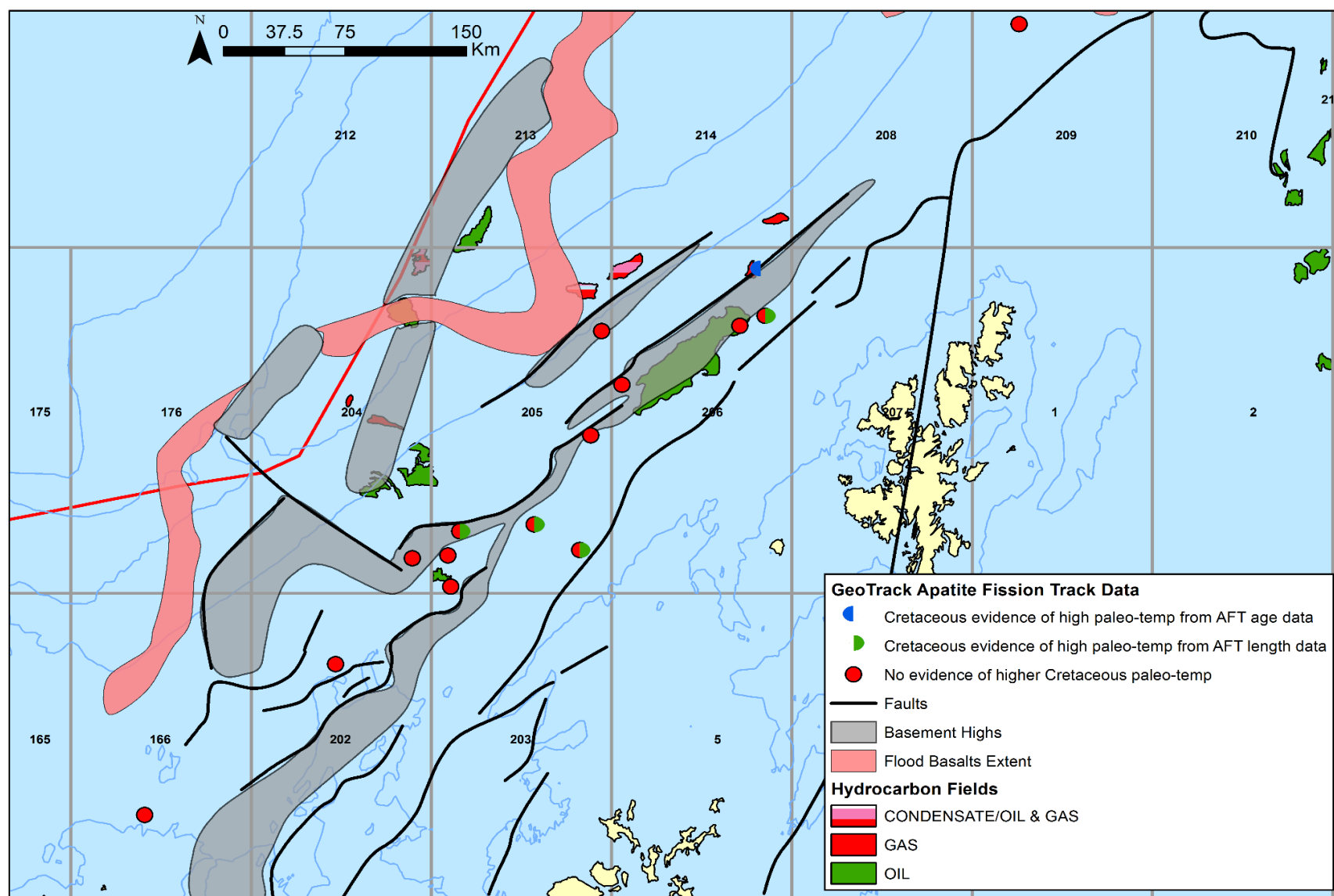


FIGURE 6.3.4 Summary map of GeoTrack legacy studies (GC503, 540, & 605) highlighting Cretaceous aged samples that Geotrack interpreted as showing evidence for cooling from AFT age and length data

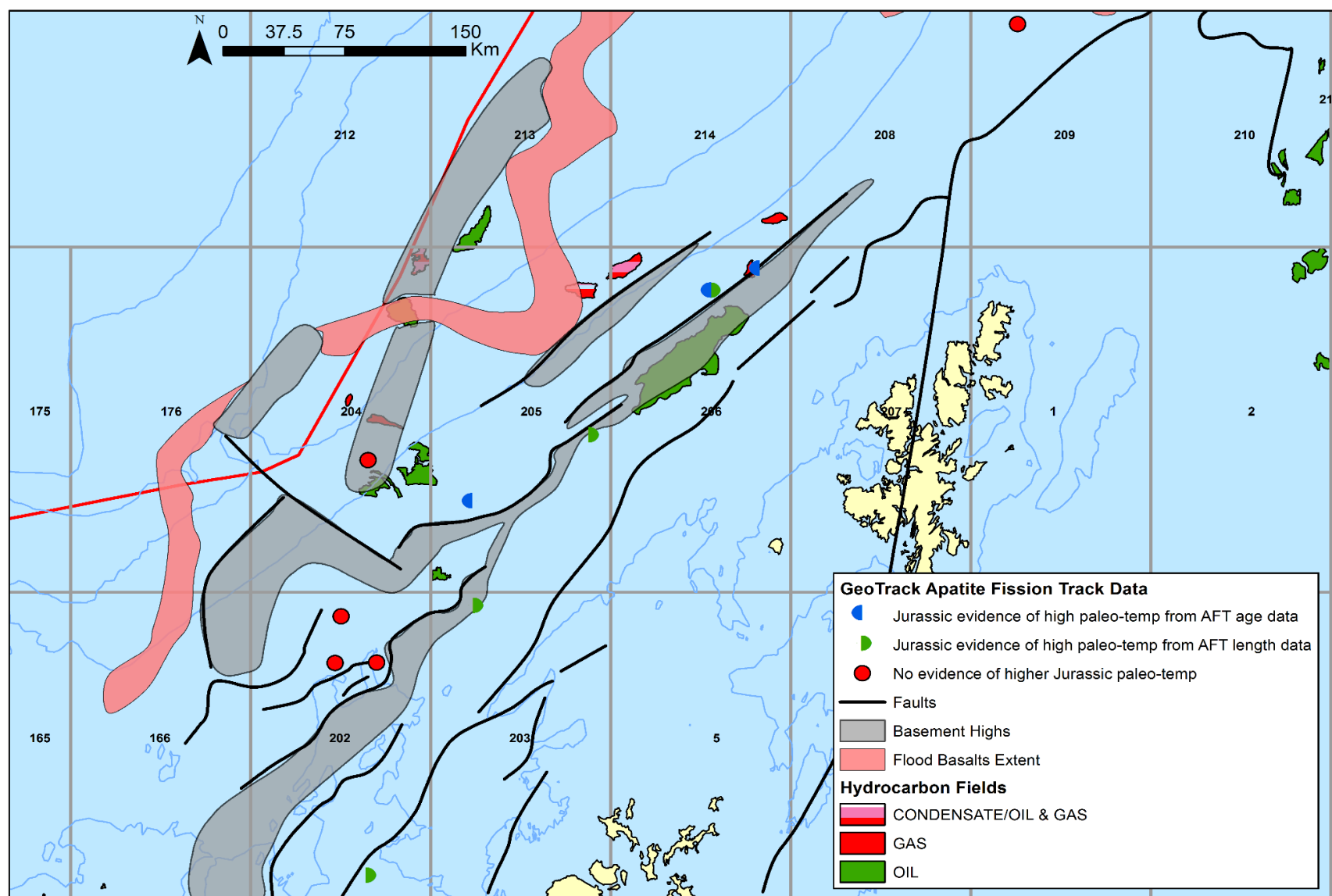


FIGURE 6.3.5 Summary map of GeoTrack legacy studies (GC503, 540, & 605) highlighting Jurassic & Triassic aged samples that GeoTrack interpreted as showing evidence for cooling from AFT age and length data

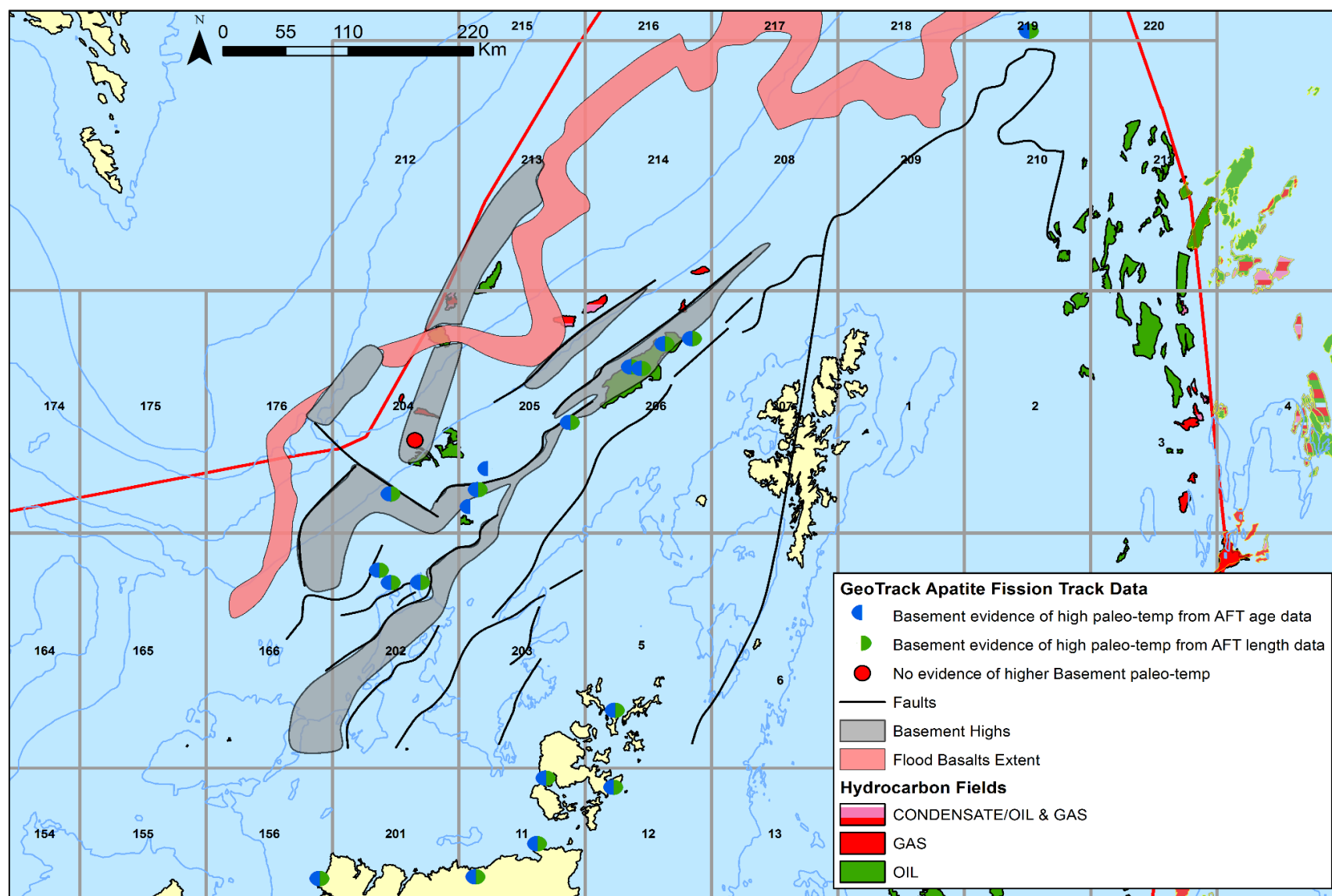


FIGURE 6.3.6 Summary map of GeoTrack legacy studies (GC503, 540, & 605) highlighting Basement aged samples that GeoTrack interpreted as showing evidence for cooling from AFT age and length data

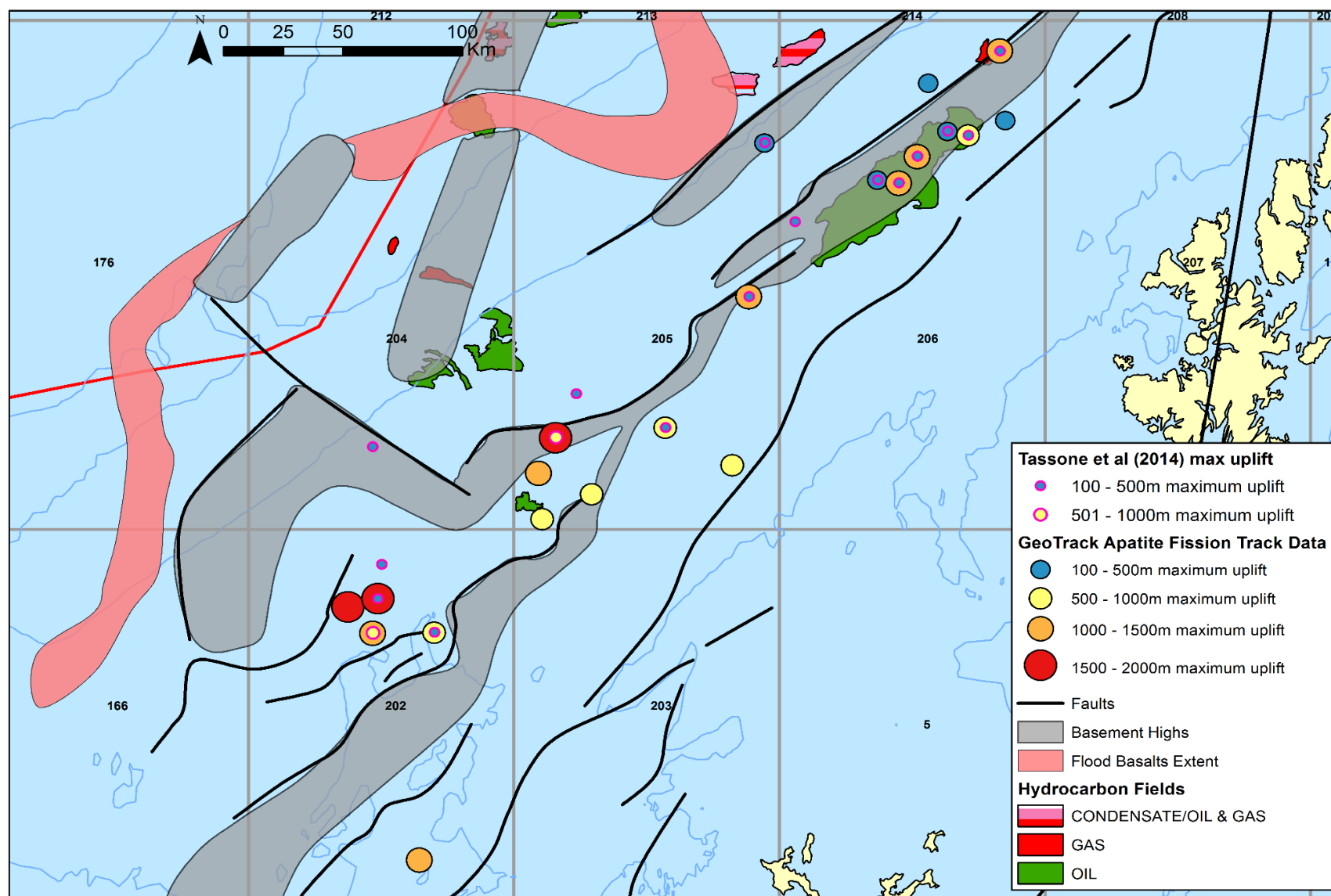


FIGURE 6.3.7 Summary map of inferred maximum uplift from GeoTrack legacy studies (GC503, 540, & 605)

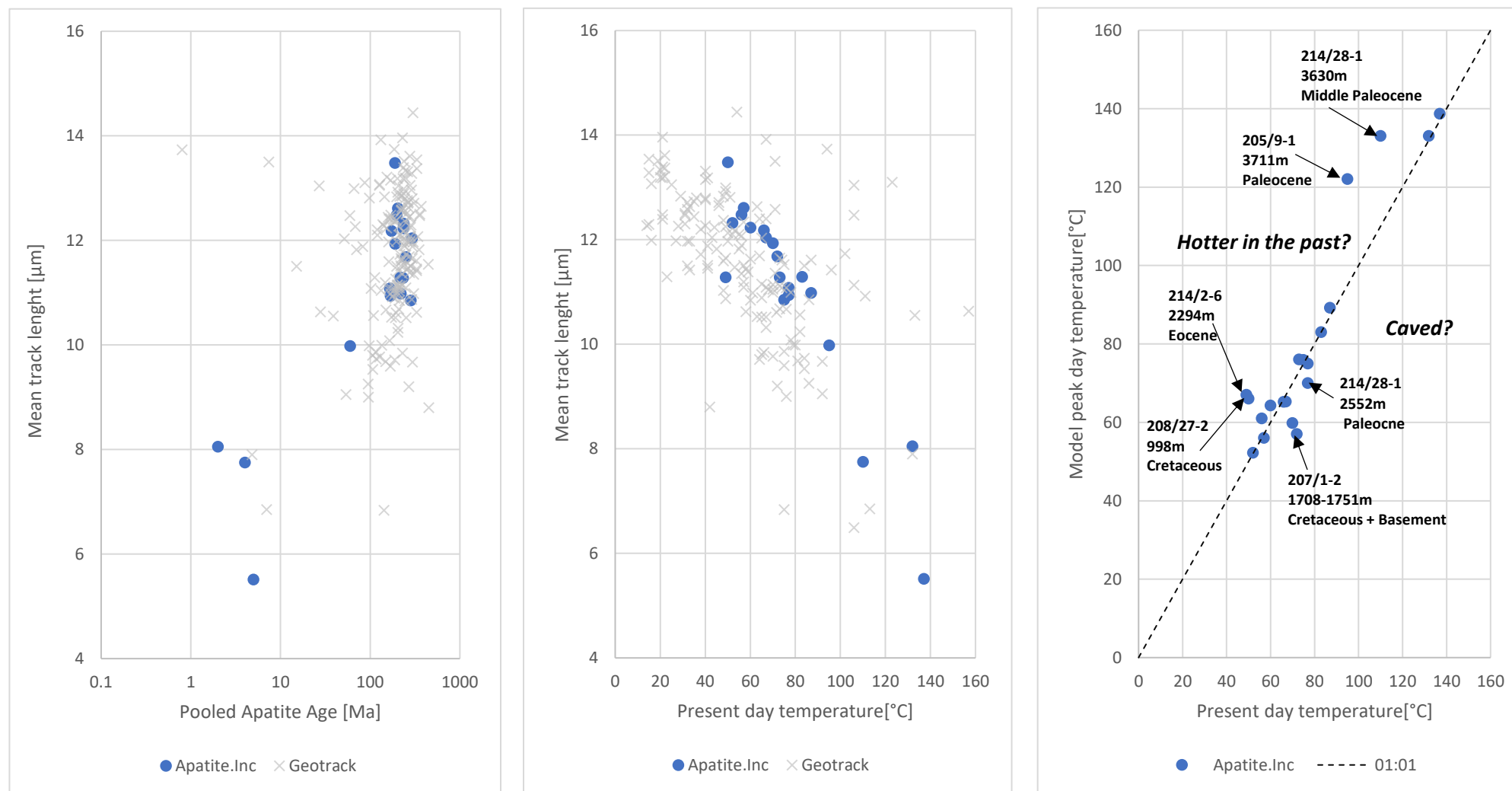


FIGURE 6.3.8 (a) 'boomerang' plot of apatite age vs mean track length (μm) for the new Apatite.Inc and the legacy GeoTrack data; (b) cross-plot of measured temperature (present-day) vs mean track length (μm); (c) cross-plot of measured temperature (present-day) vs model temperature.

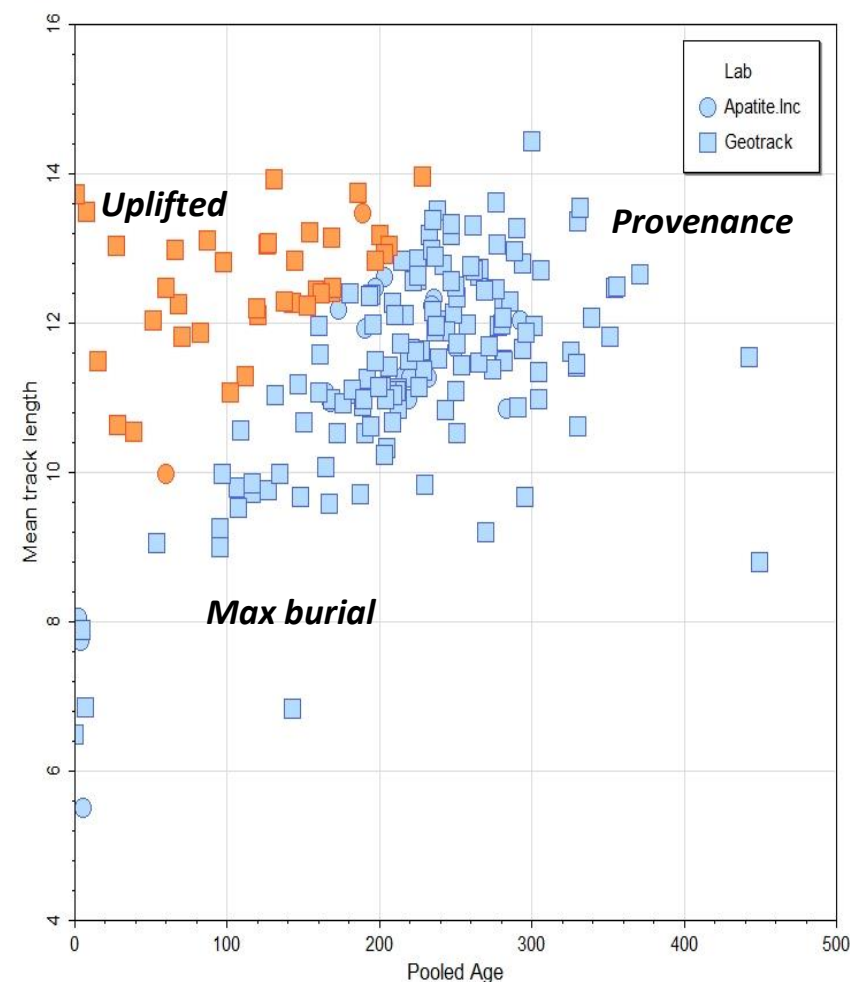
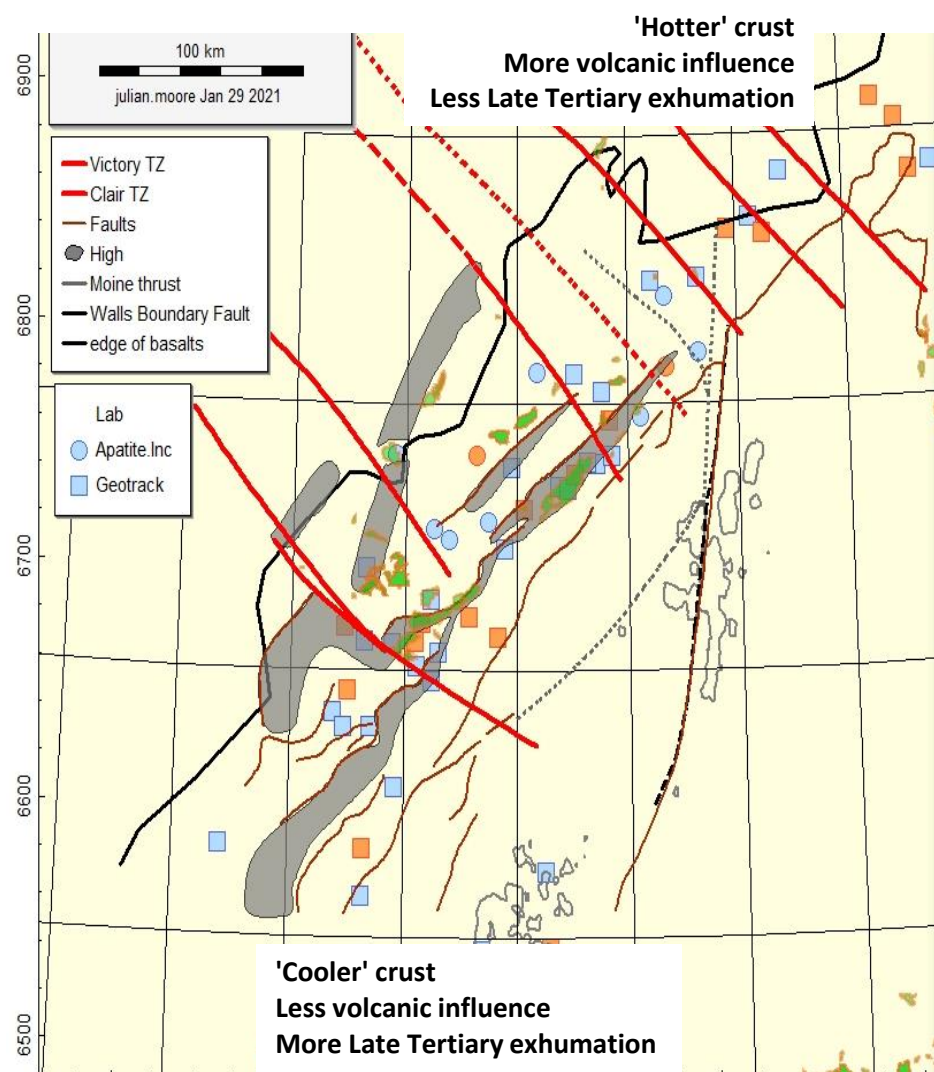


FIGURE 6.3.9 Location map and 'boomerang' plot of apatite age vs mean track length (μm) for the new Apatite.Inc and the legacy GeoTrack data highlighting samples that are potentially uplifted

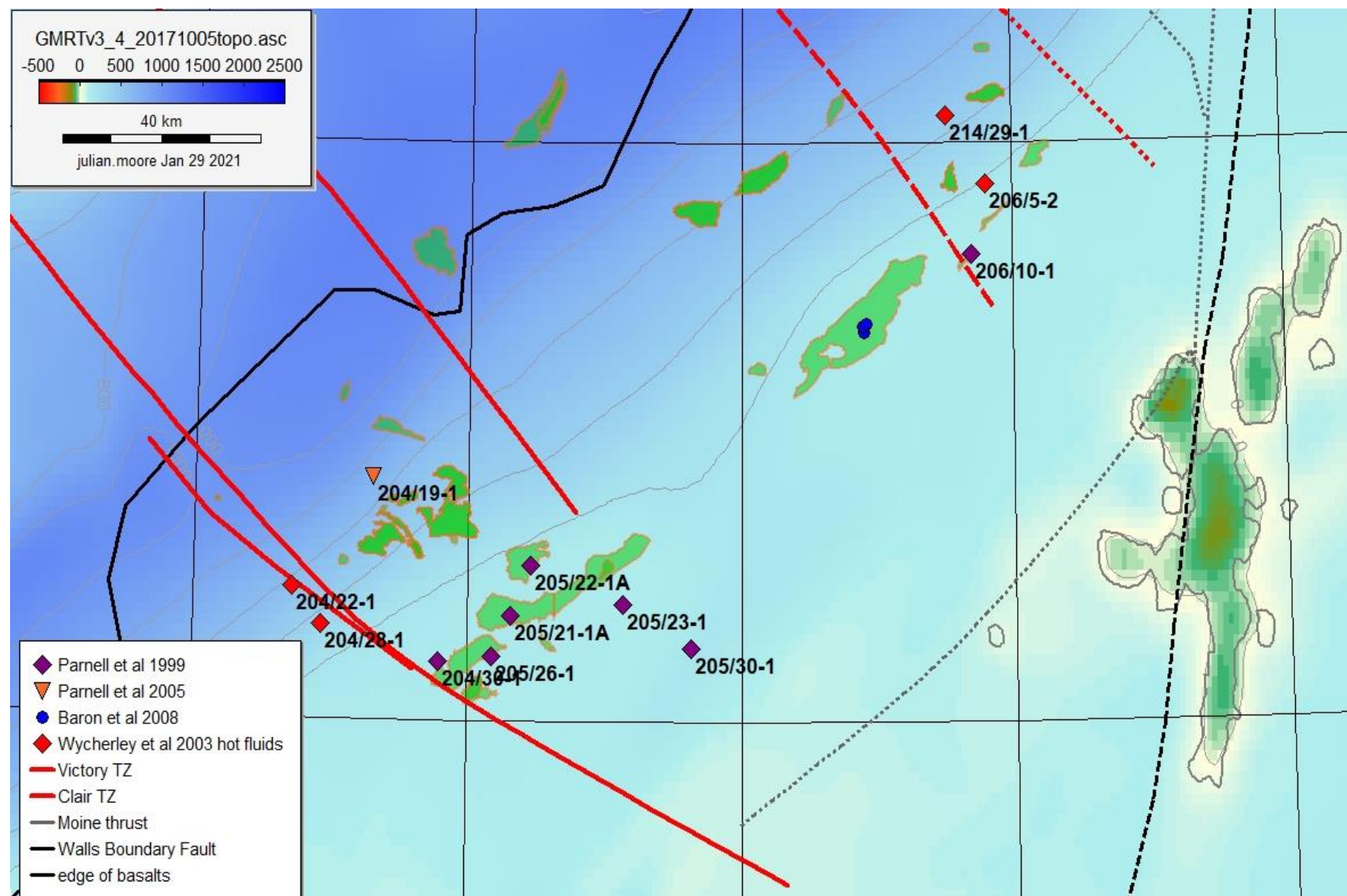


FIGURE 6.3.10 Location map of wells in studies reporting microthermomic and isotopic evidence of hot fluid movement

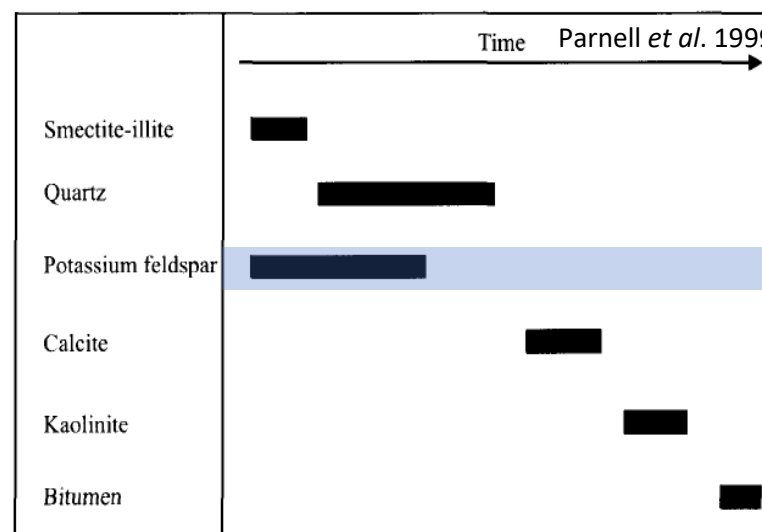
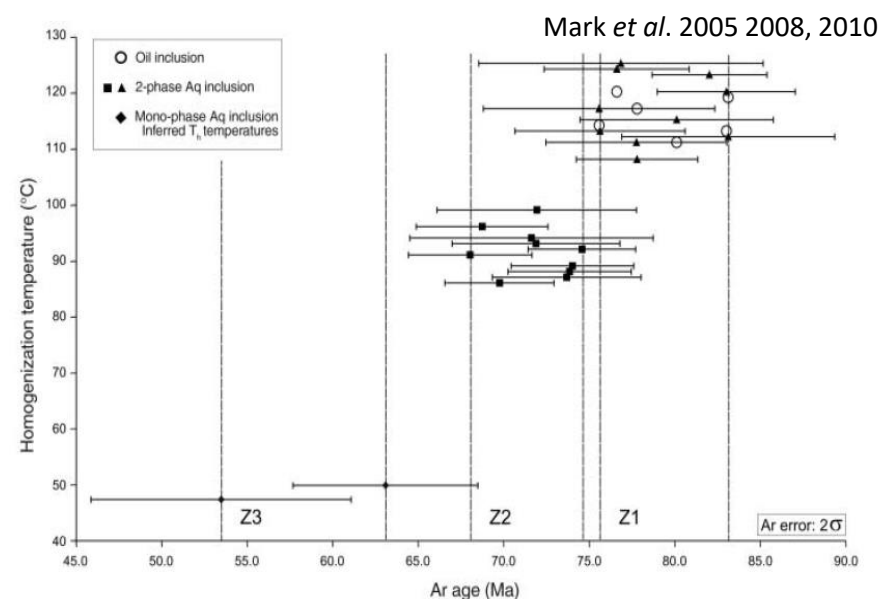
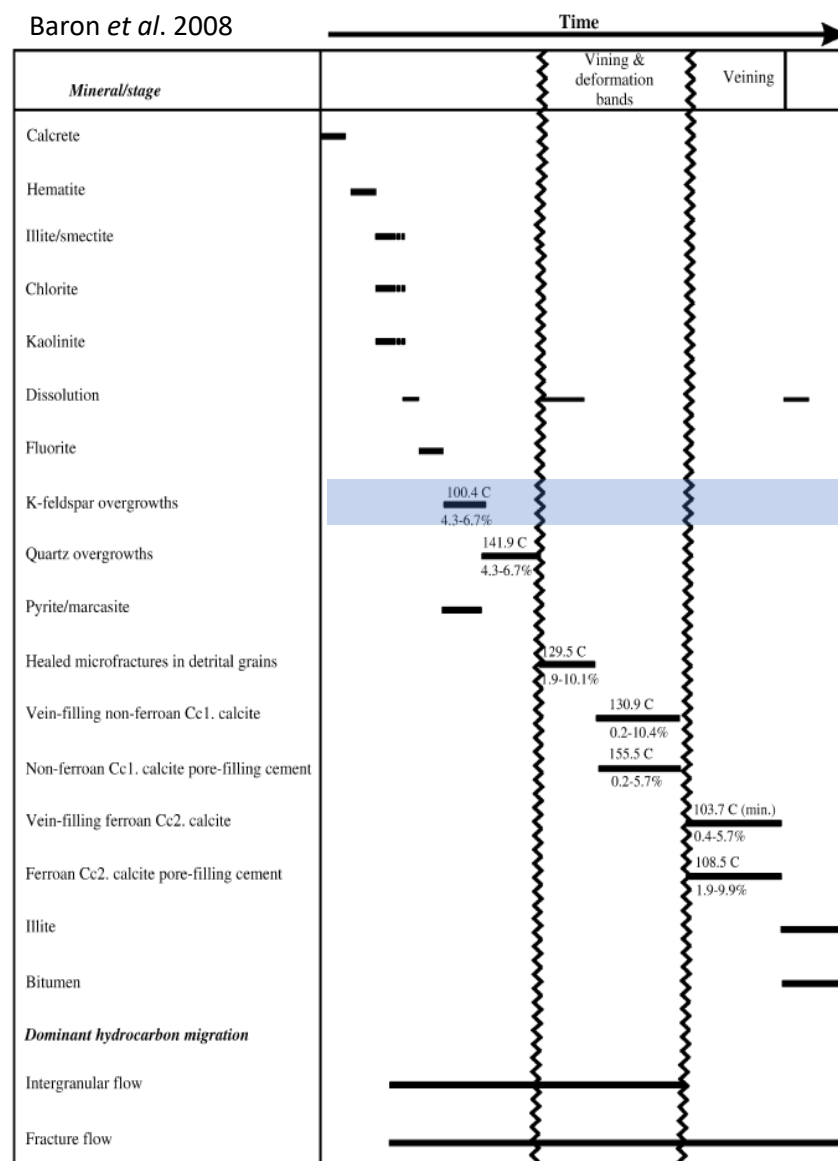


FIGURE 6.3.11 Diagenetic sequences of Baron *et al.* (2008) and Parnell *et al.* (1999) - together with K-Feldspar inclusion homogeneity temperatures from Mark *et al.* (2005, 2008, 2010).

6.4 BASIN CONTEXT & EVOLUTION

In order to build a basin model, both the geological evolution and context of the basin needs to be understood and the sources of heat in the subsurface need to be considered and parameterised. Most simply these sources are

- Mantle heat contribution (inversely proportion to the lithospheric mantle thickness ~ LAB = lithosphere-asthenosphere boundary)
- Crust heat contribution (proportional to the thickness and composition of the crust)
- Sediment heat contribution (proportional to the thickness, composition and porosity of the sediments)

Geological and geophysical aspects of the Faroe-Shetland basin that are relevant to 1D basin modelling are discussed in sections 6.4.1 to 6.4.6.

6.4.1 Lithosphere through time

The Faroe-Shetland basin has a long geological history; if we restrict our view to the Caledonian event, the basin was located in a compressional zone that would have thickened both crust and lithosphere. Streule *et al.* (2010) compared the Caledonian and Tibet-Himalayan orogenic systems and concluded they are comparable in terms of scale, the occurrence of regional Barrovian metamorphism, and the presence of calc-alkaline magmatism attributed to subduction activity prior to orogenesis. The thickened lithosphere would have resulted in reduced mantle-derived heat flow, whereas the thickened crust would likely have increased crust-derived heat flow (although this is dependent on composition, if oceanic dominated the increase could be relatively modest resulting in a net-reduction in total heat flow).

In the present-day Tibet-Himalayan orogenic zone, McKenzie & Priestly (2007) utilised shear wave velocity (V_s) as a function of depth (z) obtained from surface wave tomography (using the phase velocities of fundamental and higher mode Rayleigh waves) to map the thermal lithospheric thickness (since V_s is principally controlled by temperature, rather than by composition). This demonstrated that the orogeny had produced a thick, cool, lithospheric root. If the analogy between the Himalayan and Caledonian systems is correct then one would expect the lithosphere to have been thickened prior to the various phases of rifting. Since heat contribution from the mantle scales with lithospheric thickness:

$$Q_m = k \frac{L}{1333^\circ\text{C}}$$

where Q_m = heat flow from the mantle, k is thermal conductivity and L is lithospheric thickness with an assumed asthenosphere temperature of 1333°C . It can be seen that mantle heat flow reduces by approximately half, if lithosphere thickness (L) doubles. Thus, the early basins would have been expected to have been relatively cool.

Subsequently this Caledonian orogenic zone has been subject to a number of discrete extensional events (Dean *et al.* 1999; Lundin (2002)):

- Permo-Triassic half-grabens
- Jurassic – assumed but poorly imaged?
- Cretaceous:
- Valanginian-Barremian

- Apto-Albian (possible)
- Cenomanian-Santonian
- Campanian-Maastrichtian
- Paleocene: rift?

These events would have acted to thin the crust, that was thickened in the Caledonian event. How the thickness of the lithosphere has evolved through this series of events is harder to say. Rifting can localise to thin either the crust, the lithosphere or it may thin both equally. The Faroe-Shetland Basin was on the periphery of each of the major rift events (Figure 6.4.1) and hence we would expect each of the extensional events to be of modest magnitude (low Beta factor) – which is consistent with the basin occurring on thinned continental crust with a polyphase rift history.

To the North of the study AOI, the Lower Tertiary is of major importance, with the final rifting and separation of Greenland from Eurasia, at ~54Ma, commonly being attributed to the arrival of a mantle plume which impacted beneath Greenland. Ellis & Stoker (2014) argue that it is unlikely that this event lead to an instantaneous unzipping of the North Atlantic, and conclude that the proto-plate boundaries were likely more diffuse during their inception. They favour a dual rift model where initial attempts at North Atlantic rifting involved two opposing and almost by-passing rifts, these were the proto-Reykjanes Ridge (rift) system propagating NE along the SE Greenland margin and the SW-propagating Aegir Ridge between Norway and offshore east Greenland.

Since the principal source rock is Jurassic in age and we are predominantly focused on areas that become mature in the Tertiary, therefore the Paleocene event is thought to be of most significance. This event, in the study AOI, is not a classical rift but does relate to a thermal anomaly in the lithosphere which will have thermally eroded its base shallowing the lithosphere-asthenosphere boundary (Hole & Millet, 2016).

6.4.2 Iceland ‘plume’ and the impact on heat flow

The geodynamic origin of the North Atlantic Igneous Province is outside the scope of this project but the reader is referred to Lundin & Dore (2005) for a detailed geological discussion. For brevity it is referred to as the “Iceland plume”, even though the specific mechanisms driving it are debated. Whatever the precise origin, independent data such as igneous petrology (e.g. Hole & Millet 2016), tomography (e.g. Bijwaard & Spakman, 1999) and drainage network profile inversion (e.g. Hartley *et al.* 2011) substantiate that it is associated with thermal anomalies within the lithospheric mantle. Combining the geochronology data from Wilkinson *et al.* (2016) with the work performed by Hartley *et al.* (2011) on the river profile inversion to dynamic uplift demonstrates a temporal correlation between independent data that indicates a single underlying mechanism (Figure 6.4.2).

The origin of the thermal anomalies, their associated igneous activity and transient uplift has been discussed by Shaw Champion *et al.* (2008). The drainage network inversion results had suggested a transient uplift event of 2-3Ma, followed by rapid subsidence. The uplift could have been driven by magmatic underplating, which would induce a permanent isostatic uplift. Shaw Champion *et al.* (2008) argue that for all of the uplift to be generated by magmatic underplating, several kilometers thickness of underplating would be required, which if intruded in one batch, would generate a component of subsidence on a timescale of 10^4 – 10^5 years. While this timescale may be long enough to be within the limits of resolution of the measured subsidence,

the reconstructed vertical motions of Shaw Champion *et al.* (2008) and Hartley *et al.* (2011) show that (at least over most of the study area) the initial uplift had completely died away within 2–3 Ma. Thus, the underplating model requires that approximately half of the initial uplift is permanent, a prediction which given the rapid subsidence observed in the Late Paleocene to Eocene, is clearly not correct. Thus, while underplating is important regionally, it appears to be of limited importance in the core of the Faroe-Shetland Basin. Shaw Champion *et al.* (2008) advocate a model in which uplift is driven by emplacement of a hot, buoyant layer into the lithosphere; the rapid return to subsidence observed is too fast for dissipation of the excess heat by conduction alone and so the simplest way to account for this is to include heat loss by both conduction and convection. Understanding how this impacts the definition of the LAB in a standard industry basin model application is not trivial as commercial basin modelling packages only model the conduction component.

A reconstructed palaeogeography of the North Atlantic Ocean during Late Paleocene times from Hartley *et al.* (2011) is shown in Figure 6.4.3a. A, b and c are proposed plume centres (cf. Hartley *et al.* 2011 and refs therein); the dashed black line, approximates the location of continental break-up and the black square indicates the AOI of this study. The red shading shows the idealized extent of Icelandic plume, where variations in shading represent radial spreading of hotter annuli of plume material (Hartley *et al.* 2011). Figure 6.4.3b illustrates a map of the study area in the Early Paleocene (modified from Hole & Millet, 2016) showing the position of the onshore and offshore igneous centers, dyke swarms and projected extent of the plume influence from Lawver & Miller (1994) and Mihalffy *et al.* (2008). Studies of exhumation in Scotland (e.g. Persano *et al.* 2007) suggest the latter is more accurate and that the influence of the plume would be felt across the study AOI and into the onshore.

The challenge is that while there is ample evidence of the occurrence of the plume and its influence on the geology of the AOI, the direct impact of the plume is not generally seen except in the short-term uplift (see above) and in local effects associated with contact metamorphism from dykes and sills. As noted above, the stratigraphic data and drainage profile inversion (Shaw Champion *et al.* 2008; Hartley *et al.* 2011) suggests that the uplift was on a short timescale (~3Ma), whereas the volcanic sample geochronology suggests the associated igneous activity was longer lived (cf. Figure 6.4.2). This perhaps reflects the convective component having the most influence upon the vertical uplift, with a slower conductive component that is associated with the volcanism (and elevated background heat flow)?

The analysis of the apatite thermochronology data collected for this study, showed that the analysed basinal wells are close to their maximum temperatures present-day and thus evidence for elevated palaeo-temperatures is lacking. This may in part reflect the fact that samples out in the basin were restricted to Lower Tertiary samples which would have been shallowly buried when basal heat flow would have been expected to be elevated. However, where deeper older samples have been analysed (e.g. 206/11-1 – cf. Chapter 4, p. 4-22 – 4-23) only relatively modest increases in paleotemperature are plausible (+ 10-20°C) and are not required by the data.

From the published studies referred to above, it would seem that the Icelandic plume event is associated with thermal anomalies in the Lithosphere, but that the magnitude of these thermal anomalies in terms of elevated heat flow and hence temperatures in the sediment pile are modest and likely short lived. To investigate this further, some simple end-member models were tested in Zetaware's Genesis 1D basin modelling software. A 1D model was built for the 204/14-2,

built using our best estimates of the geological evolution of the basin (cf. section 6.5 for further details), but with a variable lithospheric thickness description. Four models were tested:

- Constant thickness – 100km
- Constant thickness – 80km
- Lithosphere thermal anomaly (Beta 1.2; τ 62Ma)
- Lithosphere thermal anomaly (Beta 1.2; τ 25Ma)

A rift type model was used for convenience and since it approximately replicates a thermal anomaly in the lithosphere. The Lower Tertiary is not a classical rift and there is no evidence of classical growth faulting; rather it is believed that it is the lithospheric mantle that is being stretched over a wider region than the crust. This would produce post-rift stratigraphic onlap at basin margins and creates a "steer's head" geometry (White & McKenzie, 1988) which is thought more akin to the shape of the Tertiary isopach. This stretching of the lithosphere is driven by the excess heat as the Icelandic plume passes, shallowing the lithosphere-asthenosphere boundary (LAB) which leads to decompression melting and the generation of magma creating the volcanism observed within the AOI.

The thermal time constant was defined by McKenzie (1979) as $\tau = (L^2/\pi^2\kappa)$ where L = lithospheric thickness and κ = the Lithospheric thermal diffusivity. The parameter controls the rate at which the lithosphere cools towards equilibrium. For standard lithosphere τ is assumed to be ~62Ma however for thinned lithosphere, as expected here, it may drop to a value of order of ~25Ma, much longer than the timescale of ~2-3Ma interpreted by Shaw Champion *et al.* (2008) and Hartley *et al.* (2011) from their data. A shorter duration for τ was not used however as it could not be calculated from physically reasonable values.

Comparison of the models described above with the temperature, % Ro data and apatite thermochronology-based tT paths are shown in Figure 6.4.4 and Figure 6.4.5 respectively. The figures illustrate a subtle difference between the models, but that the static 100km model is probably too cool (although it fits the shallow % Ro data quite well), with the 80km static model and the two dynamic LAB models fittings the data equally well. This serves to illustrate the limit of resolution of standard calibration datasets in constraining different LAB models (which are clearly non-unique). Furthermore, it suggests that in wells without significant intrusions, relatively simple models of the lithosphere can recover a reasonable thermal calibration.

6.4.3 Crustal thickness

One component that determines the basal heat flow is the type and thickness of the underlying crust. The principal source used to determine the crustal thickness for the 1D models built is the paper published by Rippington *et al.* (2015), who integrated dataset (gravity, magnetics, seismic) was used to determine the crustal architecture of the Faroe-Shetland basin. They produced a new Moho map for West of Shetlands to independently constrain the Moho position in gravity and magnetic models, where a Bouguer corrected Sandwell & Smith (2009) gravity data was inverted for Moho depth. This map was digitised and loaded into Trinity and then values for the depth to Moho for the wells selected for 1D modelling in Genesis were extracted.

This digitised Moho map (from Rippington *et al.*, 2015) was converted to a total crustal thickness map by removing estimated sediment thickness. This suggests crustal thicknesses will range between ~22km under the Southern Edge of the AOI and thin to ~14-16km in the most basinal areas. These values agree with previous studies of the crustal thickness based on regional seismic data e.g. the FAST study (England *et al.* 2005) and the iSIMM study (Roberts

et al. 2009). Interestingly according to the McKenzie rift model, if the crust thickness is less than 17.2 km then the onset of rifting would be anticipated to be marked by uplift, which is what is observed in the initial phase of Icelandic plume episode as discussed.

6.4.4 Basement composition

The measured basement compositions are discussed in detail in Chapter 3. The basement composition is of interest since it, together with the thickness, acts as a primary control on the thermal regime in sedimentary basins, with up to 50% of surface heat flow originating from radiogenic heat production (RHP) from the upper crystalline crust and basin infill (Vilà *et al.*, 2010). For “typical” Phanerozoic continental crust (including the North Sea) the RHP ranges from 2.5 – 3.2 $\mu\text{W}/\text{m}^3$ (Pollack & Chapman, 1977), with default values of upper crust RHP in most commercially available basin modelling software usually set at ca. 2.8 – 3.2 $\mu\text{W}/\text{m}^3$.

The basement underlying the Faroe-Shetland basin is composed of Neoproterozoic (ca. 2.7 – 2.8 Ga) orthogneisses (cf. Chapter 3; Holdsworth *et al.*, 2018) containing low concentrations of heat-producing radionuclides (^{40}K , ^{232}Th , ^{235}U and ^{238}U ; Pollack & Chapman, 1977) which, together with the prolonged time for radiogenic decay, are expected to result in cold (reduced RHP) basement at the time of petroleum generation. This idea has recently been further tested by Gardner *et al.* (2019), who calculated the RHP using K, Th and U concentrations following the method of Turocotte & Schubert (2014) from 3 basement samples from wells in the study area (204/10-1, 205/16-1 and 214/9-1); these calculations resulted in a mean RHP of 1.6 $\mu\text{W}/\text{m}^3$ ($\sigma = 0.74$), a reduction of up to 50% in comparison to a “typical” North Sea value of 3.2 $\mu\text{W}/\text{m}^3$ (as used in PetroMod©). Gardner *et al.* (2019) went on to demonstrate the impact of using more appropriate RHP values for the crust, which reduces the average geothermal gradient to $\sim 30.7 \pm 2.8$ $^{\circ}\text{C}/\text{km}$ across the AOI. Furthermore, this also result also means that the onset of oil expulsion will occur later than previously predicted by up to 30 Myr in the centre of the Judd sub-basin and up to 22 Myr in the centre of the Flett sub-basin (Gardner *et al.* 2019).

The present study has significantly expanded the available dataset, allowing a zonation of the crustal composition and hence radiogenic heat production to be proposed (cf. Chapter 3, Figure 3.2.6):

Zone A.	0.21 $\mu\text{W}/\text{m}^3$ (± 0.21 , n=2) [wells in Quads 154 & 164 outside of the AOI]
Zone B.	0.64 $\mu\text{W}/\text{m}^3$ (n=1) [wells in Quad 204]
Zone C.	0.75 $\mu\text{W}/\text{m}^3$ (± 0.51 , n=28) [wells in Quads 204 & 205 – SE of the Westray TZ]
Zone D.	0.86 $\mu\text{W}/\text{m}^3$ (± 0.62 , n=31) [wells in Quads 205 & 207 – NE of the Westray TZ; SE of the Victory TZ]
Zone E.	0.88 $\mu\text{W}/\text{m}^3$ (± 0.57 , n=10) [NE of the Victory TZ]
Zone F.	2.10 $\mu\text{W}/\text{m}^3$ (± 0.7 , n=12) [East / Northeast of the Moine thrust extension?]

These values, with the exception of Zone F in the Northeast of the AOI, are markedly lower than the standard defaults commonly used and range from coolest in the south West to warmest in the North East (Chapter 3, Figure 3.2.5). The values used in the 1D basin modelling performed in support of this study are, summarised in the table below. The upper crust RHP values used in model calibration were used as tuning parameters to attain a fit – they were not forced to fit the proposed basement zones, but the results were compared with the measured values to provide a test of their predictive ability. The dynamic LAB model used a variable beta factor and a τ of 25 Ma.

Well	Upper Crust (km)	Lower Crust (km)	Upper Crust RHP (μWm^3)	Lower Crust RHP (μWm^3)	LAB	Basement Heat Zone
204/10a-5	7.4	7.4	1.2	0.0	Dynamic	BC
205/09-1	7.4	7.4	1.2	0.0	Dynamic	
205/12-1	8.0	8	1.3	0.0	Dynamic	
205/14-2	7.4	7.4	0.8	0.0	Dynamic	
205/14-3	7.4	7.4	1.2	0.0	Dynamic	
205/17b-2	8.0	8.0	1.0	0.0	Dynamic	
Average: $1.12\mu\text{Wm}^3$						
206/11-1	7.4	7.4	1.6	0.0	Dynamic	
206/01-1A	8.0	8.0	1.7	0.0	Dynamic	
214/26-1	7.4	7.4	1.9	0.0	Dynamic	
214/28-1	7.4	7.4	2.4	0.0	Dynamic	
Average: $1.90\mu\text{Wm}^3$						
207/01-2	9.0	9.0	2.0	0.0	Dynamic	DE
208/17-2	6.0	6.0	1.8	0.0	Dynamic	F
208/24-1A	10.0	10.0	1.8	0.0	Dynamic	
208/27-2	10.0	10.0	2.0	0.0	Dynamic	DE
Average: $1.90\mu\text{Wm}^3$						

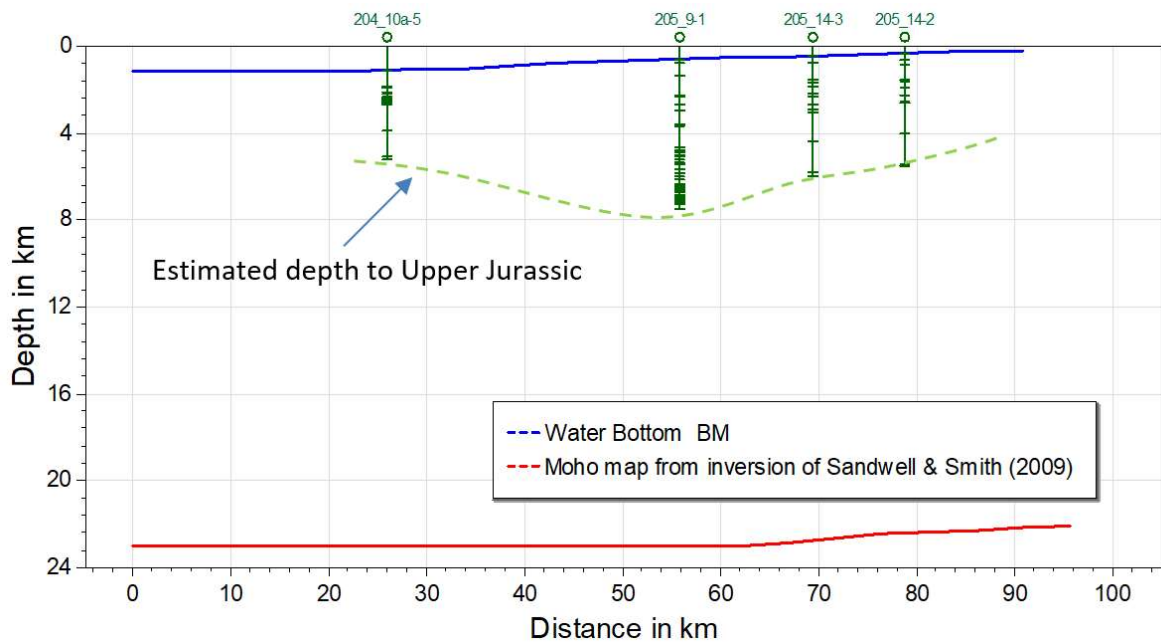
The model values used in zone BC (Average 1.12, range 0.8 – 1.3 μWm^3) are very close to the measured values in zone C 0.75 μWm^3 (± 0.51 , $n=28$), zone B was defined by only a single sample. In zone DE the model values used (Average 1.9, range 1.6 – 2.4 μWm^3) are typically higher than the measured values (D 0.86 μWm^3 (± 0.62 , $n=31$); E 0.88 μWm^3 (± 0.57 , $n=10$)). This suggests at depth in the crust there is a higher concentration of material with higher U, Th & K concentration. The most likely candidate for this material would be granitic plutonic material samples of Caledonian age (cf. Section 3.3). The models for wells 208/17-2 & 208/24-1A, in Zone F to the Northeast of the Moine thrust extension, have an average of upper crust RHP value of $1.8\mu\text{Wm}^3$, which is lower than the measured value 2.1 μWm^3 (± 0.7 , $n=12$) – this would suggest non-granitic material not measured in this study makes up a portion of the total crust in this area. Note this is only based on two wells and further investigation would be required to increase the confidence of this suggestion.

6.4.5 Depth conversion

To model the timing of generation in the Upper Jurassic source rocks in the 1D basin models, its depth needs to be estimated. However, the majority of wells TD in younger stratigraphy. Without access to depth converted seismic surfaces it is a challenge to estimate the depth to the Upper Jurassic source rock. A pragmatic approach was taken, based on information supplied in the previous APT West of Shetland non-proprietary study, regional experience and published data where the approximate TWT to the Upper Jurassic was estimated. This led to an estimate of two-way times from ~3500 to 4815ms. This has been converted to depth using the function published by Morse (2013) and is summarized below:

Well	Upper Jurassic Top (m)	Upper Jurassic Bottom (m)	Upper Jurassic TWT Top	Upper Jurassic TWT Bottom
206/11-1	4500	4800		3593
204/10a-5	5051	5252		3880
206/1-1a	5179	5379		3942
205/14-2	5400	5500		4045
205/14-3	5803	6003		4218
205/17b-2	6200	6300		4371
208/17-2	6778	6978		4563
205/12-1	7000	7100		4627
214/26-1	7094	7294		4653
205/9-1	7285	7485		4701
214/28-1	7810	8010		4815

While such an approach undoubtedly introduces error, the results will capture the timing of generation and expulsion in a general way. A sketch of the depth estimate is illustrated in the sketch below.



Sketch of a dip section showing the approximate depth of the KCF estimated in 4 of the study wells.

6.4.6 Late Tertiary uplift

The subsidence histories in the West of Shetland are complicated by multiple tectonic factors, including magmatism, inversion and regional-scale uplift and tilting, that have resulted in spatially variable exhumation. The basins here exhibit non-burial related, transient, Cenozoic heating anomalies that make thermal history interpretation and burial history reconstructions problematic.

A major mid-Cenozoic erosional unconformity across the AOI was mapped by Booth *et al.* (1993); Pliocene strata overlie Eocene strata thus (deposition) and exhumation occurred during the Oligo-Miocene. Three episodes of epeirogenic movement are identified, in the early, mid-

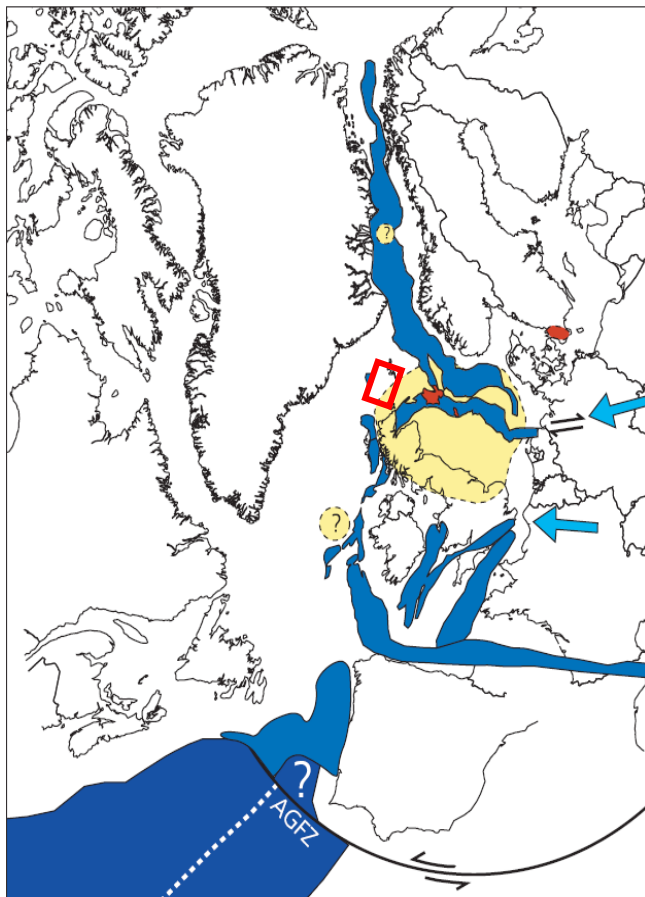
and late Cenozoic, distinct from at least one phase of compressive tectonism as discussed in Praeg *et al.* (2005). Regionally, exhumation analyses of the Chalk Group across the West of Shetland, North Sea Basin, from Britain to Denmark suggest that km-scale erosion of both the western and eastern margins of the basin took place in the late Neogene, above a mid-Miocene or an earliest Pliocene unconformity (e.g. Japsen, 1998).

The early, mid- and late Cenozoic epeirogenic episodes coincided with Atlantic plate re-organisations, but the observed km-scale tectonic movements are too large to be accounted for as flexural deflections due to intra-plate stress variations. Mantle–lithosphere interactions are implied, but the succession of epeirogenic episodes (of differing form) are difficult to reconcile with the various syn-to post-rift mechanisms of the permanent and/or transient movements proposed in the hypothetical context of a plume beneath Iceland. Here the mechanisms, while important for prediction, are perhaps less a concern for the practical application of modelling.

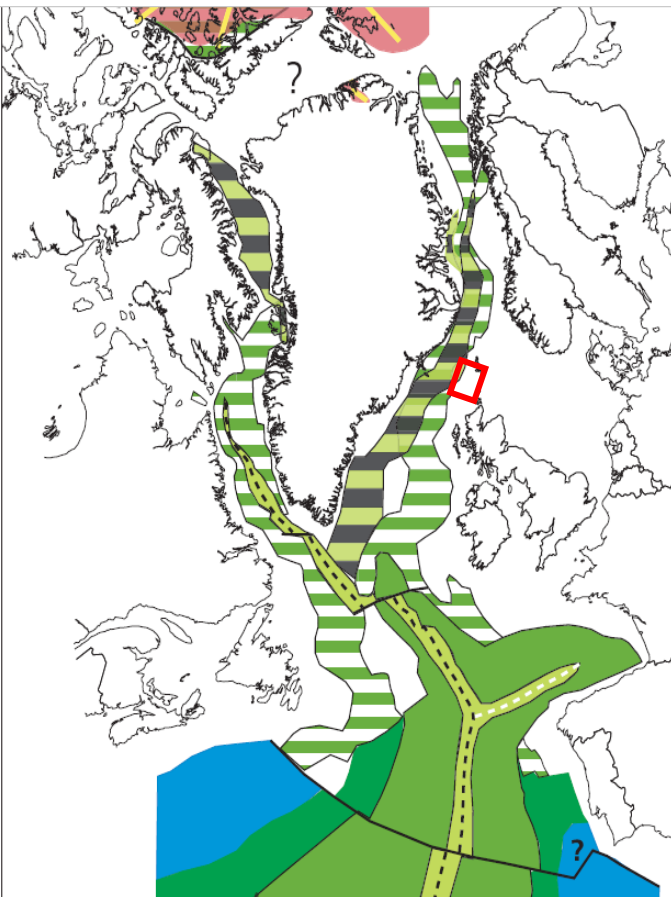
A compaction-based approach (which is less susceptible to distortions from transient heating) using sonic transit time data from Upper Cretaceous marine shales of the Shetland Group in 37 wells was applied to provide new constraints on Cenozoic burial and exhumation magnitudes in the UK sector of the Faroe-Shetland region (Tassone *et al.*, 2014). As estimates of exhumation magnitude depend critically on the form of the normal sonic transit time-depth trend, a new marine shale baseline trend was constructed from shales presently at maximum burial, consistent with other marine shale baseline trends of different ages from nearby basins.

The net exhumation (EN) estimates from Tassone *et al.* (2014) were gridded to create a exhumation map that approximately honoured the results of Tassone *et al.* (2014) from which Tertiary exhumation estimates for the 1D models could be made. This map effectively imparts a tilt to the basin orientated ~NW-SE, tilting up towards the SE. The inferred Cenozoic succession of epeirogenic tilting, sagging and tilting was proposed by Praeg *et al.* (2005) to record the episodic evolution of upper mantle convection during ocean opening, a process that may also be the underlying cause of plate re-organisations.

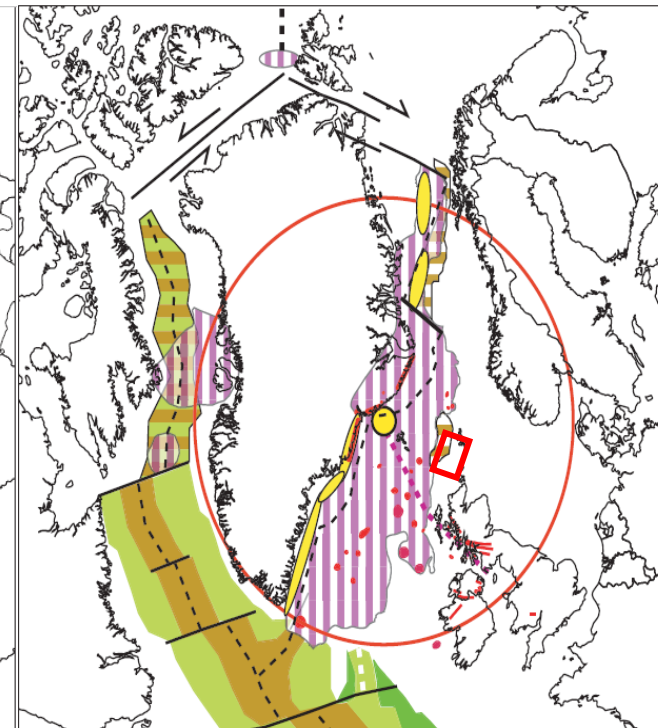
Late Jurassic plate reconstruction (150 Ma)



Late Cretaceous (80 Ma) plate reconstruction



Late Paleocene (54 Ma) plate reconstruction




 = approximate study AOI

FIGURE 6.4.1 Context and rift history (from Lundin, 2002)

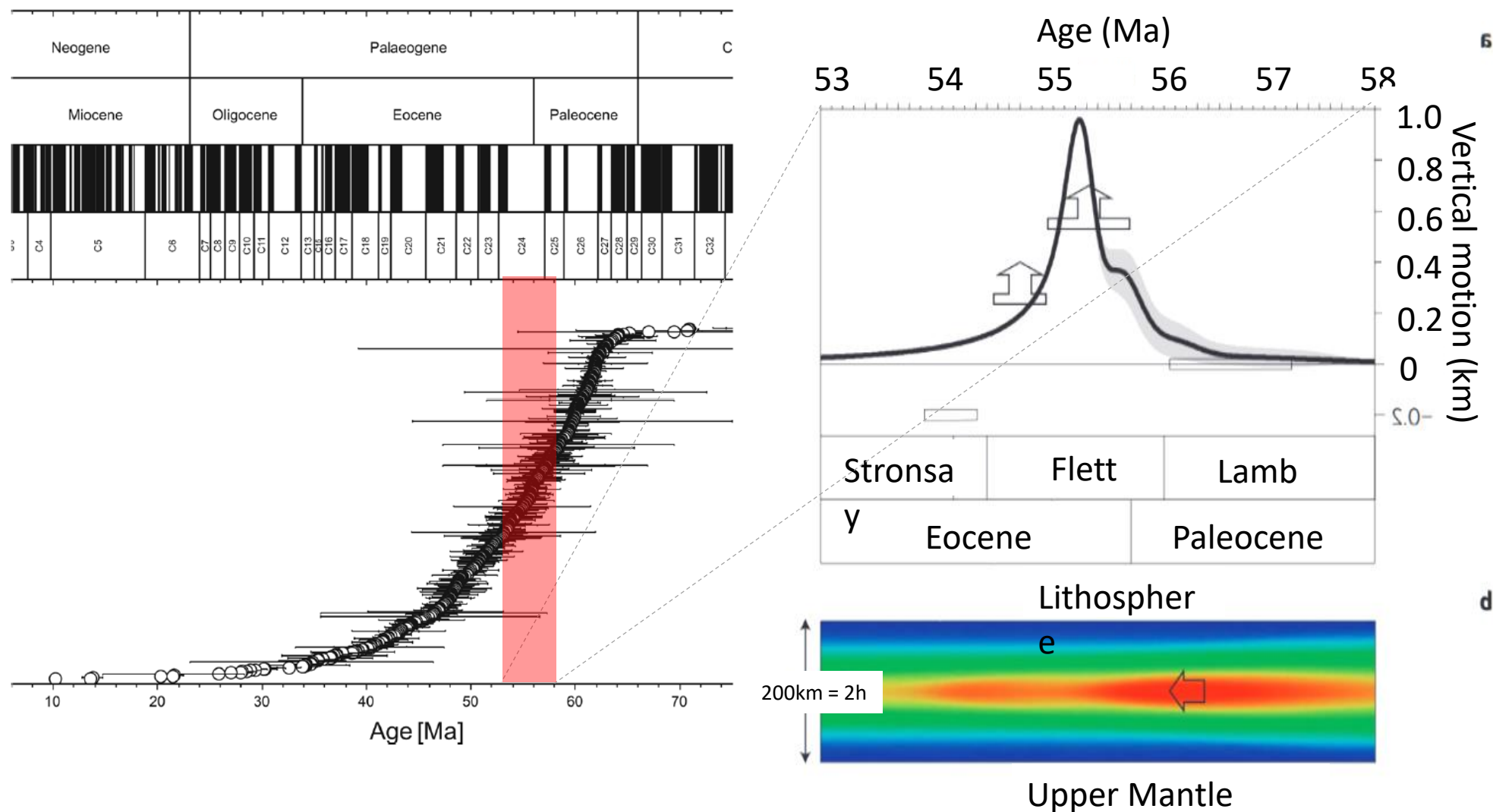


FIGURE 6.4.2 (a) North Atlantic Igneous Province sample geochronology (From Wilkinson et al. 2016); **(b)** observed and modeled uplift history and vertical slice through a dynamic model of lithosphere with radial flow (2h = 200km) (from Hartley et al. 2011)

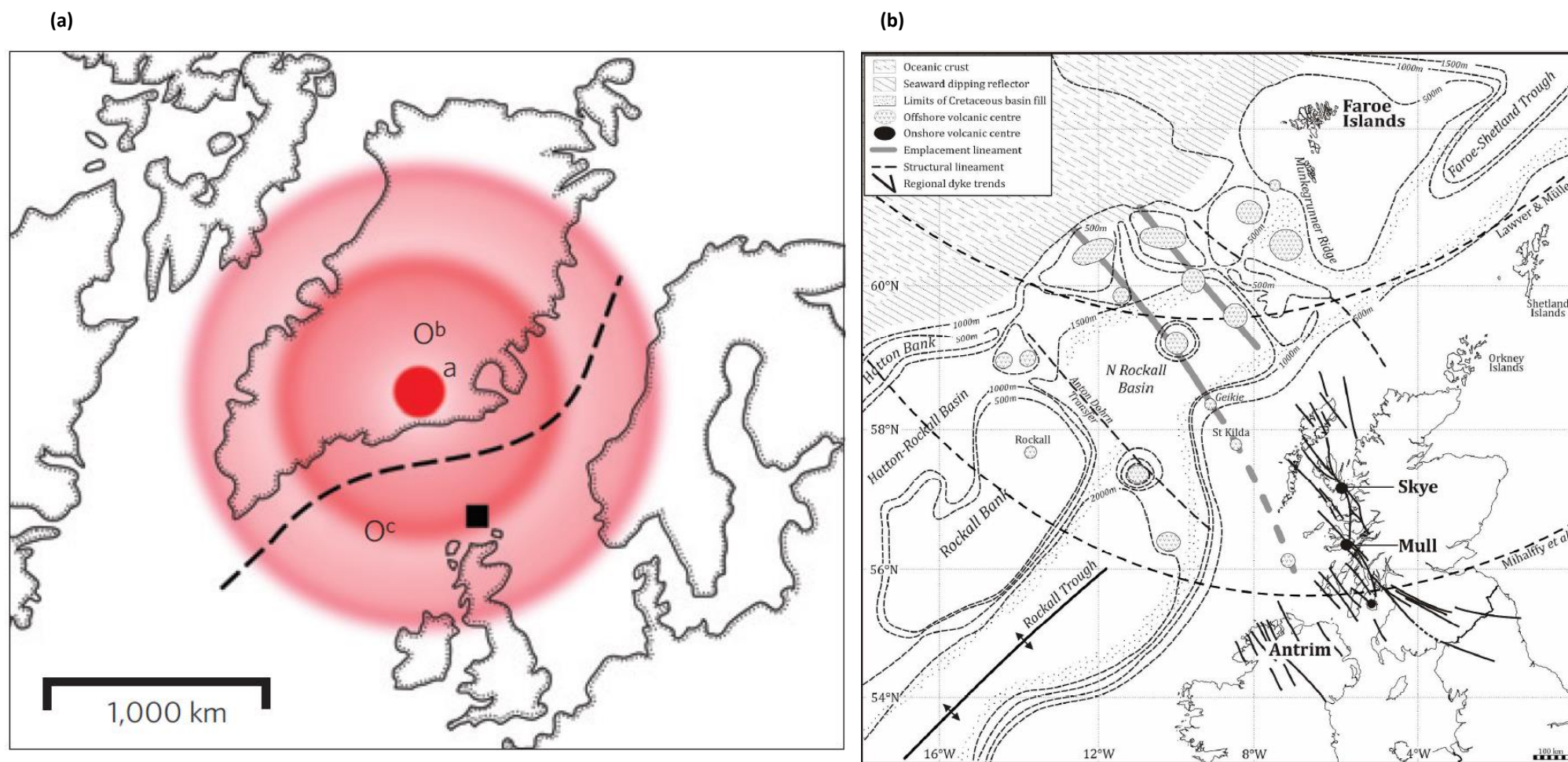


FIGURE 6.4.3 (a) Reconstructed palaeogeography of the North Atlantic Ocean during Late Paleocene times (From Hartley et al. 2011); (b) Reconstruction of the North Atlantic region at about 65 Ma giving the key features of the North Atlantic Igneous Province (from Hole & Millett, 2016)

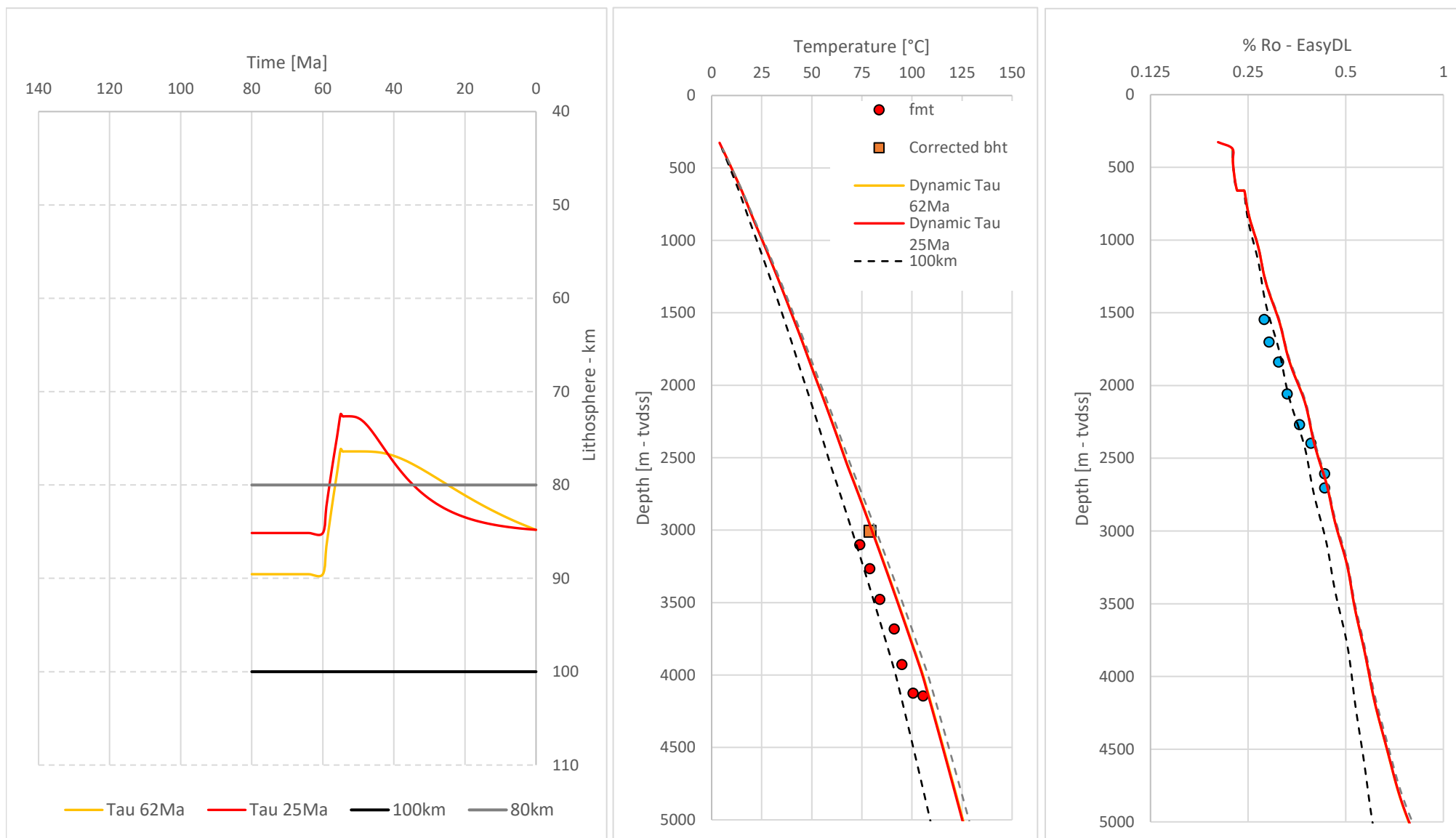


FIGURE 6.4.4 Variable LAB model tests for 205/14-2 showing 4 models results for temperature - depth and % Ro - depth (EasyDL model)

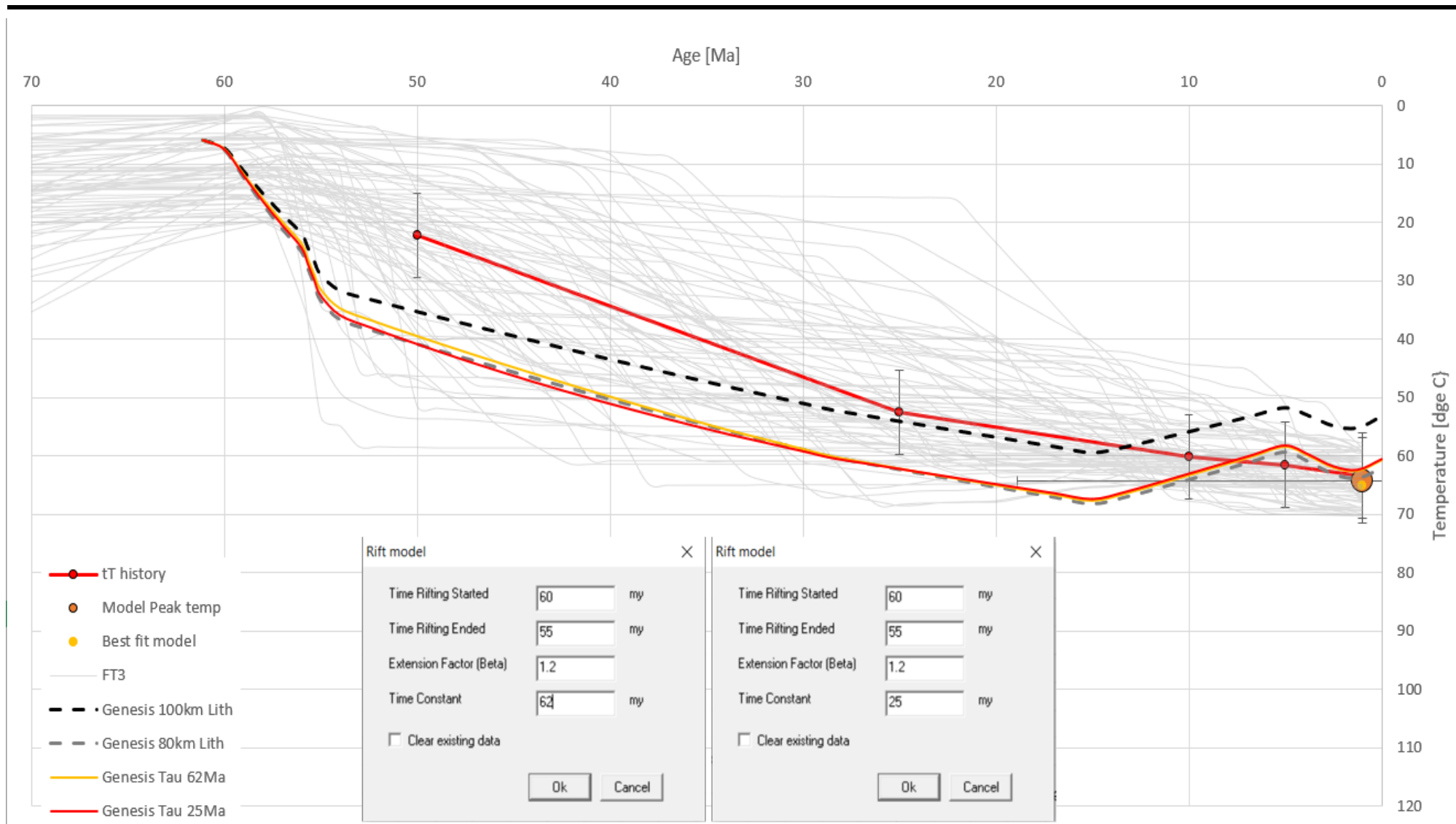


FIGURE 6.4.5 Variable LAB model tests for 205/14-2 compared with the apatite thermochronology derived tT paths

6.5 1D BASIN MODELLING

The vast majority of previous studies on the burial and thermal history of the basin (Parnell *et al.*, 1999, 2005, Tassone *et al.*, 2014) have focused on wells that are located on structural features that flank the main basins. While most wells are in such locations as they are targeting locations with a high(er) probability to find a trapping geometry, their interpretation is often complicated since these areas are also more likely to be structurally inverted and be the foci of the movement of hot basinal fluids. However, from a basin modelling perspective, such locations are atypical of the basin overall and are not especially representative of the main kitchen areas. Modelers, who are typically focused on modelling petroleum kitchens located in the basinal areas often have to use calibration data from flanking settings by necessity rather than design. Here we have attempted to select wells that will provide calibration for both basinal and flanking settings (which are still important of course to aid in understanding trap integrity and biodegradation risk).

In the following sections expulsion petroleum source rocks and how this is modelled is discussed briefly before further discussion on aspects of importance to model selection and construction.

6.5.1. Expulsion

One important but rarely considered source rock parameterisation in source rock studies is the application of an appropriate expulsion model. The defaults of many widely applied commercial modelling packages make some very simple assumptions, for example the default in Trinity is that gas will expel if and when oil does. This is a very poor description of what occurs in source rocks which have been shown in multiple unconventional studies to retain large volumes of oil and gas. The result of the simple assumption is that dry gases are expelled (instantaneous) within the gas window (Figure 6.5.1 – top row), this is often asserted but not what we see in basins with oil-prone source rocks. Taking the central North Sea as an example, the KCF is ‘gas-mature’ but highly volatile oils and rich-gas condensates are found. Similarly, large tracks of the Faroe-Shetland basin would be modelled as ‘gas-mature’ – what this means is considered further in section 6.6.

If modelled with appropriate values for storage within the source rock, Then the cumulative GOR in terms of the source rock product, as shown in Figure 6.5.1 (bottom row), shows that ‘dry’ gases are not produced directly from the source rock, but can be from migration-fractionation processes. This has important consequence for understanding petroleum systems and distribution of phases in the subsurface. A further consequence of using an appropriate expulsion model is that since more oil is retained within the source rock the amount of oil and gas expelled is reduced (since the system is less efficient at expulsion), this also results in the timing of expulsion being delayed as the oil generated needs to first exceed the internal storage of the source rock before it can be expelled. This delay has not been considered by published studies concerned with basin modelling in the West of Shetland (e.g. Iliffe *et al.* 1999).

6.5.2 Model building

Recently, Gardiner et al. (2019) have further highlighted three main factors which should be considered when undertaking basin modelling in the West of Shetland area:

1. Adding intrusive igneous material at the correct time to correctly model the subsidence history of the petroleum system. This should be considered carefully on a sub-basin scale.
2. Consider the increase in thermal conductivity that results in a sedimentary unit when more thermally conductive igneous rock is intruded into the less thermally conductive sediment.
3. Use the correct basement composition, age and RHP (calculated locally where possible), particularly in areas of ancient basement where RHP can be significantly lower than assumed values.

All these parameters together with the understanding described in section 6.3 & 6.4 have been fully integrated into the 1D modelling carried out in this study. A 1D model was built for each of the nine wells which had new apatite thermochronology data. The workflow used to build the models incorporated:

- Lithology descriptions input from Composite logs and regional analysis
- Updated crust and lithospheric mantle thermal conductivities (cf. Jaupart *et al.* 1998; Vila *et al.* 2014; McKenzie *et al.* 2005)
- Appropriate parameterisation of the radiogenic heat production (RHP) values of the basement, which due to the age and composition is much lower in this area (cf. Chapter 3).
- Explicit modelling of igneous intrusions – including impact on thermal conductivity and on the local temperature perturbation and modification of the thermal conductivity of the sediment pile.
- Explicit modelling of the lithospheric thermal anomaly (minor impact)
- Full consideration of the spatial extent and magnitude of Tertiary uplift based upon the sonic velocity-based analysis of Tassone *et al.* (2014).

In addition, expulsion is modelled explicitly using the ARCO model in the Zetaware Genesis 1D basin modelling software, as discussed in section 6.4.7. All the 1D models created, together with temperature, % Ro calibration and estimated expulsion from the KCF source rock are shown in Figures 6.5.2 to 6.5.15. The calibration to the apatite thermochronology derived tT curve were based on visual inspection and are shown in Figure 4.3.1 to 4.3.25. In a small number of wells, such as 208/17-2 (Figure 4.3.14) and 208/24-1 (Figures 4.3.15 – 16), the present-day temperature correspondence between the Genesis model and the apatite tT paths is good but the Genesis model has a more rapid heating earlier in the burial history. Since the Genesis time-temperature path is largely set by the well stratigraphy, the miss-match could have two plausible explanations.

- 1) the well stratigraphy is wrong (i.e. the older layers are thinner, the younger layers thicker than those defined in the comp log)
- 2) the FT³ code should potentially generate a wider range of tT paths to be tested.

A summary of the model geotherms and the modelled heat flow is shown in Figure 6.5.16. This Figure clearly shows the impact of the evolving crustal composition from the old and cool Southwest of the AOI to the younger, hotter Northeast of the study AOI.

An interesting outcome of using an appropriate expulsion model is that the expulsion profile through time develops multiple modes of expulsion maxima, as illustrated in Figure 6.5.17 which shows a modelled expulsion profile for well 205/14-3. A characteristic of West of Shetland oils is the presence of both biodegraded oils, presence as a UCM-hump in GC traces and apparently fresh n-alkanes. The modelling here suggests oil is expelled over ~40Ma at a variable rate. Perhaps this history accounts for the ‘multiple charge phases invoked to account for the observed geochemistry’s? The different thermal models discussed for the LAB in section all produce similar, multi-modal expulsion histories when an appropriate expulsion model is used (Figure 6.5.18), thus the behaviour does not seem to strongly depend on the thermal history. Additionally, the timing of expulsion appears to be less problematic with regards to charging oil fields with Eocene aged seals when compared with previous studies (e.g. Holmes, *et al.* 1999).

In Figure 6.5.19 a comparison is made between the modelling and analysis performed in this study with that published by Mark *at al.* (2005). This work integrates results from a pseudo-basin model in basinal location with the fluid inclusion data collected from 207/1a-5 (the discovery well for the Victory gas field). The oil-bearing fluid inclusions were dated to have formed ~83 – 72 (± 7.1) Ma based on $^{40}\text{Ar}/^{39}\text{Ar}$ dating of K-feldspars. In the paper Mark *at al.* (2005) claim that oil was generated from ~115Ma – 32Ma prior to the formation of the oil-bearing inclusions and in the published burial history, Mark *at al.* (2005) assert that oil generation (and presumably expulsion) occurs between depth of ~2100m to ~3700m (Figure 6.5.18) placing it the early to late Cretaceous. Experience would suggest that this is far too shallow and hence also too early. An offset model considered in this study for well 208/17-2, where a pseudo section was added to the extend the model to an estimated depth of ~7000m for the KCF estimates that generation occurred between 80 – 35Ma. This provides a much closer correspondence to the fluid inclusion data. Clearly the depth of the KCF is uncertain and an increase in the KCF depth estimate would make generation earlier. However, what about phase? Would this result not indicate that Victory should be oil? It is not believed so. Mark *at al.* (2005) suggested that the oil was lost through uplift and loss of trap integrity, however, they present no evidence to support this model. An alternative view is that the oil was lost as a result of increasing charge GOR and PVT behaviour. The Victory structure is small, shallow and low pressure (~2000psi); early in the charge history it is likely the field was filled with oil, but as charge GOR increased it is likely that the fluid saturation pressure would have evolved to be higher than the reservoir pressure creating a gas cap which would have progressively expanded with increasing charge GOR. This would lead to the oil leg being spilled and leaving a gas field.

6.5.1 Modelling volcanic areas

This study has explicitly modelled the impact of volcanism by considering both the shallowing of the LAB (assuming that melt is created by principally by decompression melting cf. Hole *et al.* 2016) and, where recorded, explicitly modelled the intrusion of igneous melts at elevated temperature (~1000°C).

The influence of the LAB shallowing is relatively minor based on the tests performed in this research (see section 6.4.2), although it is acknowledged that the modelling performed only considers the conductive component of heat flow and that advective heat flow will probably play a role, however this is much more difficult to model with any degree of confidence. It is thought that this component will be relatively focused around the volcanic centres.

The impact of the modelling intrusions within the Lower Tertiary package is shown in Figures 6.5.20 and 6.5.21. In Figure 6.5.20 the temperature curves through the time of intrusion are shown, illustrating the rapid conduction of heat away from the intrusions. This is most clearly seen in the Paleocene time-temperature curve (upper right, Figure 6.5.20). However, if the KCF layer is un-intruded by sills and dykes then it will be only subject to heating due to burial and the relatively modest increase in basal heat flow associated with the temporal shallowing of the LAB. A time-temperature curve for a pseudo-KCF layer for such a case is shown in the lower right-hand curve in Figure 6.5.20. Using this particular thermal history, the modelled KCF expulsion history is shown in Figure 6.5.21. In the upper expulsion profile plot the default expulsion model is used – this model only predicts gas expulsion from about 75Ma. In contrast, the ARCO model predicts that oil will be expelled from the source rock until ~55Ma (after which it will be subject to fractionation as part of the migration process – see Section 6.6.1).

The 205/9-1 well TDs in the Maastrichtian so the deeper section is unknown. For illustrative purposes the pseudo-section added for the deeper stratigraphy was modelled as being heavily intruded with dykes and sills (Figure 6.5.3). If, as assumed in the model, Cretaceous burial was insufficient to initiate generation, then the combine effects of Lower Tertiary intrusions together with the rapid subsidence representative of this period results in a relatively short generation period (still ~10Ma) which is thought to be more representative of areas close to volcanic centres and/or with a high density of intrusions within the Mesozoic section.

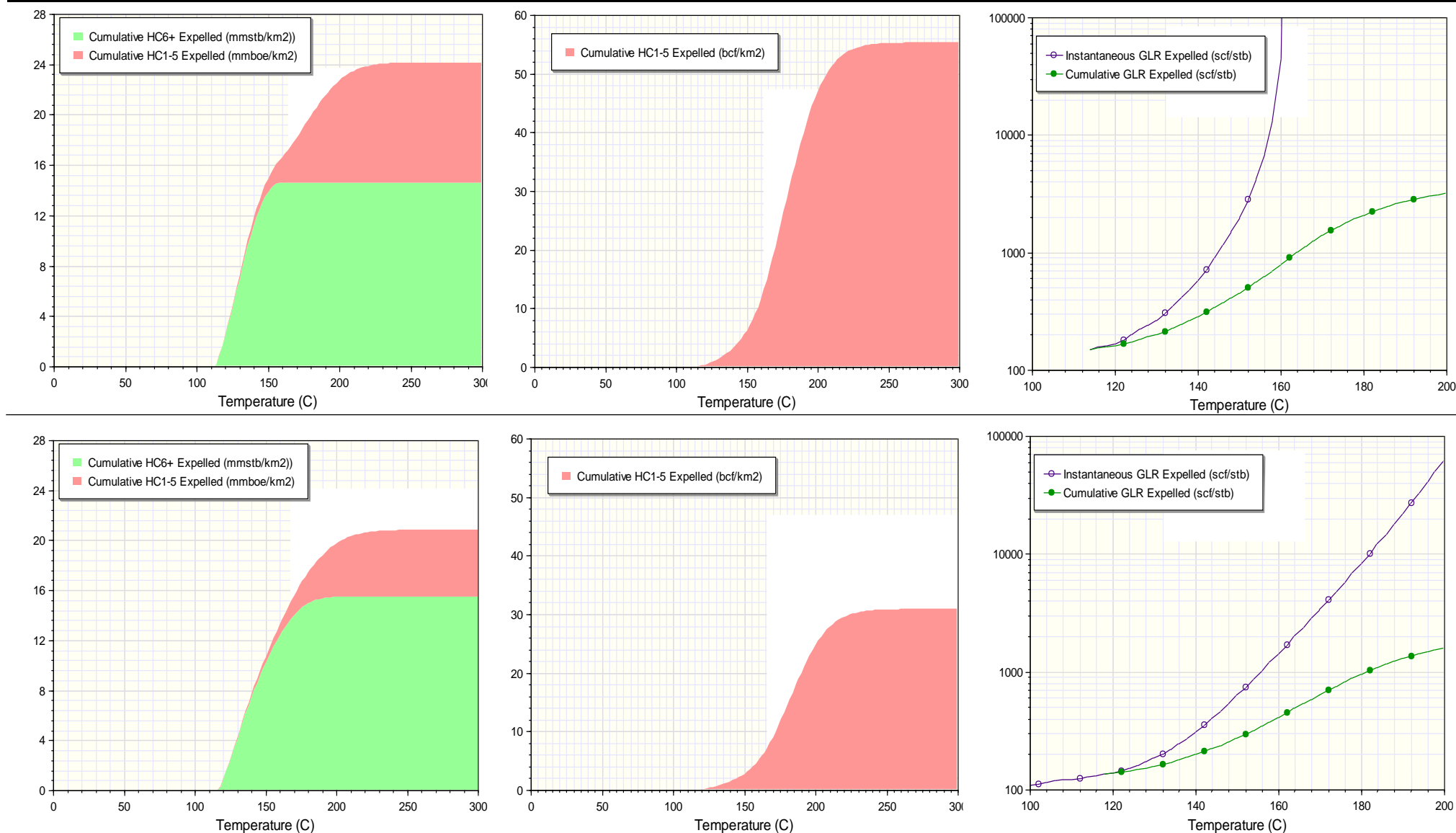


FIGURE 6.5.1 (top row) implications of assuming a simplistic ‘gas expels when oil does’ expulsion model results in the prediction of dry gases being expelled from an oil-prone source rock in the gas window (>150°C); (bottom row) application of an appropriate expulsion model with storage predicts more realistic GORs.

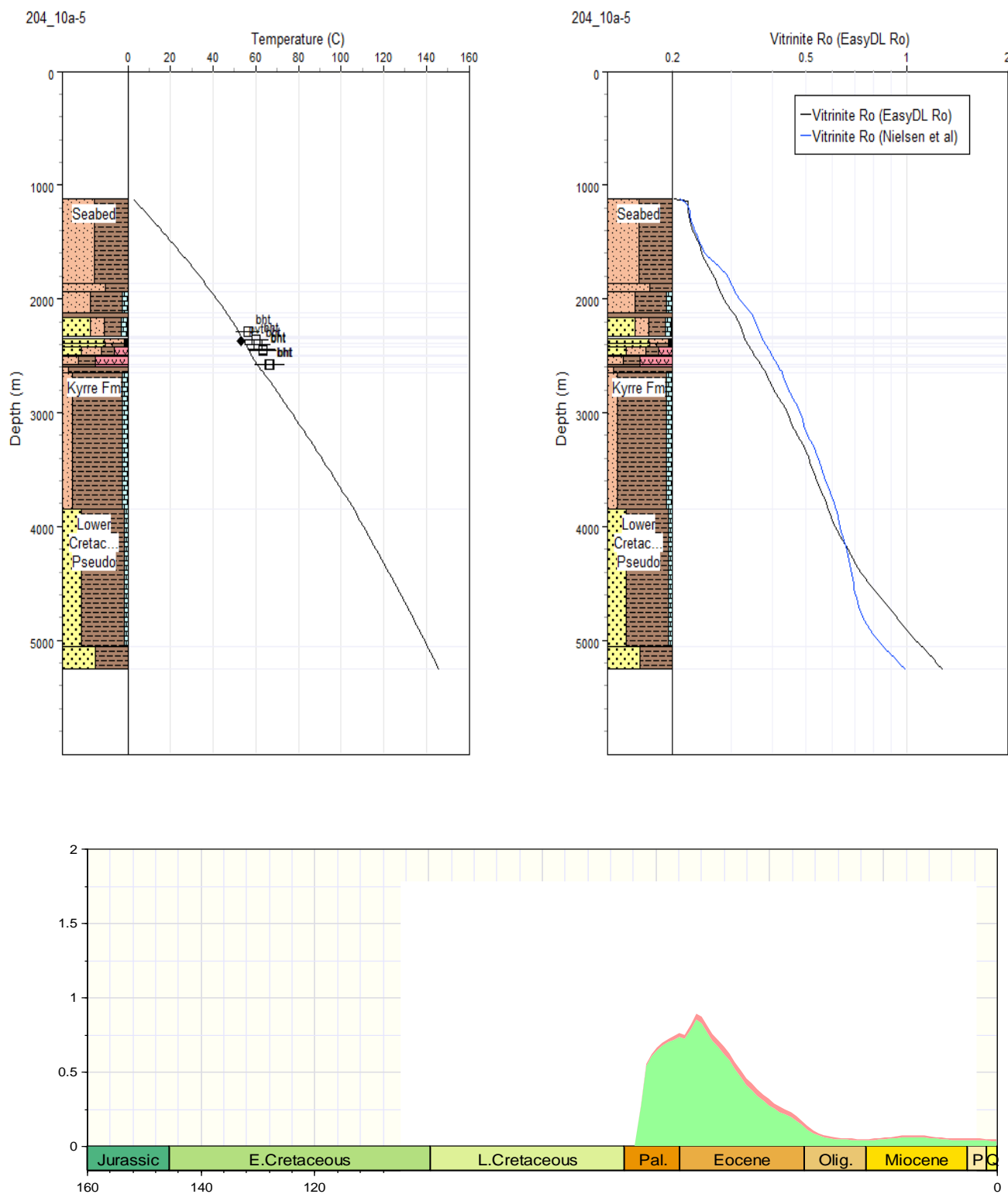


FIGURE 6.5.2 204/10a-5 1D basin model temperature calibration and modelled KCF source rock expulsion (based on a Pseudo-pick at ~5.1km TVDSS)

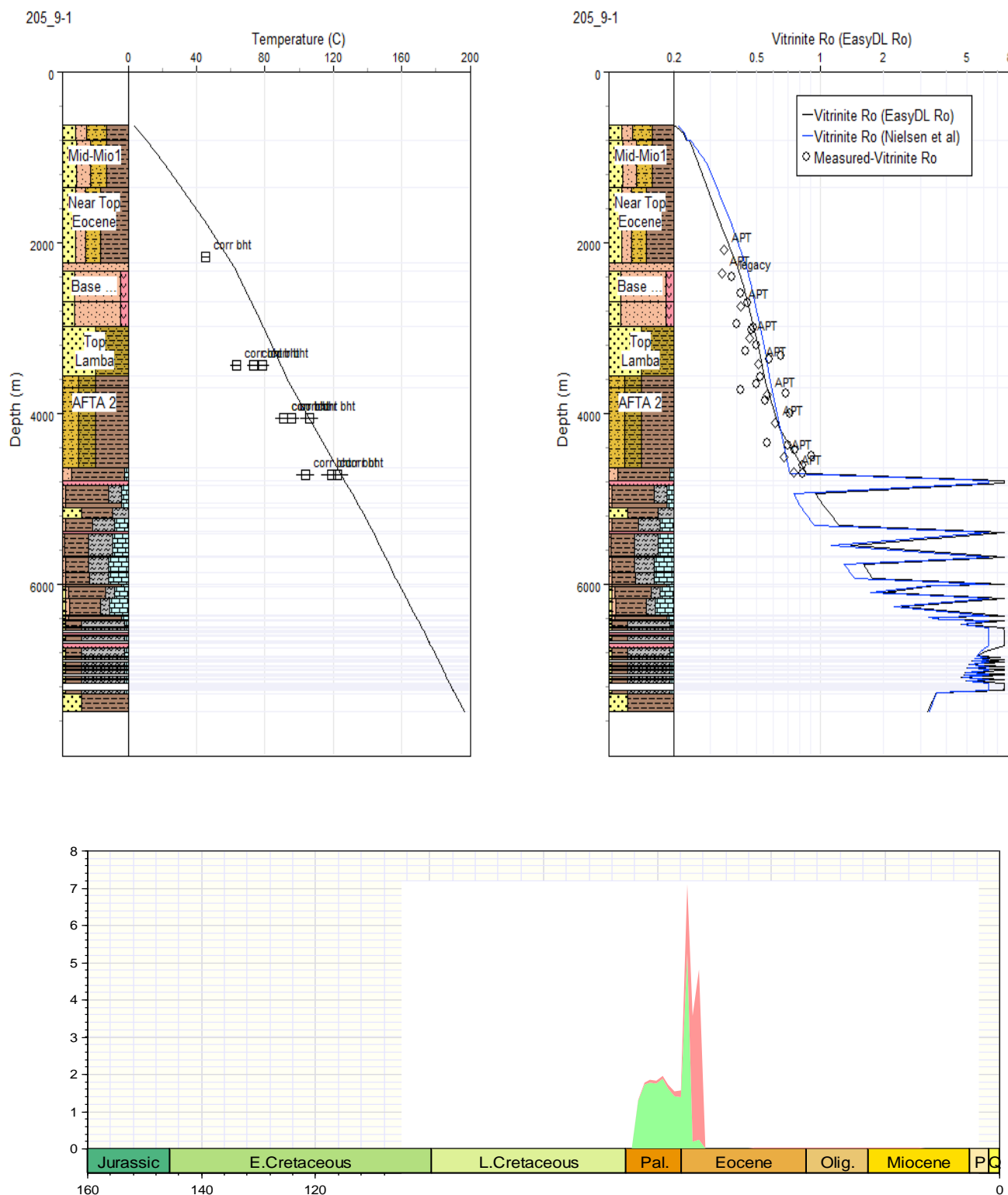


FIGURE 6.5.3 205/9-1 1D basin model temperature & vitrinite reflectivity calibration and modelled KCF source rock expulsion (based on a Pseudo-pick at ~7.5km TVDSS)

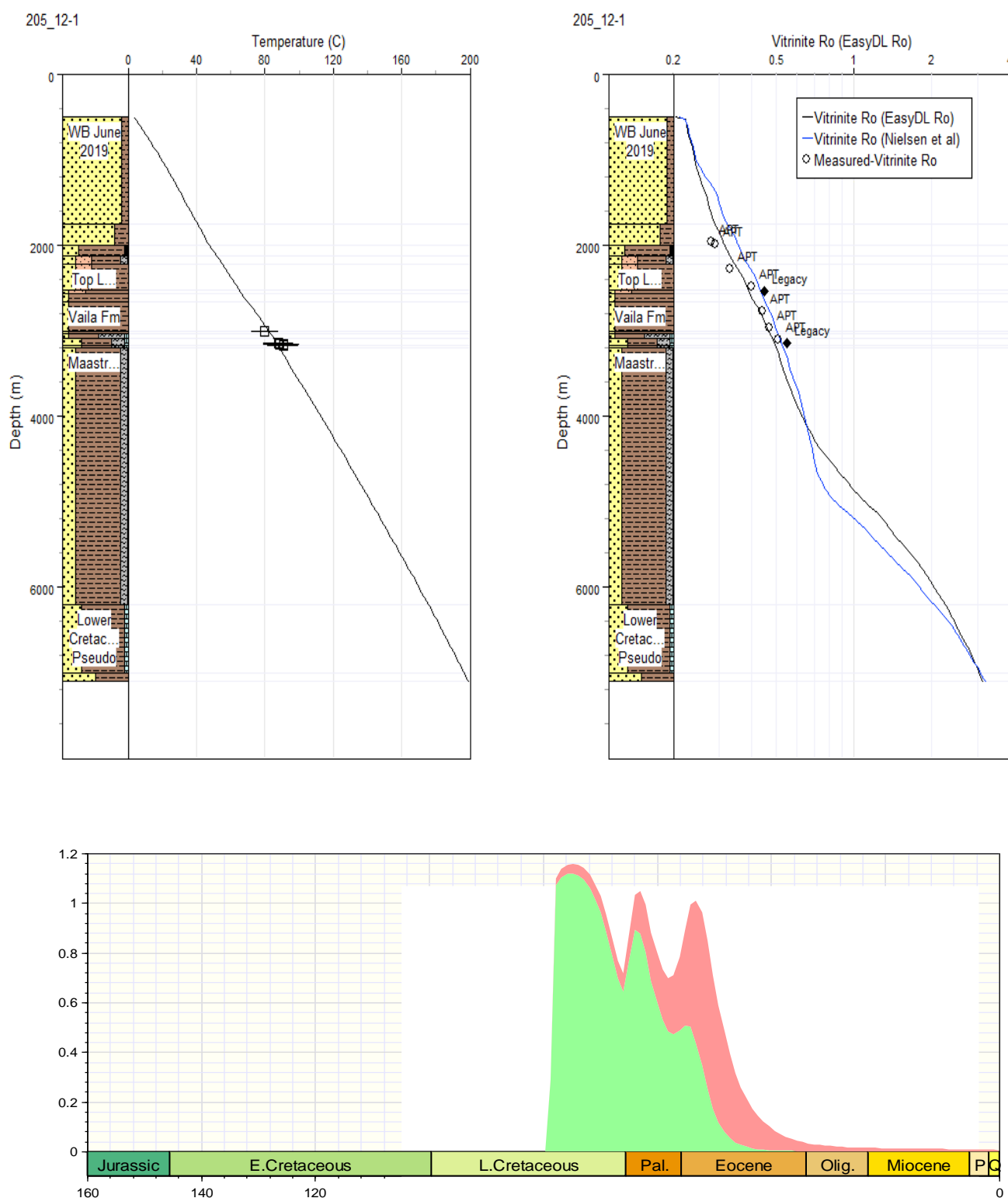


FIGURE 6.5.4 205/12-1 1D basin model temperature calibration and modelled KCF source rock expulsion (based on a Pseudo-pick at ~7.0km TVDSS)

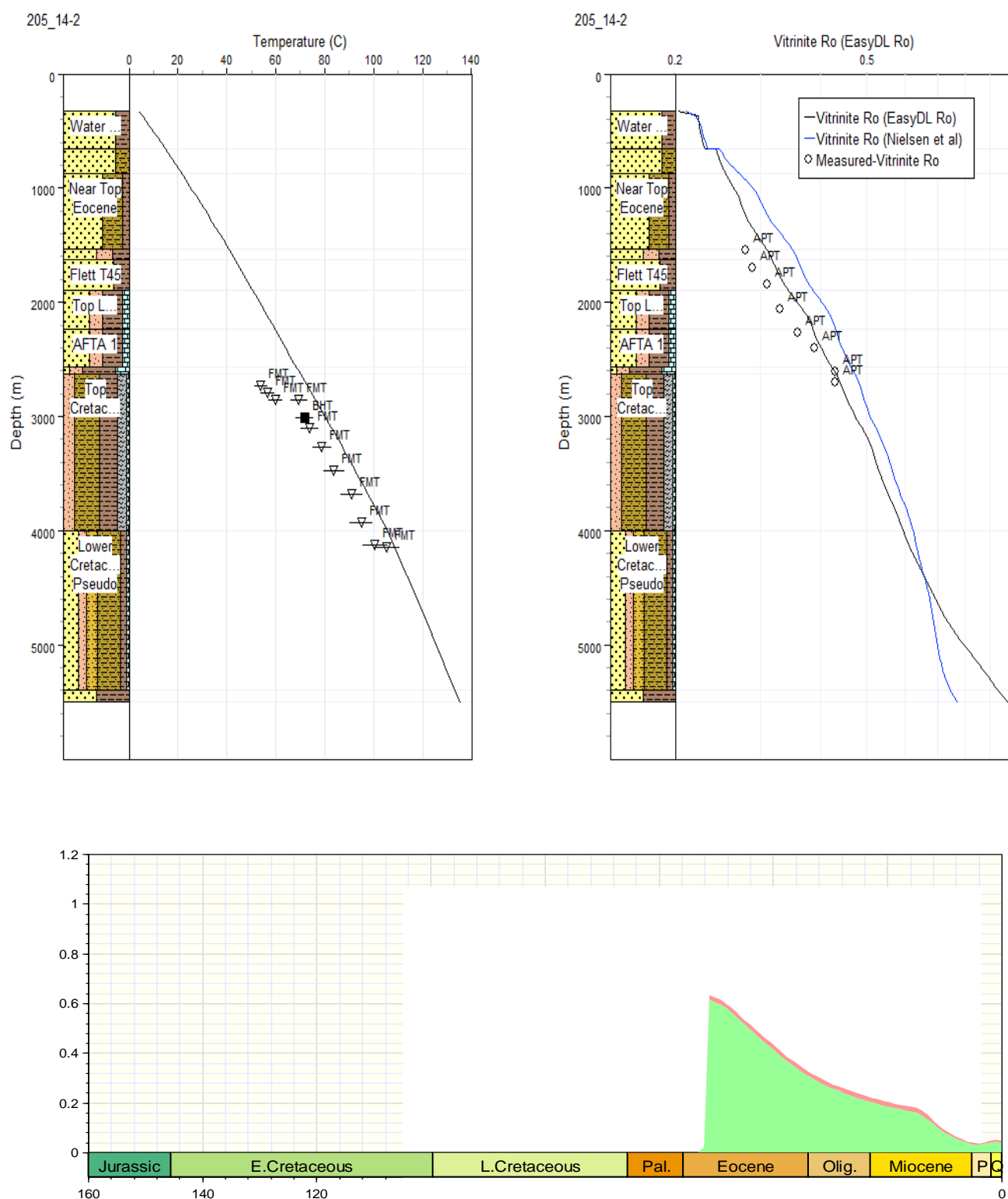


FIGURE 6.5.5 205/14-2 1D basin model temperature & vitrinite reflectivity calibration and modelled KCF source rock expulsion (based on a Pseudo-pick at ~5.4km TVDSS)

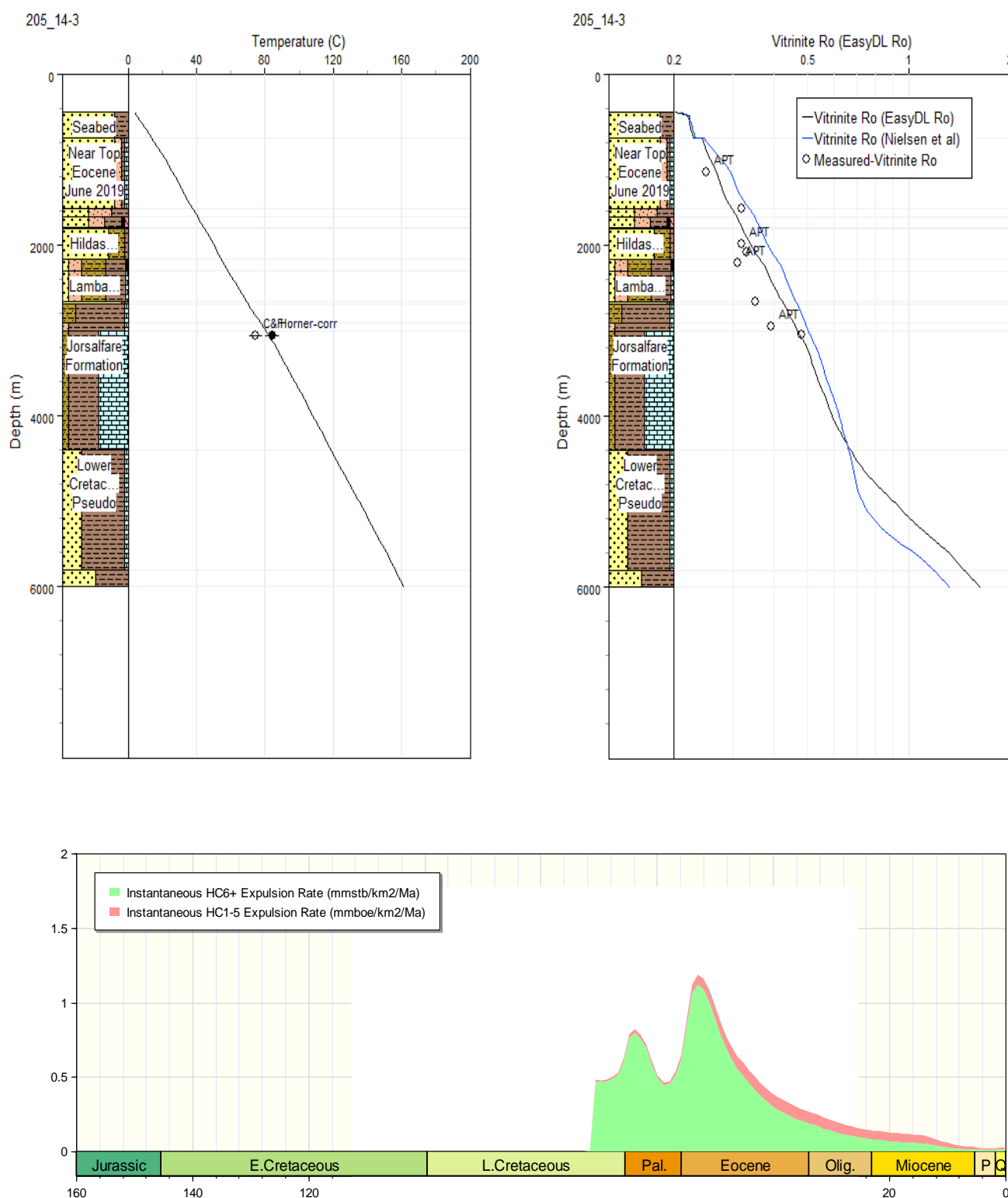


FIGURE 6.5.6 205/14-3 1D basin model temperature & vitrinite reflectivity calibration and modelled KCF source rock expulsion (based on a Pseudo-pick at ~5.8km TVDSS)

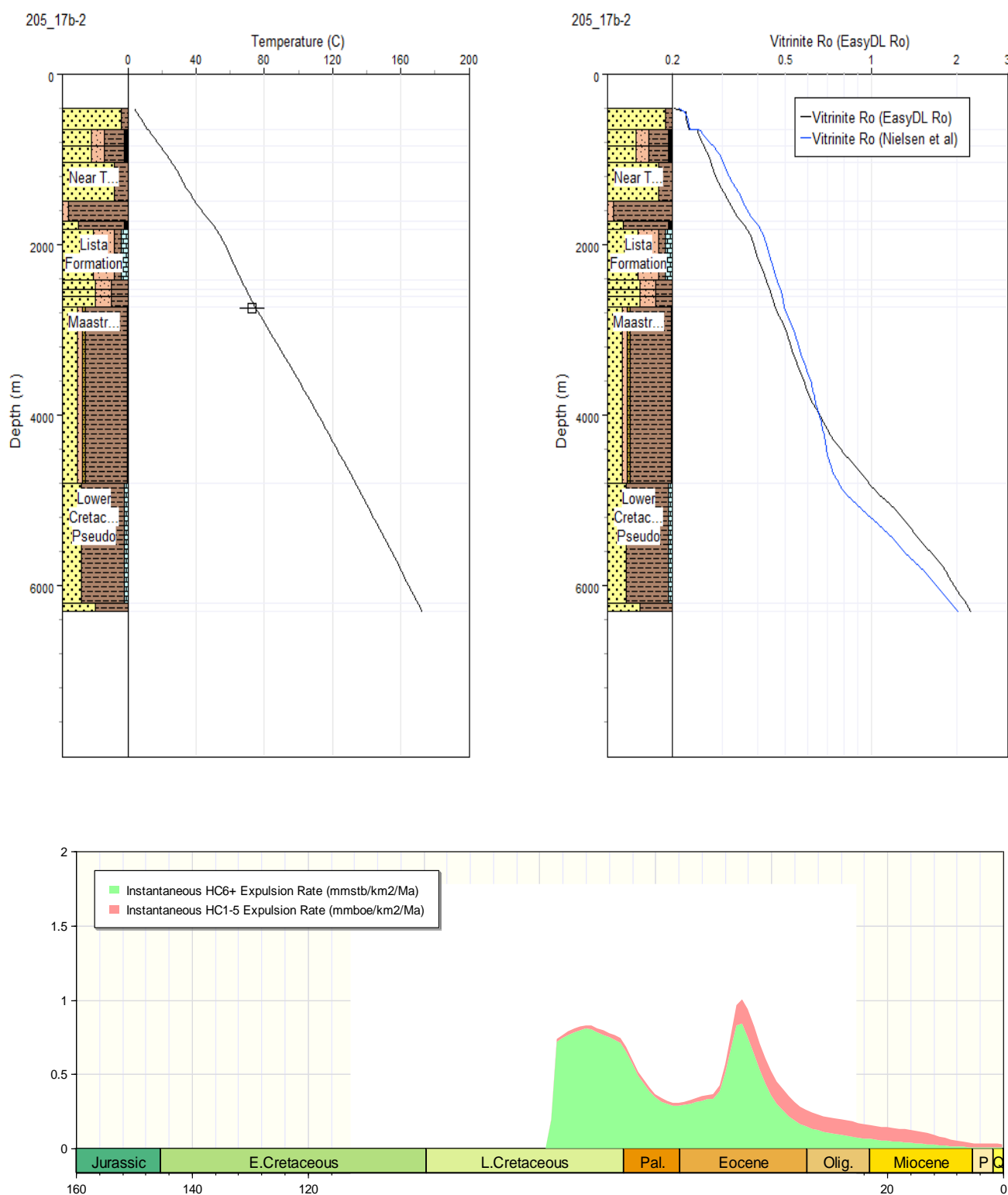


FIGURE 6.5.7 205/17b-2 1D basin model temperature & vitrinite reflectivity calibration and modelled KCF source rock expulsion (based on a Pseudo-pick at ~6.2km TVDSS)

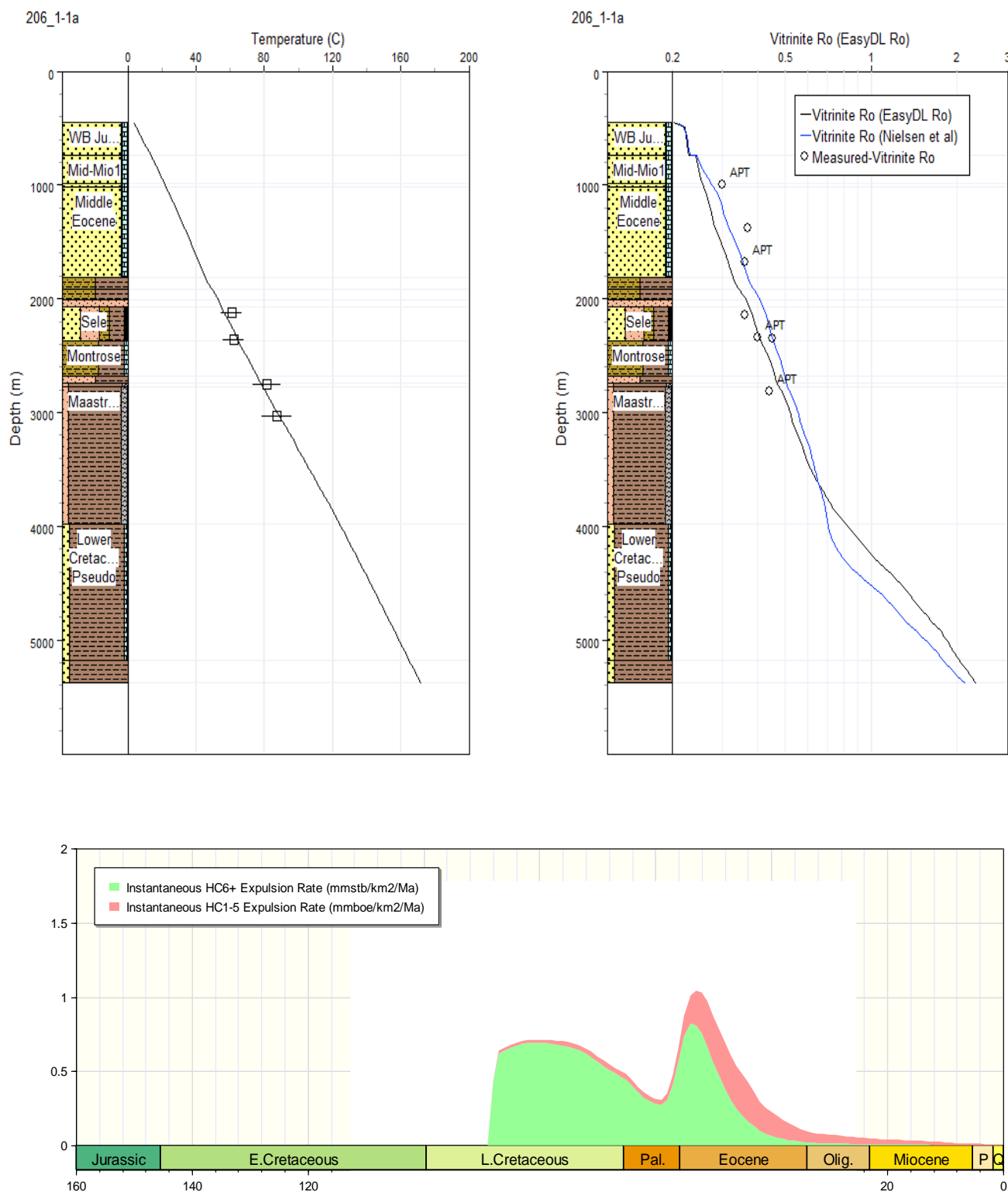


FIGURE 6.5.8 206/1-1a 1D basin model temperature & vitrinite reflectivity calibration and modelled KCF source rock expulsion (based on a Pseudo-pick at ~5.2km TVDSS)

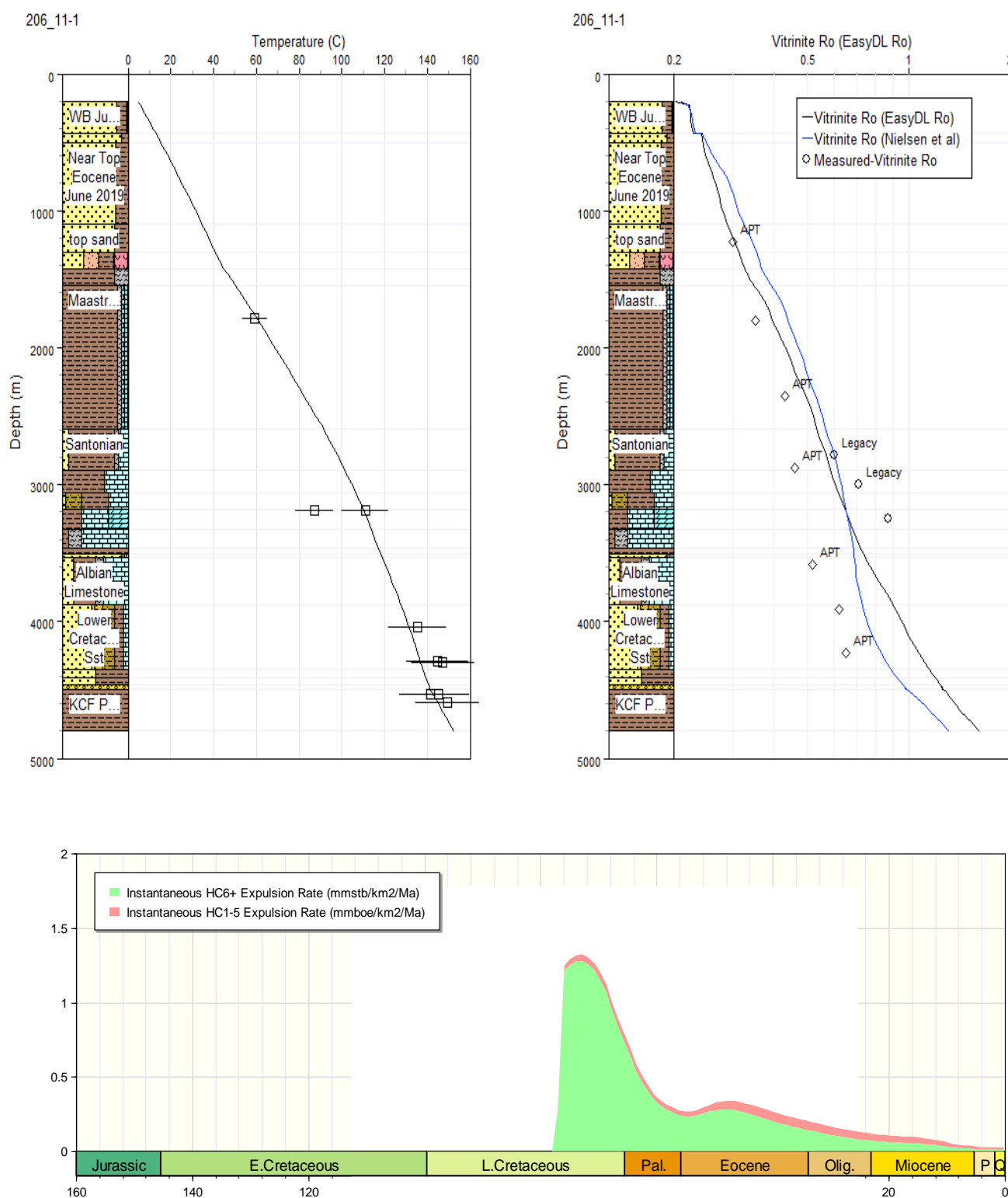
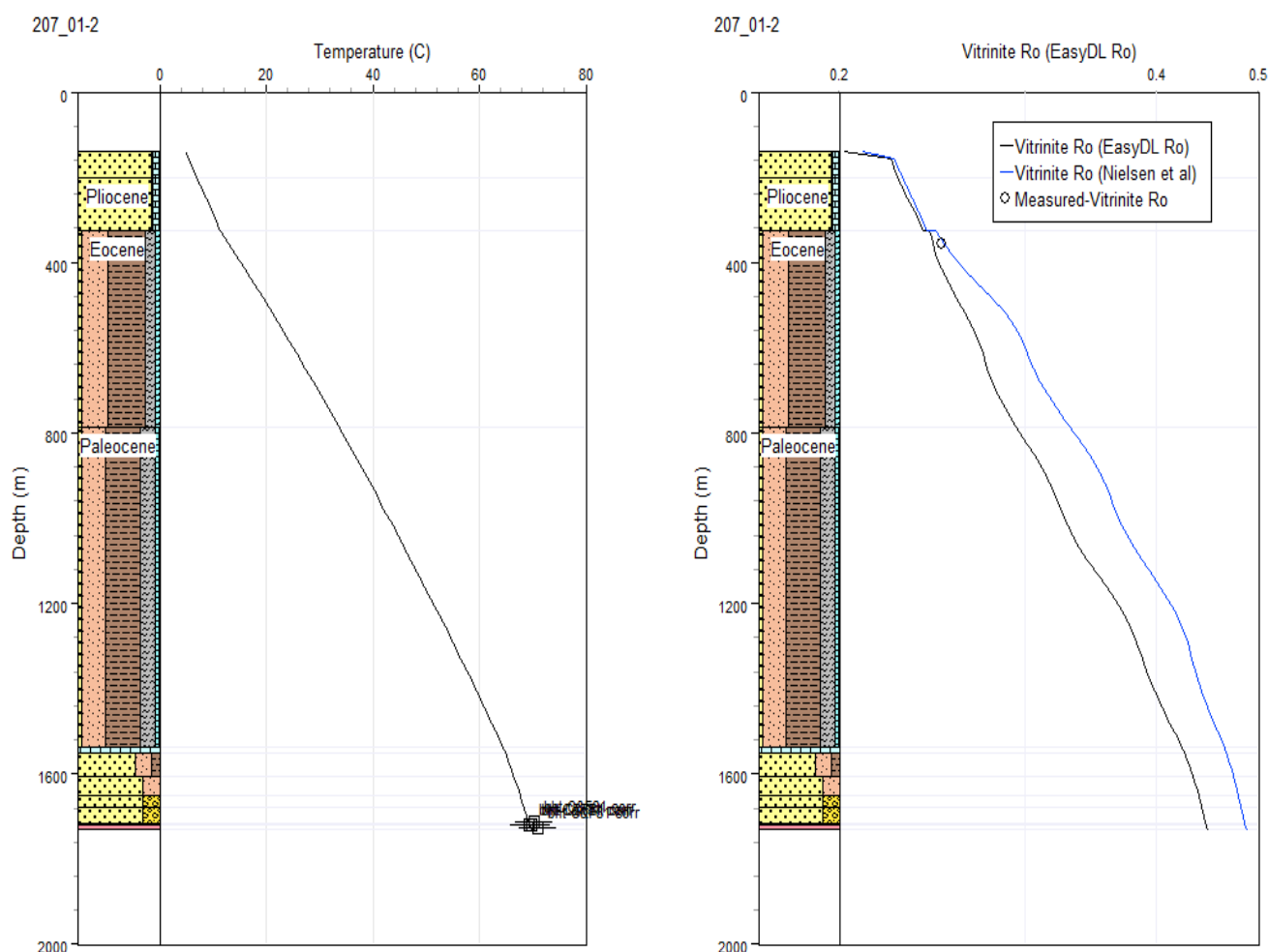


FIGURE 6.5.9 206/11-1 1D basin model temperature & vitrinite reflectivity calibration and modelled KCF source rock expulsion (based on a Pseudo-pick at ~4.5km TVDSS)



No KCF Penetrated (TD in Basement)

FIGURE 6.5.10 207/1-2 1D basin model temperature & vitrinite reflectivity calibration - KCF expulsion not modelled as depth poorly constrained

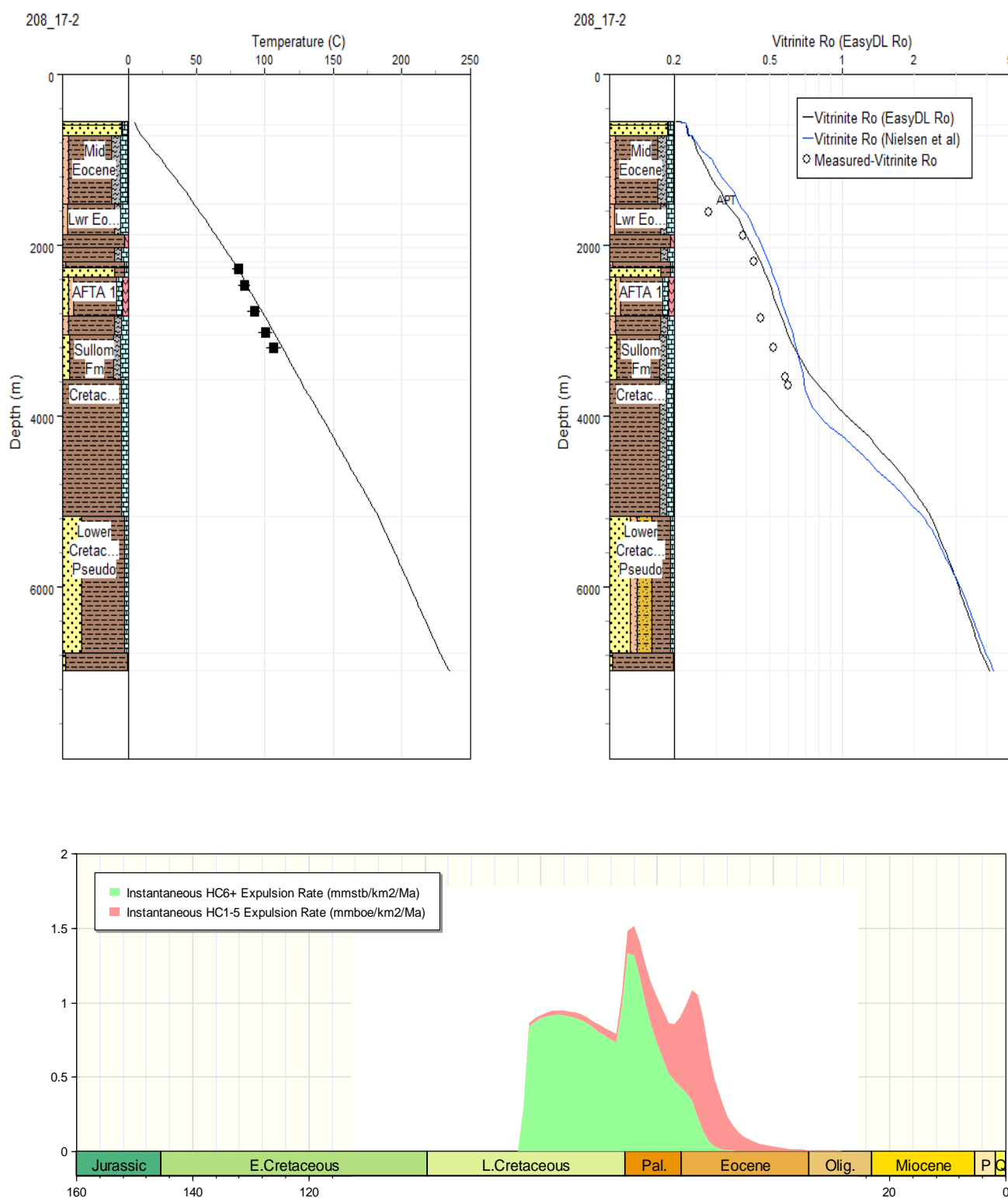
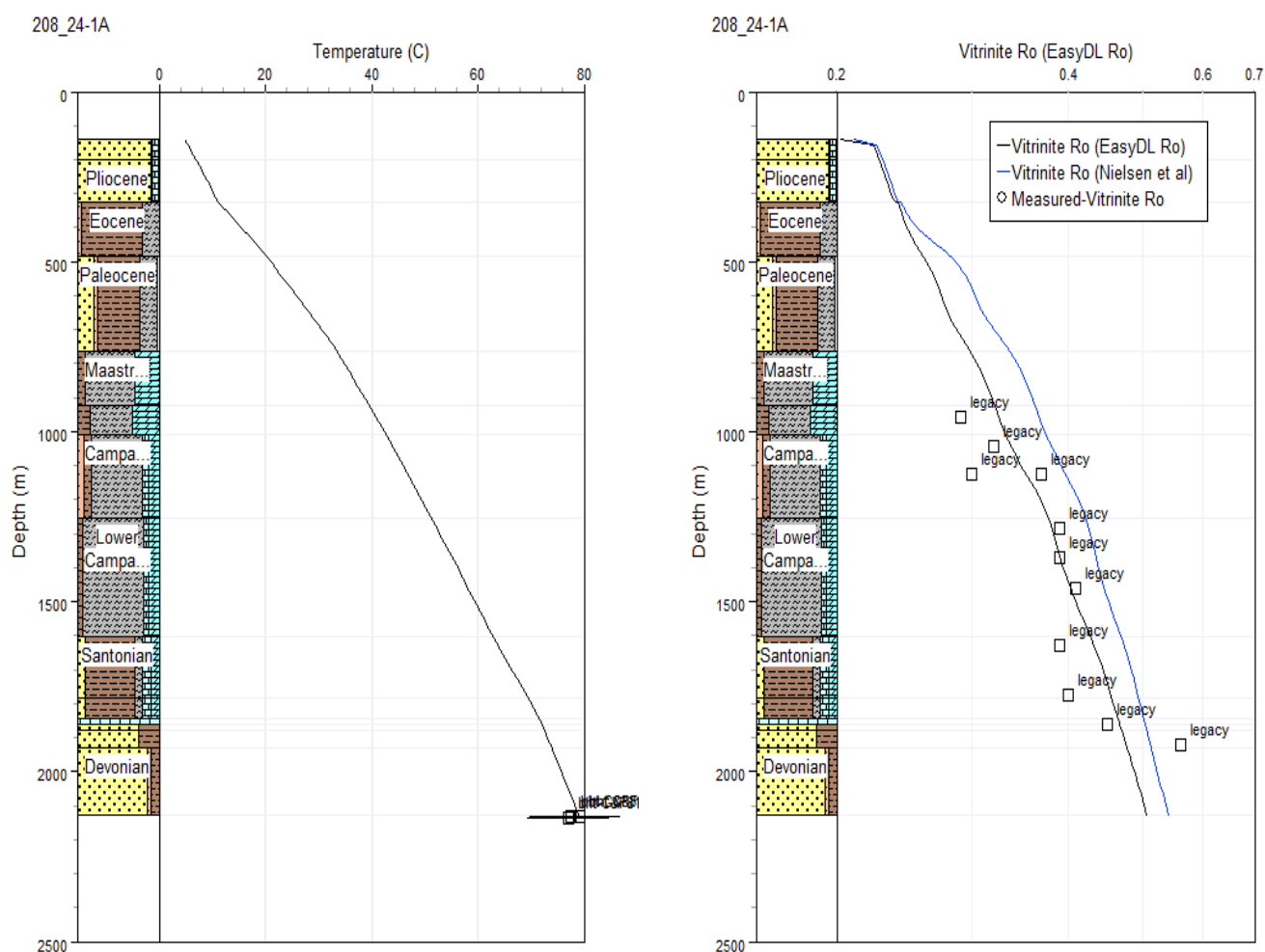
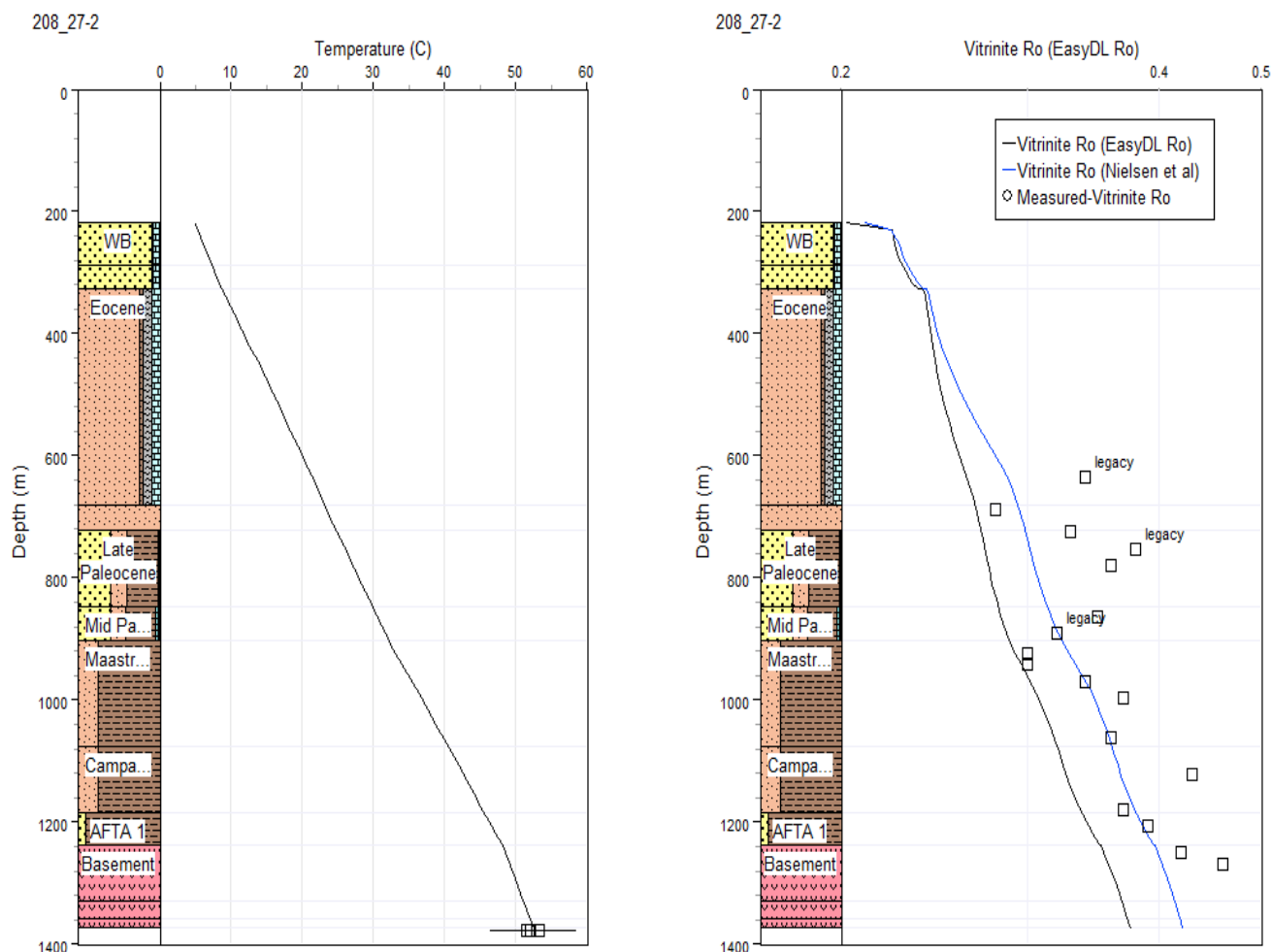


FIGURE 6.5.11 208/17-2 1D basin model temperature calibration and modelled KCF source rock expulsion (based on a Pseudo-pick at ~6.8km TVDSS)



No KCF Penetrated

FIGURE 6.5.12 208/24-1 1D basin model temperature calibration - KCF not modelled as depth poorly constrained



No KCF Penetrated (TD in Basement)

FIGURE 6.5.13 208/27-2 1D basin model temperature calibration - KCF not modelled as depth poorly constrained

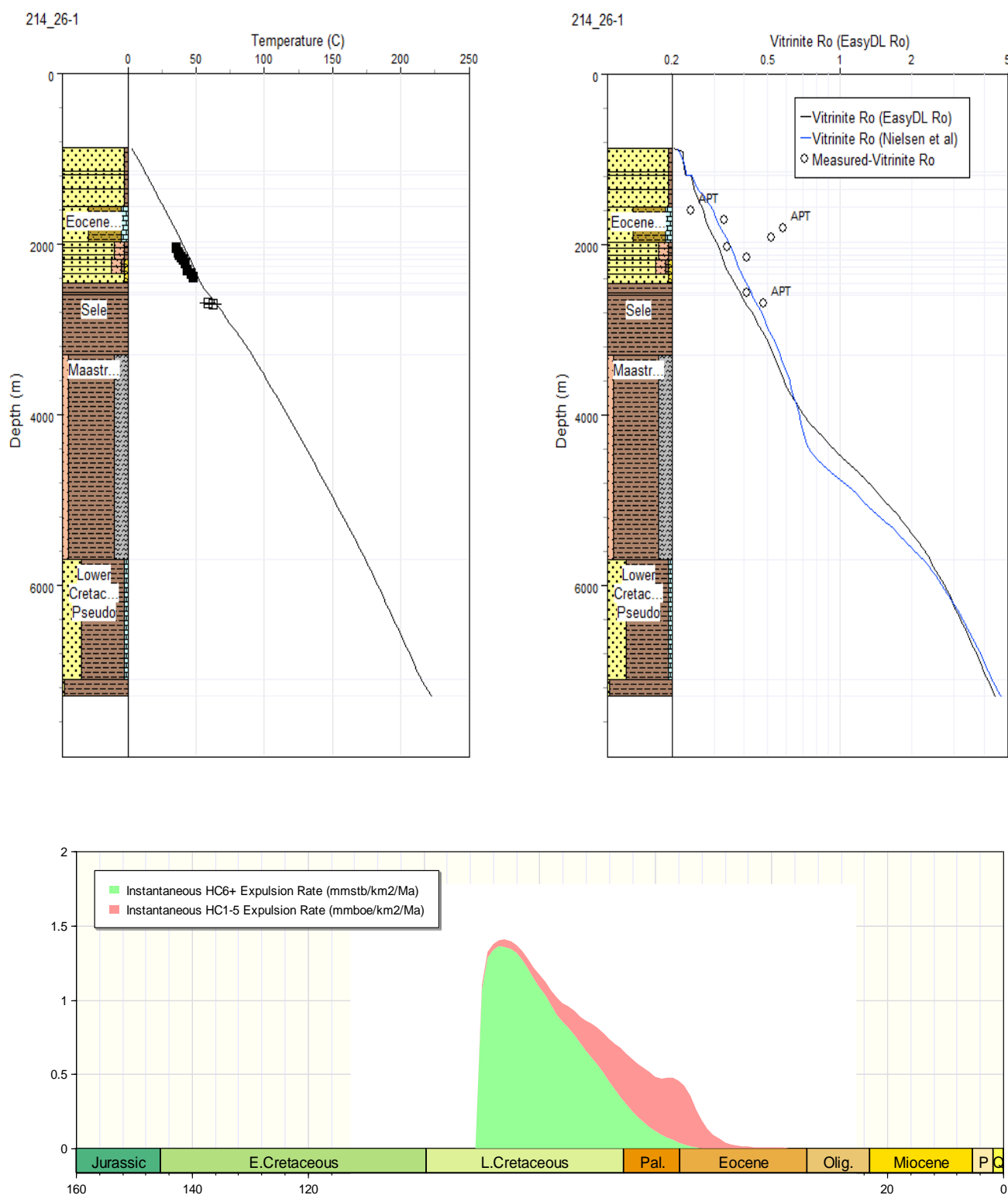


FIGURE 6.5.14 214/26-1 1D basin model temperature & vitrinite reflectivity calibration and modelled KCF source rock expulsion (based on a Pseudo-pick at ~7.1km TVDSS)

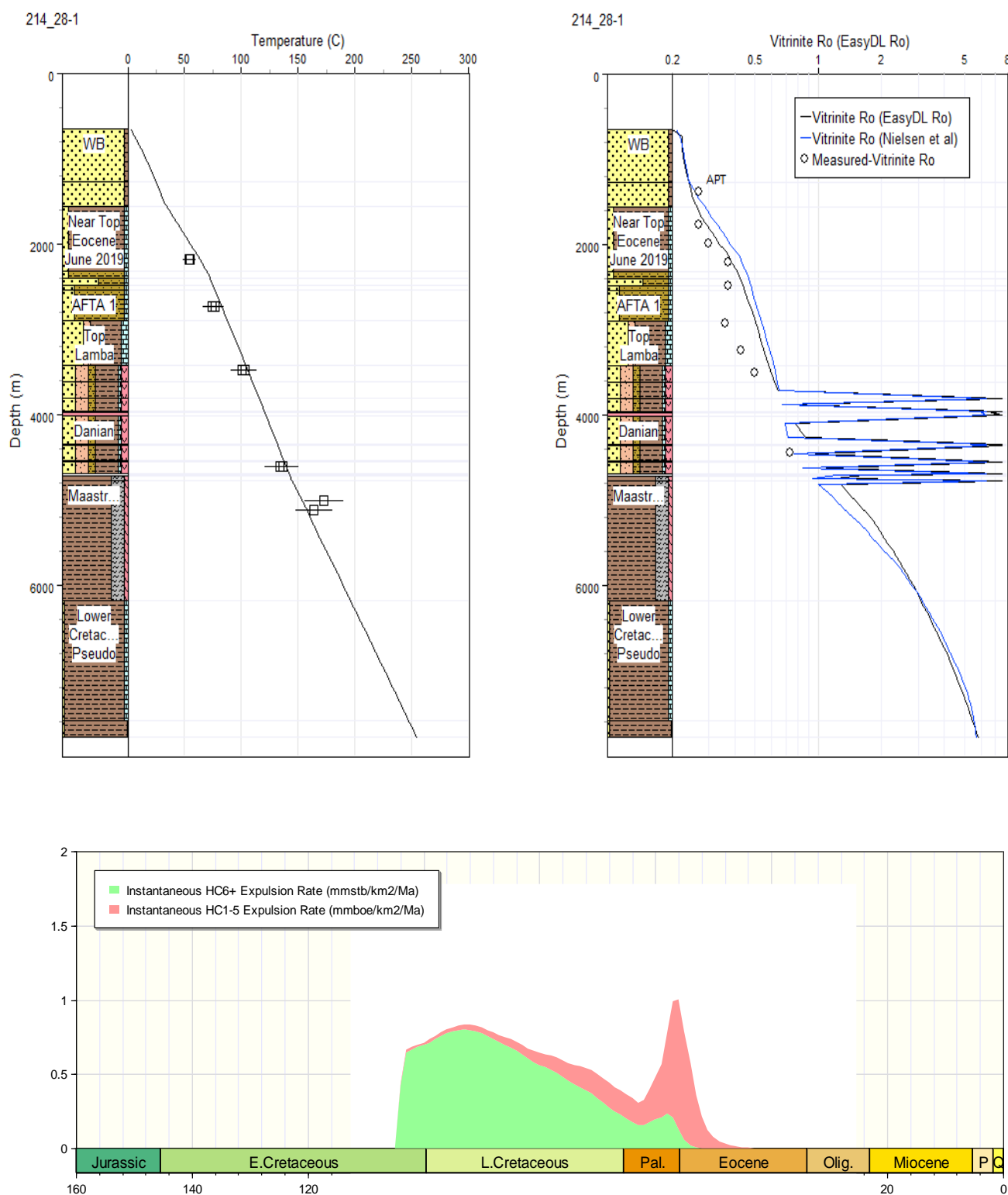


FIGURE 6.5.15 214/28-1 1D basin model temperature & vitrinite reflectivity calibration and modelled KCF source rock expulsion (based on a Pseudo-pick at ~7.6km TVDSS)

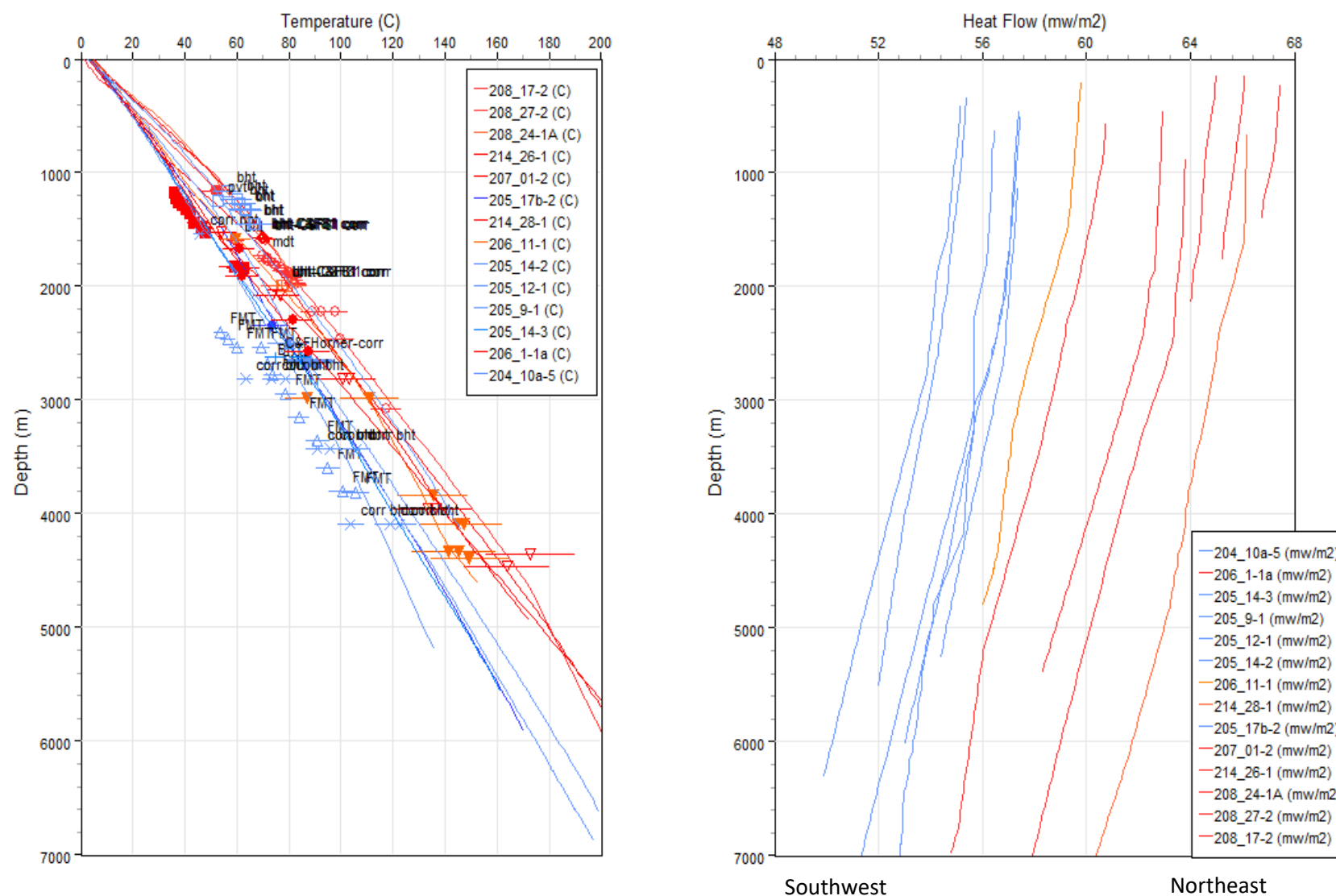


FIGURE 6.5.16 (a) All 1D model geotherms (b) modelled heat flow for the 1D models illustrating the increase in heat flow from SW to NE.

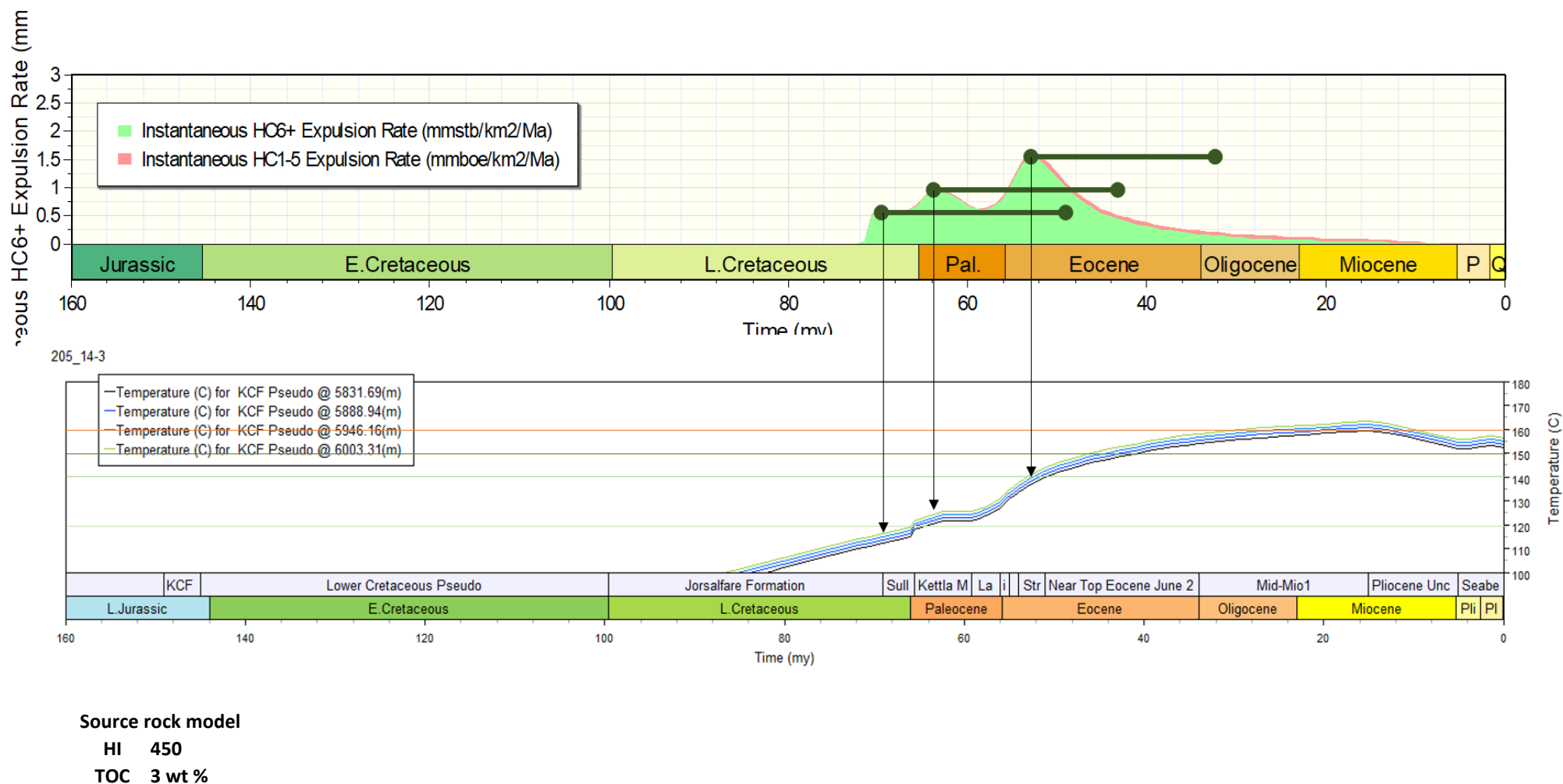


FIGURE 6.5.17 Modelled KCF expulsion profile through time versus the time-temperature history of the KCF layer in the 1D model for 205/14-3

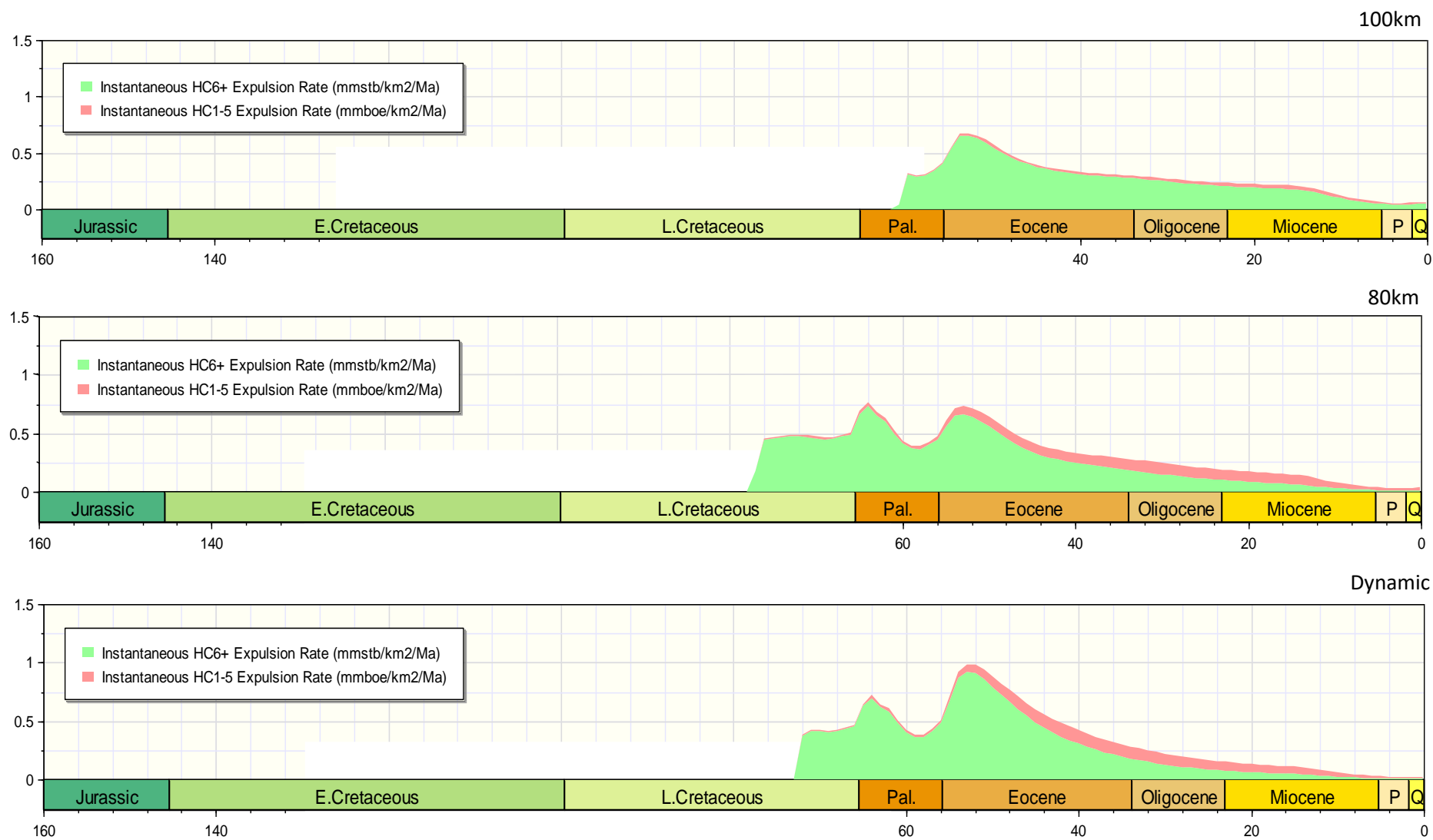


FIGURE 6.5.18 Modelled KCF expulsion profile through time for different LAB models (as shown in Figure 6.4.4) for 205/14-3

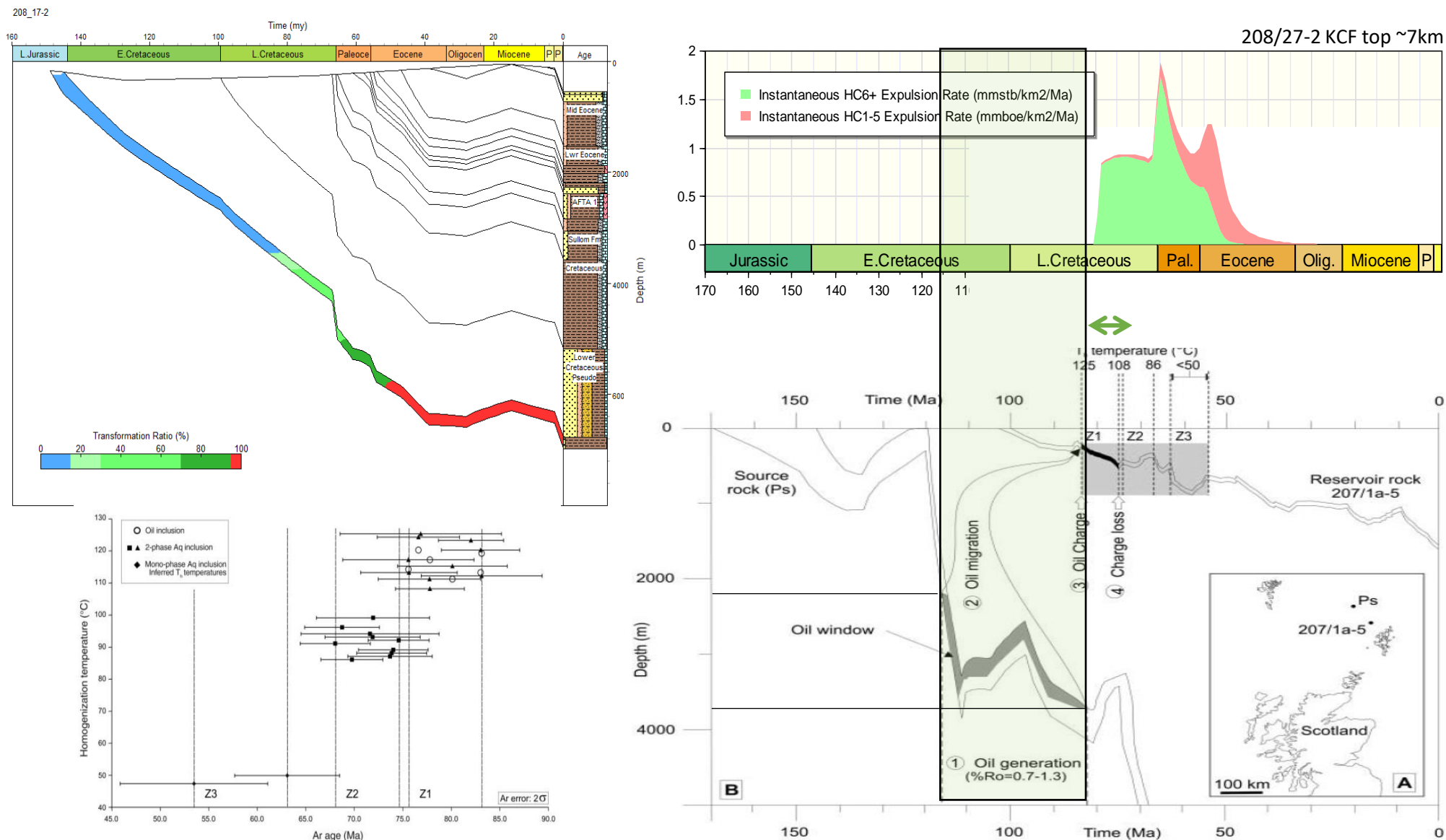


FIGURE 6.5.19 Comparison of the studying modelling with that of Mark et al. (2005)

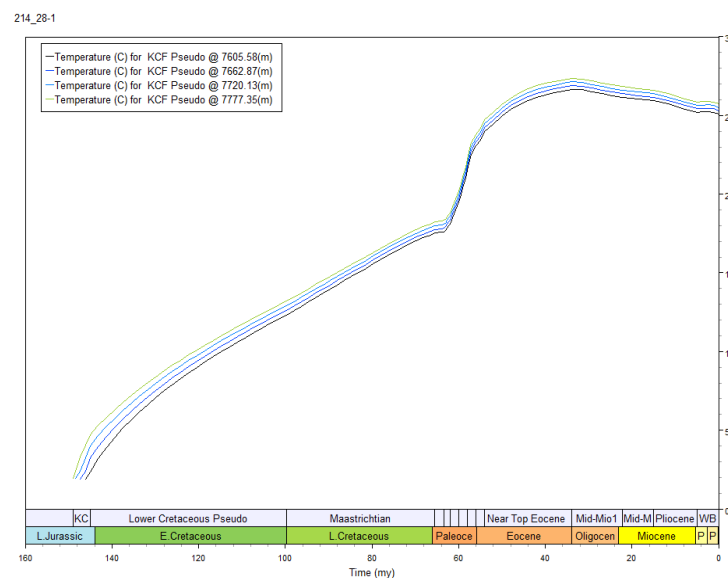
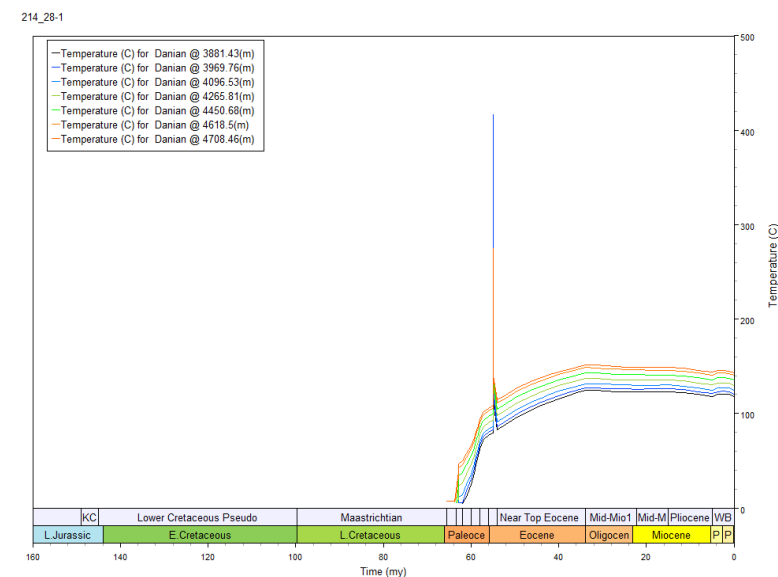
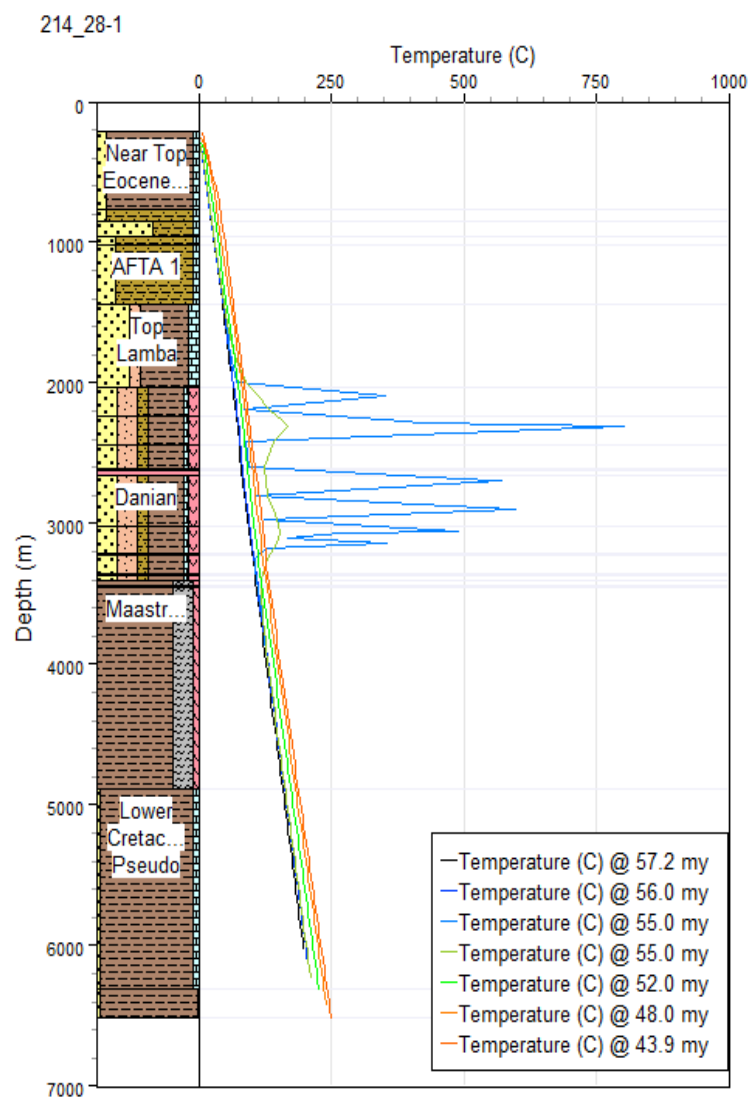
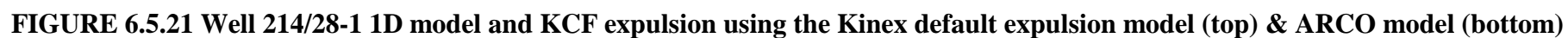


FIGURE 6.5.20 Well 214/28-1 1D model showing the explicit modelling of igneous intrusions in the Paleocene section



6.6 FAROE-SHETLAND BASIN PETROLEUM SYSTEMS

The intent of this section is not to provide a universal view of the petroleum system West of Shetland, but rather to review some misconceptions that have perhaps led to the basin being conceived as more complex than it actually is. This has been partially down to the incorrect parametrisation of basin models (in both thermal history and in expulsion behaviour) but is also due to some outdated concepts and some fundamental misunderstandings around source product and PVT behaviour.

6.6.1 Charge timing – is there a problem?

As referenced previously in this report, numerous studies have performed basin modelling in the West of Shetland and noted that generation seems to occur in the mid- to late- Cretaceous and thus pre-dating the deposition of the proven reservoirs and seals. Several explanations have been put forward to try and explain this mismatch between observed geology and modelled results, such as oil migrating into deeper holding reservoirs before re-migrating into the Palaeocene (e.g. the motel model; Lamer & Carmichael 1999) or overpressure retarding the expulsion of oil from source rock (e.g. Carr & Scotchman, 2003).

Irrespective of the thermal (or pressure) model invoked, areas where the KCF is >8km thick almost certainly have thick Cretaceous sequences, and will therefore also mature early – there is no special complexity here. Fluid inclusion data do record evidence of early charge phases and therefore, at least locally, Cretaceous generation will be expected. Our models, particularly in the Southwest of the AOI are cooler than those based on more conventional parameters and hence we thermally delay the timing of generation. By also invoking expulsion models we further retard the timing of petroleum becoming available for migration.

Additionally, at least in some areas, it seems likely that there will be some degree of migration lag. During hydrocarbon generation, the initial petroleum fluid generated is taken up by the source rock itself (by adsorption to the kerogen and partially filling the pore space in the source rock interval) – this is what is accounted for in the expulsion model. Primary migration out of the source rock then happens, where the lag time between the beginning of generation and primary migration (primary migration lag) depends on the rate of generation, and the volumes required to satisfy adsorption and saturation thresholds (He, 2016). Once the oil enters the first carrier bed, some of the initial volume is used to establish the minimum saturation needed to continue migration, and some of it is used to fill the micro and macro traps before it reaches the potential trap we may drill. This time lag depends on the rate of generation (again), and the saturation and thickness of the “waste zone” formed by the micro traps, and the size and number of larger “traps” it has to fill before reaching our target trap. The typical reservoir explored for in the west of Shetland are rather distal from the source rock. When the target trap is not at the first carrier level but shallower, then the oil has to vertically migrate some distance to reach the trap being considered. In that process, it also has to fill the sand intervals between the first carrier bed and the trap to either spill point or seal capacity. Time will again be consumed as these intermediate traps are being filled introducing a secondary migration lag. Observation and simple estimates will show this time can be very significant, e.g. He (2016) estimates between 10 – 20Ma in the GoM.

Finally, the dynamics of charge and leakage of a trap also impact what is found and can induce an apparent lag. If a field is two-phase and leaking gas then it may be interpreted as a situation

of an oil field being adjacent to a gas-mature kitchen, with the simple interpretation that the oil got there, and the gas is on its way. In actual fact, the gas could have already arrived but leaked out of the traps 'weak' point. This idea is further discussed in the following sections.

Overall, it is not believed that there is any issue with charge timing in the Faroe-Shetland basin and that the discoveries can be accounted for by some combination of:

- Delayed expulsion – due to a function of cooler models (especially in the SW) and appropriate expulsion model(s)
- Migration 'lag' (cf. He, 2016)
- Preservation of oil legs under leaking gas caps.

6.6.2 Misunderstanding of PSA, Faroe-Shetland Basin

Two aspects of petroleum systems are seemingly widely miss-understood in the exploration community. Firstly, that a 'critical' moment can be usefully identified and represented on a one-dimensional plot and secondly, that 'gas mature' means dry gas will be found as a product.

"The Critical Moment"

The 'critical moment' was defined by Magoon & Beaumont (2003) as "the time that best depicts the generation–migration–accumulation of hydrocarbons in a petroleum system; A map and cross section drawn at the critical moment best show the geographic and stratigraphic extent of the system".

The thermal histories modelled for the KCF layer (either penetrated or pseudo) in the wells shown in Figures 6.5.1 to 6.5.14 were used to model the expulsion behaviour in Zetaware's Kinex tool. All models use a standard KCF source rock model (TOC 3%, HI 450). The results are presented in Figure 6.6.1. Inspection of this figure clearly illustrates that picking a single 'critical moment' is neither correct nor helpful.

Maturity vs. Phase prediction

Scotchman *et al.* (2006) stated that "*Hydrocarbon generation modelling in the Faroe–Shetland Basin (FSB) is enigmatic in that the depth of burial suggests that the main Middle and Upper Jurassic source rocks are overmature for hydrocarbon generation. However, the reservoired hydrocarbons comprise largely oil with only minor amounts of oil-associated gases, not the high maturity gas expected from the maturation modelling.*" They went on to propose a complex model in which pressure plays a key role in retarding oil expulsion; however, while a thermodynamic argument is presented, no worked calculations are presented that give an estimation of the magnitude of the impact of this retardation. Moreover, the statement made regarding the maturity state and the fluids discovered fundamentally misunderstands the relationship between maturity and expelled product that was alluded to in section 6.4.7. For an oil-prone source rock, if modelled appropriately, the product in the 'gas-window' is primarily highly volatile oils, rich-gas condensates to wet gases at the very end of the 'gas window'. The assessment of the petroleum system benefits significantly from the integration of pressure-volume-temperature (PVT) data. As an example, in Figure 6.6.2 the PVT report gas oil ratio (GOR; usually a 'flash' GOR) is plotted against the reported saturation pressure (in psi) for a North Sea database. The majority of the samples describe an approximate curve with increasing saturation pressure with increasing GOR, known as the bubble point curve. At GORs of ~5000scf/bbl the data upticks and the saturation pressure now decreases with increasing GOR

– this is the dew point curve. The vast majority of the data fall onto the left-hand side of this inflection point since the basin is dominated by black oils. This is fundamentally a reflection of the petroleum system and that in basins dominated by oil-prone source rocks most of the mass is converted to undersaturated oils. The occurrence of leaner gas condensates at a shallow condition is best explained by the migration and fractionation of richer liquid at depth.

Thus, phase prediction, rather than simply being a simple function of source rock maturity as postulated by Scotchman *et al.* (2006), in practice it requires the integration of a number of elements:

- PT state of the trap (with respect to fluid saturation pressure; P_{sat})
- Charge GOR through time
- Trap geometry – low relief vs high relief
- Seal integrity (of all seal surfaces – top, fault, lateral etc)

Additionally, biodegradation, common in the relatively shallow, cool reservoirs in the Faroe-Shetland Basin will act to decrease a fluids saturation pressure and hence increase a fluids propensity to form a two-phase accumulation (cf. Larter & di Primio, 2005). It should be noted that most of the main oil fields West of Shetland are in fact two-phase (e.g. Clair, Foinaven, Rosebank etc) and would be all be gas fields if they hadn't leaked gas allowing significant oil legs to be preserved.

6.6.3 Oil vs. Gas Geochemistry

An exhaustive review of the fluid geochemistry of the West of Shetland area is beyond the scope of this study and may be subject to future research endeavours. However, the assertion made above that the oil fields of the West of Shetland area existed partially as a result of the leakage of gas from two phase accumulations can potentially be tested by inspection of the gas and liquid geochemistry (which in the case described would not be expected to be in equilibrium).

It is surprisingly difficult to find integrated datasets of both gas and liquid geochemistry data, the value of cross-checking these important data sources is perhaps under appreciated in the industry. The only field for which has both gas data (composition and, crucially, isotopes) and liquid geochemistry data available in the public domain is Schiehallion, which was therefore selected as an example to investigate and compare the gas and liquid geochemistry.

Figure 6.6.3a plots two Schiehallion gas samples on the Chung natural gas plot. For this plot Chung *et al.* (1988) proposed that kinetic isotope effects during kerogen thermal cracking should theoretically produce a straight-line relation between the carbon isotopic compositions of thermogenic gases (methane through butane) on a natural gas plot. Dzou & Milkov (2011) using field calibrations, developed a Chung-plot based nomogram to quantitatively estimate thermal stress of a gas which is shown as a background in Figure 6.6.3.

The Schiehallion data (Figure 6.6.3a) is compared with the data from the Marnock gas condensate field (Figure 6.6.3b) from the central North Sea. In terms of the ethane (C_2) and propane (C_3) isotopes the data are very similar, Schiehallion falls onto a standard thermal stress value of $\sim 170^\circ\text{C}$ whereas Marnock falls between 170°C and 180°C . This is much more mature than would be expected for an oil-associated gas. The pull-down of in the carbon isotope values

of methane (C_1) for the Schiehallion data likely reflects the mixing of secondary microbial methane associated with the biodegradation of the field.

For the liquid geochemistry analysis, two aromatic biomarker maturity parameters, MPR and MPDF 1, were cross plotted together with some calibrated North Sea data as shown in Figure 6.6.4. The aromatic parameters selected were used as they cover a wider range of maturation than perhaps all saturate biomarker parameters. Note, no one parameter or cross plot can universally track maturity – this particular plot is simply used illustratively. Although MPR was favoured over MPI (as the latter implicitly uses phenanthrene in its formula, which has been found to vary according to more complex factors; Szczerba & Rospondek, 2010), the MPR parameter that only uses the methylated isomers was preferred. The MPDF 1 parameter was as it was constructed to obtain an approximately linear correlation with maturity from negatively correlated components (Kvalheim *et al.*, 1987).

What is striking about Figure 6.6.4 is that data from Schiehallion and the other West of Shetland fields plotted (Clair, Foinaven, Loyal) all cluster very tightly, with only the Lancaster field sample plotting at a seemingly higher maturity. It is not known why the West of Shetland data cluster so tightly or why they seem to record a relatively lower MPR value. Notwithstanding these observations, the Schiehallion oil appears to be comparable in maturity to the plotted East Shetland basin oils, which were generated at approximately peak oil maturity ($\sim 135^\circ\text{C}$; it is undoubtedly more complex than this since ‘field’ maturity should really be tracked across a range of compound types and integrated with physical property data).

Taken together it would seem that the gas geochemistry and liquid geochemistry from the Scheihallion field are not in equilibrium, which would be consist with a model of long oil legs being preserved under leaking gas caps.

6.6.4 Re-Os Isotopes

The expulsion timings predicted in the modelling performed here (as shown in Figure 6.6.1) can be cross checked against novel methods proposed for the dating of oil charge events.

The isotopic dating of oils and fluid inclusions published to date on the Faroe-Shetland Basin indicates a range of implied petroleum generation ages, from 68 ± 13 Ma based on Rhenium-Osmium (Re-Os) isotope geochronology (Finlay *et al.*, 2011) to ~ 83 Ma from Ar-Ar dating of feldspars surrounding oil-filled inclusions (Mark *et al.*, 2005). Importantly, these studies show evidence that oil generation did not occur simultaneously across the basin. For example, further Re-Os dating combined with a spatial drill down and new statistical modelling of data presented by Finlay *et al.* (2011) provide a late Cretaceous age of oil generation for the Clair field, a Palaeocene age for the Foinaven/Schiehallion area and a Eocene age of oils in the Faroe sector (Finlay *et al.*, in prep). These estimates are compared with the model estimates performed in this study in Figure 6.6.5 from which it can be seen that there is a relatively strong agreement between these independent methods which lends confidence to both.

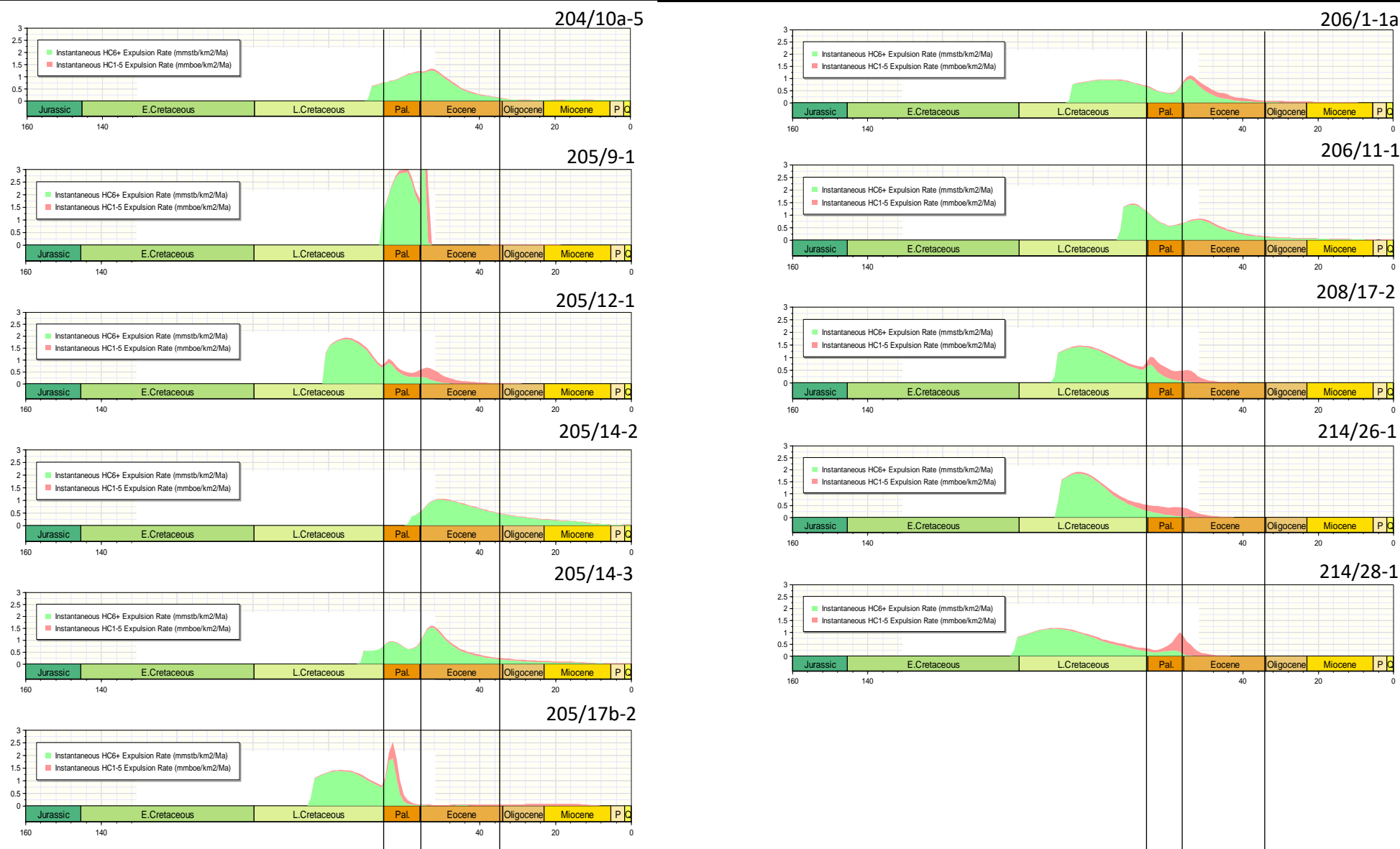


FIGURE 6.6.1 KCF expulsion modelled in Kinex using the ARCO expulsion model and thermal histories modelled for the KCF layer (either penetrated or pseudo) in the wells (Figures 6.5.1 to 6.5.14)

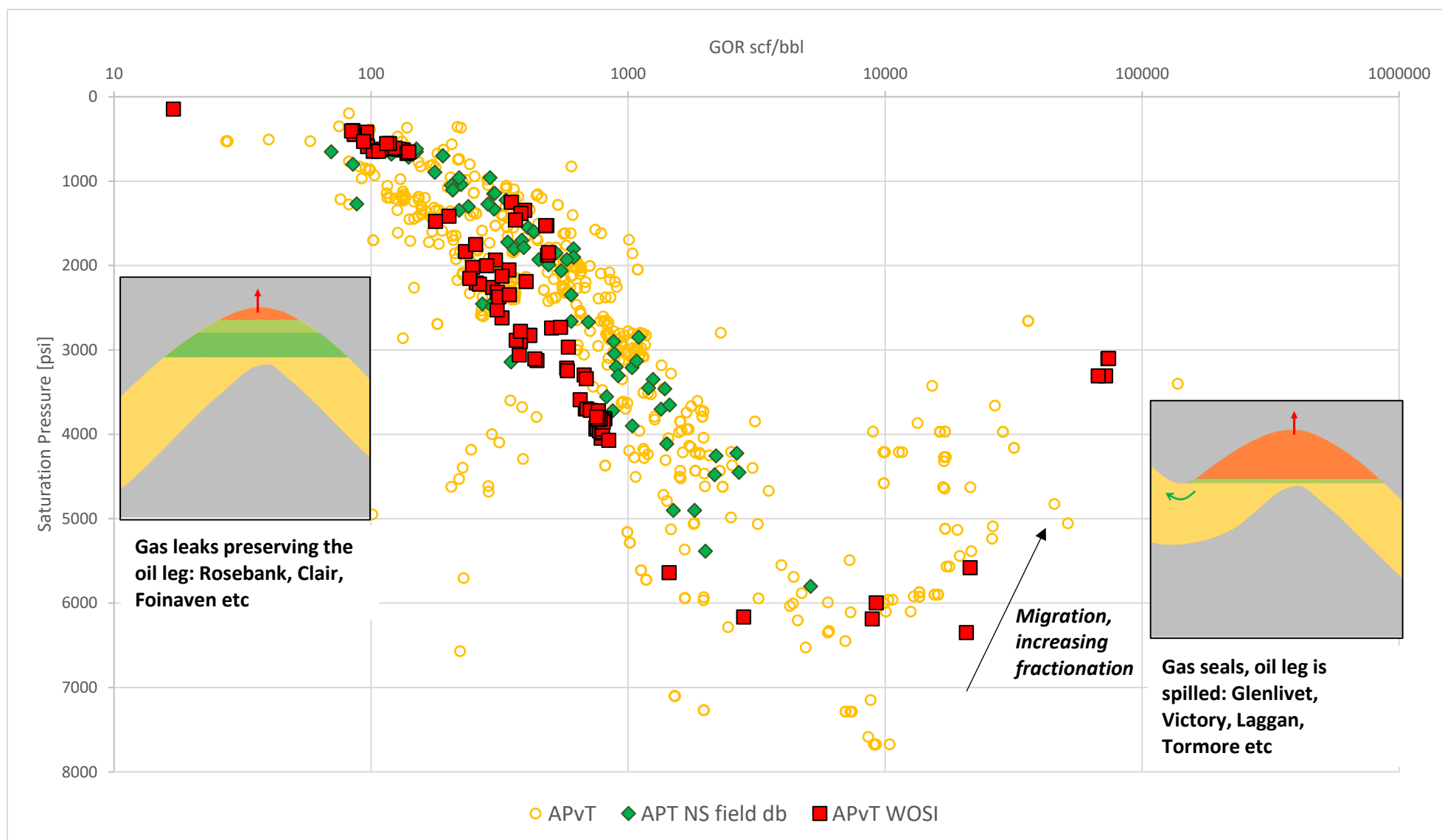


FIGURE 6.6.2 GOR (scf/bbl) vs saturation pressure for UK North Sea (from the APvT database and the APT NS field database)

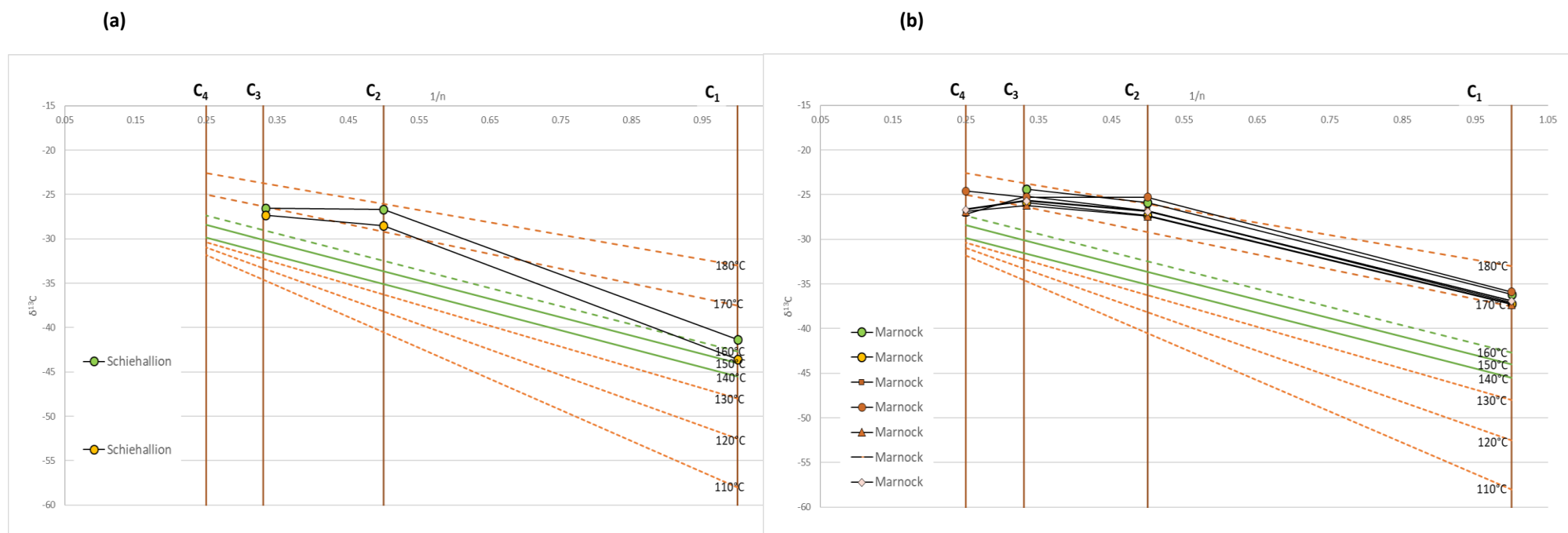


FIGURE 6.6.3 Chung natural gas plot for the (a) Schiehallion and (b) Marnock fields

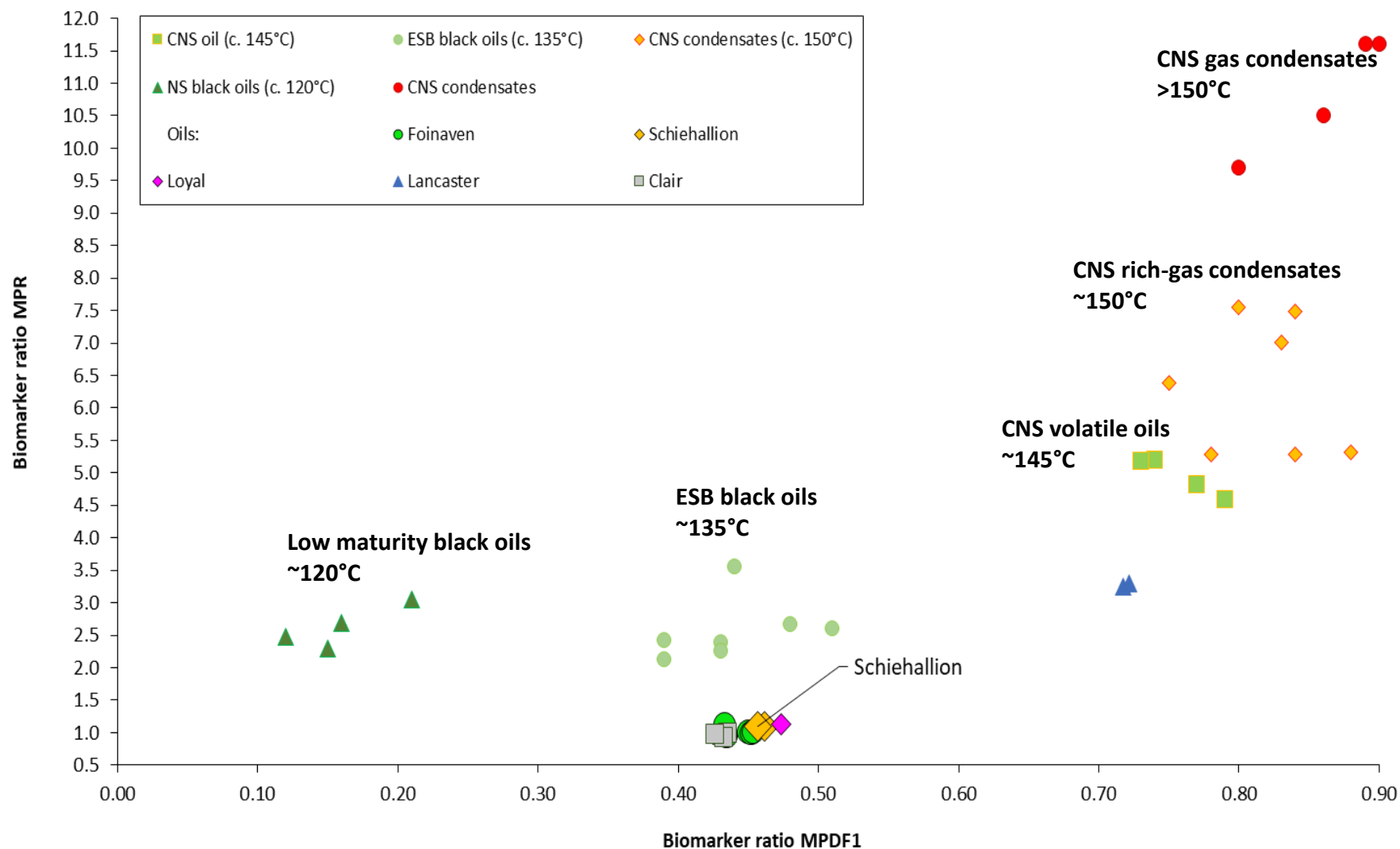


FIGURE 6.6.4 Phenanthrene aromatic biomarker maturity parameters MPR vs MPDF 1 for the North Sea & West of Shetland oils

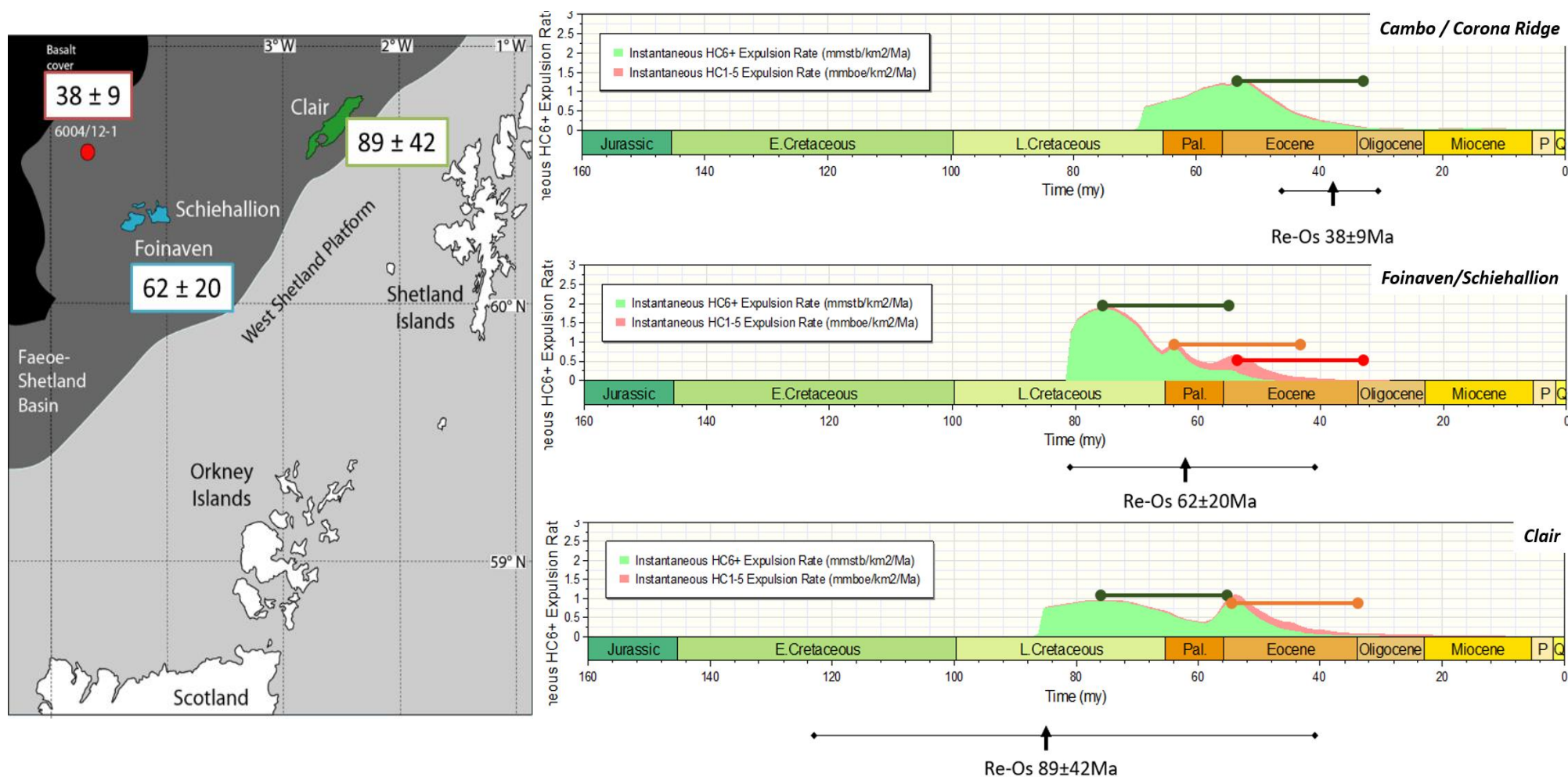


FIGURE 6.6.5 Integration of the Re-Os based oil dating method (Finlay et al. 2011) with the expulsion timing proposed in this study

CHAPTER 7

REFERENCES

- BAU, M., 1991.** Rare-earth element mobility during hydrothermal and metamorphic fluid-rock interaction and the significance of the oxidation state of europium. *Chemical Geology* v.93, no3-4, 219-230.
- BARFOD, G.H., KROGSTAD, E.J., FREI, R., AND ALBAREDE, F., 2005.** Lu-Hf and PbSL geochronology of apatites from Proterozoic terranes: A first look at Lu-Hf isotopic closure in metamorphic apatite. *Geochimica et Cosmochimica Acta*, v. 69, n. 7, 1847-1859.
- BARON, M., PARNELL, J., MARK, D., CARR, A., PRZYJALGOWSKI, M., & FEELY, M. 2008.** Evolution of hydrocarbon migration style in a fractured reservoir deduced from fluid inclusion data, Clair Field, west of Shetland, UK. *Marine and Petroleum Geology*. 25, 153–172
- BLACK, L.P., KAMO, S.L., ALLEN, C.M., DAVIS, D.W., ALEINIKOFF, J.N., VALLEY, J.W., MUNDIL, R., CAMPBELL, I.H., KORSCH, R.J., WILLIAMS, I.S., AND FOUDOULIS, C., 2004.** Improved $^{206}\text{Pb}/^{238}\text{U}$ microprobe geochronology by the monitoring of trace-element-related matrix effect; SHRIMP, ID-TIMS, ELA-ICP-MS and oxygen isotope documentation for a series of zircon standards. *Chemical Geology*, 205, 15-140
- BOYCE, J.W. AND HODGES, K.V., 2005.** U and Th zoning in Cerro de Mercado (Durango, Mexico) fluorapatite: Insights regarding the impact of recoil redistribution of radiogenic ^4He on (U-Th)/He thermochronology. *Chemical Geology*, v. 219, 261-274.
- CARR, A.D., AND SCOTCHMAN, I.C., 2003.** Thermal history modelling in the southern Faroe–Shetland Basin: *Petroleum Geoscience*, v. 9, 333–345.
- CARLSON, W.D., DONELICK, R.A. & KETCHAM, R.A. 1999.** Variability of apatite fission-track annealing kinetics: I. Experimental results. *Am. Mineral.* **84**, 1213-1223.
- CARSTENS, H., AND FINSTAD, K.G., 1981.** Geothermal gradients of the northern North Sea Basin, 59-62 N, In: **ILLING, L.V., & HOBSON, G.D.,** (eds), *Petroleum geology of the continental shelf of north-west Europe: Institute of Petroleum, London.*
- CHAMBERS, L., DARBYSHIRE, F., NOBLE, S., AND RITCHIE, D., 2005.** NW UK Continental Margin: Chronology and Isotope Geochemistry. British Geological Survey Commissioned Report, CR/05/095.
- CHEMOSTRAT REPORT., 2014.** Dating West of Shetland basement using U=Pb Zircon ages: A reconnaissance study, Unpublished report.
- CHEMOSTRAT MULTICLIENT REPORT NE118., 2013.** Chemostratigraphy of Lower Palaeogene sequences, Faroe-Shetland Basin.

CHEW, D.M., BABECHUK, M.G., COGNÉ, N., MARK, C., O’SULLIVAN, G.J., HENRICHS, I.A., DOEPKE, D., AND MCKENNA, C.A., 2016. (LA,Q)-ICPMS trace-element analyses of Durango and McClure Mountain apatite and implications for making natural LA-ICPMS mineral standards. *Chemical Geology*, v. 435, 35-48.

CHEW, D.M. AND DONELICK, R.A., 2012. Combined apatite fission track and U-Pb dating by LA-ICP-MS and its application in apatite provenance analysis. *Quantitative Mineralogy and Microanalysis of Sediments and Sedimentary Rocks: Mineralogical Association of Canada, Short Course*, v. 42, 219–247.

CHEW, D.M., DONELICK, R.A., DONELICK, M.B., KAMBER, B.S. AND STOCK, M., 2014. Apatite Chlorine Concentration Measurements by LA-ICP-MS. *Geostandards and Geoanalytical Research*, v. 38, 23-35.

CHUNG, H.M., GORMLY, J.R., SQUIRES, R.M., 1988. Origin of gaseous hydrocarbons in subsurface environments: Theoretical considerations of carbon isotope distribution. *Chemical Geology* 71, 97–104.

COGNÉ, N., CHEW, D.M., DONELICK, R.A., AND ANSBERQUE, C., 2019. LA-ICP-MS apatite fission track dating: A practical zeta-based approach. *Chemical Geology*, v. 531, no. 119302.

DONELICK, R.A., 1993. A method of fission track analysis utilizing bulk chemical etching of apatite. U.S. Patent Number 5,267,274.

DONELICK, R.A., 1995. A method of fission track analysis utilizing bulk chemical etching of apatite. Australian Patent Number 658,800.

DONELICK, R.A. AND DONELICK, M.B. Unpublished data.

DONELICK, R.A. AND DONELICK, M.B., 2014. Method of determining the concentration of an element in a solid using relative abundances of isotopes from the solid and a reference solid. U.S. Patent Number 8,901,485.

DONELICK, R.A. AND MILLER, D.S., 1991. Enhanced TINT fission track densities in low spontaneous track density apatites using ²⁵²Cf-derived fission fragment tracks: A model and experimental observations. *Nuclear Tracks and Radiation Measurements*, v. 18, no. 3,301-307.

DONELICK, R.A., O’SULLIVAN, P.B., AND DONELICK, M.B., 2009. A discordia-based method of zircon U-Pb dating from LA-ICP-MS analysis of single spots. In P.J. Williams et al., *Smart Science for Exploration and Mining*. James Cook University, Townsville, Australia,. 276-278.

DONELICK, R.A, O’SULLIVAN, P.B., AND KETCHAM, R.A., 2005. Apatite fission-track analysis. *Reviews in Mineralogy and Geochemistry, Mineralogical Society of America*, v. 58,. 49-94.

DZOU, L. & MILKOV, A. 2011. Advanced Interpretations of Stable Isotopic Composition of Gases in Working Petroleum Systems. AAPG Hedberg conference “*Natural gas geochemistry: recent developments, applications, and technologies*”. May 9-12, 2011 – Beijing, China.

ENGLAND, W.A., MACKENZIE, A.S., MANN, D.M. & QUIGLEY, T.M., 1987. The movement and entrapment of petroleum fluids in the subsurface. *Journal of the Geological Society* v. 144; 327 – 347.

ENGLAND, R. W., MCBRIDE, J. H. & HOBBS, R. W. 2005. The role of Mesozoic rifting in the opening of the NE Atlantic: evidence from deep seismic profiling across the Faroe–Shetland Trough. *Journal of the Geological Society*, 162, pp. 661–673.
<http://doi.org/10.1144/0016-764904-076>

FINLAY, A.J., CARR, A., HEDLEY, B., HOLT, B., O'NEIL, P., GARDNER, D AND DARLING, J., 2018. Calculated radioactive heat production from basement & sediments: Implications for basin & petroleum system modelling. PETEX, London.

FINLAY, A.J., SELBY, D & OSBORNE, M.J. 2011. Re-Os geochronology and fingerprinting of United Kingdom Atlantic margin oil: Temporal implications for regional petroleum systems. *Geology* 39 (5), 475-478

FLOWERS, R.M., BOWRING, S.A., TULLOCH, A.J AND KLEPEIS, K.A., 2005. Tempo of burial and exhumation within the deep roots of a magmatic arc, Fiordland, New Zealand. *Geology*, v.33.

GARDINER, D., SCHOFIELD, FINLAY, A.J., N., MARK, N., FORSTER, C., HOLT, L, GROVE, C., & MOORE, J. 2019. Modelling petroleum expulsion in sedimentary basins: the importance of igneous intrusion timing and basement control. *Geology*, v. 47.

GLEADOW, A.J.W. 1981. Fission-track dating methods - what are the real alternatives. *Nucl. Tracks Rad. Meas.* 5, 3-14.

GLEADOW, A.J.W., DUDDY, I.R., GREEN, P.F. & HEGARTY, K.A. 1986a. Fission-track lengths in the apatite annealing zone and the interpretation of mixed ages. *Earth Planet. Sc. Lett.* 78, 245-254.

GLEADOW, A.J.W., DUDDY, I.R., GREEN, P.F. & LOVERING, J.F. 1986b. Confined fission-track lengths in apatite - a diagnostic-tool for thermal history analysis. *Contrib. Mineral. Petr.* 94, 405-415.

GLEADOW, A.J.W., GLEADOW, S.J., BELTON, D.X., KOHN, B.P., KROCHMAL, M.S. & BROWN, R.W. 2009. Coincidence mapping - a key strategy for the automatic counting of fission tracks in natural minerals. *Geol. Soc. Spec. Publ.* 324, 25-36.

GREEN, P.F. 1988. The Relationship between Track Shortening and Fission-Track Age Reduction in Apatite - Combined Influences of Inherent Instability, Annealing Anisotropy, Length Bias and System Calibration. *Earth Planet. Sc. Lett.* 89, 335-352.

GREEN, P.F., DUDDY, I.R., GLEADOW, A.J.W., TINGATE, P.R. & LASLETT, G.M. 1985. Fission track annealing in apatite-track length measurements and the form of the Arrhenius plot. *Nucl. Tracks Rad. Meas.* 10, 323-328.

GREEN, P.F., DUDDY, I.R., GLEADOW, A.J.W., TINGATE, P.R. & LASLETT, G.M. 1986. Thermal annealing of fission tracks in apatite.1. A qualitative description. *Chem. Geol.* **59**, 237-253.

HARTLEY, R.A., ROBERTS, G.G., WHITE, N., & RICHARDSON, C. 2011. Transient convective uplift of an ancient buried landscape. *Nature Geoscience letters*, doi:10.1038/NEGO1191.

HE, Z., 2016. The Most Important Factors in Charge Risking & Best Practices. AAPG Hedberg Conference, “*The Future of Basin And Petroleum Systems Modelling*”, April 3-8, 2016 — Santa Barbara, California, USA.

HOLDSWORTH, R.E., MORTON, A., FREI, D., GERDES, A., STRACHAN, R.A., DEMPSEY, E., WARREN, C., AND WHITHAM, A., 2018. The nature and significance of the Faroe-Shetland Terrane: Linking Archean basement blocks across the North Atlantic: *Precambrian Research*, v. 321, 154–171

HOLE, M.J. & MILLETT, J.M. 2016. Controls of Mantle Potential Temperature and Lithospheric Thickness on Magmatism in the North Atlantic Igneous Province. *Journal of Petrology*, Vol. 57, 2, 417–436

HOLMES, A.J., GRIFFITH, C.E., AND SCOTCHMAN, I.C., 1999. The Jurassic petroleum system of the West of Britain Atlantic margin—An integration of tectonics, geochemistry and basin modelling, in Fleet, A.J., and Boldy, S.A.R., eds., *Petroleum Geology of Northwest Europe—Proceedings of the 5th Conference: Geological Society, London, Petroleum Geology Conference Series 5*, p. 1351–1365.

ILIFFE, J. E., ROBERTSON, A. G., WARD, G. H. F., WYNN, C., PEAD, S. D. M. & CAMERON, M. 1999. The importance of fluid pressures and migration to the hydrocarbon prospectivity of the Faeroe-Shetland White Zone. In: **FLEET, A. J. & BOLDY, S. A. R. (EDS.)** *Petroleum Geology of Northwest Europe: Proceedings of the 5th Conference on the Petroleum Geology of Northwest Europe*. London: The Geological Society.

JARVIS, I AND JARVIS, K.E., 1992A. Inductively coupled plasma-atomic emission spectrometry in exploration geochemistry. In: Hall, G.E.M. (eds) *Geoanalysis, Journal of Geochemical Exploration*, 44, 139-200

JARVIS, I AND JARVIS, K.E., 1992B. Plasma spectrometry in the earth sciences, techniques, applications and future trends. In: Jarvis, I. and Jarvis, K. E. (eds) *Plasma Spectrometry in the Earth Sciences, Chemical Geology*, 95, 1-33

KUIPER, K.F., DEINO, A., HILGEN, P.J., KRIJGSMAN, W., RENNE, P.R., AND WIJBRANS, J.R., 2008. Synchronizing rock clocks of Earth history. *Science*, 320, 500-504.

KVALHEIM, O.M., CHRISTY, A.A., TELNÆS, N., BJØRSETH, A., 1987. Maturity determination of organic matter in coals using the methylphenanthrene distribution. *Geochimica et Cosmochimica Acta* 51, 1883–1888. [https://doi.org/10.1016/0016-7037\(87\)90179-7](https://doi.org/10.1016/0016-7037(87)90179-7)

LAMERS, E., & CARMICHAEL, S.M.M., 1999. The Paleocene deepwater sandstone play West of Shetland, in Fleet, A.J., and Boldy, S.A.R., eds., *Petroleum Geology of Northwest Europe—Proceedings of the 5th Conference: Geological Society, London, Petroleum Geology Conference Series 5*, 645–659

LANPHERE, M.A. AND BAADSRAARD, H., 2001. Precise K-Ar, $^{40}\text{Ar}/^{39}\text{Ar}$, Rb-Sr and U-Pb mineral ages from the 27.5 Ma Fish Canyon Tuff reference standard. *Chemical Geology*, v. 175, 653-671.

LARTER, S., & di PRIMIO, R. 2005. Effects of biodegradation on oil and gas field PVT properties and the origin of oil rimmed gas accumulations. *Organic Geochemistry*, 36, pp. 299–310.

LAWVER, L.A. & MÜLLER, R.D. 1994. The Iceland hotspot track. *Geology*, 22, 311 – 314.

LUDWIG, K.R., 2008. User's manual for Isoplot 3.6: a Geochronological Toolkit for Microsoft Excel. Berkeley Geochronology Center Special Publication, Berkeley.

MAGOON, L.B. & BEAMOUNT, E.A. 1999. Petroleum Systems. In: Exploring for Oil and Gas Traps, Edward A. Beaumont and Norman H. Foster, (eds)., *Treatise of Petroleum Geology, Handbook of Petroleum Geology*.

MARK, D.F., PARNELL, J., KELLEY, S.P., LEE, M., SHERLOCK, S.C., & CARR, A., 2005. Dating of multistage fluid flow in sandstone: *Science*, v. 309, 2048–2051, doi: 10.1126/science.1116034.

MARK, D.F., GREEN, P.F., PARNELL, J., KELLEY, S.P., LEE, M.R., & SHERLOCK, S.C., 2008. Late Paleozoic hydrocarbon migration through the Clair field, west of Shetland, UK Atlantic Margin: *Geochimica et Cosmochimica Acta*, v. 72, 2510–2533, doi: 10.1016/j.gca.2007.11.037.

MCDONOUGH, W.F. AND SUN, S.S., 1995. The Composition of the Earth. *Chemical Geology*, v. 120, 223-253.

MCDOWELL, F.W., MCINTOSH, W.C., AND FARLEY, K.A., 2005. A precise $^{40}\text{Ar}/^{39}\text{Ar}$ reference age for the Durango apatite (U-Th)/He and fission-track dating standard. *Chemical Geology*, v.214, n.3-4, 249-263.

MIHALFFY, P., STEINBERGER, B. & SCHMELING, H. 2008. The effect of the large-scale mantle flow field on the Iceland hotspot track. *Tectonophysics*, 447, pp. 5 – 18.

MORSE, S.J. 2013. The supply of siliclastic input to potential late Paleocene sub-basalt reservoirs in the Faroe Shetland Basin. Unpublished MSc thesis, Royal Holloway University of London.

PACES, J.B. AND MILLER, J.D., 1993. Precise U-Pb ages of Duluth Complex and related mafic intrusions, north-eastern Minnesota: Geochronological insights to physical, petrogenic, paleomagnetic, and tectonomagmatic processes associated with the 1.1 Ga Midcontinent Rift System. *Journal of Geophysical Research*, v. 98, no. B8, p. 13997-14013.

PARK, R.G.; STEWART, A.D.; WRIGHT, D.T. 2003. The Hebridean terrane. *In*: Trewin N.H. (ed.). *The Geology of Scotland*. London: Geological Society. 45–61. ISBN 978-1-86239-126-0.

PARNELL, J., CAREY, P.F., GREEN, P., & DUNCAN, W., 1999. Hydrocarbon migration history, west of Shetland: Integrated fluid inclusion and fission track studies, *in* Fleet, A.J., and Boldy, S.A.R., eds., *Petroleum geology of Northwest Europe: Proceedings of the 5th Conference*: London, Geological Society of London, p. 613–625.

PARNELL, J., GREEN, P.F., WATT, G., & MIDDLETON, D., 2005. Thermal history and oil charge on the UK Atlantic margin: *Petroleum Geoscience*, v. 11, p. 99–112, doi: 10.1144/1354-079304-618.

PATTON, C., HELLSTROM, J., PAUL, B., WOODHEAD, J. AND HERGT, J., 2011. Lolite: freeware for the visualization and processing of mass spectrometry data. *Journal of Analytical Atomic Spectroscopy*, 26, 2508–2518.

PERSANO, C., BARFOD, D.N., STUART, F.M., BISHOP, P., 2007. Constraints on early Cenozoic underplating-driven uplift and denudation of western Scotland from low temperature thermochronometry. *Earth Planet. Sci. Lett.* 263, 404 – 419.

POLLACK, H. N. & CHAPMAN, D. S. 1977. On the regional variation of heat flow, geotherms, and lithospheric thickness. *Tectonophysics*, 38, 279–296.

PRAEG, D., STOKER, M.S., SHANNON, P.M., CERAMICOLA, S., HJELSTUEN, B., J.S., LABERG & MATHIESEN, A. 2005. Episodic Cenozoic tectonism and the development of the NW European ‘passive’ continental margin. *Marine and Petroleum Geology*, 22, 1007 – 1030.

PRENSKY, S. 1992. Temperature measurements in boreholes: An overview of engineering and scientific applications. *Log Analyst*, 33(3), pp. 313–333.

PURVIS, K., DENNIS, P., HOLT, L. & MARCA, A. 2020. The origin of carbonate cements in the Hildasay reservoir, Cambo Field, Faroe-Shetland Basin; clumped isotopic analysis and implications for reservoir performance. *Marine and Petroleum Geology*, 122, 104641.

RENNE, P.R., SWISHER, C.C., DEINO, A.L., KARNER, D.B., OWENS, T.L., AND DEPAOLO, D.J., 1998. Intercalibration of standards, absolute ages and uncertainties in $^{40}\text{Ar}/^{39}\text{Ar}$ dating. *Chemical Geology*, v. 45, p. 117–152.

RIPPINGTON, S., MAZUR, S. & WARNER, J. 2015. The crustal architecture of the Faroe–Shetland Basin: insights from a newly merged gravity and magnetic dataset. Geological Society, London, Special Publications, 421, 169–196.

RITCHIE, J. D., JOHNSON, H., QUINN, M. F. & GATLIFF, R. W. 2008. The effects of Cenozoic compression within the Faroe–Shetland Basin and adjacent areas. *In*: Johnson, H., Dore, A. G., Gatliff, R. W., Holdsworth, R. E., Lundin, E. R. & Ritchie, J. D. (eds) *The Nature and Origin of Compression in Passive Margins*. Geological Society, London, Special Publications, 306, 121–136, <http://doi.org/10.1144/SP306.5>

RITCHIE, J.D., NOBLE, D., DARBYSHIRE, F., MILLAR, I., AND CHAMBERS, L., 2011. Pre-Devonian. BGS Research Report RR/11/01 In: Ritchie, J.D., Ziska, H., Johnson, H., Evans, D. (Eds.), *Geology of the Faroe-Shetland Basin and Adjacent Areas*, 71–78.

ROBERTS, A. W., WHITE, R. S. & CHRISTIE, P. A. F. 2009. Imaging igneous rocks on the North Atlantic rifted continental margin. *Geophysical Journal International*, 179, 1024–1038.

RODEN, M.K., PARRISH, R.R., AND MILLER, D.S., 1990. The absolute age of the Eifelian Tioga ash bed. *Journal of Geology*, v. 98, 282-285.

RUDOLPH, K.W. & F.J. GOULDING., 2017. Benchmarking exploration predictions and performance using 20+ years of drilling results: One company's experience: *AAPG, Bulletin*, v. 101, pp. 161-176.

SANDWELL, D. T. & SMITH, W. H. F. 2009. Global marine gravity from retracked Geosat and ERS-1 altimetry: Ridge segmentation v. spreading rate. *Journal of Geophysical Research*, 114, B01411.

SAVITZKY, A. AND GOLAY, M.J.E., 1964. Smoothing and differentiation of data by simplified least square procedure. *Analytical Chemistry*, v. 44, no. 11, 1906-1909.

SCHOENE, B. AND BOWRING, S.A., 2006. UPb systematic of the McClure Mountain syenite: thermochronological constraints on the age of the $^{40}\text{Ar}/^{39}\text{Ar}$ standard MMhb. *Contributions to Mineralogy and Petrology*, v. 151, 615-630.

SCOTCHMAN, I.C., CARR, A.D. & PARNELL, J. 2006. Hydrocarbon generation modelling in multiple rifted and volcanic basin: A case study in the Foinaven Sub-basin, Faroe-Shetland Basin, UK Atlantic margin. *Scottish Journal of Geology*, 42, 1–19.

SIRCOMBE, K.N., 2004. Age Display: an EXCEL workbook to evaluate and display univariate geochronological data using binned frequency histograms and probability density distributions. *Computers & Geosciences*, 30, 21-31.

SHAW CHAMPION, M.E., WHITE, N.J., JONES, S.M., & LOVELL, J.P.B. 2008. Quantifying transient mantle convective uplift: An example from the Faroe-Shetland basin. *Tectonics*, Vol 27, TC1002, doi:10.1029/2007TC002106.

STRANNE, C. & O'REGAN, M. 2016. Conductive heat flow and nonlinear geothermal gradients in marine sediments—observations from Ocean Drilling Program boreholes. *Geo-Marine Letters*, 36, 25 – 33.

STREULE, M.J., STRACHAN, R.A., SEARLE, M.P., & LAW, R.D. 2010. Comparing Tibet-Himalayan and Caledonian crustal architecture, evolution and mountain building processes. *Geological Society, London, Special Publications*, 335, 207-232, <https://doi.org/10.1144/SP335.10>

SYNDES, M., FJELDSKAAR, W., GRUNNALEITE, I., FJELDSKAAR LØTVEIT, I., & MJELDE, R. 2019. Transient Thermal Effects in Sedimentary Basins with Normal Faults and

Magmatic Sill Intrusions – A Sensitivity Study. *Geosciences*, 9, 160; doi:10.3390/geosciences9040160.

SZCZERBA, M., ROSPONDEK, M.J., 2010. Controls on distributions of methylphenanthrenes in sedimentary rock extracts: Critical evaluation of existing geochemical data from molecular modelling. *Organic Geochemistry*, 41, pp. 1297–1311.

VERMEESCH, P., 2012. On the visualisation of detrital age distributions. *Chemical Geology*, 312-313, 190-194.

VILÀ, M., FERNÁNDEZ, M., AND JIMÉNEZ-MUNT, I., 2010. Radiogenic heat production variability of some common lithological groups and its significance to lithospheric thermal modelling: *Tectonophysics*, v. 490, p. 152–164, <https://doi.org/10.1016/j.tecto.2010.05.003>.

WEILL, D.F. AND DRAKE, M.J., 1973. Europium anomaly in plagioclase feldspar: experimental results and semiquantitative model. *Science* v.180 no. 4090, pp. 1059-1060.

WILKINSON, C.M., GANERØD, M., HENDRIKS, H., & EIDE, E.A. 2016. Compilation and appraisal of geochronological data from the North Atlantic Igneous Province (NAIP). In: **PERON-PINVIDIC, G., HOPPER, J. R., STOKER, M. S., GAINA, C., DOORNENBAL, J. C., FUNCK, T. & ARTING, U. E.** (eds) *The NE Atlantic Region: A Reappraisal of Crustal Structure, Tectonostratigraphy and Magmatic Evolution*. Geological Society, London, Special Publications, 447.

WYCHERLEY, H.L., PARNELL, J., WATT, G.R., CHEN, H., & BOYCE, A.J., 2003. Indicators of hot fluid migration in sedimentary basins: Evidence from the UK Atlantic Margin: *Petroleum Geoscience*, v. 9, p. 357–374, doi: 10.1144/1354-079303-569.

ZIMMERMANN, S., MARK, C., CHEW, D., AND VOICE, P.J., 2017. Maximising data and precision from detrital zircon U-Pb analysis by LA-ICPMS: The use of core-rim ages and the single-analysis concordia age. *Sedimentary Geology*, 375, 5-13.

DATA APPENDICES

APPENDIX 1	INORGANIC GEOCHEMISTRY DATA
APPENDIX 2	APATITE FISSION TRACK DATA
APPENDIX 3	OPTICAL MATURITY DATA
APPENDIX 4	PROVENANCE IMPLICATIONS SUMMARY
APPENDIX 5	METHODS

APPENDIX 1

INORGANIC GEOCHEMISTRY DATA

APPENDIX 1.1 Summary of samples analysed for inorganic geochemistry

APPENDIX 1.2 Radioactive heat production and Zircon/Apatite geochronology data

APPENDIX 1.3 Petrology and X-Ray diffraction analysis summary

APPENDIX 1.4 Mineral, fracture and bitumen point count analysis data

APPENDIX 1.1

SUMMARY OF SAMPLES ANALYSED FOR INORGANIC GEOCHEMISTRY

Tables

Ap1.1.1

Sample details – inorganic geochemistry analyses

Well	Top depth	Bottom depth	Units (m/ft)	Stratigraphy	Age	Sample type	Washed (y/n)	Basin	Mud system	Anal. reason	Anal. status
154/03-1	-	8060.0	ft	Laxford Basement	Lax	COCH	-	West Lewis	WBM (KCl/NaCl PHPA polymer)	IN GEO	P
164/25-2	2727.7	2727.8	m	Lewisian Basement	PrCam	COCH	-	North East Rockall	?WBM	IN GEO	P
202/02-1	-	3950.0	ft	Precambrian Basement	PrCam	DC	y	Solan	WBM (Seawater gel)	IN GEO	N
	-	4002.0				COCH	-			IN GEO	P
202/03-1A	-	1774.6	m	Precambrian Basement	PrCam	COCH	-	Solan	WBM (Seawater & MgSO)	IN GEO	P
202/08-1	-	5446.6	ft	Lewisian Basement	PrCam	COCH	-	Solan	?WBM	IN GEO	N
	-	5457.3				COCH	-			IN GEO	N
	-	5500.0				DC	n			IN GEO	N
	-	5510.0				DC	n			IN GEO	N
	-	5520.0				DC	n			IN GEO	N
202/09-1	-	5379.0	ft	Lewisian Basement	PrCam	COCH	-	Solan	WBM (SW gel & lignosulphonate)	IN GEO	N
204/10-1	-	2499.0	m	Precambrian Basement	PrCam	COCH	-	Corona	WBM (KCl, bentonite & Aqua Drill)	IN GEO	P
	-	2505.0				DC	y			IN GEO	N
	-	2508.0				DC	y			IN GEO	N
	-	2511.0				DC	y			IN GEO	N
	-	2514.0				DC	y			IN GEO	N
204/15-2	-	12467.0	ft	Precambrian Basement	PrCam	DC	Unkn.	Westray	WBM (KCl, Aquacol polymer)	IN GEO	P
204/23-1	-	3847.2	m	Precambrian Basement	PrCam	COCH	-	Westray	OBM (Fazeclean)	IN GEO	P
204/25-1	-	9417.0	ft	Precambrian Basement	PrCam	COCH	-	Rona	WBM (KCl polymer)	IN GEO	P
204/26-1A	-	8689.9	ft	Lewisian Basement	PrCam	COCH	-	Judd High	OBM (XP07)	IN GEO	P
204/27a-1	-	2136.3	m	Precambrian Basement	PrCam	COCH	-	Judd High	WBM (KCl polymer)	IN GEO	P
204/28-1	-	1941.6	m	Precambrian Basement	PrCam	COCH	-	Judd High	?WBM	IN GEO	P
205/16-1	4172.0	4172.2	m	Lewisian Basement	PrCam	COCH	-	Lewisian Basement	OBM (Shaledrill)	IN GEO	P
	-	4274.2				COCH	-			IN GEO	N
	-	4274.4				COCH	-			IN GEO	N
	-	4274.6				COCH	-			IN GEO	N
	-	4275.3				COCH	-			IN GEO	N
	-	4300.0				DC	y			IN GEO	N

TABLE Ap1.1.1 Sample details - inorganic geochemistry analyses

Well	Top depth	Bottom depth	Units (m/ft)	Stratigraphy	Age	Sample type	Washed (y/n)	Basin	Mud system	Anal. reason	Anal. status
205/16-1	-	4305.0	m	Lewisian Basement	PrCam	COCH	-	Rona	OBM (Shaledrill)	IN GEO	P
	-	4310.0				COCH	-			IN GEO	N
	-	4314.0				COCH	-			IN GEO	N
205/20-1	-	2017.5	m	Lewisian Basement	PrCam	COCH	-	Rona Ridge	WBM (SW & FLC-LC polymer)	IN GEO	P
205/21-1A	-	4449.0	ft	Lewisian Basement	PrCam	COCH	-	Rona Ridge	?WBM	IN GEO	N, P
	-	4465.0	ft			COCH	-			IN GEO	N, P
205/22-1A	3225.5	3225.6	m	Precambrian Basement	PrCam	COCH	-	Rona	WBM (Barite, CMC, lignite & FCL)	IN GEO	P
206/07a-2	-	2140.7	m	Lewisian Basement	PrCam	COCH	-	Clair-Victory Ridge	OBM (BCM)	IN GEO	P
	-	2141.3				COCH	-			IN GEO	P
	-	2146.7				COCH	-			IN GEO	N
	-	2147.9				COCH	-			IN GEO	N
	-	2246.4				COCH	-			IN GEO	N
	-	2438.3				COCH	-			IN GEO	P
	-	2442.6				COCH	-			IN GEO	N
	-	2443.2				COCH	-			IN GEO	P
	-	2443.2				COCH	-			IN GEO	N
	-	2506.5				COCH	-			IN GEO	N
	-	2543.7				COCH	-			IN GEO	N
	-	2593.3				COCH	-			IN GEO	N
	-	2593.3				COCH	-			IN GEO	P
	-	2593.4				COCH	-			IN GEO	P
	-	2599.4				COCH	-			IN GEO	P
	-	2596.0				COCH	-			IN GEO	N
	-	2598.0				COCH	-			IN GEO	N
206/08-1A	-	2306.4	m	Precambrian Basement	PrCam	COCH	-	Clair-Victory Ridge	WBM (Hicell & lignosulphonate)	IN GEO	L
	-	2311.0	m			COCH	-			IN GEO	P
206/08-2	-	1859.0	m	Precambrian Basement	PrCam	COCH	-	Clair-Victory Ridge	?WBM	IN GEO	P
	-	1864.6	m			COCH	-			IN GEO	P

TABLE Ap1.1.1 Sample details - inorganic geochemistry analyses

Well	Top depth	Bottom depth	Units (m/ft)	Stratigraphy	Age	Sample type	Washed (y/n)	Basin	Mud system	Anal. reason	Anal. status
206/08-7	-	2320.5	m	Basement	PrCam	COCH	-	West Shetland	OBM (Enviromul)	IN GEO	P
206/08-8	-	2499.0	m	Basement	PrCam	COCH	-	Clair-Victory Ridge	OBM	IN GEO	P
206/09-2	-	8084.0	ft	Lewisian Basement	PrCam	COCH	-	Clair-Victory Ridge	WBM (Gel, FCL & IDFLO)	IN GEO	P
206/12-1	-	5630.0	ft	Lewisian Basement	PrCam	COCH	-	Clair-Victory Ridge	WBM (Barite & lignosulphonate)	IN GEO	P
	-	5632.0	ft			COCH	-			IN GEO	P
207/01-3	-	4576.3	ft	Precambrian Basement	PrCam	COCH	-	Clair-Victory Ridge	WBM (Seawater gel & lignosulphonate)	IN GEO	N
	-	4670.0	ft			DC	y			IN GEO	N
	-	4680.0	ft			DC	y			IN GEO	N
	-	4690.0	ft			DC	y			IN GEO	N
	-	4700.0	ft			DC	y			IN GEO	N
	-	4706.0	ft			DC	y			IN GEO	N
207/02-1	-	6722.0	ft	Precambrian Basement	PrCam	COCH	-	West Shetland	?WBM	IN GEO	N
	-	6723.0	ft			COCH	-			IN GEO	N
	-	6724.0	ft			COCH	-			IN GEO	N
208/23-1	-	9795.5	ft	Lewisian Basement	PrCam	COCH	-	Clair-Victory Ridge	WBM (Seawater, gypsum & lignosulphonate)	IN GEO	P
	-	9796.5	ft			COCH	-			IN GEO	N
	-	6799.2	ft			COCH	-			IN GEO	N
	-	6803.0	ft			COCH	-			IN GEO	N
	-	6806.1	ft			COCH	-			IN GEO	N
	-	6808.0	ft			COCH	-			IN GEO	N
208/26-1	-	3894.0	m	Precambrian Basement	PrCam	COCH	-	Foula	WBM (KCl polymer)	IN GEO	P
208/27-1	-	1380.2	m	Precambrian Basement	PrCam	-	-	Clair-Victory Ridge	WBM (Polymer)	IN GEO	L
208/27-2	-	4452.5	ft	Lewisian Basement	PrCam	COCH	-	Clair-Victory Ridge	WBM (Seawater & Polymer mud)	IN GEO	P
	-	4522.2	ft			COCH	-			IN GEO	N
	-	4527.5	ft			COCH	-			IN GEO	N
	-	4528.8	ft			COCH	-			IN GEO	P
	-	4531.2	ft			COCH	-			IN GEO	N
	-	4532.0	ft			COCH	-			IN GEO	N

TABLE Ap1.1.1 Sample details - inorganic geochemistry analyses

Well	Top depth	Bottom depth	Units (m/ft)	Stratigraphy	Age	Sample type	Washed (y/n)	Basin	Mud system	Anal. reason	Anal. status
209/09-1	-	8850.0	ft	Caledonian Basement	Sil	COCH	-	Northern Faroe-Shetland	WBM (Gypsum & CMC)	IN GEO	N
	-	8854.0	ft			COCH	-			IN GEO	N
	-	8855.0	ft			COCH	-			IN GEO	N
209/12-1	-	11385.7	ft	Caledonian Basement	Sil	COCH	-	Northern Faroe-Shetland	WBM (Seawater & polymer mud)	IN GEO	N
	-	11500.0	ft			DC	y			IN GEO	N
	-	11510.0	ft			DC	y			IN GEO	N
	-	11520.0	ft			DC	y			IN GEO	N
	-	11521.0	ft			DC	Unkn.			IN GEO	L
	-	11525.0	ft			COCH	y			IN GEO	N
	-	11526.0	ft			COCH	y			IN GEO	P
	-	11527.0	ft			COCH	y			IN GEO	N
214/09-1	-	11580.7	ft	Precambrian Basement	PrCam	DC	Unkn.	Northern Faroe-Shetland	WBM (KCl silicate polymer)	IN GEO	P
220/26-1	-	5280.2	m	Caledonian Basement	Sil	COCH	y	Northern Faroe-Shetland	OBM (Energol 8313)	IN GEO	P

Abbreviations/Key

DC: Ditch cuttings
COCH: Core chip
Unkn.: Unknown
WBM: Water base mud
OBM: Oil base mud
SW: Seawater
IN GEO: Inorganic geochemistry
N: New analyses for this study
P: Published data
L: Legacy Chemostrat data

Stratigraphy/Ages/Basins

E1: Early Eocene
P3: Late Paleocene
K2: Late Cretaceous
J3: Late Jurassic
Sil: Silurian
Lax: Laxfordian Basement
PrCam: Precambrian

TABLE Ap1.1.1 Sample details - inorganic geochemistry analyses

APPENDIX 1.2

RADIOACTIVE HEAT PRODUCTION AND ZIRCON/APATITE GEOCHRONOLOGY DATA

Tables

Ap1.2.1	Radioactive heat production and Zircon/Apatite geochronology data
---------	---

Well	Bottom depth	Units (m/ft)	Stratigraphy	Age	Sample type	Radioactive Heat Production (RHP)		Zircon Geochronology				Apatite Geochronology			
						RHP (μWm^3)	Data Source	Zircon Age	$\pm 2\sigma$ (Ma)	Zircon Event	Data Source	Apatite Age	$\pm 2\sigma$ (Ma)	Apatite Event	Data Source
154/03-1	8060.0	ft	Laxford Basement	Lax	COCH	0.36	Chambers <i>et al.</i> (2005)	-	-	-	-	-	-	-	-
164/25-2	2727.8	m	Lewisian Basement	PrCam	COCH	0.06	Chambers <i>et al.</i> (2005)	-	-	-	-	-	-	-	-
202/02-1	3950.0	ft	Precambrian Basement	PrCam	DC	1.78	NEW	-	-	-	-	-	-	-	-
	4002.0				COCH	0.85	Chambers <i>et al.</i> (2005)	2829.0	46.0	Neoproterozoic	Ritchie <i>et al.</i> (2011)	-	-	-	-
202/03-1	1774.6	m	Precambrian Basement	PrCam	COCH	0.2	Chambers <i>et al.</i> (2005)	-	-	-	-	-	-	-	-
202/08-1	5446.6	ft	Lewisian Basement	PrCam	COCH	0.38	NEW	-	-	-	-	-	-	-	-
	5457.3				COCH	0.24		-	-	-	-	-	-	-	-
	5500.0				DC	0.41		-	-	-	-	-	-	-	-
	5510.0				DC	0.54		-	-	-	-	-	-	-	-
	5520.0				DC	0.43		-	-	-	-	-	-	-	-
202/09-1	5379.0	ft	Lewisian Basement	PrCam	COCH	0.71	NEW	-	-	-	-	-	-	-	-
204/10-1	2499.0	m	Precambrian Basement	PrCam	COCH	1.13	Finlay <i>et al.</i> (2018)	-	-	-	-	-	-	-	-
	2505.0				DC	0.99	NEW	Insufficient concordant Zircon recovery			NEW	1792.0	73.0	Laxfordian	NEW
	2508.0				DC	1.03									

PrCam: Precambrian

Lax: Laxfordian

COCH: Core chip

DC: Ditch cuttings

NEW: Analysed in this study

TABLE Ap1.2.1 Radioactive heat production and Zircon/Apatite geochronology data

Well	Bottom depth	Units (m/ft)	Stratigraphy	Age	Sample type	Radioactive Heat Production (RHP)		Zircon Geochronology				Apatite Geochronology			
						RHP (μWm^3)	Data Source	Zircon Age	$\pm 2\sigma$ (Ma)	Zircon Event	Data Source	Apatite Age	$\pm 2\sigma$ (Ma)	Apatite Event	Data Source
204/10-1	2511.0	m	Precambrian Basement	PrCam	DC	0.9	NEW	Insufficient concordant Zircon recovery				1792.0	73.0	Laxfordian	NEW
	2514.0				DC	0.95									
204/15-2	12467.0	ft	Precambrian Basement	PrCam	DC	0.15	Finlay <i>et al.</i> (2018)	-	-	-	-	-	-	-	-
204/23-1	3847.2	m	Precambrian Basement	PrCam	COCH	0.64	Chambers <i>et al.</i> (2005)	-	-	-	-	-	-	-	-
204/25-1	9417.0	ft	Precambrian Basement	PrCam	COCH	0.13	Chambers <i>et al.</i> (2005)	2729.0	12.0	Neoproterozoic	Holdsworth <i>et al.</i> (2019)	-	-	-	-
204/26-1A	8689.9	ft	Precambrian Basement	PrCam	COCH	-	-	2733.0	14.0	Neoproterozoic	Holdsworth <i>et al.</i> (2019)	-	-	-	-
204/27a-1	2136.3	m	Precambrian Basement	PrCam	COCH	-	-	2745.0	15.0	Neoproterozoic	Holdsworth <i>et al.</i> (2019)	-	-	-	-
204/28-1	1941.6	m	Precambrian Basement	PrCam	COCH	-	-	2762.0	13.0	Neoproterozoic	Holdsworth <i>et al.</i> (2019)	-	-	-	-
205/16-1	4172.2	m	Precambrian Basement	PrCam	COCH	1.21	Chambers <i>et al.</i> (2005)	-	-	-	-	-	-	-	-
	4274.2				COCH	0.96	NEW	-	-	-	-	-	-	-	-
	4274.4				COCH	0.41		-	-	-	-	-	-	-	-
	4274.6				COCH	2.36		2738.0	6.0	Neoproterozoic	NEW	1783.0	44.0	Laxfordian	NEW
	4275.3				COCH	0.82		-	-	-	-	-	-	-	-
	4300.0				DC	0.96		2742.0	6.0	Neoproterozoic	NEW	1905.0	41.0	Laxfordian	NEW

PrCam: Precambrian

COCH: Core chip

DC: Ditch cuttings

NEW: Analysed in this study

TABLE Ap1.2.1 Radioactive heat production and Zircon/Apatite geochronology data

Well	Bottom depth	Units (m/ft)	Stratigraphy	Age	Sample type	Radioactive Heat Production (RHP)		Zircon Geochronology				Apatite Geochronology			
						RHP (μWm^3)	Data Source	Zircon Age	$\pm 2\sigma$ (Ma)	Zircon Event	Data Source	Apatite Age	$\pm 2\sigma$ (Ma)	Apatite Event	Data Source
205/16-1	4305.0	m	Precambrian Basement	PrCam	DC	0.9	NEW	2742.0	6.0	Neoproterozoic	NEW	1905.0	41.0	Laxfordian	NEW
	4310.0				DC	0.89									
	4314.0				DC	0.67									
205/20-1	2017.5	m	Lewisian Basement	PrCam	COCH	0.90	Chambers <i>et al.</i> (2005)	2736.0	12.0	Neoproterozoic	Holdsworth <i>et al.</i> (2019)				
205/21-1A	4449.0	ft	Lewisian Basement	PrCam	COCH	0.15	Finlay <i>et al.</i> (2018)	-	-	-	-	-	-	-	-
	4465.0				COCH	0.15		-	-	-	-	-	-	-	-
205/22-1A	3225.6	m	Precambrian Basement	PrCam	COCH	0.73	Chambers <i>et al.</i> (2005)	2700.0	13.0	Neoproterozoic	Holdsworth <i>et al.</i> (2019)	-	-	-	-
206/07a-2	2140.7	m	Precambrian Basement	PrCam	COCH	-	-	2809.0	21.0	Neoproterozoic	Chemostrat (2014)	-	-	-	-
	2141.3				COCH	0.90	Chambers <i>et al.</i> (2005)	2806.0	8.0	Neoproterozoic	Holdsworth <i>et al.</i> (2019)	-	-	-	-
	2146.7				COCH	0.21	NEW	-	-	-	-	-	-	-	-
	2147.9				COCH	0.29		2851.0	18.0	Neoproterozoic	NEW	1748.2	79.6	Laxfordian	NEW
	2246.4				COCH	1.05		-	-	-	-	-	-	-	-
	2438.3				COCH	0.60	Finlay <i>et al.</i> (2018)	-	-	-	-	-	-	-	-
	2442.6				COCH	0.52	NEW	-	-	-	-	-	-	-	-

PrCam: Precambrian

COCH: Core chip

DC: Ditch cuttings

NEW: Analysed in this study

TABLE Ap1.2.1 Radioactive heat production and Zircon/Apatite geochronology data

Well	Bottom depth	Units (m/ft)	Stratigraphy	Age	Sample type	Radioactive Heat Production (RHP)		Zircon Geochronology				Apatite Geochronology			
						RHP (μWm^3)	Data Source	Zircon Age	$\pm 2\sigma$ (Ma)	Zircon Event	Data Source	Apatite Age	$\pm 2\sigma$ (Ma)	Apatite Event	Data Source
206/07a-2	2443.2	m	Precambrian Basement	PrCam	COCH	1.75	Finlay <i>et al.</i> (2018)	-	-	-	-	-	-	-	-
	2443.2				COCH	0.43	NEW	-	-	-	-	-	-	-	-
	2506.5				COCH	0.54		-	-	-	-	-	-	-	-
	2543.7				COCH	0.26		-	-	-	-	-	-	-	-
	2593.3				COCH	0.39		-	-	-	-	-	-	-	-
	2593.3				COCH	0.59	Chambers <i>et al.</i> (2005)	2753.0	6.0	Neoproterozoic	Chemostrat (2014)	-	-	-	-
	2593.4				COCH	-	-	2782.0	25.0	Neoproterozoic	Holdsworth <i>et al.</i> (2019)	-	-	-	-
	2599.4				COCH	0.42	Chambers <i>et al.</i> (2005)	-	-	-	-	-	-	-	-
	2596.0				COCH	0.59	NEW	-	-	-	-	-	-	-	-
	2598.0				COCH	0.53		2726.0	5.0	Neoproterozoic	NEW	1851.0	59.7	Laxfordian	NEW
206/08-1A	2306.4	m	Precambrian Basement	PrCam	COCH	-	-	2691.0	28.0	Neoproterozoic	Chemostrat (2014)	-	-	-	-
	2311.0				COCH	0.64	Chambers <i>et al.</i> (2005)	2802.0	5.0	Neoproterozoic	Holdsworth <i>et al.</i> (2019)	-	-	-	-
206/08-2	1859.0	m	Precambrian Basement	PrCam	COCH	2.27	Finlay <i>et al.</i> (2018)	-	-	-	-	-	-	-	-
	1864.6				COCH	1.92	Chambers <i>et al.</i> (2005)	-	-	-	-	-	-	-	-

PrCam: Precambrian

COCH: Core chip

NEW: Analysed in this study

TABLE Ap1.2.1 Radioactive heat production and Zircon/Apatite geochronology data

Well	Bottom depth	Units (m/ft)	Stratigraphy	Age	Sample type	Radioactive Heat Production (RHP)		Zircon Geochronology				Apatite Geochronology			
						RHP (μWm^3)	Data Source	Zircon Age	$\pm 2\sigma$ (Ma)	Zircon Event	Data Source	Apatite Age	$\pm 2\sigma$ (Ma)	Apatite Event	Data Source
206/08-7	2320.5	m	Basement	PrCam	COCH	0.67	Chambers <i>et al.</i> (2005)	-	-	-	-	-	-	-	-
206/08-8	2499.0	m	Basement	PrCam	COCH	0.25	Chambers <i>et al.</i> (2005)	-	-	-	-	-	-	-	-
206/09-2	8085.0	ft	Lewisian Basement	PrCam	COCH	2.68	Finlay <i>et al.</i> (2018)	-	-	-	-	-	-	-	-
206/12-1	5630.0	ft	Lewisian Basement	PrCam	COCH	0.44	Finlay <i>et al.</i> (2018)	-	-	-	-	-	-	-	-
	5632.0				COCH	-	-	2748.0	6.0	Neoproterozoic	Holdsworth <i>et al.</i> (2019)	-	-	-	-
207/01-3	4576.3	ft	Precambrian Basement	PrCam	COCH	0.94	NEW	-	-	-	-	-	-	-	-
	4670.0				DC	1.1		2738.0	16.0	Neoproterozoic	NEW	1425.0	99.0	Laxfordian	NEW
	4680.0				DC	0.89									
	4690.0				DC	1.39									
	4700.0				DC	1.03									
	4706.0				DC	1.00									
207/02-1	6722.0	ft	Precambrian Basement	PrCam	COCH	0.76	NEW	2732.0	4.0	Neoproterozoic	NEW	1761.0	25.0	Laxfordian	NEW
	6723.0				COCH	0.77		2735.0	5.0	Neoproterozoic		1761.0	28.0	Laxfordian	
	6724.0				COCH	0.86		2735.0	4.0	Neoproterozoic		1762.0	26.0	Laxfordian	

PrCam: Precambrian

COCH: Core chip

DC: Ditch cuttings

NEW: Analysed in this study

TABLE Ap1.2.1 Radioactive heat production and Zircon/Apatite geochronology data

Well	Bottom depth	Units (m/ft)	Stratigraphy	Age	Sample type	Radioactive Heat Production (RHP)		Zircon Geochronology				Apatite Geochronology			
						RHP (μWm^3)	Data Source	Zircon Age	$\pm 2\sigma$ (Ma)	Zircon Event	Data Source	Apatite Age	$\pm 2\sigma$ (Ma)	Apatite Event	Data Source
208/23-1	9795.5	ft	Lewisian Basement	PrCam	COCH	-	-	2776.0	12.0	Neoarchean	Holdsworth <i>et al.</i> (2019)	-	-	-	-
	9796.5				COCH	1.72	NEW	2782.0	6.0	Neoarchean	NEW	~450.0	75.0	LIR	NEW
	9799.2				COCH	0.56		-	-	-	-	-	-	-	-
	6803.0				COCH	0.51		-	-	-	-	-	-	-	-
	6806.1				COCH	1.97		-	-	-	-	-	-	-	-
	6808.0				COCH	1.10		-	-	-	-	-	-	-	-
208/26-1	3894.0	m	Precambrian Basement	PrCam	COCH	0.20	Finlay <i>et al.</i> (2018)	-	-	-	-	-	-	-	-
208/27-1	1380.2	m	Precambrian Basement	PrCam	-	-	-	2739.0	22.5	Neoarchean	Chemostrat (2014)	-	-	-	-
208/27-2	4452.5	ft	Lewisian Basement	PrCam	COCH	-	-	2783.0	8.0	Neoarchean	Holdsworth <i>et al.</i> (2019)	-	-	-	-
	4522.2				COCH	0.34	NEW	-	-	-	-	-	-	-	-
	4527.5				COCH	0.74		2742.0	6.0	Neoarchean	NEW	~450.0	75.0	LIR	NEW
	4528.8				COCH	1.03	Chambers <i>et al.</i> (2005)	-	-	-	-	-	-	-	-
	4531.2				COCH	0.37	NEW	-	-	-	-	-	-	-	-
	4532.0				COCH	0.49		-	-	-	-	-	-	-	-

PrCam: Precambrian

COCH: Core chip

NEW: Analysed in this study

LIR: Lower intercept range

TABLE Ap1.2.1 Radioactive heat production and Zircon/Apatite geochronology data

Well	Bottom depth	Units (m/ft)	Stratigraphy	Age	Sample type	Radioactive Heat Production (RHP)		Zircon Geochronology				Apatite Geochronology			
						RHP (μWm^3)	Data Source	Zircon Age	$\pm 2\sigma$ (Ma)	Zircon Event	Data Source	Apatite Age	$\pm 2\sigma$ (Ma)	Apatite Event	Data Source
209/09-1	3190.3	ft	Caledonian Basement	Sil	COCH	0.99	Chambers <i>et al.</i> (2005)	-	-	-	-	-	-	-	-
	8850.0				COCH	1.94	NEW	-	-	-	-	-	-	-	-
	8854.0				COCH	1.87		-	-	-	-	-	-	-	-
	8855.0				COCH	1.30		463.0	10.0	Caledonian	NEW	417.0	17.5	Caledonian	NEW
209/12-1	11385.7	ft	Caledonian Basement	Sil	COCH	3.60	NEW	-	-	-	-	-	-	-	-
	11500.0				DC	2.08		-	-	-	-	-	-	-	-
	11510.0				DC	2.18		-	-	-	-	-	-	-	-
	11520.0				DC	2.14		-	-	-	-	-	-	-	-
	11521.0				DC	-	-	-	-	-	-	425.0	21.0	Caledonian	Chemostrat (2014)
	11525.0				COCH	2.07	NEW	-	-	-	-	-	-	-	-
	11526.0				COCH	2.68	Chambers <i>et al.</i> (2005)	-	-	-	-	-	-	-	-
	11527.0				COCH	2.29	NEW	-	-	-	-	-	-	-	-
214/09-1	11580.7	ft	Precambrian Basement	PrCam	DC	2.53	Finlay <i>et al.</i> (2018)	-	-	-	-	-	-	-	-
220/26-1	5280.2	m	Caledonian Basement	Sil	COCH	0.94	Chambers <i>et al.</i> (2005)	-	-	-	-	-	-	-	-

PrCam: Precambrian

Sil: Silurian

COCH: Core chip

DC: Ditch cuttings

NEW: Analysed in this study

TABLE Ap1.2.1 Radioactive heat production and Zircon/Apatite geochronology data

APPENDIX 1.3

PETROLOGY AND X-RAY DIFFRACTION ANALYSIS SUMMARY

Tables

Ap1.3.1

Petrology and X-Ray diffraction analysis summary

Well	Bottom depth	Units (m/ft)	Stratigraphy	Age	Sample type	Petrology Technique	Crystal Size	Texture	Rock Classification (USGS)	Data Source	Sericitization of Plagioclase	Chloritization of Biotite	Carbonate Replacement of Plagioclase	Sassuritization of Plagioclase	Epidote Precipitation in Fractures	Kaolinization of Plagioclase
154/03-1	8060.0	ft	Laxford Basement	Lax	COCH	Thin section	-	Amphibolite	Amphibolite	Chambers <i>et al.</i> (2005)	-	-	-	-	-	-
164/25-2	2727.8	m	Lewisian Basement	PrCam	COCH	Thin section	-	Gneissic	Metabasic Gneiss	Chambers <i>et al.</i> (2005)	-	-	-	-	-	-
202/02-1	3950.0	ft	Precambrian Basement	PrCam	DC	-	-	-	-	-	-	-	-	-	-	-
	4002.0				COCH	Thin section	-	Gneissic	Quartzfeldspathic gneiss	Chambers <i>et al.</i> (2005)	-	-	-	-	-	-
202/03-1	1774.6	m	Precambrian Basement	PrCam	COCH	Thin section	-	-	Cataclasite	Chambers <i>et al.</i> (2005)	-	-	-	-	-	-
202/08-1	5446.6	ft	Lewisian Basement	PrCam	COCH	Thin section	Medium - Coarse	Gneissic	Monzodiorite	NEW	y	y	y	-	-	-
	5457.3				COCH	Thin section	Medium	Gneissic	Tonalite		y	y	y	y	-	-
	5500.0				DC	XRD	-	Gneissic	Granodiorite		-	-	-	-	-	-
	5510.0				DC	XRD	-	Gneissic	Granodiorite		-	-	-	-	-	-
	5520.0				DC	XRD	-	Gneissic	Granodiorite		-	-	-	-	-	-
202/09-1	5379.0	ft	Lewisian Basement	PrCam	COCH	Thin section	Medium	Gneissic	Diorite	NEW	-	y	-	y	-	-
204/10-1	2499.0	m	Precambrian Basement	PrCam	COCH	-	-	-	-	-	-	-	-	-	-	-
	2505.0				DC	XRD	-	-	-	-	-	-	-	-	-	-
	2508.0				DC		-	-	-	-	-	-	-	-	-	-
	2511.0				DC		-	-	-	-	-	-	-	-	-	-
	2514.0				DC		-	-	-	-	-	-	-	-	-	-
204/15-2	12467.0	ft	Precambrian Basement	PrCam	DC	Thin section	-	Gneissic	Tonalite	Finlay <i>et al.</i> (2018)	-	-	-	-	-	-
204/23-1	3847.2	m	Precambrian Basement	PrCam	COCH	Thin section	-	Gneissic	Quartzfeldspathic gneiss	Chambers <i>et al.</i> (2005)	-	-	-	-	-	-
204/25-1	9417.0	ft	Precambrian Basement	PrCam	COCH	Thin section	-	Gneissic	Tonalitic gneiss	Chambers <i>et al.</i> (2005)	-	-	-	-	-	-
204/26-1A	8689.9	ft	Precambrian Basement	PrCam	COCH	Thin section	-	Gneissic	Granodioritic gneiss	Holdsworth <i>et al.</i> (2019)	-	-	-	-	-	-
204/27a-1	2136.3	m	Precambrian Basement	PrCam	COCH	Thin section	-	Gneissic	Granite	Holdsworth <i>et al.</i> (2019)	-	-	-	-	-	-
204/28-1	1941.6	m	Precambrian Basement	PrCam	COCH	Thin section	-	Gneissic	Granodioritic gneiss	Holdsworth <i>et al.</i> (2019)	-	-	-	-	-	-
205/16-1	4172.2	m	Precambrian Basement	PrCam	COCH	Thin section	-	Gneissic	Dioritic gneiss	Chambers <i>et al.</i> (2005)	-	-	-	-	-	-

PrCam: Precambrian

Lax: Laxfordian

COCH: Core chip

DC: Ditch cuttings

NEW: Analysed in this study

XRD: X-Ray diffraction

TABLE Ap1.3.1 Petrology and X-Ray diffraction analysis summary

Well	Bottom depth	Units (m/ft)	Stratigraphy	Age	Sample type	Petrology Technique	Crystal Size	Texture	Rock Classification (USGS)	Data Source	Sericitization of Plagioclase	Chloritization of Biotite	Carbonate Replacement of Plagioclase	Sassuritization of Plagioclase	Epidote Precipitation in Fractures	Kaolinization of Plagioclase
205/16-1	4274.2	m	Precambrian Basement	PrCam	COCH	Thin section	Medium	Gneissic	Tonalite	-	y	y	y	-	-	-
	4274.4				COCH	Thin section	Medium - Coarse	Gneissic	Granodiorite	-	y	y	y	-	-	-
	4274.6				COCH	Thin section	Medium - Coarse	Gneissic	Granodiorite	-	y	y	y	-	-	-
	4275.3				COCH	Thin section	Medium	Gneissic	Tonalite	-	y	y	y	-	-	-
	4300.0				DC	XRD	-	Gneissic	Granite	NEW	-	-	-	-	-	-
	4305.0				DC		-	Gneissic								
	4310.0				DC		-	Gneissic								
	4314.0				DC		-	Gneissic								
205/20-1	2017.5	m	Lewisian Basement	PrCam	COCH	Thin section	-	Gneissic	Granitic gneiss	Holdsworth <i>et al.</i> (2019)	-	-	-	-	-	-
205/21-1A	4449.0	ft	Lewisian Basement	PrCam	COCH	Thin section	-	Gneissic	Granite	Finlay <i>et al.</i> (2018)	-	-	-	-	-	-
	4465.0				COCH	Thin section	-	Gneissic	Tonalite		-	-	-	-	-	-
205/22-1A	3225.6	m	Precambrian Basement	PrCam	COCH	Thin section	-	Gneissic	Dioritic gneiss	Chambers <i>et al.</i> (2005)	-	-	-	-	-	-
206/07a-2	2140.7	m	Precambrian Basement	PrCam	COCH	-	-	-	-	-	-	-	-	-	-	-
	2141.3				COCH	Thin section	-	Gneissic	Granodioritic gneiss	Holdsworth <i>et al.</i> (2019)	-	-	-	-	-	-
	2146.7				COCH	Thin section	Coarse	Gneissic	Tonalite	NEW	y	y	-	y	-	-
	2147.9				COCH	Thin section	Coarse	Gneissic	Tonalite		y	-	-	y	-	-
	2246.4				COCH	Thin section	Coarse	Gneissic	Tonalite		y	y	y	y	-	-
	2438.3				COCH	Thin section	-	Gneissic	Tonalite	Finlay <i>et al.</i> (2018)	-	-	-	-	-	-
	2442.6				COCH	Thin section	Coarse	Gneissic	Tonalite - Diorite	NEW	y	-	-	y	-	-
	2443.2				COCH	Thin section	-	Gneissic	Diorite	Finlay <i>et al.</i> (2018)	-	-	-	-	-	-
	2443.2				COCH	Thin section	Coarse	Gneissic	Tonalite	NEW	y	y	-	y	-	-
	2506.5				COCH	Thin section	Coarse	Gneissic	Granodiorite		y	y	-	y	-	-
	2543.7				COCH	Thin section	Coarse	Gneissic	Tonalite		y	y	-	y	-	-

PrCam: Precambrian

COCH: Core chip

DC: Ditch cuttings

NEW: Analysed in this study

XRD: X-Ray diffraction

TABLE Ap1.3.1 Petrology and X-Ray diffraction analysis summary

Well	Bottom depth	Units (m/ft)	Stratigraphy	Age	Sample type	Petrology Technique	Crystal Size	Texture	Rock Classification (USGS)	Data Source	Sericitization of Plagioclase	Chloritization of Biotite	Carbonate Replacement of Plagioclase	Sassuritization of Plagioclase	Epidote Precipitation in Fractures	Kaolinization of Plagioclase
206/07a-2	2593.3	m	Precambrian Basement	PrCam	COCH	Thin section	Coarse	Gneissic	Tonalite - granodiorite	NEW	y	-	-	-	-	-
	2593.3				COCH	Thin section	-	Gneissic	Granodioritic gneiss	Finlay <i>et al.</i> (2018)	-	-	-	-	-	-
	2593.4				COCH	-	-	-	-	-	-	-	-	-	-	-
	2599.4				COCH	-	-	-	-	-	-	-	-	-	-	-
	2596.0				COCH	Thin section	Coarse	Gneissic	Granodiorite	NEW	y	-	-	y	-	-
	2598.0				COCH	Thin section	Coarse	Gneissic	Syenogranite		y	y	-	y	-	-
206/08-1A	2306.4	m	Precambrian Basement	PrCam	COCH	-	-	-	-	-	-	-	-	-	-	-
	2311.0				COCH	Thin section	-	Gneissic	Dioritic gneiss	Chambers <i>et al.</i> (2005)	-	-	-	-	-	-
206/08-2	1859.0	m	Precambrian Basement	PrCam	COCH	Thin section	-	Gneissic	Granodiorite	Finlay <i>et al.</i> (2018)	-	-	-	-	-	-
	1864.6				COCH	Thin section	-	-	Protomylonite	Chambers <i>et al.</i> (2005)	-	-	-	-	-	-
206/08-7	2320.5	m	Basement	PrCam	COCH	Thin section	-	Amphibolite	Amphibolite	Chambers <i>et al.</i> (2005)	-	-	-	-	-	-
206/08-8	2499.0	m	Basement	PrCam	COCH	Thin section	-	Gneissic	Granitic gneiss	Chambers <i>et al.</i> (2005)	-	-	-	-	-	-
206/09-2	8085.0	ft	Lewisian Basement	PrCam	COCH	Thin section	-	Gneissic	Granite	Finlay <i>et al.</i> (2018)	-	-	-	-	-	-
206/12-1	5630.0	ft	Lewisian Basement	PrCam	COCH	Thin section	-	Gneissic	Granodioritic gneiss	Finlay <i>et al.</i> (2018)	-	-	-	-	-	-
	5632.0				COCH	Thin section	-	Gneissic	Granodioritic gneiss	Holdsworth <i>et al.</i> (2019)	-	-	-	-	-	-
207/01-3	4576.3	ft	Precambrian Basement	PrCam	COCH	Thin section	-	Schistose	Metasedimentary (metasandstone)	NEW	y	y	y	-	y	-
	4670.0				DC	XRD	-	Gneissic	Granodiorite	NEW	-	-	-	-	-	-
	4680.0				DC		-	Gneissic								
	4690.0				DC		-	Gneissic								
	4700.0				DC		-	Gneissic								
	4706.0				DC		-	Gneissic								
207/02-1	6722.0	ft	Precambrian Basement	PrCam	COCH	Thin section	Coarse	Gneissic	Granite	NEW	y	y	y	-	-	-
	6723.0				COCH	Thin section	Coarse	Gneissic	Syenogranite		y	-	y	-	-	-

PrCam: Precambrian

COCH: Core chip

DC: Ditch cuttings

NEW: Analysed in this study

XRD: X-Ray diffraction

TABLE Ap1.3.1 Petrology and X-Ray diffraction analysis summary

Well	Bottom depth	Units (m/ft)	Stratigraphy	Age	Sample type	Petrology Technique	Crystal Size	Texture	Rock Classification (USGS)	Data Source	Sericitization of Plagioclase	Chloritization of Biotite	Carbonate Replacement of Plagioclase	Sassuritization of Plagioclase	Epidote Precipitation in Fractures	Kaolinization of Plagioclase
207/02-1	6724.0	ft	Precambrian Basement	PrCam	COCH	Thin section	Coarse	Gneissic	Granite	NEW	y	y	-	-	-	-
208/23-1	9795.5	ft	Lewisian Basement	PrCam	COCH	Thin section	-	Gneissic	Granitic gneiss	Holdsworth <i>et al.</i> (2019)	-	-	-	-	-	-
	9796.5				COCH	Thin section	Coarse	Gneissic	Granite	NEW	y	-	y	-	-	y
	9799.2				COCH	Thin section	Coarse	Gneissic	Fractured syenogranite		y	-	y	-	-	y
	6803.0				COCH	Thin section	Coarse	Gneissic	Syenogranite		y	-	y	-	-	-
	6806.1				COCH	Thin section	Coarse	Gneissic	Tonalite		y	-	-	y	-	-
	6808.0				COCH	Thin section	Fine - Medium	Gneissic	Tonalite		y	y	y	y	-	-
208/26-1	3894.0	m	Precambrian Basement	PrCam	COCH	Thin section	-	Gneissic	Serpentinised granodiorite	Finlay <i>et al.</i> (2018)	-	-	-	-	-	-
208/27-1	1380.2	m	Precambrian Basement	PrCam	-	Thin section	-	-	-	-	-	-	-	-	-	-
208/27-2	4452.5	ft	Lewisian Basement	PrCam	COCH	Thin section	-	Gneissic	Mafic granitic gneiss	Holdsworth <i>et al.</i> (2019)	-	-	-	-	-	-
	4522.2				COCH	Thin section	Coarse	Gneissic (weathered)	Weathered granite	NEW	y	-	y	-	-	y
	4527.5				COCH	Thin section	Coarse	Gneissic (weathered)	Weathered granite		y	-	y	-	-	y
	4528.8				COCH	Thin section	-	Gneissic	Granitic gneiss	Chambers <i>et al.</i> (2005)	-	-	-	-	-	-
	4531.2				COCH	Thin section	Coarse	Gneissic (weathered)	Weathered granite	NEW	y	-	y	y	-	-
	4532.0				COCH	Thin section	Coarse	Gneissic (weathered)	Weathered syenogranite		y	y	y	-	-	-
209/09-1	3190.3	ft	Caledonian Basement	Sil	COCH	Thin section	-	Igneous	Augen gneiss	Chambers <i>et al.</i> (2005)	-	-	-	-	-	-
	8850.0				COCH	Thin section	Coarse	Igneous	Tonalite (biotite enriched)	NEW	y	y	y	-	-	-
	8854.0				COCH	Thin section	Coarse	Igneous	Granodiorite		y	y	y	-	-	-
	8855.0				COCH	Thin section	Coarse	Igneous	Gneissic quartz rich granitoid (biotite enriched)		y	y	y	-	-	-
209/12-1	11385.7	ft	Caledonian Basement	Sil	COCH	-	-	Igneous	-	NEW	-	-	-	-	-	-
	11500.0				DC	XRD	-	Igneous	Granite	NEW	-	-	-	-	-	-
	11510.0				DC		-	Igneous			-	-	-	-	-	-
	11520.0				DC		-	Igneous			-	-	-	-	-	-

PrCam: Precambrian

Sil: Silurian

COCH: Core chip

DC: Ditch cuttings

NEW: Analysed in this study

XRD: X-Ray diffraction

TABLE Ap1.3.1 Petrology and X-Ray diffraction analysis summary

Well	Bottom depth	Units (m/ft)	Stratigraphy	Age	Sample type	Petrology Technique	Crystal Size	Texture	Rock Classification (USGS)	Data Source	Sericitization of Plagioclase	Chloritization of Biotite	Carbonate Replacement of Plagioclase	Sassuritization of Plagioclase	Epidote Precipitation in Fractures	Kaolinization of Plagioclase
209/12-1	11521.0	ft	Caledonian Basement	Sil	DC	Thin section	-	Igneous	-	-	-	-	-	-	-	-
	11525.0				COCH	Thin section	Coarse	Igneous	Biotite granite - syenogranite	NEW	y	-	-	-	-	-
	11526.0				COCH	Thin section	-	-	Biotite schist	Chambers <i>et al.</i> (2005)	-	-	-	-	-	-
	11527.0				COCH	Thin section	Coarse	Igneous	Alkali feldspar biotite granite	NEW	y	y	-	-	-	-
214/09-1	11580.7	ft	Precambrian Basement	PrCam	DC	Thin section	-	Igneous	Granite	Finlay <i>et al.</i> (2018)	-	-	-	-	-	-
220/26-1	5280.2	m	Caledonian Basement	Sil	COCH	Thin section	-	Igneous	Quartzofeldspathic mylonite	Chambers <i>et al.</i> (2005)	-	-	-	-	-	-

PrCam: Precambrian

Sil: Silurian

COCH: Core chip

DC: Ditch cuttings

NEW: Analysed in this study

TABLE Ap1.3.1 Petrology and X-Ray diffraction analysis summary

APPENDIX 1.4 MINERAL, FRACTURE AND BITUMEN POINT COUNT ANALYSIS DATA

Tables

Ap1.4.1 Mineral, fracture and bitumen point count analysis data

Well	154/03-1	164/25-2	202/02-1		202/03-1	202/08-1					202/09-1	204/10-1				
Bottom Depth	8060.0	2727.8	3950.0	4002.0	1774.6	5446.6	5457.3	5500.0	5510.0	5520.0	5379.0	2499.0	2505.0	2508.0	2511.0	2514.0
Units (ft/m)	ft	m	ft		m	ft					ft	m				
Stratigraphy	Laxfordian Basement	Lewisian Basement	Precambrian Basement		Precambrian Basement	Lewisian Basement					Lewisian Basement	Precambrian Basement				
Age	Lax	PrCam	PrCam		PrCam	PrCam					PrCam	PrCam				
Sample type	COCH	COCH	DC	COCH	COCH	COCH	COCH	DC	DC	DC	COCH	COCH	DC	DC	DC	DC
Petrology Technique	Thin Section	Thin section	-	Thin section	Thin section	Thin section	Thin section	XRD	XRD	XRD	Thin section	-	XRD			
Point Count Data																
Quartz	-	-	-	-	-	2.00	18.67	-	-	-	1.00	-	-	-	-	-
K-Feldspar	-	-	-	-	-	7.33	0.33	-	-	-	0.00	-	-	-	-	-
Pagioclase Feldspar	-	-	-	-	-	52.67	40.00	-	-	-	46.67	-	-	-	-	-
Muscovite	-	-	-	-	-	0.33	0.00	-	-	-	0.67	-	-	-	-	-
Biotite	-	-	-	-	-	3.67	12.33	-	-	-	3.00	-	-	-	-	-
Amphibole/Hornblende	-	-	-	-	-	0.00	4.33	-	-	-	10.00	-	-	-	-	-
Opaque Minerals	-	-	-	-	-	0.05	0.00	-	-	-	0.33	-	-	-	-	-
Orthopyroxene	-	-	-	-	-	0.33	4.33	-	-	-	19.00	-	-	-	-	-
Clinopyroxene	-	-	-	-	-	1.00	0.00	-	-	-	4.00	-	-	-	-	-
Apatite	-	-	-	-	-	0.00	1.00	-	-	-	0.67	-	-	-	-	-
Garnet	-	-	-	-	-	0.00	0.00	-	-	-	0.00	-	-	-	-	-
Zircon	-	-	-	-	-	0.00	0.05	-	-	-	0.00	-	-	-	-	-
Olivine	-	-	-	-	-	0.00	0.00	-	-	-	0.00	-	-	-	-	-
Rutile	-	-	-	-	-	0.00	0.00	-	-	-	0.67	-	-	-	-	-
Chlorite	-	-	-	-	-	15.00	2.00	-	-	-	1.00	-	-	-	-	-
Epidote/Saussurite	-	-	-	-	-	0.00	0.33	-	-	-	4.33	-	-	-	-	-
Sericite/Illite	-	-	-	-	-	5.67	4.67	-	-	-	6.00	-	-	-	-	-
Non-resolvable clays	-	-	-	-	-	2.67	3.00	-	-	-	0.33	-	-	-	-	-
Kaolinite	-	-	-	-	-	0.00	0.00	-	-	-	0.00	-	-	-	-	-
Non-FE clays	-	-	-	-	-	4.00	3.33	-	-	-	0.00	-	-	-	-	-
FE Calcite	-	-	-	-	-	2.33	0.67	-	-	-	0.00	-	-	-	-	-
Non-FE Dolomite	-	-	-	-	-	0.00	0.00	-	-	-	0.00	-	-	-	-	-
FE Dolomite	-	-	-	-	-	0.00	0.00	-	-	-	0.00	-	-	-	-	-
Siderite	-	-	-	-	-	0.00	0.00	-	-	-	0.00	-	-	-	-	-
Bitumen (%)	-	-	-	-	-	0.05	0.33	-	-	-	0.33	-	-	-	-	-
Dissolution Porosity (%)	-	-	-	-	-	3.00	3.33	-	-	-	2.00	-	-	-	-	-
Natural Open Fracture (%)	-	-	-	-	-	0.05	1.33	-	-	-	0.00	-	-	-	-	-
Natural Void/Cavity/Druse (%)	-	-	-	-	-	0.05	0.05	-	-	-	0.05	-	-	-	-	-
Total Porosity (%)	-	-	-	-	-	3.10	4.72	-	-	-	2.05	-	-	-	-	-

PrCam: Precambrian

Lax: Laxfordian

COCH: Core chip

DC: Ditch cuttings

XRD: -Ray diffraction

TABLE Ap1.4.1 Mineral, fracture and bitumen point count analysis data

Well	204/15-2	204/23-1	204/25-1	204/26-1A	204/27a-1	204/28-1	205/16-1									205/20-1
Bottom Depth	12467.0	3847.2	9417.0	8689.9	2136.3	1941.6	4172.2	4274.2	4274.4	4274.6	4275.3	4300.0	4305.0	4310.0	4314.0	2017.5
Units (ft/m)	ft	m	ft	ft	m	m	m									m
Stratigraphy	Precambrian Basement	Precambrian Basement	Precambrian Basement	Precambrian Basement	Precambrian Basement	Precambrian Basement	Precambrian Basement									Lewisian Basement
Age	PrCam	PrCam	PrCam	PrCam	PrCam	PrCam	PrCam									PrCam
Sample type	DC	COCH	COCH	COCH	COCH	COCH	COCH	COCH	COCH	COCH	COCH	DC	DC	DC	DC	COCH
Petrology Technique	Thin section	Thin section	Thin section	Thin section	Thin section	Thin section	Thin section	Thin section	Thin section	Thin section	Thin section	XRD				Thin section
Point Count Data																
Quartz	33.67	-	-	-	-	-	-	16.33	46.00	33.67	19.00	-	-	-	-	-
K-Feldspar	3.67	-	-	-	-	-	-	7.67	14.33	18.67	0.33	-	-	-	-	-
Pagioclase Feldspar	34.00	-	-	-	-	-	-	57.00	26.33	32.67	66.33	-	-	-	-	-
Muscovite	0.33	-	-	-	-	-	-	0.33	0.00	0.33	0.00	-	-	-	-	-
Biotite	4.33	-	-	-	-	-	-	1.33	0.00	0.67	2.00	-	-	-	-	-
Amphibole/Hornblende	0.00	-	-	-	-	-	-	0.05	0.00	0.33	0.67	-	-	-	-	-
Opaque Minerals	1.00	-	-	-	-	-	-	1.33	0.33	0.33	1.67	-	-	-	-	-
Orthopyroxene	5.67	-	-	-	-	-	-	3.67	0.05	0.33	1.00	-	-	-	-	-
Clinopyroxene	0.00	-	-	-	-	-	-	0.05	0.05	0.05	0.67	-	-	-	-	-
Apatite	0.00	-	-	-	-	-	-	0.67	0.05	1.00	1.67	-	-	-	-	-
Garnet	0.00	-	-	-	-	-	-	0.00	0.00	0.00	0.00	-	-	-	-	-
Zircon	0.05	-	-	-	-	-	-	0.00	0.05	0.33	0.05	-	-	-	-	-
Olivine	0.00	-	-	-	-	-	-	0.00	0.00	0.00	?.05	-	-	-	-	-
Rutile	0.00	-	-	-	-	-	-	0.00	0.00	0.00	0.00	-	-	-	-	-
Chlorite	4.00	-	-	-	-	-	-	2.67	1.33	2.33	2.67	-	-	-	-	-
Epidote/Saussurite	0.00	-	-	-	-	-	-	0.00	0.00	0.00	0.00	-	-	-	-	-
Sericite/Illite	4.33	-	-	-	-	-	-	4.33	3.33	5.33	1.33	-	-	-	-	-
Non-resolvable clays	1.00	-	-	-	-	-	-	3.33	2.00	0.67	0.67	-	-	-	-	-
Kaolinite	0.00	-	-	-	-	-	-	0.00	0.00	0.00	0.00	-	-	-	-	-
Non-FE clays	3.33	-	-	-	-	-	-	0.05	0.00	0.00	0.33	-	-	-	-	-
FE Calcite	0.67	-	-	-	-	-	-	1.00	4.00	3.00	1.67	-	-	-	-	-
Non-FE Dolomite	0.00	-	-	-	-	-	-	0.00	0.00	0.00	0.00	-	-	-	-	-
FE Dolomite	0.00	-	-	-	-	-	-	0.00	0.00	0.00	0.00	-	-	-	-	-
Siderite	0.33	-	-	-	-	-	-	0.00	0.00	0.00	0.00	-	-	-	-	-
Bitumen (%)	0.05	-	-	-	-	-	-	0.00	0.00	0.00	0.00	-	-	-	-	-
Dissolution Porosity (%)	0.33	-	-	-	-	-	-	0.05	2.00	0.33	0.00	-	-	-	-	-
Natural Open Fracture (%)	0.05	-	-	-	-	-	-	0.33	0.05	0.05	0.00	-	-	-	-	-
Natural Void/Cavity/Druse (%)	0.00	-	-	-	-	-	-	0.05	0.33	0.00	0.00	-	-	-	-	-
Total Porosity (%)	0.38	-	-	-	-	-	-	0.43	2.38	0.38	0.00	-	-	-	-	-

PrCam: Precambrian

COCH: Core chip

DC: Ditch cuttings

XRD: X-Ray diffraction

TABLE Ap1.4.1 Mineral, fracture and bitumen point count analysis data

Well	205/21-1A		205/22-1A	206/07a-2												
Bottom Depth	4449.0	4465.0	3225.6	2140.7	2141.3	2146.7	2147.9	2246.4	2438.3	2442.6	2443.2	2443.2	2506.5	2543.7	2593.3	2593.3
Units (ft/m)	ft		m	m												
Stratigraphy	Lewisian Basement		Precambrian Basement	Precambrian Basement												
Age	PrCam		PrCam	PrCam												
Sample type	COCH	COCH	COCH	COCH	COCH	COCH	COCH	COCH	COCH	COCH	COCH	COCH	COCH	COCH	COCH	COCH
Petrology Technique	Thin section	Thin section	Thin section	-	Thin section	Thin section	Thin section	Thin section	Thin section	Thin section	Thin section	Thin section	Thin section	Thin section	Thin section	Thin section
Point Count Data																
Quartz	38.00	22.67	-	-	-	37.33	21.67	30.00	29.00	5.67	8.33	16.67	24.33	22.00	40.33	-
K-Feldspar	28.33	3.67	-	-	-	0.00	0.00	2.33	5.33	0.00	1.33	0.00	12.33	0.00	3.67	-
Pagioclase Feldspar	22.67	65.00	-	-	-	44.67	50.33	47.67	52.00	29.67	68.00	53.00	37.33	50.33	27.33	-
Muscovite	0.00	0.00	-	-	-	1.00	0.67	0.33	0.00	0.67	0.67	0.00	0.67	0.00	1.67	-
Biotite	0.67	0.33	-	-	-	0.00	5.33	3.33	2.33	8.33	4.00	4.67	6.00	6.00	2.67	-
Amphibole/Hornblende	0.00	0.33	-	-	-	0.00	0.00	0.67	0.00	2.00	0.33	0.67	1.33	2.00	0.67	-
Opaque Minerals	1.33	1.00	-	-	-	0.33	2.33	0.67	1.33	4.33	0.67	2.67	2.33	4.67	0.33	-
Orthopyroxene	1.00	0.67	-	-	-	1.00	5.00	6.67	1.67	3.67	4.33	2.00	2.67	2.00	2.00	-
Clinopyroxene	0.00	0.00	-	-	-	2.67	2.00	3.00	-	4.33	-	5.33	2.00	3.33	4.00	-
Apatite	0.33	0.67	-	-	-	0.00	0.33	0.67	0.33	0.67	1.00	1.33	0.33	0.33	0.05	-
Garnet	0.00	0.00	-	-	-	0.00	0.00	0.00	0.00	0.00	0.00	0.00	0.00	0.00	0.00	-
Zircon	0.33	0.00	-	-	-	0.00	0.05	0.33	0.05	0.00	0.05	0.67	0.05	0.33	0.33	-
Olivine	0.00	0.00	-	-	-	0.00	0.00	0.00	-	0.00	-	0.00	0.00	0.00	0.00	-
Rutile	0.00	0.00	-	-	-	0.00	0.00	0.00	0.00	0.00	0.05	0.00	0.00	0.00	0.00	-
Chlorite	3.67	2.00	-	-	-	0.00	2.67	0.33	0.00	16.00	2.33	2.00	5.33	1.33	0.00	-
Epidote/Saussurite	0.00	0.00	-	-	-	1.00	4.00	1.33	0.00	0.67	0.00	5.33	1.67	3.33	10.33	-
Sericite/Illite	1.33	1.33	-	-	-	11.00	3.67	2.00	2.00	1.67	2.33	4.33	1.67	2.33	6.67	-
Non-resolvable clays	0.33	0.00	-	-	-	0.00	0.00	0.00	0.00	1.00	0.00	0.00	0.00	0.00	0.00	-
Kaolinite	0.00	0.00	-	-	-	0.00	0.00	0.00	0.00	0.00	0.00	0.00	0.00	0.00	0.00	-
Non-FE clays	1.00	0.00	-	-	-	1.00	1.33	0.67	1.33	20.67	1.33	0.00	0.33	0.33	0.00	-
FE Calcite	0.00	0.00	-	-	-	0.00	0.00	0.00	0.00	0.00	0.67	0.00	0.00	0.33	0.00	-
Non-FE Dolomite	0.00	0.00	-	-	-	0.00	0.00	0.00	0.00	0.00	0.00	0.00	0.00	0.00	0.00	-
FE Dolomite	0.00	0.00	-	-	-	0.00	0.00	0.00	0.00	0.00	0.00	0.00	0.00	0.00	0.00	-
Siderite	0.00	0.33	-	-	-	0.00	0.00	0.00	1.33	0.00	0.33	0.00	0.00	0.00	0.00	-
Bitumen (%)	0.00	0.33	-	-	-	0.00	0.00	0.00	0.33	0.00	0.67	1.33	0.67	1.33	0.00	-
Dissolution Porosity (%)	0.33	0.00	-	-	-	0.05	0.33	0.00	0.33	0.33	1.33	0.00	1.00	0.05	0.05	-
Natural Open Fracture (%)	0.33	0.33	-	-	-	0.00	0.33	0.00	0.67	0.00	0.33	0.00	0.00	0.00	0.05	-
Natural Void/Cavity/Druse (%)	0.00	0.00	-	-	-	0.00	0.05	0.05	0.33	0.33	0.33	0.05	0.05	0.05	0.05	-
Total Porosity (%)	0.67	0.33	-	-	-	0.05	0.72	0.05	1.33	0.67	2.00	0.05	1.05	0.10	0.15	-

PrCam: Precambrian

COCH: Core chip

DC: Ditch cuttings

TABLE Ap1.4.1 Mineral, fracture and bitumen point count analysis data

Well	206/07a-2				206/08-1A		206/08-2		206/08-7	206/08-8	206/09-2	206/12-1		207/01-3		
Bottom Depth	2593.4	2599.4	2596.0	2598.0	2306.4	2311.0	1859.0	1864.6	2320.5	2499.0	8085.0	5630.0	5632.0	4576.3	4670.0	4680.0
Units (ft/m)	m				m		m		m	m	ft	ft		ft		
Stratigraphy	Precambrian Basement				Precambrian Basement		Precambrian Basement		Basement	Basement	Lewisian Basement	Lewisian Basement		Precambrian Basement		
Age	PrCam				PrCam		PrCam		PrCam	PrCam	PrCam	PrCam		PrCam		
Sample type	COCH	COCH	COCH	COCH	COCH	COCH	COCH	COCH	COCH	COCH	COCH	COCH	COCH	COCH	DC	DC
Petrology Technique	-	-	Thin section	Thin section	-	Thin section	Thin section	Thin section	Thin section	Thin section	Thin section	Thin section	Thin section	Thin section	XRD	
Point Count Data																
Quartz	-	-	27.00	21.33	-	-	25.33	-	-	-	20.00	19.33	-	52.67	-	-
K-Feldspar	-	-	13.00	51.67	-	-	3.67	-	-	-	52.67	10.00	-	2.00	-	-
Pagioclase Feldspar	-	-	48.67	13.67	-	-	32.00	-	-	-	19.00	58.67	-	6.33	-	-
Muscovite	-	-	0.67	1.33	-	-	3.67	-	-	-	1.33	2.33	-	6.00	-	-
Biotite	-	-	0.67	1.33	-	-	12.67	-	-	-	0.67	1.00	-	10.33	-	-
Amphibole/Hornblende	-	-	0.00	0.67	-	-	0.00	-	-	-	0.00	0.00	-	0.00	-	-
Opaque Minerals	-	-	0.33	0.05	-	-	0.33	-	-	-	0.33	1.33	-	1.33	-	-
Orthopyroxene	-	-	0.33	0.33	-	-	3.33	-	-	-	0.67	1.67	-	3.00	-	-
Clinopyroxene	-	-	1.33	0.67	-	-	0.00	-	-	-	0.00	0.00	-	5.33	-	-
Apatite	-	-	0.33	0.05	-	-	0.00	-	-	-	0.33	0.00	-	1.00	-	-
Garnet	-	-	0.00	0.00	-	-	0.00	-	-	-	0.00	0.00	-	0.00	-	-
Zircon	-	-	0.00	0.00	-	-	0.33	-	-	-	0.05	0.05	-	0.05	-	-
Olivine	-	-	0.00	0.00	-	-	0.00	-	-	-	0.00	0.00	-	0.00	-	-
Rutile	-	-	0.00	0.00	-	-	0.00	-	-	-	0.00	0.00	-	0.00	-	-
Chlorite	-	-	0.00	0.33	-	-	1.00	-	-	-	1.00	0.33	-	3.00	-	-
Epidote/Saussurite	-	-	2.33	3.33	-	-	6.00	-	-	-	1.00	1.00	-	0.67	-	-
Sericite/Illite	-	-	5.00	4.00	-	-	7.00	-	-	-	1.33	2.33	-	4.33	-	-
Non-resolvable clays	-	-	0.33	1.33	-	-	1.00	-	-	-	0.00	0.00	-	1.00	-	-
Kaolinite	-	-	0.00	0.00	-	-	0.00	-	-	-	0.00	0.00	-	0.00	-	-
Non-FE clays	-	-	0.00	0.00	-	-	1.67	-	-	-	0.67	0.33	-	1.00	-	-
FE Calcite	-	-	0.00	0.00	-	-	1.00	-	-	-	0.33	0.00	-	1.33	-	-
Non-FE Dolomite	-	-	0.00	0.00	-	-	0.00	-	-	-	0.00	0.00	-	0.00	-	-
FE Dolomite	-	-	0.00	0.00	-	-	0.00	-	-	-	0.00	0.00	-	0.00	-	-
Siderite	-	-	0.00	0.00	-	-	0.00	-	-	-	0.00	0.00	-	0.00	-	-
Bitumen (%)	-	-	0.00	0.00	-	-	0.33	-	-	-	0.33	0.67	-	0.00	-	-
Dissolution Porosity (%)	-	-	0.05	0.05	-	-	0.00	-	-	-	0.00	0.05	-	0.00	-	-
Natural Open Fracture (%)	-	-	0.00	0.05	-	-	0.05	-	-	-	0.33	0.33	-	0.33	-	-
Natural Void/Cavity/Druse (%)	-	-	0.05	0.05	-	-	0.00	-	-	-	0.00	0.33	-	0.00	-	-
Total Porosity (%)	-	-	0.10	0.15	-	-	0.05	-	-	-	0.33	0.72	-	0.33	-	-

PrCam: Precambrian COCH: Core chip DC: Ditch cuttings XRD: X-Ray diffraction

TABLE Ap1.4.1 Mineral, fracture and bitumen point count analysis data

Well	207/01-3			207/02-1		207/02-1	208/23-1						208/26-1	208/27-1	208/27-2	
Bottom Depth	4690.0	4700.0	4706.0	6722.0	6723.0	6724.0	9795.5	9796.5	9799.2	6803.0	6806.1	6808.0	3894.0	1380.2	4452.5	4522.2
Units (ft/m)	ft			ft		ft	ft						m	m	ft	
Stratigraphy	Precambrian Basement			Precambrian Basement		Precambrian Basement	Lewisian Basement						Precambrian Basement	Precambrian Basement	Lewisian Basement	
Age	PrCam			PrCam		PrCam	PrCam						PrCam	PrCam	PrCam	
Sample type	DC	DC	DC	COCH	COCH	COCH	COCH	COCH	COCH	COCH	COCH	COCH	COCH	-	COCH	COCH
Petrology Technique	XRD			Thin section	Thin section	Thin section	Thin section	Thin section	Thin section	Thin section	Thin section	Thin section	Thin section	Thin section	Thin section	Thin section
Point Count Data																
Quartz	-	-	-	38.67	54.67	48.33	-	33.33	41.67	19.67	43.33	35.33	21.00	-	-	-
K-Feldspar	-	-	-	16.00	32.67	23.00	-	24.00	23.67	42.33	0.05	2.33	10.00	-	-	-
Pagioclase Feldspar	-	-	-	21.33	7.33	16.67	-	15.67	12.00	14.67	28.67	17.33	48.00	-	-	-
Muscovite	-	-	-	0.33	0.05	0.05	-	0.05	0.67	0.05	4.67	5.33	0.33	-	-	-
Biotite	-	-	-	7.67	2.00	5.33	-	0.05	3.00	7.67	3.33	2.67	0.33	-	-	-
Amphibole/Hornblende	-	-	-	3.00	0.00	0.00	-	0.00	0.00	4.00	2.00	4.00	1.33	-	-	-
Opaque Minerals	-	-	-	2.00	1.00	1.33	-	1.67	2.67	2.33	1.67	2.00	1.00	-	-	-
Orthopyroxene	-	-	-	0.33	0.05	0.33	-	0.05	0.33	0.33	0.33	1.00	3.00	-	-	-
Clinopyroxene	-	-	-	0.33	0.00	0.05	-	0.00	0.00	0.00	0.33	0.33	0.00	-	-	-
Apatite	-	-	-	0.67	0.67	0.67	-	0.33	0.33	0.67	0.67	1.00	0.33	-	-	-
Garnet	-	-	-	0.00	0.00	0.00	-	0.00	0.00	0.00	0.00	0.00	0.67	-	-	-
Zircon	-	-	-	0.05	0.05	0.05	-	0.05	0.67	0.05	0.33	0.67	0.00	-	-	-
Olivine	-	-	-	0.00	0.00	0.00	-	0.00	0.00	0.00	0.00	0.00	0.00	-	-	-
Rutile	-	-	-	0.00	0.00	0.00	-	0.00	0.00	0.00	0.00	0.00	0.00	-	-	-
Chlorite	-	-	-	5.00	0.67	1.00	-	0.00	0.33	0.00	0.00	0.33	1.33	-	-	-
Epidote/Saussurite	-	-	-	0.00	0.00	0.00	-	0.00	1.33	0.00	6.33	12.00	1.67	-	-	-
Sericite/Illite	-	-	-	1.33	0.33	1.33	-	2.67	2.00	0.33	6.67	9.33	3.00	-	-	-
Non-resolvable clays	-	-	-	0.33	0.00	0.33	-	1.33	0.67	0.00	0.67	0.33	1.33	-	-	-
Kaolinite	-	-	-	0.00	0.00	0.00	-	2.33	0.33	0.00	0.00	0.00	0.00	-	-	-
Non-FE clays	-	-	-	1.33	0.00	0.00	-	0.00	0.33	0.00	0.00	3.00	0.00	-	-	-
FE Calcite	-	-	-	0.33	0.05	0.33	-	17.67	8.00	7.67	0.33	2.00	0.00	-	-	-
Non-FE Dolomite	-	-	-	0.00	0.00	0.00	-	0.00	0.00	0.00	0.00	0.00	0.00	-	-	-
FE Dolomite	-	-	-	0.00	0.00	0.00	-	0.00	0.00	0.00	0.00	0.00	0.00	-	-	-
Siderite	-	-	-	0.33	0.33	0.00	-	0.67	1.33	0.33	0.33	0.67	0.67	-	-	-
Bitumen (%)	-	-	-	0.67	0.00	0.00	-	0.33	0.67	0.00	0.33	0.00	0.33	-	-	-
Dissolution Porosity (%)	-	-	-	0.00	0.05	0.33	-	0.00	0.00	0.00	0.00	0.33	0.00	-	-	-
Natural Open Fracture (%)	-	-	-	0.33	0.33	1.00	-	0.00	0.00	0.00	0.00	0.00	0.67	-	-	-
Natural Void/Cavity/Druse (%)	-	-	-	0.05	0.05	0.05	-	0.05	0.05	0.05	0.00	0.00	0.33	-	-	-
Total Porosity (%)	-	-	-	0.38	0.43	1.38	-	0.05	0.05	0.05	0.00	0.33	1.00	-	-	-

PrCam: Precambrian

COCH: Core chip

DC: Ditch cuttings

XRD: X-Ray diffraction

TABLE Ap1.4.1 Mineral, fracture and bitumen point count analysis data

Well	208/27-2				209/09-1				209/12-1							
Bottom Depth	4527.5	4528.8	4531.2	4532.0	3190.3	8850.0	8854.0	8855.0	11385.7	11500.0	11510.0	11520.0	11521.0	11525.0	11526.0	11527.0
Units (ft/m)	ft				ft				ft							
Stratigraphy	Lewisian Basement				Caledonian Basement				Caledonian Basement							
Age	PrCam				Sil				Sil							
Sample type	COCH	COCH	COCH	COCH	COCH	COCH	COCH	COCH	COCH	DC	DC	DC	DC	COCH	COCH	COCH
Petrology Technique	Thin section	Thin section	Thin section	Thin section	Thin section	Thin section	Thin section	Thin section	-	XRD			Thin section	Thin section	Thin section	Thin section
Point Count Data																
Quartz	-	-	-	-	-	19.67	32.67	58.33	-	-	-	-	-	38.00	-	27.00
K-Feldspar	-	-	-	-	-	4.00	16.00	2.00	-	-	-	-	-	23.00	-	54.00
Pagioclase Feldspar	-	-	-	-	-	32.67	34.33	18.00	-	-	-	-	-	7.67	-	2.33
Muscovite	-	-	-	-	-	1.00	0.05	0.00	-	-	-	-	-	3.33	-	1.67
Biotite	-	-	-	-	-	21.67	8.33	13.67	-	-	-	-	-	23.33	-	12.00
Amphibole/Hornblende	-	-	-	-	-	0.00	0.00	0.00	-	-	-	-	-	0.00	-	0.00
Opaque Minerals	-	-	-	-	-	2.00	0.05	0.05	-	-	-	-	-	0.33	-	0.33
Orthopyroxene	-	-	-	-	-	1.00	0.05	0.00	-	-	-	-	-	0.33	-	0.05
Clinopyroxene	-	-	-	-	-	1.33	0.00	0.00	-	-	-	-	-	0.05	-	0.33
Apatite	-	-	-	-	-	0.67	0.33	0.33	-	-	-	-	-	0.67	-	0.33
Garnet	-	-	-	-	-	0.00	0.00	0.00	-	-	-	-	-	0.00	-	0.00
Zircon	-	-	-	-	-	0.05	0.05	0.05	-	-	-	-	-	0.33	-	0.33
Olivine	-	-	-	-	-	0.05	0.00	0.00	-	-	-	-	-	0.00	-	0.00
Rutile	-	-	-	-	-	0.00	0.00	0.00	-	-	-	-	-	0.00	-	0.00
Chlorite	-	-	-	-	-	3.67	4.00	5.00	-	-	-	-	-	0.05	-	0.33
Epidote/Saussurite	-	-	-	-	-	0.00	0.00	0.00	-	-	-	-	-	0.00	-	0.00
Sericite/Illite	-	-	-	-	-	4.00	2.33	0.67	-	-	-	-	-	3.00	-	1.33
Non-resolvable clays	-	-	-	-	-	0.00	0.00	0.00	-	-	-	-	-	0.00	-	0.00
Kaolinite	-	-	-	-	-	0.00	0.00	0.00	-	-	-	-	-	0.00	-	0.00
Non-FE clays	-	-	-	-	-	6.00	0.67	1.33	-	-	-	-	-	0.05	-	0.00
FE Calcite	-	-	-	-	-	0.33	0.67	0.67	-	-	-	-	-	0.00	-	0.00
Non-FE Dolomite	-	-	-	-	-	0.00	0.00	0.00	-	-	-	-	-	0.00	-	0.00
FE Dolomite	-	-	-	-	-	0.00	0.00	0.00	-	-	-	-	-	0.00	-	0.00
Siderite	-	-	-	-	-	0.00	0.00	0.00	-	-	-	-	-	0.00	-	0.00
Bitumen (%)	-	-	-	-	-	0.00	0.00	0.00	-	-	-	-	-	0.00	-	0.00
Dissolution Porosity (%)	-	-	-	-	-	2.00	0.67	0.00	-	-	-	-	-	0.00	-	0.00
Natural Open Fracture (%)	-	-	-	-	-	0.00	0.00	0.00	-	-	-	-	-	0.00	-	0.00
Natural Void/Cavity/Druse (%)	-	-	-	-	-	0.05	0.05	0.05	-	-	-	-	-	0.05	-	0.05
Total Porosity (%)	-	-	-	-	-	2.05	0.72	0.05	-	-	-	-	-	0.05	-	0.05

PrCam: Precambrian

Sil: Silurian

COCH: Core chip

DC: Ditch cuttings

XRD: X-Ray diffraction

TABLE Ap1.4.1 Mineral, fracture and bitumen point count analysis data

Well	214/09-1	220/26-1
Bottom Depth	11580.7	5280.2
Units (ft/m)	ft	m
Stratigraphy	Precambrian Basement	Caledonian Basement
Age	PrCam	Sil
Sample type	DC	COCH
Petrology Technique	Thin section	Thin section
Point Count Data		
Quartz	39.67	-
K-Feldspar	32.67	-
Pagioclase Feldspar	12.00	-
Muscovite	3.00	-
Biotite	3.67	-
Amphibole/Hornblende	0.00	-
Opaque Minerals	1.00	-
Orthopyroxene	1.67	-
Clinopyroxene	-	-
Apatite	0.67	-
Garnet	0.00	-
Zircon	0.05	-
Olivine	-	-
Rutile	0.00	-
Chlorite	0.67	-
Epidote/Saussurite	0.00	-
Sericite/Illite	1.00	-
Non-resolvable clays	0.00	-
Kaolinite	-	-
Non-FE clays	1.33	-
FE Calcite	0.00	-
Non-FE Dolomite	0.00	-
FE Dolomite	0.00	-
Siderite	1.00	-
Bitumen (%)	0.05	-
Dissolution Porosity (%)	0.05	-
Natural Open Fracture (%)	0.05	-
Natural Void/Cavity/Druse (%)	0.05	-
Total Porosity (%)	0.15	-

PrCam: Precambrian

Sil: Silurian

COCH: Core chip

DC: Ditch cuttings

TABLE Ap1.4.1 Mineral, fracture and bitumen point count analysis data

APPENDIX 2

APATITE FISSION TRACK DATA

APPENDIX 2.1 Summary of samples analysed for apatite fission track

APPENDIX 2.2 Apatite fission track (AFT) data

APPENDIX 2.1

SUMMARY OF SAMPLES ANALYSED FOR APATITE FISSION TRACK

Tables

Ap2.1.1 Sample details – apatite fission track analyses

Well	Top depth	Bottom depth	Units (m/ft)	Stratigraphy	Age	Sample type	Basin	Mud system	Anal. reason	Anal. status	Sample ID
204/10a-5	2361.8	2383.5	m	Hildasay	E1	COCH	Corona	WBM	AFT	N	P10012_013
205/09-1	2798.0	2807.0	m	Sele	E1	DC	Flett	WBM (Bentonite & KCl polymer)	AFT	N	P10012_001
	3704.0	3719.0	m	Lista (D1 Sand)	P3	DC			AFT	N	P10012_002
205/12-1	-	2570.0	m	Lamba	P3	DC	Flett	WBM (KCl polymer)	AFT	N	P10012_003
	-	3175.0	m	Shetland	K2	DC			AFT	N	P10012_004
205/14-2	-	7430.0	ft	Unit IV Upper	P3	DC	Flett	WBM (KCl polymer & Glycol)	AFT	N	P10012_005
205/17b-2	-	2443.8	m	Lista	P3	COCH	Flett Ridge	WBM (KCl polymer)	AFT	N	P10012_006
206/11-1	4370.0	4376.0	m	Early Cret Sands	K1	DC	Rona Ridge	WBM	AFT	N	P10012_007
207/01-2	5590.0	5620.0	ft	Victory	K1	DC	West Shetland	WBM (Seawater, CMC, barite & bentonite)	AFT	L	P10011_003
	5740.0	5750.0	ft	PrCam Basement	PrCam	DC			AFT	L	P10011_004
208/17-2	7871.0	7946.8	ft	Waterhouse	P3	COCH	N Faroe-Shetland	OBM (Aquamul)	AFT	N	P10012_008
208/24-1A	5900.0	6000.0	ft	Victory	K1	DC	Northern Faroe-Shetland	OBM (Invermul)	AFT	L	P10011_006
	6530.0	6300.0	ft	Victory	K1	DC			AFT	L	P10011_007
208/27-2	4960.0	3990.0	ft	Shetland	K2	DC	Clair-Vicotry Ridge	WBM (POLY SAL - Lignosulfonate)	AFT	L	P10011_009
	-	4540.0	ft	PrCam Basement	PrCam	DC			AFT	L	P10011_011
	4300.0	4590.0	ft	Caved Shetland	K2	DC			AFT	L	P10011_013
214/26-1	7516.0	7539.0	ft	Lewis Fan Env	E2	DC	Flett	WBM (Sewater & polyclycol)	AFT	N	P10012_009
214/28-1	-	8374.3	ft	Late Paleocene	P3	COCH	Flett Ridge	OBM (Enviromul/Invermul)	AFT	N	P10012_010
	11900.0	11920.0	ft	Middle Paleocene	P2	DC			AFT	N	P10012_011
	14310.0	14334.4	ft	E-M Paleocene	P1	COCH			AFT	N	P10012_012

Abbreviations/Key

Early Cret Sands: Early Cretaceous Sands

PrCam Basement: Precambrian Basement

Lewis Fan Env: Lewis Fan Envelope (Lobe 2)

E-M Paleocene: Early-Middle Paleocene

PrCamb: Precambrian

DC: Ditch cuttings

COCH: Core chip

N Faroe-Shetland: North Faroe-Shetland

WBM: Water based mud

OBM: Oil base mud

N: New analyses for this study

L: Legacy APT data

TABLE Ap2.1.1 Sample details - apatite fission track analyses

APPENDIX 2.2 APATITE FISSION TRACK (AFT) DATA

Tables

Ap2.2.1a	Apatite fission track age data: sub-groups
Ap2.2.1b	Apatite fission track age data: combined
Ap2.2.2a	Apatite fission track length data: sub-groups
Ap2.2.2b	Apatite fission track length data: combined

Well	Top Depth	Bottom Depth	Units (m/ft)	Stratigraphy	Age	Sample Type	Sample ID.	Sub Group	Accepted (Spots)	Pooled UFT Age (Ma)	Pooled CI-95% (Ma)	Pooled CI+95% (Ma)	Pooled Ns (SFT)	Pooled Area (μm*μm)	Pooled Rho	Pooled Sigma
204/10a-5	2361.8	2383.5	m	Hildasay	E1	COCH	P10012_013	-	33	235.4	20.72	22.68	783	93557	5620	53.6
								1	5	164.0	36.76	47.21	67	19534	694	18.6
								2A	5	245.5	62.94	84.10	47	17447	323	7.8
								2B	6	272.3	36.04	41.41	245	8075	1520	27.5
								2C	17	232.1	25.03	28.00	424	48501	3090	41.4
205/09-1	2798.0	2807.0	m	Sele	E1	DC	P10012_001	-	9	283.2	65.87	85.27	60	12228	2390	58.5
	3704.0	3719.0		Lista (D1 Sand)	P3	DC	P10012_002	2	9	283.2	65.87	85.27	60	12228	2390	58.5
								-	24	59.5	12.27	15.43	81	29516	15700	185.0
								0	6	21.1	13.35	36.30	4	7865	2190	74.7
								1	6	54.3	19.35	30.01	21	4953	4450	87.2
								2	6	117.7	28.78	37.99	54	9479	5250	120.0
								3	4	0.0	0.00	12.12	0	4709	2860	76.8
205/12-1	-	2750.0	m	Lamba	P3	DC	P10012_003	-	29	173.7	18.55	20.74	445	49043	29200	259.0
								0	3	178.9	51.96	72.83	35	5733	2230	55.4
								1	5	233.3	53.33	68.76	65	7308	3160	102.0
								2A	5	208.3	36.28	43.78	121	9092	6600	96.9
								2B	14	145.6	20.33	23.58	214	23606	16800	210.0
	-	3175.0		Shetland	K2	DC	P10012_004	-	10	219.3	41.19	50.52	101	9762	5230	92.7
								0	3	209.3	60.33	84.21	36	3675	1960	61.7
								1	3	209.3	58.98	81.60	38	2614	2060	61.6
								2	4	252.3	80.96	118.13	27	3473	1210	31.7
205/14-2	-	7430.0	ft	Unit IV Upper	P3	DC	P10012_005	-	25	234.7	30.03	34.35	273	38545	13200	204.0
								0	5	123.5	38.45	55.59	31	8383	2870	133.0
								1	7	263.7	53.88	67.36	85	9449	3650	105.0
								2	5	224.8	55.21	72.78	53	8621	2680	68.8
								3	6	292.4	55.38	67.97	100	8416	3860	90.0
205/17b-2	-	2443.8	m	Lista	P3	COCH	P10012_006	-	37	291.8	27.26	29.99	691	77996	26700	290.0
								0	6	286.6	45.48	53.84	165	10465	6510	181.0

TABLE Ap2.2.1a Apatite fission track age data: sub-groups

Well	Top Depth	Bottom Depth	Units (m/ft)	Stratigraphy	Age	Sample Type	Sample ID.	Sub Group	Zeta	1 Sigma	Chi²	P(Chi²)
204/10a-5	2361.8	2383.5	m	Hildasay	E1	COCH	P10012_013	-	1720.0	50.0	116.0	0.0000
								1			16.9	0.0020
								2A			3.5	0.4820
								2B			21.9	0.0005
								2C			64.4	0.0000
205/09-1	2798.0	2807.0	m	Sele	E1	DC	P10012_001	-	11600.0	355.0	13.0	0.1120
								2			13.0	0.1120
	3704.0	3719.0		Lista (D1 Sand)	P3	DC	P10012_002	-	11600.0	355.0	133.0	0.0000
								0			3.3	0.6550
								1			37.5	0.0000
								2			38.8	0.0000
								3			0.0	0.0000
205/12-1	-	2750.0	m	Lamba	P3	DC	P10012_003	-	11600.0	355.0	94.1	0.0000
								0			3.9	0.1410
								1			4.7	0.3150
								2A			9.7	0.0460
								2B			61.9	0.0000
	-	3175.0		Shetland	K2	DC	P10012_004	-	11600.0	355.0	18.6	0.0291
								0			1.2	0.5580
								1			11.6	0.0030
								2			4.5	0.2170
205/14-2	-	7430.0	ft	Unit IV Upper	P3	DC	P10012_005	-	11600.0	355.0	72.6	0.0000
								0			20.6	0.0004
								1			10.1	0.1200
								2			17.3	0.0017
								3			13.0	0.0238
205/17b-2	-	2443.8	m	Lista	P3	COCH	P10012_006	-	11600.0	355.0	109.0	0.0000
								0			3.6	0.6070

TABLE Ap2.2.1a Apatite fission track age data: sub-groups

Well	Top Depth	Bottom Depth	Units (m/ft)	Stratigraphy	Age	Sample Type	Sample ID.	Sub Group	Accepted (Spots)	Pooled UFT Age (Ma)	Pooled CI-95% (Ma)	Pooled CI+95% (Ma)	Pooled Ns (SFT)	Pooled Area (μm*μm)	Pooled Rho	Pooled 1 Sigma
205/17b-2	-	2443.8	m	Lista	P3	COCH	P10012_006	1	6	236.7	46.31	57.32	93	11677	4460	105.0
								2A	6	123.6	33.41	45.62	43	15249	3980	128.0
								2B	10	378.6	51.56	59.42	227	17889	6720	118.0
								2C	6	354.2	63.25	76.54	115	14632	3650	83.7
206/11-1	4370.0	4376.0	m	Early Cretaceous Sands	K1	DC	P10012_007	-	19	5.1	2.86	6.48	6	46829	13600	225.0
								1	4	0.0	0.00	20.69	0	9574	1670	57.0
								2	14	5.9	3.28	7.44	6	36572	11800	218.0
207/01-2	5590.0	5620.0	ft	Victory	K1	DC	P10011_003	-	37	190.7	14.90	16.15	1120	58943	37900	322.0
								1A	26	189.4	16.09	17.56	839	38213	28600	279.0
								1B	6	221.8	36.35	43.33	140	7857	4070	79.6
								2	1	143.1	35.23	46.57	54	2122	2450	81.4
	5740.0	5750.0	ft	Precambrian Basement	PrCam	DC	P10011_004	-	36	249.7	24.32	26.89	974	72918	47300	533.0
								1A	9	302.9	38.33	43.73	400	15633	16000	425.0
								1B	2	321.1	63.85	79.21	98	7689	3680	121.0
								2A	4	201.7	51.67	69.10	49	8336	2960	67.4
								2B	11	184.5	25.61	29.67	254	21224	16800	252.0
	7871.0	7946.8	ft	Waterhouse	P3	COCH	P10012_008	-	26	216.2	22.64	25.23	498	65289	26200	373.0
								0	6	266.1	64.87	85.22	55	23505	2340	77.7
								1A	6	262.1	44.14	52.86	138	7791	5960	149.0
								1B	7	174.3	26.21	30.77	190	17995	12400	304.0
								2	5	225.2	44.87	55.79	91	10234	4590	130.0
208/24-1A	5900.0	6000.0	ft	Victory	K1	DC	P10011_006	-	34	220.4	17.81	19.34	1004	60645	29300	292.0
								1A	17	218.0	21.99	24.41	508	26295	15000	217.0
								2B	13	225.4	23.54	26.23	455	28482	13000	186.0
								2	2	217.9	68.59	99.34	30	2776	887	45.9
	6230.0	6300.0	ft	Victory	K1	DC	P10011_007	-	36	168.2	13.62	14.80	1048	61049	40300	468.0
								1A	14	174.0	18.11	20.18	512	21835	19000	382.0
								1B	10	151.8	17.65	19.94	343	14888	14600	230.0

TABLE Ap2.2.1a Apatite fission track age data: sub-groups

Well	Top Depth	Bottom Depth	Units (m/ft)	Stratigraphy	Age	Sample Type	Sample ID.	Sub Group	Zeta	1 Sigma	Chi²	P(Chi²)
205/17b-2	-	2443.8	m	Lista	P3	COCH	P10012_006	1	11600.0	355.0	9.8	0.0821
								2A			21.9	0.0006
								2B			15.1	0.0894
								2C			14.2	0.0145
206/11-1	4370.0	4376.0	m	Early Cretaceous Sands	K1	DC	P10012_007	-	11600.0	355.0	13.6	0.7550
								1			0.0	0.0000
								2			11.5	0.5720
207/01-2	5590.0	5620.0	ft	Victory	K1	DC	P10011_003	-	6550.0	178.0	61.7	0.0049
								1A			41.9	0.0186
								1B			5.4	0.3690
								2			0.0	0.0000
	5740.0	5750.0		Precambrian Basement	PrCam	DC	P10011_004	-	12400.0	490.0	118.0	0.0000
								1A			18.2	0.0196
								1B			4.6	0.0318
								2A			5.4	0.1480
						2B	15.4	0.1190				
208/17-2	7871.0	7946.8	ft	Waterhouse	P3	COCH	P10012_008	-	11600.0	355.0	96.8	0.0000
								0			19.0	0.0019
								1A			5.1	0.4020
								1B			29.0	0.0001
								2			18.8	0.0009
208/24-1A	5900.0	6000.0	ft	Victory	K1	DC	P10011_006	-	6550.0	178.0	68.7	0.0003
								1A			29.1	0.0231
								2B			36.1	0.0003
								2			0.8	0.3660
	6230.0	6300.0		Victory	K1	DC	P10011_007	-	6550.0	178.0	194.0	0.0000
								1A			100.0	0.0000
						1B	63.3	0.0000				

TABLE Ap2.2.1a Apatite fission track age data: sub-groups

Well	Top Depth	Bottom Depth	Units (m/ft)	Stratigraphy	Age	Sample Type	Sample ID.	Sub Group	Accepted (Spots)	Pooled UFT Age (Ma)	Pooled CI-95% (Ma)	Pooled CI+95% (Ma)	Pooled Ns (SFT)	Pooled Area (μm*μm)	Pooled Rho	Pooled Sigma
208/24-1A	6230.0	6300.0	ft	Victory	K1	DC	P1001_007	2	8	197.5	33.59	40.35	129	15786	4210	88.4
208/27-2	3960.0	3990.0	ft	Shetland	K2	DC	P10011_009	-	6	189.0	41.83	53.50	67	4711	2290	45.2
								1	1	285.7	107.83	170.95	18	1494	404	17.6
								2	5	168.1	42.43	56.50	49	3218	1890	41.6
	-	4540.0		PreCambrian Basement	PrCam	DC	P10011_011	-	38	203.4	16.93	18.45	897	73981	28400	276.0
								1	4	270.5	60.86	78.05	70	7816	1660	70.8
								2A	19	210.7	20.64	22.84	532	30601	16300	179.0
								2B	15	181.3	22.44	25.56	295	35565	10500	197.0
	4300.0	4590.0		Caved Shetland	K2	DC	P10011_013	-	39	197.0	22.86	25.81	454	50385	28100	336.0
								1	3	144.1	59.96	101.90	14	3239	1190	30.8
								2A	30	201.6	24.40	27.70	387	36964	23400	264.0
								2B	6	183.7	48.29	65.18	53	10182	3520	205.0
								214/26-1	7516.0	7539.0	ft	Lewis Fan Envelope	E2	DC	P10012_009	-
1.0	8	202.3	51.24	68.25	52	10330	2000									71.2
2A	4	220.7	54.14	71.34	55	8322	1930									55.5
2B	6	290.7	60.92	76.62	87	10220	2310									89.4
2C	12	211.3	45.75	58.13	75	13944	2760									67.0
214/28-1	-	8374.3	ft	Late Paleocene	P3	COCH	P10012_010	-	29	165.0	18.64	20.98	454	63970	21400	190.0
								1A	3	226.0	41.86	51.17	114	3073	3910	100.0
								1B	15	137.1	20.32	23.82	199	35812	11300	132.0
								2C	11	177.0	29.81	35.74	141	25085	6200	92.7
	11900.0	11920.0		Middle Paleocene	P2	DC	P10012_011	-	32	4.1	1.61	2.63	17	58838	32400	360.0
								0	3	13.8	-13.79	6.88	2	2644	1140	21.6
								1	12	4.4	2.23	4.54	8	22128	14400	204.0
								2A	8	10.5	6.63	18.05	4	16928	3010	62.4
	14310.0	14334.4		Early-Middle Paleocene	P1	COCH	P10012_012	2B	9	1.7	1.17	3.74	3	17138	13800	289.0
								-	36	2.0	0.92	1.68	11	72694	43100	441.0
								0	4	51.9	25.36	49.41	9	5439	1360	33.5

TABLE Ap2.2.1a Apatite fission track age data: sub-groups

Well	Top Depth	Bottom Depth	Units (m/ft)	Stratigraphy	Age	Sample Type	Sample ID.	Sub Group	Zeta	1 Sigma	Chi²	P(Chi²)
208/24-1A	6230.0	6300.0	ft	Victory	K1	DC	P1001_007	2	6550.0	178.0	19.6	0.0064
208/27-2	3960.0	3990.0	ft	Shetland	K2	DC	P10011_009	-	6550.0	178.0	22.5	0.0004
								1			0.0	0.0000
								2			20.7	0.0004
	-	4540.0		PreCambrian Basement	PrCam	DC	P10011_011	-	6550.0	178.0	68.3	0.0013
								1			10.2	0.0172
								2A			22.4	0.2150
								2B			29.0	0.0105
	4300.0	4590.0		Caved Shetland	K2	DC	P10011_013	-	12400.0	490.0	85.9	0.0000
								1			1.6	0.4510
								2A			67.7	0.0001
								2B			16.1	0.0065
214/26-1	7516.0	7539.0	ft	Lewis Fan Envelope	E2	DC	P10012_009	-	7890.0	295.0	42.2	0.0541
								1.0			8.5	0.2900
								2A			7.3	0.0622
								2B			4.5	0.4810
								2C			18.3	0.0749
214/28-1	-	8374.3	ft	Late Paleocene	P3	COCH	P10012_010	-	7890.0	295.0	90.0	0.0000
								1A			9.8	0.0075
								1B			55.9	0.0000
								2C			15.0	0.1310
	11900.0	11920.0		Middle Paleocen	P2	DC	P10012_011	-	7890.0	295.0	69.4	0.0001
								0			7.3	0.0257
								1			32.1	0.0007
								2A			7.5	0.3750
								2B			2.9	0.9420
	14310.0	14334.4		Early-Middle Paleocene	P1	COCH	P10012_012	-	7890.0	295.0	233.0	0.0000
								0			30.8	0.0000

TABLE Ap2.2.1a Apatite fission track age data: sub-groups

Well	Top Depth	Bottom Depth	Units (m/ft)	Stratigraphy	Age	Sample Type	Sample ID.	Sub Group	Accepted (Spots)	Pooled UFT Age (Ma)	Pooled CI-95% (Ma)	Pooled CI+95% (Ma)	Pooled Ns (SFT)	Pooled Area (μm^2)	Pooled Rho	Pooled 1 Sigma
214/28-1	14310	14334	ft	Early-Middle Paleocene	P1	COCH	P10012_012	1	6	0.8	-0.83	1.66	1	10147	9490	347.0
								2	8	0.0	0.00	1.99	0	16505	11900	176.0
								3A	9	0.0	0.00	1.92	0	19080	12300	155.0
								3B	8	1.0	-1.03	2.06	1	18661	7660	132.0

Well	Top Depth	Bottom Depth	Units (m/ft)	Stratigraphy	Age	Sample Type	Sample ID.	Sub Group	Zeta	1 Sigma	Chi ²	P(Chi ²)
214/28-1	14310	14334	ft	Early-Middle Paleocene	P1	COCH	P10012_012	1	7890.0	295.0	4.0	0.5440
								2			0.0	0.0000
								3A			0.0	0.0000
								3B			7.8	0.3520

TABLE Ap2.2.1a Apatite fission track age data: sub-groups

Well	Top Depth	Bottom Depth	Units (m/ft)	Stratigraphy	Age	Sample Type	Sample ID.	Accepted (Spots)	Pooled UFT Age (Ma)	Pooled CI-95% (Ma)	Pooled CI+95% (Ma)	Pooled Ns (SFT)	Pooled Area (μm*μm)	Pooled Rho	Pooled 1 Sigma Rho	Median UPb Age (Ma)
204/10a-5	2361.8	2383.5	m	Hildasay	E1	COCH	P10012_013	39	235.65	20.67	22.62	792	114000	5679	37.9	1515.1
205/09-1	2798.0	2807.0	m	Sele	E1	DC	P10012_001	19	234.37	45.11	55.62	99	22320	4792	93.4	1399.5
	3704.0	3719.0	m	Lista (D1 Sand)	P3	DC	P10012_002	33	59.32	11.24	13.85	100	42430	19380	181.9	754.7
205/12-1	-	2570.0	m	Lamba	P3	DC	P10012_003	38	163.74	29.17	35.40	524	59690	36500	2159.0	1507.8
	-	3175.0	m	Shetland	K2	DC	P10012_004	13	222.91	41.20	50.34	105	12410	5348	65.7	564.0
205/14-2	-	7430.0	ft	Unit IV Upper	P3	DC	P10012_005	33	239.29	29.02	32.94	317	47560	15020	160.4	792.7
205/17b-2	-	2443.8	m	Lista	P3	COCH	P10012_006	42	294.12	27.30	30.02	754	90640	28950	294.0	1156.8
206/11-1	4370.0	4376.0	m	Early Cret Sands	K1	DC	P10012_007	40	4.49	1.98	3.54	12	99470	30840	399.7	1751.8
207/01-2	5590.0	5620.0	ft	Victory	K1	DC	P10011_003	41	191.24	14.73	15.94	1182	68010	39900	233.4	538.5
	5740.0	5750.0	ft	PrCam Basemen	PrCam	DC	P10011_004	42	250.59	24.30	26.85	995	87430	48170	377.5	1025.3
208/17-2	7871.0	7946.8	ft	Waterhouse	P3	COCH	P10012_008	37	225.70	22.26	24.64	598	98310	30080	276.7	574.2
208/24-1A	5900.0	6000.0	ft	Victory	K1	DC	P10011_006	41	222.98	17.91	19.44	1026	79280	29630	206.9	526.9
	6530.0	6300.0	ft	Victory	K1	DC	P10011_007	37	171.64	13.83	15.03	1077	63380	40570	343.4	563.4
208/27-2	4960.0	3990.0	ft	Shetland	K2	DC	P10011_009	12	193.76	38.23	47.46	98	16070	3265	88.3	1447.5
	-	4540.0	ft	PrCam Basemen	PrCam	DC	P10011_011	40	204.19	16.75	18.22	968	76080	30570	232.6	1467.6
	4300.0	4590.0	ft	Caved Shetland	K2	DC	P10011_013	42	196.18	22.54	25.41	470	55710	29190	238.4	1575.1
214/26-1	7516.0	7539.0	ft	Lewis Fan Env	E2	DC	P10012_009	36	235.54	31.22	35.90	279	51580	9179	101.8	1527.1
214/28-1	-	8374.3	ft	Late Paleocene	P3	COCH	P10012_010	39	165.49	18.50	20.79	471	98410	22180	135.1	613.3
	11900.0	11920.0	ft	Middle Paleocen	P2	DC	P10012_011	40	3.02	1.15	1.85	18	75900	47060	286.6	935.6
	14310.0	14334.4	ft	E-M Paleocene	P1	COCH	P10012_012	36	2.01	0.92	1.68	11	72690	43120	311.5	1738.4

TABLE Ap2.2.1b Apatite fission track age data: combined

Well	Top Depth	Bottom Depth	Units (m/ft)	Stratigraphy	Age	Sample Type	Sample ID.	Median -2 Sigma (Ma)	Median +2 Sigma (Ma)	Median U (ppm)	Median Th (ppm)	Median Sm (ppm)	Median Etch Figures	Median Dpar (µm)	Median Dper (µm)	Median Rmr
204/10a-5	2361.8	2383.5	m	Hildasay	E1	COCH	P10012_013	-232.3	232.3	5.4	0.4	27.7	8	2.41	0.79	0.8521
205/09-1	2798.0	2807.0	m	Sele	E1	DC	P10012_001	-391.5	391.5	5.0	1.0	84.0	5	1.70	0.50	0.7780
	3704.0	3719.0	m	Lista (D1 Sand)	P3	DC	P10012_002	-256.4	256.4	6.2	1.9	78.0	4	1.68	0.46	0.8032
205/12-1	-	2570.0	m	Lamba	P3	DC	P10012_003	-338.3	338.3	9.0	1.0	47.3	7	1.60	0.46	0.7804
	-	3175.0	m	Shetland	K2	DC	P10012_004	-149.9	149.9	8.9	3.8	163.6	5	1.47	0.45	0.7959
205/14-2	-	7430.0	ft	Unit IV Upper	P3	DC	P10012_005	-227.2	227.2	6.2	2.3	72.8	7	1.61	0.46	0.8118
205/17b-2	-	2443.8	m	Lista	P3	COCH	P10012_006	-304.3	304.3	6.0	4.9	100.7	9	1.65	0.45	0.8342
206/11-1	4370.0	4376.0	m	Early Cret Sands	K1	DC	P10012_007	-421.4	421.4	5.6	5.1	320.3	4	1.59	0.43	0.8305
207/01-2	5590.0	5620.0	ft	Victory	K1	DC	P10011_003	-117.7	117.7	26.2	6.7	205.1	5	1.78	0.46	0.8319
	5740.0	5750.0	ft	PrCam Basemen	PrCam	DC	P10011_004	-262.2	262.2	13.1	10.2	175.8	5	1.77	0.45	0.8414
208/17-2	7871.0	7946.8	ft	Waterhouse	P3	COCH	P10012_008	-148.2	148.2	8.6	1.3	74.0	8	1.50	0.45	0.7751
208/24-1A	5900.0	6000.0	ft	Victory	K1	DC	P10011_006	-112.3	112.3	18.8	17.5	161.0	5	2.19	0.46	0.7914
	6530.0	6300.0	ft	Victory	K1	DC	P10011_007	-131.0	131.0	20.3	23.3	243.1	6	1.85	0.44	0.8206
208/27-2	4960.0	3990.0	ft	Shetland	K2	DC	P10011_009	-293.8	293.8	13.3	9.5	126.3	6	1.57	0.50	0.8079
	-	4540.0	ft	PrCam Basemen	PrCam	DC	P10011_011	-303.8	303.8	14.1	5.2	277.3	6	1.56	0.43	0.8257
	4300.0	4590.0	ft	Caved Shetland	K2	DC	P10011_013	-317.6	317.6	9.7	2.6	336.4	5	1.82	0.46	0.7899
214/26-1	7516.0	7539.0	ft	Lewis Fan Env	E2	DC	P10012_009	-279.2	279.2	5.4	1.8	117.8	5	1.46	0.43	0.8459
214/28-1	-	8374.3	ft	Late Paleocene	P3	COCH	P10012_010	-126.4	126.4	10.6	4.5	65.5	7	1.84	0.44	0.8428
	11900.0	11920.0	ft	Middle Paleocen	P2	DC	P10012_011	-162.9	162.9	8.6	11.3	101.6	2	1.61	0.44	0.8301
	14310.0	14334.4	ft	E-M Paleocene	P1	COCH	P10012_012	-272.8	272.8	11.5	2.2	137.8	3	1.70	0.47	0.8293

TABLE Ap2.2.1b Apatite fission track age data: combined

Well	Top Depth	Bottom Depth	Units (m/ft)	Stratigraphy	Age	Sample Type	Sample ID.	Zeta	1 Sigma	Chi ²	P(Chi ²)
204/10a-5	2361.8	2383.5	m	Hildasay	E1	COCH	P10012_013	1721	49.6	128.7	0.0000
205/09-1	2798.0	2807.0	m	Sele	E1	DC	P10012_001	11550	354.9	53.0	0.0000
	3704.0	3719.0	m	Lista (D1 Sand)	P3	DC	P10012_002	11550	354.9	187.1	0.0000
205/12-1	-	2570.0	m	Lamba	P3	DC	P10012_003	11550	354.9	191.5	0.0000
	-	3175.0	m	Shetland	K2	DC	P10012_004	11550	354.9	30.6	0.0023
205/14-2	-	7430.0	ft	Unit IV Upper	P3	DC	P10012_005	11550	354.9	83.6	0.0000
205/17b-2	-	2443.8	m	Lista	P3	COCH	P10012_006	11550	354.9	117.8	0.0000
206/11-1	4370.0	4376.0	m	Early Cret Sands	K1	DC	P10012_007	11550	354.9	51.4	0.0877
207/01-2	5590.0	5620.0	ft	Victory	K1	DC	P10011_003	6553	178.1	68.6	0.0033
	5740.0	5750.0	ft	PrCam Basemen	PrCam	DC	P10011_004	12370	490.1	143.2	0.0000
208/17-2	7871.0	7946.8	ft	Waterhouse	P3	COCH	P10012_008	11550	354.9	122.7	0.0000
208/24-1A	5900.0	6000.0	ft	Victory	K1	DC	P10011_006	6553	178.1	176.1	0.0000
	6530.0	6300.0	ft	Victory	K1	DC	P10011_007	6553	178.1	207.9	0.0000
208/27-2	4960.0	3990.0	ft	Shetland	K2	DC	P10011_009	6553	178.1	58.8	0.0000
	-	4540.0	ft	PrCam Basemen	PrCam	DC	P10011_011	6553	178.1	76.0	0.0004
	4300.0	4590.0	ft	Caved Shetland	K2	DC	P10011_013	12370	490.1	89.1	0.0000
214/26-1	7516.0	7539.0	ft	Lewis Fan Env	E2	DC	P10012_009	7892	295.3	74.0	0.0001
214/28-1	-	8374.3	ft	Late Paleocene	P3	COCH	P10012_010	7892	295.3	98.7	0.0000
	11900.0	11920.0	ft	Middle Paleocen	P2	DC	P10012_011	7892	295.3	86.9	0.0000
	14310.0	14334.4	ft	E-M Paleocene	P1	COCH	P10012_012	7892	295.3	235.4	0.0000

TABLE Ap2.2.1b Apatite fission track age data: combined

Well	Top Depth	Bottom Depth	Units (m/ft)	Stratigraphy	Age	Sample Type	Sample ID.	Sub Group	Accepted (CFT's)	Mean Length (µm)	Standard Error (µm)	Standard Dev (µm)	Median Upb Age (Ma)	Median - 2 Sigma (Ma)	Median +2 Sigma (Ma)	Median U (ppm)
204/10a-5	2361.8	2383.5	m	Hildasay	E1	COCH	P10012_013	-	206	12.32	0.10	1.40	1537.7	-230.6	222.6	13.7
								1	37	13.19	0.19	1.14	482.6	-79.4	78.4	10.3
								2A	-	-	-	-	977.7	-172.0	167.5	2.0
								2B	48	11.74	0.23	1.56	1480.9	-223.8	216.3	26.5
								2C	121	12.29	0.12	1.27	1607.3	-238.3	229.8	13.9
205/09-1	2798.0	2807.0	m	Sele	E1	DC	P10012_001	-	8	10.85	0.42	1.10	1406.2	-371.4	351.0	6.4
	3704.0	3719.0		Lista (D1 Sand)	P3	DC	P10012_002	2	8	10.85	0.42	1.10	1406.2	-371.4	351.0	6.4
								-	23	9.98	0.42	1.96	1070.8	-258.5	249.8	13.9
								0	1	14.00	0.00	0.00	178.2	-116.3	150.7	4.9
								1	4	9.78	1.08	1.87	667.3	-190.3	184.7	39.0
								2	11	9.51	0.49	1.54	1006.6	-276.9	265.4	13.9
								3	7	10.26	0.93	2.28	2267.0	-473.9	441.2	10.8
205/12-1	-	2750.0	m	Lamba	P3	DC	P10012_003	-	185	12.18	0.11	1.43	1536.2	-335.4	318.7	14.1
								0	17	12.42	0.33	1.31	388.5	-85.1	83.9	16.3
								1	32	12.04	0.26	1.46	722.1	-403.8	373.6	21.9
								2A	39	12.17	0.26	1.61	1597.5	-347.1	329.4	14.7
								2B	94	12.21	0.14	1.37	1661.5	-341.7	324.5	13.1
	-	3175.0		Shetland	K2	DC	P10012_004	-	10	10.98	0.46	1.39	454.4	-120.8	118.4	10.2
								0	5	11.86	0.39	0.78	246.1	-66.3	65.6	11.1
								1	5	10.11	0.68	1.37	533.3	-126.8	124.3	21.4
								2	-	-	-	-	1552.7	-501.1	462.7	4.8
205/14-2	-	7430.0	ft	Unit IV Upper	P3	DC	P10012_005	-	65	12.23	0.21	1.64	1093.5	-275.5	252.6	10.5
								0	1	12.05	0.00	0.00	152.3	-81.2	80.2	4.6
								1	24	12.95	0.30	1.46	533.5	-132.2	129.5	12.1
								2	12	12.16	0.46	1.51	1421.4	-347.2	329.3	6.1
								3	28	11.65	0.33	1.69	2206.5	-548.1	505.0	11.9
205/17b-2	-	2443.8	m	Lista	P3	COCH	P10012_006	-	196	12.04	0.11	1.56	1419.2	-323.4	308.0	12.7
								0	32	12.29	0.20	1.11	232.1	-66.2	65.5	16.0

TABLE Ap2.2.2a Apatite fission track length data: sub-groups

Well	Top Depth	Bottom Depth	Units (m/ft)	Stratigraphy	Age	Sample Type	Sample ID.	Sub Group	Median Th (ppm)	Median Sm (ppm)	Median Etch Figures	Median Dpar (μm)	Median Dper (μm)	Median Rmr (μm)
204/10a-5	2361.8	2383.5	m	Hildasay	E1	COCH	P10012_013	-	1.3	32.7	12	1.84	0.53	0.8513
								1	2.6	62.3	12	1.84	0.58	0.8491
								2A	0.3	38.9	6	1.86	0.48	0.8574
								2B	0.5	269.5	12	1.92	0.51	0.8314
								2C	0.9	22.7	12	1.83	0.51	0.8520
205/09-1	2798.0	2807.0	m	Sele	E1	DC	P10012_001	-	1.6	75.3	7	1.63	0.49	0.7806
	3704.0	3719.0		Lista (D1 Sand)	P3	DC	P10012_002	2	1.6	75.3	7	1.63	0.49	0.7806
								-	1.4	169.4	4	1.74	0.54	0.8094
								0	36.1	214.8	4	1.90	0.61	0.8231
								1	39.3	111.2	6	1.75	0.48	0.8055
								2	1.4	163.6	6	1.75	0.54	0.7951
	3	7.5		102.9	4	1.80	0.47	0.8340						
205/12-1	-	2750.0	m	Lamba	P3	DC	P10012_003	-	1.2	73.2	8	1.75	0.46	0.8045
								0	50.0	185.9	8	1.82	0.45	0.7342
								1	12.5	94.4	9	1.73	0.45	0.7359
								2A	1.0	279.1	10	1.79	0.51	0.7490
								2B	1.3	32.2	8	1.71	0.47	0.8230
	-	3175.0		Shetland	K2	DC	P10012_004	-	14.5	176.4	9	1.60	0.47	0.7898
								0	38.0	205.9	10	1.71	0.48	0.7734
								1	4.2	164.8	12	1.57	0.44	0.7939
								2	1.6	96.6	3	1.59	0.44	0.8068
205/14-2	-	7430.0	ft	Unit IV Upper	P3	DC	P10012_005	-	3.4	98.0	8	1.79	0.47	0.8262
								0	7.5	38.7	9	1.62	0.52	0.8193
								1	0.5	133.2	6	1.88	0.47	0.8131
								2	1.1	59.6	6	1.67	0.46	0.8278
								3	8.1	123.3	10	1.79	0.47	0.8304
205/17b-2	-	2443.8	m	Lista	P3	COCH	P10012_006	-	5.6	122.1	9	1.81	0.48	0.8334
								0	53.5	227.9	9	1.73	0.46	0.8090

TABLE Ap2.2.2a Apatite fission track length data: sub-groups

Well	Top Depth	Bottom Depth	Units (m/ft)	Stratigraphy	Age	Sample Type	Sample ID.	Sub Group	Accepted (CFT's)	Mean Length (μm)	Standard Error (μm)	Standard Dev (μm)	Median Upb Age (Ma)	Median - 2 Sigma (Ma)	Median +2 Sigma (Ma)	Median U (ppm)
205/17b-2	-	2443.8	m	Lista	P3	COCH	P10012_006	1	42	12.30	0.22	1.38	433.2	-111.4	109.4	17.6
								2A	5	12.46	0.56	1.11	1037.7	-294.1	281.3	3.0
								2B	53	11.68	0.24	1.75	1793.7	-442.9	414.4	12.6
								2C	58	12.04	0.21	1.57	1969.7	-471.9	439.2	10.6
206/11-1	4370.0	4376.0	m	Early Cretaceous Sands	K1	DC	P10012_007	-	1	5.51	0.00	0.00	1290.8	-331.1	308.0	5.6
								1	-	-	-	-	524.5	-142.8	139.4	4.1
								2	1	5.51	0.00	0.00	1350.5	-349.7	329.5	5.9
207/01-2	5590.0	5620.0	ft	Victory	K1	DC	P10011_003	-	204	11.93	0.11	1.61	538.5	-116.4	114.3	28.0
								1A	130	11.87	0.15	1.68	548.6	-115.9	113.9	32.5
								1B	46	11.90	0.23	1.58	461.6	-110.0	108.2	23.2
								2	13	12.36	0.42	1.46	2709.0	-458.0	427.6	28.5
	5740.0	5750.0		Precambrian Basement	PrCam	DC	P10011_004	-	220	11.68	0.11	1.55	800.4	-208.4	201.3	15.9
								1A	113	12.12	0.11	1.13	545.3	-141.4	138.4	22.9
								1B	28	11.84	0.26	1.33	412.4	-107.6	105.8	16.6
								2A	8	10.75	0.50	1.33	1530.5	-361.2	341.9	9.8
								2B	60	10.76	0.25	1.92	1736.4	-398.6	375.3	15.4
								-	178	11.29	0.11	1.47	577.5	-150.7	147.2	22.8
208/17-2	7871.0	7946.8		Waterhouse	P3	COCH	P10012_008	0	9	11.18	0.41	1.15	260.2	-73.0	72.1	3.0
								1A	99	11.27	0.14	1.34	593.3	-152.5	149.0	27.8
								1B	50	11.16	0.24	1.69	574.2	-151.4	148.0	17.7
								2	19	11.80	0.39	1.65	1251.6	-298.3	284.0	10.8
								-	207	11.28	0.11	1.63	527.9	-116.5	114.5	24.3
208/24-1A	5900.0	6000.0		Victory	K1	DC	P10011_006	1A	144	11.37	0.14	1.68	536.6	-119.8	117.6	25.4
								2B	62	11.09	0.19	1.50	500.8	-117.4	115.4	23.8
								2	62	11.09	0.19	1.50	1472.6	-309.1	289.8	19.8
								-	205	10.94	0.12	1.67	553.0	-126.7	124.3	27.6
	6230.0	6300.0		Victory	K1	DC	P10011_007	1A	127	11.08	0.16	1.81	546.6	-122.8	120.5	32.6
								1B	58	10.67	0.18	1.37	482.3	-108.7	107.0	26.6

TABLE Ap2.2.2a Apatite fission track length data: sub-groups

Well	Top Depth	Bottom Depth	Units (m/ft)	Stratigraphy	Age	Sample Type	Sample ID.	Sub Group	Median Th (ppm)	Median Sm (ppm)	Median Etch Figures	Median Dpar (μm)	Median Dper (μm)	Median Rmr (μm)
205/17b-2	-	2443.8	m	Lista	P3	COCH	P10012_006	1	6.3	143.4	8	1.90	0.48	0.8276
								2A	2.5	88.8	8	1.77	0.51	0.8445
								2B	2.8	187.5	10	1.81	0.48	0.8398
								2C	4.4	57.4	8	1.85	0.47	0.8382
206/11-1	4370.0	4376.0	m	Early Cretaceous Sands	K1	DC	P10012_007	-	2.2	311.8	6	1.80	0.56	0.8334
								1	3.1	111.4	6	1.46	0.46	0.7406
								2	2.0	322.3	6	1.81	0.56	0.8348
207/01-2	5590.0	5620.0	ft	Victory	K1	DC	P10011_003	-	11.6	197.1	6	1.83	0.47	0.8315
								1A	9.7	222.0	6	1.79	0.47	0.8310
								1B	23.2	73.8	6	2.00	0.52	0.8302
								2	40.0	422.9	5	1.86	0.45	0.8436
	5740.0	5750.0	ft	Precambrian Basement	PrCam	DC	P10011_004	-	16.5	194.9	6	1.76	0.45	0.8439
								1A	14.8	275.4	6	1.81	0.47	0.8409
								1B	34.6	100.0	6	1.79	0.45	0.8462
								2A	7.2	51.3	5	1.77	0.42	0.8478
								2B	17.0	271.4	6	1.76	0.44	0.8418
208/17-2	7871.0	7946.8	ft	Waterhouse	P3	COCH	P10012_008	-	7.6	110.4	9	1.84	0.49	0.7745
								0	0.5	69.6	8	1.74	0.45	0.7772
								1A	7.3	217.7	10	1.89	0.52	0.7815
								1B	13.5	36.5	8	1.90	0.47	0.7553
								2	4.7	264.4	8	1.96	0.47	0.7732
208/24-1A	5900.0	6000.0	ft	Victory	K1	DC	P10011_006	-	10.3	167.6	6	1.83	0.47	0.8031
								1A	4.9	227.2	6	1.85	0.48	0.7950
								2B	34.2	107.5	6	1.76	0.48	0.8241
								2	31.3	190.6	5	1.68	0.47	0.8286
	6230.0	6300.0	ft	Victory	K1	DC	P10011_007	-	23.3	264.4	6	1.85	0.48	0.8202
								1A	16.5	383.9	6	1.81	0.48	0.8205
								1B	37.7	96.7	6	2.00	0.48	0.7971

TABLE Ap2.2.2a Apatite fission track length data: sub-groups

Well	Top Depth	Bottom Depth	Units (m/ft)	Stratigraphy	Age	Sample Type	Sample ID.	Sub Group	Accepted (CFT's)	Mean Length (µm)	Standard Error (µm)	Standard Dev (µm)	Median Upb Age (Ma)	Median - 2 Sigma (Ma)	Median +2 Sigma (Ma)	Median U (ppm)
208/24-1A	6230.0	6300.0	ft	Victory	K1	DC	P1001_007	2	13	11.38	0.44	1.53	1179.5	-267.3	255.8	46.6
208/27-2	3960.0	3990.0	ft	Shetland	K2	DC	P10011_009	-	9	13.48	0.56	1.59	1275.9	-284.4	272.3	12.3
								1	-	-	-	-	566.3	-119.9	117.7	10.8
								2	9	13.48	0.56	1.59	1441.2	-300.6	287.1	13.3
	-	4540.0		PreCambrian Basement	PrCam	DC	P10011_011	-	161	12.61	0.12	1.46	1558.0	-323.2	307.7	19.0
								1	-	-	-	-	568.6	-221.2	213.2	8.6
								2A	140	12.70	0.13	1.49	1557.7	-321.3	306.0	22.7
								2B	21	12.02	0.25	1.10	1629.6	-361.0	341.8	14.3
	4300.0	4590.0		Caved Shetland	K2	DC	P10011_013	-	206	12.48	0.12	1.67	1516.9	-314.8	300.1	12.0
								1	6	12.64	0.36	0.80	704.6	-156.8	153.1	4.8
								2A	185	12.46	0.13	1.70	1546.4	-314.7	300.1	12.5
								2B	15	12.63	0.44	1.63	1538.2	-337.2	320.3	8.7
								-	46	11.28	0.27	1.80	1619.8	-298.5	285.2	10.0
	214/26-1	7516.0		7539.0	ft	Lewis Fan Envelope	E2	DC	P10012_009	1.0	4	11.89	0.76	1.32	361.7	-73.5
2A			3							13.38	0.46	0.65	1193.5	-221.9	214.5	11.1
2B			17							11.94	0.28	1.10	1782.0	-324.4	308.8	8.3
2C			22							10.37	0.43	1.95	1678.6	-312.9	298.4	20.1
-			211							11.08	0.10	1.52	582.0	-121.2	119.0	18.3
214/28-1	-	8374.3	ft	Late Paleocene	P3	COCH	P10012_010	1A	78	11.07	0.19	1.68	453.0	-88.0	86.8	34.4
								1B	76	11.23	0.17	1.48	515.4	-95.6	94.2	13.1
								2C	57	10.87	0.18	1.34	1706.7	-285.7	273.6	16.2
								-	4	7.75	1.11	1.92	798.2	-156.8	153.1	15.1
	11900.0	11920.0		Middle Paleocene	P2	DC	P10012_011	0	-	-	-	-	151.1	-32.4	32.2	2.1
								1	3	8.18	1.49	2.10	553.8	-112.9	110.9	28.0
								2A	1	6.44	0.00	0.00	968.9	-171.9	167.4	4.7
								2B	-	-	-	-	1916.6	-312.7	298.3	17.7
	14310.0	14334.4		Early-Middle Paleocene	P1	COCH	P10012_012	-	6	8.05	1.44	3.23	1815.0	-304.7	290.6	19.7
								0	1	6.42	0.00	0.00	160.9	-32.5	32.3	7.3

TABLE Ap2.2.2a Apatite fission track length data: sub-groups

Well	Top Depth	Bottom Depth	Units (m/ft)	Stratigraphy	Age	Sample Type	Sample ID.	Sub Group	Median Th (ppm)	Median Sm (ppm)	Median Etch Figures	Median Dpar (μm)	Median Dper (μm)	Median Rmr (μm)
208/24-1A	6230.0	6300.0	ft	Victory	K1	DC	P1001_007	2	15.9	327.6	6	2.00	0.48	0.8024
208/27-2	3960.0	3990.0	ft	Shetland	K2	DC	P10011_009	-	4.8	65.9	10	1.82	0.46	0.8083
								1	31.9	133.6	5	1.77	0.44	0.8100
								2	3.3	62.2	10	1.81	0.46	0.8078
	-	4540.0		PreCambrian Basement	PrCam	DC	P10011_011	-	4.4	315.2	6	1.75	0.45	0.8302
								1	0.9	254.4	4	1.62	0.44	0.8110
								2A	4.3	393.3	6	1.83	0.47	0.8283
								2B	7.0	210.0	5	1.64	0.43	0.8477
	4300.0	4590.0		Caved Shetland	K2	DC	P10011_013	-	2.5	370.8	6	1.85	0.49	0.7992
								1	0.6	291.3	4	2.00	0.62	0.7853
								2A	2.8	416.7	6	1.83	0.48	0.7947
								2B	0.8	153.8	5	1.82	0.48	0.8241
214/26-1	7516.0	7539.0	ft	Lewis Fan Envelope	E2	DC	P10012_009	-	3.2	135.5	8	1.73	0.48	0.8467
								1.0	40.6	153.7	12	1.72	0.52	0.8356
								2A	13.8	58.8	7	1.78	0.48	0.8363
								2B	0.7	344.1	9	1.94	0.48	0.8420
								2C	3.4	101.4	8	1.67	0.48	0.8525
214/28-1	-	8374.3	ft	Late Paleocene	P3	COCH	P10012_010	-	7.0	92.0	8	1.88	0.47	0.8391
								1A	1.3	218.8	9	1.91	0.49	0.8351
								1B	3.5	31.2	8	1.87	0.48	0.8462
								2C	17.4	201.7	8	1.85	0.46	0.8391
	11900.0	11920.0		Middle Paleocen	P2	DC	P10012_011	-	26.7	140.0	4	1.69	0.48	0.8327
								0	10.9	60.5	2	1.49	0.47	0.7838
								1	51.7	177.4	4	1.69	0.46	0.8344
								2A	7.6	138.1	7	1.73	0.51	0.8125
								2B	12.8	61.8	2	1.64	0.47	0.8267
	14310.0	14334.4		Early-Middle Paleocene	P1	COCH	P10012_012	-	1.4	115.5	5	1.81	0.55	0.8246
								0	117.5	128.0	6	2.56	0.72	0.8320

TABLE Ap2.2.2a Apatite fission track length data: sub-groups

Well	Top Depth	Bottom Depth	Units (m/ft)	Stratigraphy	Age	Sample Type	Sample ID.	Sub Group	Accepted (CFT's)	Mean Length (μm)	Standard Error (μm)	Standard Dev (μm)	Median Upb Age (Ma)	Median - 2 Sigma (Ma)	Median +2 Sigma (Ma)	Median U (ppm)
214/28-1	14310	14334	ft	Early-Middle Paleocene	P1	COCH	P10012_012	1	-	-	-	-	534.1	-97.7	96.2	22.3
								2	2	7.44	5.06	5.06	1599.8	-256.9	247.0	27.7
								3A	1	6.04	0.00	0.00	2248.8	-413.4	387.1	10.1
								3B	2	10.48	2.70	2.70	1981.1	-351.4	333.0	19.7

Well	Top Depth	Bottom Depth	Units (m/ft)	Stratigraphy	Age	Sample Type	Sample ID.	Sub Group	Median Th (ppm)	Median Sm (ppm)	Median Etch Figures	Median Dpar (μm)	Median Dper (μm)	Median Rmr (μm)
214/28-1	14310	14334	ft	Early-Middle Paleocene	P1	COCH	P10012_012	1	0.7	164.4	2	1.54	0.47	0.7931
								2	2.3	129.3	8	1.58	0.48	0.8267
								3A	1.8	207.3	4	1.72	0.52	0.8246
								3B	2.0	40.8	4	1.90	0.59	0.7882

TABLE Ap2.2.2a Apatite fission track length data: sub-groups

Well	Top Depth	Bottom Depth	Units (m/ft)	Stratigraphy	Age	Sample Type	Sample ID.	Accepted (CFT's)	Mean Length (µm)	Stand Error (µm)	Stand Dev (µm)	Median Upb Age (Ma)	Median - 2 Sigma (Ma)	Median +2 Sigma (Ma)	Median U (ppm)	Median Th (ppm)
204/10a-5	2361.8	2383.5	m	Hildasay	E1	COCH	P10012_013	206	12.32	0.10	1.40	1560.3	-221	221	22.0	2.4
205/09-1	2798.0	2807.0	m	Sele	E1	DC	P10012_001	39	9.47	0.38	2.36	1413.0	-331	331	7.8	2.3
	3704.0	3719.0	m	Lista (D1 Sand)	P3	DC	P10012_002	30	10.01	0.37	2.04	1386.9	-253	253	21.7	0.9
205/12-1	-	2570.0	m	Lamba	P3	DC	P10012_003	216	12.21	0.10	1.42	1564.6	-316	316	19.2	1.5
	-	3175.0	m	Shetland	K2	DC	P10012_004	31	11.72	0.30	1.69	344.8	-89	89	11.4	25.2
205/14-2	-	7430.0	ft	Unit IV Upper	P3	DC	P10012_005	75	12.16	0.19	1.61	1394.3	-300	300	14.8	8.1
205/17b-2	-	2443.8	m	Lista	P3	COCH	P10012_006	221	12.06	0.11	1.61	1681.6	-327	327	19.4	6.3
206/11-1	4370.0	4376.0	m	Early Cret Sands	K1	DC	P10012_007	1	5.51	0.00	0.00	829.9	-217	217	5.6	0.4
207/01-2	5590.0	5620.0	ft	Victory	K1	DC	P10011_003	215	11.89	0.11	1.67	538.6	-113	113	29.9	16.6
	5740.0	5750.0	ft	PrCam Basemen	PrCam	DC	P10011_004	223	11.65	0.11	1.57	575.5	-148	148	18.7	22.8
208/17-2	7871.0	7946.8	ft	Waterhouse	P3	COCH	P10012_008	212	11.28	0.10	1.44	580.8	-150	150	36.9	14.0
208/24-1A	5900.0	6000.0	ft	Victory	K1	DC	P10011_006	212	11.33	0.11	1.67	528.9	-119	119	29.8	3.0
	6530.0	6300.0	ft	Victory	K1	DC	P10011_007	212	10.98	0.11	1.67	542.6	-120	120	34.8	23.2
208/27-2	4960.0	3990.0	ft	Shetland	K2	DC	P10011_009	19	12.78	0.31	1.36	1104.2	-263	263	11.2	0.1
	-	4540.0	ft	PrCam Basemen	PrCam	DC	P10011_011	217	12.60	0.10	1.52	1648.4	-327	327	24.0	3.6
	4300.0	4590.0	ft	Caved Shetland	K2	DC	P10011_013	219	12.48	0.11	1.64	1458.6	-297	297	14.2	2.6
214/26-1	7516.0	7539.0	ft	Lewis Fan Env	E2	DC	P10012_009	50	11.28	0.25	1.74	1712.4	-304	304	14.7	4.6
214/28-1	-	8374.3	ft	Late Paleocene	P3	COCH	P10012_010	217	11.07	0.10	1.51	550.6	-114	114	26.1	9.4
	11900.0	11920.0	ft	Middle Paleocen	P2	DC	P10012_011	6	6.39	1.05	2.57	660.9	-147	147	21.7	42.5
	14310.0	14334.4	ft	E-M Paleocene	P1	COCH	P10012_012	8	7.13	1.15	3.24	1891.6	-323	323	28.0	0.5

TABLE Ap2.2.2b Apatite fission track length data: combined

Well	Top Depth	Bottom Depth	Units (m/ft)	Stratigraphy	Age	Sample Type	Sample ID.	Median Sm (ppm)	Median Etch Figures	Median Dpar (µm)	Median Dper (µm)	Median Rmr (µm)
204/10a-5	2361.8	2383.5	m	Hildasay	E1	COCH	P10012_013	37.8	14.0	1.81	0.54	0.8505
205/09-1	2798.0	2807.0	m	Sele	E1	DC	P10012_001	66.5	13	1.74	0.50	0.7831
	3704.0	3719.0	m	Lista (D1 Sand)	P3	DC	P10012_002	260.8	7	1.90	0.56	0.8156
205/12-1	-	2570.0	m	Lamba	P3	DC	P10012_003	99.2	7	1.74	0.46	0.8287
	-	3175.0	m	Shetland	K2	DC	P10012_004	189.1	12	1.75	0.49	0.7837
205/14-2	-	7430.0	ft	Unit IV Upper	P3	DC	P10012_005	123.2	7	1.82	0.48	0.8406
205/17b-2	-	2443.8	m	Lista	P3	COCH	P10012_006	143.5	9	1.84	0.48	0.8326
206/11-1	4370.0	4376.0	m	Early Cret Sands	K1	DC	P10012_007	303.4	8	2.05	0.67	0.8363
207/01-2	5590.0	5620.0	ft	Victory	K1	DC	P10011_003	189.1	6	1.83	0.48	0.8310
	5740.0	5750.0	ft	PrCam Basemen	PrCam	DC	P10011_004	213.9	6	1.70	0.45	0.8464
208/17-2	7871.0	7946.8	ft	Waterhouse	P3	COCH	P10012_008	146.7	10	1.90	0.50	0.7739
208/24-1A	5900.0	6000.0	ft	Victory	K1	DC	P10011_006	174.3	6	1.85	0.46	0.8147
	6530.0	6300.0	ft	Victory	K1	DC	P10011_007	285.8	6	1.83	0.49	0.8199
208/27-2	4960.0	3990.0	ft	Shetland	K2	DC	P10011_009	5.4	18	1.68	0.48	0.8087
	-	4540.0	ft	PrCam Basemen	PrCam	DC	P10011_011	353.1	6	1.86	0.46	0.8347
	4300.0	4590.0	ft	Caved Shetland	K2	DC	P10011_013	405.2	6	1.92	0.48	0.8085
214/26-1	7516.0	7539.0	ft	Lewis Fan Env	E2	DC	P10012_009	153.2	10	1.84	0.50	0.8475
214/28-1	-	8374.3	ft	Late Paleocene	P3	COCH	P10012_010	118.4	7	1.89	0.48	0.8353
	11900.0	11920.0	ft	Middle Paleocen	P2	DC	P10012_011	178.4	6	1.73	0.49	0.8354
	14310.0	14334.4	ft	E-M Paleocene	P1	COCH	P10012_012	93.2	7	1.92	0.52	0.8198

TABLE Ap2.2.2b Apatite fission track length data: combined

APPENDIX 3

OPTICAL MATURITY DATA

APPENDIX 3.1 Summary of samples analysed for optical maturity

APPENDIX 3.2 Vitrinite reflectivity (VR) data

APPENDIX 3.3 Vitrinite reflectivity (VR) histograms, data and statistics

APPENDIX 3.4 Spore colour index (SCI) data

APPENDIX 3.5 List of abbreviations used in maturity data tables

APPENDIX 3.1

SUMMARY OF SAMPLES ANALYSED FOR OPTICAL MATURITY

Tables

Ap3.1.1 Sample details – optical maturity analyses

Well	Top depth	Bottom depth	Units (m/ft)	Stratigraphy	Age	Sample type	Washed (y/n)	Block No.	Basin	Mud system	Anal. reason	Anal. status
205/09-1	-	2110.0	m	Hordaland	E1	DC	y	19-862	Flett	WBM (Bentonite & KCl polymer)	MAT	NEW
	-	2384.0	m	Sele		DC	y	19-863			MAT	NEW
	-	2774.0	m			DC	y	19-864			MAT	NEW
	-	3143.0	m	Lista	P3	DC	y	19-865			MAT	NEW
	-	3452.0	m			DC	y	19-866			MAT	NEW
	-	3803.0	m			DC	y	19-867			MAT	NEW
	-	4136.0	m	Undiff.		DC	y	19-868			MAT	NEW
	-	4535.0	m	Maureen	P1	DC	y	19-869			MAT	NEW
	-	4709.0	m	Shetland	K2	DC	y	19-870			MAT	NEW
205/12-1	-	1990.0	m	Stronsay	E1	DC	y	19-871	Flett	WBM (KCl polymer)	MAT	NEW
	-	2010.0	m			DC	y	19-872			MAT	NEW
	-	2300.0	m	Lamba	P3	DC	y	19-873			MAT	NEW
	-	2515.0	m			DC	y	19-874			MAT	NEW
	-	2800.0	m	Vaila		DC	y	19-875			MAT	NEW
	-	2990.0	m			DC	y	19-876			MAT	NEW
	-	3125.0	m	Shetland	K1	DC	y	19-877			MAT	NEW
205/14-2	-	5150.0	ft	Balder	E1	DC	y	19-878	Foula	WBM (KCl polymer & Glycol)	MAT	NEW
	-	5660.0	ft			DC	y	19-879			MAT	NEW
	-	6110.0	ft	Unit II	P3	DC	y	19-880			MAT	NEW
	-	6830.0	ft			DC	y	19-881			MAT	NEW
	-	7520.0	ft	Unit IV Upper Sandstone		DC	y	19-882			MAT	NEW
	-	7940.0	ft	Unit IV Lower Sandstone		DC	y	19-883			MAT	NEW
	-	8630.0	ft	Unit V	P1	DC	y	19-884			MAT	NEW
	-	8947.0	ft	Cretaceous	K2	DC	y	19-885			MAT	NEW
205/14-3	-	3840.0	ft	Undiff.	Ter	DC	y	19-886	Flett	WBM (KCl polymer & Glycol)	MAT	NEW
	-	5250.0	ft	Stronsay		DC	y	19-887			MAT	NEW
	-	6600.0	ft	Balder	E1	DC	y	19-888			MAT	NEW
	-	6900.0	ft			DC	y	19-889			MAT	NEW

TABLE Ap3.1.1 Sample details - optical maturity analyses

Well	Top depth	Bottom depth	Units (m/ft)	Stratigraphy	Age	Sample type	Washed (y/n)	Block No.	Basin	Mud system	Anal. reason	Anal. status
205/14-3	-	7320.0	ft	Hildasay	E1	DC	y	19-890	Flett	WBM (KCl polymer & Glycol)	MAT	NEW
	-	8840.0	ft	Ketla Tuff	P3	DC	y	19-891			MAT	NEW
	-	9770.0	ft	Sullom	P2	DC	y	19-892			MAT	NEW
	-	10100.0	ft	Jorsalfare	K2	DC	y	19-893			MAT	NEW
206/01-1A	-	3350.0	ft	Undiff.	E3	DC	y	19-894	Foula	OBM (Inverkleen)	MAT	NEW
	-	4580.0	ft		E2	DC	y	19-895			MAT	NEW
	-	5570.0	ft			DC	y	19-896			MAT	NEW
	-	7100.0	ft	Sele	P3	DC	y	19-897			MAT	NEW
	-	7740.0	ft			DC	y	19-898			MAT	NEW
	-	7780.0	ft			DC	y	19-899			MAT	NEW
	-	9290.0	ft	Shetland	K2	DC	y	19-900			MAT	NEW
206/11-1	-	1250.0	m	Undiff.	Ter	DC	y	19-901	Rona Ridge	WBM	MAT	NEW
	-	1825.0	m	Late Cretaceous Shale I	K2	DC	y	19-902			MAT	NEW
	-	2380.0	m			DC	y	19-903			MAT	NEW
	-	2900.0	m			DC	y	19-904			MAT	NEW
	-	3244.0	m	Late Cretaceous Shale III		DC	y	19-905			MAT	NEW
	-	3606.0	m	Early Cretaceous Sandstone	K1	DC	y	19-906			MAT	NEW
	-	3934.0	m			DC	y	19-907			MAT	NEW
	-	4258.0	m			DC	y	19-908			MAT	NEW
	-	4586.0	ft	Early Cretaceous Turbidite		DC	y	19-909			MAT	NEW
207/01-2	1230.0	1260.0	ft	Undiff.	Ter	DC	y	19-910	West Shetland	WBM (SW, CMC, barite &	MAT	NEW
208/17-1	-	4680.0	ft	Middle Eocene	E2	DC	y	19-911	Northern Faroe-Shetland	OBM (Invert Oil Based Emulsion)	MAT	NEW
	-	5880.0	ft			DC	y	19-912			MAT	NEW
	-	6720.0	ft			DC	y	19-913			MAT	NEW
	-	7300.0	ft	Early Eocene	E1	DC	y	19-914			MAT	NEW
	-	8610.0	ft	Late Paleocene	P3	DC	y	19-915			MAT	NEW
	-	9760.0	ft			DC	y	19-916			MAT	NEW
	-	10550.0	ft			DC	y	19-917			MAT	NEW

TABLE Ap3.1.1 Sample details - optical maturity analyses

Well	Top depth	Bottom depth	Units (m/ft)	Stratigraphy	Age	Sample type	Washed (y/n)	Block No.	Basin	Mud system	Anal. reason	Anal. status
208/17-1	-	11840.0	ft	Early Paleocene	P1	DC	y	19-918	Northern Faroe-Shetland	OBM (Invert Oil Based Emulsion)	MAT	NEW
	-	12760.0	ft			DC	y	19-919			MAT	NEW
	-	13980.0	ft			DC	y	19-920			MAT	NEW
	-	14740.0	ft			DC	y	19-921			MAT	NEW
	-	15860.0	ft	Late Cret	K2	DC	y	19-922			MAT	NEW
208/17-2	-	5400.0	ft	Stronsay	Ter	DC	y	19-923	Northern Faroe-Shetland	OBM (Aquamul)	MAT	NEW
	-	6280.0	ft	Balder	E1	DC	y	19-924			MAT	NEW
	-	7290.0	ft	Flett	P3	DC	y	19-925			MAT	NEW
	-	9470.0	ft	Vaila	P2	DC	y	19-926			MAT	NEW
	-	10600.0	ft	Sullom	P1	DC	y	19-927			MAT	NEW
	-	11710.0	ft			DC	y	19-928			MAT	NEW
	-	12050.0	ft	Shetland	K2	DC	y	19-929			MAT	NEW
209/12-1	-	11383.9	ft	Humber	J3	COCH	-	19-930	Northern Faroe-Shetland	WBM (Seawater & polymer mud)	MAT	NEW
	-	11385.1	ft			COCH	-	19-931			MAT	NEW
	-	11385.7	ft			COCH	-	19-932			MAT	NEW
214/26-1	-	5350.0	ft	Hordaland	E2	DC	y	19-933	Flett	WBM (Sewater & polyglycol)	MAT	NEW
	-	5710.0	ft			DC	y	19-934			MAT	NEW
	-	6010.0	ft			DC	y	19-935			MAT	NEW
	-	6390.0	ft			DC	y	19-936			MAT	NEW
	-	6760.0	ft	Lewis Fan		DC	y	19-937			MAT	NEW
	-	7140.0	ft	Lewis Lobe		DC	y	19-938			MAT	NEW
	-	7960.0	ft			DC	y	19-939			MAT	NEW
	-	8230.0	ft	Base Lewis Lobe	E1	DC	y	19-940			MAT	NEW
	-	8510.0	ft	Balder	P3	DC	y	19-941			MAT	NEW
	-	8910.0	ft	Sele		DC	y	19-942			MAT	NEW
214/28-1	-	4560.0	ft	Lower Oligocene	O1	DC	n	19-943	Flett Ridge	OBM (Enviromul)	MAT	NEW
	-	5850.0	ft	Later Eocene	E1	DC	n	19-944			MAT	NEW
	-	6540.0	ft	Middle Eocene	E2	DC	n	19-945			MAT	NEW

TABLE Ap3.1.1 Sample details - optical maturity analyses

Well	Top depth	Bottom depth	Units (m/ft)	Stratigraphy	Age	Sample type	Washed (y/n)	Block No.	Basin	Mud system	Anal. reason	Anal. status
214/28-1	-	7300.0	ft	Middle Eocene	E2	DC	n	19-946	Flett Ridge	OBM (Enviromul)	MAT	NEW
	-	8200.0	ft	Early Eocene	E1	DC	n	19-947			MAT	NEW
	-	9630.0	ft	Middle Paleocene	P2	DC	n	19-948			MAT	NEW
	-	10660.0	ft			DC	n	19-949			MAT	NEW
	-	11540.0	ft			DC	n	19-950			MAT	NEW
	-	12510.0	ft	Early Paleocene	P1	DC	n	19-951			MAT	NEW
	-	13460.0	ft			DC	n	19-952			MAT	NEW
	-	14600.0	ft			DC	n	19-953			MAT	NEW
	-	15470.0	ft			DC	n	19-954			MAT	NEW
	-	16960.0	ft	Maastrichtian	K2	DC	n	19-955			MAT	NEW

Abbreviations/Key

DC: Ditch cuttings
COCH: Core chip
WBM: Water based mud
OBM: Oil based mud
SW: Seawater
MAT: Maturity
NEW: New analyses for this study

Stratigraphy/Ages

Undiff.: Undifferentiated
Ter: Tertiary
O1: Lower Oligocene
E3: Late Eocene
E2: Middle Eocene
E1: Early Eocene
P3: Late Paleocene
P2: Middle Paleocene
P1: Early Paleocene
K2: Late Cretaceous Shale III
K1: Early Cretaceous Turbidite
J3: Late Jurassic

TABLE Ap3.1.1 Sample details - optical maturity analyses

APPENDIX 3.2

VITRINITE REFLECTIVITY (VR) DATA

Tables

Ap3.2.1	Vitrinite reflectivity data: 205/09-1
Ap3.2.2	Vitrinite reflectivity data: 205/12-1
Ap3.2.3	Vitrinite reflectivity data: 205/14-2
Ap3.2.4	Vitrinite reflectivity data: 205/14-3
Ap3.2.5	Vitrinite reflectivity data: 206/01-1A
Ap3.2.6	Vitrinite reflectivity data: 206/11-1
Ap3.2.7	Vitrinite reflectivity data: 207/01-2
Ap3.2.8	Vitrinite reflectivity data: 208/17-1
Ap3.2.9	Vitrinite reflectivity data: 208/17-2
Ap3.2.10	Vitrinite reflectivity data: 209/12-1
Ap3.2.11	Vitrinite reflectivity data: 214/26-1
Ap3.2.12	Vitrinite reflectivity data: 214/28-1

Well	Bottom Depth (m)	Stratigraphy	Age	Sample Type	Vitrinite Reflectivity								Comments	
					Block No.	Indigenous			Other					
						No.	Avg (%Ro)	Min (%Ro)	Max (%Ro)	Type	No.	Avg (%Ro)		
205/09-1	2110.0	Hordaland	E1	DC	19-862	40	0.35	0.28	0.43	-	-	-	Fair sample with clearly recognisable vitrinite common, but milky lustre and mean reflectivity slightly above trend suggest possible oxidation.	
										-	-	-		
										-	-	-		
	2384.0	Sele		DC	19-863	40	0.34	0.28	0.41	-	-	-	Good sample, large blocky vitrinite particles abundant.	
											-	-		-
											-	-		-
	2774.0	P2	DC	19-864	44	0.42	0.36	0.50	-	-	-	Although recovery is poor, vitrinite remains fairly common.		
										-	-		-	
										-	-		-	
	3143.0		DC	19-865	40	0.46	0.35	0.56	-	-	-	Low recovery but occasional large coaly fragments present. Telinite ~0.40% Ro.		
										-	-		-	
										-	-		-	
	3452.0		DC	19-866	41	0.51	0.42	0.64	L	7	0.30	AOM predominant but well-preserved vitrinite still common. Particles typically small, rounded.		
										-	-		-	
										-	-		-	
	3803.0		DC	19-867	50	0.56	0.45	0.67	R	4	0.80	Vitrinite not abundantly sufficient for reliable data. Particles typically small, rounded.		
										-	-		-	
										-	-		-	
	4136.0		Undiff.	DC	19-868	40	0.61	0.51	0.69	L	9	0.34	Good vitrinite present but increased fusinite content. Low reflecting material may be drilling additive, if caved, it is not seen above.	
										R	4	0.75		
										-	-	-		
	4535.0		Maureen	DC	19-869	26	0.67	0.51	0.72	L	5	0.38	Good vitrinite present but increased fusinite content. Low reflecting material may be drilling additive if not caved.	
										R	14	0.79		
										-	-	-		
	4709.0	Shetland	K2	DC	19-870	27	0.75	0.67	0.84	L	15	0.42	Good vitrinite present but increased fusinite content. Low Ro material may be drilling additive if caved, vitrinite sufficient for reliable data.	
									R	4	0.95			
									-	-	-			

TABLE Ap3.2.1 Vitrinite reflectivity data: 205/09-1

Well	Bottom Depth (m)	Stratigraphy	Age	Sample Type	Vitrinite Reflectivity								Comments
					Block No.	Indigenous				Other			
						No.	Avg (%Ro)	Min (%Ro)	Max (%Ro)	Type	No.	Avg (%Ro)	
205/12-1	1990.0	Stronsay	E1	DC	19-871	30	0.28	0.21	0.36	L	2	0.19	Vitrinite fairly common, unimodal. Particles generally small, blocky. Reworked coal particles at about 0.6% Ro.
	-									-	-		
	-									-	-		
	2010.0			DC	19-872	37	0.29	0.21	0.36	-	-	-	Low recovery but sufficient vitrinite for reliable data. Particles generally small, blocky.
	-									-	-		
	-									-	-		
	2300.0	Lamba	P3	DC	19-873	40	0.33	0.27	0.44	R	3	0.53	Structured organic matter abundant. Some vitrinite has anomalously high reflectivity and is possibly pseudovitrinite.
	-									-	-		
	-									-	-		
	2515.0			DC	19-874	38	0.40	0.30	0.49	L	3	0.24	Excellent sample. Large unimodal vitrinite particles abundant.
	-									-	-		
	-									-	-		
	2800.0	Vaila		DC	19-875	34	0.44	0.36	0.54	L	10	0.27	Selection complicated by both the presence of perhydrous vitrinite and the effects of oxidation.
	R									1	0.60		
	-									-	-		
	2990.0			DC	19-876	20	0.47	0.40	0.59	L	14	0.31	Large vitrinite particles abundant.
	-									-	-		
	-									-	-		
	3125.0	Shetland	K1	DC	19-877	32	0.51	0.41	0.63	L	12	0.30	Vitrinite rare but sufficient for reliable results.
	-									-	-		
	-									-	-		

TABLE Ap3.2.2 Vitrinite reflectivity data: 205/12-1

Well	Bottom Depth (ft)	Stratigraphy	Age	Sample Type	Vitrinite Reflectivity								Comments
					Block No.	Indigenous				Other			
						No.	Avg (%Ro)	Min (%Ro)	Max (%Ro)	Type	No.	Avg (%Ro)	
205/14-2	5150.0	Balder	E1	DC	19-878	52	0.29	0.20	0.39	R	3	0.43	Abundant structured organic matter, dominantly vitrinite. Common amorphous organic matter present.
										-	-	-	
										-	-	-	
	5660.0			DC	19-879	55	0.28	0.21	0.39	-	-	-	Abundance of structured organic matter, dominated by vitrinite, some high reflecting and inert present.
									-	-	-		
									-	-	-		
	6110.0	Unit II	P3	DC	19-880	45	0.31	0.23	0.39	L	1	0.21	Lean sample. Structured organic matter smaller and clumped. Increase in amorphous organic matter and pyrite.
										R	8	0.45	
										R	1	0.77	
	6830.0			DC	19-881	47	0.33	0.26	0.43	L	2	0.23	Rich in amorphous organic matter and pyrite. Common structured organic matter. Inertinite dominates.
									R	6	0.54		
									-	-	-		
	7520.0	Unit IV Upper SS		DC	19-882	49	0.36	0.26	0.49	R	6	0.62	Rich in amorphous organic matter and pyrite. Common structured organic matter. Inertinite dominates.
										-	-	-	
										-	-	-	
	7940.0	Unit IV Lower SS		DC	19-883	43	0.39	0.28	0.48	R	11	0.59	Rich in amorphous organic matter and pyrite. Common structured organic matter. Inertinite increasingly dominant.
										-	-	-	
										-	-	-	
	8630.0	Unit V	P1	DC	19-884	19	0.43	0.33	0.52	L	1	0.29	Lean sample. Abundant amorphous organic matter and pyrite. Moderate amounts of structured organic matter, small in size. Inertinite dominates.
										R	3	0.65	
										-	-	-	
	8947.0	Cretaceous	K2	DC	19-885	29	0.43	0.33	0.54	L	1	0.30	Similar to above sample, inertinite dominates. Low and high reflecting particles common. Vitrinite common. Identification sometimes tricky.
										R	25	0.69	
										-	-	-	

TABLE Ap3.2.3 Vitrinite reflectivity data: 205/14-2

Well	Bottom Depth (ft)	Stratigraphy	Age	Sample Type	Vitrinite Reflectivity								Comments	
					Block No.	Indigenous			Other					
						No.	Avg (%Ro)	Min (%Ro)	Max (%Ro)	Type	No.	Avg (%Ro)		
205/14-3	3840.0	Undiff.	Ter	DC	19-886	22	0.25	0.20	0.33	-	-	-	Low recovery, vitrinite rare.	
										-	-	-		
										-	-	-		
	5250.0	Stronsay		DC	19-887	55	0.32	0.23	0.41	-	-	-	Large, rounded vitrinite particles common.	
										-	-	-		
										-	-	-		
	6600.0	Balder	E1	DC	19-888	40	0.32	0.25	0.40	-	-	-	Medium sized, well-preserved vitrinite common.	
										-	-	-		
										-	-	-		
	6900.0			DC	19-889	40	0.33	0.26	0.43	-	-	-	Medium sized, well-preserved vitrinite common.	
										-	-	-		
										-	-	-		
	7320.0	Hildasay		DC	19-890	40	0.31	0.24	0.35	-	-	-	Vitrinite common but particles rather small.	
									-	-	-			
									-	-	-			
	8840.0	Ketla Tuff		P3	DC	19-891	40	0.35	0.28	0.42	-	-	-	Vitrinite increasingly abundant, particles slightly larger.
										-	-	-		
										-	-	-		
	9770.0	Sullom		P2	DC	19-892	40	0.39	0.31	0.47	-	-	-	Vitrinite not abundant but sufficient for reliable data. Particles of varying size.
										-	-	-		
										-	-	-		
	10100.0	Jorsalfare		K2	DC	19-893	32	0.48	0.37	0.55	R	23	0.66	In situ vitrinite rare and swamped by reworked vitrinite.
											-	-	-	Very bright inertinite the most common structured organic matter component.
											-	-	-	

TABLE Ap3.2.4 Vitrinite reflectivity data: 205/14-3

Well	Bottom Depth (ft)	Stratigraphy	Age	Sample Type	Vitrinite Reflectivity								Comments	
					Block No.	Indigenous				Other				
						No.	Avg (%Ro)	Min (%Ro)	Max (%Ro)	Type	No.	Avg (%Ro)		
206/01-1A	3350.0	Undiff.	E3	DC	19-894	21	0.30	0.21	0.36	-	-	-	Vitrinite present but very rare, particles small.	
										-	-	-		
										-	-	-		
	4580.0		E2	DC	19-895	42	0.37	0.29	0.45	L	8	0.25	Vitrinite increasingly common. Abundant pyrite and bireflectivity (oxidation?) may have inflated readings but abundant pyrite argues against oxidation, however.	
											-	-		-
											-	-		-
	5570.0			DC	19-896	30	0.36	0.27	0.46	-	-	-	Vitrinite rare, nearly 100% amorphous organic matter but unimodal distribution gives confidence.	
											-	-		-
											-	-		-
	7100.0	Sele	P3	DC	19-897	40	0.36	0.26	0.47	-	-	-	Structured terrestrial organic matter more abundant and large vitrinite particles are common.	
											-	-		-
											-	-		-
	7740.0			DC	19-898	47	0.40	0.32	0.50	R	6	0.54	Large coaly vitrinite particles common although occasional fracturing and variation in reflectivities across surfaces of individual particles may suggest high temperature oxidation	
											-	-		-
											-	-		-
	7780.0			DC	19-899	46	0.45	0.37	0.53	L	4	0.30	Large coaly vitrinite particles common although occasional fracturing and variation in reflectivities across surfaces of individual particles may suggest high temperature oxidation	
											R	5		0.59
											-	-		-
	9290.0	Shetland	K2	DC	19-900	36	0.47	0.42	0.56	L	19	0.35	Organic facies change. Amorphous organic matter and inertinite predominant. Vitrinite population may include (and be skewed by) caved Tertiary vitrinite.	
										-	-	-		
										-	-	-		

TABLE Ap3.2.5 Vitrinite reflectivity data: 206/01-1A

Well	Bottom Depth (m)	Stratigraphy	Age	Sample Type	Vitrinite Reflectivity								Comments	
					Block No.	Indigenous			Other					
						No.	Avg (%Ro)	Min (%Ro)	Max (%Ro)	Type	No.	Avg (%Ro)		
206/11-1	1250.0	Undiff.	Ter	DC	18-901	46	0.30	0.25	0.36	-	-	-	Structured organic matter relatively abundant, vitrinite common though poorly preserved in places. Mostly moderately pyrite rich amorphous organic matter.	
										-	-	-		
										-	-	-		
	1825.0	Late Cretaceous Shale I	K2	DC	18-902	12	0.35	0.29	0.43	L	2	0.26	Structured organic matter fairly abundant, mostly reworked/oxidised particles.	
											R	8		0.52
											R	3		0.79
	2380.0			DC	18-903	13	0.43	0.34	0.53	R	13	0.62	Structured organic matter fairly abundant, mostly reworked/oxidised particles. Vitrinite is too small to measure in places.	
											R	1		0.81
											-	-		-
	2900.0			DC	18-904	12	0.46	0.37	0.54	R	7	0.66	Structured organic matter increasingly less abundant and often appears badly degraded.	
											R	5		0.82
											-	-		-
	3244.0	Late Cretaceous Shale III		DC	18-905	-	-	-	-	L	9	0.43	Low kerogen recovery. Structured organic matter uncommon, mostly reworked/oxidised particles. Unclear if indigenous vitrinite is present.	
										R	8	0.73		
										R	5	1.02		
	3606.0	Early Cretaceous Sandstone	K1	DC	18-906	17	0.52	0.44	0.64	L	5	0.36	Difficult to get a good polish. Low kerogen recovery. Structured organic matter often appears fragmented/degraded. Principally reworked/oxidised particles.	
											R	8		0.69
											R	10		0.97
	3934.0			DC	18-907	26	0.62	0.49	0.73	R	12	0.85	Structured organic matter fairly abundant, with a large vitrinite proportion of varying reflectivity possibly due to variation in preservation.	
											R	7		1.40
											-	-		-
	4258.0			DC	18-908	12	0.65	0.59	0.71	L	6	0.48	Structured organic matter abundant, dominantly reworked/oxidised particles, >1.00% Ro.	
											R	13		0.98
											R	7		1.31
	4586.0	Early Cretaceous Turbidite		DC	18-909	-	-	-	-	R	5	0.93	Principally amorphous organic matter, Structured organic matter fairly abundant but commonly inertinite, often too small to measure. Unclear if indigenous vitrinite present.	
									R	7	1.14			
									R	12	1.48			

TABLE Ap3.2.6 Vitrinite reflectivity data: 206/11-1

Well	Bottom Depth (ft)	Stratigraphy	Age	Sample Type	Vitrinite Reflectivity								Comments
					Block No.	Indigenous				Other			
						No.	Avg (%Ro)	Min (%Ro)	Max (%Ro)	Type	No.	Avg (%Ro)	
207/01-2	1260.0	Undiff.	Ter	DC	19-910	55	0.25	0.21	0.34	-	-	-	Vitrinite abundant, moderately degraded. Low reflecting particles ~0.12% Ro ?drilling additive. Semifusinite /reworked particles ~0.53% Ro and inertinite >1.00% Ro.
										-	-	-	
										-	-	-	

TABLE Ap3.2.7 Vitrinite reflectivity data: 207/01-2

Well	Bottom Depth (ft)	Stratigraphy	Age	Sample Type	Vitrinite Reflectivity								Comments
					Block No.	Indigenous			Other				
						No.	Avg (%Ro)	Min (%Ro)	Max (%Ro)	Type	No.	Avg (%Ro)	
208/17-1	4680.00	Middle Eocene	E2	DC	19-911	40	0.28	0.20	0.34	-	-	-	100% amorphous organic matter associated with framboidal pyrite, but with minor vitrinite sufficient for reliable results. Particles small, sub-rounded, wispy.
	-									-	-		
	-									-	-		
	5880.00			DC	19-912	30	0.29	0.21	0.38	-	-	-	100% amorphous organic matter associated with framboidal pyrite, but with minor vitrinite sufficient for reliable results. Particles small, sub-rounded, wispy.
	-									-	-		
	-									-	-		
	6720.00			DC	19-913	30	0.29	0.21	0.37	-	-	-	Trace amounts of vitrinite are present, particles small, rounded. Sample almost entirely amorphous organic matter.
	-									-	-		
	-									-	-		
	7300.00	Early Eocene	E1	DC	19-914	-	-	-	-	R	2	0.45	100% amorphous organic matter with trace amounts of reworked ?vitrinite.
	-									-	-		
	-									-	-		
	8610.00	Late Paleocene	P3	DC	19-915	13	0.33	0.27	0.43	-	-	-	Sample principally composed of amorphous organic matter, trace vitrinite particles observed.
	-									-	-		
	-									-	-		
	9760.00			DC	19-916	18	0.42	0.33	0.50	R	3	0.54	100% amorphous organic matter. often finely disseminated, and trace amounts of inertinite. Vitrinite very rare with high relief; measurements unreliable.
	-									-	-		
	-									-	-		
	10550.0			DC	19-917	12	0.47	0.38	0.54	R	3	0.65	100% amorphous organic matter. often finely disseminated, trace amounts of inertinite. Vitrinite very rare with high relief; measurements unreliable.
	-									-	-		
	-									-	-		
	11840.0	Early Paleocene	P1	DC	19-918	5	0.46	0.37	0.51	-	-	-	100% amorphous organic matter with traces of inertinite and almost no vitrinite.
	-									-	-		
	-									-	-		
	12760.0			DC	19-919	-	-	-	-	-	-	-	100% amorphous organic matter with pyrite framboids. No vitrinite or inertinite present.
	-									-	-		
	-									-	-		
13980.0	DC			19-920	-	-	-	-	-	-	-	100% amorphous organic matter, finely disseminated, and pyrite is rare.	
-									-	-			
-									-	-			

TABLE Ap3.2.8 Vitrinite reflectivity data: 208/17-1

Well	Bottom Depth (ft)	Stratigraphy	Age	Sample Type	Vitrinite Reflectivity								Comments
					Block No.	Indigenous				Other			
						No.	Avg (%Ro)	Min (%Ro)	Max (%Ro)	Type	No.	Avg (%Ro)	
208/17-1	14740.0	Early Paleocene	P1	DC	19-921	5	0.79	0.73	0.84	L	10	0.55	Low recovery, amorphous organic matter finely disseminated, pyrite rare. Vitrinite very rare.
										R	2	0.98	
										R	2	1.20	
	15860.0	Late Cretaceous	K2	DC	19-922	-	-	-	-	-	-	-	Low recovery. 100% amorphous organic matter. Vitrinite absent.
										-	-	-	
										-	-	-	

TABLE Ap3.2.8 Vitrinite reflectivity data: 208/17-1

Well	Bottom Depth (ft)	Stratigraphy	Age	Sample Type	Vitrinite Reflectivity								Comments
					Block No.	Indigenous			Other				
						No.	Avg (%Ro)	Min (%Ro)	Max (%Ro)	Type	No.	Avg (%Ro)	
208/17-2	5400.0	Stronsay	Ter	DC	19-923	25	0.28	0.22	0.37	-	-	-	Structured organic matter relatively rare, poorly preserved in places, particles fractured. Amorphous organic matter/mineral matter dominate sample.
										-	-	-	
										-	-	-	
	6280.0	Balder	E1	DC	19-924	23	0.39	0.32	0.50	L	2	0.22	Abundant low reflecting particles. Indigenous vitrinite relatively rare, poorly preserved in places. Amorphous organic matter super abundant.
										R	3	0.77	
										-	-	-	
	7290.0	Flett	E1	DC	19-925	38	0.43	0.35	0.54	L	9	0.25	Indigenous vitrinite rare, sample dominated by reworked and inertinite particles. Poorly preserved and oxidised in places.
										-	-	-	
										-	-	-	
	9470.0	Vaila	P2	DC	19-926	30	0.46	0.38	0.53	L	1	0.22	Significantly lesser amounts of lower reflecting particles. Vitrinite common and well preserved, identification uncertain places.
									R	4	0.86		
									-	-	-		
	10600.0	Sullom	P1	DC	19-927	12	0.52	0.47	0.60	L	8	0.35	Structured organic matter common but principally reworked or inertinite. Indigenous population well preserved.
										R	2	0.93	
										-	-	-	
	11710.0			DC	19-928	9	0.58	0.53	0.62	L	2	0.42	Indigenous vitrinite rare, sample dominated by bright mineral matter and inertinite.
		R	2							0.88			
		-	-							-			
	12050.0	Shetland	K2	DC	19-929	4	0.60	0.56	0.64	L	1	0.46	Indigenous vitrinite practically absent, bar one questionable particle. Reworked material common. Amorphous organic matter abundant.
									R	4	1.06		
									-	-	-		

TABLE Ap3.2.9 Vitrinite reflectivity data: 208/17-2

Well	Bottom Depth (ft)	Stratigraphy	Age	Sample Type	Vitrinite Reflectivity								Comments
					Block No.	Indigenous				Other			
						No.	Avg (%Ro)	Min (%Ro)	Max (%Ro)	Type	No.	Avg (%Ro)	
209/12-1	11383.9	Humber	J3	COCH	19-930	24	2.75	2.02	3.49	R	16	4.54	Sample principally composed of micrinitic amorphous organic matter. Trace amounts of structured organic matter.
	-									-	-		
	-									-	-		
	11385.1			COCH	19-931	39	2.72	1.96	3.34	R	16	4.21	Sample dominated by micrinitic amorphous organic matter, increasingly common structured organic matter. Coarse coke mosaic on some larger particles ~2.3-5.3% Ro.
										-	-	-	
										-	-	-	
	11385.7			COCH	19-932	34	2.33	1.81	2.87	R	16	3.63	Sample dominated by micrinitic amorphous organic matter, increasingly common structured organic matter. Distinctly lower reflectivities.

TABLE Ap3.2.10 Vitrinite reflectivity data: 209/12-1

Well	Bottom Depth (ft)	Stratigraphy	Age	Sample Type	Vitrinite Reflectivity								Comments	
					Block No.	Indigenous				Other				
						No.	Avg (%Ro)	Min (%Ro)	Max (%Ro)	Type	No.	Avg (%Ro)		
214/26-1	5350.0	Hordaland	E2	DC	19-933	26	0.24	0.18	0.32	R	4	0.40	Vitrinite common and well preserved. Small particles. Reworked material rare.	
										-	-	-		
	5710.0			DC	19-934	20	0.33	0.26	0.42	-	-	-	Vitrinite common, well preserved but particles small and difficult to measure in places.	
										-	-	-		
										-	-	-		
	6010.0			DC	19-935	23	0.58	0.45	0.69	R	6	0.78	Identification of indigenous population uncertain, possibly absent. Jump in SCI values not reflected in reflectivities. Reworked material common. Particles well preserved.	
										-	-	-		
										-	-	-		
	6390.0			DC	19-936	22	0.52	0.41	0.63	L	3	0.35	Reflectivity uncertain, does not match SCI data at this depth, but follows the trend. Vitrinite common, but principally reworked. Particles poorly preserved.	
										R	5	0.73		
										-	-	-		
	6760.0	Lewis Fan Envelope		DC	19-937	18	0.34	0.28	0.41	R	2	0.47	Vitrinite common and well-preserved. Amorphous organic matter and mineral matter dominate sample. Indigenous population identification uncertain in places.	
										-	-	-		
										-	-	-		
	7140.0	Lewis Lobe		DC	19-938	21	0.41	0.36	0.47	-	-	-	Organic matter abundant but principally reworked/inert particles. Vitrinite poorly preserved and oxidised in places. Vitrinite common.	
										-	-	-		
										-	-	-		
										-	-	-		
	7960.0	DC		19-939	-	-	-	-	-	-	-	-	Sample barren of organic matter.	
										-	-	-		
										-	-	-		
	8230.0	Base Lewis Fan Envelope		DC	19-940	-	-	-	-	-	-	-	-	Sample barren of organic matter.
										-	-	-		
								-	-	-				
8510.0	Balder	DC	19-941	30	0.41	0.32	0.49	-	-	-	Vitrinite common and well-preserved; occasionally very large.			
								-	-	-				
								-	-	-				
8910.0	Sele	DC	19-942	19	0.48	0.42	0.52	L	2	0.35	Vitrinite super abundant, inert particles relatively rare. Good preservation.			
								R	9	0.64				
								-	-	-				

TABLE Ap3.2.11 Vitrinite reflectivity data: 214/26-1

Well	Bottom Depth (ft)	Stratigraphy	Age	Sample Type	Vitrinite Reflectivity								Comments	
					Block No.	Indigenous				Other				
						No.	Avg (%Ro)	Min (%Ro)	Max (%Ro)	Type	No.	Avg (%Ro)		
214/28-1	4560.0	Lower Oligocene	O1	DC	19-943	45	0.27	0.20	0.35	R	10	0.45	Kerogen dominated by pyrite/?mineral rich amorphous organic matter. Sub blocky and wispy vitrinite abundant.	
										-	-	-		
										-	-	-		
	5850.0	Late Eocene	E3	DC	19-944	30	0.27	0.21	0.46	-	-	-	Dominantly by pyrite/?mineral rich amorphous organic matter. Calcite at ~0.17% Ro masquerades as vitrinite. Vitrinite generally small and often degraded.	
										-	-	-		
										-	-	-		
	6540.0	Middle Eocene	E2	DC	19-945	26	0.30	0.22	0.46	L	1	0.20	Mineral matter abundant. Vitrinite rare with varying preservation, often too small or degraded to measure accurately.	
											R	1		0.60
											-	-		-
	7300.0			DC	19-946	46	0.37	0.26	0.44	R	9	0.47	Moderately preserved vitrinite fairly abundant. Abundant mineral matter.	
										-	-	-		
										-	-	-		
	8200.0	Early Eocene	E1	DC	19-947	10	0.37	0.30	0.43	L	22	0.21	Vitrinite less abundant, and increasingly degraded. Increased proportions of reworked/oxidised particles. Low reflecting ?LCM ~0.10% Ro.	
										R	2	0.48		
										-	-	-		
	9630.0	Middle Paleocene	P2	DC	19-948	45	0.36	0.25	0.47	R	10	0.56	Structured organic matter abundant principally reworked/oxidised particles. Moderately preserved vitrinite fairly abundant.	
											-	-		-
											-	-		-
	10660.0			DC	19-949	19	0.43	0.36	0.56	L	5	0.27	Dominantly pyrite/?mineral rich amorphous organic matter. Structured organic matter abundant, but principally reworked/oxidised particles. Vitrinite rare and small.	
											R	8		0.61
											R	2		0.85
	11540.0			DC	19-950	13	0.50	0.41	0.58	L	2	0.36	Structured organic matter abundant, but too small to measure, commonly reworked/oxidised particles. Vitrinite very rare, but small ragged particles.	
											R	9		0.74
									R	4	1.11			
	12510.0	Early Paleocene	P1	DC	19-951	-	-	-	-	L	4	0.38	Cohesive amorphous organic matter abundant, structured organic matter rare and principally inertinite. Vitrinite very rare, generally small and/or degraded particles.	
											R	1		1.22
											R	3		1.68
	13460.0			DC	19-952	-	-	-	-	R	1	0.99	Very low kerogen recovery. Barren apart from occasional reworked/oxidised particles.	
										R	2	1.68		
										R	1	7.15		

TABLE Ap3.2.12 Vitrinite reflectivity data: 214/28-1

Well	Bottom Depth (ft)	Stratigraphy	Age	Sample Type	Vitrinite Reflectivity								Comments
					Block No.	Indigenous				Other			
						No.	Avg (%Ro)	Min (%Ro)	Max (%Ro)	Type	No.	Avg (%Ro)	
214/28-1	14600.0	Early Paleocene	P1	DC	19-953	2	0.73	0.71	0.75	L	2	0.40	Mineral rich amorphous organic matter abundant, structured organic matter rare and commonly reworked/oxidised particles. Vitrinite very rare and often too small to measure.
	L									5	0.55		
	R									10	1.13		
	15470.0			DC	19-954	-	-	-	-	L	1	0.48	Low kerogen recovery. Pyrite rich amorphous organic matter dominates. Abundant low reflecting calcite particles, reworked/oxidised particles common. Indigenous vitrinite very rare.
	R									6	1.06		
	R									9	1.65		
	16960.0	Maastrichtian	K2	DC	19-955	-	-	-	-	L	3	0.41	Dominated by mineral rich amorphous organic matter. Calcite particles abundant. Trace amounts of poorly preserved inertinite and low reflecting particles.
	R									1	1.62		
	R									2	2.09		

TABLE Ap3.2.12 Vitrinite reflectivity data: 214/28-1

APPENDIX 3.3

VITRINITE REFLECTIVITY (VR) HISTOGRAMS, DATA AND STATISTICS

Figures

Ap3.3.1	Histograms, data and statistics for vitrinite reflectivity - 205/09-1
Ap3.3.2	Histograms, data and statistics for vitrinite reflectivity - 205/12-1
Ap3.3.3	Histograms, data and statistics for vitrinite reflectivity - 205/14-2
Ap3.3.4	Histograms, data and statistics for vitrinite reflectivity - 205/14-3
Ap3.3.5	Histograms, data and statistics for vitrinite reflectivity - 206/01-1A
Ap3.3.6	Histograms, data and statistics for vitrinite reflectivity - 206/11-1
Ap3.3.7	Histograms, data and statistics for vitrinite reflectivity - 207/01-2
Ap3.3.8	Histograms, data and statistics for vitrinite reflectivity - 208/17-1
Ap3.3.9	Histograms, data and statistics for vitrinite reflectivity - 208/17-2
Ap3.3.10	Histograms, data and statistics for vitrinite reflectivity - 209/12-1
Ap3.3.11	Histograms, data and statistics for vitrinite reflectivity - 214/26-1
Ap3.3.12	Histograms, data and statistics for vitrinite reflectivity - 214/28-1

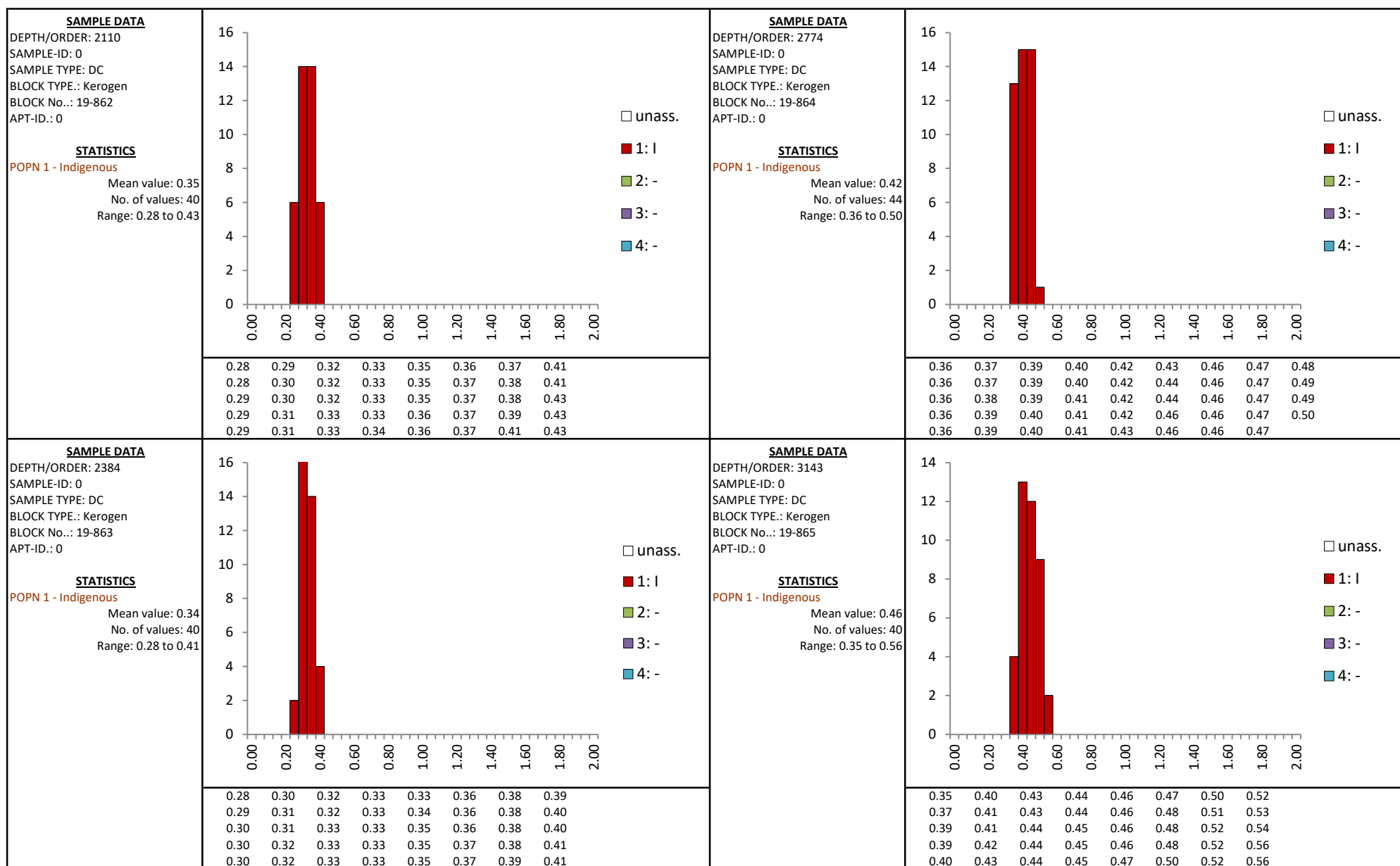


FIGURE Ap3.3.1 Histograms, data and statistics for vitrinite reflectivity - 205/09-1

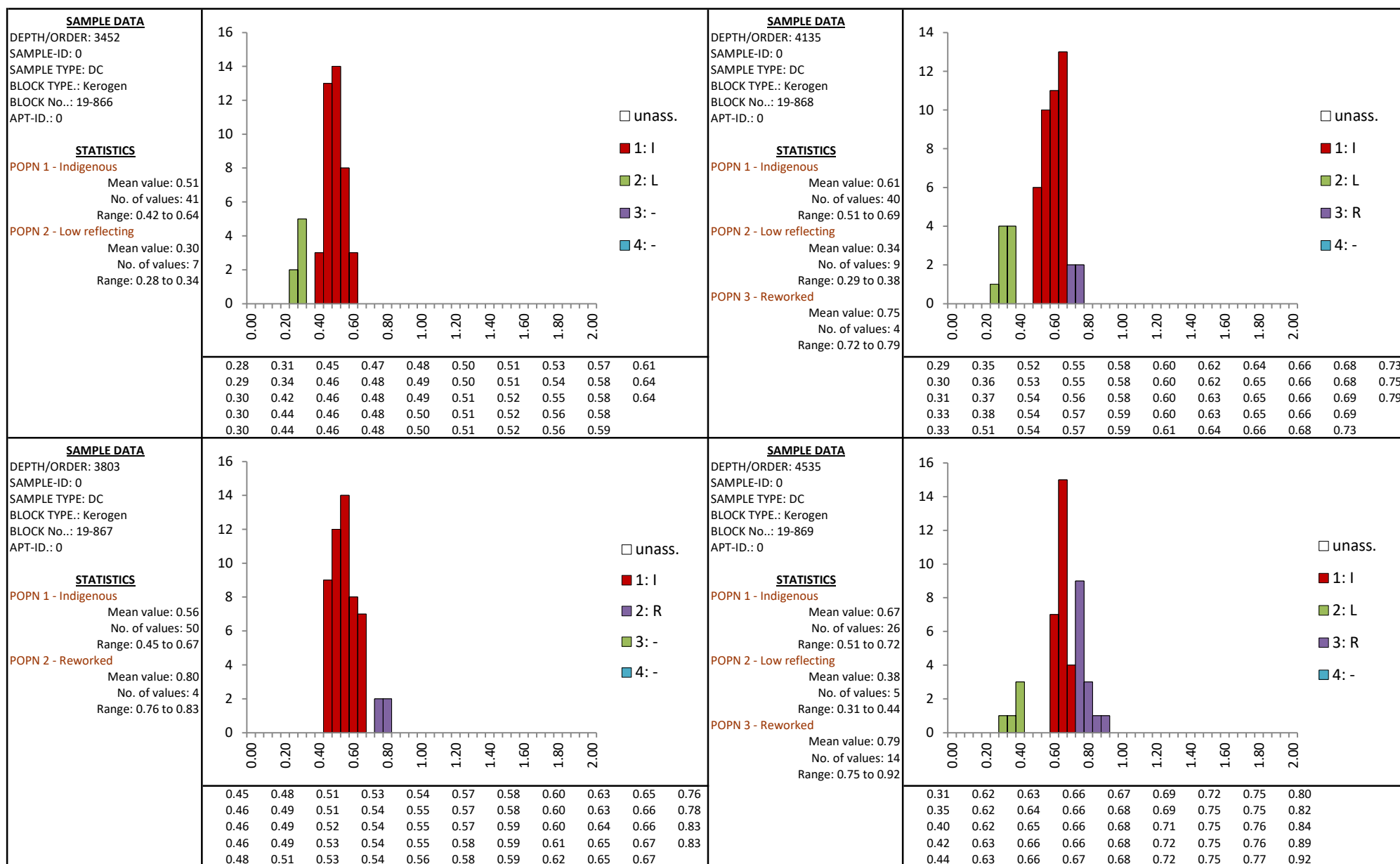


FIGURE Ap3.3.1 Histograms, data and statistics for vitrinite reflectivity - 205/09-1

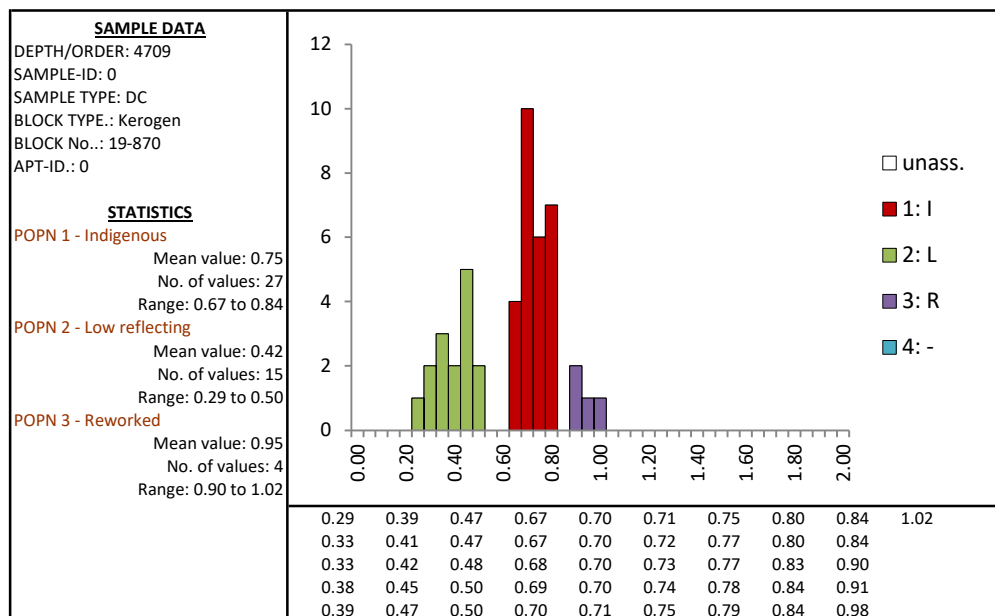


FIGURE Ap3.3.1 Histograms, data and statistics for vitrinite reflectivity - 205/09-1

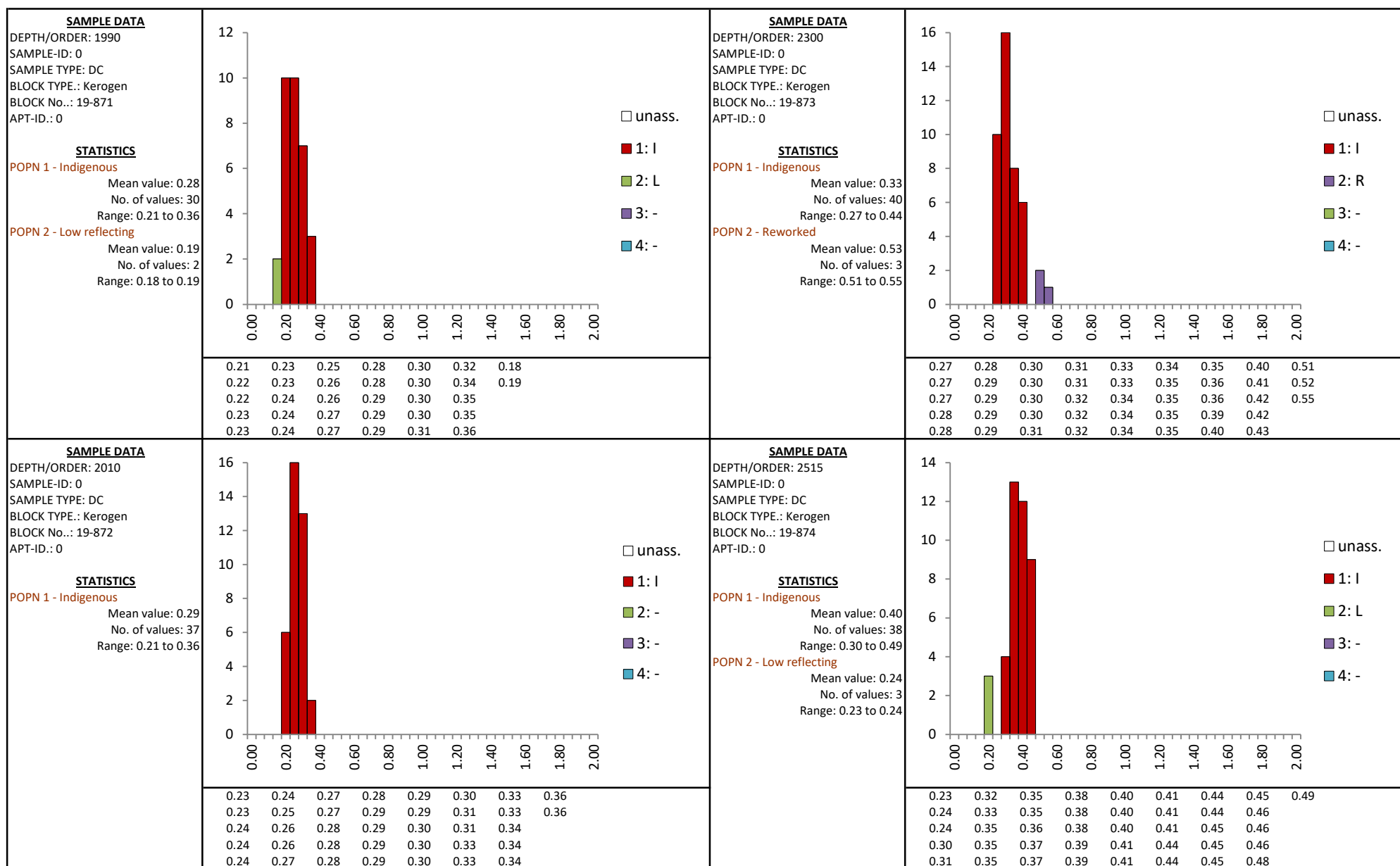


FIGURE Ap3.3.2 Histograms, data and statistics for vitrinite reflectivity - 205/12-1

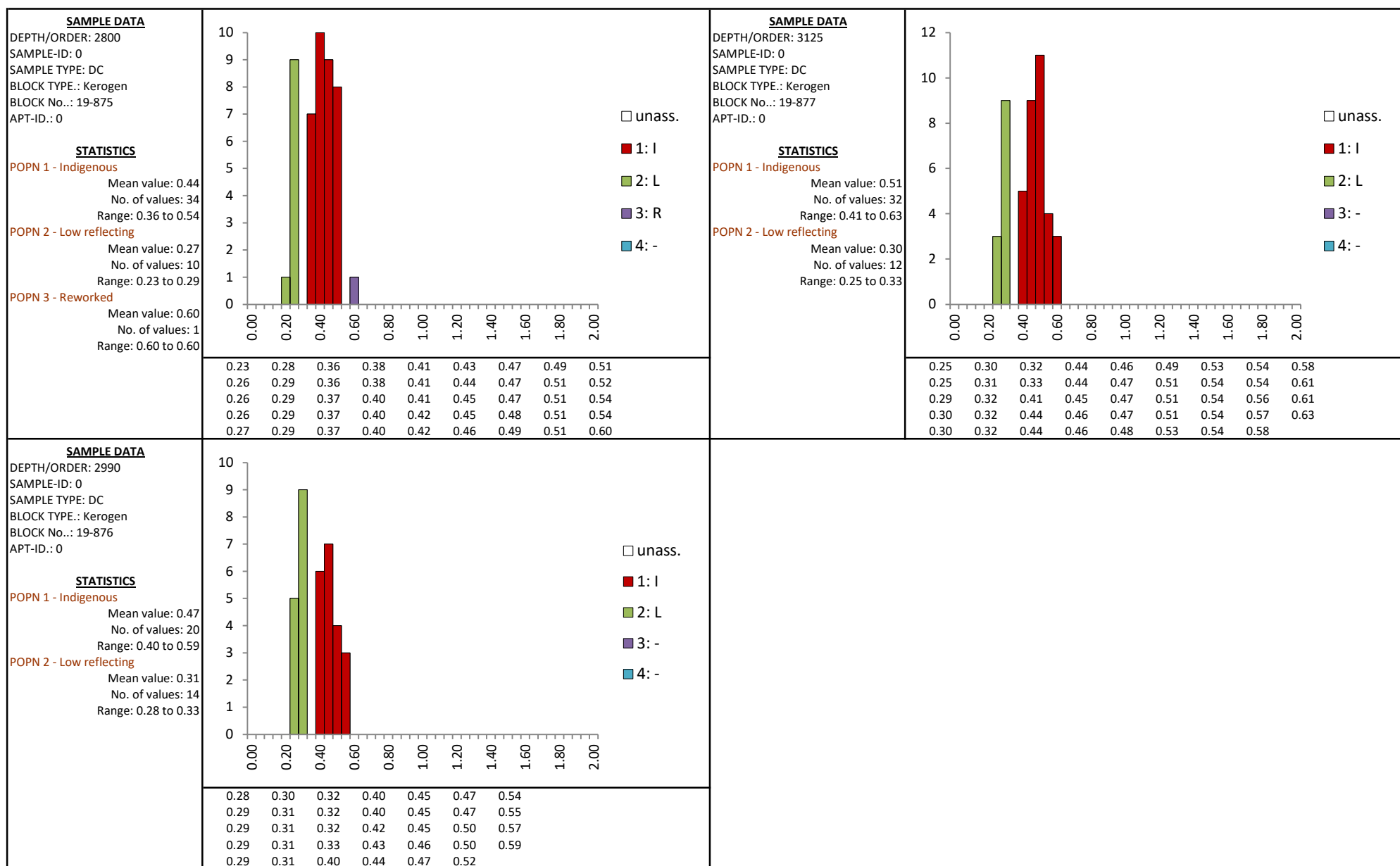


FIGURE Ap3.3.2 Histograms, data and statistics for vitrinite reflectivity - 205/12-1

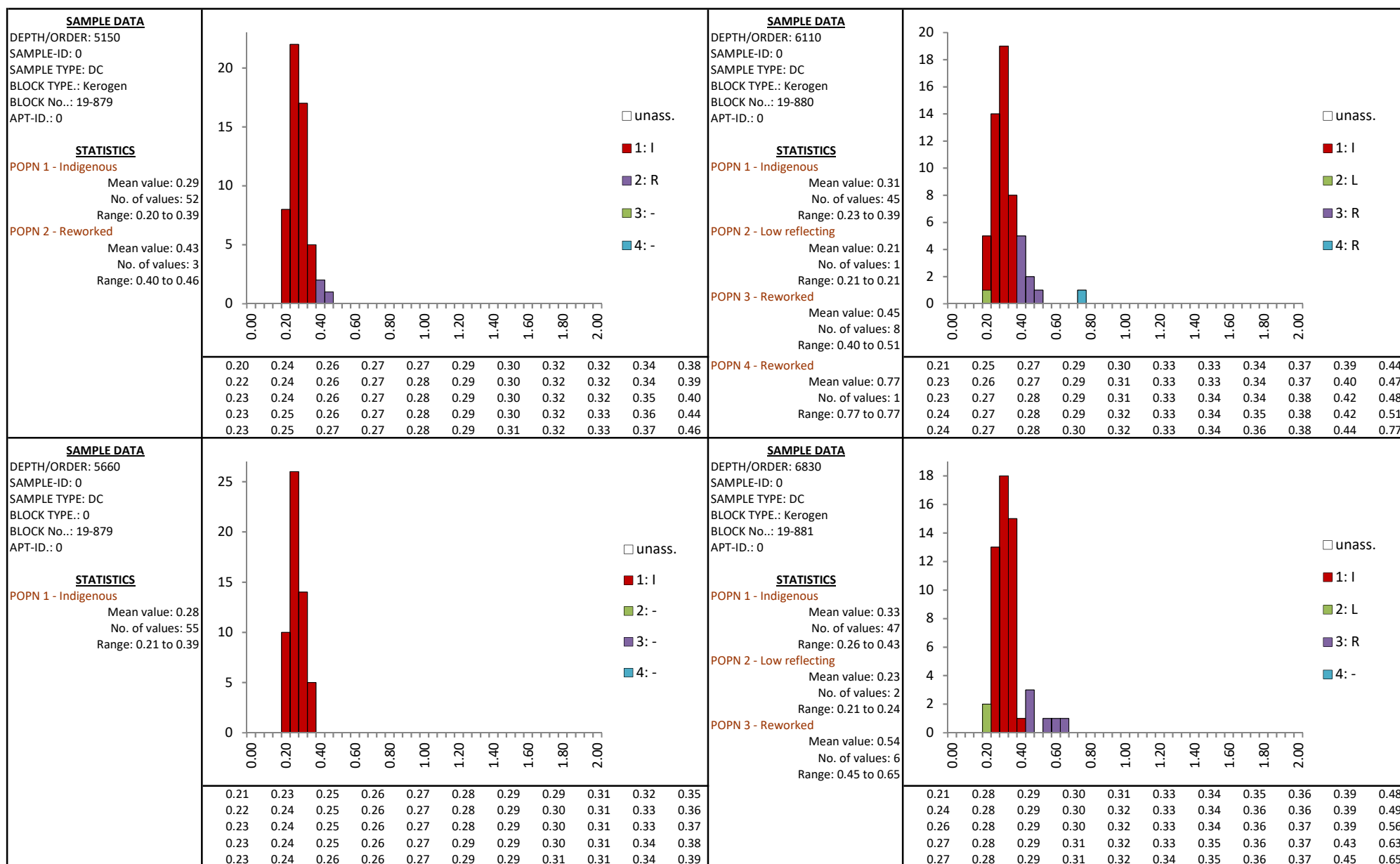


FIGURE Ap3.3.3 Histograms, data and statistics for vitrinite reflectivity - 205/14-2

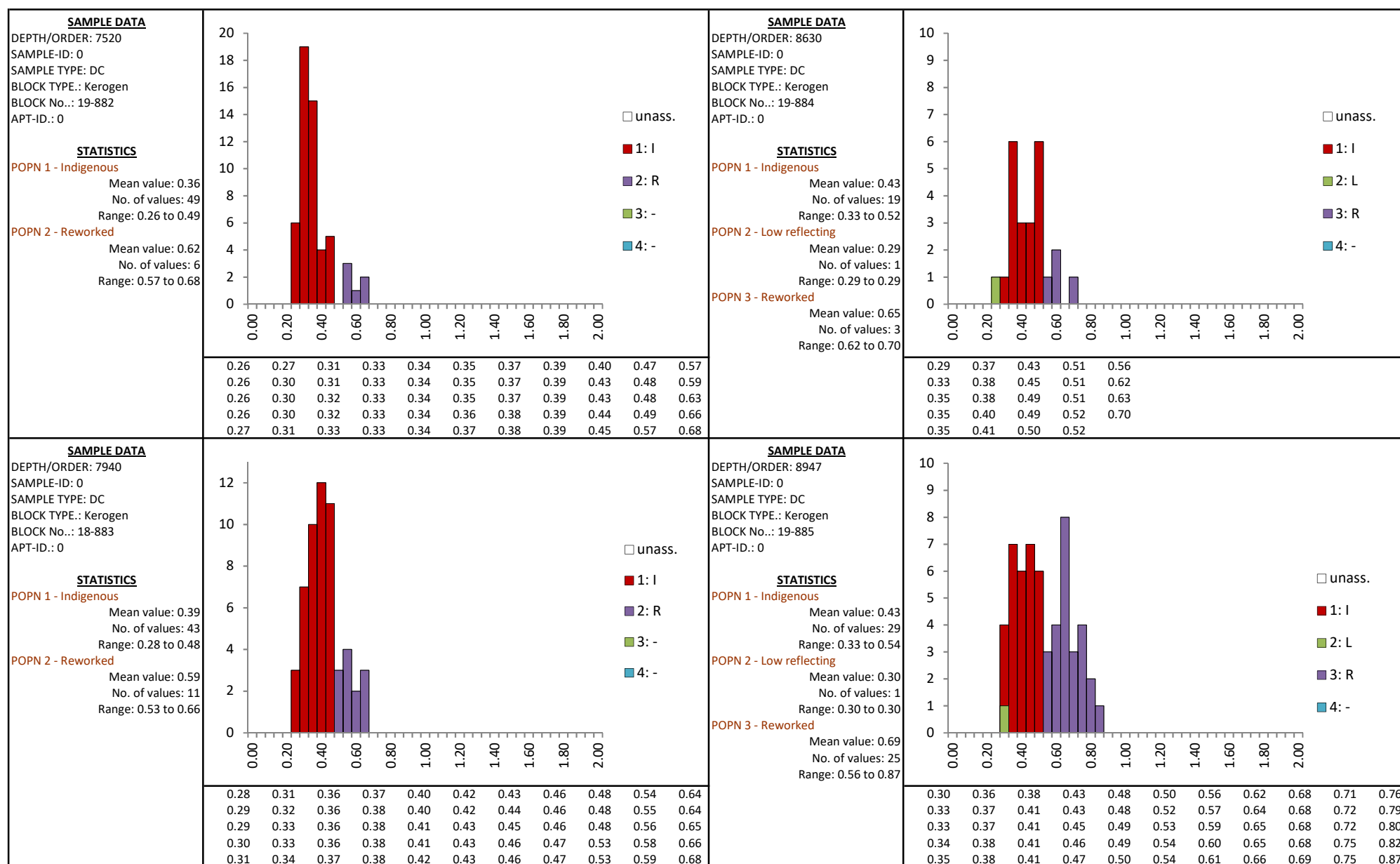


FIGURE Ap3.3.3 Histograms, data and statistics for vitrinite reflectivity - 205/14-2

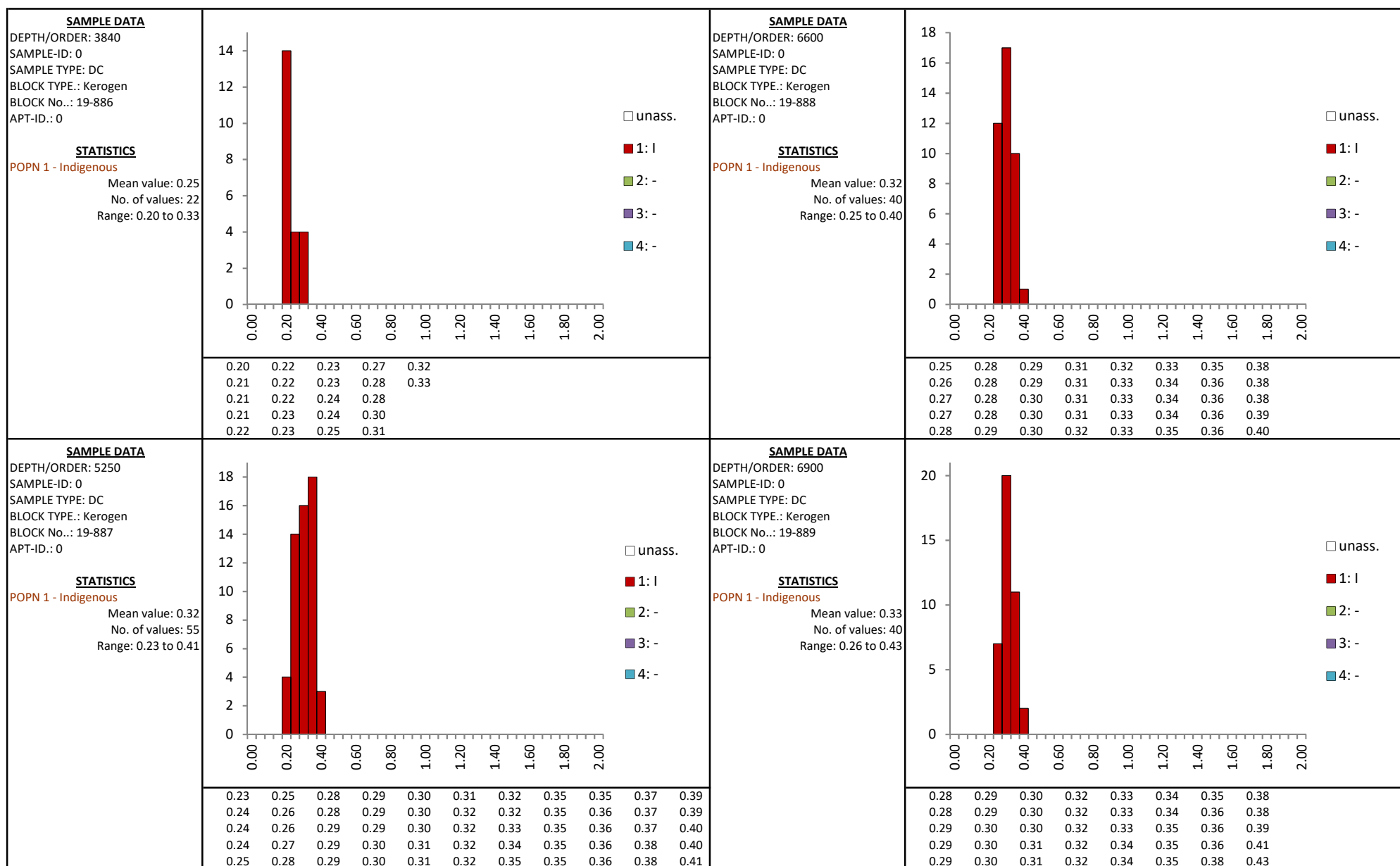


FIGURE Ap3.3.4 Histograms, data and statistics for vitrinite reflectivity - 205/14-3

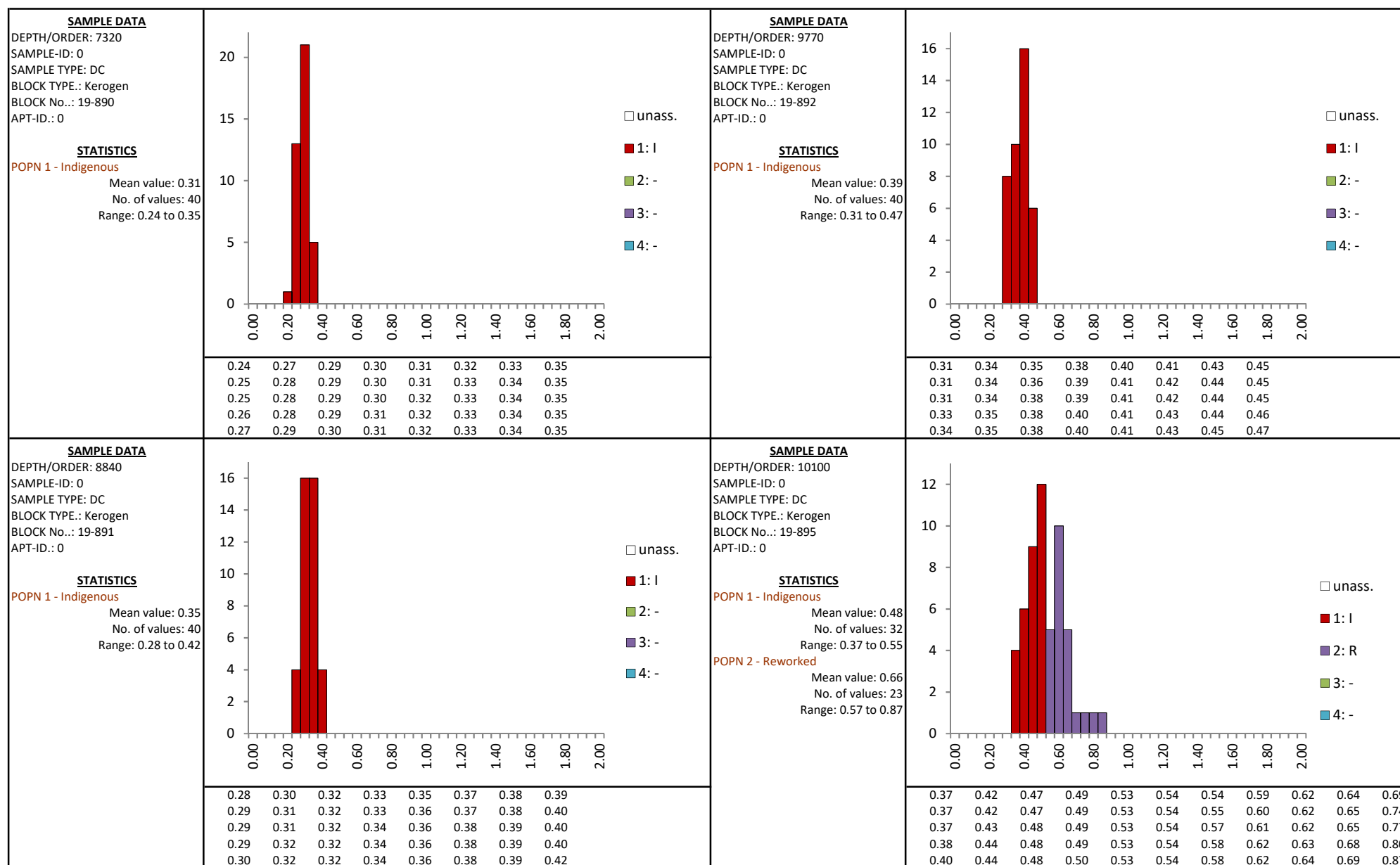


FIGURE Ap3.3.4 Histograms, data and statistics for vitrinite reflectivity - 205/14-3

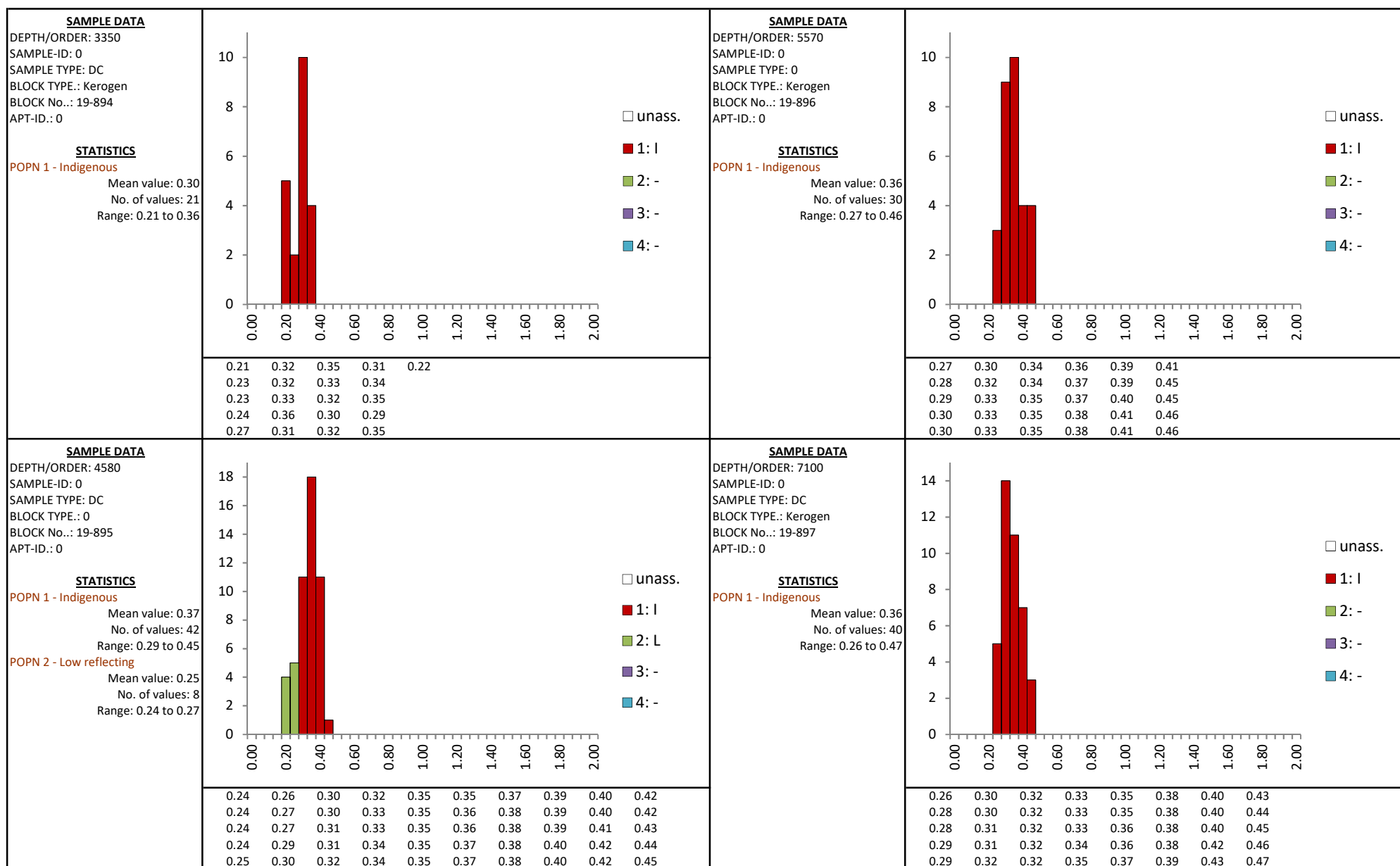


FIGURE Ap3.3.5 Histograms, data and statistics for vitrinite reflectivity - 206/01-1A

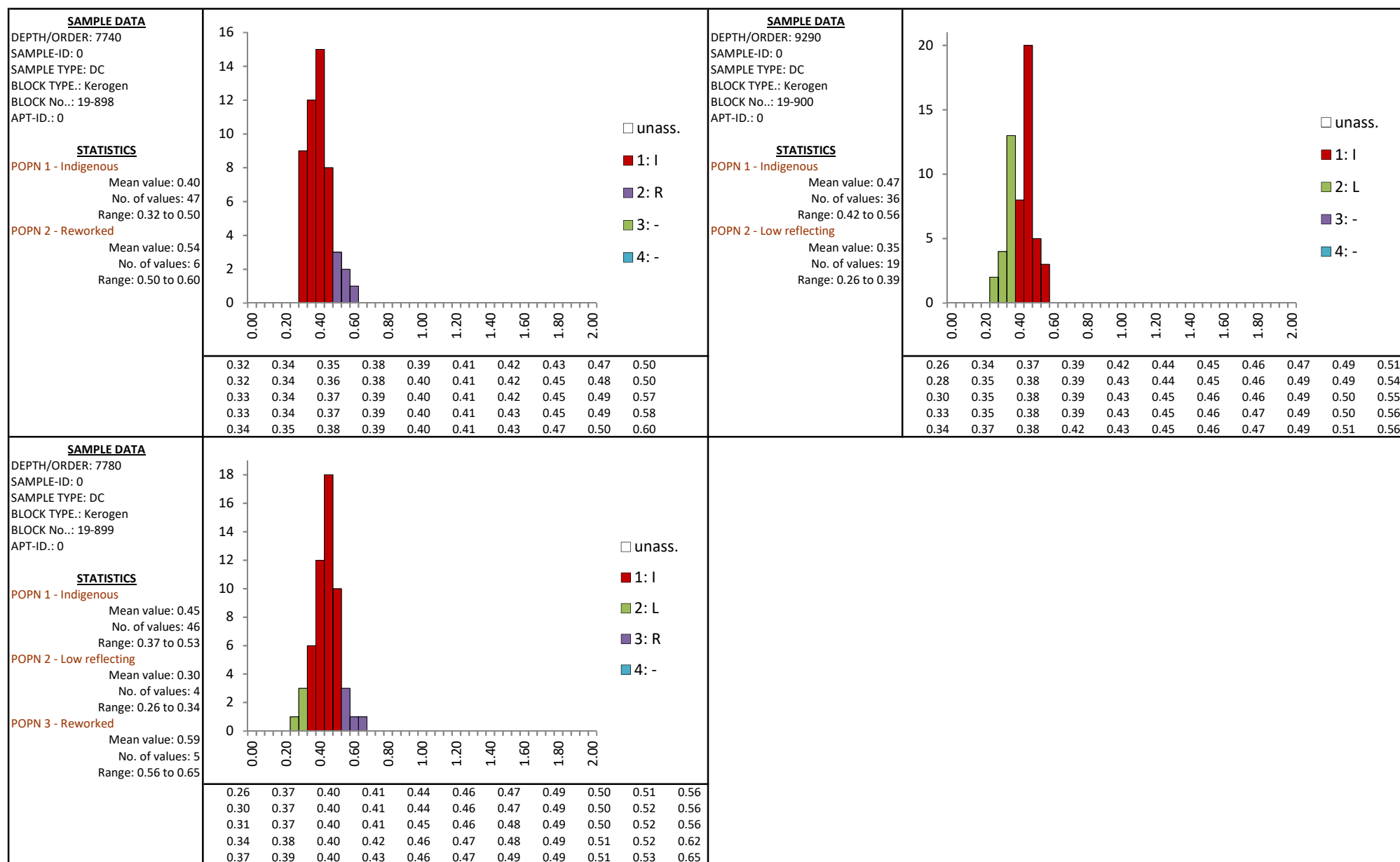


FIGURE Ap3.3.5 Histograms, data and statistics for vitrinite reflectivity - 206/01-1A

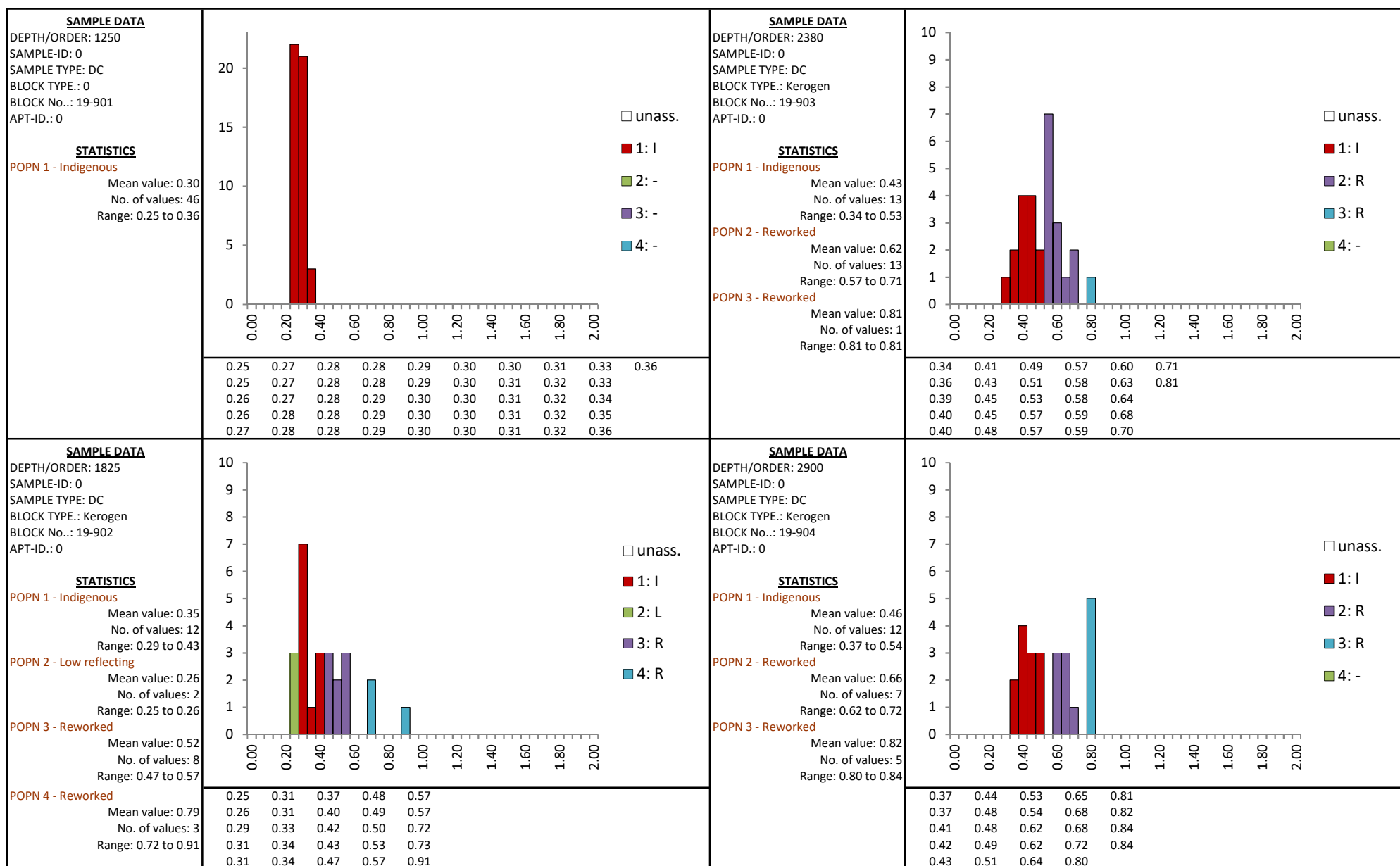


FIGURE Ap3.3.6 Histograms, data and statistics for vitrinite reflectivity - 206/11-1

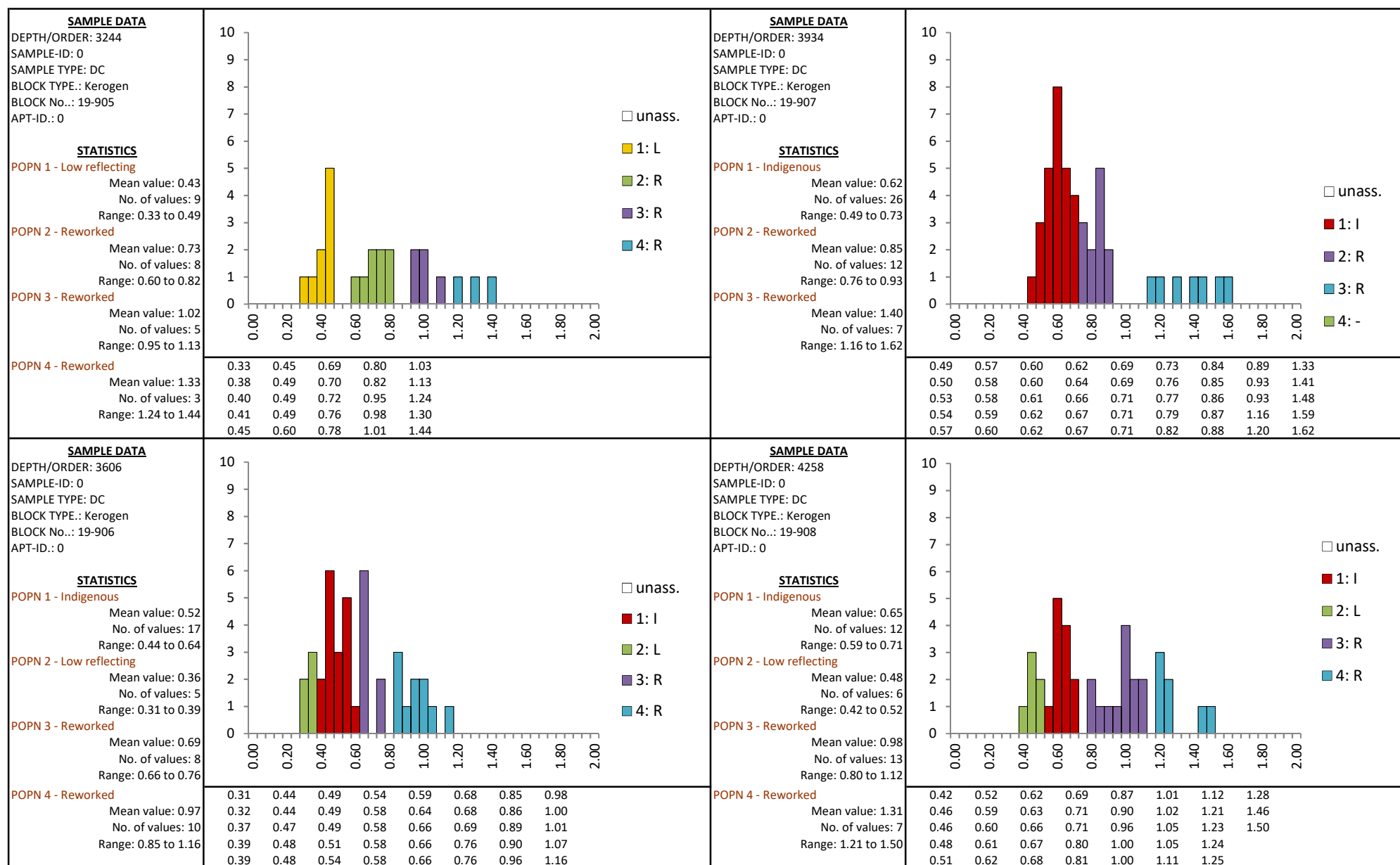


FIGURE Ap3.3.6 Histograms, data and statistics for vitrinite reflectivity - 206/11-1

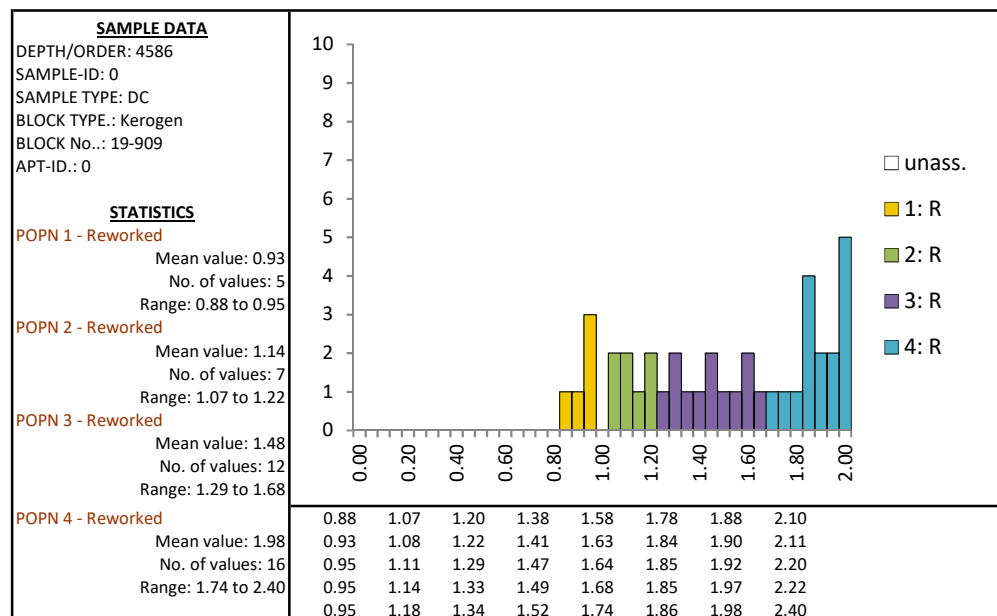


FIGURE Ap3.3.6 Histograms, data and statistics for vitrinite reflectivity - 206/11-1

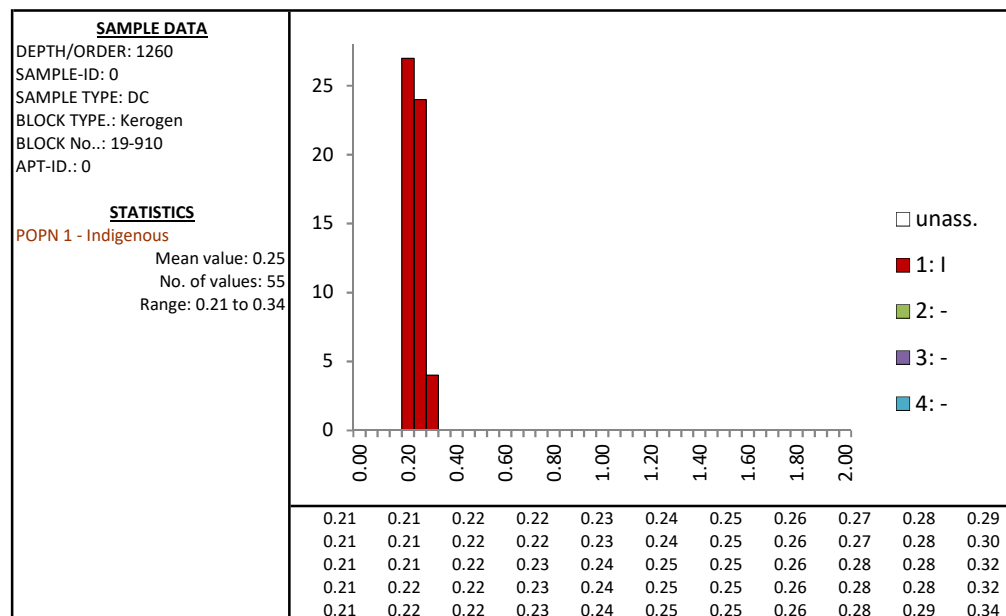


FIGURE Ap3.3.7 Histograms, data and statistics for vitrinite reflectivity - 207/01-2

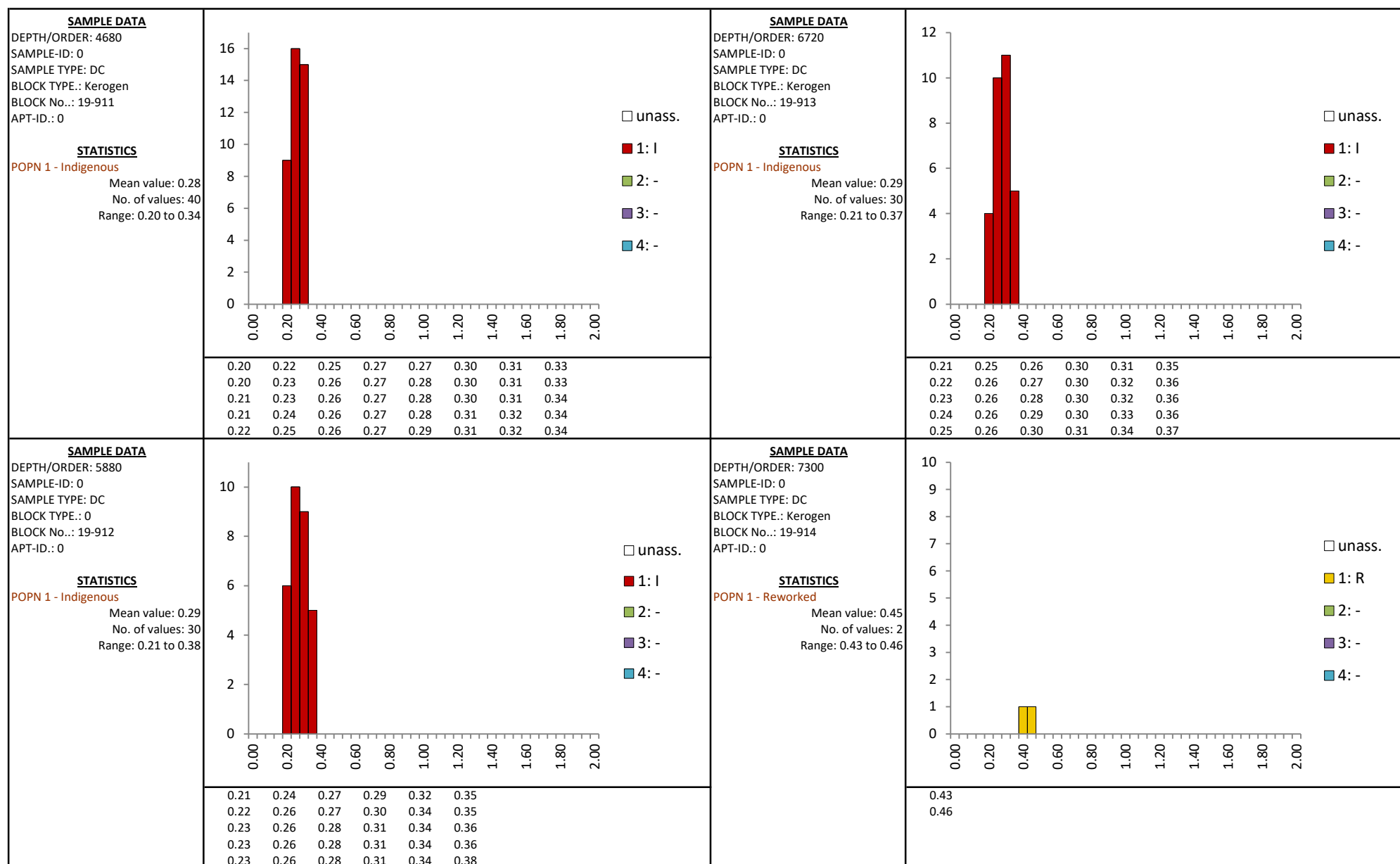


FIGURE Ap3.3.8 Histograms, data and statistics for vitrinite reflectivity - 208/17-1

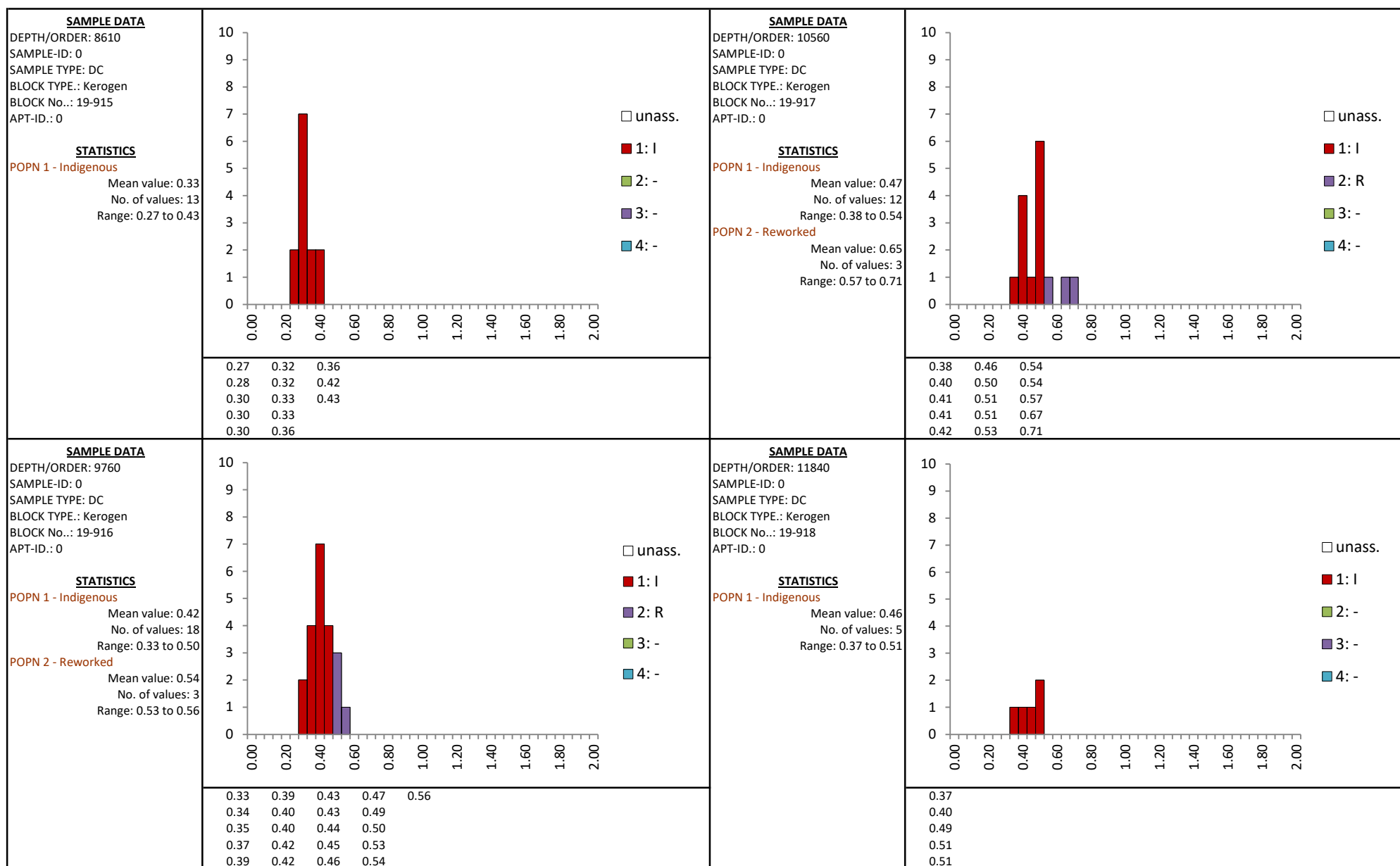


FIGURE Ap3.3.8 Histograms, data and statistics for vitrinite reflectivity - 208/17-1

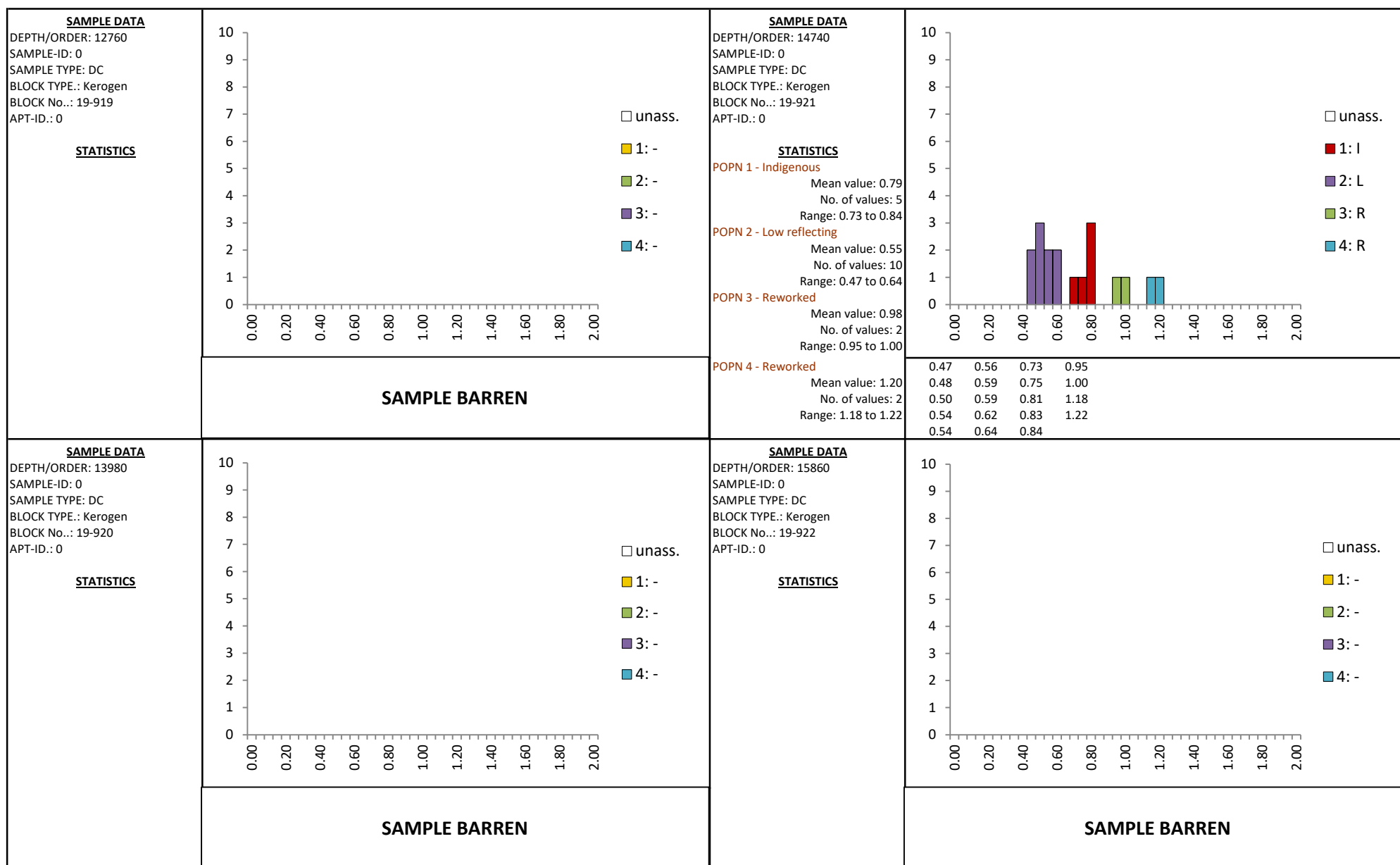


FIGURE Ap3.3.8 Histograms, data and statistics for vitrinite reflectivity - 208/17-1

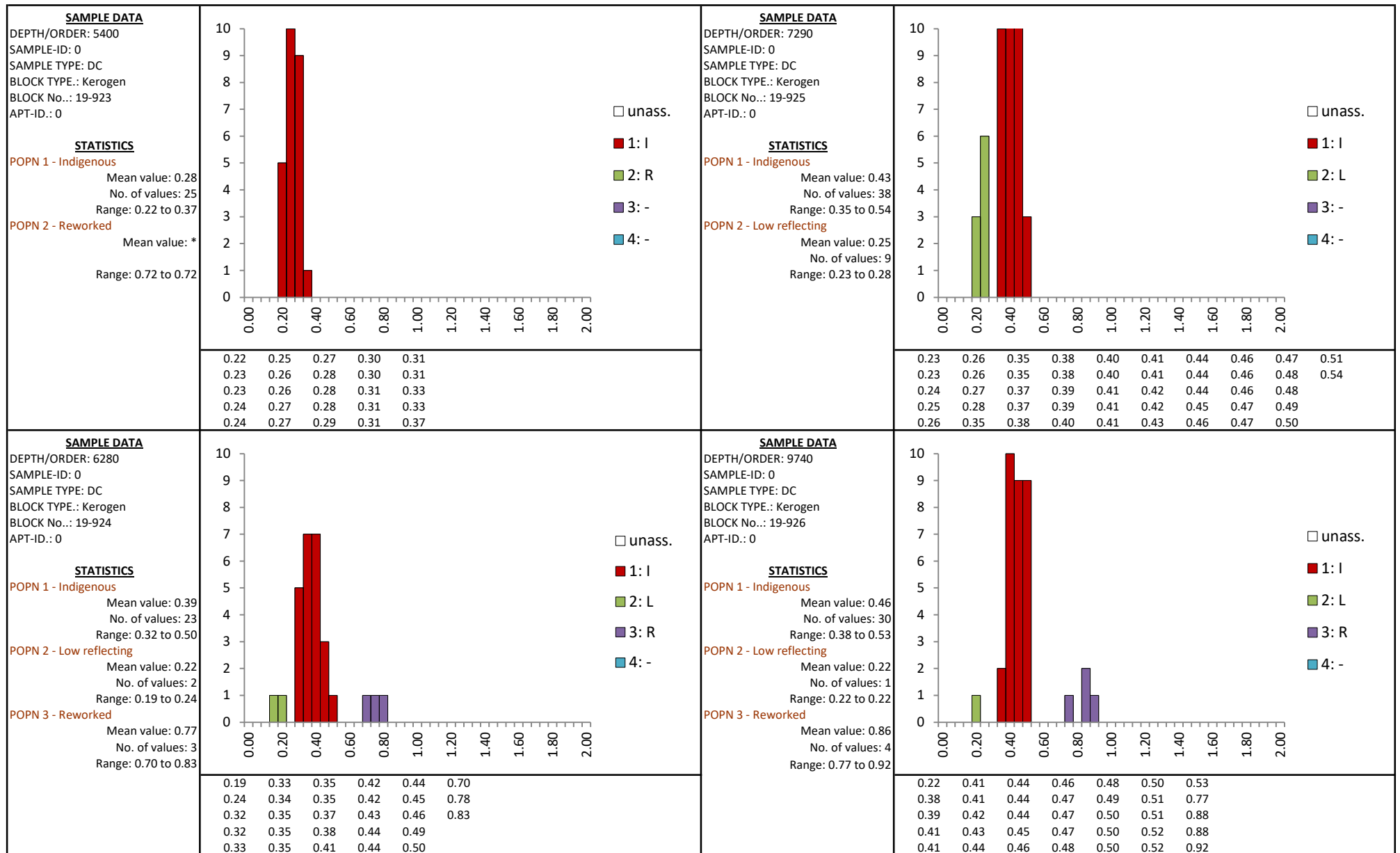


FIGURE Ap3.3.9 Histograms, data and statistics for vitrinite reflectivity - 208/17-2

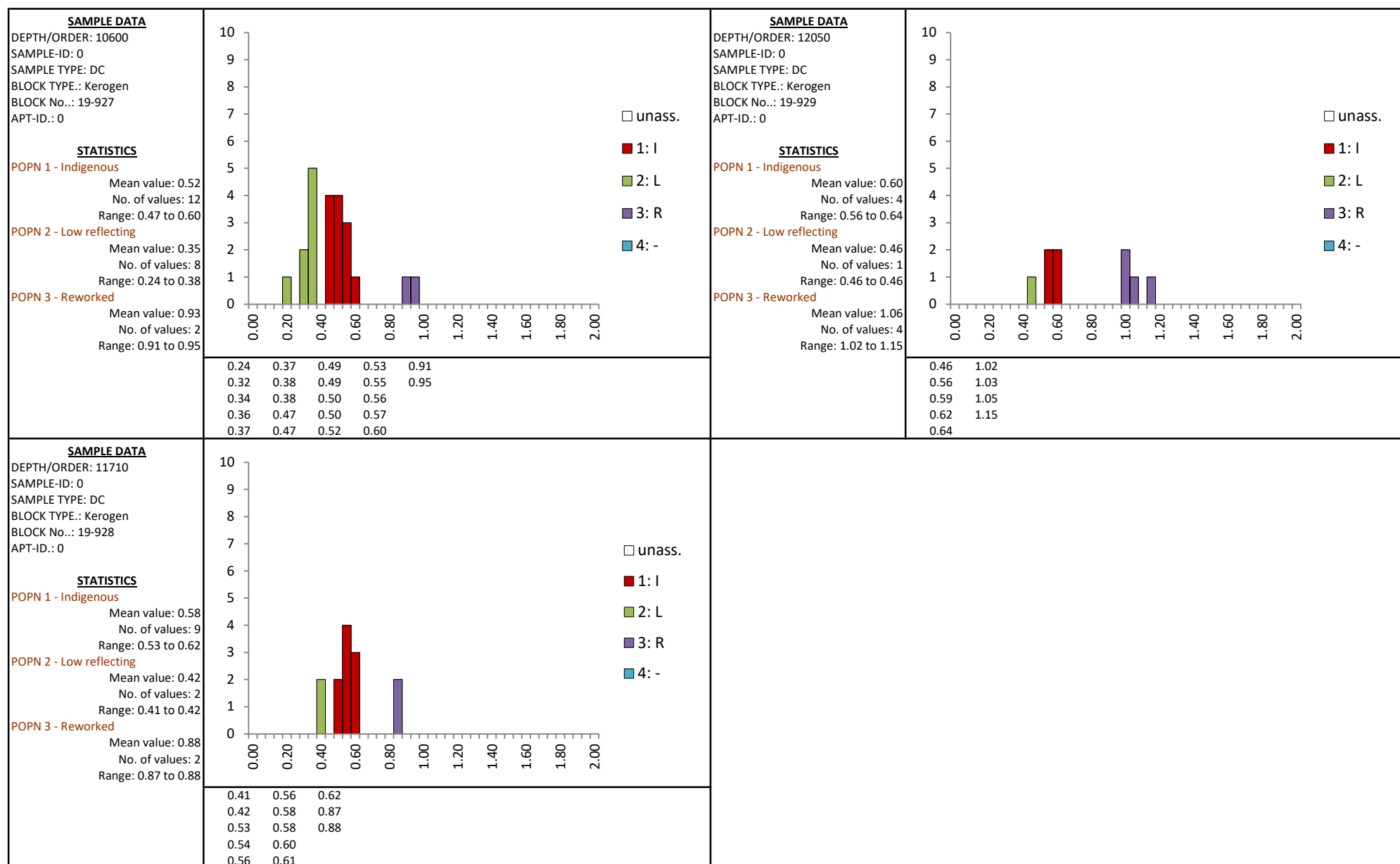


FIGURE Ap3.3.9 Histograms, data and statistics for vitrinite reflectivity - 208/17-2

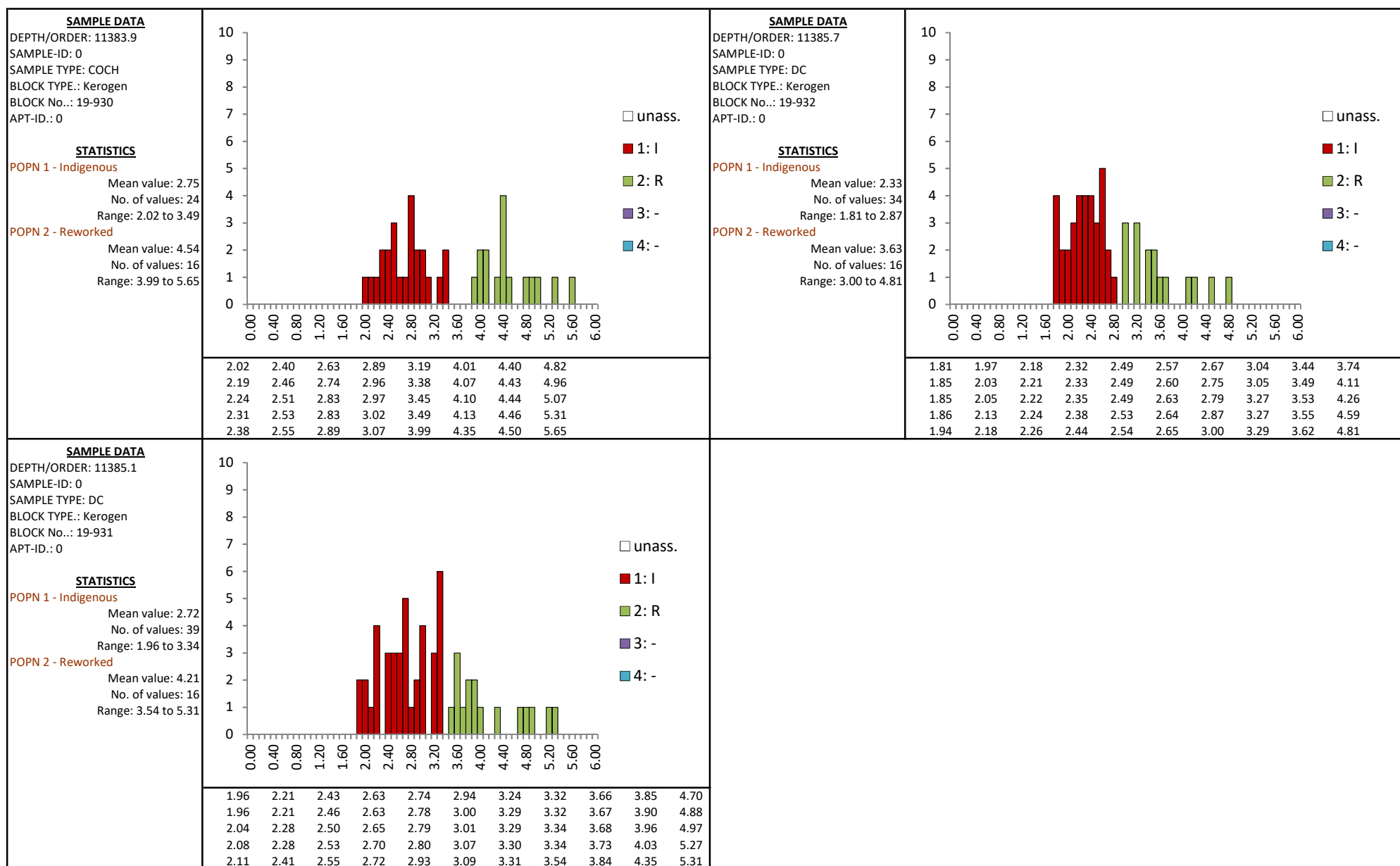


FIGURE Ap3.3.10 Histograms, data and statistics for vitrinite reflectivity - 209/12-1

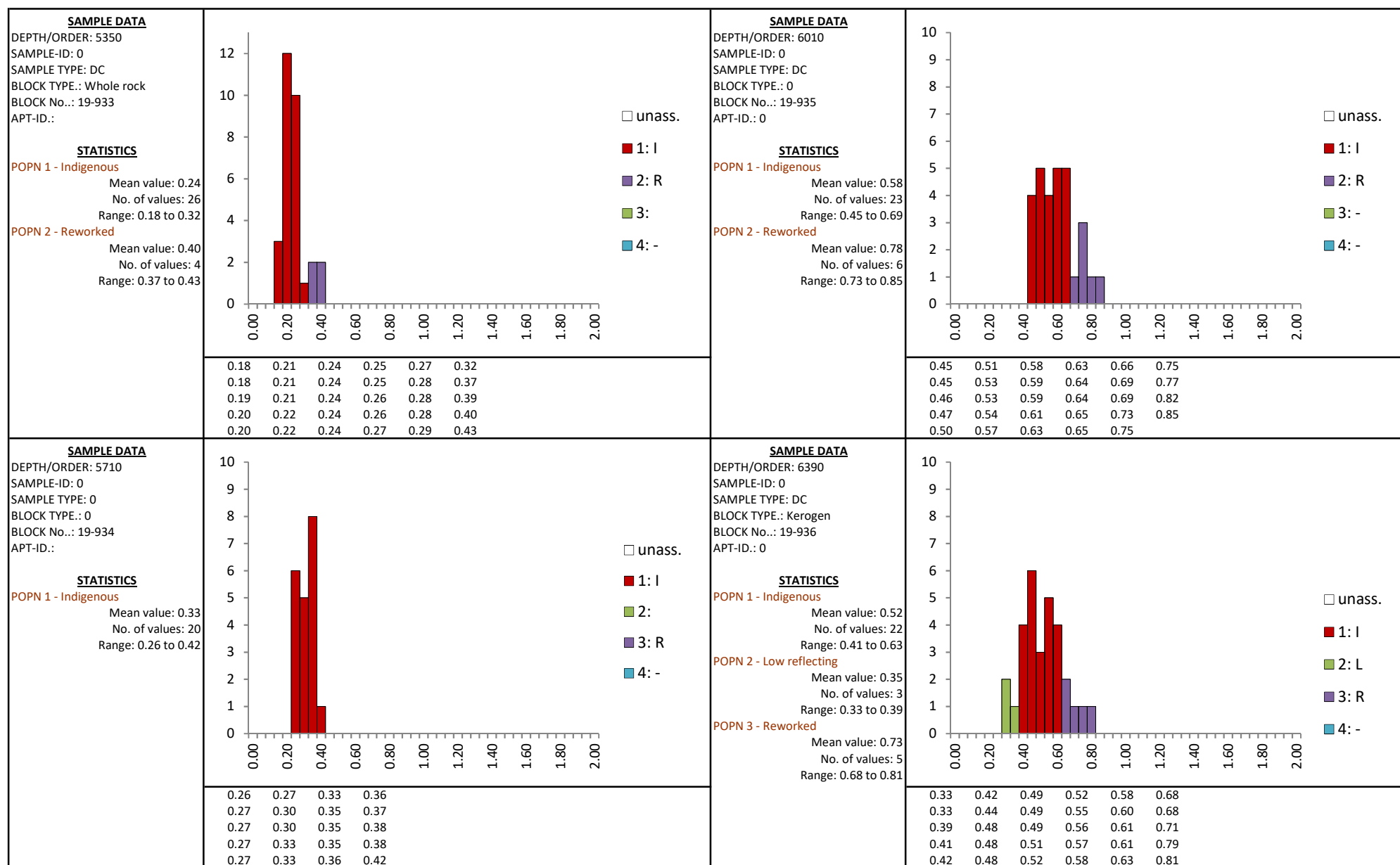


FIGURE Ap3.3.11 Histograms, data and statistics for vitrinite reflectivity - 214/26-1

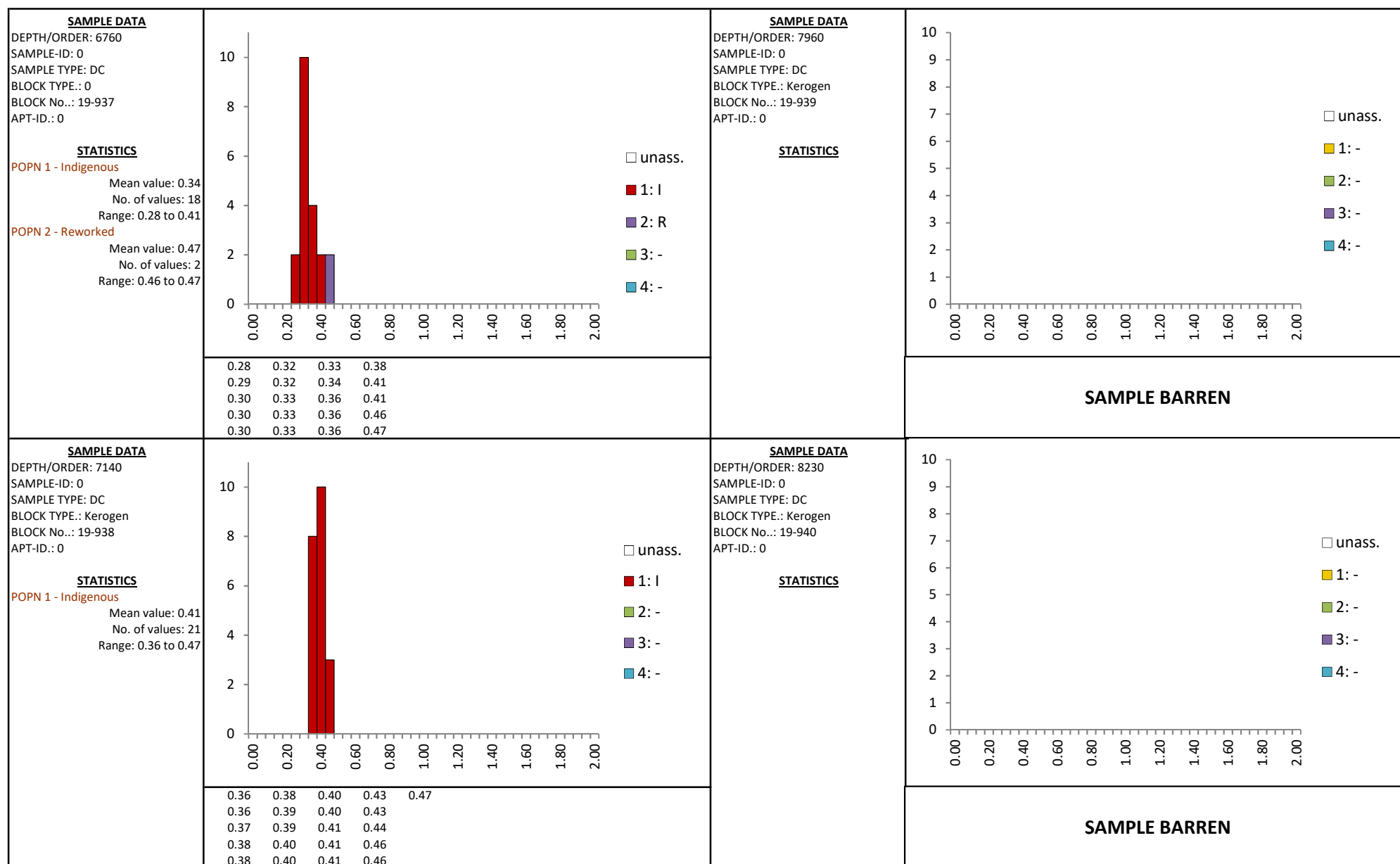


FIGURE Ap3.3.11 Histograms, data and statistics for vitrinite reflectivity - 214/26-1

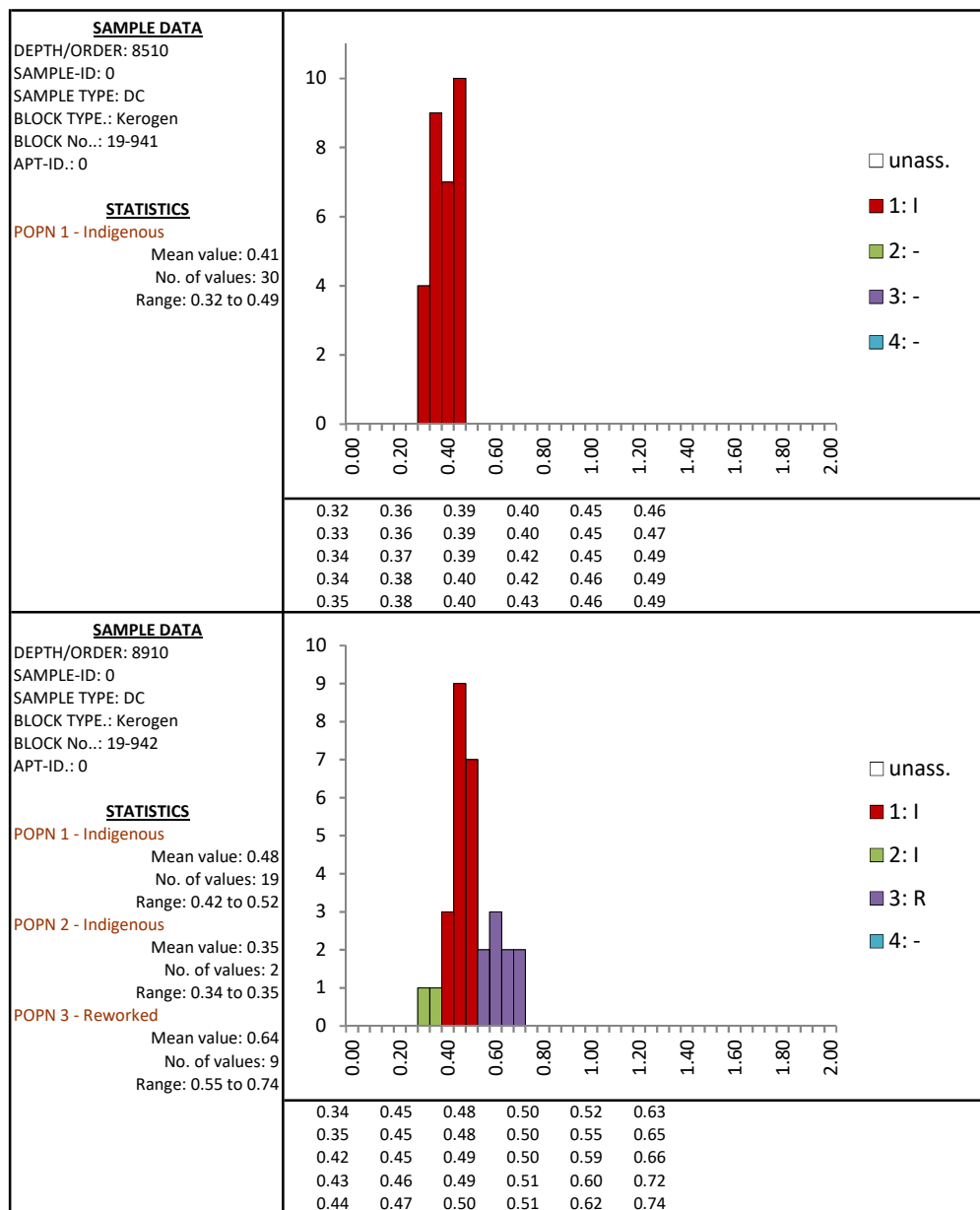


FIGURE Ap3.3.11 Histograms, data and statistics for vitrinite reflectivity - 214/26-1

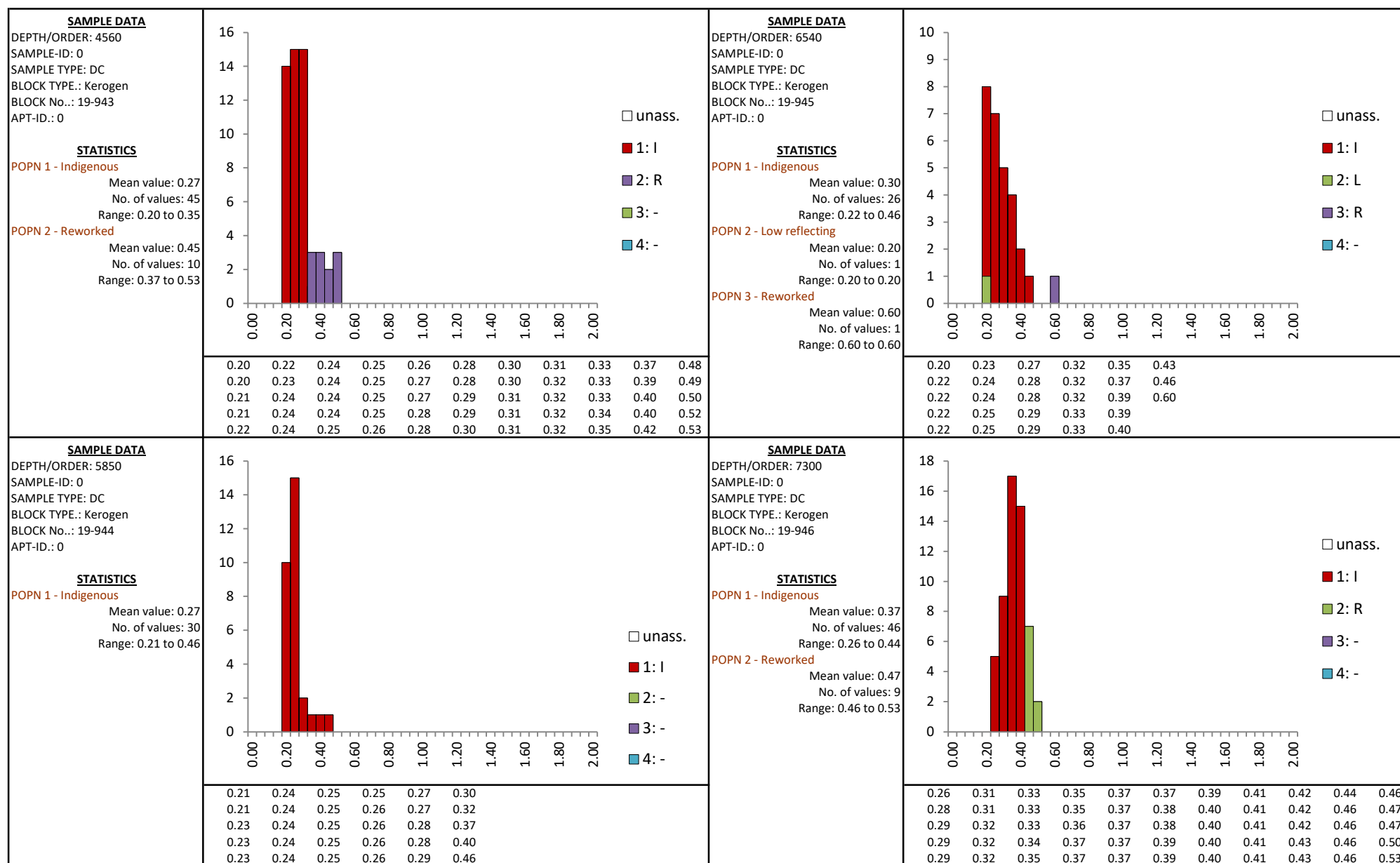


FIGURE Ap3.3.12 Histograms, data and statistics for vitrinite reflectivity - 214/28-1

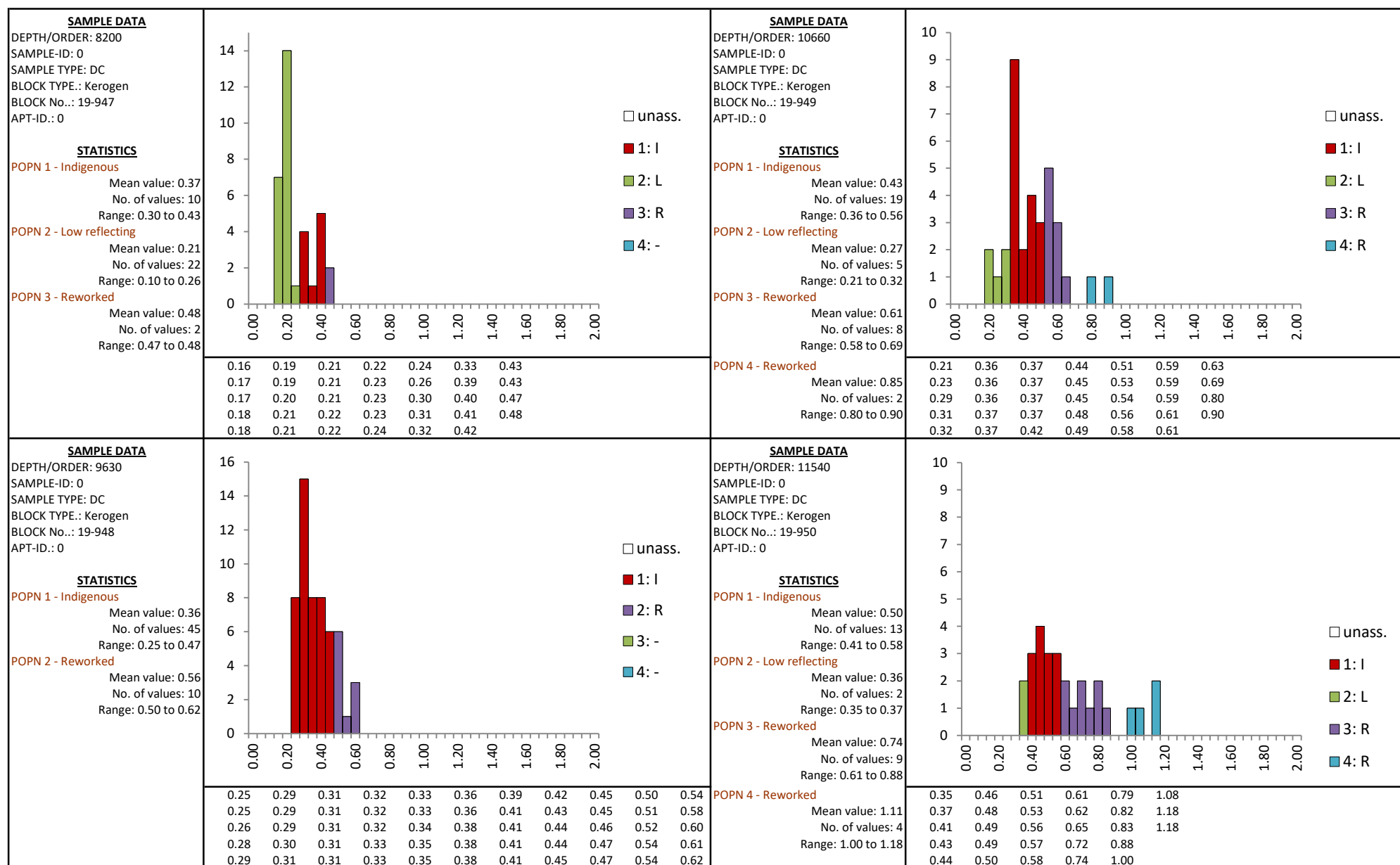


FIGURE Ap3.3.12 Histograms, data and statistics for vitrinite reflectivity - 214/28-1

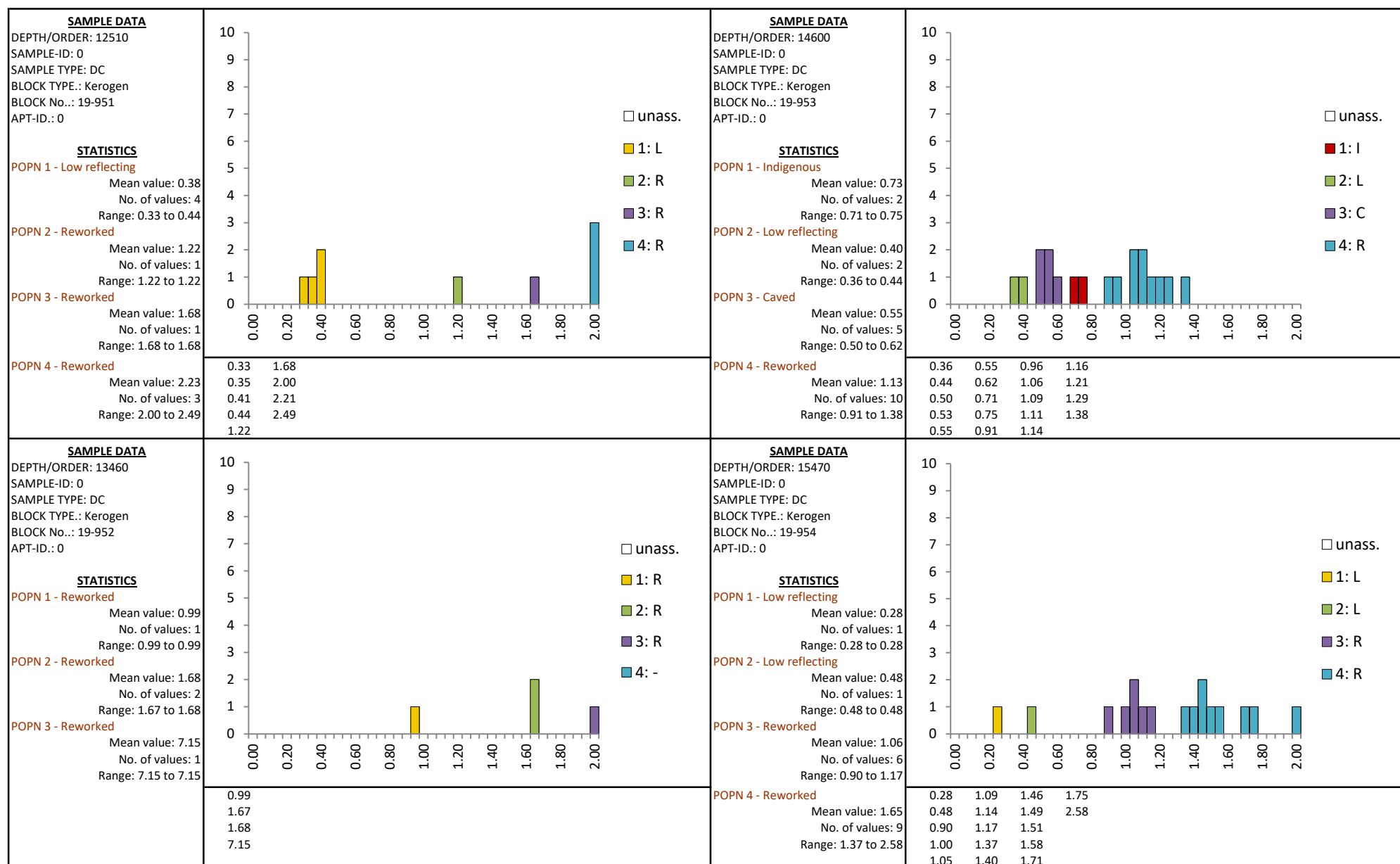


FIGURE Ap3.3.12 Histograms, data and statistics for vitrinite reflectivity - 214/28-1

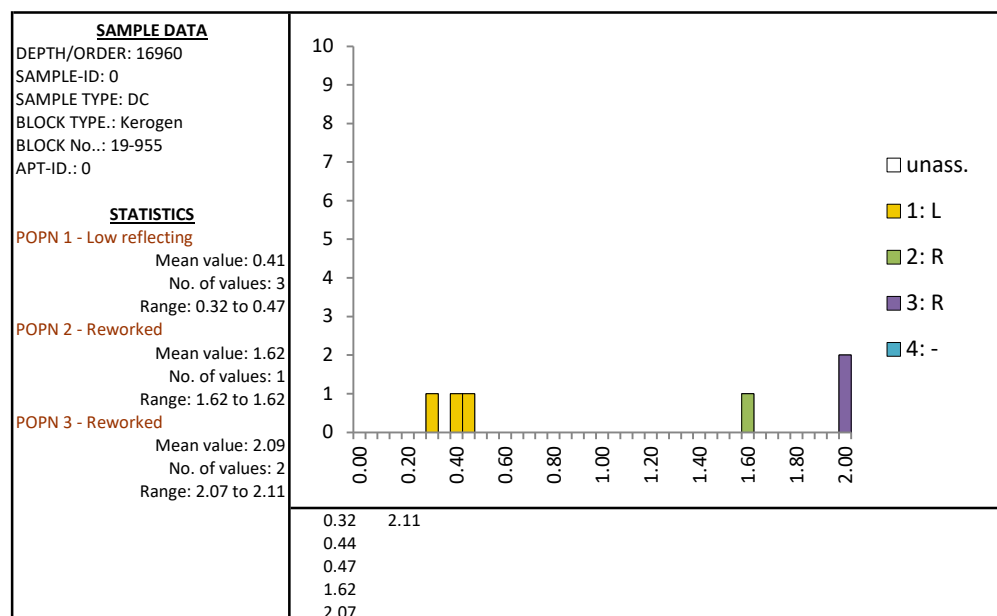


FIGURE Ap3.3.12 Histograms, data and statistics for vitrinite reflectivity - 214/28-1

APPENDIX 3.4

SPORE COLOUR INDEX (SCI) DATA

Tables

Ap3.4.1	Spore colour and kerogen composition data: 205/09-1
Ap3.4.2	Spore colour and kerogen composition data: 205/12-1
Ap3.4.3	Spore colour and kerogen composition data: 205/14-2
Ap3.4.4	Spore colour and kerogen composition data: 205/14-3
Ap3.4.5	Spore colour and kerogen composition data: 206/01-1A
Ap3.4.6	Spore colour and kerogen composition data: 206/11-1
Ap3.4.7	Spore colour and kerogen composition data: 207/01-2
Ap3.4.8	Spore colour and kerogen composition data: 208/17-1
Ap3.4.9	Spore colour and kerogen composition data: 208/17-2
Ap3.4.10	Spore colour and kerogen composition data: 209/12-1
Ap3.4.11	Spore colour and kerogen composition data: 214/26-1
Ap3.4.12	Spore colour and kerogen composition data: 214/28-1

Well	Top Depth (m)	Stratigraphy	Age	Sample Type	Slide Type	Spore Colour Index (SCI)					UV Fluorescence		Kerogen Composition (3 and 6 Component)						Comments
						Indigenous		Other			Form	Colour							
						SCI	No.	SCI	No.	Type									
205/09-1	2110.0	Hordaland	E1	DC	SCI (WK)	3.0	5	4.5	2	Rwk	Miosp	Yel orn-?brn	Sap.	Vit.	Inert.	Sieved fraction barren. Sample appears to be mostly degraded humic organic matter. Spores rare and often degraded.			
	-	-						-	Sph	Pl yel	Tr	95	5						
	-	-						-	AOM	Brn-N.F.	FA	HA	AL	HE	WO		5		
	-	-						-	-	-	-	75	Tr	?Tr	20		5		
	2384.0	Sele	DC	SCI (S/WK)	3.5	22	3.0	8	Dino	Miosp	Orn-yel	Sap.	Vit.	Inert.	Palynomorphs often thinned/degraded or fragmented. Variable SCI's ranging from ~3.0-5.0SCI, variable fluorescence. Indigenous population difficult to identify.				
	5.0						2	Rwk	Sph	Yel	Tr	95	5						
	-						-	-	Dino	Yel orn-?brn	FA	HA	AL	HE		WO	CO		
	-						-	-	AOM	Brn-N.F.	-	65	Tr	?Tr		30	5		
	2774.0		DC	SCI (S/WK)	4.0	8	4.0	2	Dino	Miosp	Yel orn-N.F.	Sap.	Vit.	Inert.	Sieved fraction lean. Spores often heavily degraded. Increased dino content.				
	5.0						1	Rwk	AOM	N.F.	Tr	95	5						
	-						-	-	-	-	FA	HA	AL	HE		WO	CO		
	-						-	-	-	-	-	75	Tr	?Tr		20	5		
	3143.0		DC	SCI (S/WK)	4.0	3	4.5	3	Dino	Miosp	Yel orn	Sap.	Vit.	Inert.	Palynomorphs very rare.				
	-						-	-	Dino	?Brn	Mn	95	5						
	-						-	-	AOM	DI brn-N.F.	FA	HA	AL	HE		WO	CO		
	-						-	-	-	-	-	65	Mn	-		30	5		
	3452.0	Lista	DC	SCI (S/WK)	4.0	14	5.5	1	Dino	Miosp	Orn	Sap.	Vit.	Inert.	Sieved fraction lean. Unclear if miospores present.				
	-						-	-	AOM	N.F.	Mn	95	5						
	-						-	-	-	-	FA	HA	AL	HE		WO	CO		
	-						-	-	-	-	-	80	Mn	-		15	5		
	3803.0		DC	SCI (S/WK)	5.0	18	4.5	2	Dino	Miosp	Orn-brn	Sap.	Vit.	Inert.	Sieved fraction very lean. Kerogen mostly humic material. Appears to be numerous, degraded ?algal palynomorphs in whole kerogen.				
	6.5						3	Rwk	Dino	Brn-N.F.	10	45	45						
	-						-	-	AOM	N.F.	FA	HA	AL	HE		WO	CO		
	-						-	-	-	-	-	25	10	?Tr		20	45		
	4136.0	Undiff.	DC	SCI (S/WK)	5.0	14	6.5	2	Dino	Miosp	?N.F.	Sap.	Vit.	Inert.	Good yield in sieved fraction. Palynomorph identification uncertain.				
	3.5						2	Cav	Dino	Wk yel orn	Mn	90	10						
	-						-	-	AOM	N.F.	FA	HA	AL	HE		WO	CO		
	-						-	-	-	-	-	85	Mn	-		5	10		

TABLE Ap3.4.1 Spore colour and kerogen composition data: 205/09-1

Well	Top Depth (ft)	Stratigraphy	Age	Sample Type	Slide Type	Spore Colour Index (SCI)					UV Fluorescence		Kerogen Composition (3 and 6 Component)						Comments
						Indigenous		Other			Form	Colour							
						SCI	No.	SCI	No.	Type									
205/09-1	4535.0	Maureen	P2	DC	SCI (S/WK)	6.0	8	5.0	2	Dino	Miosp	N.F.	Sap.		Vit.		Inert.		Miospore identification uncertain.
								8.0	1	Rwk	Dino	N.F.	-	80		20			
								-	-	-	AOM	N.F.	FA	HA	AL	HE	WO	CO	
								-	-	-	-	-	-	80	-	-	Mn	20	
	4709.0	Shetland	K2	DC	SCI (WK)	7.0	8	4.0	2	Cav	Miosp	N.F.	Sap.		Vit.		Inert.		Sieved fraction barren. Indigenous miospore identification uncertain. Palynomorph with 3.5 SCI likely caved (yellow-orange fluorescence).
								-	-	-	AOM	N.F.	Tr		20		80		
								-	-	-	-	-	FA	HA	AL	HE	WO	CO	
								-	-	-	-	-	-	20	Tr	-	Tr	80	

TABLE Ap3.4.1 Spore colour and kerogen composition data: 205/09-1

Well	Top Depth (m)	Stratigraphy	Age	Sample Type	Slide Type	Spore Colour Index (SCI)					UV Fluorescence		Kerogen Composition (3 and 6 Component)						Comments
						Indigenou		Other			Form	Colour							
						SCI	No.	SCI	No.	Type									
205/12-1	1990.0	Stronsay	E1	DC	SCI (S/WK)	2.5	23	-	-	-	Miosp	Yel	Sap.	Vit.	Inert.	Sieved fraction practically barren. Trace amounts of dinocysts present. AOM fluorescence derived from VR slide.			
	-							-	-	Dino	Yel-grn	35	60	5					
	-							-	-	AOM	Pl yel	FA	HA	AL	HE		WO	CO	
	-							-	-	-	-	30	-	Tr	5		60	5	
	2010.0	DC	SCI (S/WK)	2.5	19	6.0	2	Rwk	Miosp	Yel	Sap.	Vit.	Inert.	Increased dino content. AOM fluorescence derived from VR slide.					
						-	-	-	Dino	Yel-grn	65	25	10						
						-	-	-	AOM	Brn	FA	HA	AL		HE	WO	CO		
						-	-	-	-	-	60	-	Mn		5	25	10		
	2300.0	DC	SCI (S/WK)	3.0	17	3.5	1	Dino	Miosp	Yel-yel grn	Sap.	Vit.	Inert.	AOM fluorescence derived from VR slide.					
						1.5	1	Cav	Dino	Yel-brn	5	85	20						
						5.0	1	Rwk	AOM	N.F	FA	HA	AL		HE	WO	CO		
						-	-	-	-	-	-	20	-		5	65	20		
	2515.0	DC	SCI (S/WK)	3.5	26	-	-	-	Miosp	Yel	Sap.	Vit.	Inert.	AOM fluorescence derived from VR slide.					
						-	-	-	Dino	Yel-brn	40	30	30						
						-	-	-	AOM	Brn	FA	HA	AL		HE	WO	CO		
						-	-	-	-	-	40	-	Tr		Mn	30	30		
	2800.0	DC	SCI (S/WK)	3.5	22	7.0	5	Rwk	Miosp	Orn-yel	Sap.	Vit.	Inert.	-					
						-	-	-	AOM	N.F	5	70	25						
						-	-	-	-	-	FA	HA	AL		HE	WO	CO		
						-	-	-	-	-	-	60	Tr		5	10	25		
	2990.0	DC	SCI (S/WK)	3.5	16	5.5	2	Rwk	Miosp	N.F	Sap.	Vit.	Inert.	<i>Palaeocystodinium bulliforma</i> common. Whole kerogen nearly all humic, and amorphous organic matter is clearly degraded humics.					
						-	-	-	AOM	N.F	Tr	90	10						
						-	-	-	-	-	FA	HA	AL		HE	WO	CO		
						-	-	-	-	-	-	-	Tr		Tr	90	10		
	3125.0	Shetland	K1	DC	SCI (S/WK)	4.0	21	2.0	1	Cav	Miosp	Yel-dl orn yel	Sap.	Vit.	Inert.	<i>Aquillapollenites</i> spp . at 3.0 SCI with orange yellow fluorescence.			
								-	-	-	AOM	N.F	10	30	60				
								-	-	-	-	-	FA	HA	AL		HE	WO	CO
								-	-	-	-	-	-	20	5		5	10	60

TABLE Ap3.4.2 Spore colour and kerogen composition data: 205/12-1

Well	Top Depth (ft)	Stratigraphy	Age	Sample Type	Slide Type	Spore Colour Index (SCI)					UV Fluorescence		Kerogen Composition (3 and 6 Component)						Comments
						Indigenou		Other			Form	Colour							
						SCI	No.	SCI	No.	Type			Sap.	Vit.	Inert.	FA	HA	AL	
205/14-2	5150.0	Balder	E1	DC	SCI (S/WK)	3.0	14	6.0	7	Rwk	Miosp	DI yel-dl orn	Sap.	Vit.	Inert.	Amorphous organic matter rare in sieved slide. Plenty of light/medium brown phytoclasts. 'Pacman' present at 3.5 SCI; orange fluorescence.			
	-							-	-	AOM	DI orn	10	50	40					
	-							-	-	-	-	FA	HA	AL	HE		WO	CO	
	-							-	-	-	-	10	-	-	Tr		50	40	
	5660.0			DC	SCI (S/WK)	3.0	36	5.5	6	Rwk	Miosp	DI yel-dl orn	Sap.	Vit.	Inert.	Dark squashed/moderately preserved spores present. Amorphous organic matter weakly fluorescent and probably not oil-prone, given its immaturity.			
								-	-	-	AOM	DI orn	30	40	30				
								-	-	-	-	-	FA	HA	AL		HE	WO	CO
								-	-	-	-	-	20	-	-		10	40	30
	6110.0	Unit II	P3	DC	SCI (S/WK)	3.5	27	6.0	3	Rwk	Miosp	N.F.	Sap.	Vit.	Inert.	Organic matter becoming less abundant. Miospores all becoming less common but still in abundant.			
								-	-	-	AOM	N.F.	10	40	50				
								-	-	-	-	-	FA	HA	AL		HE	WO	CO
								-	-	-	-	-	5	-	-		5	40	50
	6830.0			DC	SCI (S/WK)	3.5	19	6.0	2	Rwk	Miosp	N.F.	Sap.	Vit.	Inert.	Miospores increasingly rare. Rare foram fragments present.			
								-	-	-	AOM	N.F.	10	40	50				
								-	-	-	-	-	FA	HA	AL		HE	WO	CO
								-	-	-	-	-	10	-	-		-	40	50
	7520.0	Unit IV Upper SS		DC	SCI (S/WK)	4.0	15	2.5	5	Cav	Miosp	Orn-brn	Sap.	Vit.	Inert.	Amorphous organic matter increasingly abundant, appears less preserved and degraded. ?Warty spores at 4.5 SCI. phytoclasts light brown.			
								5.0	4	Rwk	AOM	Brn	5	75	20				
								-	-	-	-	-	FA	HA	AL		HE	WO	CO
								-	-	-	-	-	-	45	-		5	30	20
	7940.0	Unit IV Lower SS		DC	SCI (S/WK)	4.0	24	2.5	7	Cav	Miosp	Orn	Sap.	Vit.	Inert.	Bright fluorescence. Miospore fragments and bisaccates more abundant than above. Reworked Jurassic spore; <i>Callialasporites</i> at 4.5 SCI, determines upper SCI limit.			
								5.5	3	Rwk	AOM	Brn	20	25	55				
								-	-	-	-	-	FA	HA	AL		HE	WO	CO
								-	-	-	-	-	20	-	-		-	25	55
	8630.0	Unit V	P1	DC	SCI (S/WK)	4.0	27	3.0	1	Dino	Miosp	Orn-brn	Sap.	Vit.	Inert.	Similar to above. Spores appear lighter, ?Bleaching. Foram fragments present. ?Warty spore at 5.5 SCI. Dino fragments 3.0 SCI.			
								2.5	2	Cav	Dino	DI yel	75	5	20				
								6.0	5	Rwk	AOM	?Brn	FA	HA	AL		HE	WO	CO
								-	-	-	-	-	70	-	-		5	5	20

TABLE Ap3.4.3 Spore colour and kerogen composition data: 205/14-2

Well	Top Depth (ft)	Stratigraphy	Age	Sample Type	Slide Type	Spore Colour Index (SCI)					UV Fluorescence		Kerogen Composition (3 and 6 Component)						Comments
						Indigenous		Other			Form	Colour							
						SCI	No.	SCI	No.	Type									
205/14-2	8947.0	Cretaceous	K2	DC		4.5	6	3.0	1	Dino	Miosp	Brn	Sap.		Vit.		Inert.		Lean sample. Sieved dominated by coaly material. Dinos present. 4.0 SCI specimens are uncertain.
								6.5	1	Rwk	Dino	DI orn	5	20	75				
								-	-	-	AOM	DI brn-N.F.	FA	HA	AL	HE	WO	CO	
								-	-	-	-	-	5	-	-	-	20	75	

TABLE Ap3.4.3 Spore colour and kerogen composition data: 205/14-2

Well	Top Depth (ft)	Stratigraphy	Age	Sample Type	Slide Type	Spore Colour Index (SCI)					UV Fluorescence		Kerogen Composition (3 and 6 Component)						Comments								
						Indigenous		Other			Form	Colour															
						SCI	No.	SCI	No.	Type																	
205/14-3	3840.0	Undiff.	Ter	DC	SCI (S/WK)	2.0	15	3.5	1	Rwk	Miosp	Orn yel-yel	Sap.	Vit.	Inert.												
								-	-	-	AOM	N.F.	5	90	5												
								-	-	-	-	-	FA	HA	AL							HE	WO	CO			
								-	-	-	-	-	-	-	5							90	5				
	5250.0	Stronsay	Ter	DC	SCI (S/WK)	3.0	23	6.5	4	Rwk	Miosp	Orn-yel	Sap.	Vit.	Inert.	Deflandrea phosphoritica and Wetzeliella articulata confirm Eocene age.											
								-	-	-	Dino	Grn	Mn	95	5												
								-	-	-	AOM	Wk brn	FA	HA	AL							HE	WO	CO			
								-	-	-	-	-	-	75	Mn							Mn	20	5			
	6600.0	Balder	E1	DC	SCI (S/WK)	3.0	19	-	-	-	Miosp	Yel	Sap.	Vit.	Inert.												
									-	-	-	AOM	Orn brn-yel	65	20							15					
									-	-	-	-	-	FA	HA							AL	HE	WO	CO		
									-	-	-	-	-	65	-							-	Mn	20	15		
	6900.0	Hildasay		DC	SCI (S/WK)	3.5	18	1.5	1	Cav	Miosp	Yel	Sap.	Vit.	Inert.												
									7.0	5	Rwk	AOM	Orn brn-yel	65	20							15					
									-	-	-	-	-	FA	HA							AL	HE	WO	CO		
									-	-	-	-	-	65	-							-	Mn	20	15		
	7320.0	Ketla Tuff		P3	DC	SCI (S/WK)	3.5	19	-	-	-	Miosp	Yel orn	Sap.	Vit.	Inert.											
										-	-	-	AOM	N.F.	80	15							5				
										-	-	-	-	-	FA	HA							AL	HE	WO	CO	
										-	-	-	-	-	80	-							-	-	15	5	
	8840.0	Sullom	P2		DC	SCI (S/WK)	3.5	20	6.0	1	Rwk	Miosp	Yel orn	Sap.	Vit.	Inert.											
										-	-	-	AOM	Brn-yel-orn	10	60							30				
										-	-	-	-	-	FA	HA							AL	HE	WO	CO	
										-	-	-	-	-	10	40							-	Mn	20	30	
	9770.0	Sullom			P2	DC	SCI (S/WK)	3.5	20	-	-	-	Miosp	Yel-orn	Sap.	Vit.	Inert.										
											-	-	-	AOM	Orn-N.F.	10	65							25			
											-	-	-	-	-	FA	HA							AL	HE	WO	CO
											-	-	-	-	-	10	65							-	-	Mn	25

TABLE Ap3.4.4 Spore colour and kerogen composition data: 205/14-3

Well	Top Depth (ft)	Stratigraphy	Age	Sample Type	Slide Type	Spore Colour Index (SCI)					UV Fluorescence		Kerogen Composition (3 and 6 Component)						Comments
						Indigenous		Other			Form	Colour							
						SCI	No.	SCI	No.	Type									
205/14-3	10100.0	Jorsalfare	K2	DC	SCI (S/WK)	4.5	19	7.0	2	Rwk	Miosp	Orn	Sap.		Vit.		Inert.		
								-	-	-	AOM	N.F	Mn	85	15				
								-	-	-	-	-	FA	HA	AL	HE	WO	CO	
								-	-	-	-	-	-	85	Tr	Mn	Mn	15	

TABLE Ap3.4.4 Spore colour and kerogen composition data: 205/14-3

Well	Top Depth (ft)	Stratigraphy	Age	Sample Type	Slide Type	Spore Colour Index (SCI)					UV Fluorescence		Kerogen Composition (3 and 6 Component)						Comments																																																																																																																																																																																																																																																																																																																																																																																																																																																																																																																																																																																																																																																																																																																																																																																																																																																																																																																																																																																																																																																																																																																																																																																																																																																																																																																																																																																								
						Indigenous		Other			Form	Colour																																																																																																																																																																																																																																																																																																																																																																																																																																																																																																																																																																																																																																																																																																																																																																																																																																																																																																																																																																																																																																																																																																																																																																																																																																																																																																																																																																																															
						SCI	No.	SCI	No.	Type																																																																																																																																																																																																																																																																																																																																																																																																																																																																																																																																																																																																																																																																																																																																																																																																																																																																																																																																																																																																																																																																																																																																																																																																																																																																																																																																																																																																	
206/01-1A	3350.0	Undiff.	E3	DC	SCI (S/WK)	2.5	2	2.5	1	Dino	Miosp	Yel	Sap.	Vit.	Inert.																																																																																																																																																																																																																																																																																																																																																																																																																																																																																																																																																																																																																																																																																																																																																																																																																																																																																																																																																																																																																																																																																																																																																																																																																																																																																																																																																																																												</

TABLE Ap3.4.5 Spore colour and kerogen composition data: 206/01-1A

Well	Top Depth (m)	Stratigraphy	Age	Sample Type	Slide Type	Spore Colour Index (SCI)					UV Fluorescence		Kerogen Composition (3 and 6 Component)						Comments		
						Indigenou		Other			Form	Colour									
						SCI	No.	SCI	No.	Type											
206/11-1	1250.0	Undiff.	Ter	DC	SCI (S/WK)	3.0	10	4.5	3	Dino	Miosp	DI yel orn	Sap.	Vit.	Inert.	Organic matter lean in sieved fraction. Miospores rare and identification uncertain.					
								7.0	1	Rwk	Sph	Grn	Mn	85	15						
								-	-	-	Dino	N.F.	FA	HA	AL	HE	WO	CO			
								-	-	-	AOM	N.F.	-	75	Mn	-	10	15			
	1825.0	Late Cretaceous Shale I	K2	DC	SCI (S/WK)	3.5	8	4.5	9	Dino	Miosp	Yel orn-N.F.	Sap.	Vit.	Inert.	Organic matter lean in sieved fraction. Miospores degraded. <i>Aquillapollinites</i> at 3.0 SCI.					
									2.5	2	Cav	Sph	Pl yel	Mn	80	20					
									5.5	2	Rwk	Dino	Yel orn-orn	FA	HA	AL	HE	WO	CO		
									-	-	-	AOM	N.F.	-	80	Tr	Mn	Mn	20		
	2380.0			DC	SCI (S/WK)	4.0	14	5.0	10	Dino	Miosp	DI yel orn-N.F.	Sap.	Vit.	Inert.	Palynomorphs appear mostly marine in nature. <i>Aquillapollinites</i> at 3.5 SCI.					
										2.5	5	Cav	Dino	N.F.	Mn	60	40				
										6.0	1	Rwk	AOM	N.F.	FA	HA	AL	HE	WO	CO	
										-	-	-	-	-	-	55	Mn	Mn	5	40	
	2900.0			DC	SCI (S/WK)	4.5	2	4.5	3	Dino	Miosp	Yel orn-dl orn	Sap.	Vit.	Inert.	Sieved fraction dominantly cohesive amorphous organic matter. Indigenous spores may be absent. Spore with 5.0 SCI and better preservation possible reworked?					
										7.0	2	Rwk	Dino	Orn	Mn	90	10				
										-	-	-	AOM	N.F.	FA	HA	AL	HE	WO	CO	
										-	-	-	-	-	-	90	Tr	Mn	Tr	10	
	3244.0			DC	SCI (S/WK)	4.5	3	4.0	3	Dino	Miosp	Yel orn-dl orn	Sap.	Vit.	Inert.	Organic matter lean in sieved fraction. Palynomorphs rare and often appear heavily degraded. 5.0 SCI identification uncertain.					
										-	-	-	Dino	?N.F.	Tr	70	30				
										-	-	-	AOM	N.F.	FA	HA	AL	HE	WO	CO	
										-	-	-	-	-	-	65	Tr	Tr	5	30	
	3606.0	Early Cretaceous Sandstone	K1	DC	SCI (S/WK)	5.0	6	4.5	7	Dino	Miosp	DI orn-N.F.	Sap.	Vit.	Inert.	Good kerogen recovery, poor palynomorph preservation.					
									3.0	1	Cav	Dino	N.F.	Tr	60	40					
									7.5	2	Rwk	AOM	N.F.	FA	HA	AL	HE	WO	CO		
									-	-	-	-	-	-	55	Tr	Tr	5	40		
	3934.0			DC	SCI (S/WK)	5.0	1	7.0	4	Dino	Miosp	Brn-N.F.	Sap.	Vit.	Inert.	-					
								4.0	4	Cav	Sph	?Yel orn	Tr	70	30						
								8.0	3	Rwk	Dino	?N.F.	FA	HA	AL	HE	WO	CO			
								-	-	-	AOM	N.F.	-	70	Tr	Tr	Tr	30			

TABLE Ap3.4.6 Spore colour and kerogen composition data: 206/11-1

Well	Top Depth (m)	Stratigraphy	Age	Sample Type	Slide Type	Spore Colour Index (SCI)					UV Fluorescence		Kerogen Composition (3 and 6 Component)						Comments
						Indigenous		Other			Form	Colour							
						SCI	No.	SCI	No.	Type									
206/11-1	4258.0	Early Cretaceous Sandstone	K1	DC	SCI (S/WK)	6.5	6	6.0	7	Dino	Miosp	Brn-N.F.	Sap.	Vit.	Inert.	Palynomorphs often appear severely degraded and/or thinned. Dinocysts abundant. Spores rare and/or too degraded to identify.			
								4.5	5	Cav	Sph	DI yel orn	Mn	45	55				
								7.5	1	Rwk	AOM	N.F.	FA	HA	AL		HE	WO	CO
								-	-	-	-	-	-	40	Mn		Tr	5	55
	4586.0	Early Cretaceous Turbidite		DC	SCI (S/WK)	7.5	7	4.0	1	Dino	Miosp	N.F.	Sap.	Vit.	Inert.	Sieved and whole kerogen fractions comprised of mostly humic material.			
								8.5	1	Rwk	Dino	N.F.	-	25	75				
								-	-	-	AOM	N.F.	FA	HA	AL		HE	WO	CO
								-	-	-	-	-	-	10	-		-	15	75

TABLE Ap3.4.6 Spore colour and kerogen composition data: 206/11-1

Well	Top Depth (ft)	Stratigraphy	Age	Sample Type	Slide Type	Spore Colour Index (SCI)					UV Fluorescence		Kerogen Composition (3 and 6 Component)						Comments
						Indigenous		Other			Form	Colour							
						SCI	No.	SCI	No.	Type									
207/01-2	1260.0	Undiff.	Ter	DC	SCI (S/WK)	3.0	5	6.0	1	Rwk	Miosp	Pl yel-yel orn	Sap.		Vit.		Inert.		Sieved fraction mostly humic material. Spores rare. Kerogen mostly degraded vitrinite.
								-	-	-	AOM	N.F.	Tr		95		5		
								-	-	-	-	-	FA	HA	AL	HE	WO	CO	
								-	-	-	-	-	-	5	-	Tr	90	5	

TABLE Ap3.4.7 Spore colour and kerogen composition data: 207/01-2

Well	Top Depth (ft)	Stratigraphy	Age	Sample Type	Slide Type	Spore Colour Index (SCI)					UV Fluorescence		Kerogen Composition (3 and 6 Component)						Comments
						Indigenou		Other			Form	Colour							
						SCI	No.	SCI	No.	Type									
208/17-1	4680.0	Middle Eocene	E2	DC	SCI (S/WK)	3.0	3	?	3.0	2	Dino	Miosp	Orn-yel	Sap.	Vit.	Inert.	Yellow live hydrocarbon fluorecence, ?additive.		
	-							-	-	Sph	Yel	Tr	100	Mn					
	-							-	-	Dino	Yel	FA	HA	AL	HE	WO		CO	
	-							-	-	AOM	N.F.	-	100	Tr	Tr	Tr		Mn	
	5880.0			DC	SCI (S/WK)	2.5	1	-	-	-	Miosp	Yel	Sap.	Vit.	Inert.	Yellow live hydrocarbon fluorecence, ?additive.			
	-							-	-	AOM	N.F.	Tr	100	Mn					
	-							-	-	-	-	FA	HA	AL	HE		WO	CO	
	-							-	-	-	-	-	100	Tr	Tr		Tr	Mn	
	6720.0			DC	SCI (S/WK)	-	-	-	-	-	AOM	N.F.	Sap.	Vit.	Inert.	Very strong yellow live hydrocarbon fluorecence, ?additive.			
								-	-	-	-	-	-	100	Tr				
								-	-	-	-	-	FA	HA	AL		HE	WO	CO
								-	-	-	-	-	-	100	-		-	Tr	Tr
	7300.0	Early Eocene	E1	DC	SCI (S/WK)	-	-	-	-	-	AOM	N.F.	Sap.	Vit.	Inert.	Sample barren of identifiable organic matter.			
								-	-	-	-	-	-	100	-				
								-	-	-	-	-	FA	HA	AL		HE	WO	CO
								-	-	-	-	-	-	100	-		-	-	-
	8610.0	Late Paleocene	P3	DC	SCI (S/WK)	-	-	-	-	-	AOM	N.F.	Sap.	Vit.	Inert.	Some hydrocarbon fluorecence but reduced amounts compared to above.			
								-	-	-	-	-	-	100	-				
								-	-	-	-	-	FA	HA	AL		HE	WO	CO
								-	-	-	-	-	-	100	-		-	Tr	-
	9760.0			DC	SCI (S/WK)	-	-	-	-	-	AOM	N.F.	Sap.	Vit.	Inert.	Some hydrocarbon fluorecence but reduced amounts compared to above and increased amounts of structured organic matter.			
								-	-	-	-	-	-	100	-				
								-	-	-	-	-	FA	HA	AL		HE	WO	CO
								-	-	-	-	-	-	100	-		-	-	-
	10550.0			DC	SCI (S/WK)	5.0	4	8.0	2	Rwk	Miosp	N.F.	Sap.	Vit.	Inert.	Reduced hydrocarbon fluorecence. Miospore identification uncertain.			
								-	-	-	AOM	N.F.	Tr	100	-				
								-	-	-	-	-	FA	HA	AL		HE	WO	CO
								-	-	-	-	-	-	100	-		Tr	-	-

TABLE Ap3.4.8 Spore colour and kerogen composition data: 208/17-1

Well	Top Depth (ft)	Stratigraphy	Age	Sample Type	Slide Type	Spore Colour Index (SCI)					UV Fluorescence		Kerogen Composition (3 and 6 Component)						Comments
						Indigenous		Other			Form	Colour							
						SCI	No.	SCI	No.	Type									
208/17-1	11840.0	Early Paleocene	P1	DC	SCI (S/WK)	6.0	6	4.5	3	Dino	Miosp	N.F.	Sap.	Vit.	Inert.	Palynomorph identification uncertain, SCI should be interpreted cautiously.			
	7.5							2	Rwk	Dino	Brn	Mn	100	Mn					
	-							-	-	AOM	N.F.	FA	HA	AL	HE		WO	CO	
	-							-	-	-	-	-	100	Mn	Mn		Tr	Mn	
	12760.0			DC	SCI (S/WK)	-	-	7.5	2	Rwk	AOM	N.F.	Sap.	Vit.	Inert.	No hydrocarbon fluorescence.			
	-							-	-	-	-	-	100	-					
	-							-	-	-	-	FA	HA	AL	HE		WO	CO	
	-							-	-	-	-	-	100	-	-		-	-	
	13980.0			DC	SCI (S/WK)	-	-	5.5	1	Cav	AOM	N.F.	Sap.	Vit.	Inert.				
	-							-	-	-	-	-	100	-					
	-							-	-	-	-	FA	HA	AL	HE		WO	CO	
	-							-	-	-	-	-	100	-	-		-	-	
	14740.0			DC	SCI (S/WK)	-	-	-	-	-	AOM	N.F.	Sap.	Vit.	Inert.	Kerogen appears lighter than previous samples.			
	-							-	-	-	-	Mn	100	-					
	-							-	-	-	-	FA	HA	AL	HE		WO	CO	
	-							-	-	-	-	-	100	Mn	-		-	-	
	15860.0	Late Cretaceous	K2	DC	SCI (S/WK)	-	-	-	-	-	AOM	N.F.	Sap.	Vit.	Inert.	Kerogen appears darker.			
	-							-	-	-	-	-	100	-					
	-							-	-	-	-	FA	HA	AL	HE		WO	CO	
	-							-	-	-	-	-	100	-	-		-	-	

TABLE Ap3.4.8 Spore colour and kerogen composition data: 208/17-1

Well	Top Depth (ft)	Stratigraphy	Age	Sample Type	Slide Type	Spore Colour Index (SCI)					UV Fluorescence		Kerogen Composition (3 and 6 Component)						Comments	
						Indigenou		Other			Form	Colour								
						SCI	No.	SCI	No.	Type										
208/17-2	5400.0	Stronsay	Ter	DC	SCI (S/WK)	3.5	5	-	-	-	Miosp	Yel-?orn	Sap.	Vit.	Inert.	Brown clumps amorphous organic matter dominates, cohesive and opaque in places. Rare brown structured woody particles. Miospores and inertinite rare.				
								-	-	-	AOM	?Ft orn	90	5	5					
								-	-	-	-	-	FA	HA	AL	HE	WO	CO		
								-	-	-	-	-	90	-	-	Tr	5	5		
	6280.0	Balder	E1	DC	SCI (S/WK)	4.0	16	3.5	4	Dino	Miosp	Yel-orn	Sap.	Vit.	Inert.	Brown cuticle particles common. Increased amounts of opaque inert material. Medium to dark brown amorphous material dominates unsieved.				
								6.0	4	Rwk	Dino	Ft orn	10	80	10					
								-	-	-	AOM	Yel-orn	FA	HA	AL	HE	WO	CO		
								-	-	-	-	-	10	70	Tr	Tr	10	10		
	7290.0	Flett		DC	SCI (S/WK)	4.0	24	2.5	2	Cav	Miosp	?Brn-orn	Sap.	Vit.	Inert.	Unsieved composed of black to opaque amorphous organic matter; cohesive/finely disseminated. Miospores very rare. Abundant 5.0-6.0 spores, ?reworked.				
								5.5	7	Rwk	AOM	Orn-yel	15	75	10					
								-	-	-	-	-	FA	HA	AL	HE	WO	CO		
								-	-	-	-	-	15	70	-	Tr	5	10		
	9470.0	Vaila	P2	DC	SCI (S/WK)	4.5	17	?4.5	1	Dino	Miosp	Brn-bt orn	Sap.	Vit.	Inert.	Unsieved dominated by medium brown to black cohesive amorphous material, finely disseminated in places, commonly fluoresces.				
								7.0	2	Rwk	Dino	Orn-yel	20	70	10					
								-	-	-	AOM	Bt orn-N.F.	FA	HA	AL	HE	WO	CO		
								-	-	-	-	-	20	65	Tr	Tr	5	10		
	10600.0	Sullom	P1	DC	SCI (S/WK)	5.0	9	3.5	6	Cav	Miosp	Orn-brn	Sap.	Vit.	Inert.	Sample dominated by non-fluorescing amorphous organic matter. Opaque inert material increasingly common. Sieved dominated by opaque inert material.				
									6.5	8	Rwk	AOM	?Brn-orn	10	75	15				
									-	-	-	-	-	FA	HA	AL	HE	WO	CO	
									-	-	-	-	-	10	75	-	Tr	Tr	15	
	11710.0			DC	SCI (S/WK)	?6.5	2	5.0	5	Dino	Miosp	?Brn	Sap.	Vit.	Inert.	Sieved dominated by opaque inert material. Miospores poorly preserved in places, SCI difficult to determine. Unsieved dominated by black cohesive amorphous organic matter.				
								-	-	-	Dino	N.F.	Tr	90	10					
								-	-	-	AOM	Ra orn-N.F.	FA	HA	AL	HE	WO	CO		
								-	-	-	-	-	Tr	90	-	Tr	Tr	10		
	12050.0	Shetland	K2	DC	SCI (S/WK)	-	-	7.5	4	Dino	Dino	N.F.	Sap.	Vit.	Inert.	Sieved dominated by opaque inert material. Miospores absent. Dinocysts look <i>in situ</i> but only explanation could be localised volcanism at this high SCI.				
								8.0	1	Rwk	AOM	Ra ft brn-N.F	Tr	80	20					
								-	-	-	-	-	FA	HA	AL	HE	WO	CO		
								-	-	-	-	-	Tr	80	-	-	Mn	20		

TABLE Ap3.4.9 Spore colour and kerogen composition data: 208/17-2

Well	Top Depth (ft)	Stratigraphy	Age	Sample Type	Slide Type	Spore Colour Index (SCI)					UV Fluorescence		Kerogen Composition (3 and 6 Component)						Comments
						Indigenous		Other			Form	Colour							
						SCI	No.	SCI	No.	Type									
209/12-1	11383.9	Humber	J3	COCH	SCI (S/WK)	-	-	-	-	-	AOM	N.F.	Sap.		Vit.		Inert.		Miospores absent but dark brown to black amorphous organic matter are consistent with an ~8.5-9.5 SCI.
	-							-	-	-	-	Tr	100	Tr					
	-							-	-	-	-	FA	HA	AL	HE	WO	CO		
	-							-	-	-	-	-	100	-	-	Tr	Tr		
	11385.1			COCH	SCI (S/WK)	-	-	-	-	-	AOM	N.F.	Sap.		Vit.		Inert.		Miospores absent but dark brown to black amorphous organic matter are consistent with an ~8.5-9.5 SCI.
								-	-	-	-	-	-	85	15				
								-	-	-	-	-	FA	HA	AL	HE	WO	CO	
								-	-	-	-	-	-	80	-	-	5	15	
	11385.7			COCH	SCI (S/WK)	-	-	-	-	-	AOM	N.F.	Sap.		Vit.		Inert.		Miospores absent but dark brown to black amorphous organic matter are consistent with an ~8.5-9.5 SCI.
								-	-	-	-	-	-	85	5				
								-	-	-	-	-	FA	HA	AL	HE	WO	CO	
								-	-	-	-	-	-	80	-	-	5	5	

TABLE Ap3.4.10 Spore colour and kerogen composition data: 209/12-1

Well	Top Depth (ft)	Stratigraphy	Age	Sample Type	Slide Type	Spore Colour Index (SCI)					UV Fluorescence		Kerogen Composition (3 and 6 Component)						Comments
						Indigenou		Other			Form	Colour							
						SCI	No.	SCI	No.	Type									
214/26-1	5350.0	Hordaland	E2	DC	SCI (S/WK)	3.0	20	6.0	5	Rwk	Miosp	Yel-orn	Sap.	Vit.	Inert.	Amorphous organic matter rare in sieved, abundant in unsieved, variable fluorescence. Miospores very rare. Abundant light coloured woody material. Tracheid fragments.			
	-							-	-	AOM	Orn-brn-N.F.	Tr	90	10					
	-							-	-	-	-	FA	HA	AL	HE		WO	CO	
	-							-	-	-	-	-	70	-	Tr		20	10	
	5710.0			DC	SCI (S/WK)	3.5	7	3.5	5	Dino	Miosp	Orn	Sap.	Vit.	Inert.	Organic matter lean in sieved fraction, miospores rare and poorly preserved. Unsieved dominated by small clumps of light coloured amorphous material.			
								7.0	6	Rwk	Dino	Orn	?60	30	10				
								-	-	-	AOM	Orn-N.F.	FA	HA	AL		HE	WO	CO
								-	-	-	-	-	?60	20	Tr		Tr	10	10
	6010.0			DC	SCI (S/WK)	7.0	15	6.0	3	Dino	Miosp	?N.F.	Sap.	Vit.	Inert.	SCI unlikely, ?heating event. Eocene <i>Phthanoperidinium ?geminatum</i> : 7.0 SCI and <i>P. amoenem</i> : 5.0 and 8.0 SCI. Reworked Classopollis: 7.0 SCI and Chitinozoan.			
								8.5	3	Rwk	Dino	?Orn-brn	Tr	90	10				
								-	-	-	AOM	Ra yel-orn	FA	HA	AL		HE	WO	CO
								-	-	-	-	-	-	75	Tr		Tr	15	10
	6390.0	DC		SCI (S/WK)	6.5	2	5.5	2	Dino	Miosp	N.F.	Sap.	Vit.	Inert.	SCI unlikely, ?heating event. Eocene <i>Palaeocystodinium golwenze</i> , <i>Ennyodacysta arcuata</i> , a <i>Wetzelia</i> type and a degraded tricolpate form all 7.0 SCI. <i>E. levimurum</i> : 7.5 SCI, but <i>E. dityoplokus</i> : 3.5 SCI.				
							8.5	4	Rwk	Dino	?Bl	Tr	90	10					
							-	-	-	AOM	?Ft orn-N.F.	FA	HA	AL		HE	WO	CO	
							-	-	-	-	-	-	85	Tr		Tr	5	10	
	6760.0	DC		SCI (S/WK)	3.5	19	5.0	1	Dino	Miosp	Orn-yel	Sap.	Vit.	Inert.	Miospore SCI appears distinctly lower than above. Amorphous organic matter rare in sieved. Unsieved dominated by cohesive, fluorescent amorphous organic matter.				
							5.5	1	Rwk	Dino	Ft orn	75	20	5					
							-	-	-	AOM	Orn	FA	HA	AL		HE	WO	CO	
							-	-	-	-	-	70	-	Tr		5	20	5	
	7140.0	DC		SCI (S/WK)	4.0	6	4.0	1	Dino	Miosp	Orn-brn-N.F	Sap.	Vit.	Inert.	Miospores rare, organic matter lean in sieved. Large laths of brown woody material common in unsieved. Dominated by cohesive amorphous organic matter.				
							6.5	12	Rwk	Dino	Orn	5	85	10					
							-	-	-	AOM	?Bt orn-brn	FA	HA	AL		HE	WO	CO	
							-	-	-	-	-	5	80	Tr		Tr	5	10	
	7960.0	DC		SCI (S/WK)	4.0	11	6.0	1	Dino	Miosp	Orn-N.F.	Sap.	Vit.	Inert.	Low kerogen recovery, swamped by woody LCM. Reworked <i>Stereisporites</i> spp. (Jurassic/ Cretaceous): 6.5 SCI.				
							6.5	4	Rwk	Dino	N.F.	20	60	20					
							-	-	-	AOM	Brn-yel-orn	FA	HA	AL		HE	WO	CO	
							-	-	-	-	-	20	30	Tr		Tr	30	20	

TABLE Ap3.4.11 Spore colour and kerogen composition data: 214/26-1

Well	Top Depth (ft)	Stratigraphy	Age	Sample Type	Slide Type	Spore Colour Index (SCI)					UV Fluorescence		Kerogen Composition (3 and 6 Component)						Comments
						Indigenou		Other			Form	Colour							
						SCI	No.	SCI	No.	Type									
214/26-1	8230.0	Base Lewis Fan Envelope	E1	DC	SCI (S/WK)	4.5	10	6.0	19	Dino	Miosp	Ft orn-N.F.	Sap.	Vit.	Inert.	Abundant dinocysts, fragments in places. Super abundant Early Eocene, <i>Cordosphaeridium gracillis</i> , thick walled which are darker than usual. Miospores very rare.			
								6.5	9	Rwk	Dino	ft orn-brn-N.F.	10	85	5				
								-	-	-	AOM	Orn-brn-N.F.	FA	HA	AL		HE	WO	CO
								-	-	-	-	-	Tr	80	10		Tr	5	5
	8510.0	Balder		DC	SCI (S/WK)	4.0	7	5.5	12	Dino	Miosp	Brn-Ft orn-N.	Sap.	Vit.	Inert.	Miospores appear slightly bleached in places. Appears less mature than above sample.			
								6.0	13	Rwk	Dino	Orn-brn	10	60	30				
								-	-	-	AOM	Orn-N.F.	FA	HA	AL		HE	WO	CO
								-	-	-	-	-	5	10	5		Tr	50	30
	8910.0	Sele		DC	SCI (S/WK)	4.5	9	6.0	5	Dino	Miosp	Orn-brn-N.F.	Sap.	Vit.	Inert.	Fragments of miospores common, ?bleached in places. SCI determination uncertain with wide range of colours.			
								6.5	17	Rwk	Dino	Brn	5	75	20				
								-	-	-	AOM	Orn-brn	FA	HA	AL		HE	WO	CO
								-	-	-	-	-	Tr	65	Tr		5	10	20

TABLE Ap3.4.11 Spore colour and kerogen composition data: 214/26-1

Well	Top Depth (ft)	Stratigraphy	Age	Sample Type	Slide Type	Spore Colour Index (SCI)					UV Fluorescence		Kerogen Composition (3 and 6 Component)						Comments					
						Indigenou		Other			Form	Colour												
						SCI	No.	SCI	No.	Type														
214/28-1	4560.0	Lower Oligocene	O1	DC	SCI (S/WK)	3.0	4	3.0	3	Dino	Miosp	?Yel orn	Sap.	Vit.	Inert.	Sieved fraction dominated by cohesive amorphous organic matter, mostly non-fluorescent. Spores very rare.								
								-	-	-	Dino	?Yel orn	Mn	90	10									
								-	-	-	AOM	N.F.	FA	HA	AL	HE	WO	CO						
								-	-	-	-	-	-	90	Mn	-	Tr	10						
	5850.0	Late Eocene	E3	DC	SCI (S/WK)	3.5	1	3.5	3	Dino	Miosp	?Orn	Sap.	Vit.	Inert.	Sieved fraction dominated by cohesive amorphous organic matter, mostly non-fluorescent. Unclear if indigenous spores present.								
								-	-	-	Sph	Yel-yel orn	10	85	5									
								-	-	-	Dino	?Yel orn	FA	HA	AL	HE	WO	CO						
								-	-	-	AOM	Yel-brn-N.F.	10	85	Mn	-	?Tr	5						
	6540.0	Middle Eocene	E2	DC	SCI (S/WK)	3.5	4	4.0	6	Dino	Miosp	?Orn	Sap.	Vit.	Inert.	Cohesive amorphous organic matter in sieved, determining fluorescing distinction difficult due to mineral matter abundance. Minor marine/algal palynomorphs present.								
								6.5	1	Rwk	Sph	Yel-yel orn	10	85	5									
								-	-	-	Dino	?Yel orn	FA	HA	AL	HE	WO	CO						
								-	-	-	AOM	Yel-brn-N.F.	10	85	Mn	-	Tr	5						
	7300.0			DC	SCI (S/WK)	3.5	10	6.0	14	Dino	Miosp	Yel orn-?orn	Sap.	Vit.	Inert.	Dinos & algal palynomorphs abundant. Spore identification uncertain in places. Abundant mineral matter in the whole kerogen fraction								
								-	-	-	Sph	Yel-dl yel orn	80	-	20									
								-	-	-	Dino	Yel orn-orn	FA	HA	AL	HE	WO	CO						
								-	-	-	AOM	N.F.	70	-	10	-	-	20						
	8200.0	Early Eocene	E1	DC	SCI (S/WK)	3.0	34	5.0	1	Dino	Miosp	Yel orn-orn	Sap.	Vit.	Inert.	Abundant palynomorphs, appear degrade/thinned. Organic matter poorly preserved. 1st occurrence of 2.0-3.0 SCI miospores so unlikely caved.								
								5.0	5	Rwk	Sph	Yel-yel orn	10	75	15									
								-	-	-	Dino	Yel orn	FA	HA	AL	HE	WO	CO						
								-	-	-	AOM	DI brn-N.F.	-	65	Mn	10	10	15						
	9630.0	Middle Paleocene	P2	DC	SCI (S/WK)	4.0	12	5.0	2	Dino	Miosp	Yel orn	Sap.	Vit.	Inert.	Sieved fraction dominated by humic material.								
								2.5	2	Cav	Sph	Yel-yel orn	Mn	55	45									
								7.5	2	Rwk	Dino	DI yel orn	FA	HA	AL	HE	WO	CO						
								-	-	-	AOM	Orn-N.F.	-	50	Tr	Mn	5	45						
	10660.0			DC	SCI (S/WK)	4.5	4	3.5	2	Cav	Miosp	Orn-N.F.	Sap.	Vit.	Inert.	Mineral (?calcite) abundant in sieved. Spores rare and occasionally degraded/thinned.								
								6.0	1	Dino	Sph	Yel orn	Mn	85	15									
								-	-	-	AOM	Ra dl brn-N.F	FA	HA	AL	HE	WO	CO						
								-	-	-	-	-	-	-	85	Mn	-	Mn	15					

TABLE Ap3.4.12 Spore colour and kerogen composition data: 214/28-1

Well	Top Depth (ft)	Stratigraphy	Age	Sample Type	Slide Type	Spore Colour Index (SCI)					UV Fluorescence		Kerogen Composition (3 and 6 Component)						Comments	
						Indigenous		Other			Form	Colour								
						SCI	No.	SCI	No.	Type										
214/28-1	11540.0	Middle Paleocene	P2	DC	SCI (S/WK)	5.0	2	3.5	2	Cav	Miosp	DI orn-N.F.	Sap.	Vit.	Inert.	Cohesive amorphous organic matter dominates sieved. Poor preservation makes spore identification uncertain. Caved miospores with bright yellow fluorescence.				
								-	-	-	Sph	?Orn	Tr	70	30					
								-	-	-	AOM	N.F.	FA	HA	AL	HE	WO	CO		
								-	-	-	-	-	-	70	Tr	-	-	30		
	12510.0	Early Paleocene	P1	DC	SCI (S/WK)	4.5	4	3.0	1	Cav	Miosp	Brn-N.F.	Sap.	Vit.	Inert.	Sieved fraction mostly humic material and abundant mineral matter. Spores very rare and identification uncertain. Green-yellow fluorescing ?contaminants present.				
										-	-	-	Sph	DI orn-N.F.	Mn	95	5			
										-	-	-	AOM	N.F.	FA	HA	AL	HE	WO	CO
										-	-	-	-	-	-	95	Mn	-	-	5
	13460.0			DC	SCI (S/WK)	4.5	1	5.5	1	Rwk	Miosp	?Brn	Sap.	Vit.	Inert.	Very low kerogen recovery. Spore identification uncertain. Composition estimate uncertain due to lean whole kerogen fraction.				
										-	-	-	AOM	N.F.	-	90	10			
										-	-	-	-	-	FA	HA	AL	HE	WO	CO
										-	-	-	-	-	-	90	-	-	Tr	10
	14600.0			DC	SCI (S/WK)	?4.5	1	-	-	-	Miosp	?DI brn	Sap.	Vit.	Inert.	Mineral matter abundant in both fractions. Sieved dominated by humic material. Palynomorphs practically absent or too degraded to identify.				
										-	-	-	AOM	N.F.	-	60	40			
										-	-	-	-	-	FA	HA	AL	HE	WO	CO
										-	-	-	-	-	-	60	-	-	-	40
	15470.0			DC	SCI (S/WK)	5.0	3	3.5	1	Cav	Miosp	N.F.	Sap.	Vit.	Inert.	Spores very rare and identification uncertain. Amorphous organic matter tends to coalesce as spheres, ?degraded. Moderate orange liptodetrinite fluorescence.				
										7.5	2	Rwk	AOM	N.F.	-	85	15			
										-	-	-	-	-	FA	HA	AL	HE	WO	CO
										-	-	-	-	-	-	85	-	-	-	15
	16960.0	Maastrichtian	K2	DC	SCI (S/WK)	-	-	-	-	-	AOM	N.F.	Sap.	Vit.	Inert.	Mineral matter dominates sieved, super abundant in unsieved. Amorphous organic matter appears heavily degraded. Likely barren of palynomorphs.				
								-	-	-	-	-	-	100	-					
								-	-	-	-	-	FA	HA	AL	HE	WO	CO		
								-	-	-	-	-	-	95	-	-	5	-		

TABLE Ap3.4.12 Spore colour and kerogen composition data: 214/28-1

APPENDIX 3.5

LIST OF ABBREVIATIONS USED IN MATURITY DATA TABLES

Tables

Ap3.5KEY Optical maturity summary table - key

Population type: Vitrinite reflectivity

N.D.P.: No determination possible
I: Indigenous
C: Caved
L: Low reflecting
R: Reworked
B: Bitumen
E: Excinite
Z: Zooclast

Population type: Spore colouration

N.D.P.: No determination possible
Indg: Indigenous
Cav: Caved/bleached
St: Stained
Rwk: Reworked
e: estimate based on acritarch or overall kerogen colour/fluorescence

Colour

lt: Light
pl: Pale
bt: Bright
dl: Dull
wk: Weak
dk: Dark
brn: Brown
orn: Orange
yl: Yellow
grn: Green
rd: Red
ra: Rare
N.F: Non Fluorescent

Form

AOM: Amorphous organic matter
Paly: Palynomorphs
Indet: Indeterminate
Mio: Misopores
Dino: Dinocysts
Sph: Sphaeromorphs
Bisa: Bisaccate
Acrit: Acritarchs
FDOM: Finely disseminated organic matter
SOM: Structured organic matter

Kerogen types: six component system

FA: Fluoramorphinite - fluorescent amorphous material
HA: Hebamorphinite - non-fluorescent or weakly fluorescent amorphous material.
AL: Algal organic matter/phytoplankton - identifiable algae and phytoplankton, including dinocysts
HE: Herbaceous Organic Matter - identifiable species and fragments of spores, pollen and cuticles
WO: Woody Organic Matter - translucent, structured woody tissues
CO: Coaly Organic Matter - completely opaque, usually angular material
SP: Identifiable species and fragments of spores and pollen
CUT: Cuticular organic matter (cutinite)
Humic: Structured humic organic matter (huminite, vitrinite) - translucent, structured woody tissues.
Inert: Inert organic matter (inertinite)- completely opaque, usually angular material

Kerogen types: three component system

Sap: Includes alginite, sporinite, cuticle and liptodetrinite and organic matter interpreted to have originated as fluoramorphinite.
Vit: Includes vitrinite and vitridetrinite and organic matter interpreted to have originated as hebamorphinite.
Inert: Inert organic matter (inertinite)- completely opaque, usually angular material.
Am: Amorphous organic matter (used as a modifier for sapropel and vitrinite).

Quantities

Tr: Trace
Mn: Minor
V: Very
Abn: abundant

TABLE Ap3.5KEY Optical maturity summary table - key

APPENDIX 4

PROVENANCE IMPLICATIONS

APPENDIX 4.1 Zircon provenance

APPENDIX 4.2 Apatite provenance

APPENDIX 4.1 ZIRCON PROVENANCE

APPENDIX 4.1 ZIRCON PROVENANCE

Detrital zircon studies (e.g. Chemostrat 2013) consistently show that Palaeocene sands in the FSB contain both Laxfordian and Neoarchaen zircon families. It has commonly been assumed that these are sourced from local basement. However, as demonstrated in this study, local basement does not contain any Laxfordian aged zircons, and so the Palaeocene sands are likely to not be sourced only from local basement highs. Likely sources for these zircons are reworked Torridonian and Carboniferous sediments.

A full provenance analysis workup is outside of the scope of this study, however, due to the way the apatite data has been collected for this study enables further provenance information to be established.

APPENDIX 4.2

APATITE PROVENANCE

Figures

Ap4.1.1	Location map of wells with provenance Group A sediments
Ap4.1.2	Probability plots of U, Th and Sm concentration (ppm) and the Rmr0 apatite kinetic parameter for the A Group.
Ap4.1.3	Location map of wells with provenance Group B sediments
Ap4.1.4	Probability plots of U, Th and Sm concentration (ppm) and the Rmr0 apatite kinetic parameter for the B Group.
Ap4.1.5	Location map of wells with provenance Group B1 sediments
Ap4.1.6	Location map of wells with provenance Group B2 sediments
Ap4.1.7	Location map of wells with provenance Group C sediments
Ap4.1.8	Probability plots of U, Th and Sm concentration (ppm) and the Rmr0 apatite kinetic parameter for the C Group.
Ap4.1.9	Location map of wells with provenance Group C1 sediments
Ap4.1.10	Location map of wells with provenance Group C21 sediments
Ap4.1.11	Location map of wells with provenance Group C22 sediments
Ap4.1.12	Location map of wells with provenance Group D sediments
Ap4.1.13	Probability plots of U, Th and Sm concentration (ppm) and the Rmr0 apatite kinetic parameter for the D Group.
Ap4.1.14	Location map of wells with provenance Group D1 sediments
Ap4.1.15	Location map of wells with provenance Group D2 sediments

APPENDIX 4.2 APATITE PROVENANCE

The apatite data (U-Pb isotope age and rare earth element data; REE) collected during the LA-ICP-MS analysis have been used in two ways:

1. To optimise group selection to recovery time-temperatures histories (the focus of the main section of this report)
2. To optimise grouping for resolution with respect to provenance groups.

For use in provenance studies the apatite data has been interrogated to identify groups of apatite's based on their age and sub groups of data based on the size of their Eu anomaly. The groups and sub groups identified are summarised in the table below.

Group	Sub Group	Age (Ma)	Event	Eu Anomaly
A		<~325	Tertiary, Carb' & Permian igneous events	N/A
B	B1	~325-800	Caledonian orogenic igneous bodies and orogenic heating	Strong negative
	B2	~325-800		Weak negative
C	C1	800-1300	Early Laxfordian	N/A
	C1-1	800-1300		Strong negative
	C1-2	800-1300		Weak negative
	C2	1300-1750	Later Laxfordian	N/A
	C2-1	1300-1750		Strong negative
	C2-2	1300-1750		Weak negative
D	D1	>1750	Neoproterozoic high grade metamorphism (basement)	Strong negative
	D2	>1750		Weak negative

The U-Pb dating is described in the associated Apatite.Inc methods (Appendix 4.2). Briefly, the ages presented in table above reflect the time that each apatite cooled below ~450-500°C (its closing temperature; Flowers *et al.*, 2005 either during igneous or metamorphic events.

The enrichment or depletion of Europium (Eu) is generally attributed to europium's tendency to be incorporated into plagioclase preferentially over other minerals. For example, if a magma crystallizes stable plagioclase, most of the Eu will be incorporated into this mineral, causing a higher than expected concentration of Eu in the mineral versus other REE in that mineral (a positive anomaly). The rest of the magma will then be relatively depleted in Eu with a concentration of Eu lower than expected versus the concentrations of other REEs in that magma. Conversely, if the Eu-depleted magma is then separated from its plagioclase crystals and subsequently solidifies, its chemical composition will display a negative Eu anomaly (because the Eu is locked up in the plagioclase left in the magma chamber). When a magma

accumulates plagioclase crystals before solidification, its rock composition will display a relatively positive Eu anomaly (Weill & Drake, 197 and Bau, 1991).

When compared spatially, there is an approximate correspondence between the Basement types recognised (Chapter 6) and the sediment provenance groups shown in the table below.

Basement Group	RHP $\mu\text{W}/\text{m}^3$	Basement history	Sandstone Provenance Group: Tentative Correspondence
A	Zone A $0.21 \mu\text{W}/\text{m}^3 (\pm 0.21)$ $n=2$	Neoproterozoic Tonalitic facies SW of the "Laxfordian front"	None
B	Zone B $0.64 \mu\text{W}/\text{m}^3$ $n=1$	Neoproterozoic Granitic-Granodioritic NE of "Laxfordian front"	C-D
C	Zone C $0.75 \mu\text{W}/\text{m}^3 (\pm 0.51)$ $n=28$	Neoproterozoic Tonalitic-Granitic-Granodioritic with medium temperature Laxfordian event	
D	Zone D $0.86 \mu\text{W}/\text{m}^3 (\pm 0.62)$ $n=31$	Neoproterozoic Granitic-Granodioritic with medium temperature Laxfordian event	
E	Zone E $0.88 \mu\text{W}/\text{m}^3 (\pm 0.57)$ $n=10$	Neoproterozoic with Caledonian deformation	B
F	Zone F $2.1 \mu\text{W}/\text{m}^3 (\pm 0.7)$ $n=12$	Caledonian Granite	A

A full provenance analysis workup is outside of the scope of this study, and so only broad stratigraphic divisions (based on data available from public domain sources, principally NDR) have been applied. It is not known if this is due to the variation in basement groups is controlling later basin formation or is just coincidence. However, the figures below do demonstrate that this data set is spatially variable and so can be applied to future provenance studies if required. To do this a more detailed studies incorporating both higher resolution stratigraphic designation and integration with poro-perm data would be desirable.

A Group

The A sub-group is typified by relatively young U-Pb ages (<325Ma) and are thought to relate to Acadian/Variscan related source material. No unique properties in terms of U, Th, Sm concentration and apatite kinetics are indicated (Figure Ap4.1.2).

A Group sediments occurs in the following wells (all Palaeocene in age):

- 205/9-1
- 205/14-2
- 205/19b-2
- 208/17-2
- 214/28-1

And from the Lower Cretaceous in:

- 205/12-1

A map showing the distribution of sediments with A Group provenance is shown in Figure Ap4.1.1.

B Group

The B sub-group is typified by U-Pb ages in the range of 325-800Ma and are thought to relate to Neoarchian material with a Caledonian re-working with some possible overprint of younger events (Acadian-Variscan) source material. No unique properties in terms of U, Th, Sm concentration and apatite kinetics are indicated (Figure Ap4.1.4).

B Group sediments are widespread occurring in all wells sampled.

Basement:

- 207/1-2
- 208/27-2

Lower Cretaceous:

- 205/12-1
- 206/11-1
- 207/1-2
- 208/24-1

Paleocene:

- 204/10a-5
- 205/9-1
- 205/12-1
- 205/14-2
- 205/17b-2
- 208/17-2
- 208/27-2
- 214/28-1

Eocene:

- 214/26-1

A map showing the distribution of sediments with B Group provenance is shown in Figure Ap4.1.3.

B1 Sub-Group

The B1 sub-group is typified by U-Pb ages in the range of 325-800Ma and are thought to relate to Neoarchian material with Caledonian reworking with some possible overprint of younger events (Acadian-Variscan) source material with a strong negative Eu anomaly.

B1 Group sediments occur in the following wells:

B1 Basement:

- 207/1-2

B1 Lower Cretaceous:

- 207/1-2
- 208/24-1

B1 Paleocene:

- 208/17-2
- 214/28-1

A map showing the distribution of sediments with B1 Sub-Group provenance is shown in Figure Ap4.1.5.

B2 Sub-Group

The B2 sub-group is typified by U-Pb ages in the range of 325-800Ma and are thought to relate to Neoarchian material with Caledonian reworking with some possible overprint of younger events (Acadian-Variscan) source material with a weak negative Eu anomaly.

B2 Group sediments occur in the following wells:

B2 Basement:

- 207/1-2

B2 Lower Cretaceous:

- 207/1-2
- 208/24-1

B2 Paleocene:

- 208/17-2
- 214/28-1

A map showing the distribution of sediments with B2 Sub-Group provenance is shown in Figure Ap4.1.6.

C Group

The C sub-group is typified by U-Pb ages in the range of 800-1750Ma and are thought to relate to Neoarchian material with a Laxfordian overprint. No unique properties in terms of U, Th, Sm concentration and apatite kinetics are indicated (Figure Ap4.1.8).

C Group sediments are widespread, occurring in all wells bar Paleocene samples in Quad 205 (205/9-1; 205/14-2; but does occur in 205/12-1 & 205/17b-2).

C Group samples occur in the following wells sampled.

Basement:

- 207/1-2
- 208/27-2

Lower Cretaceous:

- 205/12-1
- 206/11-1
- 207/1-2
- 208/24-1

Paleocene:

- 204/10a-5
- 205/12-1
- 205/17b-2
- 208/17-2
- 208/27-2
- 214/28-1

Eocene:

- 214/26-1

A map showing the distribution of sediments with C Group provenance is shown in Figure Ap4.1.7.

C1 Sub-Group

The C1 sub-group is typified by U-Pb ages in the range of 800-1300Ma and are thought to relate to Neoarchian material with a Laxfordian overprint.

C1 Group sediments occur in the following wells:

C1 Basement:

- 207/1-2

C1 Lower Cretaceous:

- 207/1-2

C1 Paleocene:

- 204/10a-5
- 205/17b-2

C1 Eocene:

- 214/26-1

A map showing the distribution of sediments with C1 Sub-Group provenance is shown in Figure Ap4.1.9.

C21 Sub-Group

The C2-1 sub-group is typified by U-Pb ages in the range of 1300-1750Ma and are thought to relate to Neoarchian material with no Laxfordian overprint with a strong negative Eu anomaly.

C21 Group sediments occur in the following wells:

Paleocene:

- 204/10a-5
- 205/17b-2

Eocene:

- 214/26-1

A map showing the distribution of sediments with C21 Sub-Group provenance is shown in Figure Ap4.1.10.

C22 Sub-Group

The C22 sub-group is typified by U-Pb ages in the range of 1300-1750Ma and are thought to relate to Neoarchian material with a Laxfordian overprint with a weak negative Eu anomaly.

C22 Group sediments occur in the following wells:

Paleocene:

- 204/10a-5
- 205/12-1
- 205/17b-2
- 214/28-1

Eocene:

- 214/26-1

A map showing the distribution of sediments with C21 Sub-Group provenance is shown in Figure Ap4.1.11.

D Group

The D sub-group is typified by U-Pb ages >1750Ma and are thought to relate to Neoarchian material with no Laxfordian overprint. No unique properties in terms of U, Th, Sm concentration and apatite kinetics are indicated (Figure Ap4.1.13).

D Group sediments are only found in the Paleocene in the following wells:

- 205/09-1
- 205/14-2
- 214/28-1

A map showing the distribution of sediments with D Group provenance is shown in Figure Ap4.1.12.

D1 Sub-Group

The D1 sub-group is typified by U-Pb ages >1750Ma and are thought to relate to Neoarchian material with no Laxfordian overprint with a strong Eu anomaly.

The D1 sub-group is only recognised in the Paleocene interval of the 214/28-1 well.

A map showing the distribution of sediments with D1 Sub-Group provenance is shown in Figure Ap4.1.13.

D2 Sub-Group

The D2 sub-group is typified by U-Pb ages $>1750\text{Ma}$ and are thought to relate to Neoarchian material with no Laxfordian overprint with a weak Eu anomaly.

The D2 sub-group is only recognised in the Paleocene interval of 214/28-1 well.

A map showing the distribution of sediments with D2 Sub-Group provenance is shown in Figure Ap4.1.14.

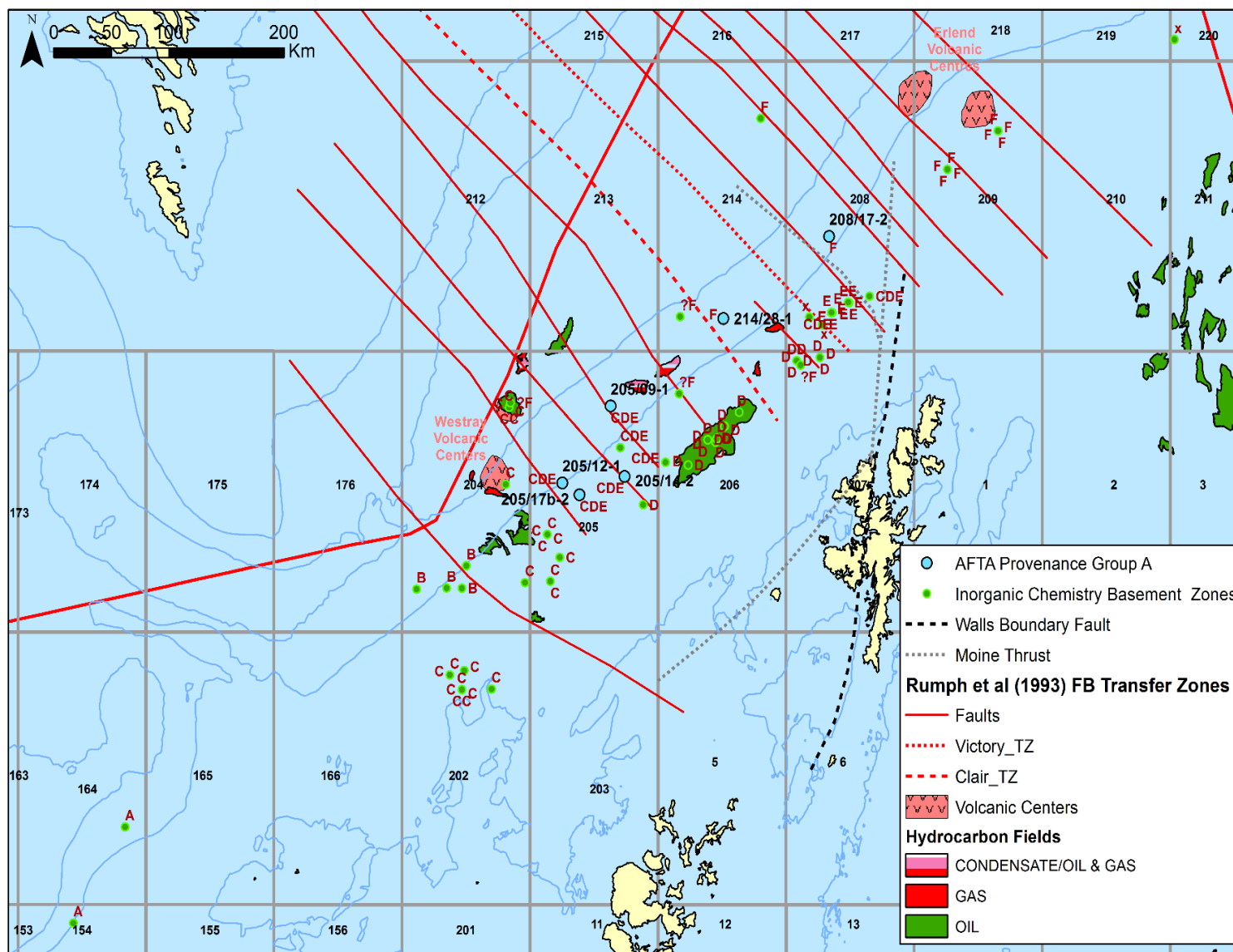


FIGURE Ap4.1.1 Location map of wells with provenance Group A sediments

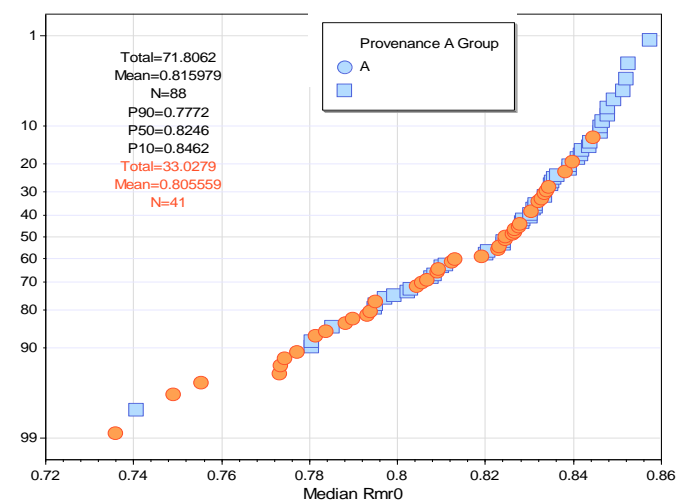
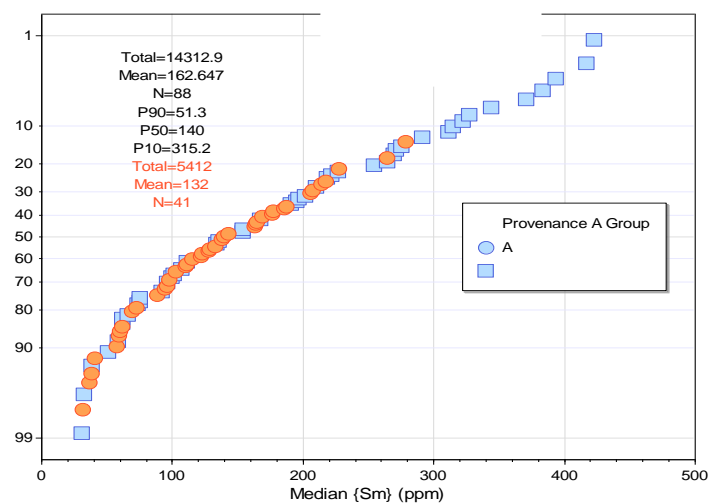
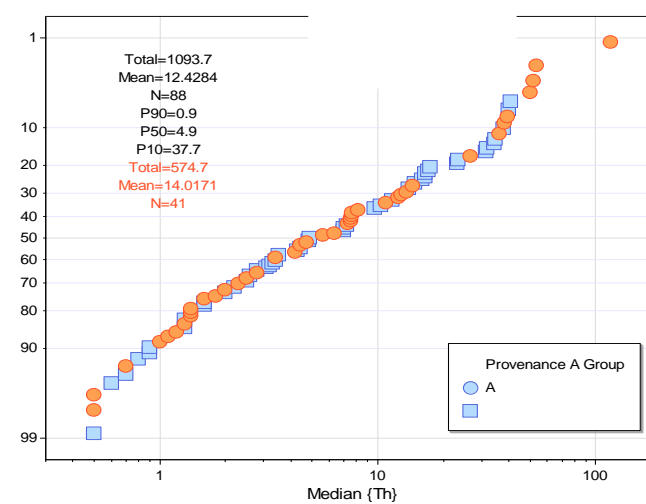
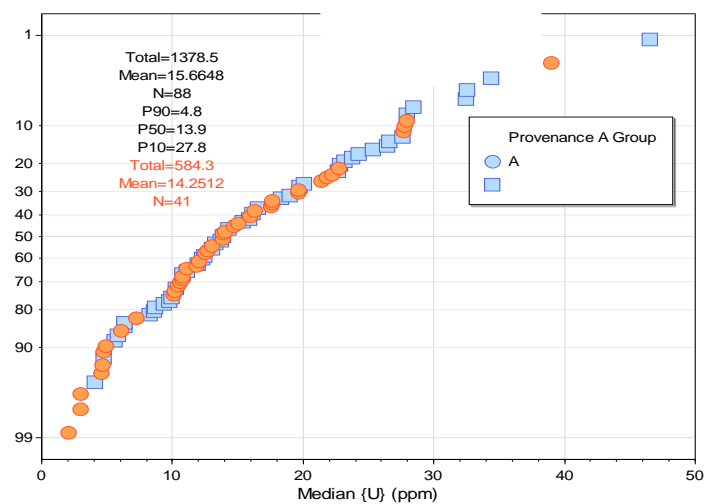


FIGURE Ap4.1.2 Probability plots of U, Th and Sm concentration (ppm) and the Rmr0 apatite kinetic parameter for the A Group.

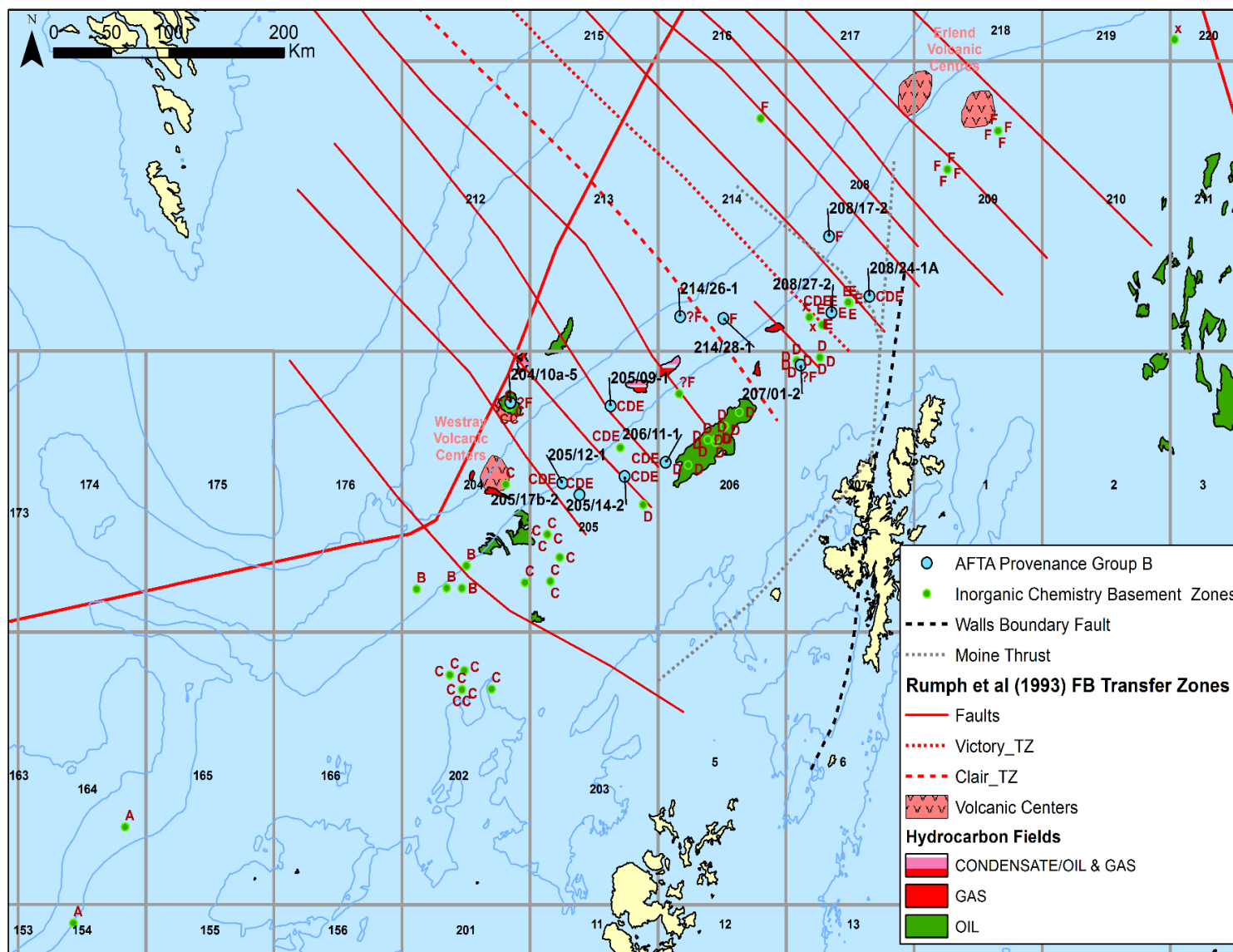


FIGURE Ap4.1.3 Location map of wells with provenance Group B sediments

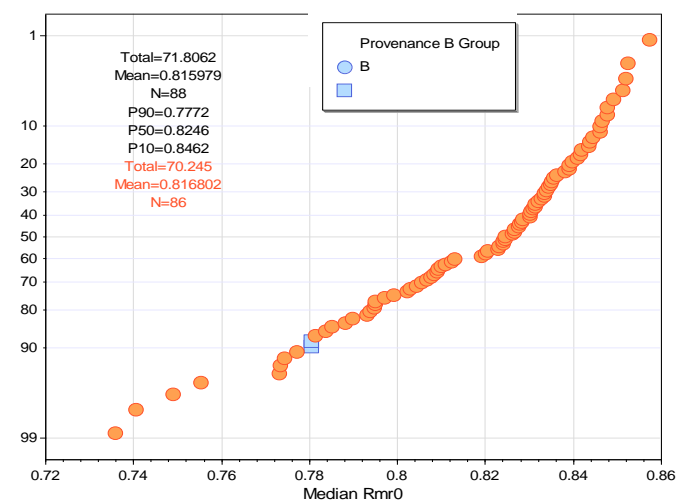
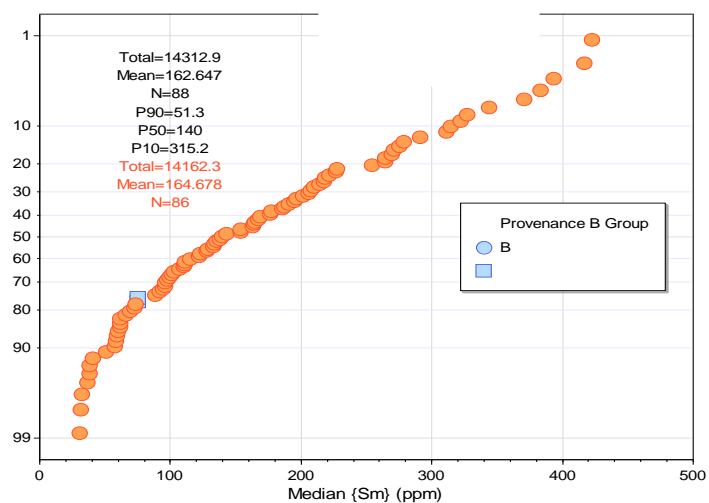
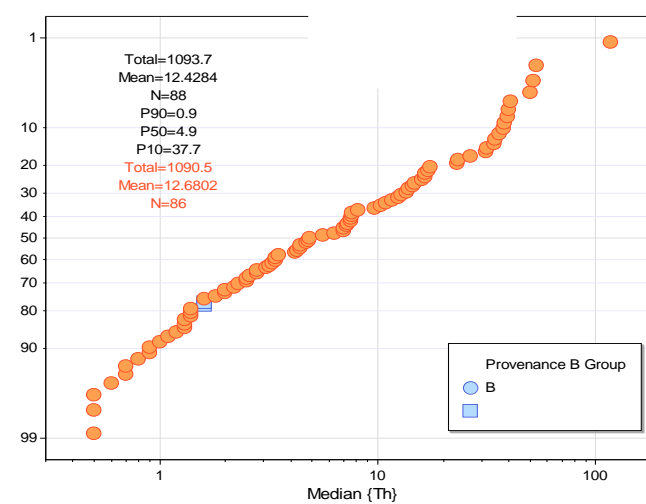
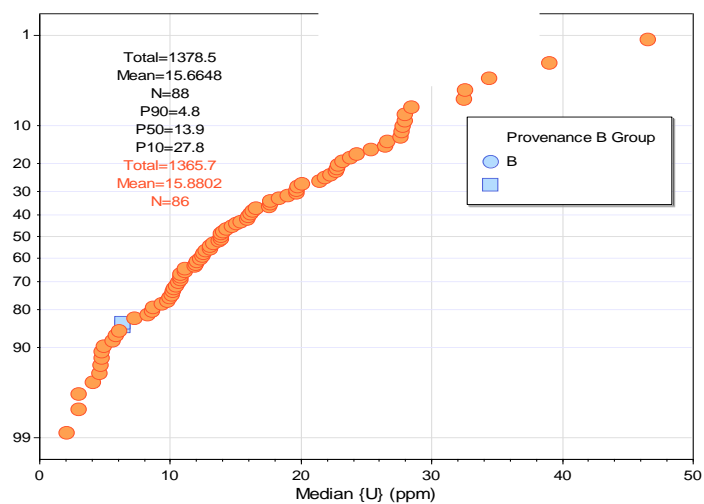


FIGURE Ap4.1.4 Probability plots of U, Th and Sm concentration (ppm) and the Rmr0 apatite kinetic parameter for the B Group.

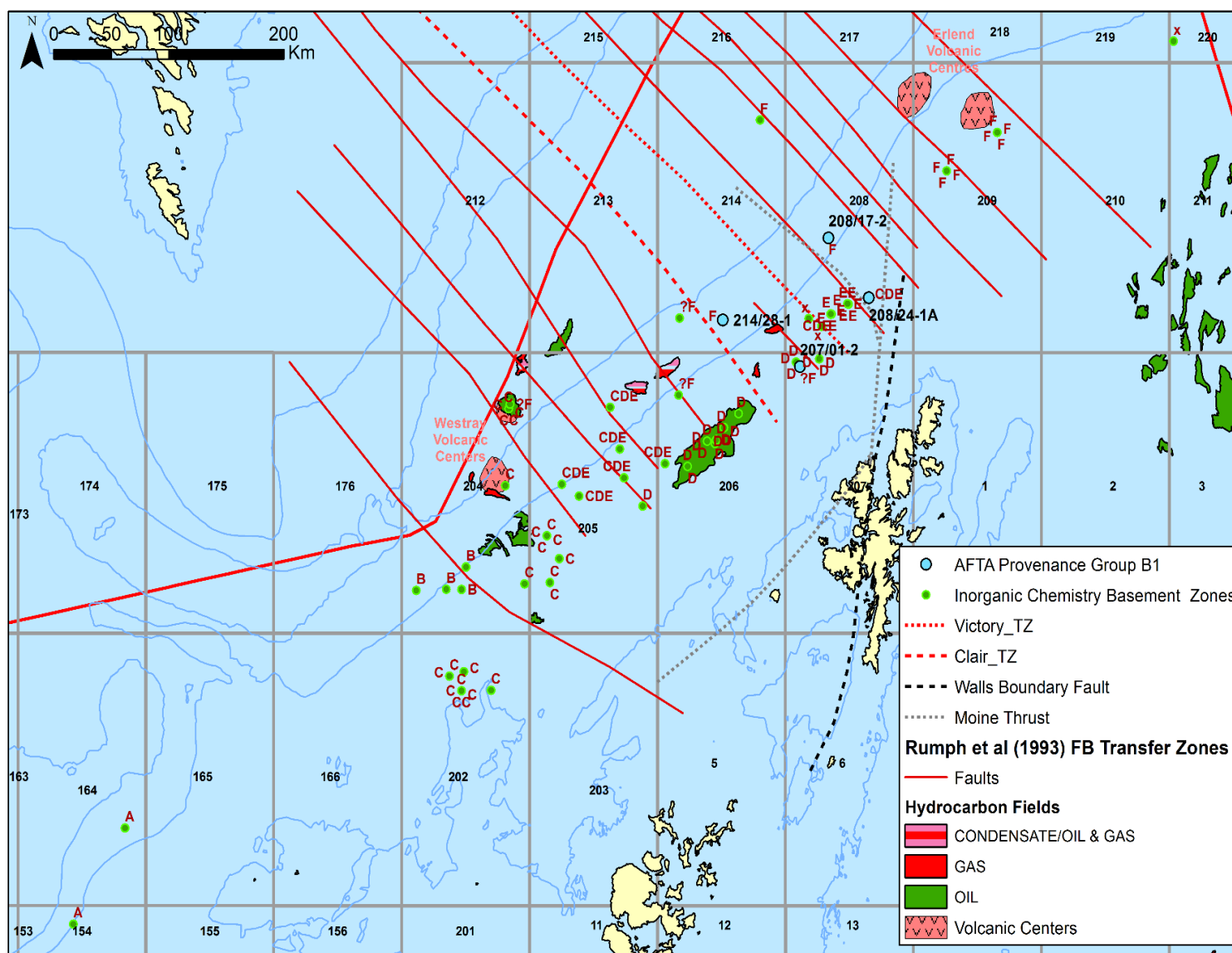


FIGURE Ap4.1.5 Location map of wells with provenance Group B1 sediments

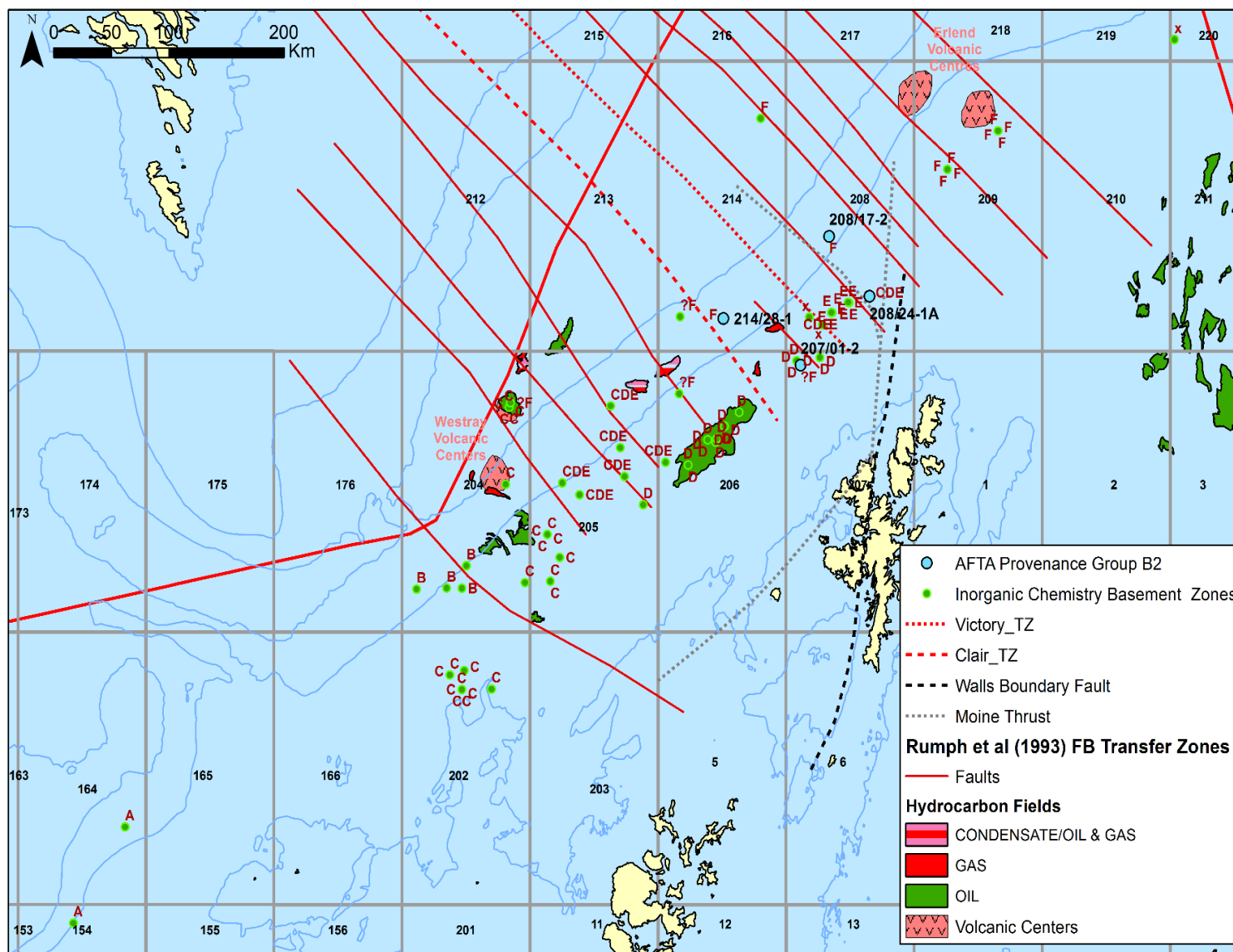


FIGURE Ap4.1.6 Location map of wells with provenance Group B2 sediments

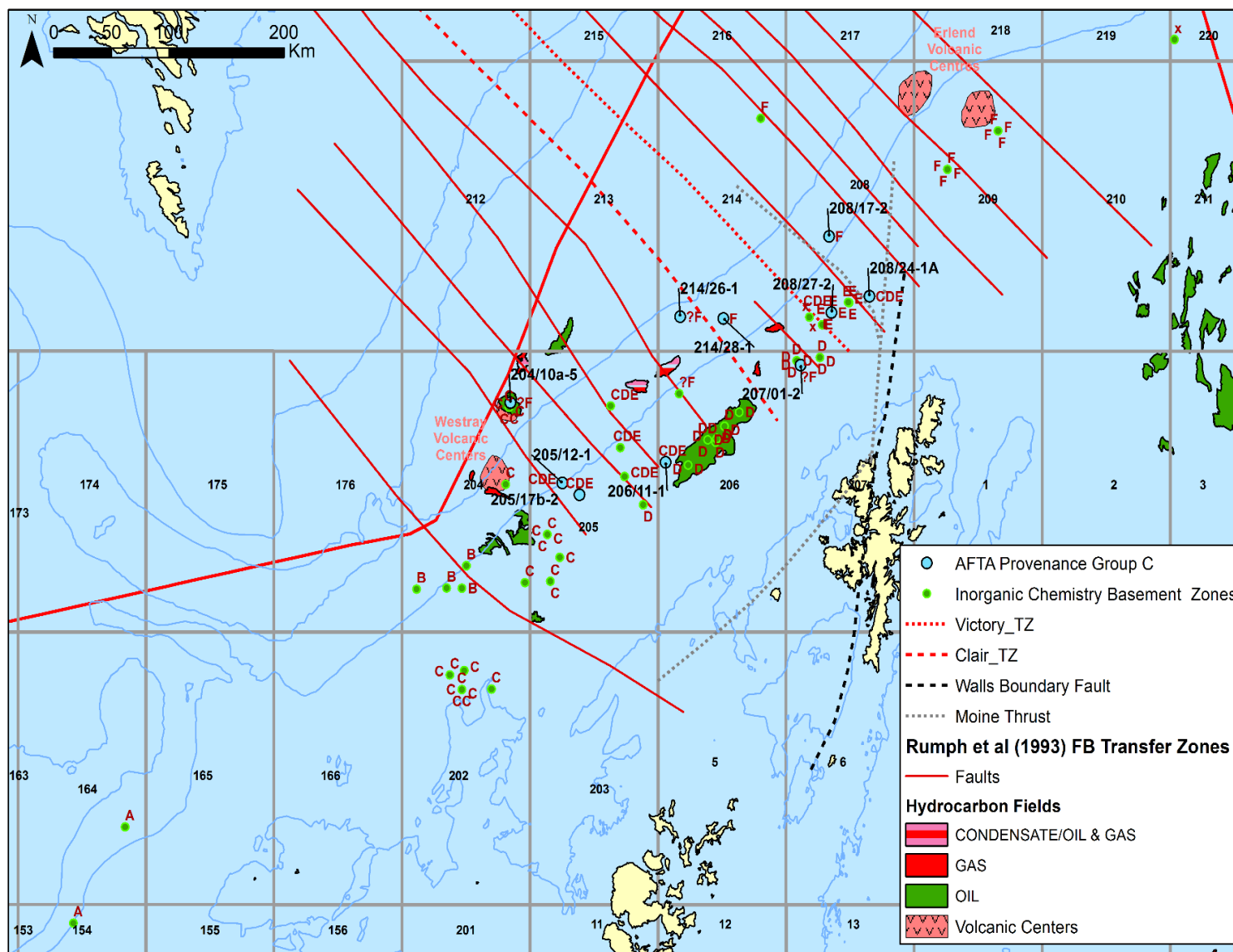


FIGURE Ap4.1.7 Location map of wells with provenance Group C sediments

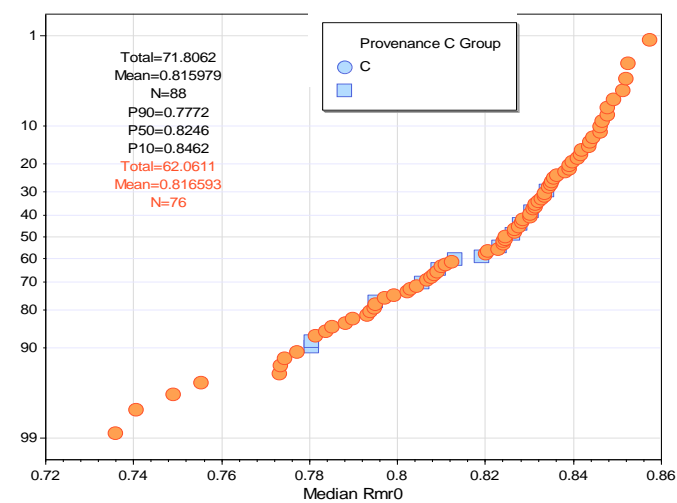
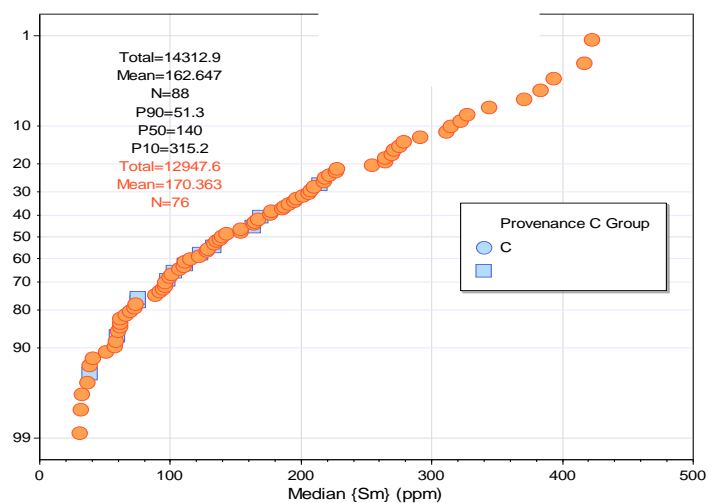
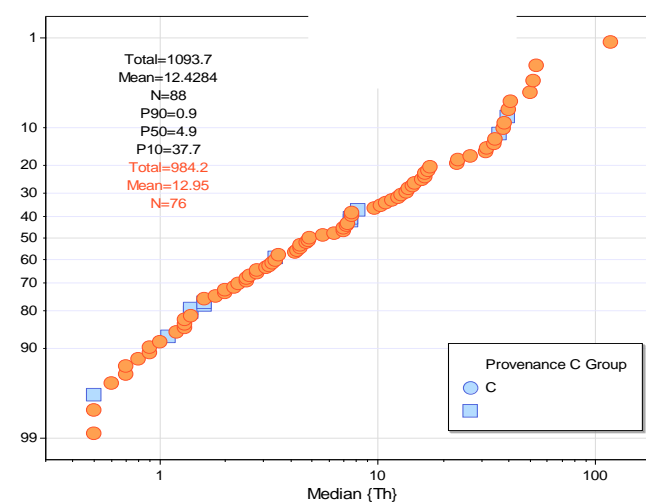
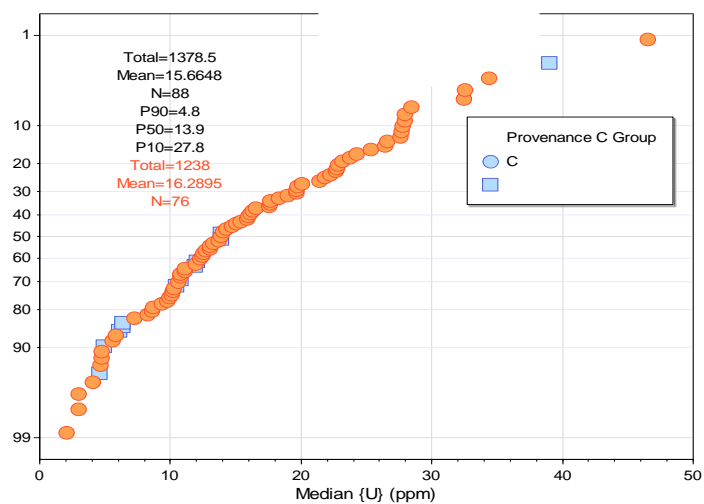


FIGURE Ap4.1.8 Probability plots of U, Th and Sm concentration (ppm) and the Rmr0 apatite kinetic parameter for the C Group.

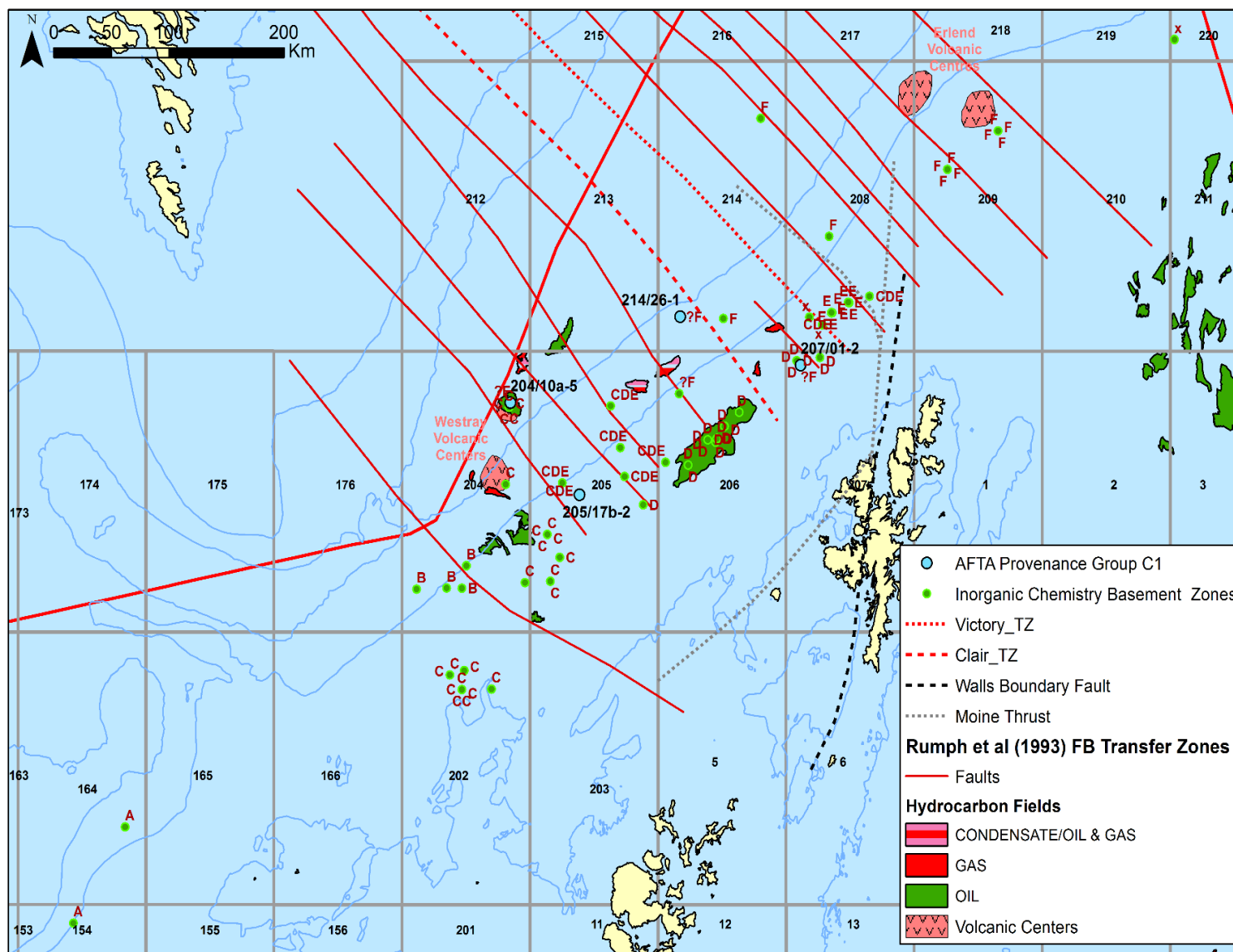


FIGURE Ap4.1.9 Location map of wells with provenance Group C1 sediments

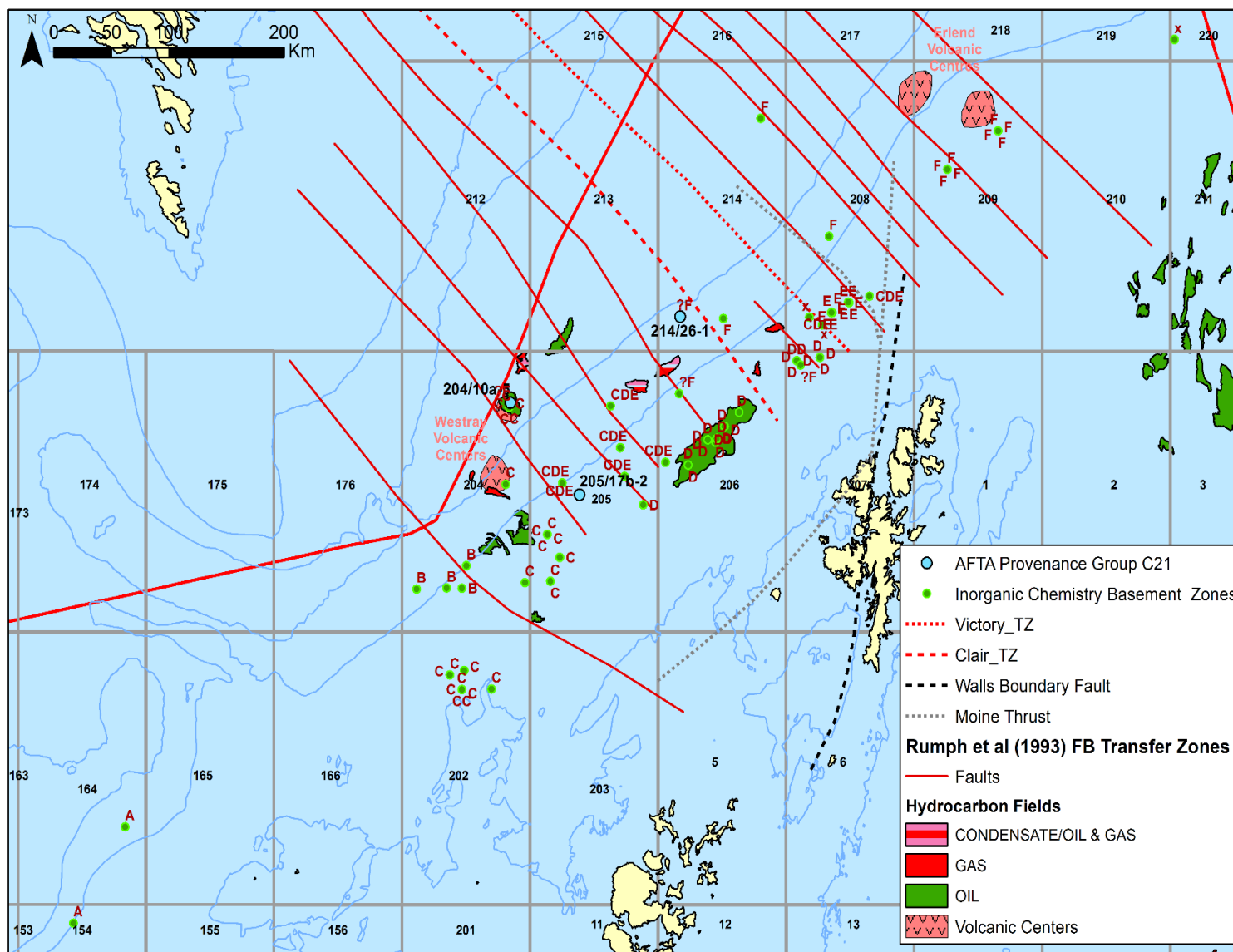


FIGURE Ap4.1.10 Location map of wells with provenance Group C21 sediments

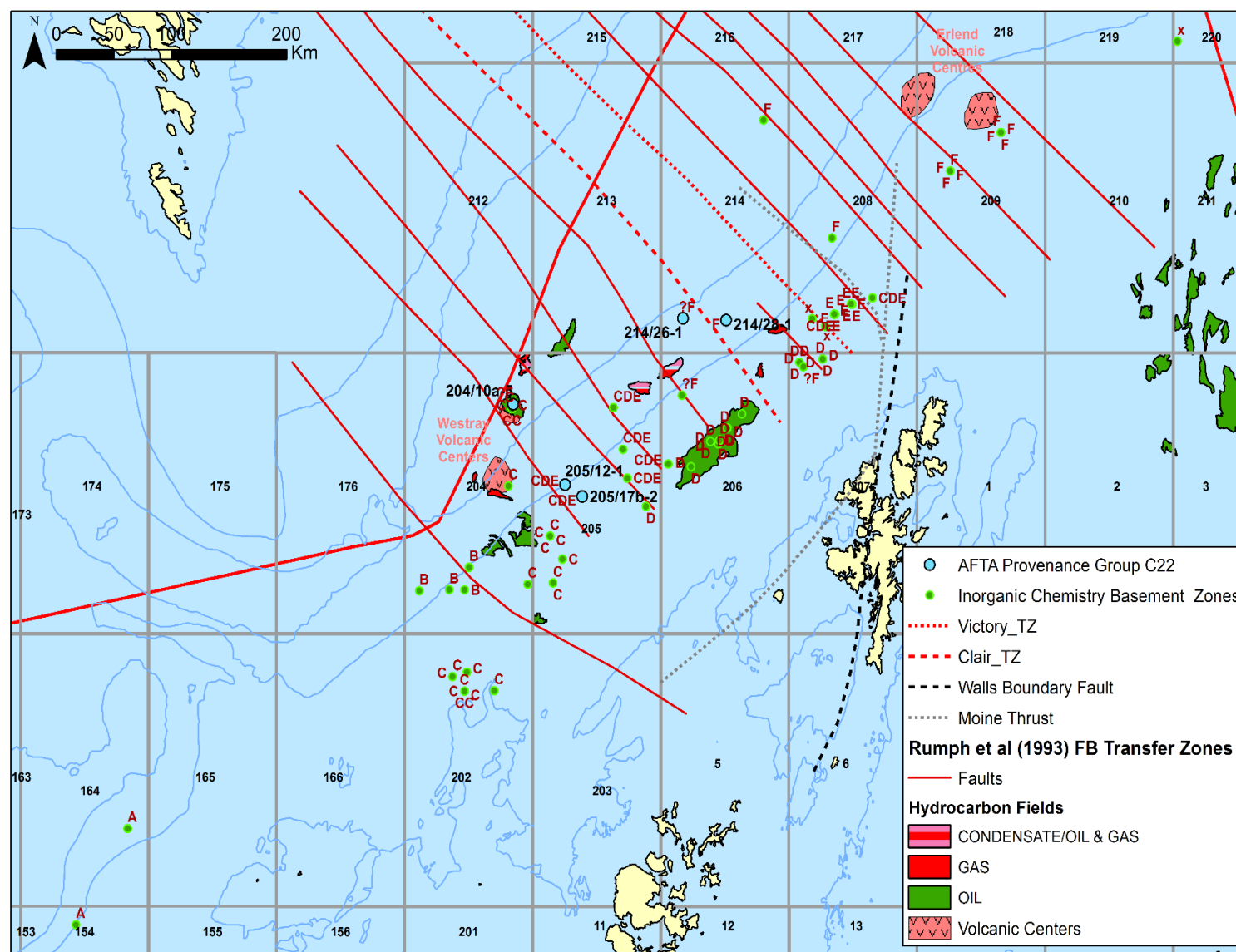


FIGURE Ap4.1.11 Location map of wells with provenance Group C22 sediments

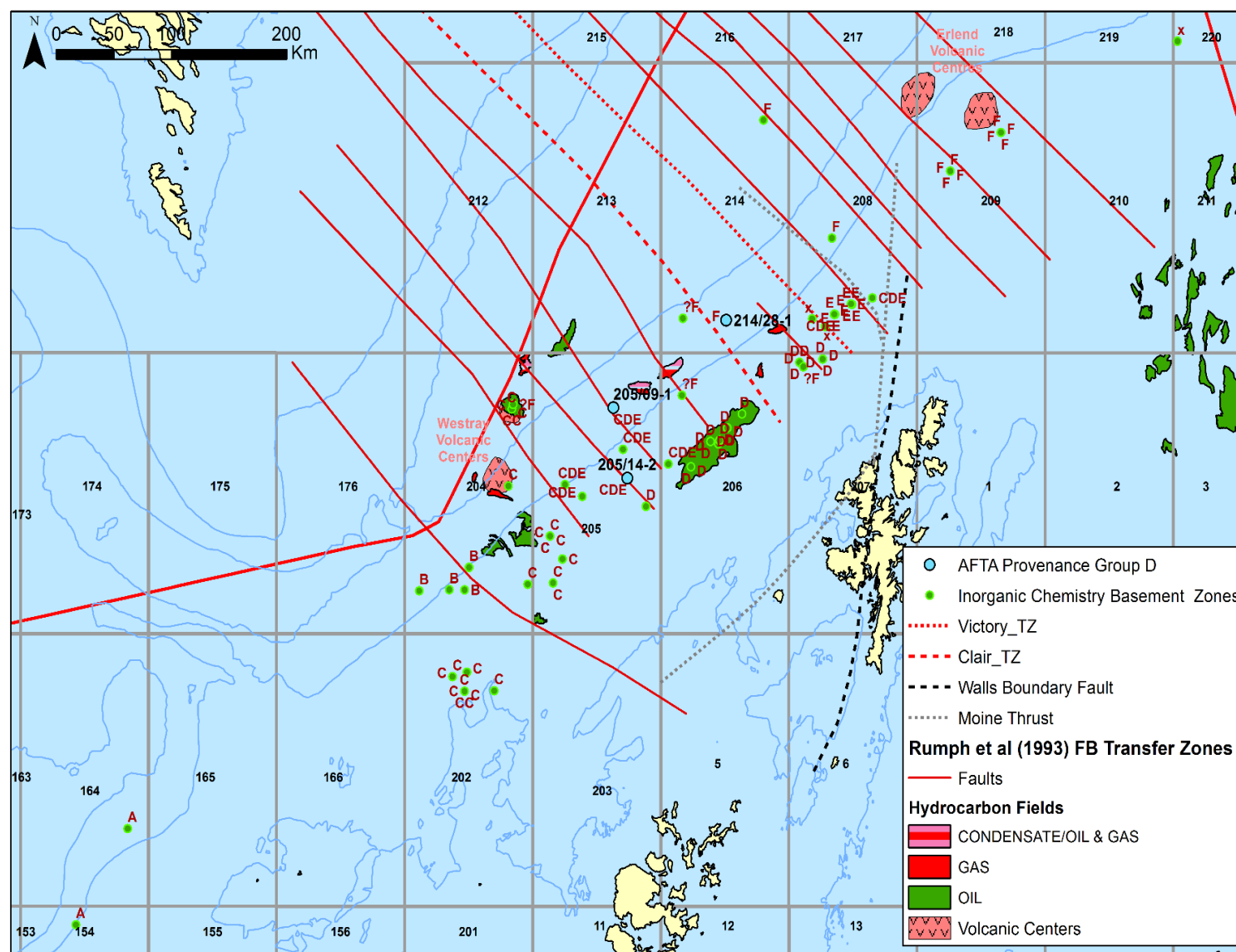


FIGURE Ap4.1.12 Location map of wells with provenance Group D sediments

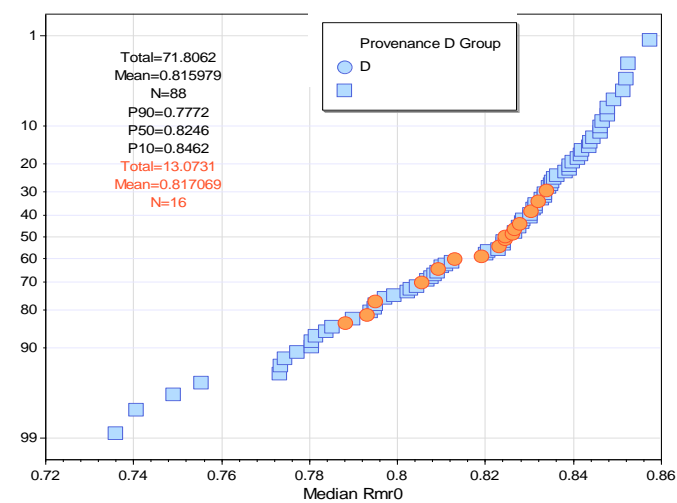
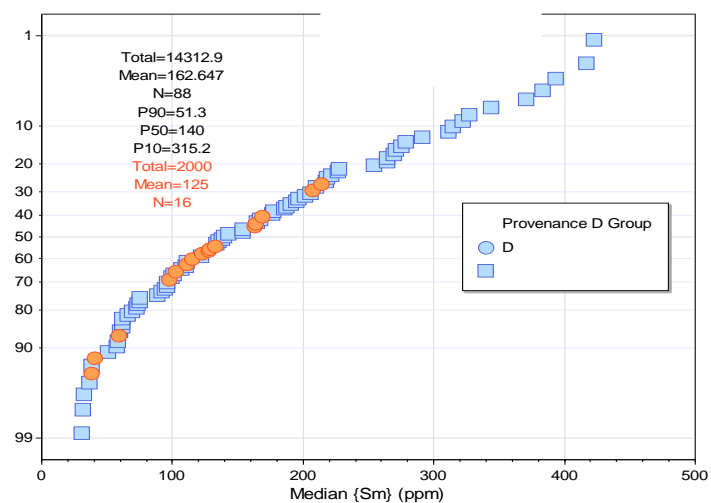
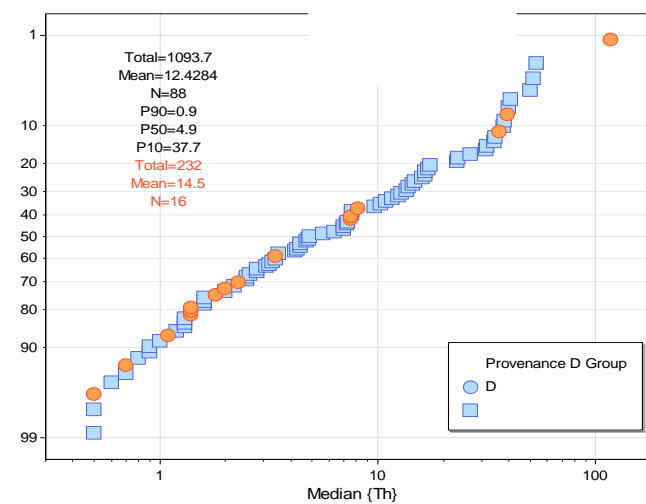
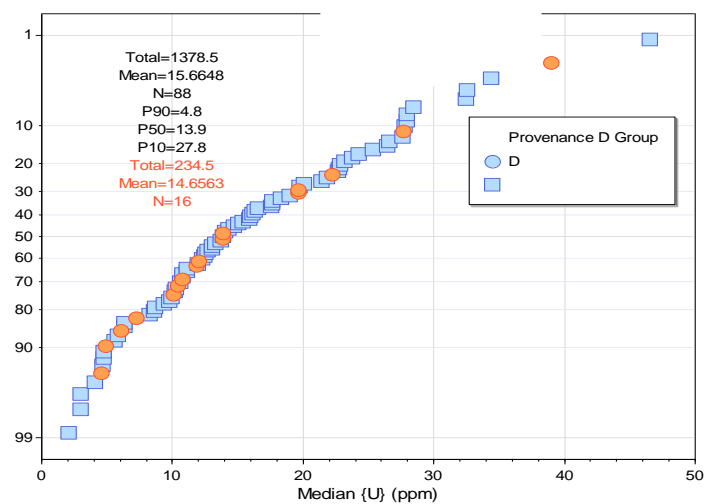


FIGURE Ap4.1.13 Probability plots of U, Th and Sm concentration (ppm) and the Rmr0 apatite kinetic parameter for the D Group.

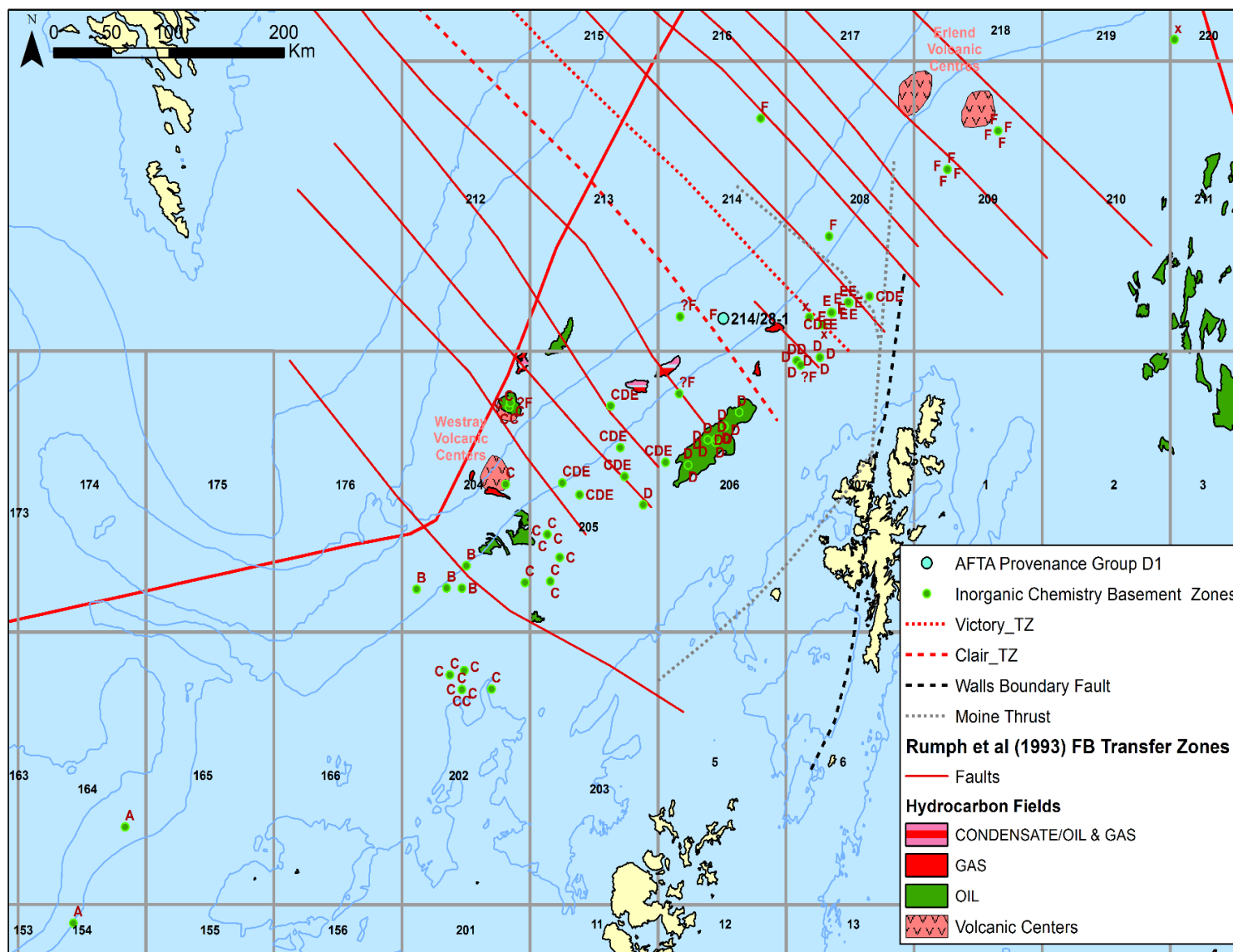


FIGURE Ap4.1.14 Location map of wells with provenance Group D1 sediments

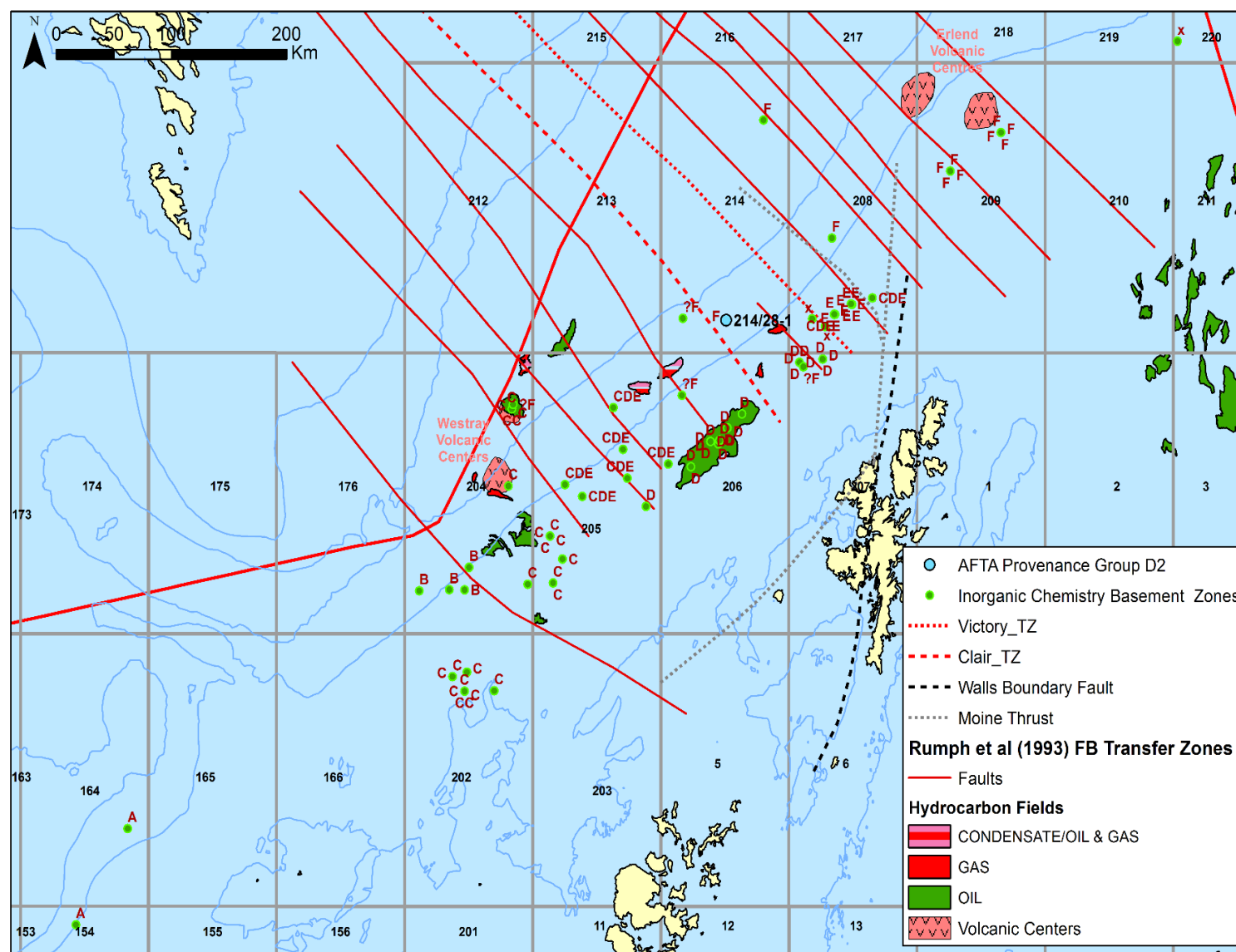


FIGURE Ap4.1.15 Location map of wells with provenance Group D2 sediments

APPENDIX 5

METHODS

APPENDIX 5.1 Analytical methods used in the Chemostrat laboratory (UK)

APPENDIX 5.2 Analytical methods used in the Apatite.com laboratory (USA)

APPENDIX 5.3 Analytical methods used in the APT AS laboratories (Norway) and APT UK laboratories (UK)

APPENDIX 5.1 ANALYTICAL METHODS USED IN THE CHEMOSTRAT LABORATORY (UK)

APPENDIX 5.1.1	ELEMENTAL DATA AND RADIOACTIVE HEAT PRODUCTION
APPENDIX 5.1.2	MINERALOGICAL DATA
APPENDIX 5.1.3	GEOCHRONOLOGICAL DATA

Analytical methods used in the Chemostrat laboratory (UK)

APPENDIX 5.1.1 ELEMENTAL DATA AND RADIOACTIVE HEAT PRODUCTION

Radioactive heat production was calculated from Potassium (K), Thorium (Th) and Uranium (U) elemental data using an in house Chemostrat method. The elemental data was either collected from the published literature (see results tables) or generated from new analysis as part of this study.

Each sample was washed and dried to remove any surface mud and/or contaminants. Prior to analysis, all prepped cuttings samples were then ground to a fine powder in agate mortars. Following preparation, the cuttings samples were prepared for ICP analyses by using the lithium metaborate (alkali) fusion procedure, as advocated by Jarvis & Jarvis (1992a and 1992b). The prepared samples were then analysed using ICP-OES and ICP-MS instruments, with quantitative data being acquired for fifty elements, which include ten major elements, e.g., Al, Si, Ti, Fe, Mn, Mg, Ca, Na, K and P, twenty-two trace elements, e.g., Ba, Be, Co, Cr, Cs, Cu, Ga, Hf, Mo, Nb, Ni, Pb, Rb, S, Sc, Sr, Ta, Tl, Th, U, V, W, Y, Zn and Zr, and fourteen rare earth elements, e.g., La, Ce, Pr, Nd, Sm, Eu, Gd, Tb, Dy, Ho, Er, Tm, Yb and Lu.

The precision of the geochemical data acquired by the ICP analyses is determined by replicate analyses of multiple preparations of certified rock standard reference materials (SRMs), along with duplicate preparations of three unknown samples, which are analysed on a routine basis along with each of the samples. With reference to the SRMs, the absolute accuracy of all the data are generally considered to lie within the range of error achieved for multi-determinations of the same sample.

APPENDIX 5.1.2 MINERALOGICAL DATA

Mineralogical data was either collected through point counting of 300 crystals from a thin section or by X-ray Diffraction (XRD). For XRD analysis the sample is first disaggregated gently using a pestle and mortar. A 2g split of this material is then 'micronised' using a McCrone Micronising Mill to obtain an x-ray diffraction 'powder' with a mean particle diameter of between 5 - 10 microns. The sample as a slurry can then be treated in one of the following ways: If sample quantity is limited the slurry is dried overnight at 80°C, re-crushed to a fine powder and back-packed into an aluminium cavity mount, producing a randomly orientated sample for presentation to the x-ray beam. When appropriate, and with samples where 5-10g are available, the (water-based) slurry is sprayed under pressure into an oven where it is instantly dried into a powder comprising microspherical aggregates of mineral particles. This powder is front-packed into an aluminium cavity mount, producing a randomly orientated sample for presentation to the x-ray beam. Samples are then analysed by XRD between 4.5° and 75° 2 θ (theta) at a step size of 0.013 and nominal time per step of 0.2 s (continuous scanning mode) using x-ray radiation from a copper anode at 40kV, 40mA. Data is then interpreted through in house "Traces" and "Search Match" or Reitveld analysis in Siroquant.

APPENDIX 5.1.3 GEOCHRONOLOGICAL DATA

Zircon and Apatite grains were separated using LST heavy mineral separation and then analysed by laser ablation inductively-coupled plasma mass spectrometry (LA-ICP-MS). The non-magnetic fraction (>1.2A) was mounted in araldite resin blocks and polished. The resin blocks

were then placed into a Scanning Electron Microscope (SEM) and mapped using electron dispersive spectroscopy to identify zircons and apatites in the sample (elevated Hf & P content). U-Pb age dating was performed using quadrupole-based LA-ICP-MS.

Mass bias and instrument drift were monitored constantly and accounted for by using sample-standard bracketing. Raw data were processed using Iolite software (Patton et al. 2011). All analytical errors in the text are quoted at 2 σ level.

All zircon analyses were displayed on concordia diagrams (Ludwig, 2008) to check the data for any major peculiarities and for geologically significant discordia arrays. The single analysis concordia age (op. cit.) was calculated for each analysis and these ages were used for plotting and interpreting the data. This age has the advantage of being more precise than both the $^{206}\text{Pb}/^{207}\text{Pb}$ ages and the $^{206}\text{Pb}/^{238}\text{U}$ ages (Zimmermann et al., 2017) and therefore removes the need to switch between isotope systems at a given age (typically 1.0 Ga). The data were filtered using a threshold of >0.001 for the probability of concordance, a statistic which is calculated simultaneously to the concordia age. Accepted data from each sample were then plotted on histograms (25 Ma bin width), kernel density estimation (KDE; 20 Ma bandwidth) plots (Vermeesch, 2012) and probability density plots (Sircombe, 2004).

APPENDIX 5.2

ANALYTICAL METHODS USED IN THE APATITE.COM LABORATORY (USA)

APPENDIX 5.2.1	Apatite fission track analysis methods
APPENDIX 5.2.2	Laser ablation-inductively coupled plasma-mass spectrometry sessions
APPENDIX 5.2.3	Lase ablation settings
APPENDIX 5.2.4	Inductively coupled plasma-mass spectrometry settings
APPENDIX 5.2.5	Apatite U, Th and Pb age standards
APPENDIX 5.2.6	Durango apatite (Chew et al., 2016) and C1 chondrite (McDonough and Sun, 1995) Rare Earth Element (REE) reference elements
APPENDIX 5.2.7	Age ranges for apatite U, Th & Pb
APPENDIX 5.2.8	Apatite UFT U, Th & Pb 20190910 results for primary standard MM
APPENDIX 5.2.9	Apatite UFT U, Th & Pb 20190910 results for primary standard DR
APPENDIX 5.2.10	Apatite UFT U, Th & Pb 20190910 results for primary standard MD
APPENDIX 5.2.11	Apatite UFT U, Th & Pb 20190912 results for primary standard MM
APPENDIX 5.2.12	Apatite UFT U, Th & Pb 20190912 results for primary standard DR
APPENDIX 5.2.13	Apatite UFT U, Th & Pb 20190912 results for primary standard MD
APPENDIX 5.2.14	Apatite UFT U, Th & Pb 20191109 results for primary standard MM
APPENDIX 5.2.15	Apatite UFT U, Th & Pb 20191109 results for primary standard DR
APPENDIX 5.2.16	Apatite UFT U, Th & Pb 20191109 results for primary standard MD
APPENDIX 5.2.17	Apatite UFT U, Th & Pb 20191110 results for primary standard MM
APPENDIX 5.2.18	Apatite UFT U, Th & Pb 20191110 results for standard DR
APPENDIX 5.2.19	Apatite UFT U, Th & Pb 20191110 results for standard MD
APPENDIX 5.2.20	Apatite UFT U, Th & Pb 20191216 results for primary standard MM
APPENDIX 5.2.21	Apatite UFT U, Th & Pb 20191216 results for standard DR
APPENDIX 5.2.22	Apatite UFT U, Th & Pb 20191216 results for standard MD

Analytical methods used in the Apatite.com laboratory (USA)

APPENDIX 5.2.1 Apatite fission track analysis methods

Introduction

Thermochronology methods use Time-temperature histories extracted from rock or mineral samples to understand how rates of heating (burial) or cooling (rock uplift: vertical motion of rock relative to the geoid) and exhumation (displacement of rock relative to Earth's surface) have varied spatially and temporally in different geological settings (Reiners *et al.*, 2005).

Fission track dating is based on the spontaneous fission decay of ^{238}U which produces linear defects in the lattice of U-bearing minerals. These linear defects are commonly referred to as fission tracks and are enlarged using a standardized chemical etching process so they can be observed under an optical microscope. By comparing the density of fission tracks with the U content of the mineral, an apparent fission track age can be calculated. The U content used to have to measured using a nuclear reactor ('the external detector method') which was slow and difficult. It is now done with LA-ICP-MS, this also allows collection of other useful data, especially for provenance studies (e.g. rare earth elements, U-Pb dates).

Fission tracks are semi-stable features that are progressively shortened as temperature increases over a specific range, this shortening is referred to as annealing, whereby displaced atoms and electrons can migrate back to their original sites. This process is dependent on both temperature and time. Enough exposure to elevated temperatures will progressively shorten the tracks until they are entirely annealed, and the AFT clock is reset. To go from a track length distribution to a thermal history we need to know the controls on the rate of annealing. This rate is determined by the apatite composition, in particular the Cl content (Green *et al.* 1985), subsequently Mn, Sr, OH, Fe, and the rare earth elements, have also been suggested as significantly influencing track-retention in apatite e.g. Ketcham *et al.* 2007). Two parameters, the r_{m0} and the Dpar are key inputs into the thermal history modelling, they are briefly introduced below:

Ketcham *et al.* (1999) showed that the laboratory annealing results for any two apatite's annealed at the same conditions can be described by the relation:

$$r_{lr} = \left(\frac{r_{mr} - r_{m0}}{1 - r_{m0}} \right)^k$$

Where r_{lr} and r_{mr} are the reduced track lengths of the less resistant and more resistant apatite and the r_{m0} and k are fitted parameters. The parameter r_{m0} has a physical meaning as the reduced track length of the more resistant apatite at the conditions where the less-resistant apatite first becomes fully annealed.

Dpar is the the arithmetic mean fission track etch figure diameter parallel to the crystallographic c-axis (in μm). It is an estimator of annealing rate of an individual apatite grain (Barbarand *et al.*, 2003a). Dpar essentially works as a proxy for composition, and thus track-retentively, as the etching efficiency is a function of composition; increased etch-pit size correlates with increased Cl-content. Donelick (1993) demonstrated a correlation between grain composition and etch pit size. A function that relates measurable parameters such as Dpar to chemical composition is critical to understanding the significance of fission track age and length data.

A fission track age provides an estimate of the time that has elapsed since the mineral cooled through a specific temperature window (referred to as the partial annealing zone or PAZ apatite is ~60-110°C, temperatures above 120°C lead to the tracks being annealed).

The apatite fission track method also yields information on the nature of the cooling path, this information is obtained from the distribution of confined fission track lengths in a sample (Gleadow *et al.* 1986a). Confined fission tracks are horizontal (or <10° from horizontal) tracks that lie in a c-axis prismatic section, such that both ends of the track are visible entirely within the polished and etched apatite crystal without altering the focal depth. Unannealed, spontaneous fission track lengths in natural apatite grains typically range between ~14.5 and 15.5µm depending on its chemical composition (Gleadow *et al.* 1986a). For example, an apatite grain which exhibits a fission track population with mean track lengths in this range and a narrow variation in track length distribution (e.g., <1.5µm), would be interpreted to have cooled relatively rapidly from a temperature $\geq 110^{\circ}\text{C}$ to a temperature $\leq 60^{\circ}\text{C}$ at the time indicated by the apparent apatite fission track age. A shorter mean track length with a broad standard distribution indicates that the sample resided in the PAZ for a significant period of time since the formation of the oldest fission tracks (Gleadow *et al.* 1986b). The apatite fission track age and track length distribution can be combined to construct time–temperature paths by inverse and/or forward modelling of the fission track age and length data (e.g., Gallagher 1995, Ketcham 2005).

Sample Preparation

The samples were prepared for analysis following the detailed description of Donelick *et al.* (2005). Each cuttings sample was crushed by hand, the crushate was sieved using 300 micron nylon mesh, the <300 micron fraction was washed with tap water and dried at room temperature in air, and apatite was isolated using standard gravimetric and magnetic mineral separation techniques. Apatite grains were mounted in epoxide resin and polished to a fine finish using 0.3 micron alumina slurry. Apatite grain mounts were stirred vigorously in reagent grade 5.5 molar nitric acid for 20 seconds at 21°C and rinsed with distilled water to etch natural AFTs and to remove any common lead contamination on the grain mount surfaces.

AFT Data Collection

AFT data were collected and ages calculated following the detailed description of Donelick *et al.* (2005). AFTs were viewed and measured by analyst Ray Donelick using a Nikon E600 optical microscope affixed with a Ludl Kinetec XY-stage, ASI Z-drive, Lumenera Infinity1 digital camera, and operated by Apatite.com Partners' Sample_Scanner.py software package. The 50x objective was used for counting surface fission tracks (SFTs) for age dating, the 100x objective was used to measure confined fission tracks (CFTs) and etch figure dimensions (parameters Dpar, Dper). The number of CFTs available for measurement was enhanced by irradiating the apatite grain mounts with ^{252}Cf -derived fission fragments.

LA-ICP-MS Data Collection

The two laser ablation-inductively coupled plasma-mass spectrometry (LA-ICP-MS) sessions that were run in this study are summarized in Table A.1. LA and ICP-MS settings for each session are detailed in Tables A.2 and A.3, respectively. Masses measured for each session are detailed in Table A.4. Age standards used in this study are summarized in Table A.5. Age ranges measured for selected age standards are detailed in Table A.6. Results for selected UThPb age standards are shown in Figure A.1 and Figure A.2.

LA-ICP-MS Data Modelling

The data for each spot is characterized by a series of data scans, each scan representing one measurement for each mass in order of increasing mass. The series data scans may be divided into background and signal & background segments. Background represents data collected prior to firing the laser. Signal & background represents data collected during laser ablation of the spot. The following steps are taken to determine background-corrected signal intensities for each mass analysed for each spot:

- The true time is calculated at which each measurement was collected for each mass for each scan.
- The time at which background ends and signal & background begins is determined using selected masses listed in Table A.4 (for which Search Last Background? is TRUE).
- A line is fitted to all background values for each mass prior to the time at which background ends. For a negative slope, the background value for the current mass is set equal to the value of the line at the time at which background ends; the error is set equal to the standard deviation of the background values about the fitted line. For zero or positive slope, the background value for the current mass is set equal to the mean of the fitted background values; the error is set equal to the standard deviation of the background values about the mean.
- Signal & background values are smoothed (versus scan number) for each mass using a Savitzky and Golay (1964) filter based on the median of fitted polynomials; the error of each signal & background value is set equal to the standard deviation of the signal & background values about the smoothed curve.
- Signal & background values are corrected for background noise by subtracting background.

Fission track ages were calculated using the equations of Donelick *et al.* (2005). UThPb ages were calculated for each spot using the general principles described in Donelick *et al.* (2009). Chemical composition values were calculated using the methods described in Donelick and Donelick (2014).

High resolution AFT Analysis using UPb Ages and REEs

In sedimentary rocks and modern sediments, mineral grains such as apatite and zircon from multiple provenance sources may be mixed together. A practical example of where this may be important is the interpretation of apatite fission track (AFT) data from a sandstone. To properly interpret AFT data from such a mixture of sources, it is necessary to bin apatite grains, and their associated AFT data, into discrete groups based on AFT-independent data such as chemical composition or isotopic age.

The Radial Plot uses the AFT ages and age errors to produce one or more vectors that point to an age or ages of presumed geological significance. Algorithm BinomFit deconvolves the AFT age probability density function into one or more age peaks, each peak yielding an age of presumed geological significance. Neither of these approaches requires any AFT-independent data. O'Sullivan *et al.* (2018) use laser ablation-inductively coupled plasma-mass spectrometry (LA-ICP-MS) to measure rare earth element (REE) concentrations and uranium-lead (UPb) ages for apatite grains and sort them into groups using principle component analysis.

For High-Resolution AFT (HR AFT), apatite grains are sorted into groups using the following steps: 1) for each of approximately 9 different apatite standard species analysed during a LA-ICP-MS session, measure REE concentrations and UPb ages and calculate the mean and

standard deviation for each measured value for each standard, 2) derive a session-specific, best-fit line for each measured value that gives standard deviation as a function of mean among all standards, 3) for each unknown apatite grain (from an unknown group), use the derived best-fit lines to define an apatite grain group centered at the measured values for the unknown grain and bounded by 2 standard deviations about the measured values, and 4) search for and isolate other unknown apatite grains that exhibit measured values that fall within the bounds of the defined apatite grain group.

Thermal history modelling

The geological significance of fission track ages strongly depends on the time-temperature (tT) history of the samples (Wagner, 1981). Exploration of the thermal history of a sample is based on a modelling programme, where measured FT ages, kinetic parameters and track length data form the input. The modelling procedure employs annealing models that aim to describe the quantitative relationship between the FT age kinetic parameters, track length parameters, temperature and time; annealing models are used to predict fission track ages for predefined track length distributions, or track length statistics for randomly generated thermal histories. Modelling starts with predefined Time-temperature points based on available geological constraints; e.g. the depositional age of a sampled sedimentary rock. These Time-temperature points, joined by linear tie lines, provide starting points for a random exploration of Time-temperature space. Each of the randomly generated Time-temperature path predicts a set of FT ages and lengths that can be compared against the measured data. A goodness of fit (GOF) criterion is used to assess how well predicted thermal histories match the observed data. Model results are displayed in a time-temperature plot, where the goodness of fit of a particular model cooling history to the data is indicated with a colour code.

FT3 is Apatite.com Partners' software package for calculating thermal histories based on conventional AFT and HR-AFT data. The philosophy of this software is similar to that of AFTSolve (Ketcham et al., 2000). FT3 uses the experimental data of Donelick (1988, 1991), Donelick et al. (1990), Vrolijk et al. (1992), Carlson et al. (1999), and the calibration of Rmr0 provided by Ketcham et al. (1999). All CFT data are projected onto the c-axis using the model of Donelick (1991) and Donelick et al. (1999).

APPENDIX 5.2.2 Laser ablation-inductively coupled plasma-mass spectrometry sessions

Session Name	Laboratory	Hardware	Laboratory Scientist	Collected By
Apatite UFT UThPb 20190907	Chronuscamp Research, Itapira, Sao Paulo State, Brazil	LA: NWR UP-213 213 nm ICP-MS: Agilent 7800 quadrupole	Dr. Cleber Soares	Dr. Cleber Soares and Dr. Ray Donelick
Apatite UFT UThPb 20190909	Chronuscamp Research, Itapira, Sao Paulo State, Brazil	LA: NWR UP-213 213 nm ICP-MS: Agilent 7800 quadrupole	Dr. Cleber Soares	Dr. Cleber Soares and Dr. Ray Donelick

APPENDIX 5.2.3 Lase ablation settings

Setting	Apatite UFT UThPb 20190907	Apatite UFT UThPb 20190909
Background	16 s	18 s
Laser ablation	27 s	27 s
Washout	25 s	27 s
Laser rate	10 Hz	10 Hz
Laser spot size	30 μ m	30 μ m
Energy	45% transmission	45% transmission
He carrier gas	900 ml/minute	1700 ml/minute
Ultra high purity N ₂ gas	4.5 ml/minute	4.5 ml/minute

APPENDIX 5.2.4 Inductively coupled plasma-mass spectrometry settings

Setting	Apatite UFT UThPb 20190907	Apatite UFT UThPb 20190909
Ar plasma gas	800 ml/minute	800 ml/minute

APPENDIX 5.2.5 Apatite U, Th and Pb age standards

Standard Name	Type	Accepted Age	Reference
MM = McClure Mtn.	primary	523.98 \pm 0.12 Ma	Schoene and Bowring (2006)
B4 = Bamble	secondary	~1128 Ma	Donelick and Donelick (unpublished data)
T2 = Temora 2	secondary	416.78 \pm 0.33 Ma	Black <i>et al.</i> (2004)
IF = Fish Canyon Tuff	secondary	28.201 \pm 0.012 Ma	Lanphere and Baadsraard (2001) Kuiper <i>et al.</i> (2008)
F5 = Duluth anorthosite	secondary	1099.0 \pm 0.6 Ma	Paces <i>et al.</i> and Miller (1993)
MD = Mount Dromedary	secondary	99.12 \pm 0.14 Ma	Renne <i>et al.</i> (1998)
OL = Otter Lake	secondary	913 \pm 7 Ma	Barfod <i>et al.</i> (2005)
TI = Tioga Bed B	secondary	390.5 \pm 0.5 Ma	Roden <i>et al.</i> (1990)
DR = Durango	secondary	31.44 \pm 0.18 Ma	McDowell <i>et al.</i> (2005) Boyce and Hodges (2005)

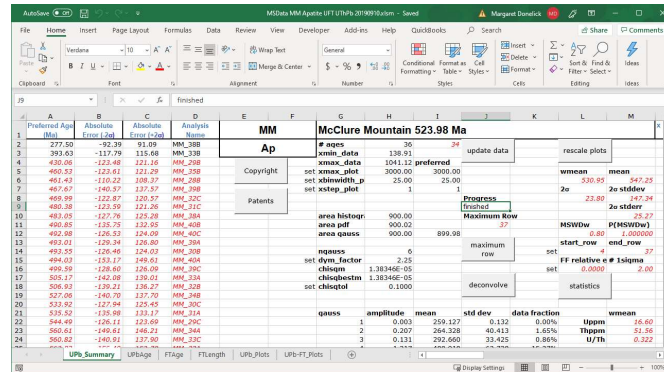
APPENDIX 5.2.6 Durango apatite (Chew *et al.*, 2016) and C1 chondrite (McDonough and Sun, 1995) Rare Earth Element (REE) reference elements

REE	Durango Apatite Reference Concentration (ppm)	C1 Chondrite Reference Concentration (ppm)
La	3786.00	0.2370
Ce	5306.00	0.6130
Pr	472.50	0.0928
Nd	1534.00	0.4570
Sm	215.20	0.1480
Eu	18.90	0.0563
Gd	186.90	0.1990
Tb	24.25	0.0361
Dy	129.90	0.2460
Ho	26.35	0.0546
Er	68.69	0.1600
Tm	8.75	0.0247
Yb	45.10	0.1610
Lu	5.17	0.0246

APPENDIX 5.2.7 Age ranges for apatite U, Th & Pb

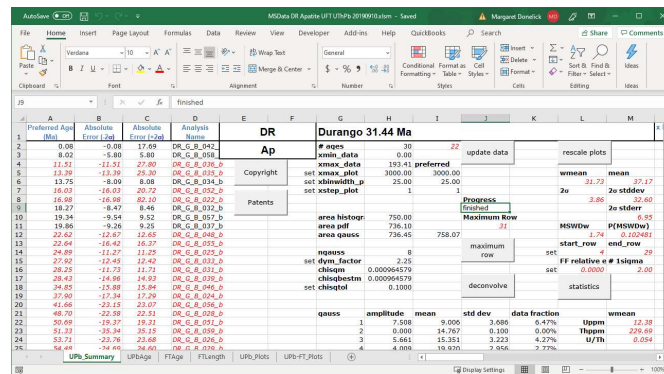
Session Name	DR 31.44 Ma	MD 99.12 Ma	MM 523.98 Ma
Apatite UFT UThPb 20190910	0.08-82.25 Ma	26.62-354.47 Ma	277.50-732.01 Ma
Apatite UFT UThPb 20190912	2.91-355.13 Ma	74.33-224.74 Ma	470.54-658.52 Ma
Apatite UFT UThPb 20191109	3.21-57.95 Ma	42.49-173.05 Ma	428.62-691.65 Ma
Apatite UFT UThPb 20191110	2.55-77.71 Ma	43.51-260.44 Ma	426.94-682.63 Ma
Apatite UFT UThPb 20191216	18.11-42.64 Ma	83.86-150.58 Ma	391.48-613.16 Ma

APPENDIX 5.2.8 Apatite UFT U, Th & Pb 20190910 results for primary standard MM



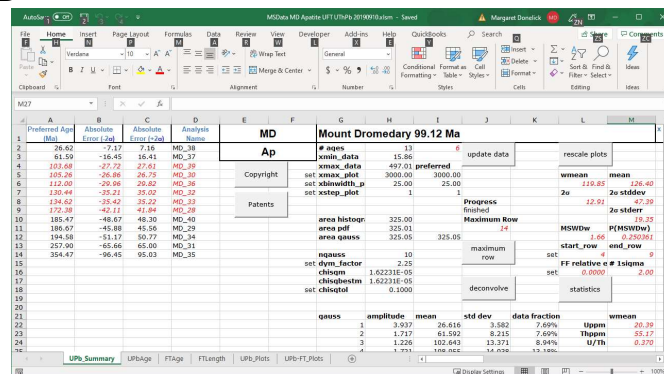
Preferred Age (Ma)	Absolute Error (2 σ)	Absolute Error (1 σ)	Analysis Name
277.50	-92.39	91.09	MM_388
293.63	-117.79	115.68	MM_338
430.06	-122.68	121.16	MM_298
460.52	-122.61	121.29	MM_298
461.43	-110.22	108.37	MM_298
467.67	-140.57	137.57	MM_298
469.69	-122.67	120.57	MM_298
480.38	-122.59	121.26	MM_21C
481.03	-127.79	125.08	MM_384
480.65	-128.79	125.85	MM_408
492.08	-126.53	124.09	MM_40C
493.01	-129.34	126.80	MM_384
493.25	-126.56	124.02	MM_308
494.02	-133.17	130.61	MM_404
499.59	-128.60	126.09	MM_29C
505.17	-148.68	146.01	MM_314
506.63	-139.21	136.27	MM_528
507.68	-140.39	137.70	MM_308
533.92	-127.94	125.45	MM_29C
535.52	-135.99	133.17	MM_314
544.40	-176.11	173.68	MM_29C
560.01	-140.61	136.21	MM_344
560.82	-140.91	137.80	MM_29C

APPENDIX 5.2.9 Apatite UFT U, Th & Pb 20190910 results for primary standard DR



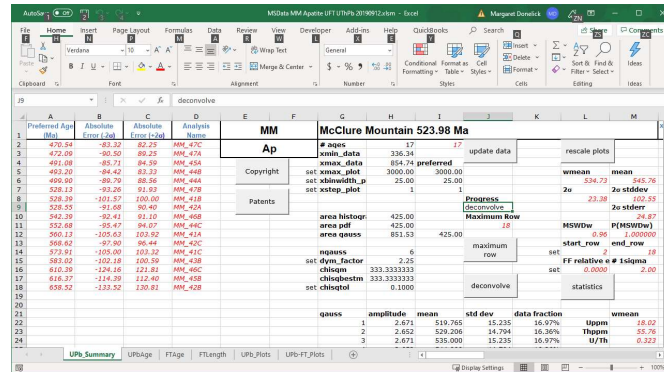
Preferred Age (Ma)	Absolute Error (2 σ)	Absolute Error (1 σ)	Analysis Name
0.08	-0.08	17.69	DR_G_042
8.03	-8.89	8.49	DR_G_039
11.51	-11.51	27.80	DR_G_036
13.39	-13.39	25.30	DR_G_035
13.75	-8.09	8.08	DR_G_031
16.03	-16.03	20.72	DR_G_052
16.68	-16.68	62.10	DR_G_052
18.27	-8.47	8.46	DR_G_032
19.34	-9.54	9.52	DR_G_057
19.86	-9.26	9.25	DR_G_037
22.62	-12.67	12.65	DR_G_046
22.64	-16.42	16.37	DR_G_055
24.68	-11.27	11.25	DR_G_025
27.52	-12.63	12.42	DR_G_051
28.25	-11.73	11.71	DR_G_031
28.43	-14.96	14.93	DR_G_052
29.85	-15.88	15.84	DR_G_046
37.90	-17.34	17.29	DR_G_051
41.66	-23.13	23.07	DR_G_056
46.70	-22.58	22.51	DR_G_051
50.69	-19.37	19.31	DR_G_051
51.51	-35.94	35.89	DR_G_046
53.71	-23.76	23.68	DR_G_026
54.46	-29.46	29.41	DR_G_026

APPENDIX 5.2.10 Apatite UFT U, Th & Pb 20190910 results for primary standard MD



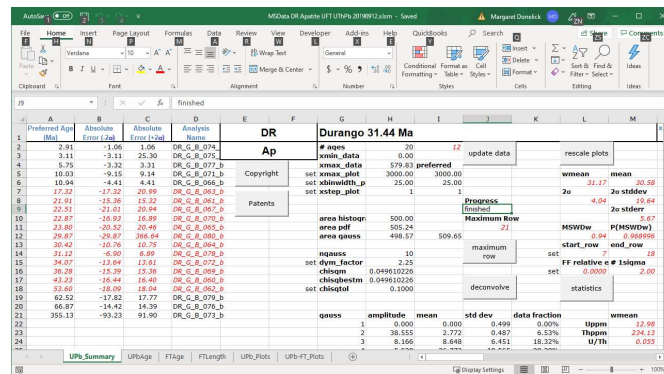
Preferred Age (Ma)	Absolute Error (2 σ)	Absolute Error (1 σ)	Analysis Name
26.42	-7.17	7.16	MD_38
41.59	-16.45	16.41	MD_37
103.68	-27.72	27.61	MD_39
105.26	-26.86	26.75	MD_39
112.00	-20.06	20.02	MD_36
130.44	-35.21	35.02	MD_35
134.62	-35.62	35.02	MD_35
172.58	-42.11	41.84	MD_29
185.47	-46.67	46.30	MD_40
188.67	-45.88	45.56	MD_29
194.58	-51.17	50.77	MD_34
257.90	-65.66	65.00	MD_31
354.47	-96.45	95.03	MD_35

APPENDIX 5.2.11 Apatite UFT U, Th & Pb 20190912 results for primary standard MM



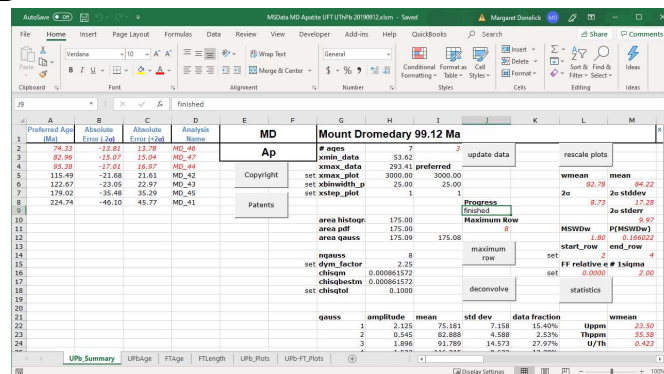
Preferred Age (Ma)	Absolute Error (2σ)	Absolute Error (1σ)	Analysis Name
476.54	48.52	82.25	MM_476
472.09	-80.50	89.25	MM_476
491.08	-85.71	84.59	MM_491
493.20	-84.42	83.23	MM_493
490.90	-89.79	88.56	MM_491
528.13	-93.26	91.93	MM_478
528.39	-101.57	100.00	MM_478
528.55	-91.68	90.40	MM_494
542.39	-92.41	91.10	MM_498
552.68	-95.67	94.07	MM_49C
560.13	-105.63	103.92	MM_414
568.62	-97.60	96.44	MM_49C
573.81	-105.00	103.32	MM_41C
583.02	-102.16	100.59	MM_418
610.39	-124.16	121.81	MM_49C
616.57	-114.99	112.40	MM_498
658.52	-133.52	130.81	MM_498

APPENDIX 5.2.12 Apatite UFT U, Th & Pb 20190912 results for primary standard DR



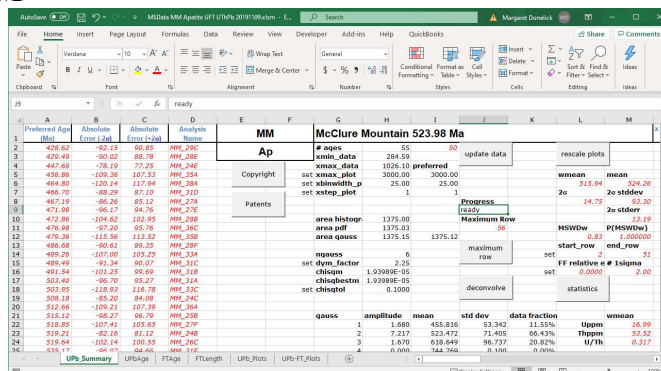
Preferred Age (Ma)	Absolute Error (2σ)	Absolute Error (1σ)	Analysis Name
2.91	-1.06	1.06	DR_G_074
3.11	-3.11	25.30	DR_G_074
5.75	-3.32	3.31	DR_G_077_b
10.63	-9.15	9.14	DR_G_071_b
15.94	-4.41	4.41	DR_G_068_b
17.32	-17.32	20.99	DR_G_063_b
21.91	-15.36	15.32	DR_G_061_b
22.51	-21.01	20.94	DR_G_067_b
22.87	-16.93	16.89	DR_G_076_b
23.80	-20.52	20.46	DR_G_095_b
26.87	-26.87	36.64	DR_G_098_b
30.42	-10.76	10.75	DR_G_064_b
31.22	-6.60	6.89	DR_G_078_b
36.07	-13.64	13.61	DR_G_072_b
38.28	-15.39	15.36	DR_G_099_b
43.23	-16.44	16.40	DR_G_066_b
53.60	-18.09	18.04	DR_G_062_b
62.52	-17.62	17.77	DR_G_079_b
66.87	-14.42	14.39	DR_G_076_b
355.13	-93.23	91.90	DR_G_073_b

APPENDIX 5.2.13 Apatite UFT U, Th & Pb 20190912 results for primary standard MD

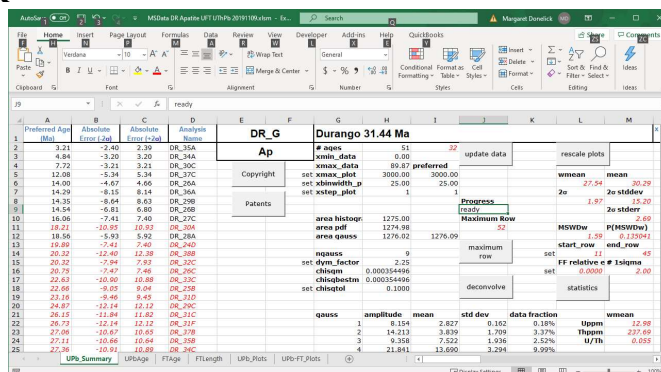


Preferred Age (Ma)	Absolute Error (2σ)	Absolute Error (1σ)	Analysis Name
74.33	-13.81	13.79	MD_48
83.96	-15.07	15.04	MD_47
85.38	-17.01	16.97	MD_44
115.49	-21.68	21.61	MD_43
122.67	-23.05	22.97	MD_43
179.92	-35.48	35.29	MD_45
224.74	-46.10	45.77	MD_41

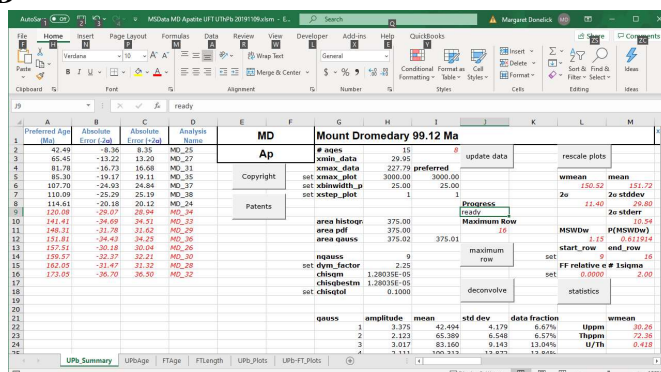
APPENDIX 5.2.14 Apatite UFT U, Th & Pb 20191109 results for primary standard MM



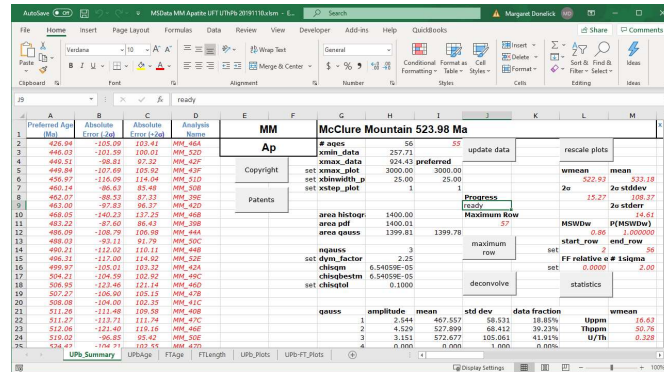
APPENDIX 5.2.15 Apatite UFT U, Th & Pb 20191109 results for primary standard DR



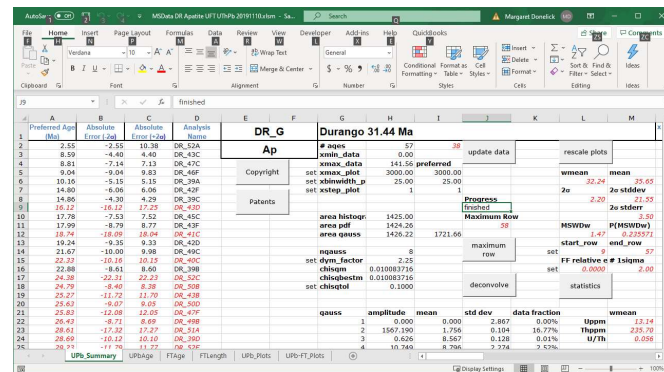
APPENDIX 5.2.16 Apatite UFT U, Th & Pb 20191109 results for primary standard MD



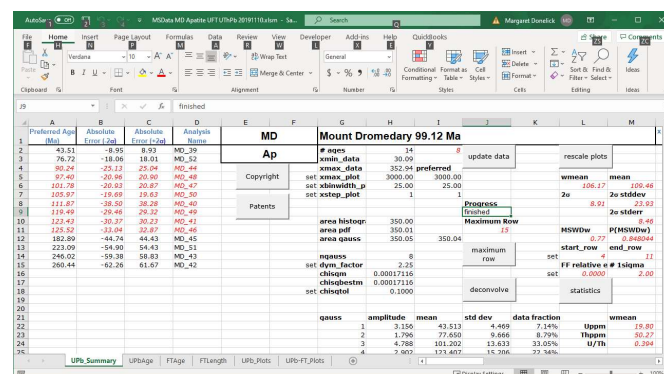
APPENDIX 5.2.17 Apatite UFT U, Th & Pb 20191110 results for primary standard MM



APPENDIX 5.2.18 Apatite UFT U, Th & Pb 20191110 results for standard DR



APPENDIX 5.2.19 Apatite UFT U, Th & Pb 20191110 results for standard MD



APPENDIX 5.2.20 Apatite UFT U, Th & Pb 20191216 results for primary standard MM

[illegible]

APPENDIX 5.2.21 Apatite UFT U, Th & Pb 20191216 results for standard DR

APPENDIX 5.2.22 Apatite UFT U, Th & Pb 20191216 results for standard MD

[illegible]

APPENDIX 5.3 ANALYTICAL METHODS USED IN THE APT UK LABORATORY (UK)

- APPENDIX 5.3.1 Introduction
- APPENDIX 5.3.2 Microscopy analysis methods

Analytical methods used in the APT UK laboratory (UK)

APPENDIX 5.3.1 INTRODUCTION

Microscopy analyses are carried out by APT UK in their laboratory in Colwyn Bay, North Wales, United Kingdom. Descriptions of the techniques employed are given below.

APPENDIX 5.3.2 MICROSCOPY ANALYSIS METHODS

Kerogen microscopy is carried out by APT UK in both reflected and transmitted light as described below:

Microscopes

Reflectivity measurements are made using a Zeiss Universal microscope equipped with an Epi 40X Pol oil immersion objective and 10.0X eyepieces, giving a total visual magnification of 400X. The immersion oil used is Cargille Type A (refractive index = 1.515° at 23°C). Measurements are made in light at a wavelength of 546nm (green), which is the ICCP standard. The measuring aperture is circular with a diameter of 1.6 micron or 0.8 microns; the choice of measuring aperture size is dependent on the size and quality of the organic material being measured.

Kerogen colouration and fluorescence analyses are conducted in transmitted white light using a Zeiss Axioplan microscope fitted with Zeiss Epiplan – Neofluar 10X, 40X and 63X objectives and 10X eyepieces, which gives a total visual magnification of 100X, 400X and 630X. Ultra-violet fluorescence colours are observed in reflected short wavelength blue light using an excitation filter passing light of 365nm wavelength, a barrier filter of 397nm, and a dichromatic beam splitter of 395nm wavelength.

Reflected light studies

The reflectivity studies have been carried in the first instance out using polished samples of isolated kerogen mounted in resin blocks. Grinding and polishing were carried out on a rotating lap wheel. The surface of the blocks was ground flat on carborundum papers using progressively finer grinding stages of 120, 240, 600 and 1200 grit. Polishing was carried out in three stages; 5/20, 3/50 and gamma alumina (.05µ) on magnetically attached polishing pads using water as lubricant. The finished blocks were mounted on microscope slides using a hand press and a small lump of plasticine, ensuring that the polished surface is normal to the incident light.

Measurements made are of Ro(random), which means they are made in nominally unpolarised light; as against Ro(max), which are made in polarised light. Two of three standards are normally used: Spinel (Ro = 0.588%), Yttrium-Aluminium-Garnet (Ro = 0.879%) and Gadolinium-Gallium-Garnet (Ro = 1.696%). The choice of standards used is dependent on the expected range of reflectivity of the samples being examined.

Spore colouration studies

The slides used for spore colouration work are prepared using standard palynological techniques (hydrochloric and hydrofluoric acids) but omitting any oxidative stages. The kerogen is floated in zinc bromide after agitation with ultrasonic energy to disaggregate the kerogen components to remove mineral matter. The floated kerogen is then split into unsieved total kerogen and sieved >10µ fractions, each of which are mounted on separate cover slips,

which are then affixed to the same microscope slide using Norland Optical Adhesive. Unused kerogen is retained in water for use in preparing polished kerogen blocks for reflectivity studies.

Spore colours are determined using the $>10\mu$ fraction while kerogen description is carried out using the total kerogen. Spore colour and kerogen typing analyses are supplemented by observation of exinite fluorescence under reflected blue light excitation.